1227706
[00829504]

OFFICE OF RIVER PROTECTION
P.O. Box 450, MSIN H6-60
Richland, Washington 99352

DEC 03 2014

14-TF-0128

Ms. Jane A. Hedges, Program Manager
Nuclear Waste Program
Washington State
Department of Ecology
3100 Port of Benton Blvd
Richland, Washington 99354

RECEIVED
DEC 08 2014
EDMC

Ms. Hedges:

COMPLETION OF HANFORD FEDERAL FACILITY AGREEMENT AND CONSENT ORDER TARGET DATE M-045-91G-T04, DUE JANUARY 30, 2015

Reference: WRPS letter L.D. Olson to K.W. Smith, ORP, "Washington River Protection Solutions LLC Submittal of Hanford Federal Facility Agreement and Consent Order Target M-045-91G-T04 Deliverable," WRPS-1404777, dated November 13, 2014.

This letter documents the completion of the Hanford Federal Facility Agreement and Consent Order target date M-045-91G-T04. This target date requires that the U.S. Department of Energy, Office of River Protection:

> Provide to Ecology the Structural Analyses of Record final documentation of SSTs for: 55,000 gallon tanks (B, C, T, and U farms).

The enclosed document, RPP-RPT-49993, *Single-Shell Tank Integrity Project Analysis of Record Hanford Type I Single-Shell Tank Thermal and Operating Loads and Seismic Analysis*, meets the requirements of M-045-91G-T04. RPP-RPT-49993 was prepared using the criteria specified in RPP-46442, *Single-Shell Tank Structure Evaluation Criteria.*

If you have questions, please contact Mr. Jeremy M. Johnson at 376-1866.

K. W. Smith

Kevin W. Smith
Manager

TPD:JMJ

Attachment

Distribution: See Page 2

340

cc w/attach:
Environmental Portal, LMSI
TPA Administrative Record
WRPS Correspondence

cc w/o attach:
S. Harris, CTUIR
J.M. Alzheimer, Ecology
J.J. Lyon, Ecology
J.B. Price, Ecology
N.H. Uziemblo, Ecology
D.A. Faulk, EPA
G. Bohnee, NPT
S.E. Hudson, HAB
R.E. Piippo, MSA
J.G. Woolard, MSA
K.Niles, ODOE
R.Buck, Wanapum
J.J. Luke, WRPS
R.Jim, YN
D. Rowland, YN

ATTACHMENT

14-TF-0128

RPP-RPT-49993

Single-Shell Tank Integrity Project Analysis of Record Hanford Type I Single-Shell Tank Thermal and Operating Loads Seismic Analysis

Rev. 0

DOCUMENT RELEASE AND CHANGE FORM

Prepared For the U.S. Department of Energy,
Assistant Secretary for Environmental Management
By Washington River Protection Solutions, LLC., PO Box 850, Richland, WA 99352
Contractor For U.S. Department of Energy, Office of River Protection, under Contract DE-AC27-08RV14800

1a. Doc No: RPP-RPT-49993 **Rev.** 00

1b. Project Number: ☒ N/A

TRADEMARK DISCLAIMER: Reference herein to any specific commercial product, process, or service by trade name, trademark, manufacturer, or otherwise, does not necessarily constitute or imply its endorsement, recommendation, or favoring by the United States government or any agency thereof or its contractors or subcontractors.

Printed in the United States of America.

Release Stamp

2. Document Title

Single-Shell Tank Integrity Project Analysis of Record Hanford Type I Single-Shell Tank Thermal and Operating Loads and Seismic Analysis

3. Design Verification Required

☐ Yes ☐ No

4. USQ Number ☐ N/A
TF-14-1956-D_R0

5. PrHA Number ☒ N/A
Rev.

6. USQ Screening:

a. Does the change introduce any new failure modes to the equipment? ☐ **Yes** ☒ **No**
Basis is required for Yes:_____

b. Does the change increase the probability of existing failure modes? ☐ **Yes** ☒ **No**
Basis is required for Yes:

c. For Safety Significant equipment, does the change require a modification to Chapter 4 of the DSA and/or FRED? ☐ **Yes** ☐ **No** ☒ **N/A**
Basis is required for Yes:

7. Description of Change and Justification (Use Continuation pages as needed)

Initial Issue

8. Approvals

Title	Name	Signature	Date
Checker	SCOTT, MARK A	MISIAK, THOMAS A for SCOTT, MARK A per telecon	10/22/2014
Clearance Review	BRATTON, GAYLA E	BRATTON, GAYLA E	11/04/2014
Design Authority	GAUCK, GREGORY J	GAUCK, GREGORY J	10/23/2014
Document Control Approval	WASHINGTON, MARGUERITE	WASHINGTON, MARGUERITE	11/04/2014
Originator	MISIAK, THOMAS A	MISIAK, THOMAS A	10/22/2014
Other Approver	VOOGD, JEFFRY A	VOOGD, JEFFRY A	10/23/2014
Other Approver	BINGHAM, JAMES D	BINGHAM, JAMES D	10/23/2014
Other Approver	BERGMAN, SCOTT M	BERGMAN, SCOTT M	10/23/2014
Responsible Engineer	MISIAK, THOMAS A	MISIAK, THOMAS A	10/22/2014
Responsible Manager	BAIDE, DAN	BAIDE, DAN	11/03/2014

Please see continuation sheet

9. Clearance Review:

Restriction Type:

☒ Public
☐ Undefined
☐ Unclassified Controlled Nuclear Information (UCNI)
☐ Export Control Information (ECI)
☐ Official Use Only Exemption 2-Circumvention of Statute (OUO-2)
☐ Official Use Only Exemption 3-Statutory Exemption (OUO-3)
☐ Official Use Only Exemption 4-Commercial/Proprietary (OUO-4)
☐ Official Use Only Exemption 5-Privileged Information (OUO-5)
☐ Official Use Only Exemption 6-Personal Privacy (OUO-6)
☐ Official Use Only Exemption 7-Law Enforcement (OUO-7)

DOCUMENT RELEASE AND CHANGE FORM

Doc No: RPP-RPT-49993 **Rev.** 00

10. Distribution:

Name	Organization
BAIDE, DAN	TFP ENGINEERING
BERGMAN, SCOTT M	ELECTRICAL/AREA/242A-EVAP ENG
BINGHAM, JAMES D	ELECTRICAL/AREA/242A-EVAP ENG
BOOMER, KAYLE D	TANK AND PIPELINE INTEGRITY
CASTLEBERRY, JIM L	TFP PROJECT MANAGEMENT
GAUCK, GREGORY J	WASTE STORAGE/TRANSFER ENG
HAASS, MATT J	
JOHNSON, JEREMY	
LITTLE, DAVID B	ENGINEERING
MISIAK, THOMAS A	ENGRNG PROGRAMS & STANDARDS
SCOTT, MARK A	ENGRNG PROGRAMS & STANDARDS
TURKNETT, JERRY C	COGNIZANT SYSTEM ENGINEERING
VENETZ, TED J	TANK AND PIPELINE INTEGRITY
VOOGD, JEFFRY A	BASE OPS ENV COMPLIANCE

11. TBDs or Holds ☒ N/A

12. Impacted Documents – Engineering ☐ N/A

Document Number	Rev.	Title
RPP-11802	03A	ANALYSIS OF RECORD SUMMARY FOR SINGLE-SHELL TANKS

13. Other Related Documents ☐ N/A

Document Number	Rev.	Title
RPP-RPT-49989	00	SINGLE-SHELL TANK INTEGRITY PROJECT ANALYSIS OF RECORD HANFORD TYPE II SINGLE-SHELL TANK THERMAL AND OPERATING LOADS AND SEISMIC ANALYSIS
RPP-RPT-49990	00	SINGLE-SHELL TANK INTEGRITY PROJECT ANALYSIS OF RECORD HANFORD TYPE III SINGLE-SHELL TANK THERMAL AND OPERATING LOADS AND SEISMIC ANALYSIS
RPP-RPT-49991	00	Single-Shell Tank Integrity Project Analysis of Record Tank to Tank Interaction Study of the Hanford Single-Shell Tanks
RPP-RPT-49992	00	Single-Shell Tank Integrity Project Analysis of Record Hanford Type IV Single-Shell Tank Thermal and Operating Loads and Seismic Analysis

14. Related Systems, Structures, and Components:

14a. Related Building/Facilities ☐ N/A	14b. Related Systems ☐ N/A	14c. Related Equipment ID Nos. (EIN) ☒ N/A
241-B 241-C 241-T 241-U	241-WST	

DOCUMENT RELEASE AND CHANGE FORM CONTINUATION SHEET

Document No: RPP-RPT-49993 **Rev.** 00

8. **Approvals**			
Title	**Name**	**Signature**	**Date**
USQ Evaluator	LOPEZ, RAFAEL	LOPEZ, RAFAEL	10/22/2014

N/A

RPP-RPT-49993, Rev. 0

SINGLE-SHELL TANK INTEGRITY PROJECT ANALYSIS OF RECORD HANFORD TYPE I SINGLE-SHELL TANK THERMAL AND OPERATING LOADS AND SEISMIC ANALYSIS

Author Name:
T.A. Misiak
Washington River Protection Solutions
Richland, WA 99352
U.S. Department of Energy Contract DE-AC27-08RV14800

EDT/ECN: DRCF UC:
Cost Center: Charge Code:
B&R Code: Total Pages: 337 mw 11/4/2014

Key Words: Single-Shell Tank, SST, structural, analysis of record, AOR, thermal, operating, seismic, concrete, rebar, soil-structure interaction, finite element analysis, ANSYS, Type I, dome, load

Abstract: This report documents the structural analysis of record (AOR) of Hanford 55,000 gallon (Type I) Single-Shell Tanks (SSTs). The analysis concludes that for the imposed loading, the reinforced concrete tank structure meets the requirements of the American Concrete Institute (ACI) 349 code and thereby the International Building Code (IBC). Analyses include the effects and combinations of seismic, dead, live, soil, thermal, hydrostatic, and concentrated loads. Limit load and buckling analyses are also performed to provide insight as to the response of the tank structure to increased concentrated and distributed loads applied at the ground surface. This AOR has been peer reviewed by recognized industry experts.

TRADEMARK DISCLAIMER. Reference herein to any specific commercial product, process, or service by trade name, trademark, manufacturer, or otherwise, does not necessarily constitute or imply its endorsement, recommendation, or favoring by the United States Government or any agency thereof or its contractors or subcontractors.

Release Approval Date Release Stamp

Approved For Public Release

U.S. DEPARTMENT OF ENERGY

Prepared for the U.S. Department of Energy
under Contract DE-AC05-76RL01830

RPP-RPT-49993, Rev. 0
PNNL-23745

Single-Shell Tank Integrity Project Analysis of Record

Hanford Type I Single-Shell Tank Thermal and Operating Loads and Seismic Analysis

Report to Washington River Protection Solutions

KI Johnson
JE Deibler
FG Abatt
BM Larsen
NK Karri
SE Sanborn
KL Stoops
LJ Julyk

October 2014

Pacific Northwest
NATIONAL LABORATORY
Proudly Operated by Battelle Since 1965

DISCLAIMER

This report was prepared as an account of work sponsored by an agency of the United States Government. Neither the United States Government nor any agency thereof, nor Battelle Memorial Institute, nor any of their employees, makes **any warranty, express or implied, or assumes any legal liability or responsibility for the accuracy, completeness, or usefulness of any information, apparatus, product, or process disclosed, or represents that its use would not infringe privately owned rights**. Reference herein to any specific commercial product, process, or service by trade name, trademark, manufacturer, or otherwise does not necessarily constitute or imply its endorsement, recommendation, or favoring by the United States Government or any agency thereof, or Battelle Memorial Institute. The views and opinions of authors expressed herein do not necessarily state or reflect those of the United States Government or any agency thereof.

PACIFIC NORTHWEST NATIONAL LABORATORY
operated by
BATTELLE
for the
UNITED STATES DEPARTMENT OF ENERGY
under Contract DE-AC05-76RL01830

This document was printed on recycled paper.
(9/2003)

RPP-RPT-49993, Rev. 0
PNNL-23745

Single-Shell Tank Integrity Project Analysis of Record

Hanford Type I Single-Shell Tank Thermal and Operating Loads and Seismic Analysis

Report to Washington River Protection Solutions

KI Johnson
JE Deibler
FG Abatt[a]
BM Larsen[a]
NK Karri
SE Sanborn
KL Stoops[a]
LJ Julyk[a]

October 2014

Prepared for
the U.S. Department of Energy
under Contract DE-AC05-76RL01830

Pacific Northwest National Laboratory
Richland, Washington 99352

(a) Becht Engineering
Richland, Washington 99352

This page intentionally left blank.

Executive Summary

This report, prepared by Pacific Northwest National Laboratory and Becht Engineering for Washington River Protection Solutions, documents the Type I (55-kgal storage capacity) single-shell tank (SST) detailed modeling results for the thermal and operating loads analysis (TOLA) and seismic analysis under the Single-Shell Tank Analysis of Record (SST AOR) Project.

The SST AOR project supports the U.S. Department of Energy's (DOE's) Office of River Protection mission for obtaining a better understanding of the structural integrity of Hanford SSTs. Phase I of the SST AOR Project included the Evaluation Criteria report (Johnson et al. 2010) to guide the AOR of the Hanford SSTs, and the Preliminary Modeling Plan for Thermal and Operating Loads, found in Rinker et al. (2010), to determine the number of analyses required for adequate bounding of each of the SST types. Phase II of the SST AOR performs detailed modeling of thermal, operating, and seismic loads for each of the Hanford SST types. This Type I SST report is one of the Phase II deliverables for the SST AOR Project.

The analyses documented in this report used modern finite element modeling techniques with ANSYS®,[(a)] version 13.0 (ANSYS, 2010). The ANSYS® software was fully verified and validated per the project quality assurance requirements on each of the computers used in the structural analyses.

The TOLA static model includes the Type I geometry and the steel reinforcement detailed in the tank drawings. The static analysis evaluated the effects of waste level, waste temperature, and soil overburden loads. The effects of temperature on material properties, concrete cracking, and soil properties were also considered. The effects of time (creep) on the concrete were not considered. Previous SST AORs have demonstrated that creep leads to reduced demands on the concrete. A tank limit load analysis was also conducted with the TOLA static model. Tank buckling was also evaluated using theoretical buckling solutions with appropriate knockdown factors for geometric imperfections, creep, cracking of reinforced concrete, and inelastic concrete deformation.

The SSTs are categorized as and evaluated as Performance Category 2 (PC-2) structures, and DOE-STD-1020-2002, Section 2 (DOE 2002), requires that the ground motions for PC-2 shall be developed following the 2000 International Building Code requirements. The Tank Operations Contractor standard (TFC-ENG-STD-06) recognizes the State of Washington Administrative Code 51-50-003, which adopted the 2009 edition of the International Building Code at the time that the structural evaluation criteria for the SSTs were developed (Johnson et al. 2010).

Consistent with Johnson et al. (2010), IBC (2009), and DOE (2002), the MCE ground motions are defined as the ground motions with a mean annual frequency of exceedance of 4×10^{-4} (2% probability of exceedance in 50 years). In this analysis, the site-specific design response spectra (DRS) for the SST facilities site uses the Rohay and Reidel (2005) Hanford Waste Treatment Plant (WTP) design spectra as a reasonable assessment of the current state of knowledge of the hazard levels at the 200 East and 200 West areas. The 2005 spectra are conservative relative to data documented in Geomatrix (2007), but this choice was made to protect against the chance that Hanford seismic hazard levels could be increased in

(a) ANSYS® is a registered trademark of ANSYS, Inc., Canonsburg, Pennsylvania.

the near future. The dynamic seismic model evaluated a range of soil properties, and evaluated tanks with and without waste during a seismic event using degraded concrete properties as determined in TOLA.

While the International Building Code (IBC) does not explicitly address underground tanks, provisions are made within the code to satisfy its requirements by demonstrating compliance with the requirements of the American Concrete Institute (ACI) code for concrete structures. Chapter 19 of the IBC states that structural concrete shall be designed in accordance with the requirements of ACI 318. The commentary on ACI 349 describes the additional conservatisms for nuclear structures that exceed those in ACI 318. Therefore, the Evaluation Criteria report (Johnson et al. 2010) specified that the American Concrete Institute code for nuclear safety-related structures (ACI 349-06) be used to evaluate the SST reinforced concrete structures. ACI 349-06 defines specific combinations of static, thermal, and seismic loads that must be checked. For the static plus seismic load combination, the concrete forces and moments from the dynamic seismic analyses were added to the static TOLA results as prescribed in ACI-349-06. The SST Type I results documented in this report demonstrate that the steel reinforced concrete SSTs meet the requirements of ACI 349-06 and by inference the IBC (2009).

The structural evaluations completed with the TOLA and seismic tank models do not reveal any significant deficiencies with the structural integrity of the Type I SSTs. Very minor rebar yielding (0.05% strain) was predicted at the edge of the flat roof as the tank thermal history was applied. However, this yielding did not increase under application of the LC1 (factored static load) or LC4 (unfactored static plus seismic) load combinations. The analyses evaluate 67 years of use, which extends from 1947 when the Type-I tanks were initially filled to the present. The temperature records for the Type I tanks are very limited, so a maximum temperature of 250°F was imposed to include the potential for storing high-heat generating wastes. Bounding material properties were also selected to analyze the most limiting combinations.

The soil overburden is the largest load on the tank and the largest contributor to the static tank demands. Waste and soil surface loads produced only secondary effects. Thermal loads were significant in the slab and lower wall where the temperatures were highest (250°F). There was little variation in concrete section demands with the different material combinations.

The Type I tank model was subjected to a 142 kip concentrated load on the soil surface, a 40 lb/ft^2 uniform surface load for snow and ash, a typical waste load history, and a 67-year thermal history that peaked at 250°F. Soil at 125 lb/ft^3 was modeled over the flat tank roof to bound the maximum 11.45-ft soil depth measured over the B-201 through B-204, Type I tanks (Rifaey 2002). The ACI 349-06 code evaluations show that tank demands are lower than the capacities for all locations in the roof, upper haunch, and wall. The peak non-seismic ACI 349-06 load demands are 52%, 22%, and 38% of the meridional, hoop, and shear capacities, respectively, at any section in the roof, upper haunch, and wall.

The maximum tank section forces and moments over the time history were extracted from the seismic model and combined with the non-seismic forces and moments to evaluate the ACI seismic load combination. Again, the seismic ACI evaluation results indicate that tank demands are lower than the ACI 349-06 capacities for all locations in the roof, upper haunch, and wall. The peak seismic ACI load combination resulted in demands that were 45%, 26%, and 32% of the meridional, hoop, and shear capacities, respectively, in the roof, upper haunch, and wall. The seismic loads are small, representing only about 10% of the section capacities. This increases the maximum D/C ratios for the unfactored thermal and operating loads from 0.35 to 0.45.

Tank-to-tank interaction effects were considered but not specifically evaluated for the Type I tanks because the 50-ft center-to-center spacing gives 3 radii of soil between adjacent tanks. Furthermore, all the D/C ratios are significantly less than 0.8, so adding the maximum $\Delta D/C=0.2$ for tank-to-tank effects would still result in D/C ratios well below 1.0.

The TOLA analyses and the combined case of TOLA and seismic loads did show several locations in the bottom slab where section demands are predicted to be higher than capacities. This indicates that cracking of the slab likely occurred from radial thermal expansion followed by contraction under the bounding thermal history. However, cracks in the slab do not affect the structural stability of the tank roof, walls, and footing. The slab removal study evaluated the effect of possible cracking and shear offset between the footing and slab. This analysis predicted that the maximum shear offset would be less than one-half of the nominal steel liner thickness. The slab removal study concluded that neither the structural stability nor the liner integrity would be affected by the potential shear offset at the footing to slab interface.

Tank limit load and buckling analyses are also included in the Type I SST analysis of record. The limit load analysis evaluated both uniform and concentrated loads over the tank roof. The tank limit load analyses, as applied with a conservative plastic strain limit criterion, produce safety factors less than the recommended value of 3.0. However, the load-displacement curves continue to increase beyond the plastic strain criterion, indicating that the tanks are able to support further increased loads. The use of the concrete crushing criterion increases the safety factors to 2.9 and 3.0 for the local and uniform surface loads respectively. Additional more refined analysis is recommended if the need for an over-tank concentrated load arises. The buckling analysis evaluated the tank wall with the 11.45 ft soil overburden at 125 lbf/ft^3 plus uniform and concentrated surface loads. The combined vertical and lateral soil pressures on the tank wall only comprise about 17% of the buckling capacity. The analysis shows that the tank wall is very stable and would fail first by plastic limit load rather than elastic buckling.

Appendix A provides load contribution plots showing the effects of individual load components and force and moment plots for Run #6 with nominal strength concrete to gain a more complete understanding of the Type I SST loads. Appendices B and C document the buckling analyses using Mathcad™ and the details of the ACI evaluations. Appendix D documents the independent review assessment of this analysis. Attachment 1 contains the seismic analysis report prepared by Becht Engineering.

This page intentionally left blank.

Acknowledgments

Project Management would like to thank the static and seismic modeling teams for their tenacity in the completion of task deliverables. In addition, appreciation is extended to the following individuals for their dedicated administrative, contracts, scheduling and budget support, technical editing and formatting, and peer review support, respectively: Lori Bisping, Kelle Airhart, Kay Hass, and Ray Shippell.

This page intentionally left blank.

Acronyms

ACI	American Concrete Institute
AOR	analysis of record
ASA	Accelerated Safety Analysis
ASCE	American Society of Civil Engineers
ASME	American Society of Mechanical Engineers
ASTM	American Society for Testing and Materials
AWS	American Welding Society
BBI	Best-Basis Inventory
BES	best estimate soil
CTL	Construction Technology Laboratory
DBE	design-basis (event/earthquake)
D/C	demand/capacity ratio
DF	damping factor
DOE	U.S. Department of Energy
DOE-RL	U.S. Department of Energy's Richland Operations Office
DRS	design response spectra
DW	dead weight
EDP	Extended Drucker-Prager
EPA	U.S. Environmental Protection Agency
FCC	fully cracked concrete
FE	finite element
FIRS	foundation input response spectra
HEW	Hanford Engineering Works
HW	Hanford Works
HWS	Hanford Works Specification
IBC	International Building Code
IDMS	Integrated Data Management System
kip	thousand pounds
LBS	lower bound soil
LC1	ACI Load Combination 1
LC4	ACI Load Combination 4
LC9	ACI Load Combination 9
MP	material properties
NRA	not readily available
ORP	DOE Office of River Protection
PNNL	Pacific Northwest National Laboratory

QA	Quality Assurance
QAPD	Quality Assurance Program Description
SACS	Surveillance Analysis Computer System
SSI	soil-structure interaction
SST	single-shell tank
TOLA	Thermal and Operating Loads Analysis
TTI	tank to tank interaction
TWINS	Tank Waste Information Network System
UBS	upper bound soil
WRPS	Washington River Protection Solutions

Contents

Executive Summary iii
Acknowledgments vii
Acronyms ix
1.0 Introduction and Objective 1.1
1.1 Quality Assurance 1.1
2.0 Scope 2.1
2.1 TOLA and Seismic Results Roadmap 2.1
3.0 Type I SST Background 3.1
3.1 Design 3.1
3.2 Temperature and Waste Height Profiles 3.5
4.0 Guidance 4.1
4.1 Acceptance Criteria 4.1
4.1.1 Material Properties 4.1
4.1.2 Loads 4.2
4.1.3 Static Load Combinations 4.3
4.2 Post Design Evaluation Input 4.6
5.0 Static Thermal and Operating Loads Analysis 5.1
5.1 Introduction 5.1
5.2 ANSYS® Model Construction 5.1
5.3 Real Constants 5.6
5.4 Loads and Boundary Conditions 5.8
5.5 The TOLA Run Matrix 5.9
5.6 Temperature Profile and the Thermal Model 5.10
6.0 Seismic Analysis 6.1
7.0 Static Modeling Results 7.1
7.1 Introduction 7.1
7.2 Steel Reinforcement Plastic Strain 7.1
7.3 ACI Evaluations – Structural Concrete 7.2
7.4 Run 2, Baseline Case with Best Estimate Material Properties 7.7
7.5 Run 4, Low Soil Modulus, High Concrete Modulus, and Near Zero Concrete Tensile Strength 7.14
7.6 Run 7, Low Soil Modulus, Nominal Concrete Modulus, and Near Zero Concrete Tensile Strength 7.22
7.7 Slab Removal Study 7.28
7.8 TOLA Run Matrix Conclusions 7.32
8.0 Seismic Results 8.1
9.0 Combined Static and Seismic Results 9.1

9.1 TOLA and Seismic Combination Procedure 9.1
9.2 ACI Load Combination 4 Results 9.2
10.0 Tank Limit Analysis 10.1
11.0 Concrete Shell Buckling Analysis 11.1
11.1 Unfactored Theoretical Buckling Loads for a Cylindrical Wall Under Axial Compression and External Pressure 11.2
11.2 Buckling Load-Reduction Factors 11.3
11.3 Buckling Load-Interaction and Safety Factors 11.7
11.4 Results of the Type I Tank Wall Buckling Evaluation 11.9
11.5 Summary of the Type I Tank Buckling Evaluation 11.10
12.0 Conclusions 12.1
13.0 References 13.1
Appendix A – Run 1, Baseline Case with Best Estimate Material Properties: Load Contributions A.1
Appendix B – Buckling Calculations in Mathcad B.1
Appendix C – Details of ACI-349 Demand/Capacity Calculations C.1
Appendix D – External Reviewer Comments and Resolutions D.1
Attachment 1 – Seismic Analysis Report Att.1

Figures

3.1 Cross-Section View of the Type I, Series 200 SSTs 3.2
3.2 Aerial View of the Four Type I Tanks at the West Edge of B-Farm 3.2
3.3 Typical 55,000-Gallon Single-Shell Waste Tank and Riser Configuration for Type I Tanks 241B, 241C, 241T, and 241U. 3.3
3.4 The Temperature (°F) and Waste Height (inches) Profiles used in the Type I AOR 3.6
4.1 Typical Layout of a Type I Single-Shell Tank Model 4.5
4.2 TOLA Flow Plan for Type I SST AOR 4.6
5.1 Finite Element Mesh of Tank and Soil Element-Type Plot 5.3
5.2 Close-up of Roof and Wall Reinforced Concrete Elements (ANSYS Real Constant Plot) 5.4
5.3 Close-up of Footing with Reinforced Concrete Elements (ANSYS Real Constant Plot) 5.4
5.4 ANSYS Model Showing Type I SST and Surrounding Soil (Material-Type Plot) 5.5
5.5 Final ANSYS Type I Model (Material-Type Plot) 5.5
5.6 ANSYS Model – Hatchway Details (Element-Type Plot) 5.6
5.7. Thermal Model 5.11
5.8 Peak (250°F) Temperature Distribution in Concrete Tank 5.12
5.9 Peak (250°F) Temperature Distribution 5.13
7.1 Steel Reinforcement Plastic Strain 7.2
7.2 Reinforced Concrete ACI Evaluated Sections 7.4
7.3 ACI Demand/Capacity Ratio Definition 7.7
7.4 Run 2, Meridional ACI D/C Ratios at Peak Temperature 7.7
7.5 Run 2, Hoop ACI D/C Ratios at Peak Temperature 7.8
7.6 Run 2, Shear ACI D/C Ratios at Peak Temperature 7.8
7.7 Run 2, In-Plane Shear ACI D/C Ratios at Peak Temperature 7.8
7.8 Run 2, Meridional ACI D/C Ratios at LC1 ..... 7.9
7.9 Run 2, Hoop ACI D/C Ratios at LC1 ..... 7.9
7.10 Run 2, Shear ACI D/C Ratios at LC1 ..... 7.9
7.11 Run 2, In-Plane Shear ACI D/C Ratios at LC1 ..... 7.10
7.12 Run 2, Meridional ACI D/C Ratios at LC4 (TOLA only) 7.10
7.13 Run 2, Hoop ACI D/C Ratios at LC4 (TOLA only) 7.10
7.14 Run 2, Shear ACI D/C Ratios at LC4 (TOLA only) 7.11
7.15. Run 2, In-Plane Shear ACI D/C Ratios at LC4 (TOLA only) 7.11
7.16 Run 2, Meridional ACI D/C Ratios at LC9 ..... 7.11
7.17 Run 2, Hoop ACI D/C Ratios at LC9 ..... 7.12
7.18 Run 2, Shear ACI D/C Ratios at LC9 ..... 7.12
7.19 Run 2, In-Plane Shear ACI D/C Ratios at LC9 ..... 7.12
7.20 Run 2, Sections 18 – 20 Shear ACI D/C Ratios at LC9 ..... 7.13
7.21 Run 2, Section 19 Shear ACI D/C Ratios at LC9 ..... 7.14

7.22 Run 4, Meridional ACI D/C Ratios at Peak Temperature 7.14
7.23 Run 4, Hoop ACI D/C Ratios at Peak Temperature 7.15
7.24 Run 4, Shear ACI D/C Ratios at Peak Temperature 7.15
7.25 Run 4, In-Plane Shear ACI D/C Ratios at Peak Temperature 7.15
7.26 Run 4, Meridional ACI D/C Ratios at LC1 ..... 7.16
7.27 Run 4, Hoop ACI D/C Ratios at LC1 ..... 7.16
7.28 Run 4, Shear ACI D/C Ratios at LC1 ..... 7.16
7.29 Run 4, In-Plane Shear ACI D/C Ratios at LC1 ..... 7.17
7.30 Run 4, Meridional ACI D/C Ratios at LC4 (TOLA only) 7.17
7.31 Run 4, Hoop ACI D/C Ratios at LC4 (TOLA only) 7.17
7.32 Run 4, Shear ACI D/C Ratios at LC4 (TOLA only) 7.18
7.33 Run 4, In-Plane Shear ACI D/C Ratios at LC4 (TOLA only) 7.18
7.34 Run 4, Meridional ACI D/C Ratios at LC9 ..... 7.18
7.35 Run 4, Hoop ACI D/C Ratios at LC9 ..... 7.19
7.36 Run 4, Shear ACI D/C Ratios at LC9 ..... 7.19
7.37 Run 4, In-Plane Shear ACI D/C Ratios at LC9 ..... 7.19
7.38 Run 4, Section 19 Shear ACI D/C Ratios at LC9 ..... 7.20
7.39 Run 4, Section 19 ACI Shear Demand and Capacity at LC9 ..... 7.21
7.40 Run 4, Section 19 and 20 Meridional Moment at LC9 ..... 7.21
7.41 Run 7, Meridional ACI D/C Ratios at Peak Temperature 7.22
7.42 Run 7, Hoop ACI D/C Ratios at Peak Temperature 7.22
7.43 Run 7, Shear ACI D/C Ratios at Peak Temperature 7.23
7.44 Run 7, In-Plane Shear ACI D/C Ratios at Peak Temperature 7.23
7.45 Run 7, Meridional ACI D/C Ratios at LC1 ..... 7.23
7.46 Run 7, Hoop ACI D/C Ratios at LC1 ..... 7.24
7.47 Run 7, Shear ACI D/C Ratios at LC1 ..... 7.24
7.48 Run 7, In-Plane Shear ACI D/C Ratios at LC1 ..... 7.24
7.49 Run 7, Meridional ACI D/C Ratios at LC4 (TOLA only) 7.25
7.50 Run 7, Hoop ACI D/C Ratios at LC4 (TOLA only) 7.25
7.51 Run 7, Shear ACI D/C Ratios at LC4 (TOLA only) 7.25
7.52 Run 7, In-Plane Shear ACI D/C Ratios at LC4 (TOLA only) 7.26
7.53 Run 7, Meridional ACI D/C Ratios at LC9 ..... 7.26
7.54 Run 7, Hoop ACI D/C Ratios at LC9 ..... 7.26
7.55 Run 7, Shear ACI D/C Ratios at LC9 ..... 7.27
7.56 Run 7, In-Plane Shear ACI D/C Ratios at LC9 ..... 7.27
7.57 Slab Detachment – Section 19 ..... 7.29
7.58 ACI Meridional D/C Ratios, Slab Detachment 7.30
7.59 ACI Hoop D/C Ratios, Slab Detachment 7.30
7.60 ACI Shear D/C Ratios, Slab Detachment 7.31

7.61 ACI In-Plane Shear D/C Ratios, Slab Detachment 7.31
9.1 Example P-M Diagram with Four Possible Seismic Combinations 9.2
9.2 Meridional ACI D/C Ratios at LC4 ..... 9.3
9.3 Hoop ACI D/C Ratios at LC4 ..... 9.3
9.4 Shear ACI D/C Ratios at LC4 ..... 9.4
9.5 In-Plane Shear ACI D/C Ratios at LC4 ..... 9.4
10.1 Equivalent Uniform Surface Load Definition 10.2
10.2 Local (Concentrated) Load Definition 10.2
10.3 Equivalent Uniform Surface Load Calculation 10.3
10.4 Equivalent Local Surface Load Calculation 10.4
10.5 Load-Displacement Response under Uniform Surface Load 10.5
10.6 Load-Displacement Response under Local Load 10.5
11.1 Values of ψ for Effect of Concrete Cracking and Amounts and Type of Reinforcement (Figure 4 of Scordelis 1981) 11.5
11.2 Effect of Geometric Imperfections on Buckling Load (Figure 3 of Scordelis 1981) 11.5
11.3 Reduction Factor α_3 for Concrete Cracking and Amounts and Type of Reinforcement (Figure 5 of Scordelis 1981) 11.6

Tables

3.1 Type I SST Geometry 3.4
3.2 Type I SST Waterproofing Description 3.4
3.3 Type I SST Waste Design Parameters 3.4
3.4 Specified Backfill Soil Properties for the Type I SSTs 3.5
4.1 TOLA Run Matrix (Material Combination Strategy) Used in the Type II SST AOR 4.2
4.2 SST Analysis Load Conditions 4.3
4.3 Comparison of the SST Concentrated Load Limits 4.3
4.4 Load Combinations 4.4
4.5 TOLA Load Step Numbers for Reference 4.6
5.1 Source Drawings for Type I ANSYS® Model Construction 5.1
5.2 Roof Concrete Rebar Volume Ratios 5.7
5.3 Wall Concrete Rebar Volume Ratios 5.8
5.4 Foundation Concrete Rebar Volume Ratios 5.8
5.5 TOLA Run Matrix (Material Combination Strategy) for Type I SST AOR 5.10
5.6 Temperature History and Waste Height Data Used in the Type I Tank AOR 5.11
7.1 Section Properties in Meridional Direction 7.5
7.2 Section Properties in Circumferential Direction 7.6
7.3 Section 18 and 19 Peak ACI Shear Ratios 7.28
10.1 Summary of Limit Load Analysis 10.6
11.1 Buckling Safety Factors from Kollar and Dulacska (1984) 11.7
11.2 Tank Dimensions for the Wall Buckling Analysis 11.9
11.3 Summary Results of the Wall Buckling Analysis 11.11

1.0 Introduction and Objective

The U.S. Department of Energy (DOE) Office of River Protection has determined the need to better understand the structural integrity of the single-shell tanks (SSTs) on the Hanford Site in Washington state. To address this need, Pacific Northwest National Laboratory (PNNL) with support from Becht Engineering has performed an SST Analysis of Record (AOR) for Washington River Protection Solutions (WRPS). Completion of this work supports the Hanford Federal Facility Agreement and Consent Order and the Tri-Party Agreement Milestone, M-45-10-01.

The primary objective of the SST AOR Project is to perform a comprehensive structural AOR for the SSTs in order to understand the existing SST structural integrity as a result of past usage and potential future natural hazard phenomena. Seismic analysis is included to assess the structural integrity of the tanks in the event that a design basis earthquake occurs in the future. PNNL has performed the static analysis of the thermal and operating loads while Becht Engineering was subcontracted to perform the seismic analysis of the SSTs.

The first phase of the SST AOR Project, preliminary analysis documentation, conducted an extensive review of SST reports, specifications, drawings, and supporting documents, followed by finite element model development, exploratory calculations, and benchmarking resulting in recommendations for subsequent phases. Phase II of the SST AOR project is to perform detailed analyses of the thermal and operating loads and the seismic loads for each of the four tank types. The analyses described in this report document the structural integrity assessment for the Type I (55,000-gal storage capacity) SSTs.

This report summarizes the AOR detailed modeling results for the Type I SSTs. The Hanford Type I SSTs are located at the B, C, T, and U Tank Farms. Acceptance criteria and recommendations given in Johnson et al. (2010) guided the modeling effort. The AOR evaluates the structural consequences of both the static and seismic loads. Attachment 1 contains the Type I SST seismic analysis report in its entirety. The combined TOLA and seismic demands are evaluated in the body of this report.

1.1 Quality Assurance

The PNNL Quality Assurance Program is based upon the requirements as defined in DOE Order 414.1D, Quality Assurance and 10 CFR 830, Energy/Nuclear Safety Management, Subpart A -- Quality Assurance Requirements (a.k.a., the Quality Rule). PNNL has chosen to implement the following ASME-NQA-1 (ASME, 2000) consensus standards in a graded approach in the Quality Assurance Program Description (QAPD):

- ASME NQA-1-2000, Quality Assurance Requirements for Nuclear Facility Applications, Part 1, Requirements for Quality Assurance Programs for Nuclear Facilities.
- ASME NQA-1-2000, Part II, Subpart 2.7, Quality Assurance Requirements for Computer Software for Nuclear Facility Applications.
- ASME NQA-1-2000, Part IV, Subpart 4.2, Graded Approach Application of Quality Assurance Requirements for Research and Development.

The implementing procedures and processes, described in the DOE-approved PNNL QAPD, are made available in a web-based system for the delivery of PNNL requirements and laboratory-level workflow and procedures.

Because the efforts of the SST AOR Project are beyond those defined as research and development, such as Subpart 4.2 of NQA-1, a Quality Assurance Program to Parts I and II of NQA-1 (using a graded approach) is necessary and is required per the project Statement of Work. PNNL-NQA-EQAM-1 (PNNL, 2010), Energy and Environment Directorate Quality Assurance Plan, provides that NQA-1 Quality Assurance Program (plan). PNNL-NQA-EQAM-1 provides the general, or high-level, overview of the implementation of NQA-1-2008 (ASME, 2008). Therefore, the SST AOR uses the more recent 2008 edition compared to PNNL's program based on the 2000 edition. PNNL-NQA-EQAM-1 is supported by administrative procedures (APs) that provide the more specific requirements for implementation of NQA-1 requirements. The Project Quality Assurance Plan (PQAP), Single Shell Tank Type I AOR (66259-QAP, Revision 0), is subordinate to PNNL-NQA-EQAM-1 and uses the processes and procedures of PNNL-NQA-EQAM-1 to provide the applicable quality assurance requirements for the specific work activities for the Project, based on client requirements and PNNL requirements, and is compliant with the QAPD. For the parts of the project that are safety-software related, the requirements of NQA-1, Subpart 2.7 were applied.

The requirements contained in the PQAP will satisfy the requirements of DOE Order 414.1D and 10 CFR 830 (when applicable).

2.0 Scope

The objective of the Single-Shell Tank Analysis of Record (SST AOR) Project is to perform a comprehensive structural analysis of record for each of the four tank types of the Hanford single-shell tanks (SSTs). This report provides the detailed finite element (FE) modeling results and code evaluation for the Type I SSTs. The Type I SST structural integrity was evaluated by performing thermal and operating loads analysis, as well as seismic analysis. These analyses include the following load conditions described in the Evaluation Criteria report (Johnson et al. 2010): waste thermal and hydrostatic pressure loads, soil overburden, uniform and concentrated surface loads, and seismic loads; temperature effects on material properties; creep; concrete cracking; tank appurtenances; and tank limit loads. Additional closed form calculations were performed for the buckling analysis. Two types of models were used—one addressed the static thermal and operating loads analysis (TOLA), and the second addressed seismic loads. The seismic analysis is documented in an independent report (Abatt et al. 2014), which is included as Attachment 1 in this report. The TOLA and seismic models were analyzed independently, and then selected TOLA and seismic results were combined to obtain demand-to-capacity ratios in accordance with the American Concrete Institute code, ACI 349-06 (ACI 2007). The resulting demands on the FE models of the Type I tanks were compared to the capacities at various locations on the tank profile to evaluate the structural integrity of the Type I SSTs.

Tank-to-tank interaction effects are not evaluated for the Type I tanks because the 50-ft center-to-center spacing gives 3 radii of soil between adjacent tanks. Furthermore, adding the maximum $\Delta D/C=0.2$ for tank-to-tank effects (Johnson et al. 2014) to the maximum Type I D/C ratio of 0.52 is still significantly less than 1.0. Tank-to-tank interaction was previously evaluated for the Type IV tanks because the Type IVc tanks in AX Farm are spaced less than 0.5 radii apart.

2.1 TOLA and Seismic Results Roadmap

Two structural models (TOLA and seismic) were used to evaluate the structural integrity of Type I SSTs. Given the number of TOLA and seismic analyses conducted on the Type I FE models, this section describes the sequence in which the analyses and their results are presented in this report.

Independent run matrices were established for the TOLA and seismic models to evaluate results' sensitivities to material property variations and loading scenarios. TOLA and seismic results were then combined for selected best estimate and bounding combinations.

The analytical portion of the report begins with background information on the Type I SSTs in Chapter 3.0. This section summarizes the design information including tank dimensions, dates of construction and specifications, and design parameters.

Chapter 4.0 lists the applicable codes and standards, acceptance criteria, and loads described in the Evaluation Criteria report, which apply to both the TOLA and seismic modeling efforts. The TOLA material property run matrix (Table 4.1) used in the Type II AOR (Rinker et al. 2010) is presented for reference as the starting point for the TOLA Type I SST run matrix. The material property run matrix evaluates the sensitivity of the analysis results to the expected variations in soil, concrete, and waste properties, and their combinations. The TOLA Type I SST run matrix is presented in Table 5.5.

Chapter 4.0 also presents the ACI 349-06 load combinations and load factors that are applicable to the SST TOLA and seismic analyses.

Chapter 5.0 describes the TOLA model, including the geometry, boundary conditions, material properties, and the applied loads. Material property combinations are summarized in the TOLA run matrix (Table 5.5). Figure 3.4 shows the temperature and waste-level histories that were applied in the TOLA analyses.

Chapter 6.0 references the seismic model which is described in the seismic report found in Attachment 1.

Chapter 7.0 presents the TOLA model results for the TOLA material run matrix. The ACI 349-06 meridional, hoop, and through-wall shear demand to capacity (D/C) ratios are reported for each of the TOLA runs (refer to Sections 7.4 through 7.6). Section 7.7 presents the slab removal study.

Chapter 8.0 references the seismic modeling results that are presented in the seismic report found in Attachment 1.

Chapter 9.0 summarizes the combined TOLA + Seismic (ACI LC-4) results.

Chapter 10.0 summarizes the tank limit load analysis performed for Type I SSTs. The limit loads were evaluated for both uniform and concentrated loads over the tank roof. The uniform load was applied over the entire soil surface, while the concentrated load was applied over a 10-ft-diameter area on the soil above the center of the tank. The limit loads were estimated by increasing the load until the tank model offered little or no resistance to additional load. The limit load results are summarized in Table 10.1.

Chapter 11.0 presents the buckling analyses performed for the Type I SSTs. Results for the buckling analysis are discussed in Section 11.4.

Chapter 12.0 gives the overall conclusions of the tank modeling results.

The references cited in the report are listed in Chapter 13.0.

Appendix A provides examples of the force, moment, and shear loads on the tank sections from the various load components applied to the Type I tank. Appendix B presents the Mathcad™ buckling calculations. Appendix C illustrates an example of the ACI evaluation methodology. Appendix D contains the external reviewer comments on this report. Finally, Attachment 1 contains the Type I seismic analysis prepared by Becht.

3.0 Type I SST Background

In response to Hanford's plutonium production, a total of 149 underground tanks were constructed between 1943 and 1964 to contain the nuclear waste in twelve separate tank farms in the 200 East and West areas of the Hanford Site. The SSTs were constructed with a single wall, carbon steel liner backed by reinforced concrete. They are classified as types I through IV in order of increasing waste capacity. Sixteen Type I, 55,000-gallon tanks were constructed in 1943-1944; four each at tank farms B, C, T, and U (Boomer 2009). Waste discharges to the SSTs ended by 1980 as mandated by congress, and interim stabilization was completed by 2004 when target supernate and interstitial liquids were removed from all SSTs (Berman 2009). Subsequent sections in this chapter summarize the Type I SST design information.

3.1 Design

Unlike the larger domed tanks, the Type I tanks have flat roofs with a large hatchway structure that bridges over and supports the roof (Figure 3.1). The Type I tanks are located in rows of four (50-ft center-to-center spacing) along the edge of tank farms B, C, T, and U (Figure 3.2). The Type I tanks have a 20-ft inner diameter and a floor-to-ceiling height of 26 ft (Figure 3.3). The welded carbon steel liner extends to a height of approximately 25.5 ft, and the maximum waste height is 24.5 ft (294 inches).

Table 3.1 summarizes the geometric features of the Type I SSTs, while Table 3.2 describes the asphaltic waterproofing of the tanks. Note that the waterproofing layers and the steel liner were not included in the structural models because neither provides significant strength to the reinforced concrete tanks (Rinker et al. (2010). Waste loading characteristics obtained from the construction specifications and technical drawings are presented in Table 3.3. Current tank contents are not presented in this report, but tank-specific data and current status are provided in the Best-Basis Inventory (BBI) within the Tank Waste Information Network System (TWINS). The BBI is the official database for tank waste inventory estimates at the DOE Hanford Site. Although Table 3.3 lists a waste specific gravity of 1.25, a higher value of 1.7 was used in the analysis (see Table 4.2 in the next chapter).

The load types evaluated in the Type I AOR are defined in the Evaluation Criteria report (Johnson et al. 2010). Table 4.2 in the next chapter lists the bounding loads that were used in this analysis. These are defined from the current maximum-allowable dome loads for the Type I tanks that are defined in Mackey (2012) as a function of the measured soil overburden depth for a conservative soil density of 125 lb_f/ft^3.

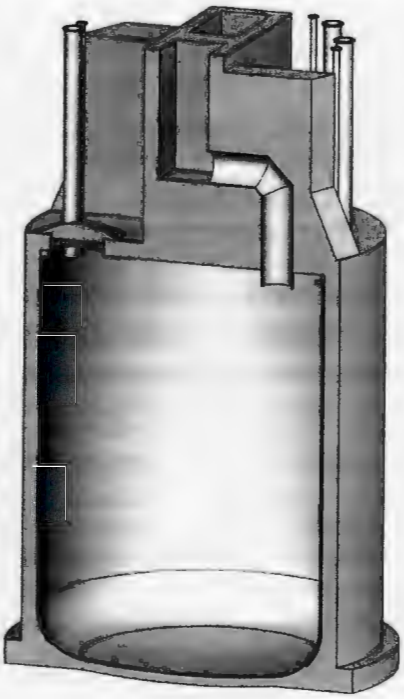

Figure 3.1. Cross-Section View of the Type I, Series 200 SSTs

Figure 3.2. Aerial View of the Four Type I Tanks at the West Edge of B-Farm

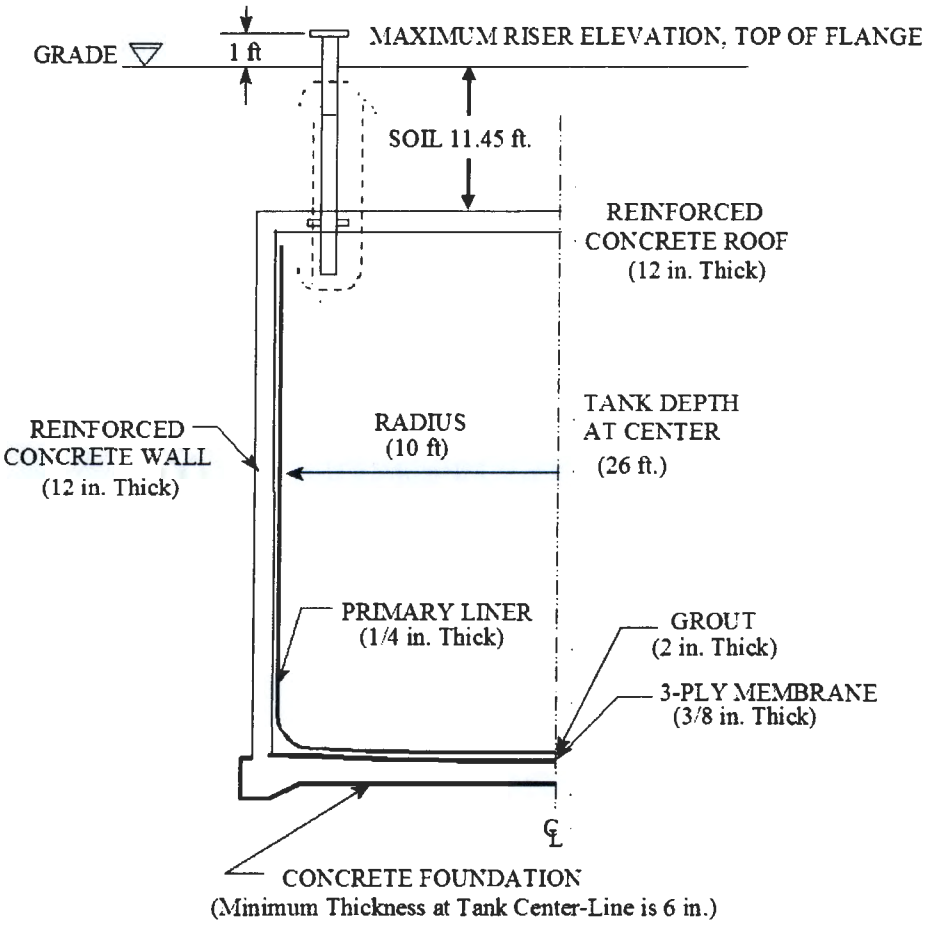

Figure 3.3. Typical 55,000-Gallon Single-Shell Waste Tank and Riser Configuration for Type I Tanks 241B, 241C, 241T, and 241U.

Table 3.1. Type I SST Geometry

Tank Farm	Footing Thickness (in.)	Concrete Slab Centerline Thickness (in.)	Reinforced Concrete Wall Thickness in.)	Reinforced Concrete Roof Thickness (in.)	Steel Liner Height (in.)	Reference (Drawings)	Steel Liner Thickness (in.)
B,C,T, and U	18	6[a]	12	12	300	Centerline slab concrete thickness, steel liner height and thickness: HW-72417; Wall thickness: D-21; and Roof thickness: D-20	0.25

(a) Dished bottom

Table 3.2. Type I SST Waterproofing Description

Tank Farm	Between Steel Liner and Concrete Foundation	Between Steel Liner and Concrete Wall	Concrete Exterior	Reference
B,C,T, and U	1-in. grout layer – 1943_NA_Specifications 1961, and Drawing HW-72417	1-ft thick Banrock wire mesh blanket, style #102 covered with ½-in. cement mortar or gunite – Drawing D-20	3-ply membrane waterproofing covered with ¾ in. (½ in. on vertical surfaces) protective cement grout or gunite with chicken wire reinforcement; covers just the top of the tank, not the sides	Drawings HW-72417, D-20

Table 3.3. Type I SST Waste Design Parameters

Tank Farm	Max Specific Gravity	Reference	Max Height (in.)	Reference	Storage Pressure (psi)	Reference	Max Liquid Temperature (°F)	Reference	pH	Reference
B,C,T, and U	1.25	Drawing HW-72417	294	Drawings D-20, HW-72417	Atmospheric	1943_NA_ Specifications 1961	220	Drawing HW-72417	10	Drawing HW-72417

Table 3.4 summarizes the specified soil conditions. Mackey and Julyk (2004) provides measured soil cover depths from a detailed soil survey of the double-shell tanks and the SSTs at the Hanford Site. Mackey (2012) lists these soil cover depths with conservative values of soil density, 125 lb_f/ft^3, and maximum concentrated load, 142 kip (see Table 4.2).

Table 3.4. Specified Backfill Soil Properties for the Type I SSTs

Tank Farm	Soil Quantity	Reference
	Soil Density (lb_f/ft^3)	
B, C, T, and U	125	Mackey (2012)
	Soil Overburden Depths, Flat Roof to Backfill Grade (ft)	
B, C, T, and U	11.45, 10.7, 10.0, and 9.5	Mackey (2012)
	Backfill Placement	
B,C,T, and U	Backfill will be placed in layers from 6 in. to 24 in.	1943_NA_Specifications and 1944_NA_Specifications

3.2 Temperature and Waste Height Profiles

The temperature and waste height data for the Type I tanks is less complete than those for the Type II, III, or IV tanks. No temperature data are available for the Type I tanks prior to 1975, and most of these tanks were out of service by 1977. Temperature data available for all Type I tanks from 1975 onwards indicate that the temperatures have been around 100°F, except for the B-204 tank, which experienced a peak temperature of 220°F in 1989 according to Rifaey (2002). However, the B-204 peak temperature is not visible in the temperature plots in Brevick et al. (1997), which is the reference provided by Rifaey. Communications with WRPS indicate that the C-200 series tanks were filled with potential high heat-generating waste, which may support temperatures in the 220°F to 250°F range. Therefore, 250°F was used as a conservative upper-bound for the maximum waste temperature of the Type I tanks.

Several of the Type I tanks (notably those in the B and C farms) were filled to near capacity. Figure 3.4 shows the C-201 waste height history with a maximum value of 284 inches (Brevick et al. 1996). Although Tank C-201 was later drained, the TWINS-SACS database shows that Tank B-203 currently has a waste height of about 265 inches. Therefore, the 284-inch maximum waste height of Tank C-201 was maintained throughout the full history to conservatively bound the waste height through time.

The temperature and waste height profile shown in Figure 3.4 was used in the Type I AOR. This combines the maximum waste height of 284 inches throughout the history, with the possible high temperature limit of 250°F during the years before temperature data is available. The high temperature was reduced to 100°F in 1972 to represent the typical maximum recorded values during the years 1975–1997 when temperature measurements were recorded.

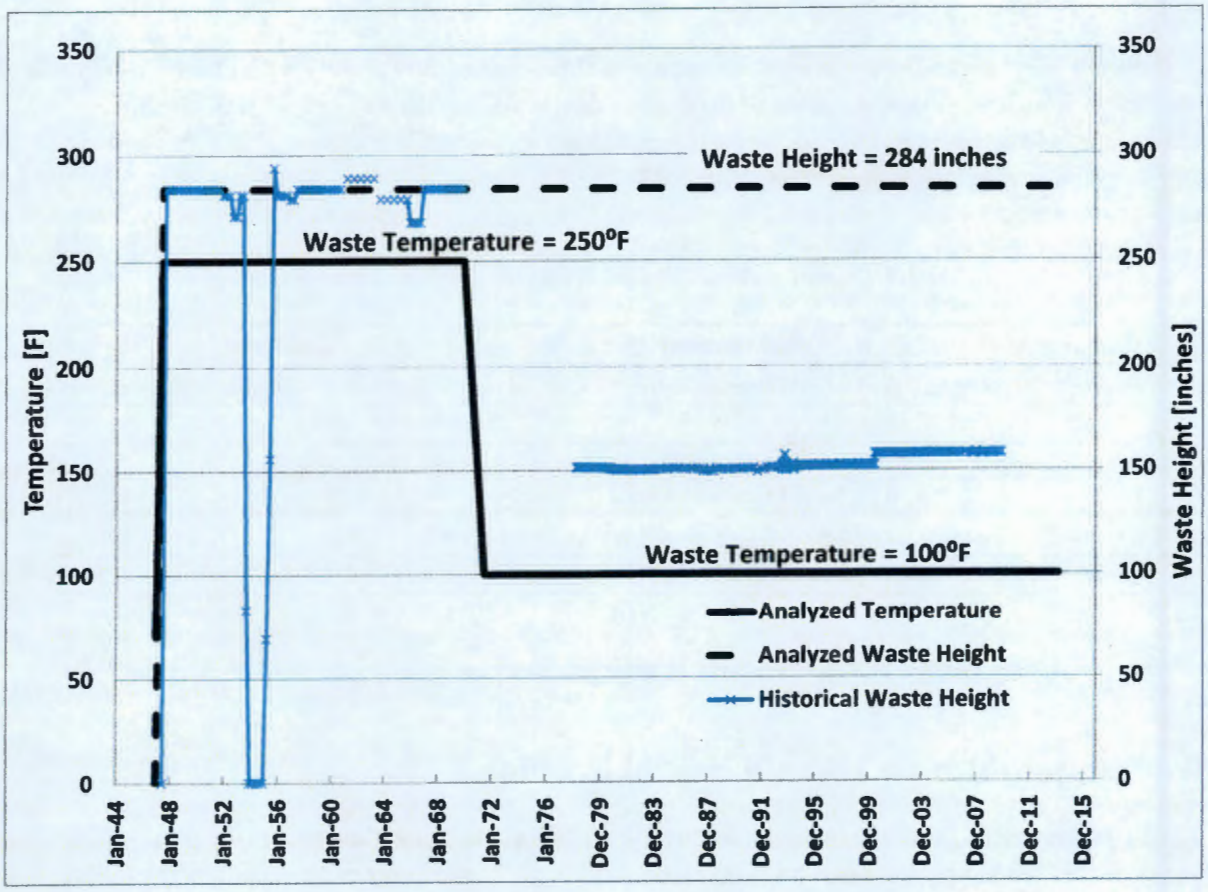

Figure 3.4. The Temperature (°F) and Waste Height (inches) Profiles used in the Type I AOR

4.0 Guidance

This chapter summarizes the guidance documents and design input used in the detailed finite element (FE) models of the Type I single-shell tanks.

4.1 Acceptance Criteria

The Evaluation Criteria report by Johnson et al. (2010) provides the acceptance criteria, codes and standards, and the recommended analysis methods for application in the SST structural integrity evaluations. Subsequent sections of this chapter describe the material properties, loads, and load combinations considered in the Type I tank analyses in this report.

4.1.1 Material Properties

Material property data for concrete, soil, and reinforcing steel are provided in the Evaluation Criteria report (Johnson et al. 2010). Best estimate, lower bound, and upper bound concrete strength and elastic modulus are provided as a function of temperature. Elastic modulus versus temperature is provided for the reinforcing steel. Best estimate, lower bound, and upper bound values are provided for the static stiffness properties of Hanford soils. The nominal concrete density of 145 lb_f/ft^3 used in the analysis is representative of unreinforced Hanford concrete. The added weight of the rebar was accounted for by the ANSYS software in the reinforcement layers. However, the steel volume is a small fraction of the total tank section volume so this has a very small effect on the overall density of the reinforced concrete.

Rinker et al. (2010) conducted material property sensitivity studies to develop the recommended TOLA run matrix for the detailed analyses of record. The matrix covered the uncertainty in concrete strength and modulus and the soil modulus. This material property sensitivity matrix was updated in the Type II report (Rinker et al. 2011a) based on the literature review and reviewer recommendations on the use of concrete tensile strength in finite element models. Table 4.1 shows the TOLA run matrix used in the Type II SST AOR. Table 4.1 was further updated for the SST Type I analysis based on initial screening cases that showed the structural demands versus section capacities to be lower than those of the larger tanks. The final Type I TOLA run matrix is presented in Section 5.6.

Table 4.1. TOLA Run Matrix (Material Combination Strategy) Used in the Type II SST AOR

Case/ Run	Soil Modulus	Concrete Modulus	Concrete Tensile Strength	Concrete Creep		Notes
1	N	N	Near Zero (10 psi)	Yes		Best Estimate Properties
2	N	N	Near Zero (10 psi)	No	"Worst-Case Combinations" using available material property bounds	
3	N	H	Near Zero (10 psi)	No		Depending on depth, low soil modulus is lower by 20% to 50% when compared to best estimate values.
4	L	H	Near Zero (10 psi)	No		
5	L	N	Near Zero (10 psi)	No		Depending on temperature, high concrete modulus is higher by 15% to 30% when compared to best estimate values.
6	N	N	N	Yes		
7	L	N	Near Zero (10 psi)	Yes		

H = High.
L = Low.
N = Nominal/Mean (Best Estimate).

4.1.2 Loads

The design and operating loads for the SSTs are established by their construction specifications, safety analysis reports, or other basis documents for the tank farm of interest (Johnson et al. 2010). The load types for evaluation at each of the SST farms were summarized in several reports, including Chapter 2 of Johnson et al. (2010) and Appendix A of Rifaey (2002). The SST design loads include those associated with normal operation, abnormal conditions, and extreme conditions. Table 4.2 lists the loading conditions used in the Type I AOR. The 1.7 specific gravity is significantly higher than the 1.25 operating limit on specific gravity given in Rifaey (2002) for the Type I tanks.

The 142 kip maximum concentrated surface load for the Type I tanks was calculated using finite element analysis (Julyk and Mackey 2003b). A 2D axisymmetric model (ANSYS PLANE42 elements) with linear elastic concrete and 11.5 ft. of soil at 125 lb/ft^3 gave a peak hoop stress of 49 psi tension at the center inside surface of the tank roof. The concentrated surface load (distributed within a 10-ft diameter circle above the tank center) was increased until the peak stress reached 176.5 psi, the 300 psi tensile limit ($f_t = 6\sqrt{f'_c}$ where f'_c=2500 psi) divided by the 1.7 ACI load factor. The total resultant load was 142 kips. Comparing the mass of the hatchway structure with the weight of the displaced soil gives a combined net weight of 32 kip above the Type I tanks. Therefore, the Type I AOR models apply an additional 110 kips to achieve the 142 kip total concentrated load above the tanks.

Table 4.3 compares the concentrated loads used in each of the SST AORs. The 110 kip added surface load is large considering the 20-ft diameter of the Type I tanks compared to the 75-ft diameter of the Type II, III, and IV tanks.

The Type I tanks are also different from the large 75-ft diameter SSTs in that the hatchways extend above the surface of the soil and they occupy a large fraction of the 10-ft concentrated load circle. The Type I AOR conservatively applies the concentrated load directly to the full 10-ft surface of the tank roof as described in Section 5.4.

Table 4.2. SST Analysis Load Conditions

Design Load	Value	Notes
Design Life	25 to 35 years	A 67-year (1947–2014) design life is used
Soil Cover	11.45 ft @ 125 lb/ft^3	
Hydrostatic	variable height @ SpG = 1.7	Specific gravity (SpG) = 1.7
Live Load	40 lb/ft^2	Uniform surface load
	142,000 lb	Concentrated (proportionately distributed on hatchway and soil over 5 ft radius circle above tank center)
Thermal	250°F	Maximum temperature of waste (tank center bottom)
Seismic	--	See Attachment 1

Table 4.3. Comparison of the SST Concentrated Load Limits

SST Type	Tank Inner Diameter (ft)	Soil Depth (ft)	Net Pit Weight (kip)	Total Concentrated Load (kip)	Net Surface Load (kip)
I	20	11.45	32	142	110
II	75	10	124.8	200	75.2
III	75	11	140.8	200	59.2
IV	75	7.51	115.5	270	154.5

4.1.3 Static Load Combinations

The classification of loading conditions and events is key to determining the appropriate load factors and combinations to analyze in the tank structural integrity evaluations. Section 9.2 of the American Concrete Institute (ACI) 349-06 code (ACI 2007) specifies the factored load combinations that must be used in evaluating the required design strength. The Evaluation Criteria report provides a complete list of load combinations followed by a short list of load combinations applicable to the SSTs. In summary, the applicable load combinations from the Evaluation Criteria report are:

Load Combination 1 (LC1). $$U = 1.4D + 1.4F + 1.7L + 1.7H \quad (4.1a)$$

Load Combination 4 (LC4). $$U = D + F + L + H + T_o + E_{ss} \quad (4.1b)$$

Load Combination 9 (LC9). $$U = 1.05D + 1.05F + 1.3L + 1.3H + 1.05T_o \quad (4.1c)$$

where D = Dead loads including tank self weight, piping and equipment dead loads. (Where the structural effects of differential settlement, creep, or shrinkage may be significant, they shall be included with the dead load D.)

L = Live loads, including impact effects of moving loads

F = Lateral and vertical pressure of liquids

H = Loads due to weight and pressure of soil, water in soil, or other materials, or related internal moments and forces

T_o = Internal moments and forces caused by temperature distribution within the concrete during normal operation and shutdown

E_{ss} = Safe Shutdown Earthquake (SSE) effects = Design-Basis Event/Earthquake (DBE) effects

When applying the SST load combinations from the Evaluation Criteria report, the sub-classification of soil loads over and around the tanks into dead or live loads is somewhat open to interpretation. The previous analysis of the C-106 tank provides a detailed discussion of the classification of soil and other loads (Bander et al. 1994). That analysis, along with the guidance from the tank operating contractor (WRPS), was considered when defining the dead and live loads. Table 4.4 lists the loading conditions and the corresponding load factors used in the Type I SST analysis of record. Figure 4.1 shows a typical layout of an SST along with the soil boundaries used in the load and load factor definitions applicable to the ACI 349-06 evaluation of the thermal and operating loads.

Table 4.4. Load Combinations

Loading Type	Load	Nominal Value (LC4)	Load Factor (LC1)	Load Factor (LC9)	Alternative Load Factors
Structure	Body Load (D)	1 g	1.4	1.05	1.4
Structure	Soil Cover (D)	11.45 ft	N/A (density is factored)	N/A (density is factored)	N/A (density is factored)
Structure	Soil Density – backfill overburden (D)	125 lb_f/ft^3	1.4	1.05	1.4
	Soil Density – backfill side soil (H)	125 lb_f/ft^3	1.7	1.3	0.9
	Soil Density – undisturbed	110 lb_f/ft^3	N/A	N/A	N/A
Normal Op	Uniform Surface Load (L)	40 lb_f/ft^2	1.7	1.3	1.7
Extended Op	Concentrated Load above tank center (L)	142 kip	1.7	1.3	1.7
Normal Op	Waste Specific Gravity (F)	1.7	1.4	1.05	1.4
Normal Op	Waste Level	284 in	N/A (density is factored)	N/A (density is factored)	N/A (density is factored)
Normal Op	Thermal cycle as shown in Figure 3.4	Peak of 250°F (all waste)	N/A	1.05	N/A
Seismic	Horizontal	See Attachment 1	N/A	N/A	N/A
	Vertical		N/A	N/A	N/A

N/A = Not applicable.

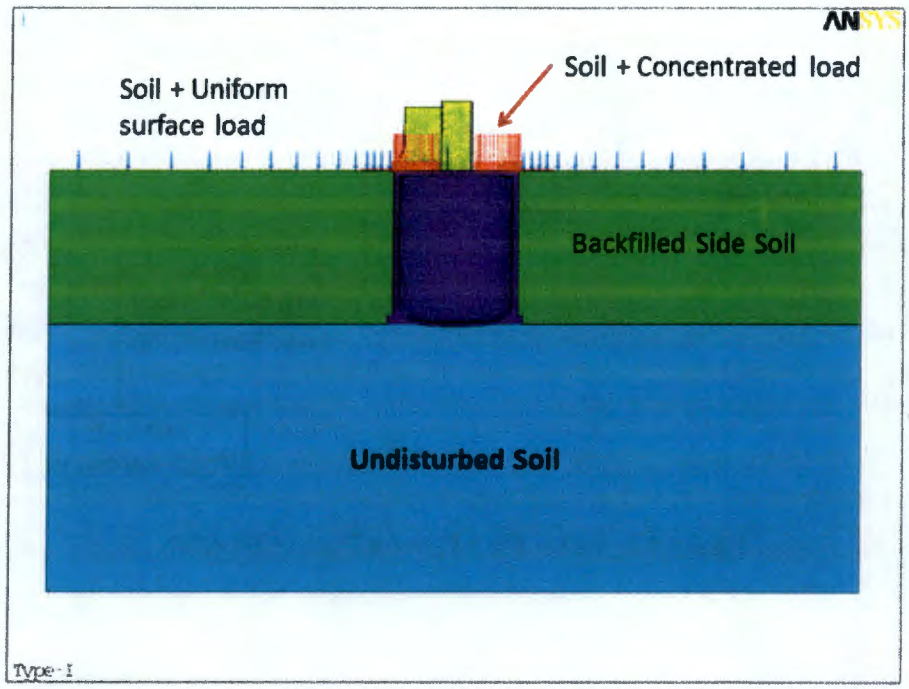

Figure 4.1. Typical Layout of a Type I Single-Shell Tank Model

Figure 4.2 shows the flow chart used to model the 67 years of thermal loads with appropriate intervals for the ACI structural evaluation. Mechanical loads (gravity, waste load, and concentrated load) were applied in load steps 1 through 3. Thermal and waste-level histories were applied in load steps 4 through 11, with load step 6 corresponding to a maximum waste temperature of 250°F. Details of the waste temperature and level are provided in Section 5.6. The analyses were then carried in two separate steps for respective ACI evaluations. In one step, the entire model was cooled down to 53°F (the initial stress-free temperature) after which the ACI load combination 1 load factors (LC1) were applied for tank evaluation. In the other step, the waste was cooled to 80°F (the current temperature) during which the ACI load combination 4 (LC4) was evaluated followed by the evaluation of ACI load combination 9 (LC9). Table 4.5 shows the load step numbers and the corresponding thermal and waste-level history. Figure 4.2 illustrates the temperature and waste height profiles used for the detailed analysis of the Type I tanks.

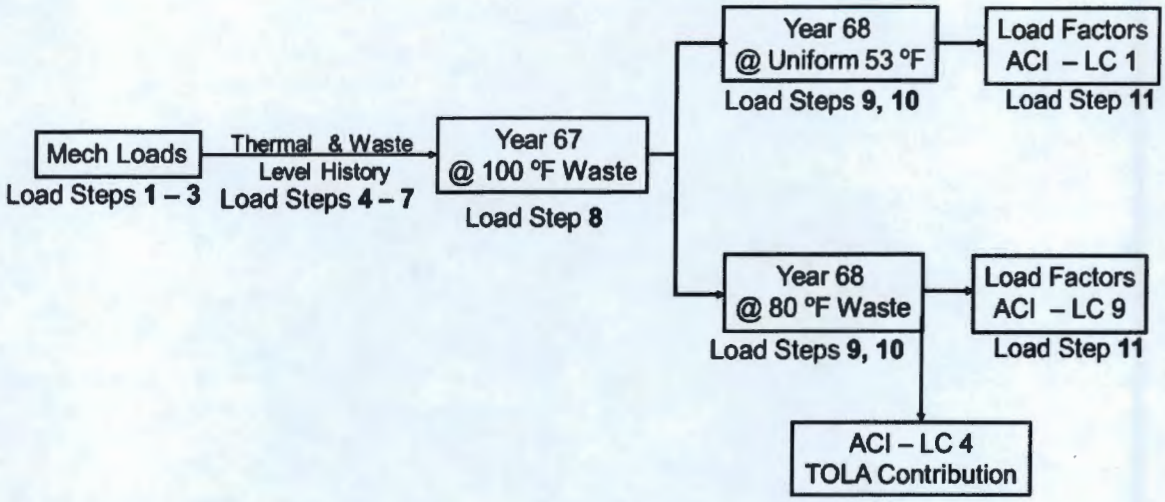

Figure 4.2. TOLA Flow Plan for Type I SST AOR

Table 4.5. TOLA Load Step Numbers for Reference

Load Step No.	Time Days	Time Years	Max Temp (tank center bottom) (°F)		Waste Height (inches)	Notes	
1	1	0.003	53		0	Gravity	Mech Loads
2	2	0.005	53		284	Waste Load	
3	3	0.008	53		284	Conc. and Live Loads	
4	184	0.50	250		284	-	Thermal & Waste Level History Loads
5	8404	23	250		284	-	
6	8405	23	250		284	Material Property Change	
7	8951	24.5	100		284	-	
8	24566	67.3	↙ 100 ↘		284	-	
9	24930	68.3	53 (LC1)	80 (LC9)	284	Back to Initial/Current Temperature	-
10	25295	69.3	53 (LC1)	80 (LC9)	284	Steady State at 53°F/80°F	-
11	25296	69.3	53 (LC1-LF)	80 (LC9-LF)	284	Load Factors	ACI Load Factors

LC = Load Combination.
LF = Load Factors.

4.2 Post Design Evaluation Input

The current dome load limits in Mackey (2012) were used for the Type I AOR. The maximum 11.45-ft soil overburden bounds the Type I tanks in the B, C, T, and U tank farms. The prescribed soil density of 125 lbf/ft^3 is an upper bound estimate recommended by Johnson et al. (2010). The concentrated load limit of 142 kip over a 5-ft radius above the tank center is specified in Mackey (2012) for 11.45-ft of soil at 125 lbf/ft^3.

5.0 Static Thermal and Operating Loads Analysis

5.1 Introduction

This chapter describes the ANSYS® finite element model developed for the Type I SST Thermal and Operating Loads Analysis (TOLA).

Section 5.2 and following describe the steps involved in developing the model: tank and soil geometry, element types, material properties, and the loads and boundary conditions applied for the structural and thermal models. The geometric details of the Type I tanks were taken from the pertinent construction drawings database collected during Phase I of the Single-Shell Tank Analysis of Record (SST AOR) Project.

The Type I SSTs differ from the larger SSTs in having a flat roof with a large hatchway structure that supports the roof as shown in Figure 3.1. A simple 2-degree slice model similar to those used in the other SST AORs was desirable for analysis, but would not account for the effects of the hatchway on the roof stiffness and strength. Initial analyses of the simple model without the hatchway showed that the hatchway is required for adequate strength. Consequently, a 180-degree symmetry model including the hatchway was developed and is described in the following sections.

5.2 ANSYS® Model Construction

ANSYS® Version 13.0 was used in all the TOLA analyses of the Type I SSTs. The FE model was developed using ANSYS® parametric design language macros and input files. The geometric details of the Type I tanks were taken from the construction drawings listed in Table 5.1. The Type I FE model is a 180-degree 3-D symmetry model including the hatchway. The hatchway structure is not symmetric, but the assumption of symmetry is conservative in the resulting unsupported roof area and reduces the analysis run time required by a full 360-degree model. While building the 3-D model, the 2-D geometry was initially created to represent the cross section, and it was swept (rotated) about the central axis through 180 degrees in 3 degree increments. Figures 5.1 through 5.3 show various details of the 2-D geometry.

Table 5.1. Source Drawings for Type I ANSYS® Model Construction

Tank Farm	Composite Tank Details	Wall and Floor Reinforcement	Roof Reinforcement
B, C, T and U	D-20, Rev 6	D-21, Rev 8	D-22, Rev 1

Similar to other SSTs, the steel liner in the Type I tanks is not attached to the cylindrical wall and does not contribute significantly to the structural integrity of the reinforced concrete tank shell. The purpose of the liner is only to serve as a leak barrier and hence it is not included in the structural analysis.

The Type I tanks were modeled with a soil overburden of 11.45 ft, bounding the maximum value reported for the Type I tanks. The sub-grade undisturbed soil depth was specified at 48 ft below the

foundation, consistent with the recommendation of the Evaluation Criteria report (Johnson et al. 2010). The radial extent of the soil (lateral soil dimension) was modeled to a radial distance of 72.5 ft, which is 6 times the footing radius as in the Type II, III, and IV AORs. Similar to the Type II, III, and IV AORs, the compacted backfill excavation slope boundary that distinguishes backfill soil from undisturbed soil was not modeled in the TOLA analysis and instead the backfill soil (with lower stiffness than the undisturbed soil) was conservatively modeled throughout the radial extent of the soil. The Type I model includes six layers of backfill soil above the tank foundation level. The undisturbed soil underneath the tanks was modeled with five stratigraphic soil layers to a depth of 48-ft. The material properties for the concrete and soil are summarized in the SST Evaluation Criteria report (Johnson et al. 2010). Figure 5.4 shows the FE model with the corresponding soil layers.

The soil above the tank was initially modeled using layers of finite elements. However, low soil pressure on the tank roof occurred due to soil bridging. The soil bridging results because the small tank 11 ft outer radius) is covered by relatively deep soil (11.45 ft) with regard to the soil friction angle. Therefore, the soil elements were removed and replaced by an equivalent soil pressure equal to the soil overburden depth times the soil density. Accordingly, all analyses were conducted with the FE model shown in Figure 5.5.

Details of the hatchway are shown in Figure 5.6. Bonded contact elements were used between the hatchway and tank roof to connect the dissimilar meshes.

The ANSYS® SOLID65 (3-D Reinforced Concrete Solid) elements were used to represent concrete regions with and without reinforcement bars (rebars). SOLID65 elements have the ability to simulate concrete cracking in tension, crushing in compression and creep. The reinforced concrete is divided into regions that have different steel reinforcement ratios, where it is assumed that each reinforcing layer is 1-in. thick (approximately the thickness of the crossed meridional and hoop rebar layers). The reinforcement model in the SOLID65 elements is a smeared model and requires specifying the amount of steel in each element as a volume fraction of the total element volume. The volume fractions of steel and concrete near the inner and the outer faces of the tank cross section were calculated at various locations around the tank cross section and assigned to the elements in the 1-in.-thick reinforced layers (designated as "rebar elements" in Figures 5.2 and 5.3). The reinforcement properties are input as real constants, which include the material number, the volume ratio, and the orientation angles. In these regions the element coordinate system is defined such that the element x-axis is parallel to the direction of a vector connecting the centroids of the current and adjacent elements and the y-axis is defined normal to this vector. These local coordinate systems are defined on the plane passing through the z-centroids (the plane passing through half the three-degree angle of the slice) of the elements. The z-axis (for hoop reinforcement) for these elements is automatically defined normal to the x-y plane.

Because the rebar was not explicitly modeled, it is not required to prescribe the exact location of each rebar. While calculating the volume fraction of steel for real constants, careful consideration was given to match the total amount of steel in the meridional and the hoop directions. The locations of the 1-in.-thick reinforcement layers ("rebar elements" in Figures 5.2 and 5.3) were also accurately defined in the cross-section thickness to accurately model the bending resistance of the reinforcing bars.

Previous double-shell tank and SST models with SOLID65 concrete elements experienced solution convergence difficulties because of the decrease in stiffness after cracking. The problem can persist even with the implementation of the ANSYS® tensile stress relaxation option. In order to overcome the

convergence issues, the unreinforced concrete elements were given insignificant but non-zero reinforcement by assigning a reinforcement volume fraction of 0.01% of the element volume. The use of this augmented stiffness greatly enhanced the numerical stability of the model and it was demonstrated to have no significant impact on the resulting force, moment, stress, or strain calculations. This method is standard practice for tank models with ANSYS® SOLID65 concrete elements.

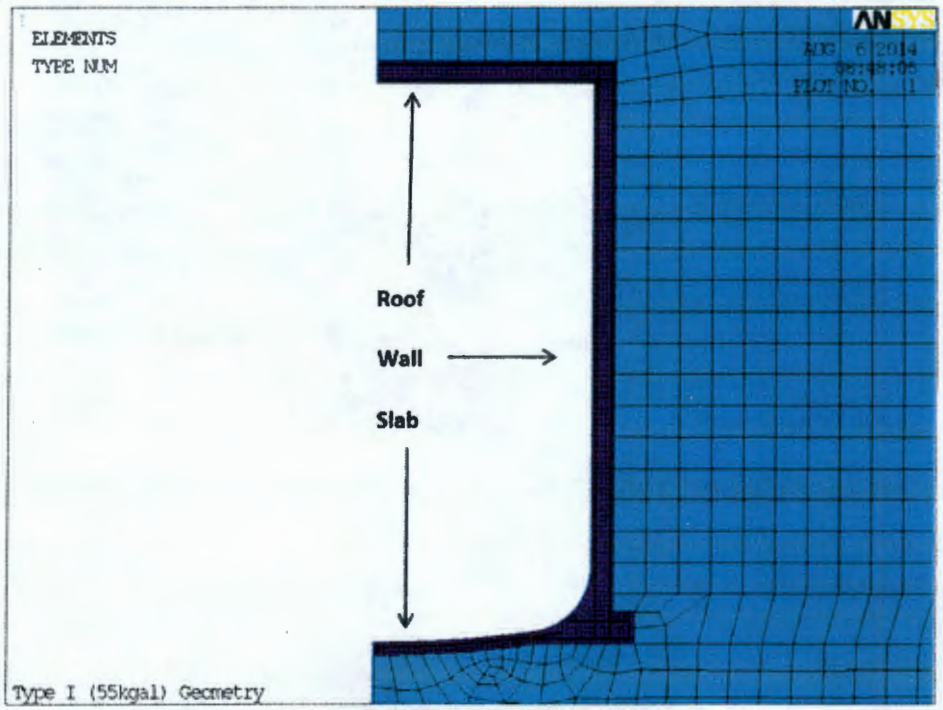

Figure 5.1. Finite Element Mesh of Tank and Soil Element-Type Plot

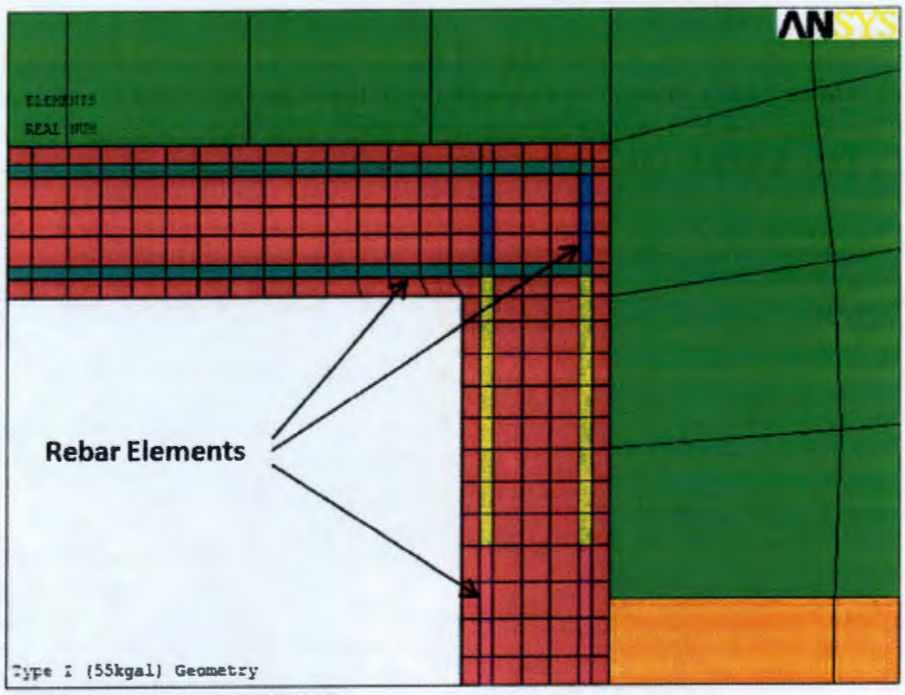

Figure 5.2. Close-up of Roof and Wall Reinforced Concrete Elements (ANSYS Real Constant Plot)

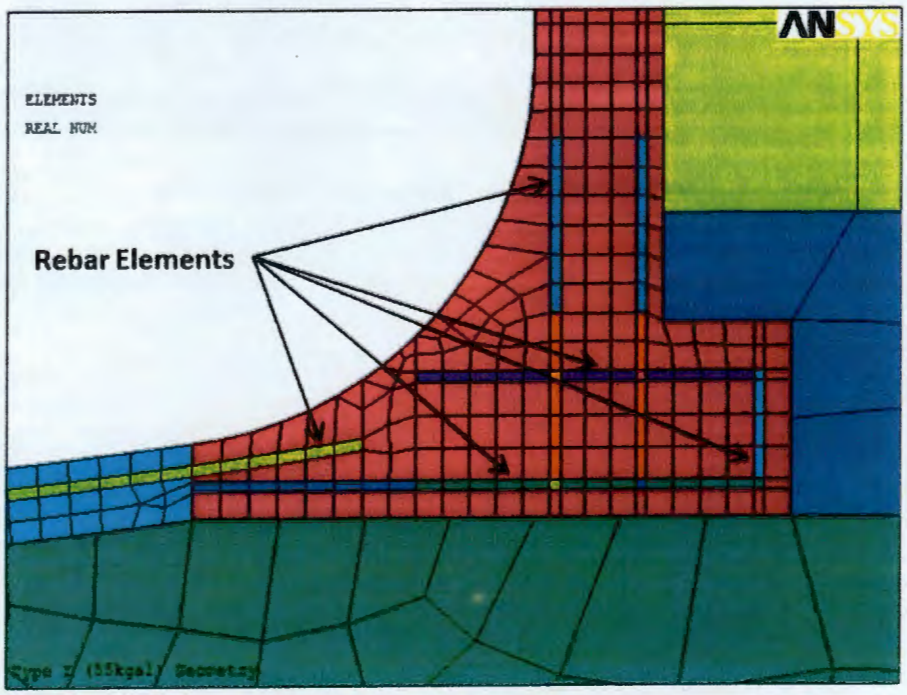

Figure 5.3. Close-up of Footing with Reinforced Concrete Elements (ANSYS Real Constant Plot)

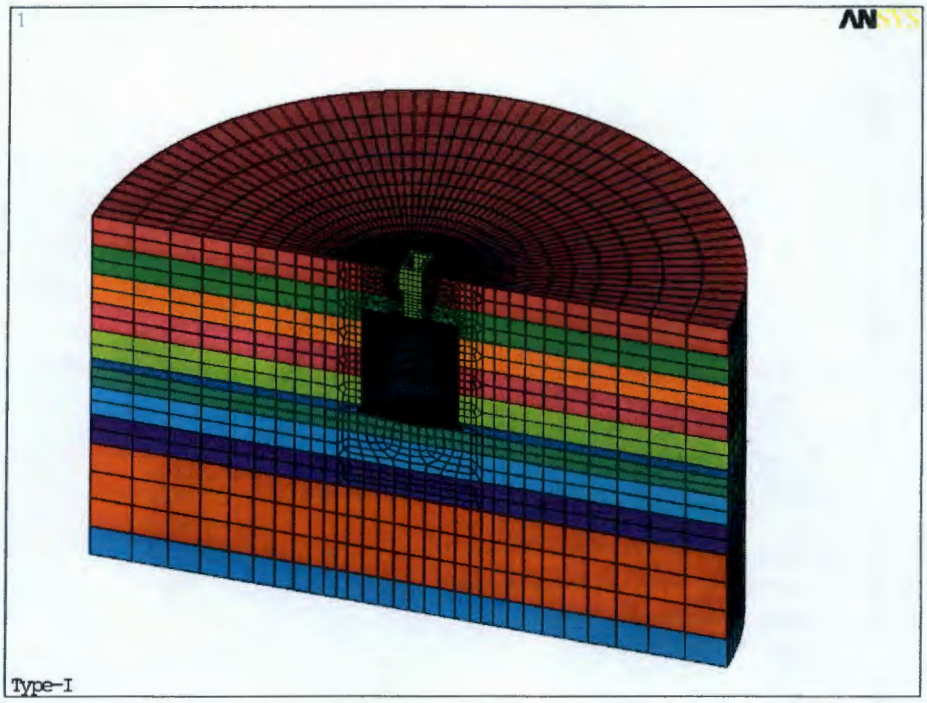

Figure 5.4. ANSYS Model Showing Type I SST and Surrounding Soil (Material-Type Plot)

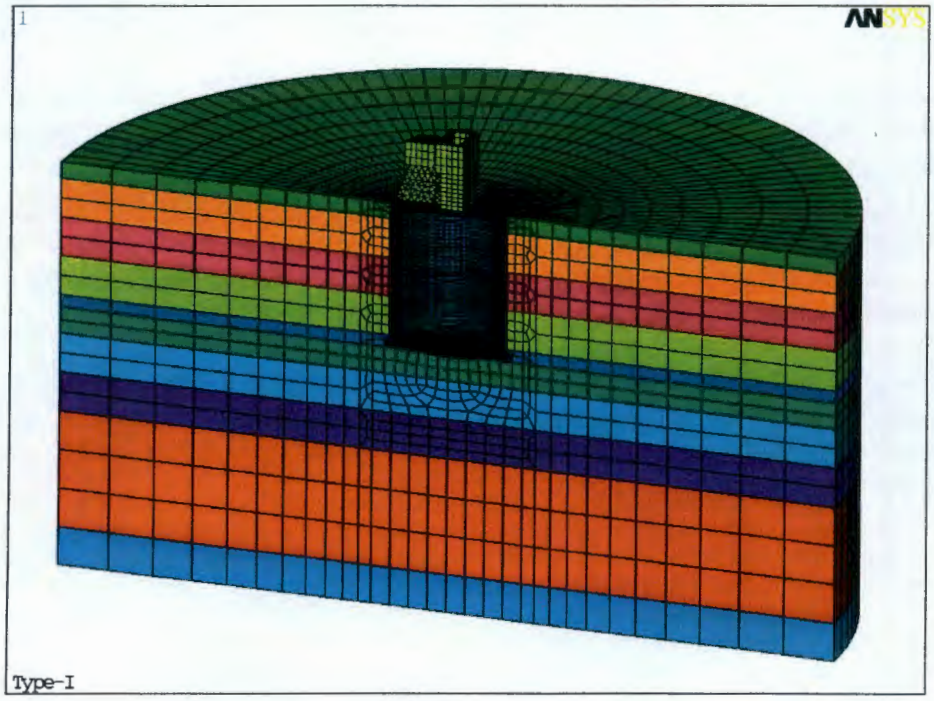

Figure 5.5. Final ANSYS Type I Model (Material-Type Plot)

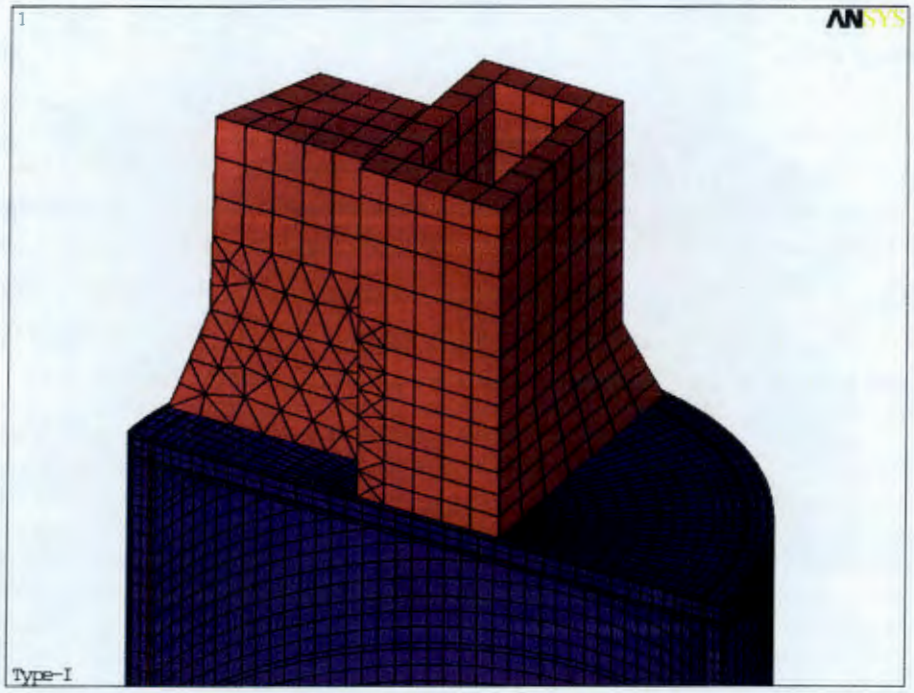

Figure 5.6. ANSYS Model – Hatchway Details (Element-Type Plot)

The ANSYS® concrete material model that allows for cracking and crushing, as well as variable shear transfer for open/closed cracks, is used for the SOLID65 elements.

The soil surrounding the tank is modeled with SOLID185 elements. The soil elements use the Extended Drucker-Prager (EDP) constitutive model, which has an internal friction angle, cohesion, and dilatancy angle as material properties. A small positive value of cohesion is used to represent the Hanford cohesionless soils. As per Johnson et al. (2010), the dilatancy angle is defined as 13° and the internal friction angle is defined as 35°. The ANSYS® EDP material model also requires specification of yield surface and flow potentials. A linear yield function and linear flow potential function are prescribed for the soil EDP material behavior in these analyses models.

The nonlinear contacts at the concrete and the soil interface use TARGE170 and CONTA173 elements. The soil-structure interaction (SSI) between the tank and surrounding soil is modeled using these surface-to-surface contact elements with sliding friction coefficient values prescribed in Section A.5.6 of the Evaluation Criteria report (Johnson et al. 2010).

5.3 Real Constants

ANSYS® uses real constants to define element properties for certain element types (e.g., thickness for shell elements, friction for contacts, steel-to-concrete volume fractions for reinforced concrete elements). The concrete reinforcing steel is modeled by using rebar capabilities of the ANSYS® SOLID65 element. Elements of 1-in. thickness were defined in the appropriate location in the roof, haunch, wall, knuckle, and foundation slab to model the steel reinforcement at those locations. There are three possible rebar

directions in ANSYS® for rebar elements, and each of these directions include the following real constants:

- The rebar material ID number
- Steel volume ratio
- Two angles used to orient the rebar directions relative to the element coordinate system.

Tables 5.2 through 5.4 show the calculated steel volume ratios of the concrete rebar elements. Initially these real constants are defined in the model input file and are then assigned to the reinforcement elements by location. The following nomenclature is applicable to Tables 5.2 through 5.4:

- Elevation: The height of any section from the tank's origin that is at the top of slab along the tank's axis in the model.
- Radius: The radial distance of any section where the rebar volume fraction is calculated.
- Spacing: The distance between the reinforcement bars along hoop or meridional direction.
- Volume Ratio: The ratio of the steel volume to the total volume (concrete + steel) at any section when the rebar steel is assumed to be distributed in a 1-in.-thick element as shown in Figure 5.2 or in Figure 5.3. In the tables, the Top/Bottom refers to top or bottom layup of reinforcements in the roof and similarly Inner/Outer refers to inner or outer layup of reinforcement in the wall or floor.
- Real Constant: The real constant number assigned to a section in the ANSYS® model that contains details of volume fractions of steel in the meridional and hoop directions.

Table 5.2. Roof Concrete Rebar Volume Ratios

Description:	Roof							
Elevation[a] (in.)	**Radius (in.)**	**Size**	**Meridional Spacing[b] (in.)**	**Volume Ratio (Top=Bot)**	**Size[c]**	**Hoop Spacing (in.)**	**Volume Ratio (Top=Bot)**	**Real Constant**
N/A	0–133	6	12.0	0.0368	6	12	0.0368	44

(a) Considering top of the slab at centerline is origin.
(b) The drawings used to obtain this information specify radial rebar by spacing at 38 ft 2⅝ in. radius reference circle; therefore, the meridional spacing for steel volume fraction is taken as the average of spacing the beginning and end of the radii range and the number of bars are calculated by dividing the circumference at 38 ft 2⅝ in. radial reference circle with specified spacing.
(c) Bar size given in eighths of an inch; i.e., 6×1/8 = ¾ in. bars.

Table 5.3. Wall Concrete Rebar Volume Ratios

Description: Wall									
Elevation[a] (in.)	Radius[b] (in.)	Size	Meridional Spacing[c] (in.)	# Bars[c]	Vol. Ratio (In=Out)	Size[d]	Hoop Spacing (in.)	Volume Ratio (Inner=Outer)	Real Constant
2.5–18	452	6	15	NA	0.0295	NA	NA	0.0001	36
18–35	470	6	12	NA	0. 0368	5	8.5	0. 0361	37
35–89	452	6	12	NA	0.0368	5	6	0.0511	38
89–137	464	6	12	NA	0.0368	5	8	0.0383	39
137–197	470	6	12	NA	0.0368	5	10	0.0307	40
197–293	452	6	12	NA	0.0368	5	12	0.0256	41
293–313	464	6	12	NA	0.0368	5	6	0.0511	42
308–322.5	470	6	12	NA	0.0368	NA	NA	0.0001	43

(a) Considering bottom of the slab at centerline is origin.
(b) The radial distance to inner, outer and or middle rebar in the wall.
(c) The drawings used to obtain this information specify wall rebar by spacing; therefore, the number of bars are not recorded.
(d) Bar size given in eighths of an inch, i.e., 6×1/8 = ¾ in. bars.
NA = Not applicable.

Table 5.4. Foundation Concrete Rebar Volume Ratios

Description: Slab									
Elevation[a] (in.)	Radius (in.)	Size	Meridional Spacing[b] (in.)	# Bars[b]	Volume Ratio	Size[c]	Hoop Spacing (in.)	Volume Ratio	Real Constant
NA	0–105	4	12	NA	0.0164	4	12	0.0164	31
Description: Footing									
Elevation (in.)	**Radius (in.)**	**Size**	**Meridional Spacing (in.)**	**# Bars**	**Volume Ratio**	**Size**	**Hoop Spacing (in.)**	**Volume Ratio**	**Real Constant**
Footing-bottom	89–110	4	15		0.0131			0.0001	32
Footing-bottom	110–142	4	15		0.0131	1" sq	10	0.1000	33
Footing-side		4	15		0.0131			0.0001	34
Footing-top	110–142	4	15		0.0131	1"sq	10	0.1000	35
Footing-middle		6	15		0.0295			0.0001	36

(a) Considering bottom of the slab at centerline is origin.
(b) The drawings used to obtain this information specify radial rebar by spacing at 38 ft 2⅝ in. radius reference circle; therefore, the number of bars are calculated by dividing the circumference of 38 ft 2⅝ in. radial reference circle with the specified rebar spacing.
(c) Bar size given in eighths of an inch, i.e.,size 6 = 6×1/8 = ¾ in. bars. 1" sq indicate 1" x 1" square bars.
NA = Not applicable.

5.4 Loads and Boundary Conditions

The Type I TOLA models consider the following mechanical live and dead loads.

- Equivalent soil pressure (soil overburden of 11.45 ft at 125 lb/ft^3) and self-weight of the tank applied by gravity.

- Historical hydrostatic loads due to waste (variable height at specific gravity of 1.7) applied as pressure loads on the inner surface of the tank
- 40 lb/ft^2 uniform surface live load to account for snow and ash fall applied as pressure on the top surface of the soil
- 142 kip concentrated live load distributed over a 10-ft radius circular area concentric with the tank applied as a pressure load. This pressure was applied to the full tank roof, including the roof under the hatchway and is thus viewed as extremely conservative.

The concentrated load for the Type I tanks has been specified as 142 kip over a 5-ft radius area (Julyk and Mackey 2003b) applied at the soil surface. The 11.45 ft soil depth in concert with the 35 degree soil friction angle and the 10-ft tank radius, results in an effective load radius on the tank that exceeds 10 ft. Because the ANSYS® model does not include any soil elements above the tank but represents the soil load with an equivalent pressure, the concentrated load was conservatively applied as an added pressure over the 10-ft radius.

The mechanical loads were applied to the model in three load steps; the first load step applies the gravity load (self weight and soil pressure), the second load step applies the initial hydrostatic waste load, and the third load step applies the additional surface live loads. The transient thermal loads along with variable hydrostatic waste loads were applied to the model in several load steps beginning from load step four. The historical thermal and waste load profiles are shown in Figure 4.2, and these loads are solved in steps 4 through 8 in the analysis.

In the FE model, the base of the soil column is constrained in the vertical direction. Similarly, the soil column is confined radially at the outer (72.5 ft.) radial surface. The front and back faces of the model are given symmetric boundary conditions (constrained circumferentially). These boundary conditions are applicable to structural models with mechanical as well as thermal loads.

The thermal loads on the tank (temperature profiles) at any point of time during the tank's operating history are dependent on the waste temperature and level in the tank. These thermal loads were determined from the transient thermal model that was developed to bound the operational histories of the Type I tanks. Section 5.6 describes in detail the transient thermal analysis models.

The temperature distributions in the tank and soil from the transient thermal model were mapped onto the structural model at specific times of interest using the ANSYS® BFINT command.

The model considers the thermal degradation of concrete properties during the tank's service history. The property degradation is incorporated in the model by locking in the degraded material properties when the tank sections reach the peak temperatures in time. This prevents the degradation from reversing as the tank cools.

5.5 The TOLA Run Matrix

The initial TOLA run matrix for the Type I SST AOR was developed based on the results of the Type II AOR (Rinker et al. 2011a). The number of ANSYS analyses was reduced to those material combination that have consistently given the highest structural demand in the Type II, III, and IV analyses of record. Results from the Type I Seismic Analysis, described in Attachment 1, also demonstrate that a

single bounding case is defensible. The reduced Run Matrix for Type I is shown in Table 5.5. TOLA results for Runs 2, 4, and 7 are reported in Chapter 7.0. Combined TOLA + seismic results for Run 7 are reported in Chapter 9.0. Run 6 is used in the Tank Limit Load analysis as reported in Chapter 10.0.

Concrete creep was not considered in any of the analyses. Analysis execution times with creep enabled were prohibitive. Previous (Type II, III and IV) AORs have consistently demonstrated that creep serves to reduce the concrete section demands. Conducting the ANSYS analyses without the creep enabled will result in conservative ACI D/C ratios.

Table 5.5. TOLA Run Matrix (Material Combination Strategy) for Type I SST AOR

		Concrete			
Case/ Run	**Soil Modulus**	**Concrete Modulus**	**Tensile Strength**	**Concrete Creep**	**Notes**
2	N	N	Near Zero (10 psi)	No	Best Estimate Properties
4	L	H	Near Zero (10 psi)	No	Establish degraded concrete for Limit Load Analysis
6	N	N	Nominal	No	
7	L	N	Near Zero (10 psi)	No	

H = High.
L = Low.
N = Nominal/Mean (Best Estimate).

5.6 Temperature Profile and the Thermal Model

Type I single-shell tanks have a capacity to hold 55,000 gallons of waste and are located in the B, C, T, and U Tank Farms. The temperature history used in the Type I AOR is defined in Section 3.2. A transient thermal finite element model was used to calculate the temperature history inputs for the TOLA.

Thermal analysis was carried out using a 180-degree 3-D model including the hatchway. The soil extent in the model was the same as that shown in Figure 5.4. Resulting temperatures were mapped onto the structural model using the ANSYS BFINT routine.

One addition to the thermal model was the waste surface as shown in Figure 5.7. This waste surface was added to simulate radiation and convection heat transfer from the waste surface to the tank roof and walls. The waste surface in the model is not physically linked to the rest of the tank elements. Therefore, there is no conduction between the waste surface elements and the tank elements. The radiation surface has been identified in Figure 5.7 with the aid of red and blue arrows. ANSYS® calculates the radiation view factors for all element surfaces based on the axisymmetric model.

Loads on the thermal model were specified in the form of uniform temperatures (either 250°F, 100°F, or 80°F) on the inner surface of the tank. Waste temperatures were imposed in the model by assigning the waste temperature values to the nodes on the inner surface of the tank that are located at or below the waste height. The temperature specifications (thermal load) on the tank inner surface and the liquid

surface were imposed in the form of ramped boundary conditions. That is, the imposed temperature within a step is ramped (increased or decreased) linearly with time over the time period of the step.

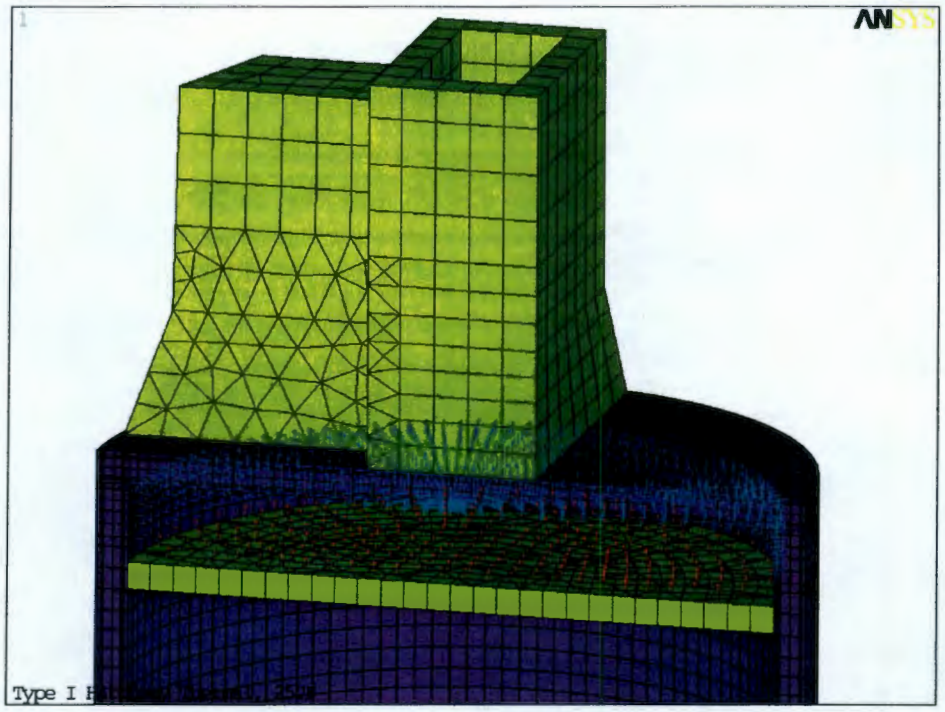

Figure 5.7. Thermal Model

Boundary conditions were imposed on the top and the bottom surfaces of the soil in the model. The bottom surface was assigned an isothermal boundary condition with a temperature value of 53°F (the far-field soil temperature) and the top surface was assigned a heat transfer coefficient of 2 Btu/h-ft^2-F convecting heat to the atmosphere at 53°F. There was no specified boundary condition on the right end of soil in the model. ANSYS® assumes an adiabatic boundary condition (default) on this surface.

Table 5.6 shows the data in Figure 3.4 in a tabulated form.

Table 5.6. Temperature History and Waste Height Data Used in the Type I Tank AOR

Thermal Step #	Date	Waste Height (in.)	Waste Temperature (°F)
--	1/1/1947	0	53
1	7/1/1947	284	250
2	1/1/1970	284	250
3	6/21/1971	284	100
4	3/31/2014	284	100

Nodal temperatures obtained from the thermal analysis were imposed as body forces on the nodes of the structural models in the thermal stress analysis. The nodal temperatures at the end of each time step were read into the structural analysis to define the temperature dependent material properties and calculate the thermal stresses.

Figure 5.8 shows the temperature distribution in the tank at the peak temperature value of 250°F. The temperature distribution for the full model is shown in Figure 5.9.

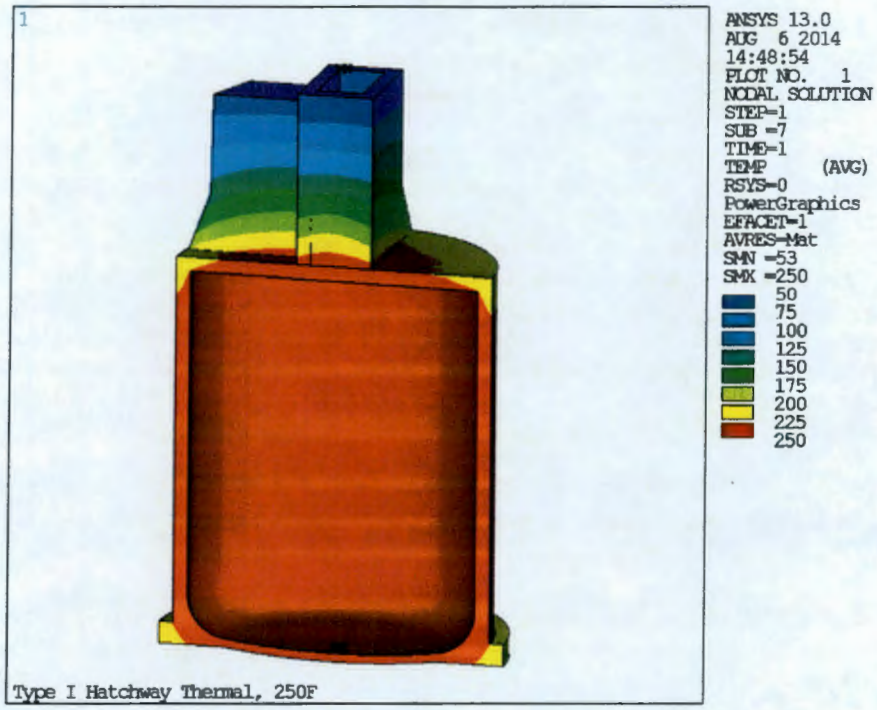

Figure 5.8. Peak (250°F) Temperature Distribution in Concrete Tank

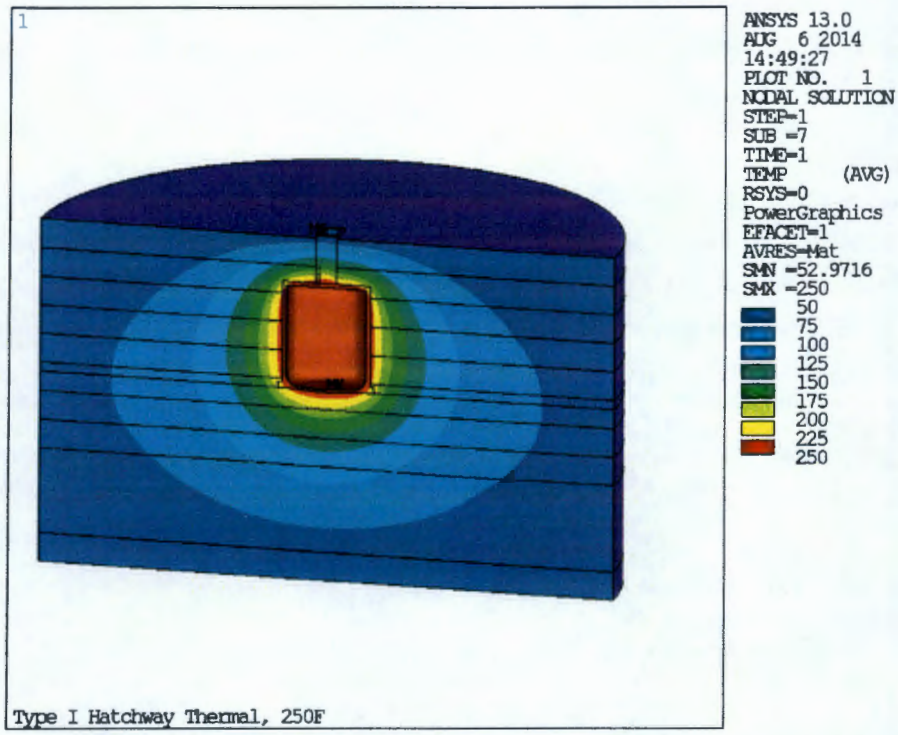

Figure 5.9. Peak (250°F) Temperature Distribution

This page intentionally left blank.

6.0 Seismic Analysis

Becht Engineering was subcontracted by PNNL to perform the seismic analysis of the Type I single-shell tanks (SSTs) for the Analysis of Record (AOR). The seismic model is described in a separate report from Becht entitled, "Hanford Type I Single Shell Tank Seismic Analysis." Attachment 1 contains the seismic analysis report in its entirety. Chapters 6 and 7 of Attachment 1 give the modeling details of the seismic analysis.

This page intentionally left blank.

7.0 Static Modeling Results

This chapter presents the TOLA static modeling results (without seismic) for the TOLA matrix runs given in Section 5.5 of Chapter 5.0.

7.1 Introduction

This section summarizes the results from the three different TOLA runs described in Chapter 5.0 of this document. The primary focus is structural evaluation of the SST according to the criteria developed by Johnson et al. (2010) and summarized in Chapter 4.0 of this report. The ACI concrete evaluation for each run in Table 5.5 is presented. Run 2 is the baseline model with best estimate properties. TOLA matrix Runs 4 and 7 are combinations of bounding material property variations. These are called worst-case combinations because they are combined to bound the possible scenarios.

Each run was conducted in several steps as shown in Figure 4.2. The ACI evaluations are conducted at different points depending on the particular ACI load combination. Load combination 1 (LC1) is a separate load path and is always conducted after the final 53°F load step. Load combinations 4 (LC4) and 9 (LC9) include temperature effects.

Load step numbers and years are referenced in various plots in the following evaluation sections. Table 4.5 gives the load step numbers as related to the year of the analysis and individual thermal load steps.

The remainder of Chapter 7.0 is organized as follows. Section 7.2 discusses the plastic strain observed in the steel reinforcement. Section 7.3 describes the ACI evaluation of the 22 sections around the profile of the Type I tank. Section 7.3 also presents the ACI D/C ratios for the individual cases in the material run matrix. Section 7.8 summarizes the conclusions of the TOLA run matrix analyses.

7.2 Steel Reinforcement Plastic Strain

The material property data for the reinforcing steel includes a non-linear stress strain curve as recommended in the Evaluation Criteria report (Johnson et al. 2010). Previous AORs of the Type II, III, and IV SSTs have not observed any plastic strain during the loads required by the ACI evaluation. Rebar plastic strain was observed in the Type I analyses during the increase in temperature early in the thermal cycle. The tensile plastic strain accompanied by concrete cracking is localized in the edge of the roof in the region unsupported by the hatchway as shown in Figure 7.1. The maximum plastic strain of 0.05% is very low compared to the maximum tensile strain of 40 ksi rebar which typically exceeds 10%.

This plastic deformation is thermally induced and consequently is self-limiting. The rebar does not continue to plastically deform through the remainder of the thermal cycle. The larger SSTs feature a dome rather than a flat roof. The soil loads in the domed tanks are supported through dome compression rather than bending as in the Type I flat roof. The presence of small plastic strains in the Type I tank analysis is not regarded to be of structural concern.

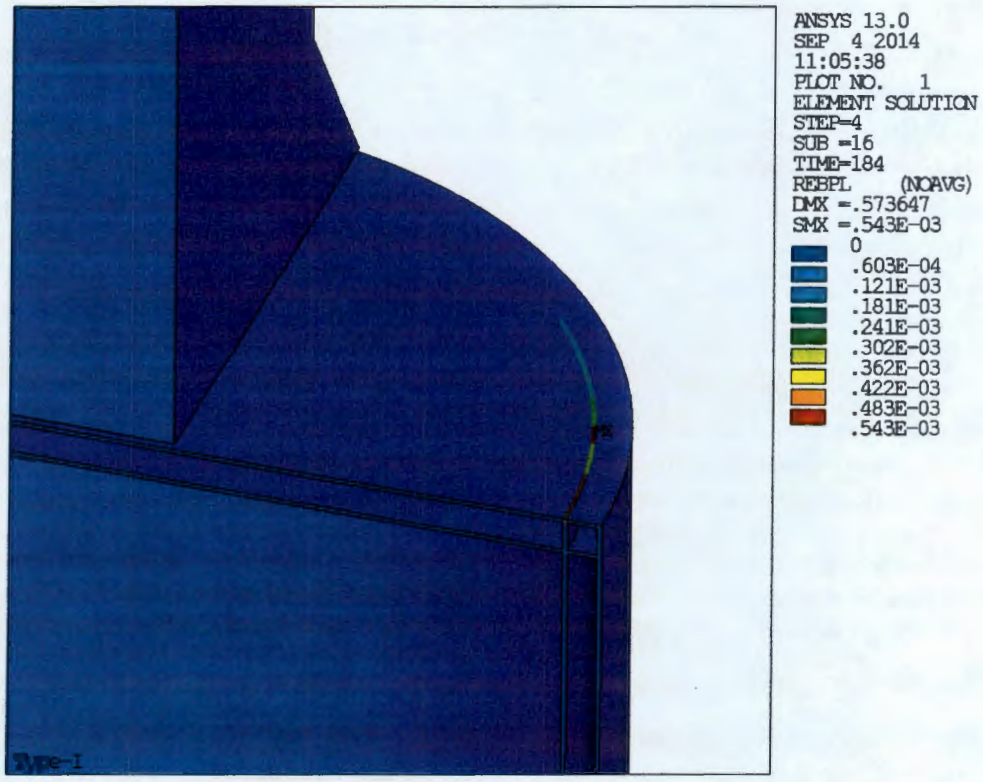

Figure 7.1. Steel Reinforcement Plastic Strain

7.3 ACI Evaluations – Structural Concrete

The Evaluation Criteria report (Johnson et al. 2010) specifies that the reinforced concrete structure of the tanks shall be evaluated to the standards of ACI 349-06 (ACI 2007). The load factors to be applied in this analysis are a subset of the possible combinations specified in ACI 349-06. Chapter 4.0 of this report indicates that load combinations 1, 4, and 9 are relevant for this analysis.

Load combination 1 [U = 1.4D + 1.4F + 1.7L + 1.7H] was achieved by running the model for an additional load step after the 53°F load step of thermal and waste-level history. This combination requires, in part, a factor of 1.4 on dead loads and a factor of 1.7 on live loads and lateral soil loads. This was achieved by placing the 1.4 factor on the gravitational acceleration and scaling the soil densities by the ratio of 1.7/1.4. The soil pressure above the tank was increased by a factor of 1.4 and the pressure increment for the concentrated load was increase by a factor of 1.7. Outboard of the tank, the soil pressure was increased by a factor of 1.7 to increase the lateral soil load.

Load combination 4 (without seismic) [$U = D + F + L + H + T_o + E_{ss}$] has load factors of 1.0 and includes thermal effects. This was achieved by cooling the waste temperature to 80°F (the estimated current temperature) after the thermal and waste-level history. The LC4 without seismic is provided to assess the effect of the seismic contribution on the LC4 D/C ratios when seismic is included.

Load combination 9 [U = 1.05D + 1.05F + 1.3L + 1.3H + 1.05T_o] was achieved by running the load combination 4 model for an additional load step after the 80°F load step. This combination requires, in part, a factor of 1.05 on dead loads and a factor of 1.3 on live loads and lateral soil loads. This was achieved by placing the 1.05 factor on the gravitational acceleration and scaling the soil densities by the ratio of 1.3/1.05 except for soil overburden above roof. The live loads were also scaled up by a factor of 1.3. In addition, the temperature difference (tank temperature – the initial stress-free temperature) was multiplied by 1.05 T_o.

An ANSYS® macro, paciX.inp, was developed to compute shear, meridional, and circumferential (hoop) forces and moments at 22 locations in the concrete tank. The macro then increments 61 times to achieve the full 180-degrees of the model. Figure 7.2 shows the locations of the ACI evaluated sections on the 0-degree section. The sections in the concrete tank begin at the center of the roof and traverse through the haunch, down the wall, and back across the slab. No sections were included within the footing as it is shorter than the ACI specified "D-distance" (the minimum distance between the compressize face and the the tensile rebar). Force-moment diagrams of all the 22 sections were developed using the ACI methodology described in the Evaluation Criteria report. The section properties used in the ACI capacity calculations are described in Table 7.1 and Table 7.2. The ACI evaluation is performed for sections in the roof, wall, and floor of the tank that form the waste containment boundary. The hatchway structure is not evaluated.

Figure 7.3 shows a typical force-moment diagram along with the definition of the demand/capacity ratio. The demand/capacity ratio is defined as the ratio of the vector length from the origin to the force-moment demand coordinate to the vector length from the origin to the capacity curve assuming the same ratio of force to moment. A demand/capacity ratio exceeding 1.0 indicates that the ACI requirements are not met. Caution should be observed to not interpret the demand/capacity ratio as a measure of safety factor, which is only applicable if the same ratio of force to moment is maintained under changing loads. Appendix C shows the implementation of the ACI methodology in Mathcad™ using section 5 under peak temperature as an example. The results for the 61 sections are combined on a single plot (e.g., Figure 7.4) using MATLAB™.

The ACI capacity curves change with temperature, and the capacities plotted in these figures correspond to the maximum temperature experienced by the section. Because high temperature irreversibly degrades the strength and stiffness of concrete, the ACI capacity curves are always calculated for the maximum temperature that the tank has experienced up to that point in time.

The results presented in this section are the demand/capacity ratios for each of the three ACI load combinations (1, 4-TOLA loads only, and 9) and the peak temperature load step for TOLA runs 2, 4, and 7. Run 6 was conducted to establish the degraded concrete condition at the start of the tank limit analysis described in Chapter 10.0. Run 6 was not evaluated using ACI because of the inconsistency between the ACI evaluation which does not take credit for concrete tensile strength and the analysis which used nominal tensile strength.

The overall results presented in this chapter show that the ACI D/C ratios are significantly below 0.6 in the roof, haunch, and wall of the Type I tanks. However, there are locations in the slab where the D/C ratios exceed 1.0. This includes through-section shear where the slab and lower knuckle intersect inside the wall (Section 19). Further analysis with the slab detached from the inner footing shows that the tank is still structurally stable without shear transfer across Section 19.

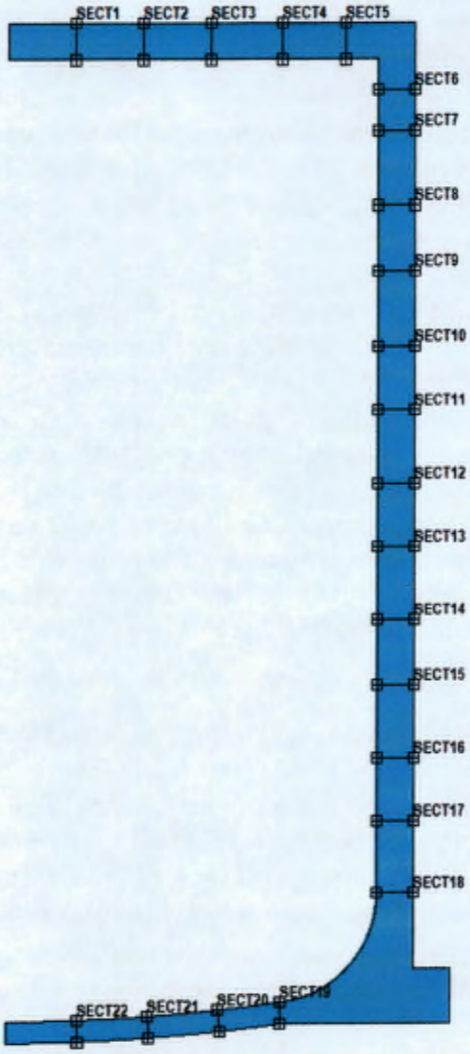

Figure 7.2. Reinforced Concrete ACI Evaluated Sections

Table 7.1. Section Properties in Meridional Direction

	Concrete Section	External Rebar			Internal Rebar			Middle Rebar		
			Depth	Spacing		Depth	Spacing		Depth	Spacing
No.	Thick (in.)	Bar Size	d_1 (in.)	s (in.)[a]	Bar Size	d_2 (in.)	s (in.)	Bar Size		Notes/Schematic
1	12	6	2.375	12	3	9.625	12			
2	12	6	2.375	12	6	9.625	12			
3	12	6	2.375	12	6	9.625	12			
4	12	6	2.375	12	6	9.625	12			
5	12	6	2.375	12	6	9.625	12			
6	12	6	2.375	6	6	9.625	12			
7	12	6	2.375	12	6	9.625	12			
8	12	6	2.375	12	6	9.625	12			
9	12	6	2.375	12	6	9.625	12			
10	12	6	2.375	12	6	9.625	12			
11	12	6	2.375	12	6	9.625	12			
12	12	6	2.375	10	6	9.625	12			
13	12	6	2.375	10	6	9.625	12			
14	12	6	2.375	8	6	9.625	12			
15	12	6	2.375	8	6	9.625	12			
16	12	6	2.375	6	6	9.625	12			
17	12	6	2.375	6	6	9.625	12			
18	12	6	2.375	6	6	9.625	12			
19	7	3	3.813	10000	8	4.75	12			
20	6.96	3	1.688	10000	8	4.71	12			
21	6.98	3	1.688	10000	8	4.73	12			
22	7	3	1.688	10000	8	4.75	12			

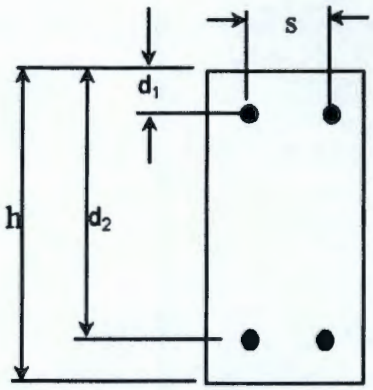

(a) 10000 inch spacing is entered to make external rebar contribution negligible. Only one rebar layer exists in the slab (see Figure 5.3).

Table 7.2. Section Properties in Circumferential Direction

		External Rebar			Internal Rebar			Middle Rebar			
Concrete Section No.	Thick (in.)	Bar Size	Depth d_1 (in.)	Spacing s (in.)[a]	Bar Size	Depth d_2 (in.)	Spacing s (in.)	Bar Size	Depth d (in.)	Spacing s (in.)	Notes
1	12	6	3.125	12	6	8.875	12				
2	12	6	3.125	12	6	8.875	12				
3	12	6	3.125	12	6	8.875	12				
4	12	6	3.125	12	6	8.875	12				
5	12	6	3.125	12	6	8.875	12				
6	12	5	3.063	6	5	8.94	6				
7	12	5	3.063	12	5	8.94	12				
8	12	5	3.063	12	5	8.94	12				
9	12	5	3.063	12	5	8.94	12				
10	12	5	3.063	12	5	8.94	12				
11	12	5	3.063	12	5	8.94	12				
12	12	5	3.063	10	5	8.94	10				
13	12	5	3.063	10	5	8.94	10				
14	12	5	3.063	8	5	8.94	8				
15	12	5	3.063	8	5	8.94	8				
16	12	5	3.063	6	5	8.94	6				
17	12	5	3.063	6	5	8.94	6				
18	12	5	3.063	6	5	8.94	6				
19	7	3	4.1875	10000	4	4.25	12				
20	6.96	3	2.0625	10000	4	4.21	12				
21	6.98	3	2.0625	10000	4	4.23	12				
22	7	3	2.0625	10000	4	4.25	12				

(a) 10000 inch spacing is entered to make external rebar contribution negligible. Only one rebar layer exists in the slab (see Figure 5.3).

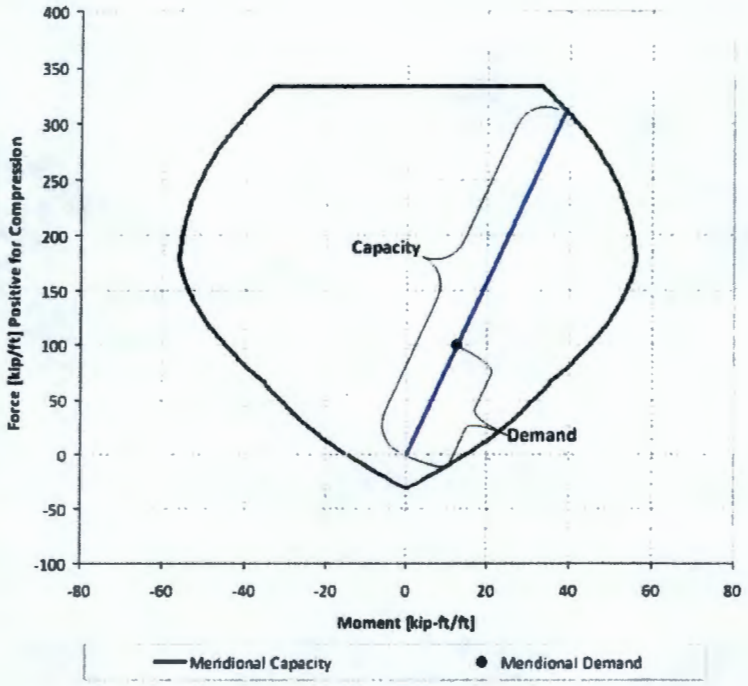

Figure 7.3. ACI Demand/Capacity Ratio Definition

7.4 Run 2, Baseline Case with Best Estimate Material Properties

This run uses the best estimate material properties (nominal soil modulus, nominal concrete modulus and near zero concrete tensile strength) and is considered to be the baseline analysis. Figures 7.4 through 7.19 show the demand/capacity ratios at peak temperature, LC1, LC4 (TOLA only) and LC9 in the meridional, circumferential, shear, and in-plane shear directions for the baseline material combination, Run 2.

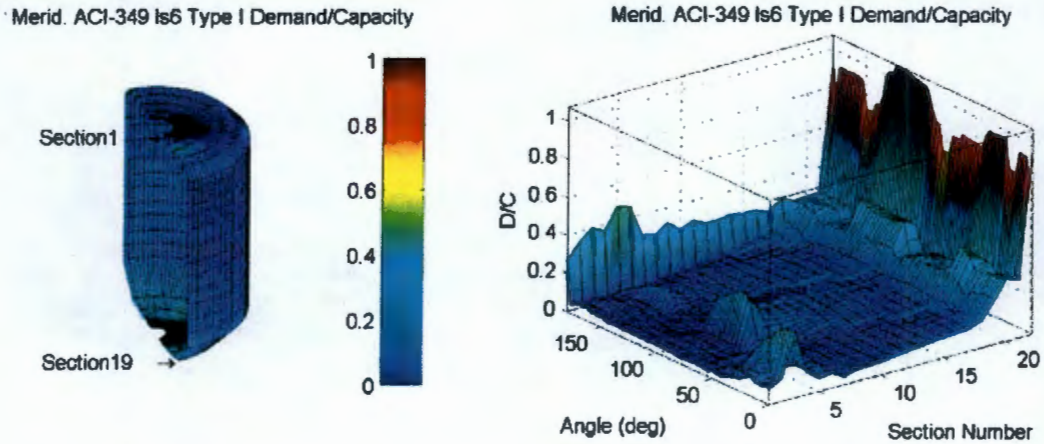

Figure 7.4. Run 2, Meridional ACI D/C Ratios at Peak Temperature

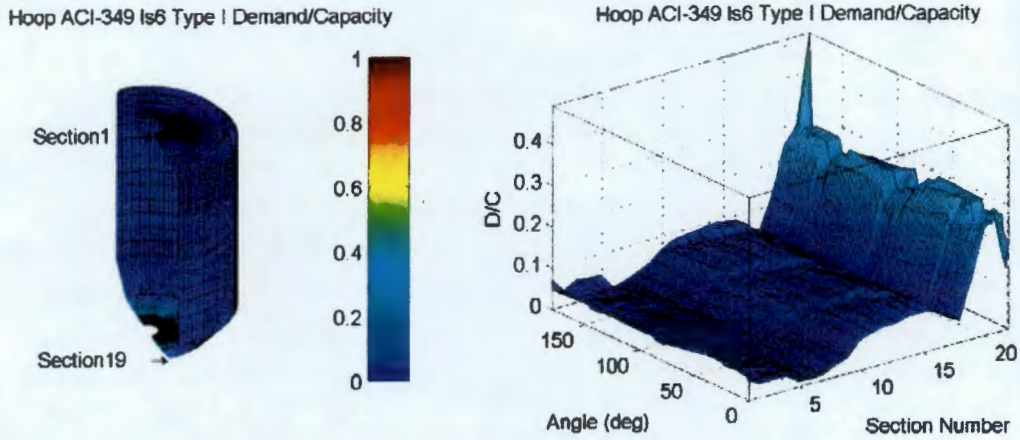

Figure 7.5. Run 2, Hoop ACI D/C Ratios at Peak Temperature

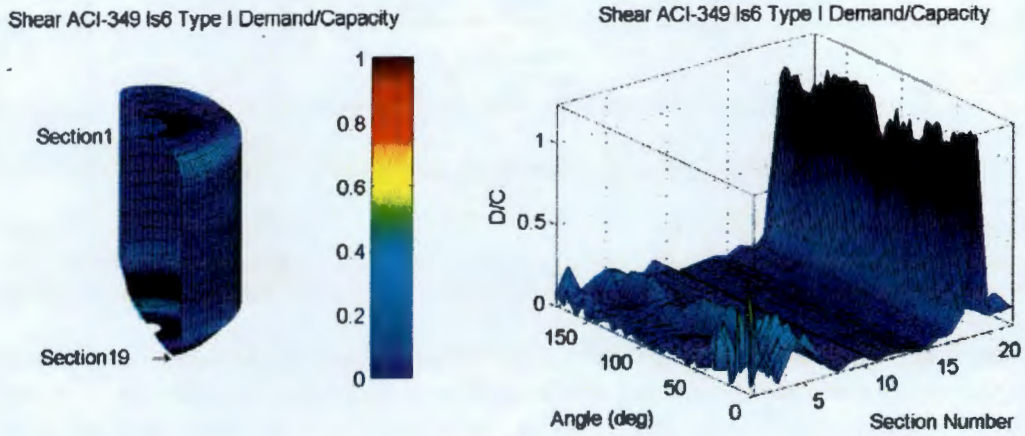

Figure 7.6. Run 2, Shear ACI D/C Ratios at Peak Temperature

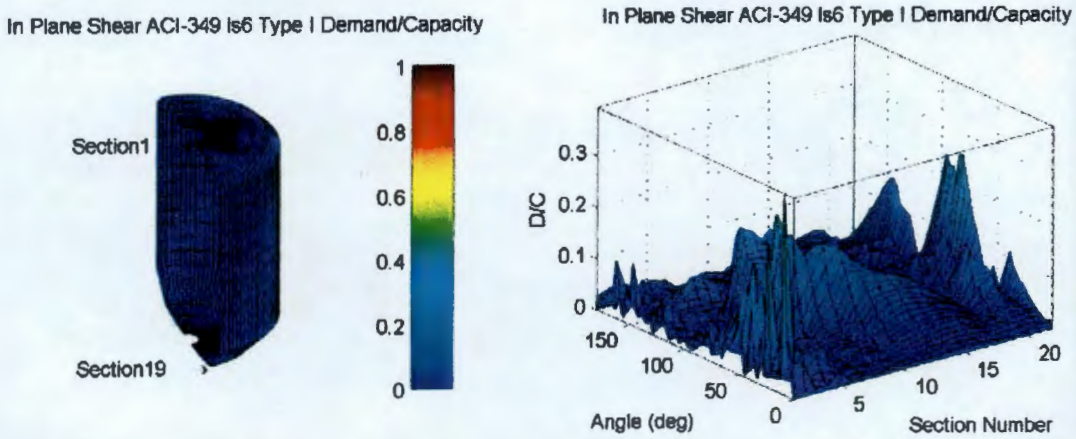

Figure 7.7. Run 2, In-Plane Shear ACI D/C Ratios at Peak Temperature

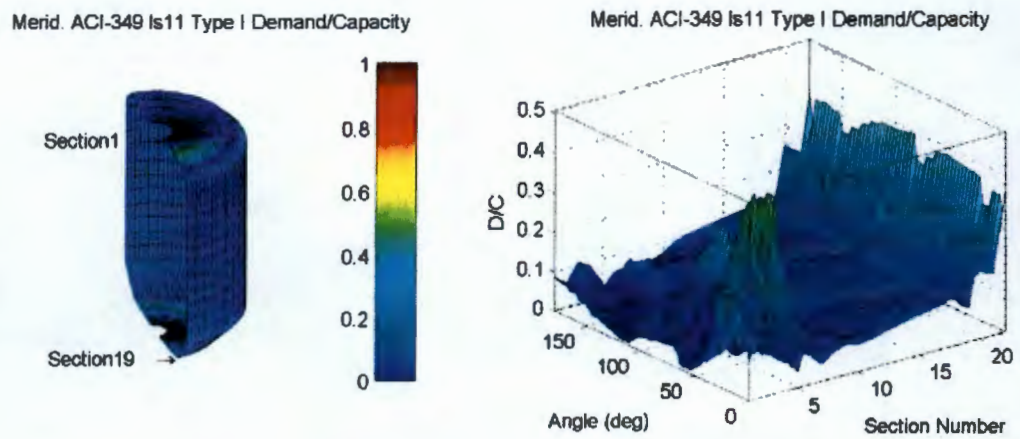

Figure 7.8. Run 2, Meridional ACI D/C Ratios at LC1

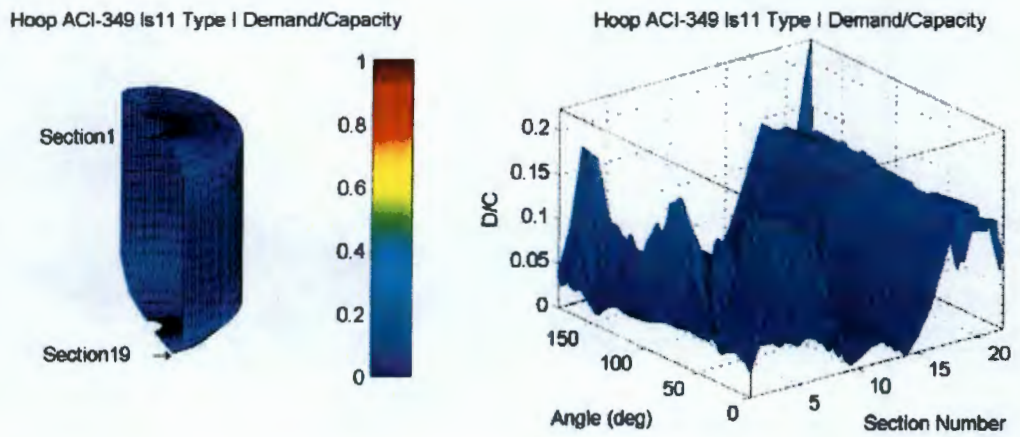

Figure 7.9. Run 2, Hoop ACI D/C Ratios at LC1

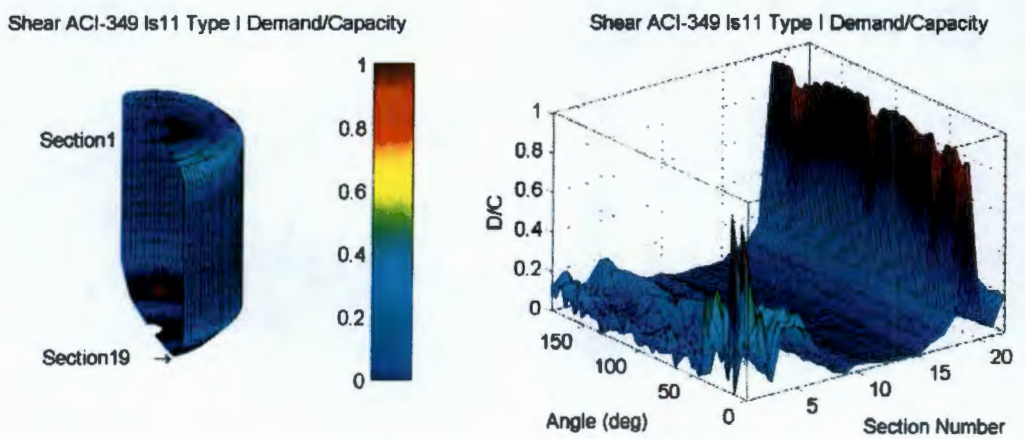

Figure 7.10. Run 2, Shear ACI D/C Ratios at LC1

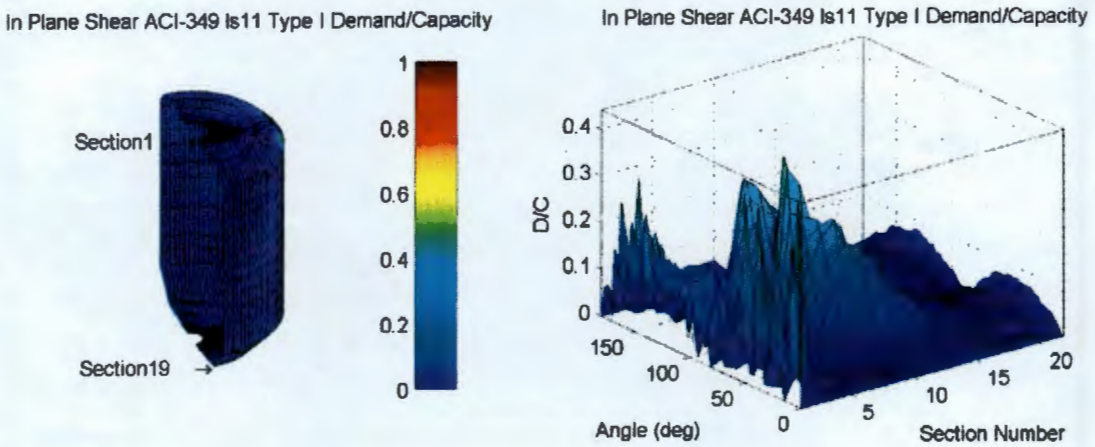

Figure 7.11. Run 2, In-Plane Shear ACI D/C Ratios at LC1

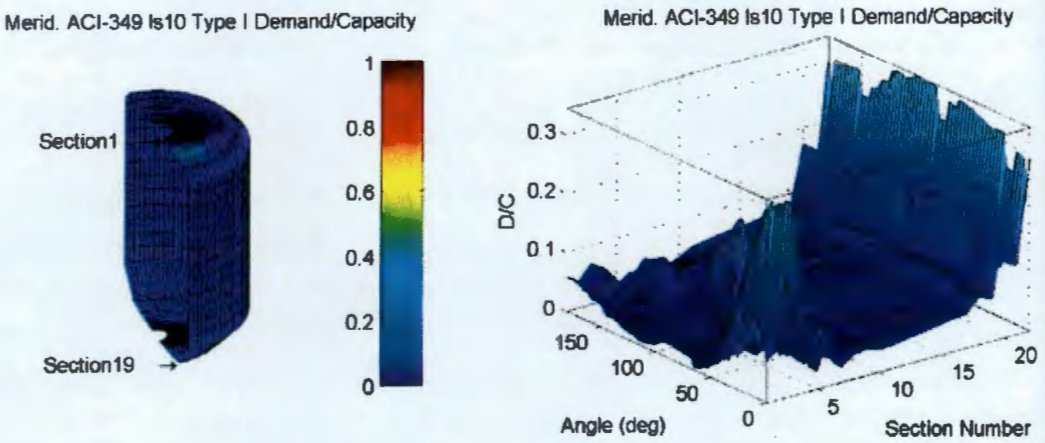

Figure 7.12. Run 2, Meridional ACI D/C Ratios at LC4 (TOLA only)

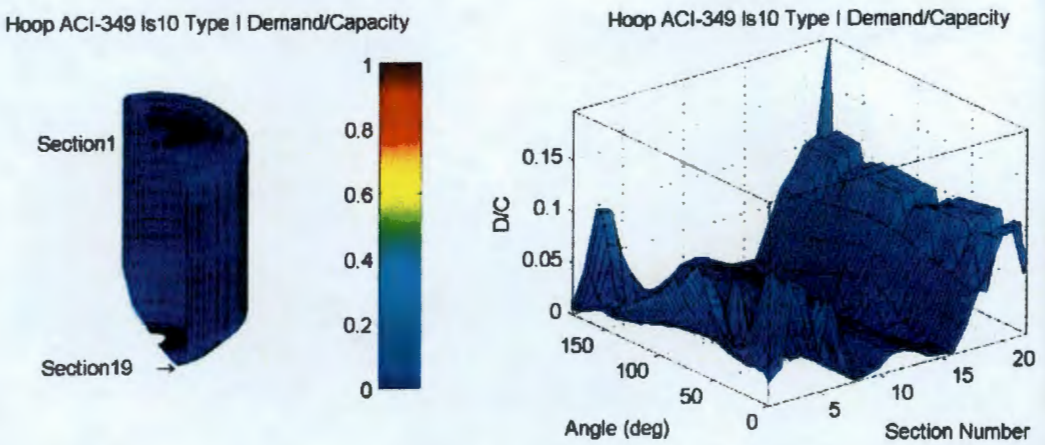

Figure 7.13. Run 2, Hoop ACI D/C Ratios at LC4 (TOLA only)

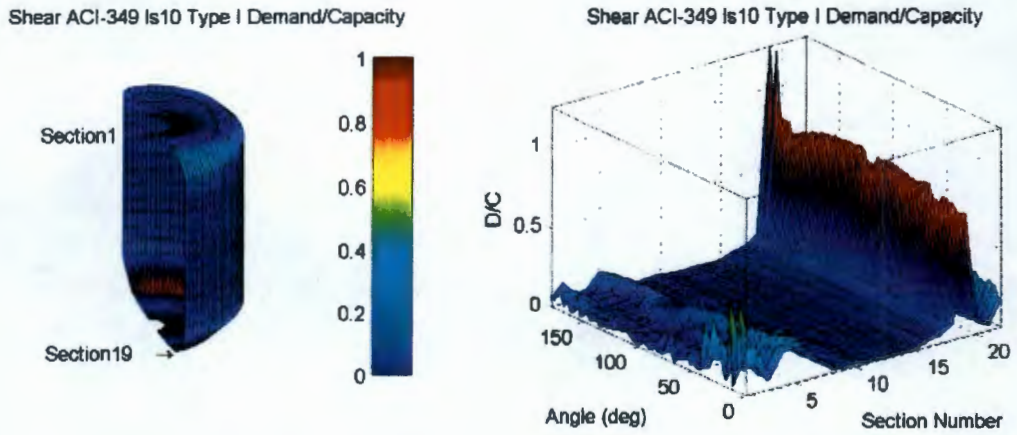

Figure 7.14. Run 2, Shear ACI D/C Ratios at LC4 (TOLA only)

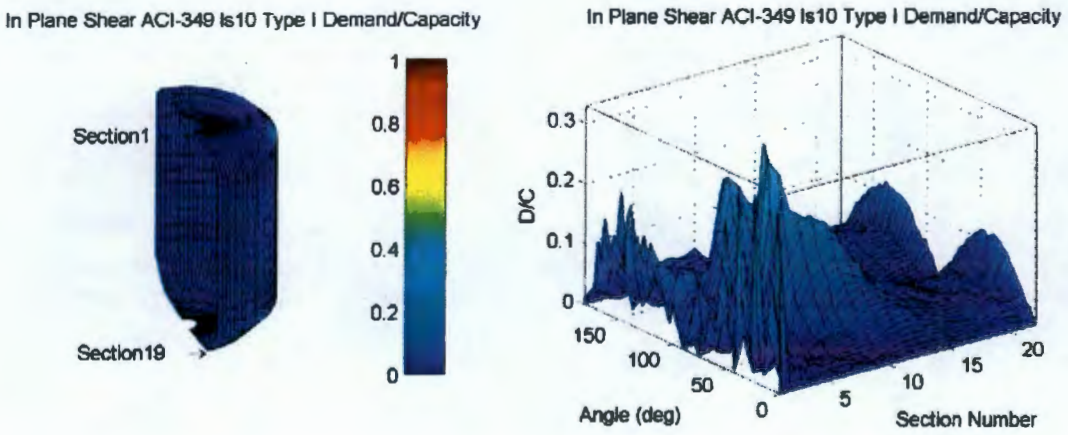

Figure 7.15. Run 2, In-Plane Shear ACI D/C Ratios at LC4 (TOLA only)

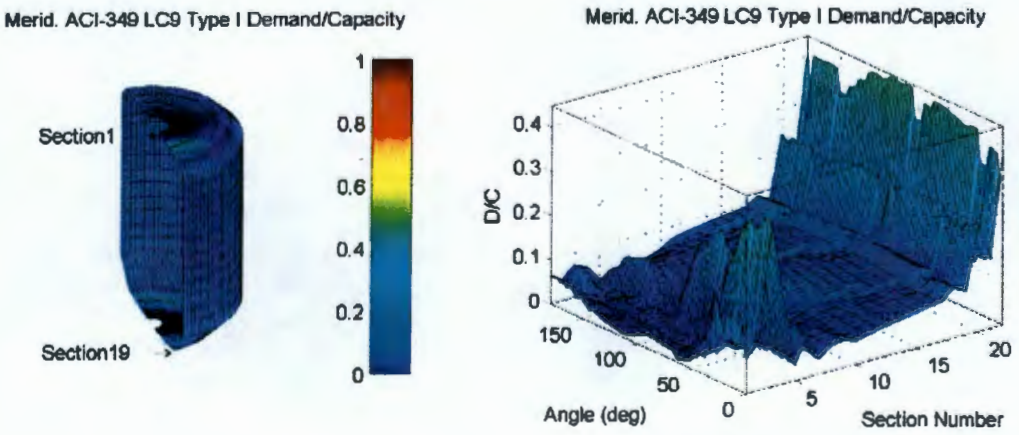

Figure 7.16. Run 2, Meridional ACI D/C Ratios at LC9

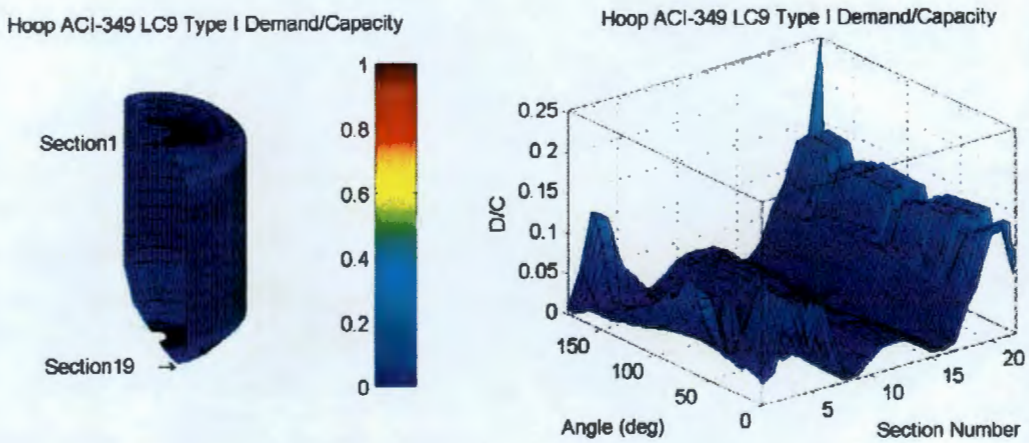

Figure 7.17. Run 2, Hoop ACI D/C Ratios at LC9

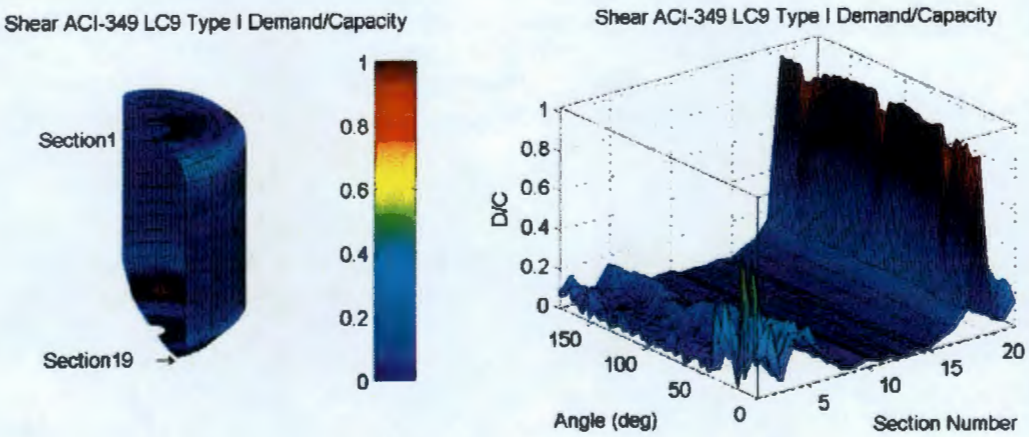

Figure 7.18. Run 2, Shear ACI D/C Ratios at LC9

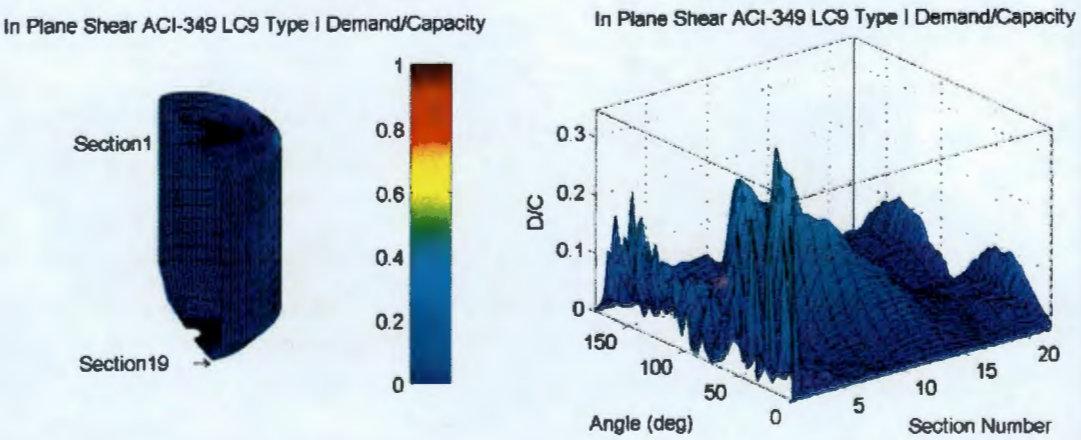

Figure 7.19. Run 2, In-Plane Shear ACI D/C Ratios at LC9

The shear D/C ratio plots, Figures 7.6, 7.10, 7.14, and 7.18 consistently show D/C ratios near 1.0 in the vicinity of section 19, the first ACI section in the slab. This provides the motivation for the detached slab analysis mentioned above and described in Chapter 7.7. Details of the shear D/C ratios, however, may be obscured by the volume of data in the 3D plots. Figure 7.20 is a 2D plot showing the ACI D/C ratios in shear for sections 18 (bottom of wall), 19 (first slab section), and 20 (second slab section) at peak temperature. This plot clearly demonstrates that section 19 is the only section experiencing elevated D/C ratios. Figure 7.21 is also a 2D plot showing all 22 ACI sections along the 60-degree slice (the slice with the highest D/C ratio) at peak temperature. Once again, this plot clearly shows that only section 19, the first section in the slab, experiences the high D/C ratio.

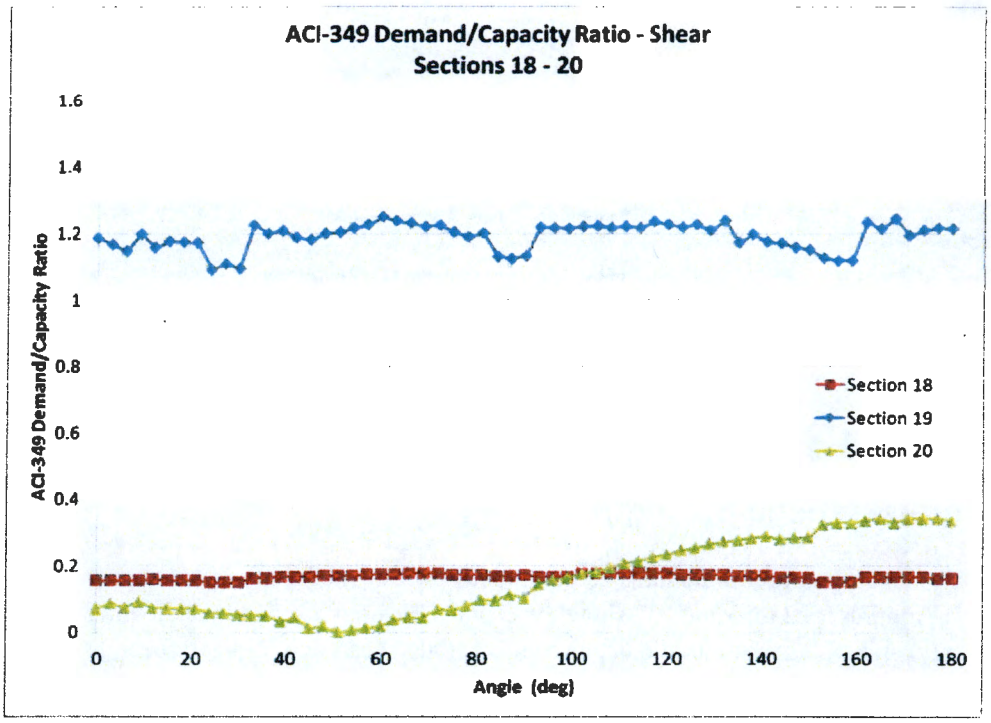

Figure 7.20. Run 2, Sections 18 – 20 Shear ACI D/C Ratios at LC9

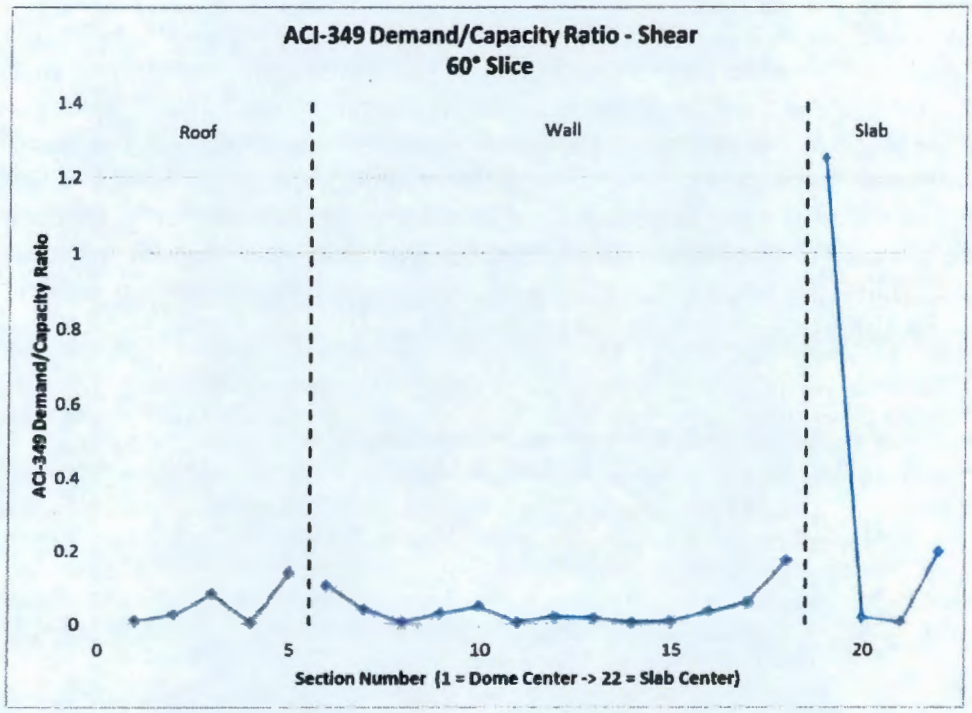

Figure 7.21. Run 2, Section 19 Shear ACI D/C Ratios at LC9

7.5 Run 4, Low Soil Modulus, High Concrete Modulus, and Near Zero Concrete Tensile Strength

This run uses lower bound soil modulus, upper bound concrete modulus and near zero concrete tensile strength. Figures 7.22 through 7.37 show the demand/capacity ratios at peak temperature, LC1, LC4 (TOLA only) and LC9 in the meridional, circumferential, shear, and in-plane shear directions for this material combination, Run 4.

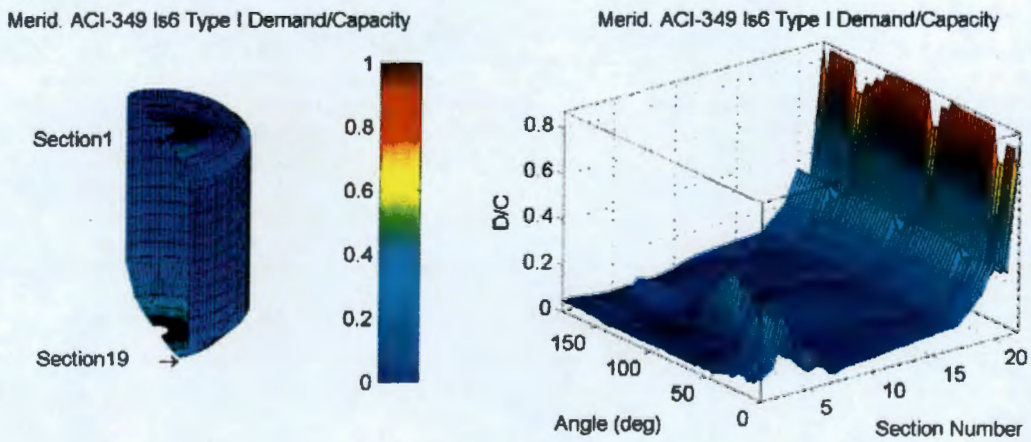

Figure 7.22. Run 4, Meridional ACI D/C Ratios at Peak Temperature

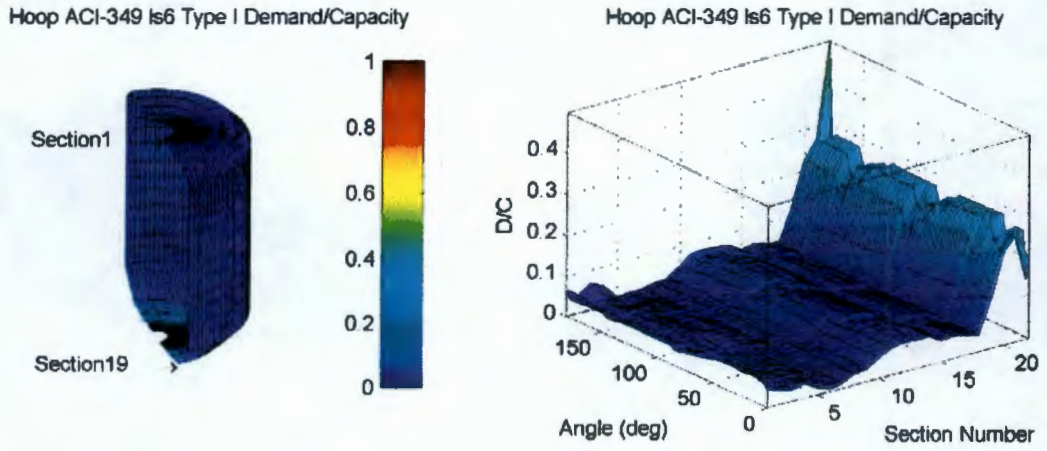

Figure 7.23. Run 4, Hoop ACI D/C Ratios at Peak Temperature

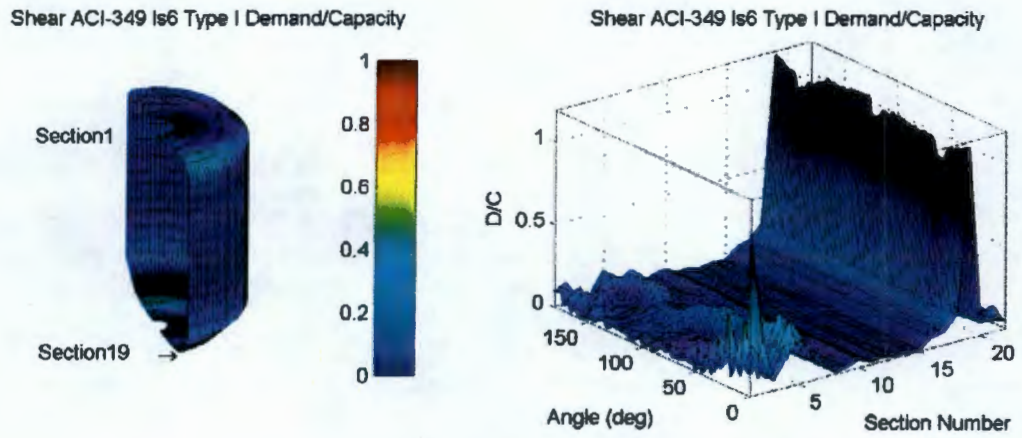

Figure 7.24. Run 4, Shear ACI D/C Ratios at Peak Temperature

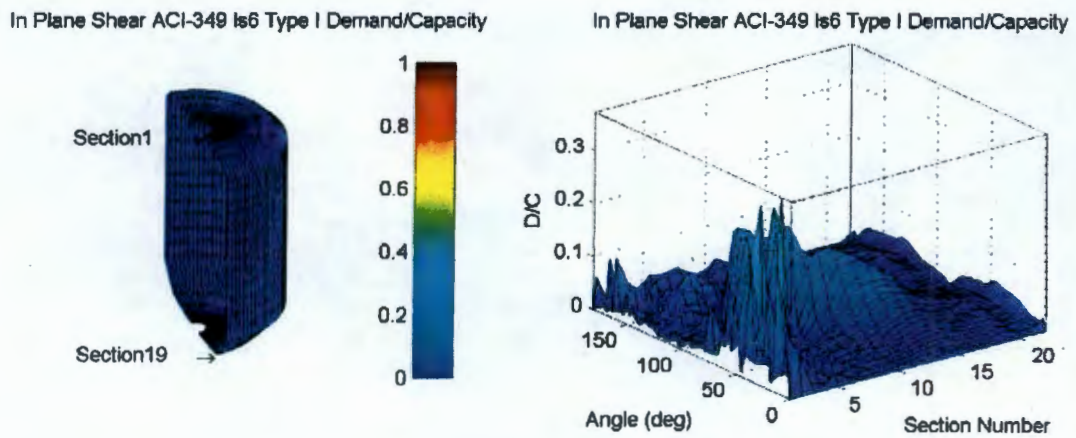

Figure 7.25. Run 4, In-Plane Shear ACI D/C Ratios at Peak Temperature

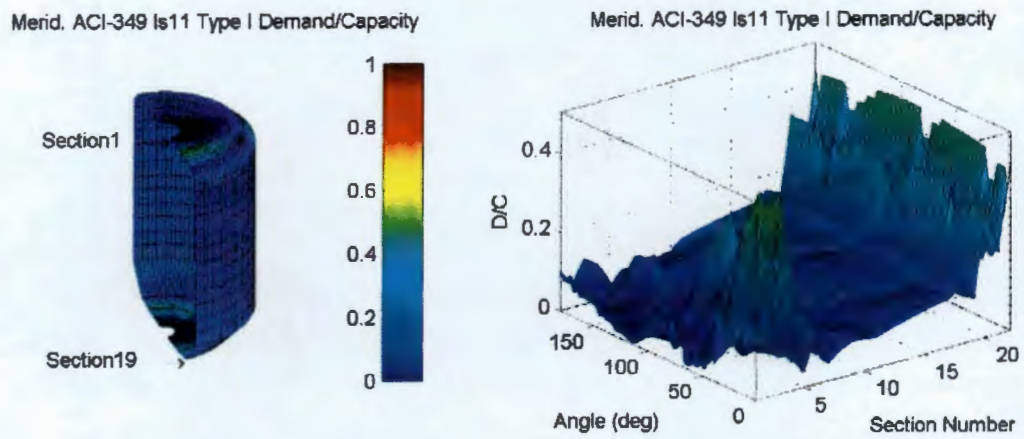

Figure 7.26. Run 4, Meridional ACI D/C Ratios at LC1

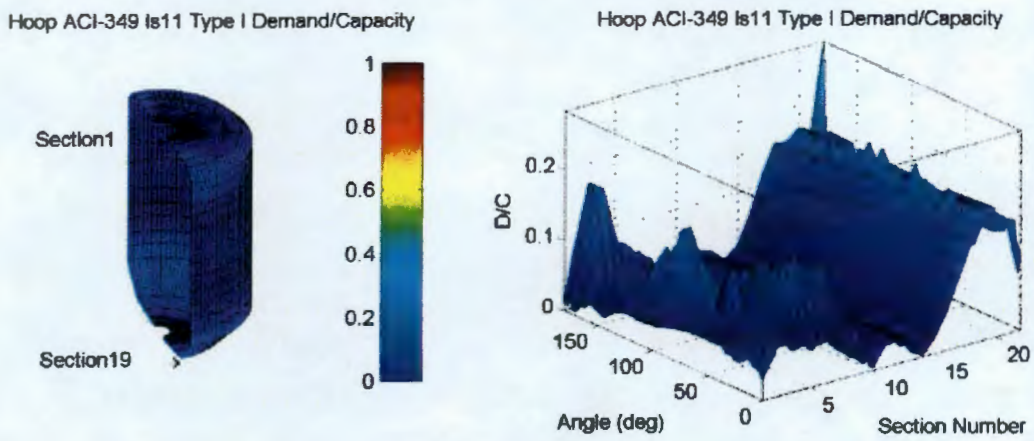

Figure 7.27. Run 4, Hoop ACI D/C Ratios at LC1

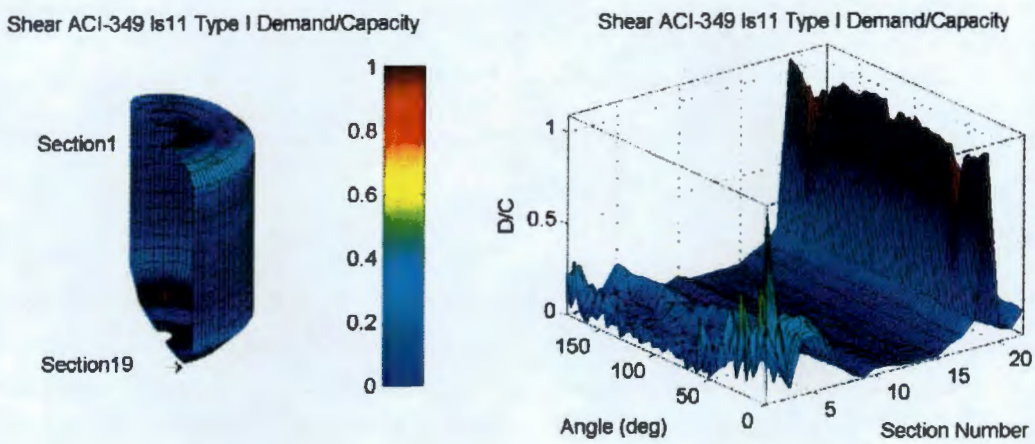

Figure 7.28. Run 4, Shear ACI D/C Ratios at LC1

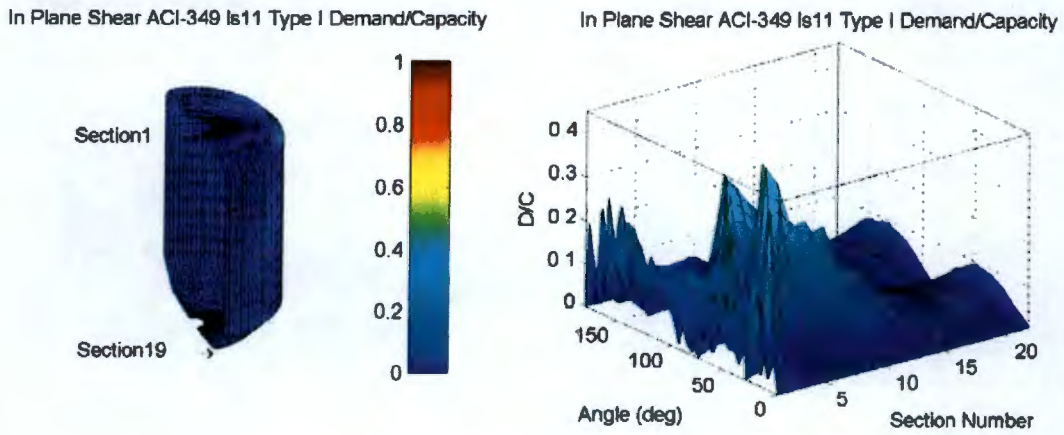

Figure 7.29. Run 4, In-Plane Shear ACI D/C Ratios at LC1

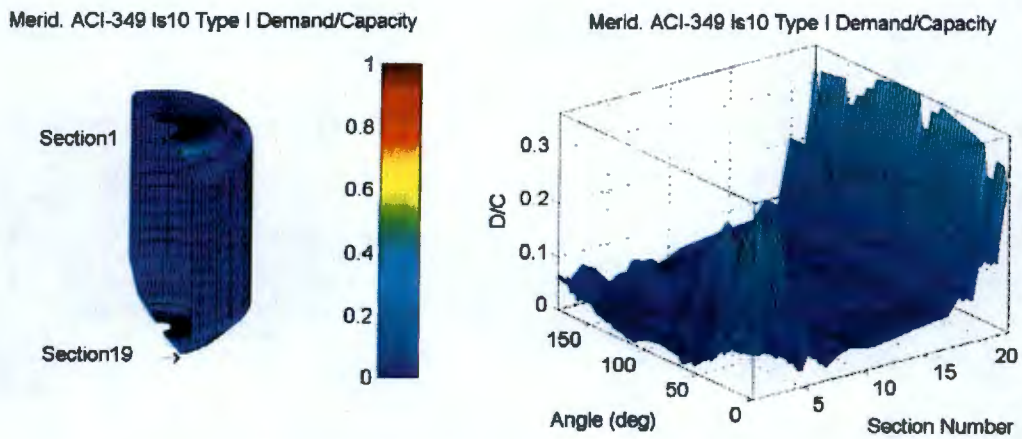

Figure 7.30. Run 4, Meridional ACI D/C Ratios at LC4 (TOLA only)

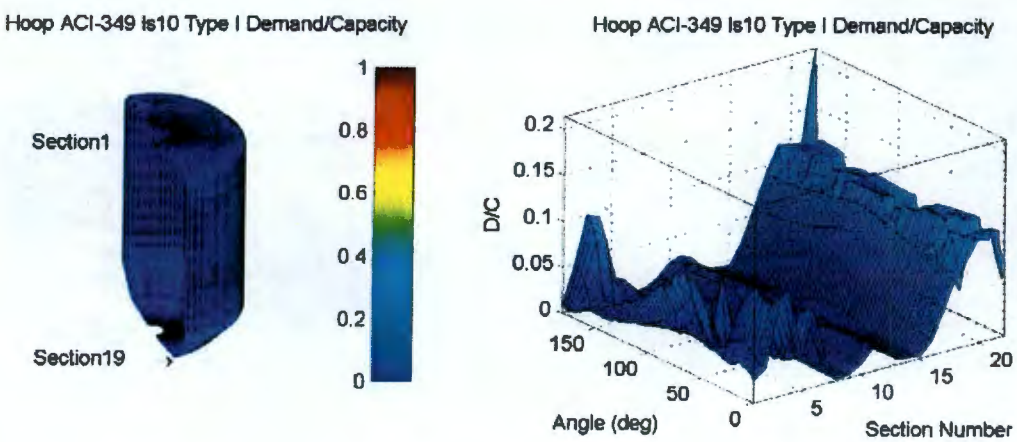

Figure 7.31. Run 4, Hoop ACI D/C Ratios at LC4 (TOLA only)

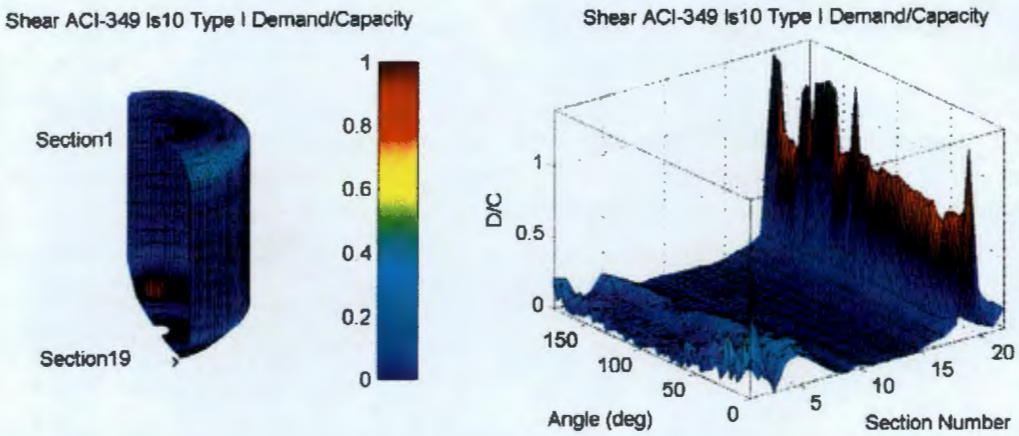

Figure 7.32. Run 4, Shear ACI D/C Ratios at LC4 (TOLA only)

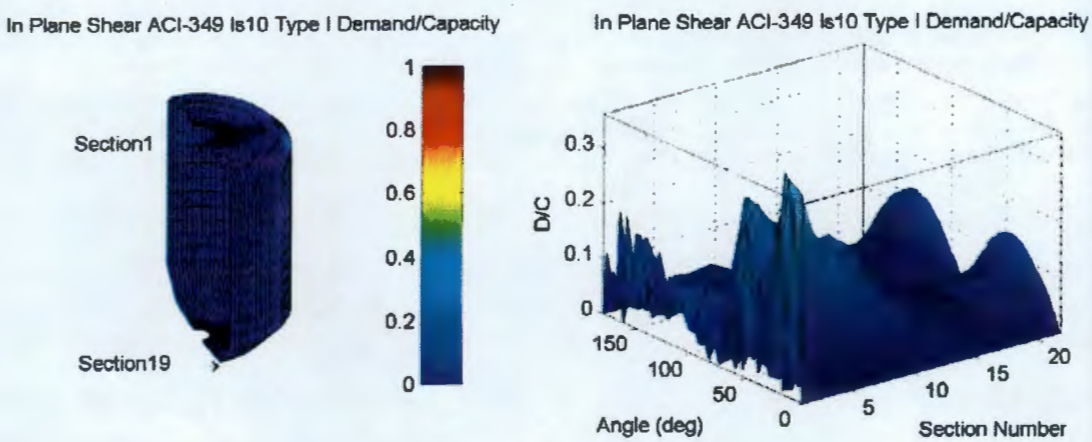

Figure 7.33. Run 4, In-Plane Shear ACI D/C Ratios at LC4 (TOLA only)

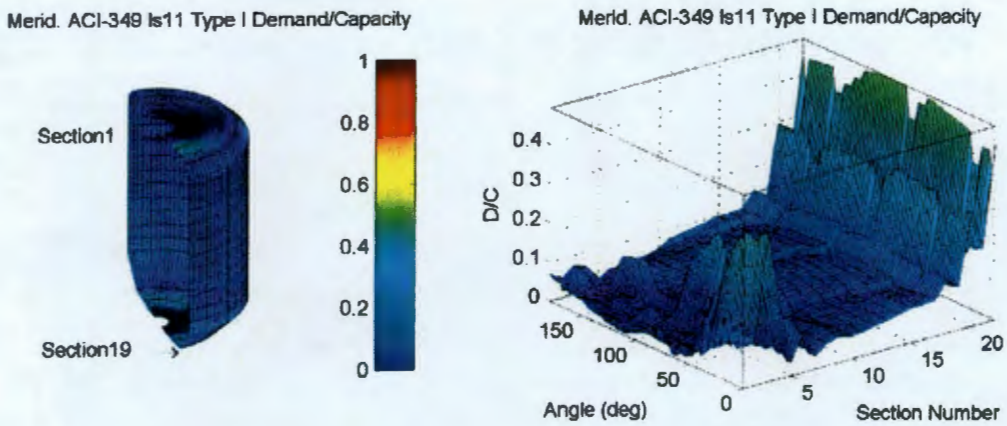

Figure 7.34. Run 4, Meridional ACI D/C Ratios at LC9

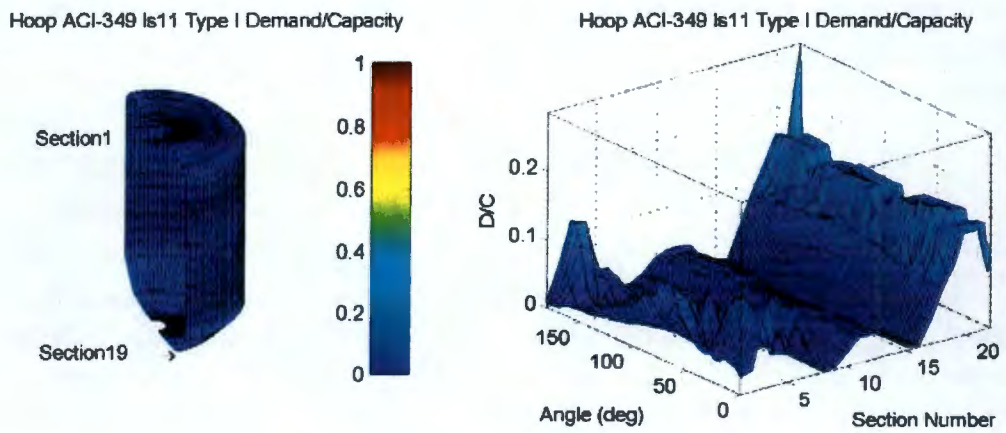

Figure 7.35. Run 4, Hoop ACI D/C Ratios at LC9

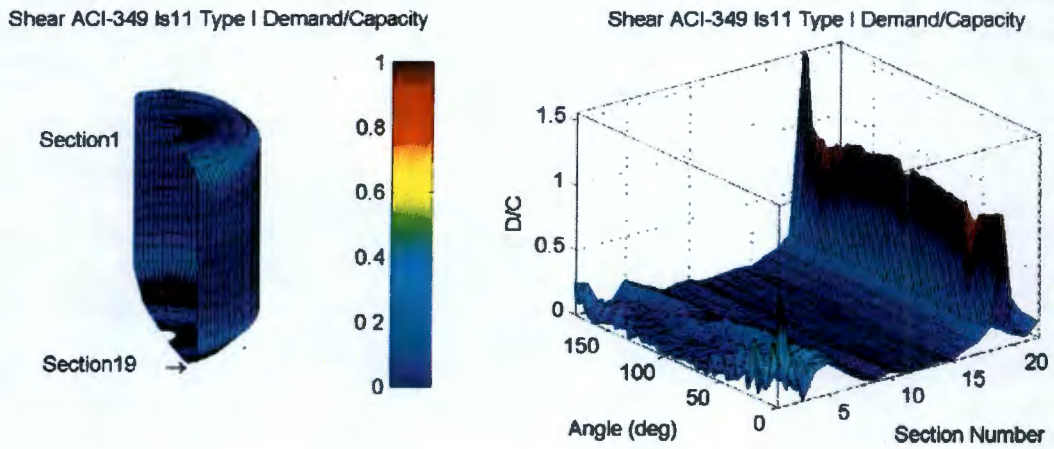

Figure 7.36. Run 4, Shear ACI D/C Ratios at LC9

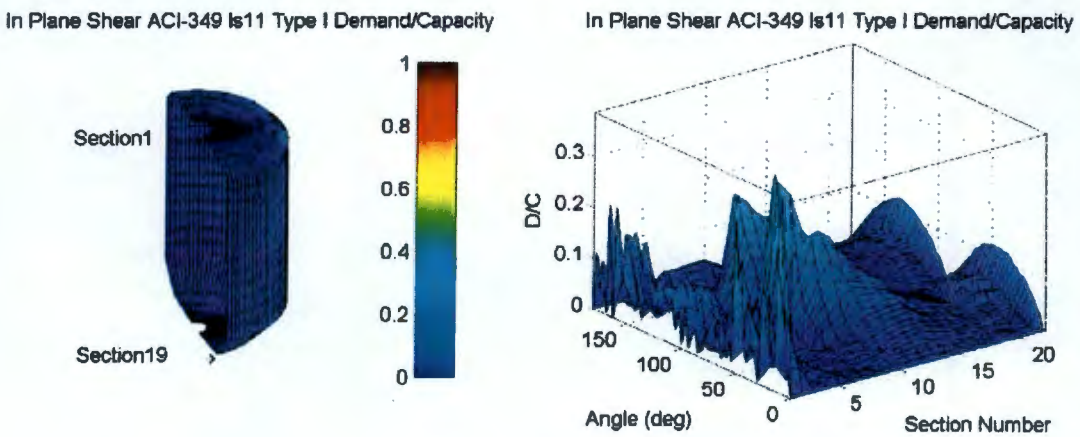

Figure 7.37. Run 4, In-Plane Shear ACI D/C Ratios at LC9

Figure 7.36 shows nearly a 50% spike in ACI D/C ratio in shear in section 19 near the 180-degree slice. This is shown more clearly in the 2D plot shown in Figure 7.38. The shear demands for section 19 are approximately constant at 12 kip/ft around the tank as shown in Figure 7.39. The capacity is also nearly constant at 12 kip/ft around the tank, but drops to 8 kip/ft at the final two slices (177 and 180 degree), thus giving rise to the spike in D/C ratios. This drop in capacity is the result of the conservative method of calculating shear capacities in the Mathcad™ ACI routine.

The shear capacity depends in part on the dimension, *d*, defined as the "distance from extreme compression fiber to centroid of longitudinal tension reinforcement." Section 19 contains only a single layer of reinforcing steel, not located at the center of the section, as shown in Figure 5.3. The Mathcad™ shear capacity calculation conservatively considers only the meridional moment when assessing the value of *d*. The meridional moment for sections 19 and 20 are plotted in Figure 7.40. The moments for section 19 are very low as seen by comparison with section 20. But the moment changes sign for the final two slices (177 and 180 degrees). This change in sign triggers the Mathcad™ routine to take the other, smaller leg of section 19 as the *d* dimension, thus giving rise to the lower capacity. This condition does not occur in the roof or wall sections of the tank because there are symmetric inner and outer courses of rebar there. Review of the meridional moment data driving the shear capacity in the other ACI shear D/C plots that show spikes in the D/C at section 19 (Figures 7.14, 7.32, and 7.51), confirms that the spikes are driven by the change in the sign of the already low moment values.

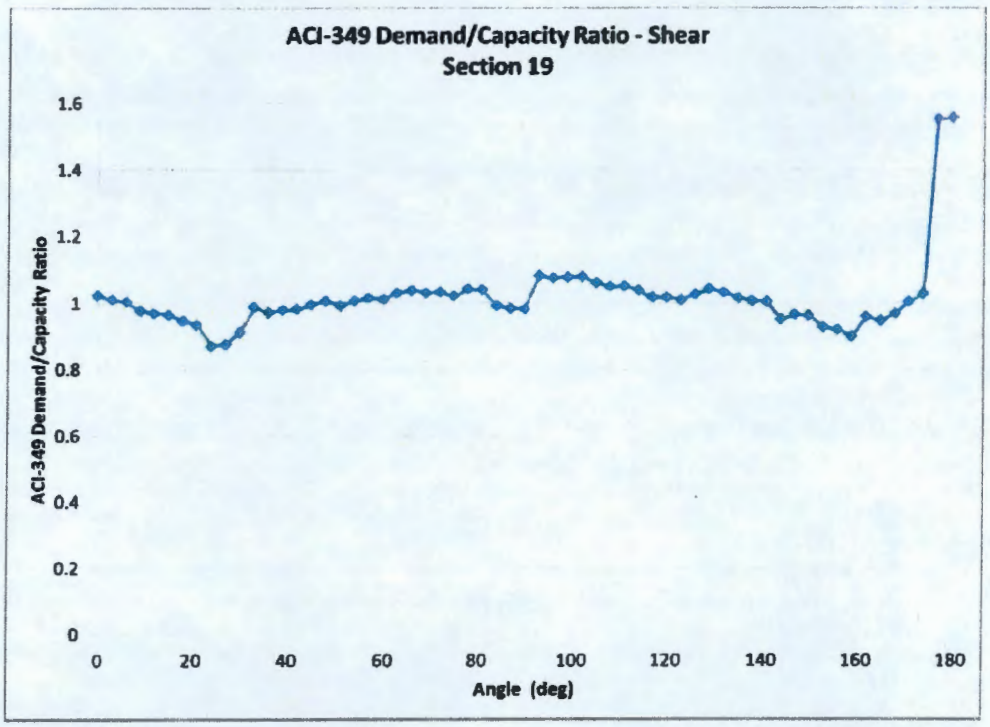

Figure 7.38. Run 4, Section 19 Shear ACI D/C Ratios at LC9

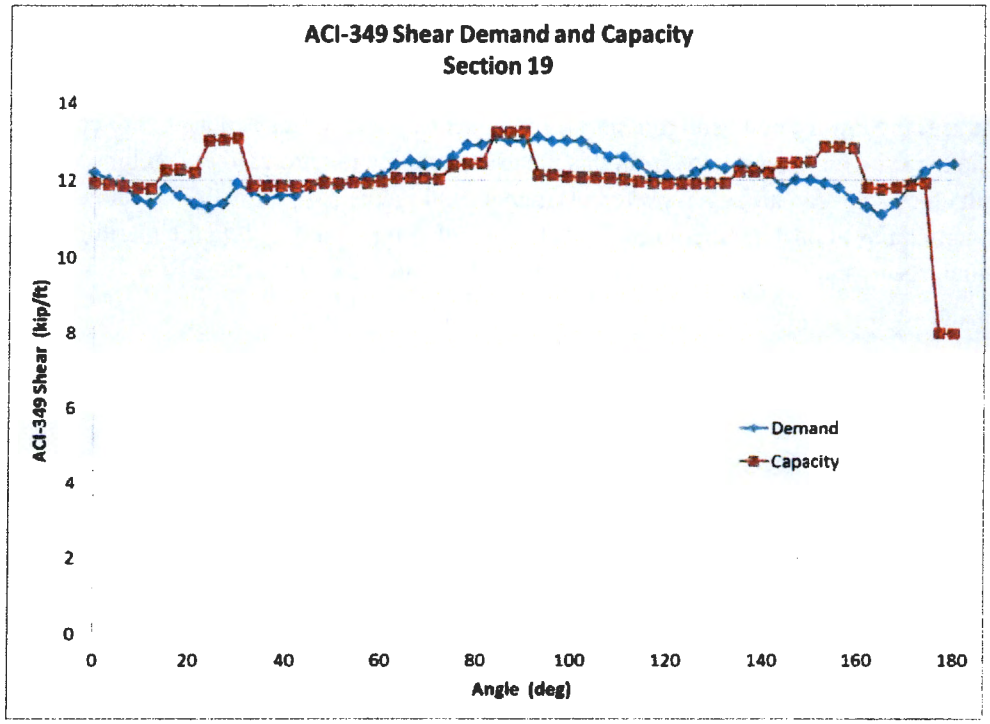

Figure 7.39. Run 4, Section 19 ACI Shear Demand and Capacity at LC9

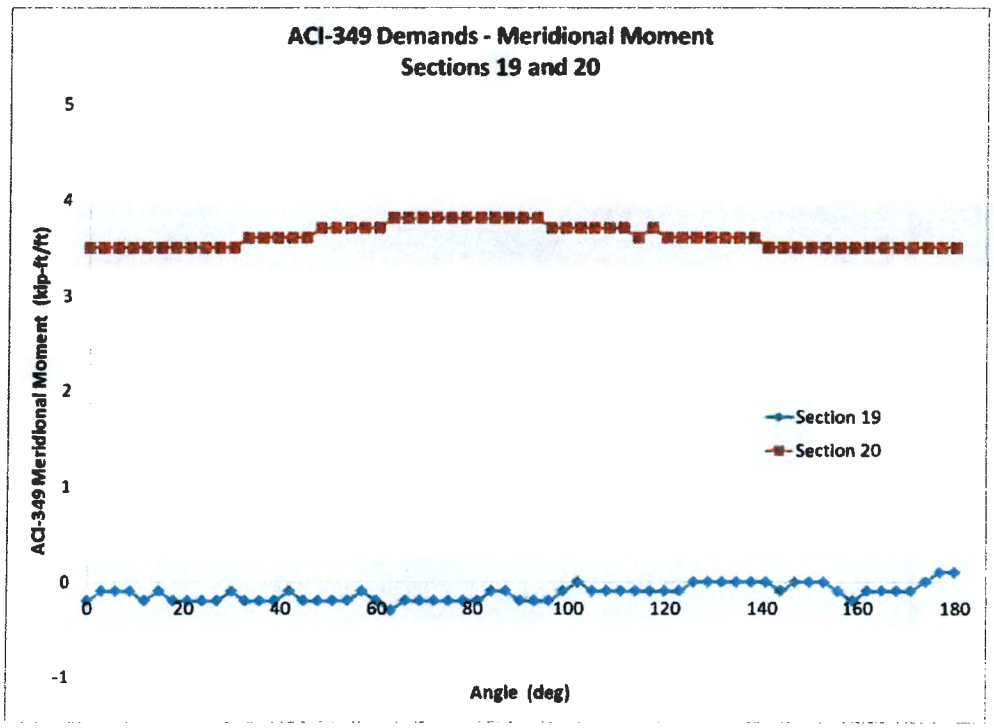

Figure 7.40. Run 4, Section 19 and 20 Meridional Moment at LC9

7.6 Run 7, Low Soil Modulus, Nominal Concrete Modulus, and Near Zero Concrete Tensile Strength

This run uses the lower bound soil modulus, nominal concrete modulus and near zero concrete tensile strength. The load and moment results from this material combination are used to combine with the seismic results for ACI LC-4 and are reported in Chapter 9. Figures 7.41 through 7.51 show the demand/capacity ratios at peak temperature, LC1, LC4 (TOLA only) and LC9 in the meridional, circumferential, shear, and in-plane shear directions for this material combination, Run 7.

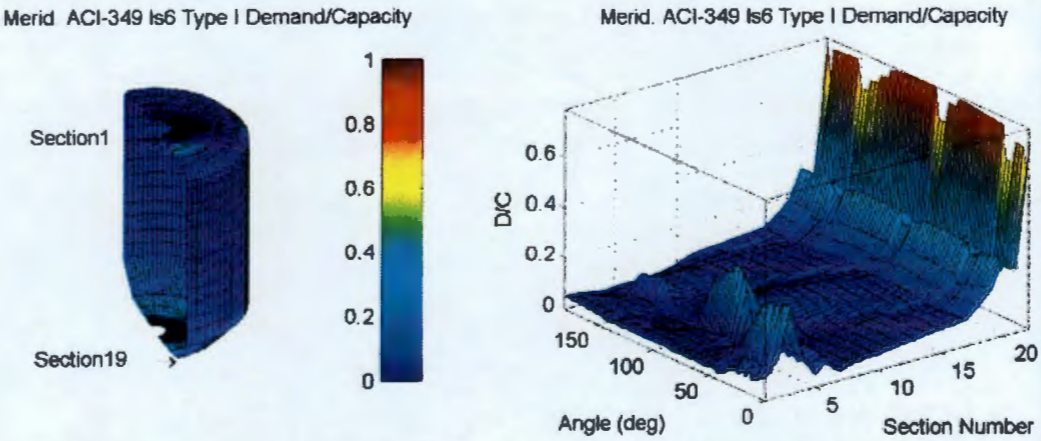

Figure 7.41. Run 7, Meridional ACI D/C Ratios at Peak Temperature

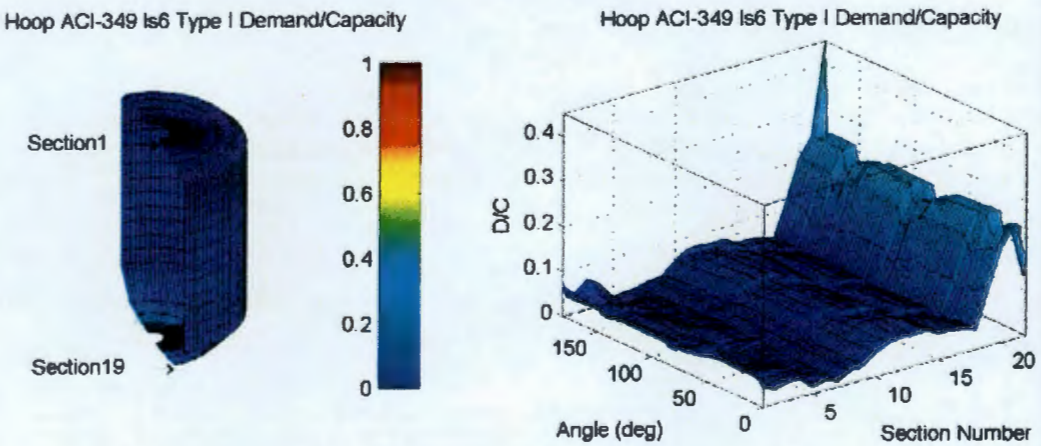

Figure 7.42. Run 7, Hoop ACI D/C Ratios at Peak Temperature

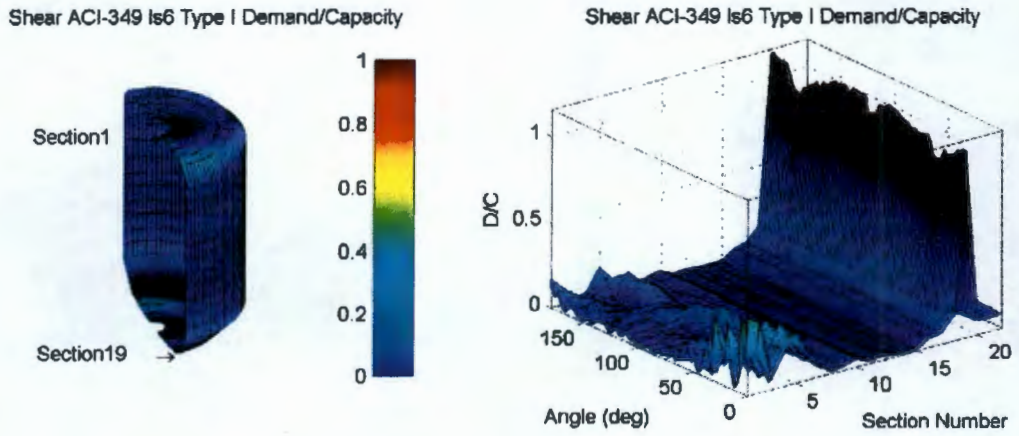

Figure 7.43. Run 7, Shear ACI D/C Ratios at Peak Temperature

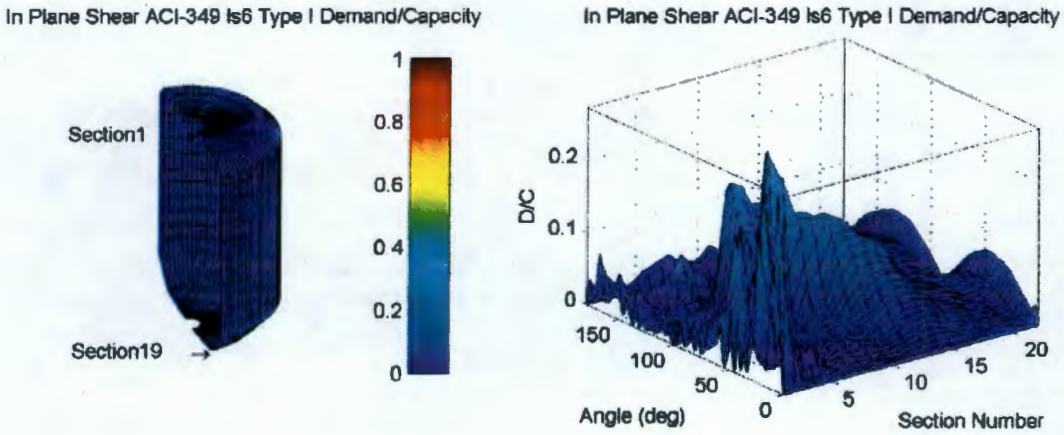

Figure 7.44. Run 7, In-Plane Shear ACI D/C Ratios at Peak Temperature

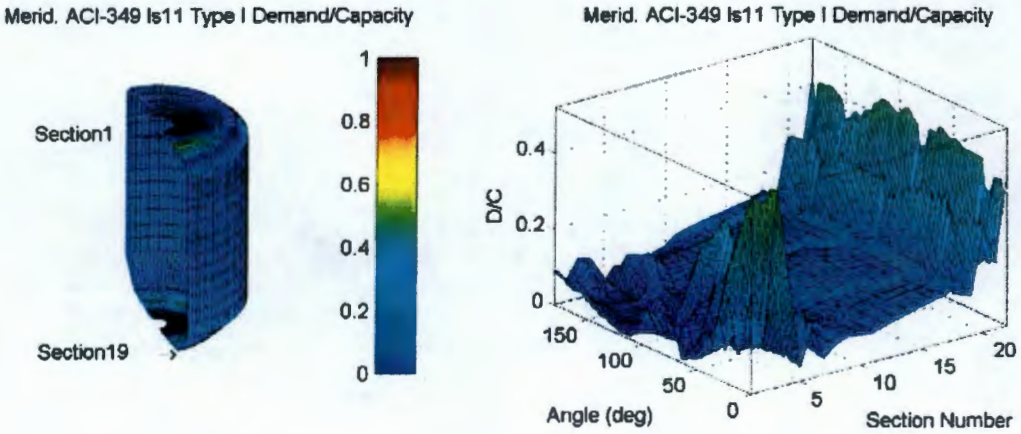

Figure 7.45. Run 7, Meridional ACI D/C Ratios at LC1

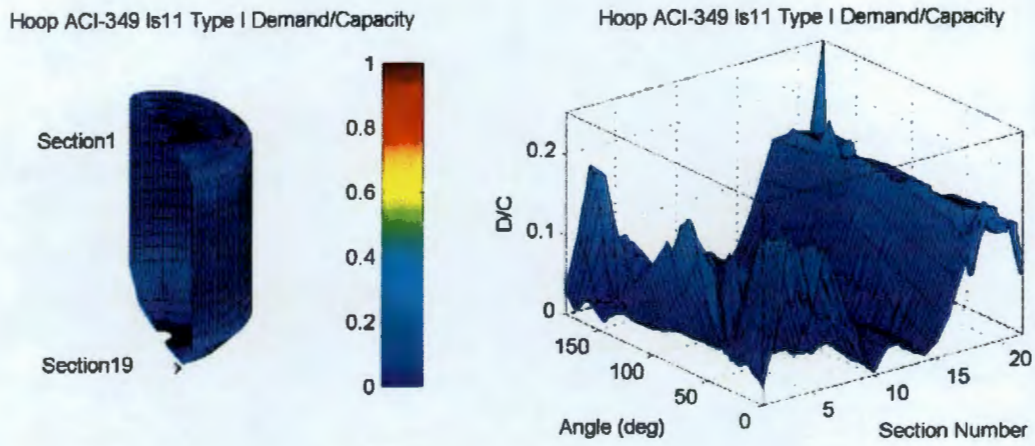

Figure 7.46. Run 7, Hoop ACI D/C Ratios at LC1

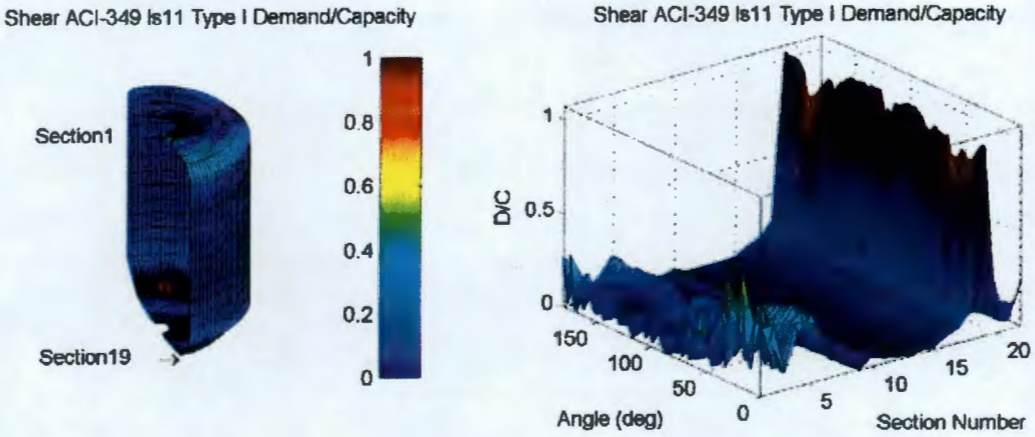

Figure 7.47. Run 7, Shear ACI D/C Ratios at LC1

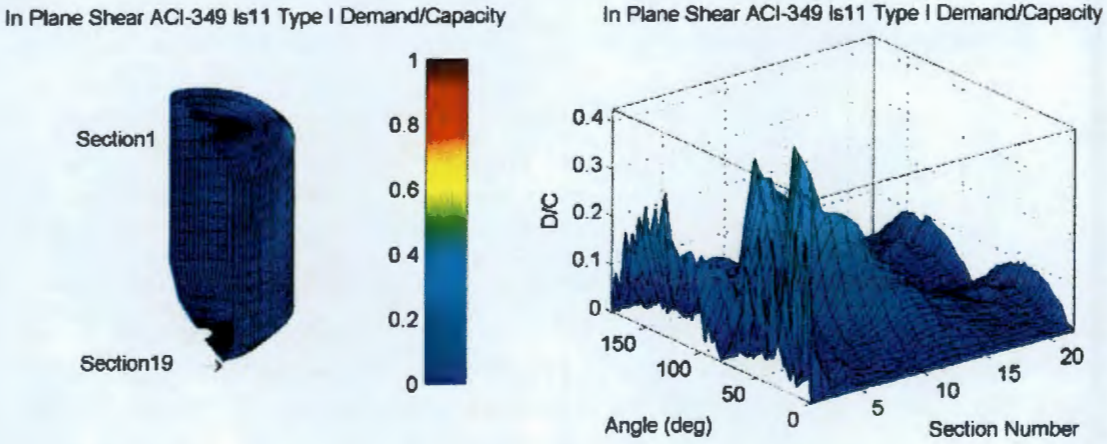

Figure 7.48. Run 7, In-Plane Shear ACI D/C Ratios at LC1

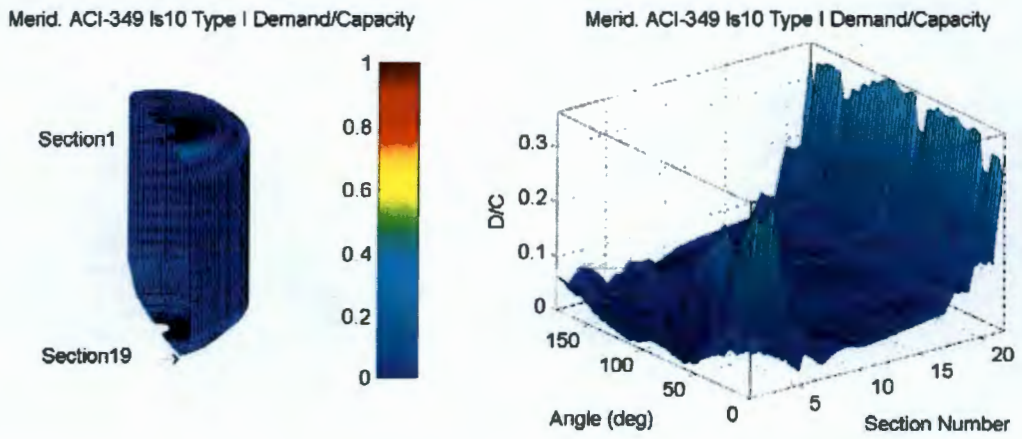

Figure 7.49. Run 7, Meridional ACI D/C Ratios at LC4 (TOLA only)

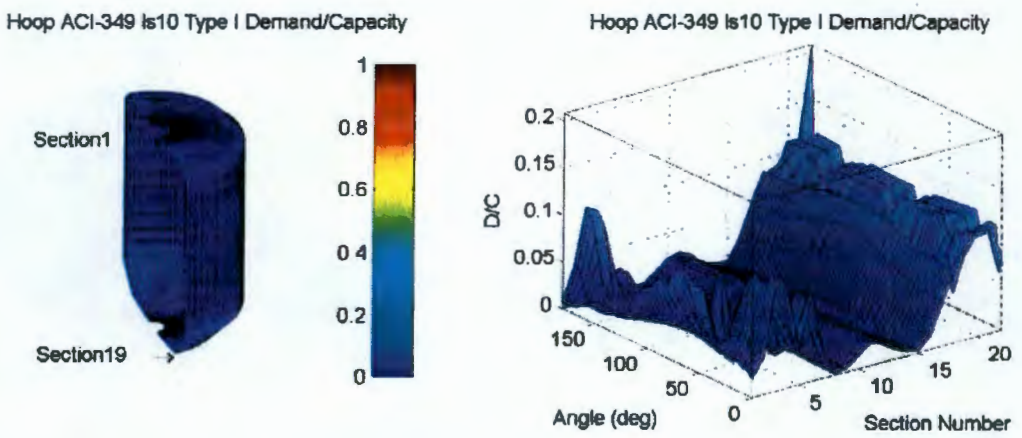

Figure 7.50. Run 7, Hoop ACI D/C Ratios at LC4 (TOLA only)

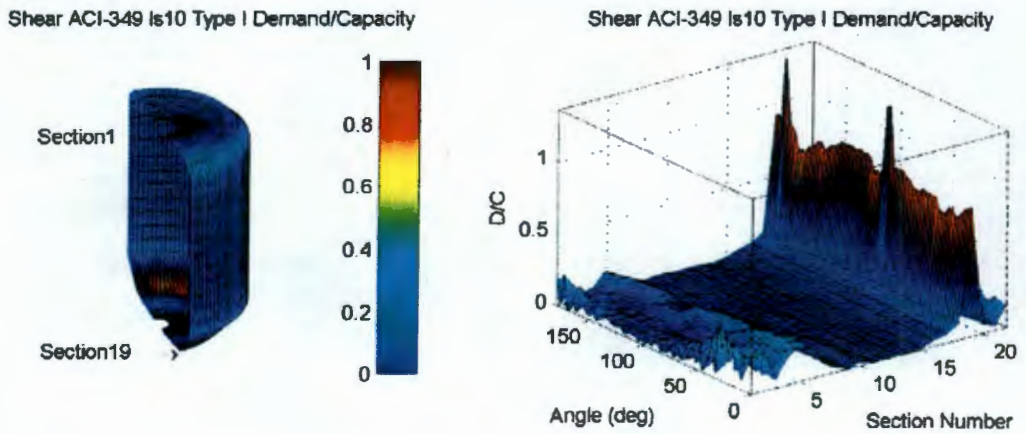

Figure 7.51. Run 7, Shear ACI D/C Ratios at LC4 (TOLA only)

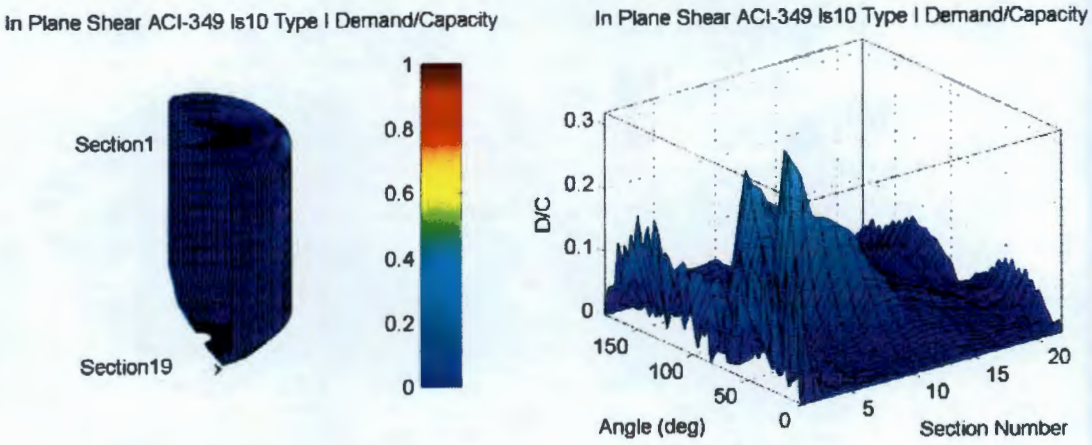

Figure 7.52. Run 7, In-Plane Shear ACI D/C Ratios at LC4 (TOLA only)

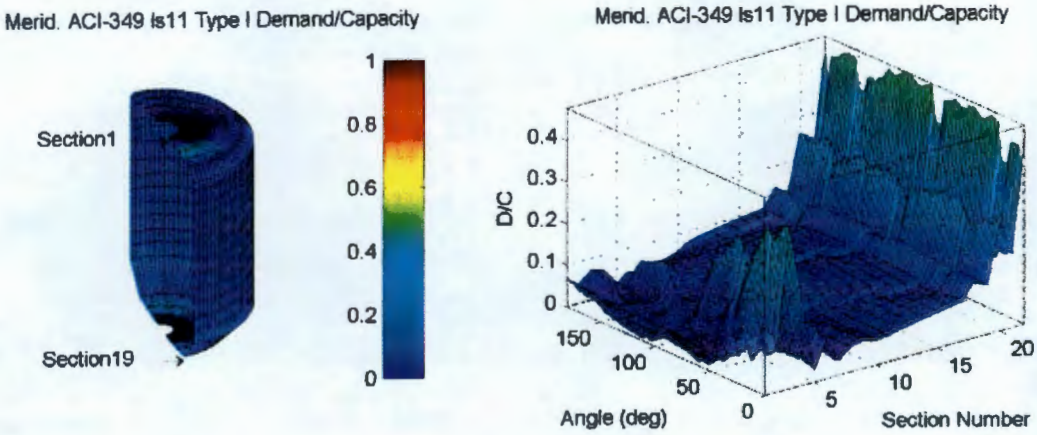

Figure 7.53. Run 7, Meridional ACI D/C Ratios at LC9

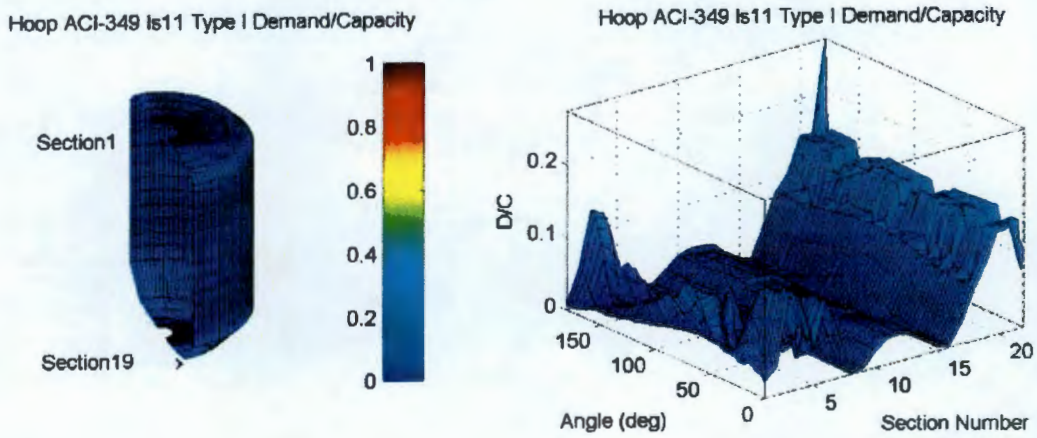

Figure 7.54. Run 7, Hoop ACI D/C Ratios at LC9

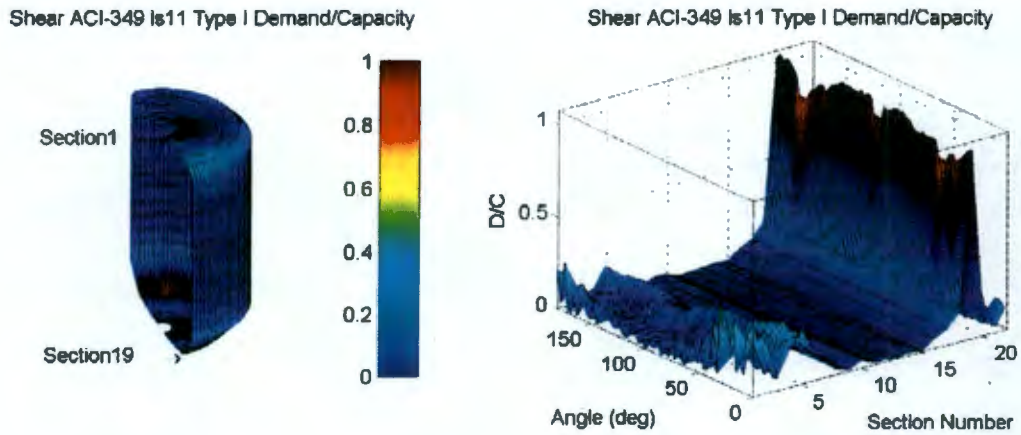

Figure 7.55. Run 7, Shear ACI D/C Ratios at LC9

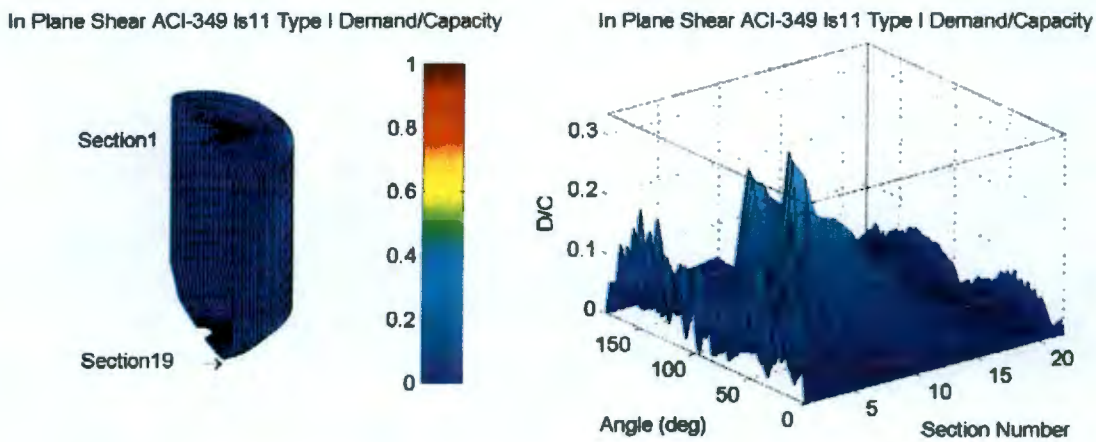

Figure 7.56. Run 7, In-Plane Shear ACI D/C Ratios at LC9

For clarification, Table 7.3 gives the peak ACI shear D/C ratios for sections 18 and 19 for each material combination run.

The D/C ratios show similar trends for the three material combinations with only minor differences. It is important to note that the D/C ratios in the roof, haunch, and wall are all less than 1.0 for each of these material and ACI load combinations. Therefore, all the tank regions that are critical to the structural stability of the Type I tanks pass the ACI 349-06 acceptance criteria for the design of new structures. This is true for the conservative combination of maximum recorded thermal loads and maximum soil overburden depth in combination with the run matrix of bounding material property combinations. Note that the LC4 evaluation of combined TOLA and seismic forces and moments also shows all D/C ratios to be less than 1.0 (Chapter 9.0).

Table 7.3. Section 18 and 19 Peak ACI Shear Ratios

Run	Section 18	Section 19
Run 2, peak temperature	0.18	1.25
Run 2, LC-1	0.17	1.00
Run 2, LC-4 (TOLA only)	0.12	1.25
Run 2, LC-9	0.17	1.02
Run 4, peak temperature	0.18	1.19
Run 4, LC-1	0.17	1.09
Run 4, LC-4 (TOLA only)	0.13	1.39
Run 4, LC-9	0.19	1.56
Run 7, peak temperature	0.16	1.15
Run 7, LC-1	0.17	1.07
Run 7, LC-4 (TOLA only)	0.13	1.36
Run 7, LC-9	0.18	1.06

Figures 7.10 through 7.51 demonstrate that the ACI D/C ratios may exceed 1.0 in the slab. Section 19 at the intersection of the slab and lower knuckle may exceed 1.0 in shear. Additionally, section 22 near the slab centerline may exceed 1.0 in the meridional direction at peak temperature. These results are consistent with results reported in the SST Type II, III and Type IV AORs (Rinker et al. 2011a, b). The high temperature in the slab degrades the concrete strength (reduced capacity) while also creating high compressive stress due to thermal expansion (increased demand). The combination results in D/C ratios that may exceed 1.0 in the slab. However, exceedance in the slab does not impact the overall structural stability of the tank. Slab removal studies conducted as part of the Type II, Type III, and Type IV AORs show that the differential shear deflection in the event of a shear failure is less than one-half the steel liner thickness. These slab removal studies consistently demonstrated that potential slab failures do not adversely affect the structural integrity of the single shell tank. The Type I slab removal study is described in the following section.

7.7 Slab Removal Study

The demand/capacity ratios at section 19 may exceed 1.0 in shear at peak temperature and LC1 for all material combinations (Figures 7.6 through 7.47). The consequence of potential slab failure was evaluated in the slab removal study following the methodology of the Type II, III, and Type IV AORs.

The previous slab removal analyses demonstrated that any ACI exceedance in shear, meridional, or circumferential directions in the slab region does not reduce the capacity of the tank structure to support the thermal and operating loads. The worst case of low soil modulus showed no significant differences from the nominal soil condition. The Type I slab removal study was based on the Run 4 (low soil modulus, high concrete modulus) to retain the conservative nature of this analysis.

Detachment of the slab at ACI section 19, the first section inward from the wall, was accomplished with the ANSYS® EKILL command. This command deactivates the specified elements by multiplying the element stiffness by 1.0E-6. The tank elements immediately outward of section 19 were deactivated,

effectively isolating the slab from the rest of the tank such that it provides no structural support. Figure 7.57 illustrates this procedure.

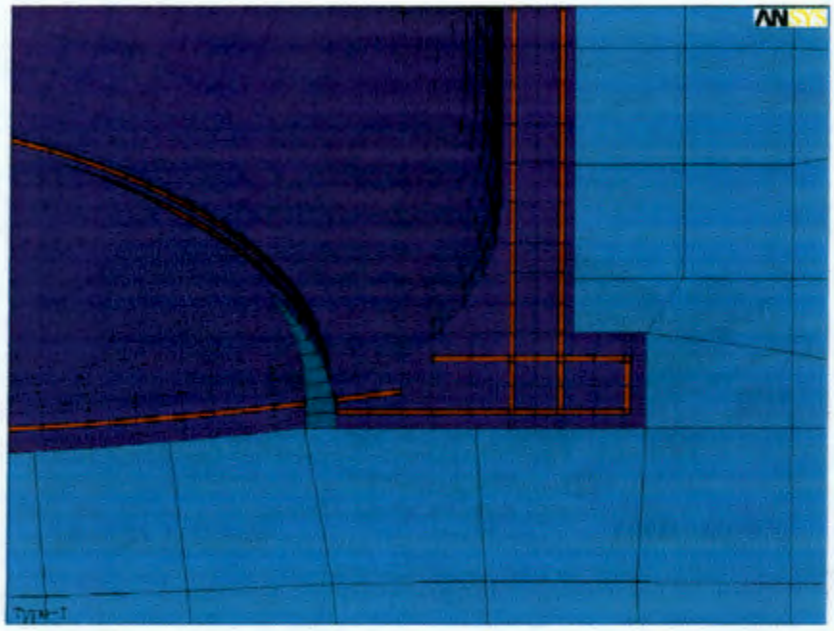

Figure 7.57. Slab Detachment – Section 19

Upon application of ACI 349-06 LC1 load factors, D/C ratios were calculated through the dome, haunch, and wall. Because the slab is isolated from the rest of the tank, no section D/C ratios were calculated in the slab after section 18. Figures 7.58 through 7.61 shows the D/C ratios for this analysis. Comparison of the slab removal results with nominal Run 4 results in Figures 7.26 through 7.29 shows practically no difference.

Clearly the removal of section 19 does not adversely affect the structural integrity of the tank from an ACI 349-06 perspective.

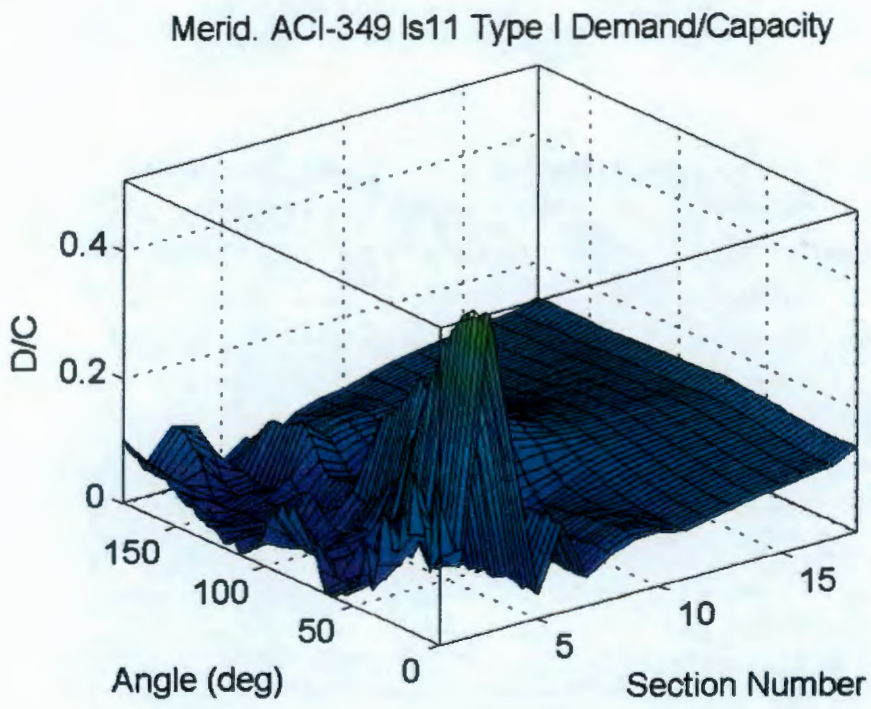

Figure 7.58. ACI Meridional D/C Ratios, Slab Detachment

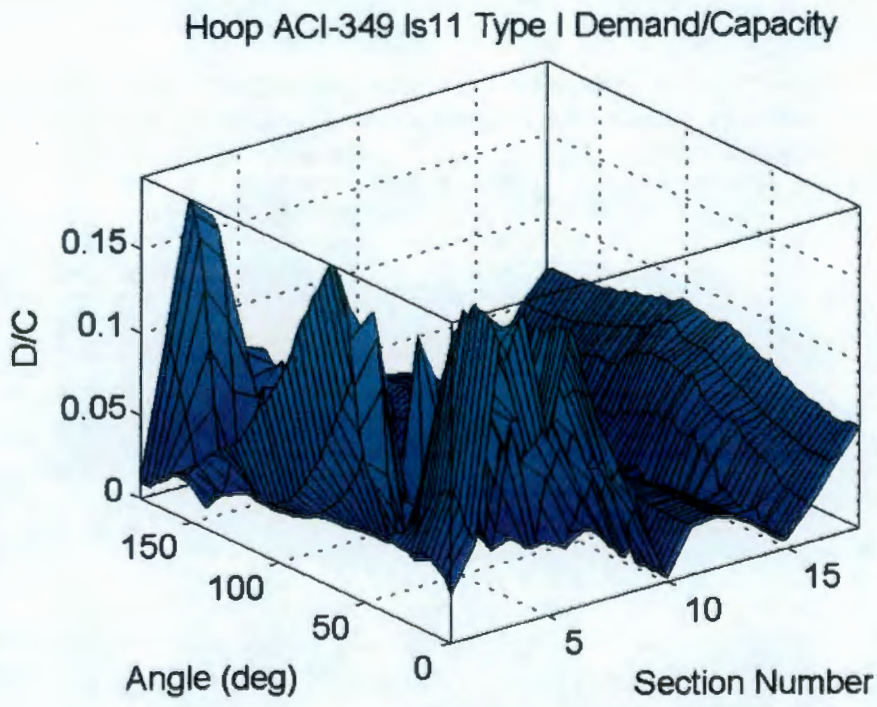

Figure 7.59. ACI Hoop D/C Ratios, Slab Detachment

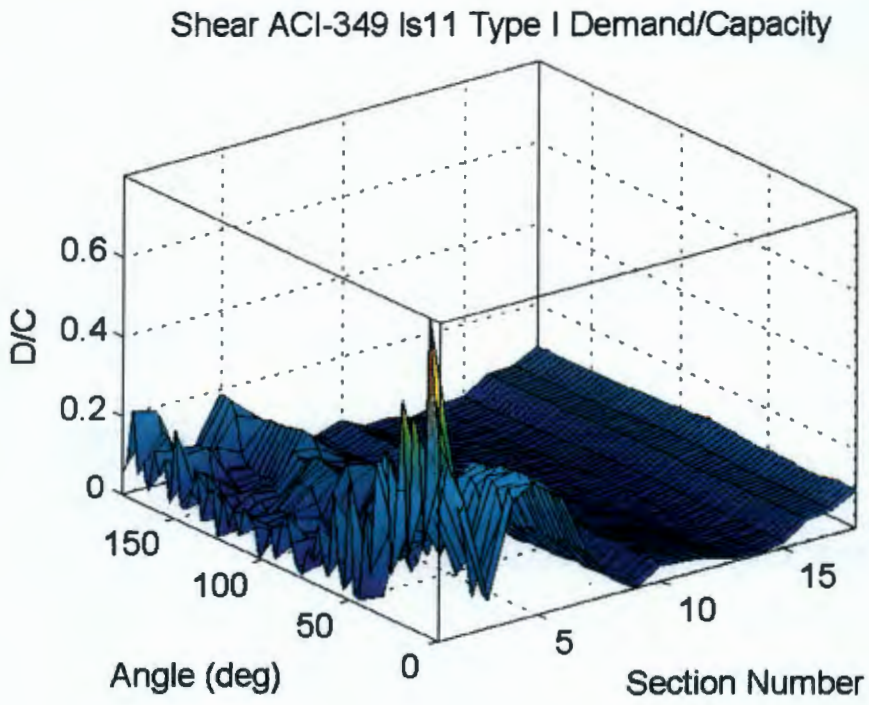

Figure 7.60. ACI Shear D/C Ratios, Slab Detachment

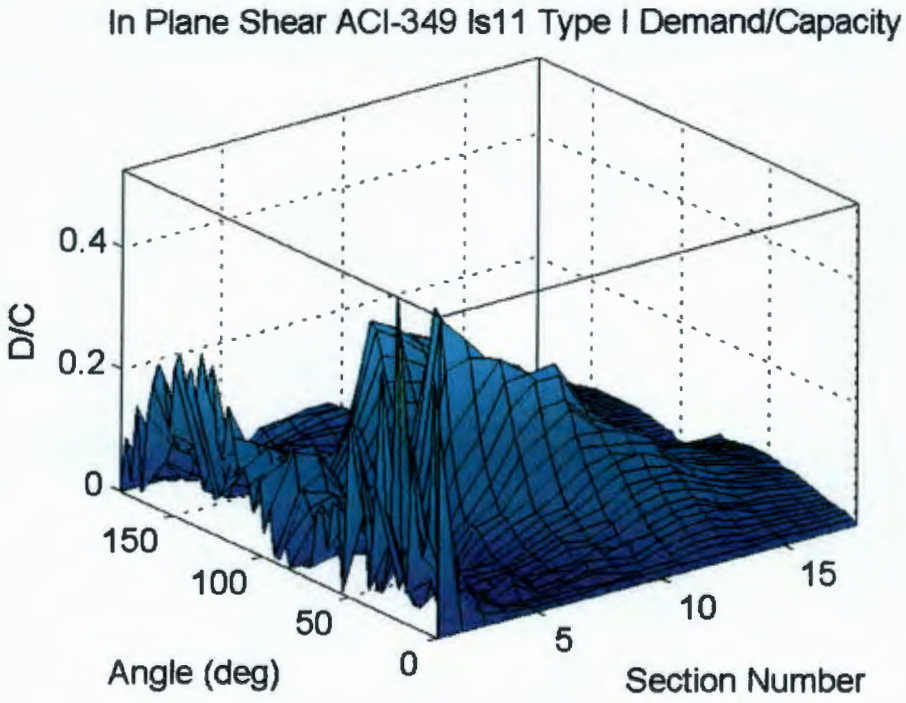

Figure 7.61. ACI In-Plane Shear D/C Ratios, Slab Detachment

Upon removal of the slab, or isolation of the slab from the rest of the tank, the tank wall and footing may now be free to punch into the soil below. To assure this is not the case, the total vertical displacement of the bottom of the wall of Run 4 with section 19 removed was compared to the corresponding displacement for the nominal Run 4. Total vertical displacement of the bottom of the wall for Run 4 under ACI 349-06 LC1 is –0.624 inches. The total vertical displacement of the bottom of the wall for Run 4 with the detached slab under ACI 349-06 LC1 is –0.638 inches. This insignificant difference of 0.014 inches in displacement indicates that the remaining soil support is sufficient to prevent the wall and footing from punching into the soil. In addition, the relative vertical displacement across the gap in section 19 under ACI 349-06 LC1 is only 0.085 inches, which is 34% of the 0.25-in. thick steel liner bottom plate. Again, this minor relative displacement indicates that the wall and footing are not expected to punch into the soil.

The slab removal analysis demonstrates that any ACI exceedance in the slab is considered to be of no structural significance.

7.8 TOLA Run Matrix Conclusions

Figures 7.4 through 7.51 show the ACI D/C ratios in meridional, circumferential, shear, and in-plane shear. It is important to note that the D/C ratios are less than 1.0 in the roof, haunch, and wall for all load steps and load combinations. Therefore, all the tank regions that are critical to the structural stability of the Type I tanks pass the ACI 349-06 acceptance criteria for the design of new structures. This is true for the conservative combination of maximum recorded thermal loads and maximum soil overburden depth combined with the run matrix of bounding material property combinations.

8.0 Seismic Results

The seismic model is described in a separate report by Becht Engineering entitled "Hanford Type I Single Shell Tank Seismic Analysis." For completeness this report in its entirety is included in Attachment 1 of this document. Within this separate report, Chapter 8 presents the major tank demands resulting from the seismic modeling.

This page intentionally left blank.

9.0 Combined Static and Seismic Results

This chapter presents the demand to capacity ratios for the tanks subjected to the ACI LC4 demands. First the procedure for applying the LC4 unfactored TOLA plus seismic demands is reviewed. Then the demand to capacity ratios are presented.

9.1 TOLA and Seismic Combination Procedure

From Section 4.1.3, load combination LC4 is the only applicable ACI load combination that contains seismic demands. The seismic analysis report (Attachment 1) demonstrates that the lower bound soil, full tank, section A-A hatchway configuration was the bounding case and could be used as a "representative" seismic case. The seismic demands from this analysis must be combined with the appropriate TOLA demands. TOLA Run 7 is identified as the applicable analysis.

Because the earthquake ground motions are reversible, the seismic forces and moments must be combined with the TOLA forces and moments in both a positive and negative way. This leads to four combinations for ACI LC4 for both the meridional and hoop demands:

- F+M+: TOLA force + seismic force and TOLA moment + seismic moment
- F+M-: TOLA force + seismic force and TOLA moment – seismic moment
- F-M+: TOLA force – seismic force and TOLA moment + seismic moment
- F-M-: TOLA force – seismic force and TOLA moment – seismic moment

The highest D/C ratio of these four combinations for both meridional and hoop directions is reported as the D/C ratio. Figure 9.1 shows an example P-M diagram with these four demand combinations as well as the TOLA-only demand. The upper right point in this case would have the highest D/C ratio based on the demand and capacity definitions defined in Figure 7.3. In addition, the through-wall shear capacity depends on the meridional force and moment values. Again, four through wall shear D/C ratios are calculated and the highest values are reported in the next section.

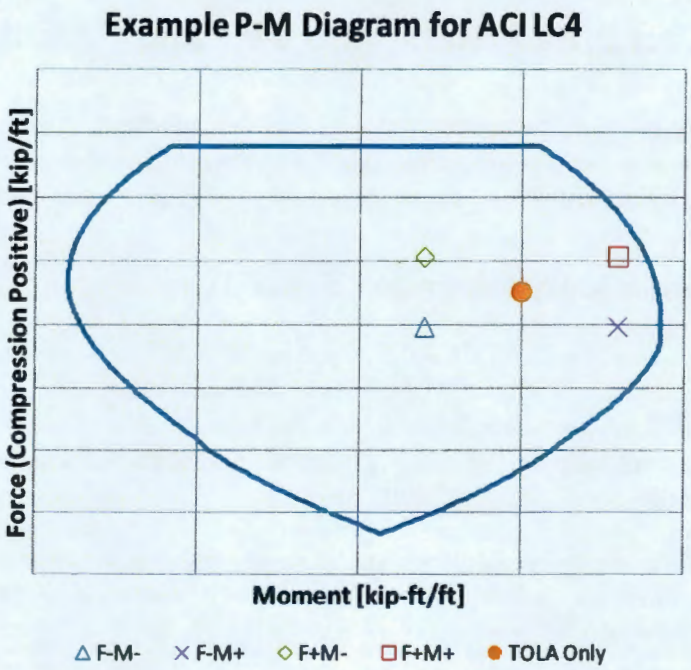

Figure 9.1. Example P-M Diagram with Four Possible Seismic Combinations

Finally, unlike the axisymmetric TOLA runs that only had axisymmetric loading, in-plane shear is present as a result of the non-symmetric seismic loads. As recommended in the Structural Evaluation Criteria (Johnson et al. 2010), the in-plane shear capacity is evaluated by ACI 349-06 equation 11-29. D/C ratios for in-plane shear are also reported in the next section.

9.2 ACI Load Combination 4 Results

The ACI 349-06 LC4 meridional, hoop, shear, and in-plane shear D/C ratios for the combined TOLA plus seismic analysis are summarized in Figures 9.2 through 9.5. These figures show that all the ACI D/C ratios in the roof, haunch, and wall are considerably less than one. The D/C ratio at section 19 is near 1.0 indicating that shear cracking may have occurred at the transition between the footing and the slab. This was noted earlier for the peak temperature condition, and the seismic loads do not significantly increase this condition. Comparing Figures 9.2 through 9.5 to Figures 7.44 through 7.48 shows that the seismic loads contribute only about 10% of the section capacities, increasing the maximum TOLA only D/C ratios from 0.35 to 0.45.

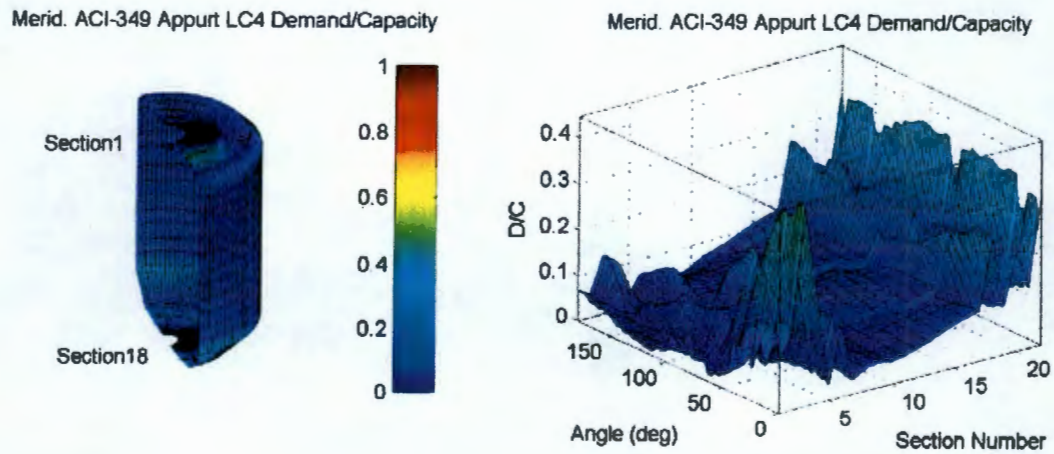

Figure 9.2. Meridional ACI D/C Ratios at LC4

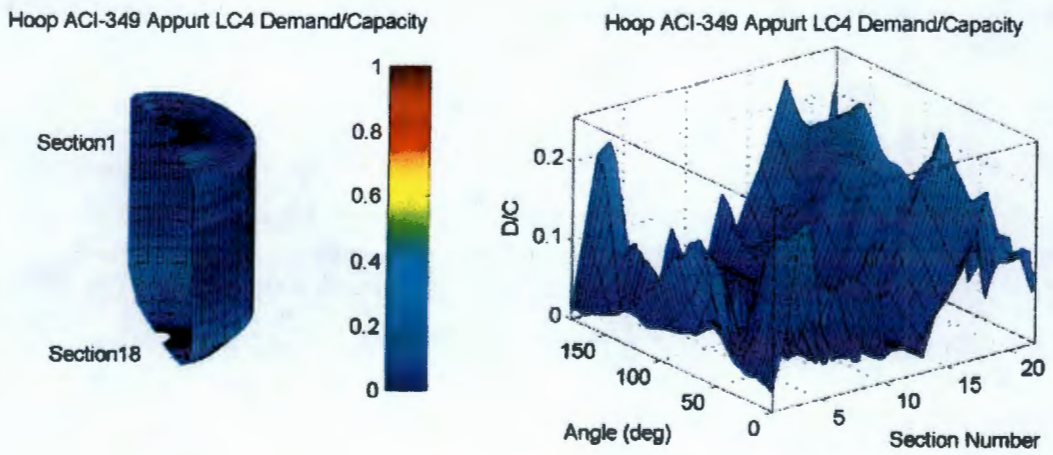

Figure 9.3. Hoop ACI D/C Ratios at LC4

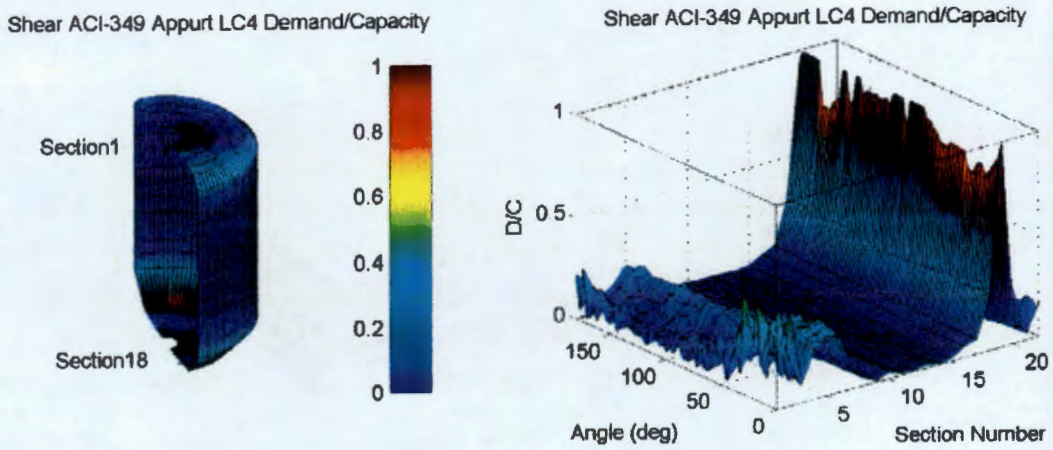

Figure 9.4. Shear ACI D/C Ratios at LC4

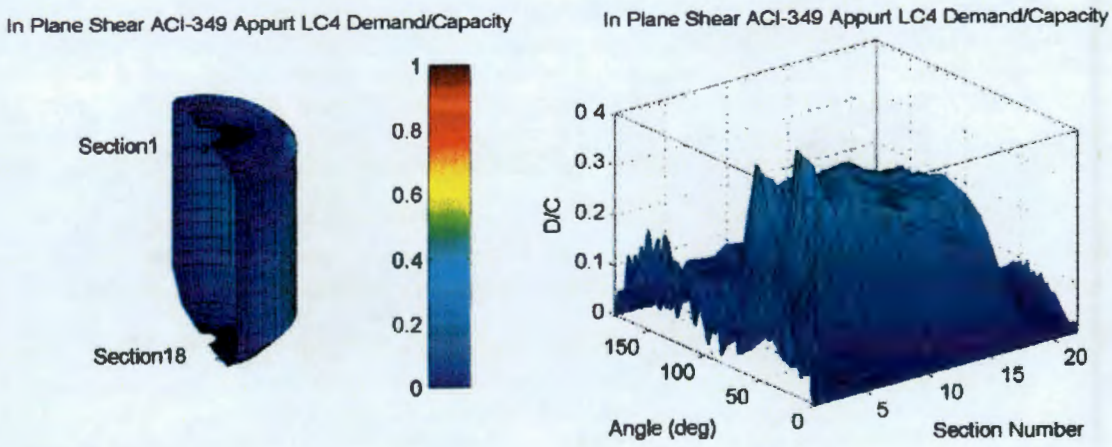

Figure 9.5. In-Plane Shear ACI D/C Ratios at LC4

10.0 Tank Limit Analysis

The methodology for assessing the tank limit loads is described in the Evaluation Criteria report (Johnson et al. 2010). The specifics of that methodology were developed in the C-106 Structural Integrity Evaluation (Bander et al. 1994). The tank limit loads were evaluated relative to both the in situ soil-load condition and relative to future loading conditions. The in situ limit load was determined by applying a uniformly distributed load over the entire model at the plane of the tank roof. The load includes the equivalent pressure of the soil overburden and it was increased until the tank offered little or no resistance to additional load. The tank limit load relative to future loading conditions was determined by applying a local load over a 20-ft diameter area above the center of the tank. Again, the load was increased until the tank offered little or no resistance to additional load.

The load-displacement curve for each analysis is presented in addition to the tabular limit load results. The displacement in these curves is the vertical displacement of the roof center relative to the top of the wall. It is anticipated that these may be of value in on-going dome monitoring programs.

The tank limit loads were applied following the full thermal history shown in Table 5.6. The tank limit loads were applied at a uniform 53°F. The 53°F temperature corresponds to the initial stress-free temperature of the model at the beginning of the 67-year thermal analysis.

The limit load analyses were conducted with lower bound concrete properties. The concrete tensile strength was prescribed as lower bound, rather than the near zero value prescribed in Chapter 4.0. In addition, the concrete moduli and compressive strengths were selected to be lower bound estimates of currently existing concrete. The Type I tank limit load is governed by tensile yielding of the rebar as discussed below.

The in situ limit load analysis presented in this chapter differs from previous analyses (Bander et al. 1994) in that the load was applied over the entire effective soil surface rather than being limited to the projected area of the roof. This load distribution was deemed more representative of the natural phenomena loads. In addition, potential barrier covers would most likely cover the whole farm and extend out beyond the farm. The equivalent soil pressure represented the nominal soil overburden depth of 11.45 ft as specified in Section 4.2.

The uniform surface pressure was applied to the soil surface and tank roof beyond the hatchway as shown in Figure 10.1. Figure 10.2 shows the concentrated limit load applied inside the 10-ft radius and outside the hatchway.

The limit load safety factor is defined as the ratio of the limit load plus the equivalent surface load divided by the equivalent surface load. The equivalent surface load is defined as the load that results in the same roof center deflection as the in situ loads of soil and roof weight. For the uniform surface load, this is an equivalent uniform pressure applied at the surface of the soil. For the local surface load, this is the equivalent local pressure over a 20-ft diameter that also gives the in situ roof deflection. This equivalent load was determined for each case by extrapolating the roof load-displacement curve back to zero displacement. This procedure is illustrated in Figure 10.3 for the uniform surface load.

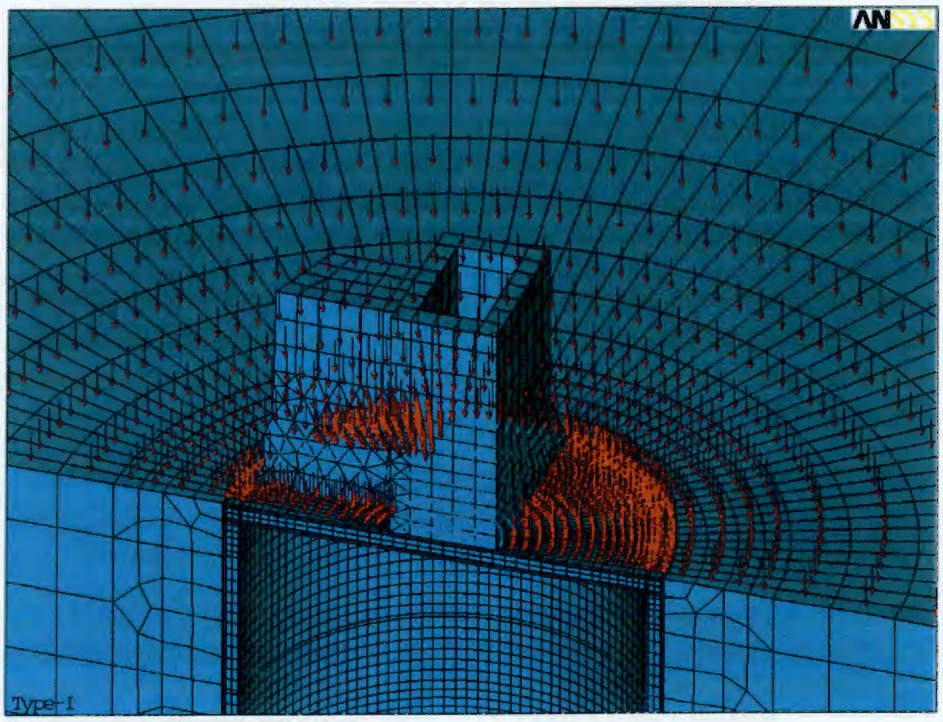

Figure 10.1. Equivalent Uniform Surface Load Definition

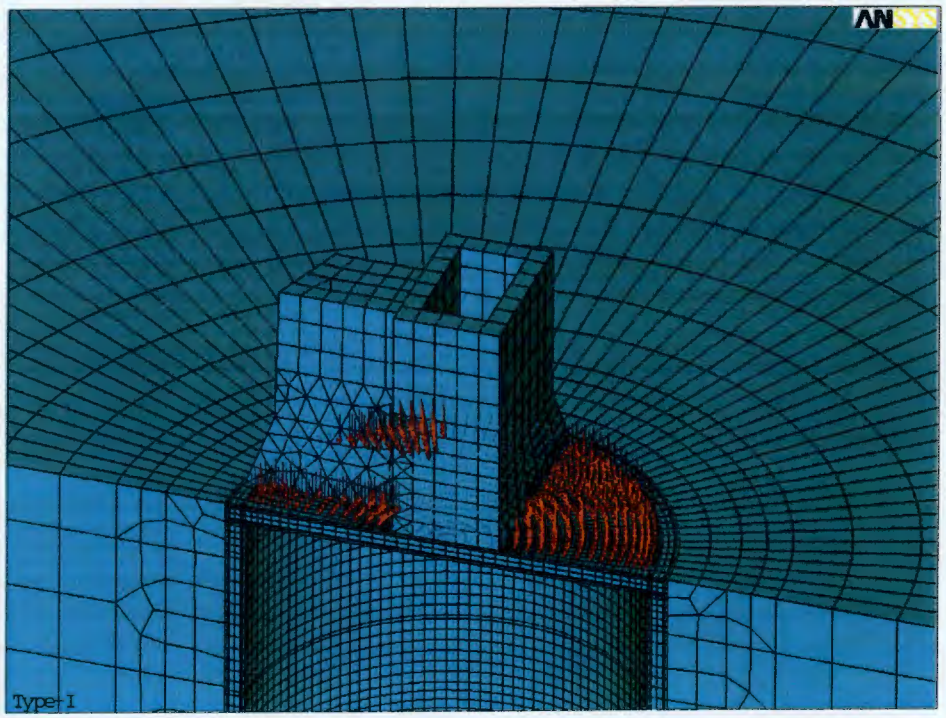

Figure 10.2. Local (Concentrated) Load Definition

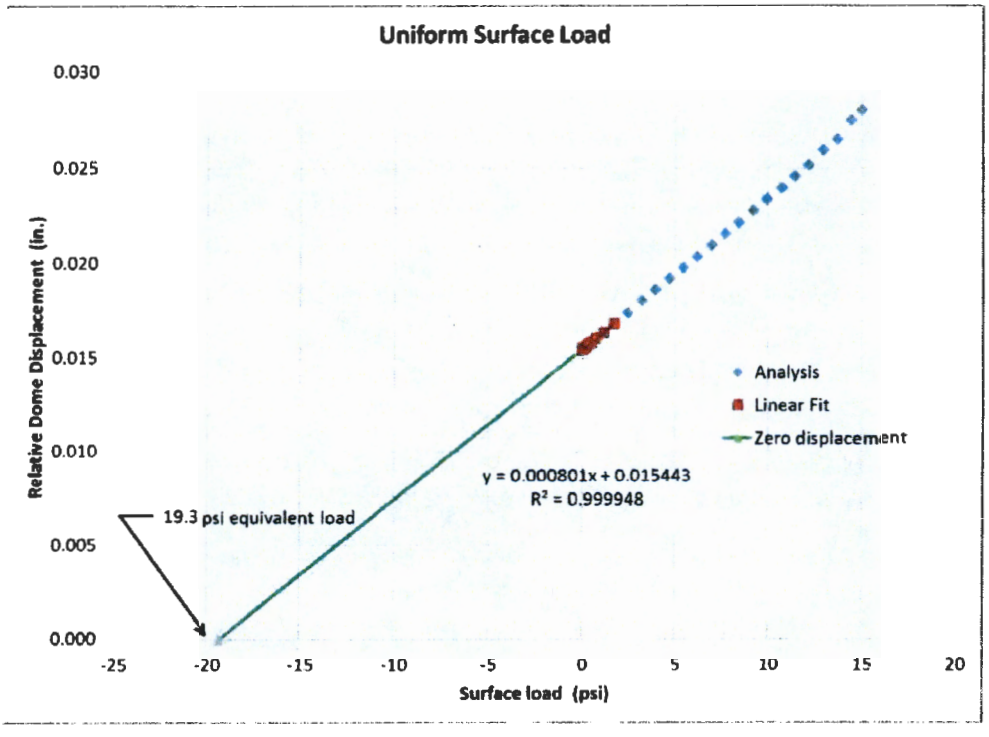

Figure 10.3. Equivalent Uniform Surface Load Calculation

In Figure 10.3, the "analysis" data is the displacement response of the roof centerline (relative to the top of the wall) as the uniform surface load is increased on the slice model with undegraded lower bound concrete. The 0.015-in. relative displacement at zero load reflects the in-situ displacement of the roof under the effects of gravity on the roof and 11.45-ft soil overburden. A "linear fit" is established through the initial portion of the load-displacement data. The slope of this line is affected by both the soil overburden depth, concrete stiffness (i.e., elastic modulus), and load distribution (uniform surface vs. local). The "analysis" data are then extrapolated using this slope to "zero displacement." The 19.3 psi load at the 0.0-in. intercept is defined as the equivalent surface load for this case.

This procedure was repeated using the hatchway model for the local load distribution case. The equivalent local load calculation is illustrated in Figure 10.4 The equivalent local is 813 kips.

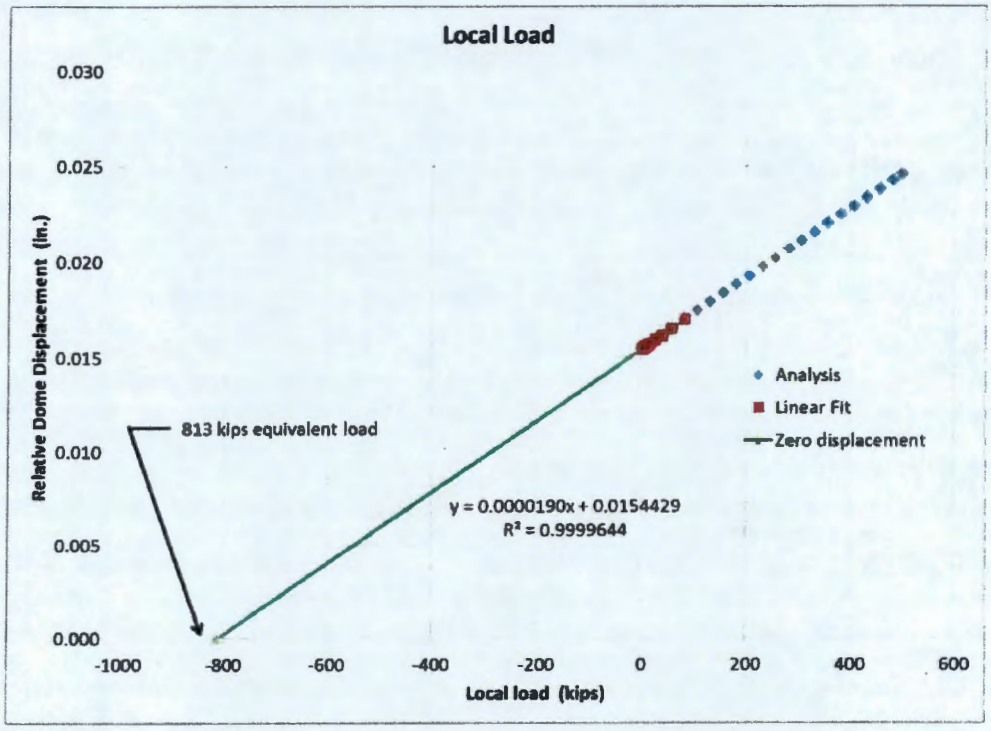

Figure 10.4. Equivalent Local Surface Load Calculation

The Evaluation Criteria report, in keeping with previous analyses, recommends use of the ASME Boiler & Pressure Vessel Code methodology of identifying the limit load as the intersection of the load-displacement curve with a line drawn through the origin at two times the slope of the initial linear portion of the load-displacement curve. The ASME methodology proved to be difficult to apply consistently in both the current analyses and the C-106 Structural Integrity Evaluation as reported by Bander et al. (1994). Bander et al. (1994) and the reviewers of the SST Type II AOR [Appendix A-2 of Rinker et al. (2011a)] comment that, "the combination of concrete crushing and rebar yielding is the critical failure mode." The Type I limit load definition is complicated by the rebar yielding which has already occurred during the thermal cycle as described in Section 7.2. Accordingly, the limit load was taken to be the load at the increase of rebar plastic strain.

Results from the uniform surface load case are shown in Figure 10.5. The limit load of 15.8 psi is established by the increase in plastic strain in the outer rebar in the roof near the wall. This gives a safety factor of 1.8, which is lower than the required 3.0. The onset of concrete crushing is also noted for reference.

Results from the local load case are shown in Figure 10.6. The limit load of 879 kips is established by the increase in plastic strain in the outer rebar in the roof near the wall. This gives a safety factor of 2.1, which is also lower than the required 3.0. The onset of concrete crushing is also noted for reference.

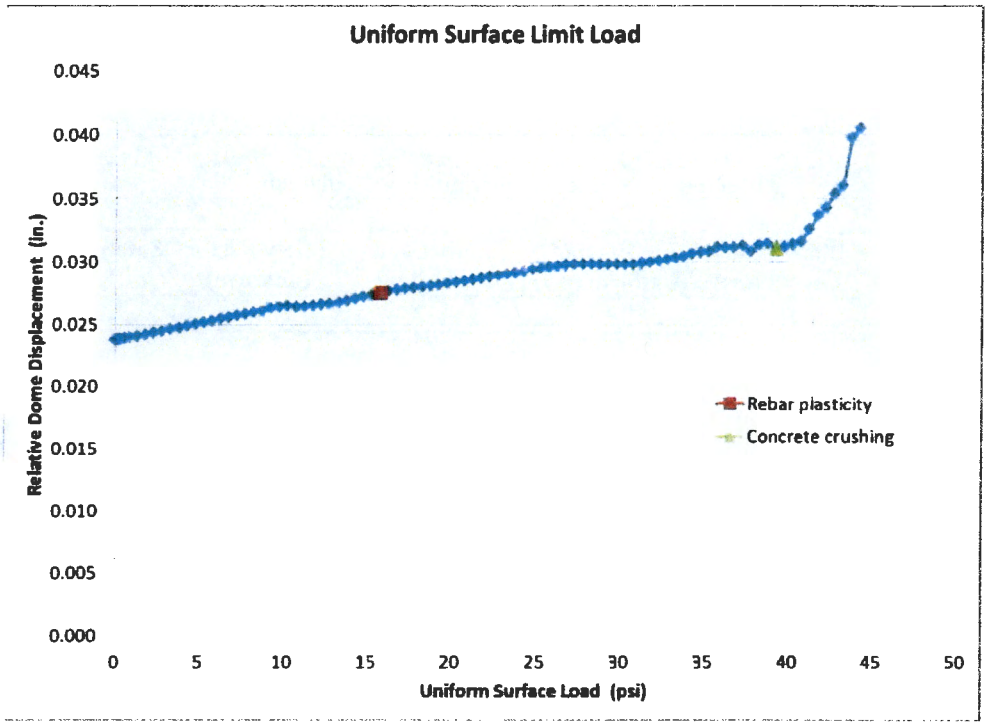

Figure 10.5. Load-Displacement Response under Uniform Surface Load

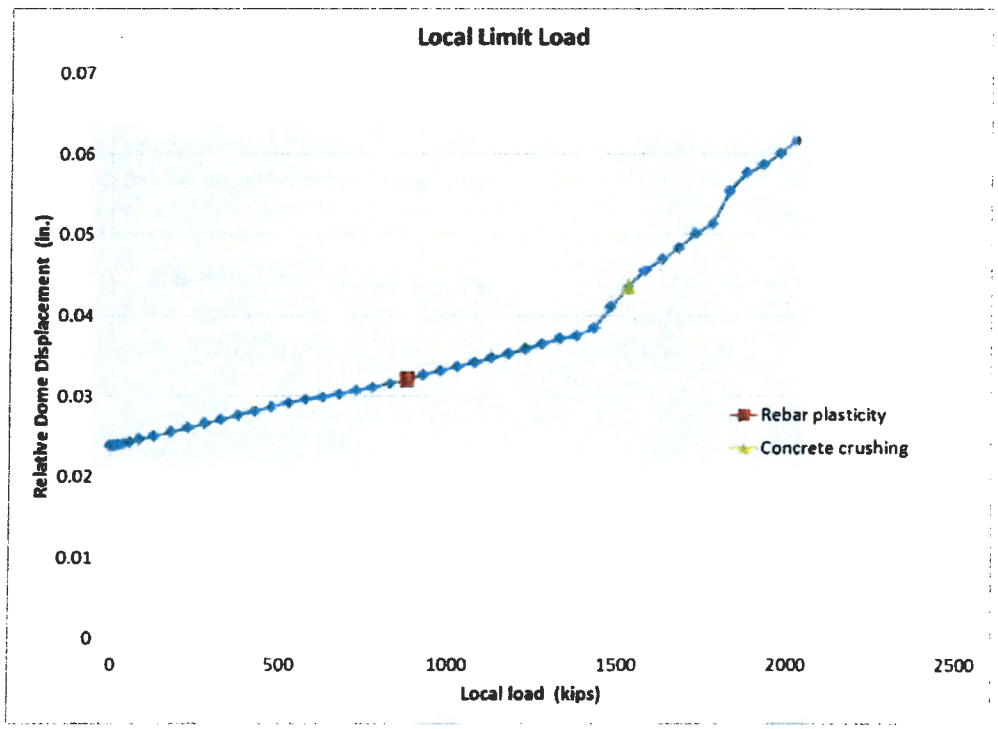

Figure 10.6. Load-Displacement Response under Local Load

The limit loads and safety factors are summarized in Table 10.1. The safety factors are calculated as: (total load + equivalent load)/equivalent load. The safety factors based on increasing rebar plastic strain are less than the 3.0 recommended in the Evaluation Criteria report.

Table 10.1. Summary of Limit Load Analysis

Limit Load - Uniform (psi)	Limit Load - Local (kips)	Equiv Load - Uniform (psi)	Equiv Load - Local (kips)	Safety Factor (uniform)	Safety Factor (local)
15.8	879	19.3	813	1.8	2.1

However, review of the load-displacement responses in Figures 10.5 and 10.6 demonstrate that the load continues to increase beyond the plastic strain criterion in a nearly linear manner. If the onset of concrete crushing was used as the limit load criterion, the safety factors for uniform limit load and local limit load would be 2.9 and 3.0 respectively for uniform and local loads. If the ASME methodology of two times the slope of the load-displacement curve were applied, the safety factors would be even higher.

The conservatism of applying the limit loads as pressures directly on the tank roof should also be noted. The Dome Load Capacity report (Julyk and Mackey 2003a) note that, "concentrated or distributed loadings on top of the tanks do not have a significant affect unless the tanks are less than 5 ft below ground level. 200 series Single Shell Tanks buried below 5 ft may be able to support substantial concentrated and distributed loads located above ground."

The definition of the size and location of the concentrated load is also complicated for the Type I tanks. RPP-11802 defines the 200 Series concentrated load as applied over a 10-ft radius and RPP-16660 defines it applied over a 5-ft radius. Applying the concentrated load over the center of the tank suggests the load is applied directly to the hatchway, a load which is likely not allowed by Tank Farm Operations. Configuring a concentrated load over the 10-ft radius centered on the tank but lying outside the hatchway is unlikely (see Figure 10.2). It is also recognized that the need for an over-tank concentrated load is mitigated by the relatively small diameter of the tank. Surface equipment could be placed outside the tank walls and need not be located over the roof.

While the tank limit load analysis, as conservatively applied, did not demonstrate the desired safety factors of the evaluation criteria, it does demonstrate additional margin nearly equal to the applied loads. Additional more refined analysis is recommended if the need for an over-tank concentrated loads arises.

11.0 Concrete Shell Buckling Analysis

This chapter presents the concrete shell buckling analysis for the Type I single-shell tanks. Only buckling of the tank wall is considered because the flat roof supported by the hatchway would fail by limit loading not buckling. The analysis shows that the tank wall is also very stable and would fail first by compressive crushing rather than buckling.

Buckling occurs when a structure is subjected to a compressive load and a small increase in the load causes a large increase in the deflection of the structure or a large change in the equilibrium configuration. The mode of buckling may be characterized either by a split in the equilibrium path to an adjacent equilibrium configuration (bifurcation) or by a sudden jump to a new equilibrium configuration (snap-through) as the applied load is increased infinitesimally. In general for thin-shell structures, the magnitude of the buckling load depends on the shell geometry, boundary restraints, material properties, and the type of load. The effects of large displacements and geometric imperfections are important considerations in correlating experimental results with theoretical analyses. For concrete shell structures like the SSTs, the effects of inelastic behavior, creep, reinforcement, and cracking need to be considered.

There are two interacting buckling modes that must be addressed for the cylindrical tank wall: (1) buckling under uniform axial compression and (2) buckling under external lateral pressure. Parameters of potential significance to the buckling capacity of the tank roof and the cylindrical tank wall include the following:

- Type of loading: uniform, concentrated, axisymmetric, or asymmetric
- Post-buckling behavior
- Initial geometric imperfection
- Creep
- Cracking and the amount and type of reinforcement
- Nonlinear behavior of concrete in compression.

Chapter 19 of ACI 349-06 (ACI 2007) requires the investigation of thin shells for instability, including consideration of the possible reduction in buckling capacity caused by large deflections, creep effects, temperature, cracking, and deviations between the actual and theoretical shell geometry. Referring to the commentary in Chapter 19 of ACI 318-05, ACI 349-06 identifies ACI SP-67, *Concrete Shell Buckling* (ACI 1981), as a source of approaches for determining the critical buckling loads of reinforced concrete shells. A practical procedure for determining critical buckling loads of reinforced concrete shells, as given by the International Association for Shell and Spatial Structures (IASS) Working Group No. 5, *Recommendations for Reinforced Concrete Shells and Folded Plates*, is discussed in the ACI SP-67 document (ACI 1981).

Scordelis (1981) summarizes the IASS recommendations in SP-67 with the following equations:

$$P_b^{red} = \propto_1 \propto_2 \propto_3 \propto_4 P_b^{lin} = \propto P_b^{lin} \tag{11.1}$$

$$P_b^{allow} = P_b^{red} / SF_b \tag{11.2}$$

where P_b^{red} = Reduced buckling load
P_b^{lin} = Linear "classical" critical buckling load
P_b^{allow} = Allowable buckling load
$\propto_1$ = Geometric imperfection-sensitivity reduction factor
$\propto_2$ = Creep reduction factor
$\propto_3$ = Reduction factor to account for cracking and amount and type of reinforcement
$\propto_4$ = Reduction factor to account for material nonlinearity of concrete under high stresses
$\propto$ = Combined buckling load-reduction factor = $\propto_1 \propto_2 \propto_3 \propto_4$
SF_b = Buckling safety factor

11.1 Unfactored Theoretical Buckling Loads for a Cylindrical Wall Under Axial Compression and External Pressure

Computation of the "classical" buckling load as predicted by linear buckling theory for an ideal shell geometry assuming gross uncracked concrete is based on the end-of-life degraded concrete modulus. The critical buckling load for axial compression in the tank cylindrical wall, $P_{b_a}^{lin}$, is derived from the equation for the critical buckling stress presented by Seide (1981):

$$\sigma_{b_a}^{lin} = \frac{1}{\sqrt{3\left(1-\nu^2\right)}} E\left(\frac{t}{R}\right) \tag{11.3}$$

which is transformed to the corresponding total roof load

$$P_{b_a}^{lin} = 2\pi R t \sigma_{b_a}^{lin} = \frac{2\pi}{\sqrt{3\left(1-\nu^2\right)}} E t^2 \tag{11.4}$$

where E = Young's modulus for concrete
ν = Poisson's ratio for concrete
t = Tank minimum wall thickness
R = Tank cylinder mid-wall radius of curvature

The theoretical buckling pressure of the cylindrical wall loaded by external lateral pressure is given by Flugge (1960) as:

$$P_{bL}^{lin} = \frac{E}{1-\nu^2}\sqrt{12\cdot k}\cdot\varphi_{cr} \tag{11.5}$$

where:

$$\varphi_{cr} = \frac{\left(1-\nu^2\right)\cdot(n\cdot\lambda)^4 + k\left[\left[(n\cdot\lambda)^2+m^2\right]^4 - 2\cdot\left[\begin{array}{l}\nu\cdot(n\cdot\lambda)^6+3(n\cdot\lambda)^4\cdot m^2\ldots\\ +(4-\nu)\cdot(n\cdot\lambda)^2\cdot m^4+m^6\end{array}\right]\ldots\right.}{\left.+2\cdot(2-\nu)\cdot(n\cdot\lambda)^2\cdot m^2+m^4\right]}{m^2\cdot\left[(n\cdot\lambda)^2+m^2\right]^2 - m^2\cdot\left[3\cdot(n\cdot\lambda)^2+m^2\right]} \tag{11.6}$$

$$\lambda = \pi\cdot\frac{R}{L} \tag{11.7}$$

$$k = \frac{t^2}{12\cdot R^2} \tag{11.8}$$

n = the integer describing the half wave buckling mode along the length.
2m = the integer describing the half wave buckling mode along the circumference.

Whereas the critical buckling load for external lateral pressure is determined for a uniform distribution along the length of the cylindrical wall, the actual distribution of pressure is linearly varying from a minimum value at the top to a maximum value at the base of the wall. Seide et al. (1979) identify theoretical results for a pressure distribution that varies linearly in the longitudinal direction. The critical equivalent uniform pressure is found to be the length average of the positive pressure distribution. If the lateral pressure is entirely positive along the full length of the cylinder, this corresponds to the average lateral pressure. Therefore, the at-rest soil pressure at the mid-height of the tank wall was used in the buckling calculations.

11.2 Buckling Load-Reduction Factors

The buckling load-reduction factor, α_1, accounts for the imperfection sensitivity (i.e., deviation between the actual and theoretical shell geometry) of the structure. Seide (1981) develops a lower bound correlation equation as a function of radius-to-thickness ratio based on experimental buckling data for axially loaded cylindrical shells. The use of this lower bound correlation is appropriate when imperfections are unknown. Experimental values presented for axially compressed cylindrical shells, while exhibiting considerable scatter, indicate that the discrepancy between theory and experiment tends to increase as the R/t of the shell increases. Seide attributes this phenomenon to decreased bending stiffness of the relatively thinner shells, which renders them more susceptible to imperfections during construction. Seide (1981) presents the following conservative design formula as a lower bound representation of the experimental data:

$$\alpha_1 = 1 - 0.9\left(1 - e^{\frac{-1}{16}\sqrt{\frac{R}{T}}}\right) \tag{11.9}$$

for cylinders with 100 < R/t < 3,000 and 0.5 < L/R < 5, where L is the length of the cylinder. The applicability of knockdown factors developed for axially compressed cylinders to the roof under radial pressure is recognized by Popov and Medwadowski (1981) in their account of the IASS recommendations. They state that if no solution is available for shells of a given geometry and load, the curves applicable to an axially compressed cylinder and a spherical cap should be used.

The upper bound R/t for the Type I SSTs is 10.6, which is outside the range where Eq. (11.9) is applicable. By taking R/t at the lower bound of the acceptable range (R/t = 100), a very conservative value of α_1 is calculated to be 0.58 for the wall under axial compression. A conservative value of α_1 for the wall under external lateral pressure is based on Seide's (1981) recommendation of 0.75.

The buckling load-reduction factor, α_2, accounts for concrete creep. The creep reduction factor is defined as E_{c2}/E_c where E_c is the initial concrete modulus at the time of first loading and $E_{c2} = E_c/(1 + C_u)$ is the reduced concrete modulus resulting from creep strains. The ultimate creep coefficient for the concrete, C_u, is the ratio of the ultimate creep strain divided by the initial elastic strain. The values of C_u should be based on a creep analysis for an upper bound thermal history of the structure. If a creep analysis is not available, Popov and Medwadowski (1981) recommend that the ultimate creep coefficient be estimated as $C_u = 4 - 2\log(f_c)$, where f_c is the concrete compressive strength at the time of loading in MPa. Both methods of calculating C_u were checked in the current buckling analysis and the maximum C_u was applied to conservatively calculate the minimum creep reduction factor. The C_u value calculated from finite element creep strains governed for the Type I SST with the bounding thermal history. The same creep reduction factor (α_2) was applied conservatively to all loads during the tank service period despite the fact that for short-term loads such as live loads, the effect of creep is considered to be insignificant.

$$\dot{\varepsilon}_{cr} = C_1 \sigma^{c_2} t^{c_2} e^{-c_4/T} \tag{11.10}$$

The buckling load-reduction factor, α_3, accounts for the effect of cracking and the amount and type of reinforcement in the cross-section. Following the IASS procedure cited in SP-67 (Popov and Medwadowski 1981), $n = E_s/E_{c2}$ where E_s is the elastic modulus of the steel reinforcement and E_{c2} is the reduced concrete modulus caused by creep computed as before, except that a conservative initial concrete modulus corresponding to the end-of-life degraded concrete is applied. The steel ratio $p = A_s/A_c$ is determined, where A_s is the total steel area per unit width of shell in one direction and A_c is the concrete area. The product $\eta\rho$ is used to determine a Ψ factor from Figure 11.1 ((Scordelis 1981), p. 100). From Figure 11.2 (Scordelis 1981), a value of w_o/h (the ratio of the imperfection size divided by the wall thickness) is selected that corresponds to α_1. Finally, α_3 is estimated from Figure 11.3 (Scordelis 1981) as a function of w_o/h.

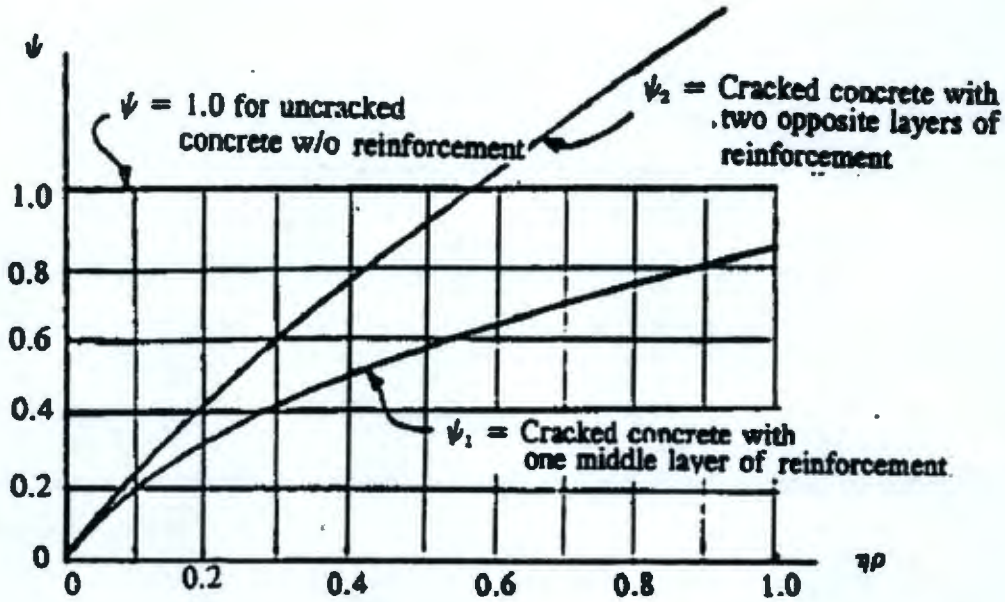

Figure 11.1. Values of ψ for Effect of Concrete Cracking and Amounts and Type of Reinforcement (Figure 4 of Scordelis 1981)

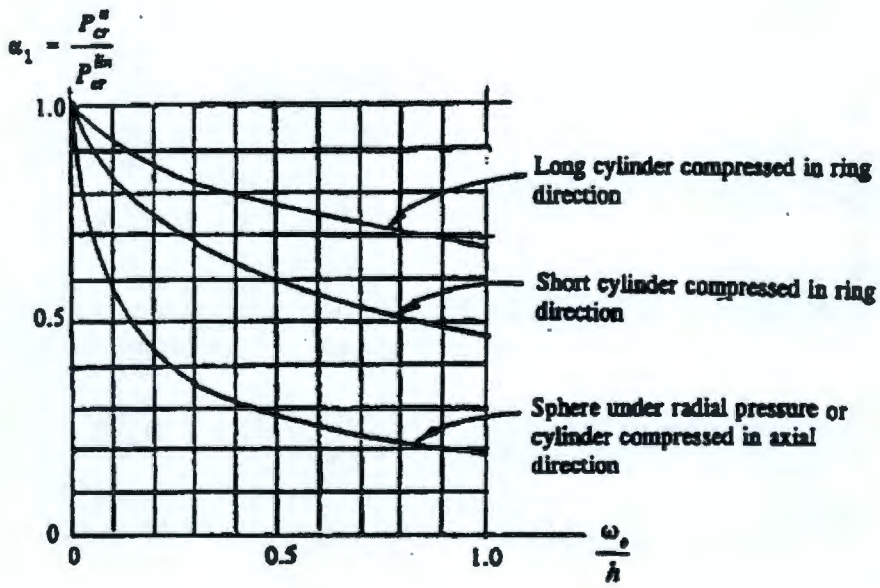

Figure 11.2. Effect of Geometric Imperfections on Buckling Load (Figure 3 of Scordelis 1981)

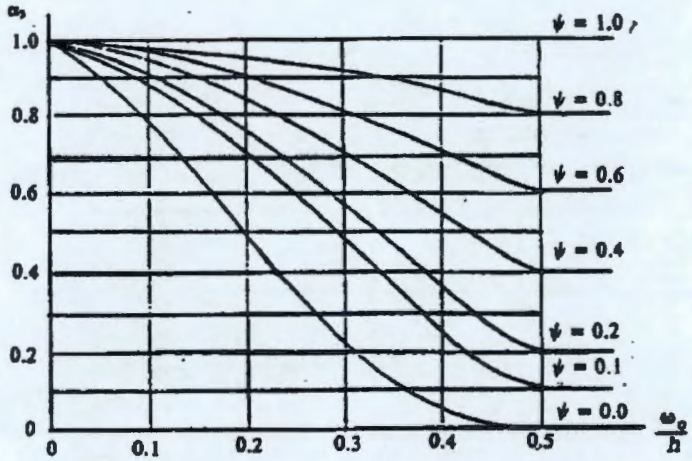

Figure 11.3. Reduction Factor α_3 for Concrete Cracking and Amounts and Type of Reinforcement (Figure 5 of Scordelis 1981)

The buckling load-reduction factor, α_4, is associated with material nonlinearity of the concrete under high stresses. The α_4 is determined from the semi-quadratic interaction equation (Scordelis 1981):

$$\left(\frac{P_b^{red}}{P_{ult}}\right)^2 + \left(\frac{P_b^{red}}{P_3}\right) = 1 \tag{11.11}$$

or

$$\alpha_4^2\left(\frac{P_3}{P_{ult}}\right)^2 + \alpha_4 = 1 \tag{11.12}$$

where $P_3 = \alpha_1\alpha_2\alpha_3 P_b^{lin}$

P_{ult} = ultimate externally applied load that the shell can carry as governed by the ultimate strength of the reinforced concrete shell section, independent of any buckling consideration.

P_{ult_u} = for the SST roof under uniform pressure may be based on predictions from the limit load analysis for a uniform load applied at the soil surface.

P_{ult_c} = for the SST roof under concentrated loading is based on predictions from the limit load analysis for loads applied at the soil surface over a local region about the center of the tank.

P_{ult_a} = for the SST cylindrical wall under axial compressive loading is computed based on obtaining a uniform circumferential compressive stress equal to the predicted degraded concrete compressive strength of the cylindrical wall at the end of its service.

P_{ult_L} = for the SST cylindrical wall under uniform external lateral pressure is computed based on obtaining a uniform circumferential compressive stress equal to the predicted degraded concrete compressive strength of the cylindrical wall at the end of its service.

11.3 Buckling Load-Interaction and Safety Factors

Choosing the appropriate buckling safety factors requires consideration of the type of shell structure, its characteristic post-buckling behavior, and the type of loads that are applied. The evaluation must also assess the combination of the uniform pressure and concentrated loads on the roof. The SST Type-II AOR (Rinker et al. 2011a) used the guidance of SP-67 (ACI 1981) to define safety factors for the uniform pressure and concentrated roof loads. Conservative safety factors of 3.5 were chosen for both load types, because it was estimated from elastic buckling solutions that both conditions may result in unstable post-buckling responses. However, further investigation determined that these safety factors are quite conservative and are more appropriate for thin shells (diameter/thickness > 300) where elastic buckling is the expected response. The Hanford Type I tank walls are much thicker (diameter/thickness = 21), where plastic buckling is the more likely failure mode.

The literature on concrete shell buckling subsequent to SP-67 (i.e., after 1981) was reviewed for further guidance on choosing more appropriate safety factors. Both Kollar and Dulacska (1984) and Medwadowski (2004) discuss the implications of elastic and plastic buckling modes on the determination of safety factors and were particularly useful.

Kollar and Dulacska (1984) compiled information from concrete shell buckling research plus actual buckling failures in the field, and determined that different safety factors are warranted depending on: a) the failure mode (elastic or plastic), b) the type of load (dead or live), and c) the stability in the post-buckling condition. The interaction of different loads must also be accounted for. Table 11.1 summarizes their recommended safety factors.

Table 11.1. Buckling Safety Factors from Kollar and Dulacska (1984)

Buckling Mode	Safety Factor	Post Buckling Stability / Load Condition
Elastic Buckling	$k_{el} = 3.5$	Unstable post buckling
	$k_{el} = 1.75$	Stable post buckling
Plastic Buckling	$k_{pl} = 1.5$	Dead load = Uniform soil loads
	$k_{pl} = 1.7$	Live loads = Concentrated surface loads

The allowable load for each load type (uniform dead load and concentrated live load) can be determined using the quadratic Dunkerley type relation:

$$\left(\frac{k_{el} \cdot p_{cr_allow}}{p_{cr_el_upper}}\right)^2 + \left(\frac{k_{pl} \cdot p_{cr_allow}}{p_{pl}}\right)^2 = 1 \qquad (11.13)$$

$$p_{cr_allow} = \frac{p_{cr_el_upper}}{k_{el}} \sqrt{\frac{1}{1+\left(\frac{k_{pl}}{k_{el}} \cdot \frac{p_{cr_el_upper}}{p_{pl}}\right)^2}} \quad \lambda = \frac{p_{pl}}{p_{cr_el_upper}} = \frac{p_{ult}}{p_3} \tag{11.14}$$

The interaction between the dead load and the concentrated live load must also satisfy

$$\frac{p_{u_applied}}{p_{u_allow}} + \frac{p_{c_applied}}{p_{c_allow}} \le 1 \tag{11.15}$$

The detailed implementation of these equations is fully described in the Mathcad ™ worksheets contained in Appendix B of this report.

In 2004, Stefan Medwadowski, one on the editors of ACI special publication SP-67 (ACI 1981), published an updated review of buckling analysis methods for concrete shells (Medwadowski 2004). In that article he proposed a buckling evaluation method that compares the elastic buckling load with the ultimate limit load to determine if elastic or plastic buckling is the expected failure mode. He proposed that the point of separation between the buckling failure mode and limit load failure occurs then the elastic buckling load divided by the buckling safety factor is equal to the limit load divided by a safety factor based on material strength.

$$\frac{\alpha_1 \cdot p_{cr_lin}}{k_{buckling}} = \frac{p_{ult}}{k_{material}} \qquad k_{buckling} := 3.5 \qquad k_{material} := 1.75 \tag{11.16}$$

Substituting the buckling and material safety factors shows that buckling is the expected failure mode when the buckling load divided by the limit load is less than 2. For the Type I tank wall, this ratio is 5.9, showing that the plastic limit load would be reached long before elastic buckling is an issue. Therefore, the material safety factor of 1.75 could be substituted for the elastic and plastic safety factors in Eq. (11.17) to calculate the allowable uniform and concentrated loads. That is:

$$k_{pl_c} : k_{material} = 1.75 \qquad k_{pl_u} : k_{material} = 1.75$$
$$k_{el_c} : k_{material} = 1.75 \qquad k_{el_u} : k_{material} = 1.75 \tag{11.17}$$

Medwadowski (2004) also presents a suggested procedure for evaluating buckling in concrete shell structures that is based on the general SP-67 methodology described by Eqs. (11.1) and (11.2). He recommends an updated equation for the inelastic reduction factor, α_4, and the safety factors are defined based on Eq. (11.16) considering if the shell is likely to fail by buckling or plastic collapse. The safety factor is 1.75 if plastic collapse governs, otherwise the buckling safety factor is calculated by the following equation with w_o/h being the imperfection size defined as a fraction of the shell thickness. For w_o/h=0.1, the buckling safety factor is 3.36 compared to the value of 3.5 previously used.

$$\text{Safety Factor} = 2.5 + e^{\left[-1.5\frac{w_0}{h}\right]} \tag{11.18}$$

The above investigation of updated safety factors and load combination methods leads to three similar but different buckling evaluation methods:

1. The Kollar and Dulacska method of combining elastic/plastic effects and dead and live loads,
2. Medwadowski's safety factors used in the Kollar and Dulacska load combination equations, and
3. Medwadowski's updated method that is similar to the SP-67 procedure.

All three methods were implemented in the Mathcad™ worksheets presented in Appendix B. The maximum buckling D/C ratios of the three methods are reported in the next section.

11.4 Results of the Type I Tank Wall Buckling Evaluation

The maximum loading condition was considered in the buckling evaluation of the Type I SSTs. The Type I thermal history was analyzed with the maximum soil overburden depth of 11.45 ft, soil density of 125 lb/ft^3, and the 142 kip concentrated load specified in RPP-16363 (Julyk and Mackey 2003b).

The analysis used the 95/95 lower bound concrete strength and elastic modulus degraded at the maximum temperature of 250°F in the roof and wall concrete. The unfactored critical buckling loads are a direct function of the concrete elastic modulus. Therefore, thermal degradation of the concrete modulus directly reduces the critical buckling loads. The steel properties correspond to 80°F, which is the estimated current and future operating temperature of the Type I tanks. The steel modulus is constant within the temperature range of interest. The creep model for Hanford concrete documented in the Evaluation Criteria report (Johnson et al. 2010) was used to conservatively estimate the axial creep at the mid-wall height after 67 years at 250°F.

The buckling analysis methods outlined in Sections 11.1 through 11.3 were implemented the Mathcad™ worksheet listed in Appendix B. Table 11.2 lists the Type I tank dimensions that were used and Table 11.3 summarizes the buckling analysis results. The wall buckling analysis applied the higher safety factors for live loads to the total axial compression loads even though only a small fraction of the total load is the concentrated live load. The dead load safety factors were applied to the lateral soil pressure on the outside of the tank wall.

Table 11.2. Tank Dimensions for the Wall Buckling Analysis

Item	Value
Tank mid-wall radius, ft	10.6
Minimum wall thickness, inch	12
Height of cylindrical wall, inch	313
Total tank height, footing to top of flat roof, inch	325
Soil density, lb/ft^3	125
Soil internal friction angle, φ, °	35
At-rest soil pressure coefficient [1-sin(φ)]	0.426
Soil overburden depth, ft	11.45
Soil depth from surface to mid-wall, ft	25.5

The applied axial load at the mid-wall of the tank (20.8 kip/ft) was obtained from the finite element model of the Type I tank with 11.45-ft of soil overburden. The models include the 40 lb/ft^2 uniform live load across the entire soil surface plus the maximum concentrated loads of 142 kip. The applied lateral pressure on the outside of the wall (9.4 psi) was calculated as the at-rest soil pressure at the mid-wall soil depths of 25.5 ft.

Table 11.3 shows that maximum D/C ratio for wall buckling was 0.17 for the three methods evaluated. The applied axial compression on the wall is only 9% of the limit load at the concrete compressive strength. Therefore, buckling of the Type I tank wall under 11.45 ft of soil and 142 kip concentrated load is not of concern.

11.5 Summary of the Type I Tank Buckling Evaluation

A buckling analysis was performed for the Type I tank wall. The tank roof was not considered because the flat roof is supported by the hatchway and it will not fail by buckling. The buckling analysis methods summarized in the Evaluation Criteria report (Johnson et al. 2010) were augmented by more recent references on concrete shell buckling that better represent the geometry and loading conditions of the tanks. The theoretical buckling loads were reduced by factors that account for geometric imperfections, concrete creep, cracking and loading of the reinforcing steel, and the nonlinear stress-strain behavior of concrete at high compressive stress. The evaluation considered combined axial compression plus lateral soil pressure on the outside of the tank. The axial buckling load for the tank is nearly 6 times the limit load, so the tank wall would fail by plastic collapse rather than buckling. The maximum D/C ratio was calculated to be 0.17. Therefore, buckling is not of concern for the Type I SSTs.

Table 11.3. Summary Results of the Wall Buckling Analysis

Item	Value
Maximum Wall Temperature, T_{max}, °F	250
Current and Future Wall Temperature, T_{oper}, °F	80
Overburden Depth, ft	11.45
Concrete Compressive Strength, f_c, psi	3568
Concrete elastic modulus at T_{max}, 10^6 psi	2.5
Concrete Poisson's ratio at T_{max}	0.15
Concrete density, lb/ft^3	145
Steel elastic modulus at T_{oper} = 80°F, 10^6 psi	29.4
Steel Poisson's ratio at T_{oper} = 80°F	0.30
Axial Compression on Cylinder	
Theoretical axial buckling load, lb	1.32×10^9
α_1, geometric reduction factor	0.58
α_2, creep reduction factor	0.15
α_3, cracking reduction factor	0.98
α_4, nonlinear material reduction factor	0.26
Total Reduction Factor, $\alpha_1 \times \alpha_2 \times \alpha_3 \times \alpha_4$	0.022
Reduced axial buckling load, lb	2.94×10^7
External Lateral Pressure on Cylinder	
Theoretical lateral buckling pressure, psi	2668
α_1, geometric reduction factor	0.75
α_2, creep reduction factor	0.15
α_3, cracking reduction factor	0.92
α_4, nonlinear material reduction factor	0.69
Total Reduction Factor, $\alpha_1 \times \alpha_2 \times \alpha_3 \times \alpha_4$	0.071
Reduced lateral buckling pressure, psi	189
Ultimate creep strain in wall	16.3×10^{-5}
Initial elastic strain in wall	2.9×10^{-5}
Ultimate axial wall load, lbf	3.42×10^7
Ultimate lateral wall pressure, psi	337.1
Axial wall force at mid-wall section 10, lbf	1.38×10^6
At-Rest Soil Pressure at mid-wall depth, psi	9.4
Combined Buckling Demand/Capacity for Lateral Pressure and Axial Loads	0.17
Applied Axial Compression / Max. Axial Compression	0.09

This page intentionally left blank.

12.0 Conclusions

The structural analyses discussed in this report do not reveal any significant deficiencies with the structural integrity of the Type I Hanford single-shell tanks. Very minor rebar yielding (0.05% strain) was predicted at the edge of the flat roof as the tank thermal history was applied. However, this yielding did not increase under application of the LC1 (factored static load) or LC4 (unfactored static plus seismic) load combinations. The analyses represent 67 years of use. The loads imposed on the finite element tank model are more severe than any service loads to date or currently planned for the future. The analyses treated the most severe combinations of soil and concrete stiffness and based the structural evaluation on lower bound concrete strength.

The soil overburden is the largest load on the tank and it is the largest contributor to the static tank demands. Waste and soil surface loads produced only secondary effects. Thermal loads were significant in the slab and lower wall where the temperatures were highest (250°F). The material combination of upper bound concrete modulus and lower bound soil modulus increased the concrete section demands compared to the baseline case with best estimate material properties.

The Type I tank model was subjected to a 142-kip concentrated load on the soil surface, a 40 lb/ft^2 uniform surface load, a 284 inch waste load at 1.7 specific gravity, 11.45 ft of soil overburden, and a 67-year thermal history that peaked at 250°F. The reinforced concrete structure was evaluated in the manner required by ACI 349. Load combinations 1, 4 (which includes the seismic load), and 9 of the ACI codes were evaluated for each variation of soil and concrete properties. The force and moment pairs in the meridional and hoop directions were evaluated on the force-moment diagrams for each individual cross-section.

The ACI 349-06 code evaluations show that tank demands are lower than the capacities for all locations in the roof, upper haunch, and wall for all load combinations. The peak non-seismic ACI 349-06 load demands are 52%, 22%, 33% of the meridional, hoop, and shear capacities, respectively, in the roof, upper haunch, and wall. In addition, the maximum tank section forces and moments over the time history were extracted from the seismic model and combined with the non-seismic forces and moments to evaluate the ACI seismic load combination. The seismic ACI evaluation results indicate that tank demands are lower than the ACI 349-06 capacities for all locations in the roof, upper haunch, and wall. The peak seismic ACI load combination resulted in demands that were 45%, 26%, and 32% of the meridional, hoop, and shear capacities, respectively, in the roof, upper haunch, and wall. The seismic loads are small, representing only about 10% of the section capacities. This increases the maximum D/C ratios for the unfactored thermal and operating loads from 0.35 to 0.45.

Tank-to-tank interaction effects were considered but not specifically evaluated for the Type I tanks because the 50-ft center-to-center spacing gives 3 radii of soil between adjacent tanks. Furthermore, all the D/C ratios are significantly less than 0.8, so adding the maximum $\Delta D/C=0.2$ for tank-to-tank effects would still result in D/C ratios well below 1.0.

The TOLA analyses and the combined case of TOLA and seismic loads do show several locations in the bottom slab where section demands are predicted to be higher than capacities. This indicates that cracking of the slab likely occurred from radial thermal expansion followed by contraction under the bounding thermal history. However, cracks in the slab do not affect the structural stability of the tank

roof, walls, and footing. A slab removal analysis with the slab separated from the tank footing was conducted to further evaluate the effect of possible cracking and shear offset of the concrete in the slab. This analysis predicted that the maximum shear offset between the slab and footing would be less than one-half of the nominal liner thickness. The slab removal study concluded that neither the SST structural stability nor the liner integrity would be affected by the potential shear offset at the footing to slab interface.

Tank limit load analyses with uniform surface loads and concentrated (local) loads were also conducted. The tank limit load analyses, as applied with a conservative plastic strain limit criterion, have safety factors less than the recommended value of 3.0. However, the load-displacement curves continue to increase beyond the plastic strain criterion, indicating that the tanks are able to support further increased loads. The use of the concrete crushing criterion increases the safety factors to 2.9 and 3.0 for the local and uniform surface loads respectively. The small diameter of these tanks will likely preclude the necessity to apply significant concentrated loads directly above the Type I tanks. Additional more refined analysis is recommended if the need for an over-tank concentrated load arises.

A buckling analysis was also performed for the Type I tank wall. The tank roof was not considered since the flat roof is supported by the hatchway and it will not buckle. The evaluation considered combined axial compression plus lateral soil pressure on the outside of the tank. The axial buckling load for the tank is nearly 6 times the limit load, so the tank wall would fail by plastic collapse rather than buckling. The maximum D/C ratio was calculated to be 0.17. Therefore, buckling is not of concern for the Type I SSTs.

Appendix A provides load contribution plots showing the effects of individual load components to gain a more complete understanding of the Type I SST loads and structural response. Appendix B documents the buckling analyses using Mathcad™ and Appendix C documents the ACI evaluation methods. The final appendix, D, contains the external reviewer comments from the Type I AOR review. Attachment 1 at the end of the report contains the seismic analysis prepared by Becht.

13.0 References

Abatt FG, KL Stoops, BM Larsen and LJ Julyk. 2014. *Hanford Type I Single Shell Tank Seismic Analysis*. 20906-R-001, Revision 0, Becht Engineering Company, Inc., Richland, Washington.

ACI. 1981. *Concrete Shell Buckling*. ACI SP-67, American Concrete Institute (ACI), Detroit, Michigan. EP Popov and SI Medwadowski (eds).

ACI. 2007. *American Concrete Institute Code Requirements for Nuclear Safety Related Concrete Structures*. ACI 349-06, American Concrete Institute (ACI), Farmington Hills, Michigan.

Bander TJ, JP Day, AD Dyrness, RJ James, LJ Julyk, RS Marlow, CJ Moore, EW Pianka, YR Rashid, JS Shulman and MP Weis. 1994. *Tank 241-C-106 Structural Integrity Evaluation for In situ Conditions*. WHC-SD-W320-ANAL-001, Revision 0, Volumes I and II, Westinghouse Hanford Company, Richland, Washington.

Berman HS. 2009. "Hanford Single-Shell Tank Integrity Program." Presented at *Single-Shell Tank Integrity Project-Workshop, WRPS-40224-VA*, July 29, 2009, Richland, Washington.

Boomer KD. 2009. "Presentations to the Single-Shell Tank Integrity Panel - Single-Shell Tank History." Presented at *Single-Shell Tank Integrity Project-Workshop, WRPS-40224-VA*, January 26-28, 2009, Richland, Washington.

Brevick CH, RL Newell and JW Funk. 1996. *Supporting Document for the Historical Tank Content Estimate for C-Tank Farm*. WHC-SD-WM-ER-313, Rev. 1, ICF Kaiser Hanford Company, Richland, Washington.

Brevick CH, JL Stroup and JW Funk. 1997. *Supporting Document for the Historical Tank Content Estimate for B-Tank Farm*. WHC-SD-WM-ER-310, Rev. 1, Fluor Daniel Northwest, Richland, Washington.

DOE. 2002. *Natural Phenomena Hazards Design and Evaluation Criteria for Department of Energy Facilities*. DOE-STD-1020-2002, U.S. Department of Energy (DOE), Washington, D.C.

Flugge W. 1960. *Stresses in Shells*. Springer-Verlag, New York.

Geomatrix. 2007. *Updated Site Response Analyses for the Waste Treatment Plant, DOE Hanford Site Washington*. GMX-9995.002-001, Rev. 00, Geomatrix Consultants, Inc., Oakland, California.

IBC. 2009. *International Building Code 2009*. International Code Council, Inc., Washington, D.C.

Johnson KI, SP Bapanapalli, JE Deibler, FG Abatt, KL Stoops, NK Karri, SE Sanborn, SP Pilli, BM Larsen and LJ Julyk. 2014. *Tank to Tank Interaction Study of the Hanford Single-Shell Tanks*. RPP-RPT-49991, Rev. 0; PNNL-23328, Rev. 0, Pacific Northwest National Laboratory, Richland, Washington.

Johnson KI, JE Deibler, FG Abatt and MW Rinker. 2010. *Single-Shell Tank Evaluation Criteria*. RPP-46442, Rev. 0; PNNL-18837, Pacific Northwest National Laboratory, Richland, Washington.

Julyk LJ and TC Mackey. 2003a. *200-Series Single-Shell Tank Dome Load Capacity (200, B, C, T, and U)*. RPP-16660, Rev. 0, CH2M HILL Hanford Group, Inc., Richland, Washington.

Julyk LJ and TC Mackey. 2003b. *Tank-Specific Allowable Dome Load for Hanford-Site 100-Series Single-Shell Tanks*. RPP-16363, Rev. 0, CH2M HILL Hanford Group, Inc., Richland, Washington.

Kollar L and E Dulacska. 1984. *Buckling of Shells for Engineers*. Wiley-Interscience, John Wiley & Sons, New York.

Mackey TC. 2012. *Analysis of Record Summary for Single-Shell Tanks*. RPP-11802, Rev. 3, CH2M HILL Hanford Group, Inc., Richland, Washington.

Mackey TC and LJ Julyk. 2004. *Soil Load Above Hanford Waste Storage Tanks*. WHC-SD-WM-TI-665, Rev. 0D, CH2M HILL Hanford Group, Inc., Richland, Washington.

Medwadowski SJ. 2004. "Buckling of Concrete Shells: An Overview." *Journal of the International Association for Shell and Spatial Structures* 45(1):51-63.

Popov EP and SJ Medwadowski. 1981. "Stability of Reinforced Concrete Shells: State-of-the-Art Overview." In *Concrete Shell Buckling, ACI SP-67*. American Concrete Institute, Detroit, Michigan.

Rifaey SH. 2002. *Single Shell Tank System Integrity Assessment Report*. RPP-10435, Rev. 0, CH2M HILL Hanford Group, Richland, Washington.

Rinker MW, SP Bapanapalli, JE Deibler, CE Guzman-Leong, KI Johnson, NK Karri, SP Pilli and SE Sanborn. 2010. *Single-Shell Tank Integrity Project Analysis of Record - Preliminary Modeling Plan for Thermal and Operating Loads*. RPP-46644, Rev. 0; PNNL-19338, Pacific Northwest National Laboratory, Richland, Washington.

Rinker MW, KI Johnson, SP Bapanapalli, NK Karri, JE Deibler, SP Pilli, CE Guzman-Leong, SE Sanborn, FG Abatt, JA Dewberry, BM Larsen, KL Stoops and LJ Julyk. 2011a. *Single-Shell Tank Integrity Project Analysis of Record: Hanford Type II Single-Shell Tank Thermal and Operating Loads and Seismic Analysis*. RPP-RPT-49989, Rev. 0; PNNL-20424, Pacific Northwest National Laboratory, Richland, Washington.

Rinker MW, KI Johnson, SP Bapanapalli, NK Karri, JE Deibler, SP Pilli, CE Guzman-Leong, SE Sanborn, FG Abatt, JA Dewberry, BM Larsen, KL Stoops and LJ Julyk. 2011b. *Single-Shell Tank Integrity Project Analysis of Record: Hanford Type III Single-Shell Tank Thermal and Operating Loads and Seismic Analysis*. RPP-RPT-49990, Rev. 0; PNNL-20739, Pacific Northwest National Laboratory, Richland, Washington.

Rohay AC and SP Reidel. 2005. *Site-Specific Seismic Site Response Model for the Waste Treatment Plant, Hanford, Washington*. PNNL-15089, Pacific Northwest National Laboratory, Richland, Washington.

Scordelis AC. 1981. "Stability of Reinforced Concrete Domes and Hyperbolic Paraboloid Shells." In *Concrete Shell Buckling, ACI SP-67*. American Concrete Institute, Detroit, Michigan.

Seide P. 1981. "Stability of Cylindrical Reinforced Concrete Shells." In *Concrete Shell Buckling, ACI SP-67*. American Concrete Institute, Detroit, Michigan.

Seide P, V Weingarten and S Masri. 1979. *Buckling Criteria and Application of Criteria to Design of Steel Containment Shell. Final Report. January 1978-March 1979*. NUREG/CR-0793, U.S. Nuclear Regulatory Commission, Washington, D.C.

Appendix A

Run 1, Baseline Case with Best Estimate Material Properties: Load Contributions

This page intentionally left blank.

Appendix A

Run 1, Baseline Case with Best Estimate Material Properties: Load Contributions

A.1 Individual Load Effect on Tank Forces and Moments

To understand the effect of each individual load on the tank demands, Figures A.1 through A.10 show the total forces and moments as well as the incremental forces and moments in the tank sections for each of the loads. The total force and moment figures (A.1, A.3, A.5, A.7, and A.9) show the total force or moment under the load steps for gravity only, ls2, ls3, peak, 53F, LC1, 80F, and LC9. Ls2 includes the effects of gravity and the waste load. Ls3 includes the effects of all mechanical loads – that is, gravity, waste load, and the concentrated load and surface load. Peak includes the effects of these mechanical loads and the thermal cycle up to peak temperature. 53F or 80F include the effects of these mechanical loads and the thermal cycle through the cool-down to stress-free temperature (53°F) or to the present day temperature (80°F). LC1 includes the effect of the mechanical loads through cool-down to stress-free temperature plus the effect of the ACI 349-06 (ACI 2007) load combination 1 load factors. LC9 includes the effect of the mechanical loads through cool-down to present-day temperature plus the effect of the ACI 349-06 load combination 9 load factors.

The incremental force and moment figures (A.2, A.4, A.6, A.8, and A.10) show the incremental force or moment demands for these load steps. To show the effect of adding a particular load to the tank, the force or moment of prior loads are subtracted. The TOLA model has non-linearities so the effect of the loading would be different if the loading order was different. The forces and moments of the gravity load remain the same as the total force and moment plots as the gravity load is the first applied.

Figure A.2 shows the incremental meridional force. Gravity load is shown to introduce large compressive forces in the slab, and smaller compressive forces in the roof and wall. Adding waste load (ls2) to the tank reduces the meridional force in the roof and wall to near zero and adds tensile forces in the slab. Adding the concentrated surface load and uniform surface load (ls3) adds some meridional compression to the roof, wall, and slab. Heating the tank to the peak temperature (ls6) has little effect in the roof, adds some compression in the wall, and adds significant compression in the slab. As the tank heats up, the slab, exposed to the hottest waste (described in Section 5.6) expands. This expansion is resisted by the surrounding soil and compression is introduced into the slab. The figure shows the thermal cycle through cool-down (to either 53°F or 80°F) by subtracting the mechanical loads (gravity, waste, and surface loads) from these cool-down steps (53F or 80F). The effect of the entire thermal cycle through cool-down is to add meridional tension to the roof, wall, and slab. However, this added tension is small compared to the compression added by the mechanical loads; therefore, as seen in Figure A.1, the roof, wall and slab remain in compression. The addition of load factors for ACI 349-06 LC1 adds compression to the roof, wall, and slab. The addition of load factors for ACI 349-06 LC9 also adds compression to the roof, wall and slab.

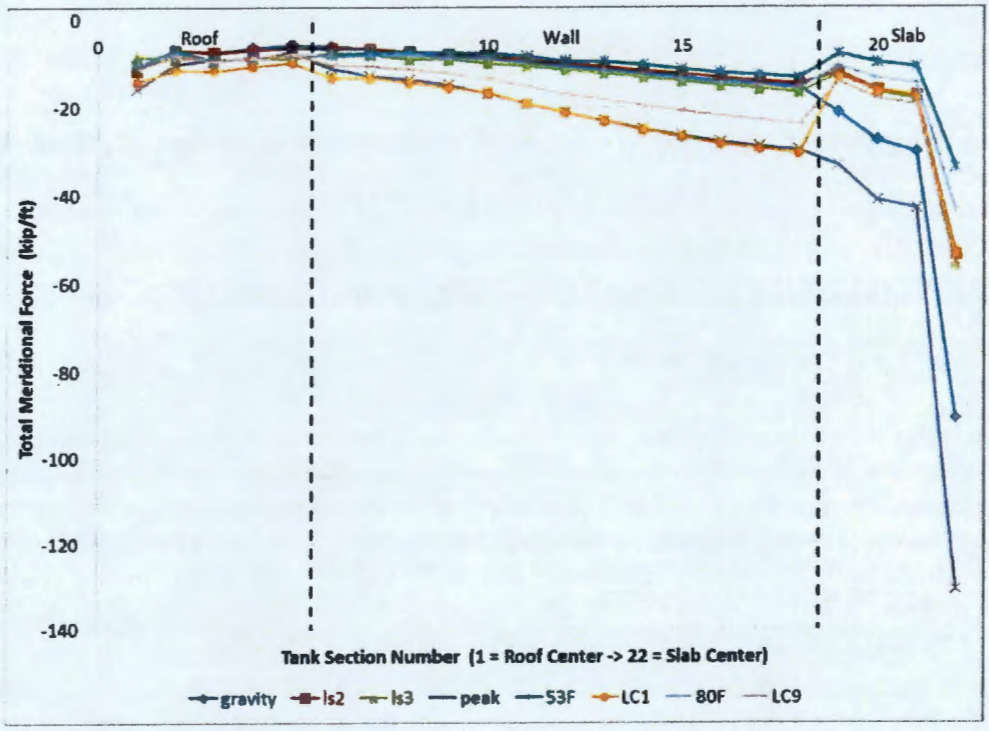

Figure A.1. Total Meridional Force for Run 1

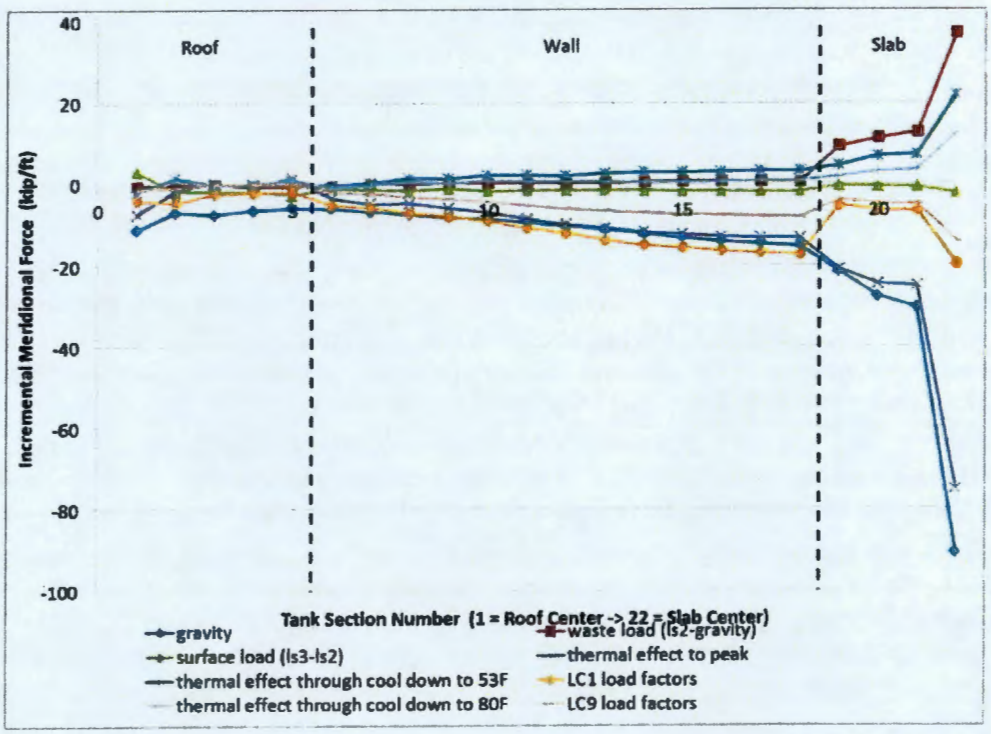

Figure A.2. Incremental Meridional Force for Run 1

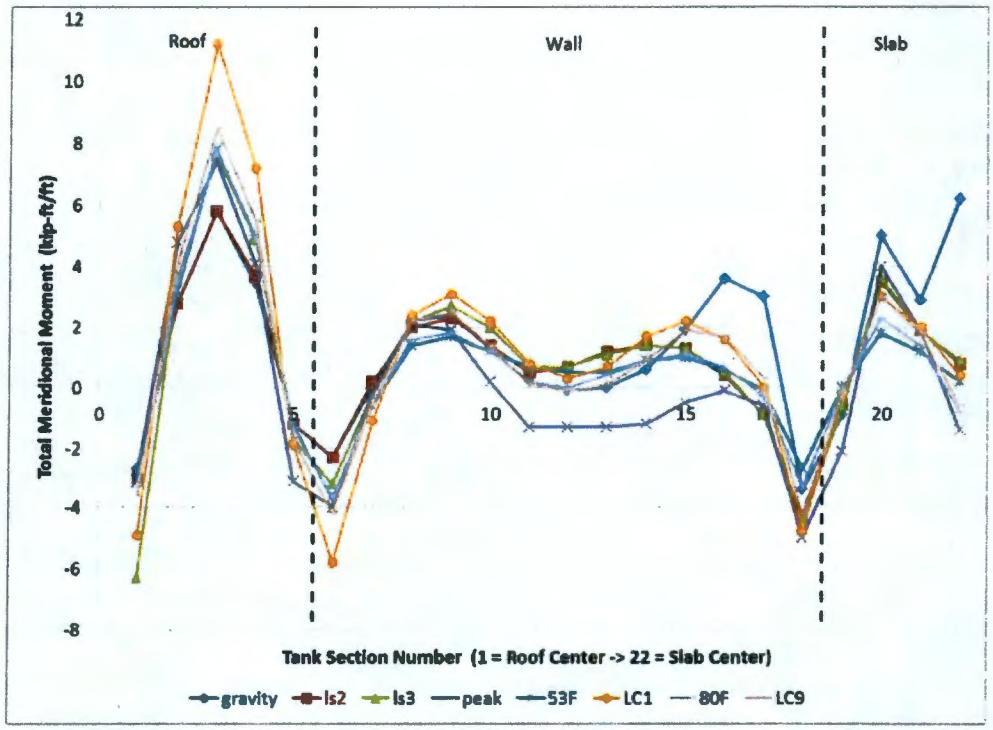

Figure A.3. Total Meridional Moment for Run 1

Figure A.4 shows the incremental meridional moment. Gravity load adds moment to the roof, wall and slab. Waste loads and concentrated and uniform surface loads reduce the moment in the roof, wall and slab. The effect of the thermal cycle through peak temperature is to change the sign of the moment in the mid and lower wall with only small changes in the roof and slab. The effect of the thermal cycle through either of the two cool down temperatures is to reduce the moment in the wall and only small changes in the roof and slab. The load factors from both ACI 349-06 LC1 and LC9 tend to add a small moment to the roof and wall with little effect on the slab.

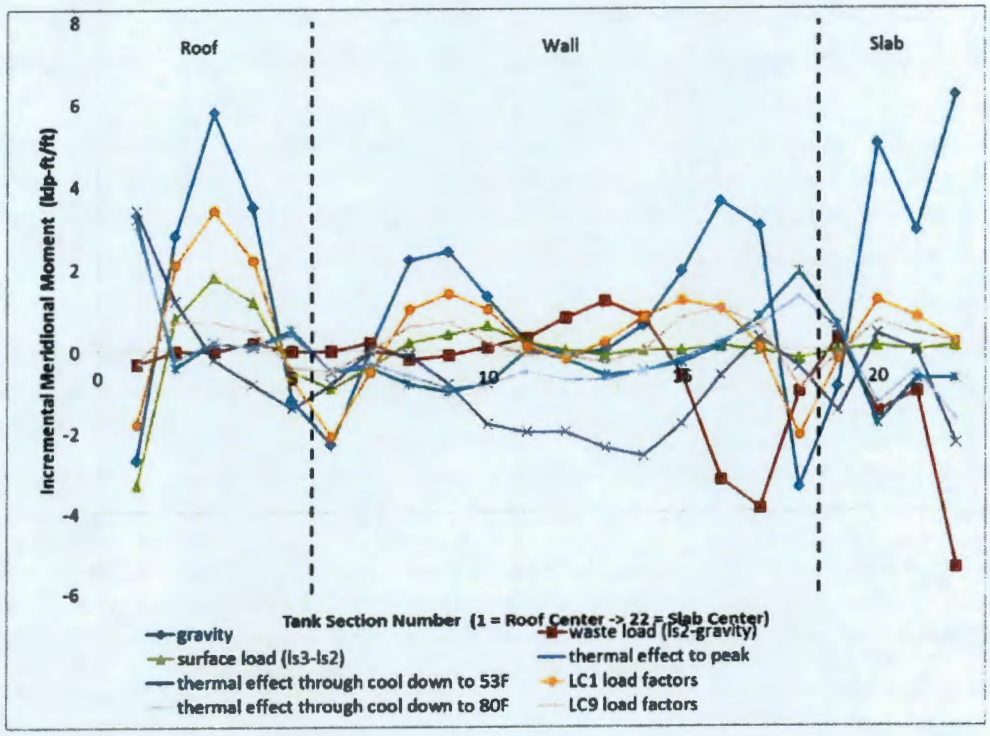

Figure A.4. Incremental Meridional Moment for Run 1

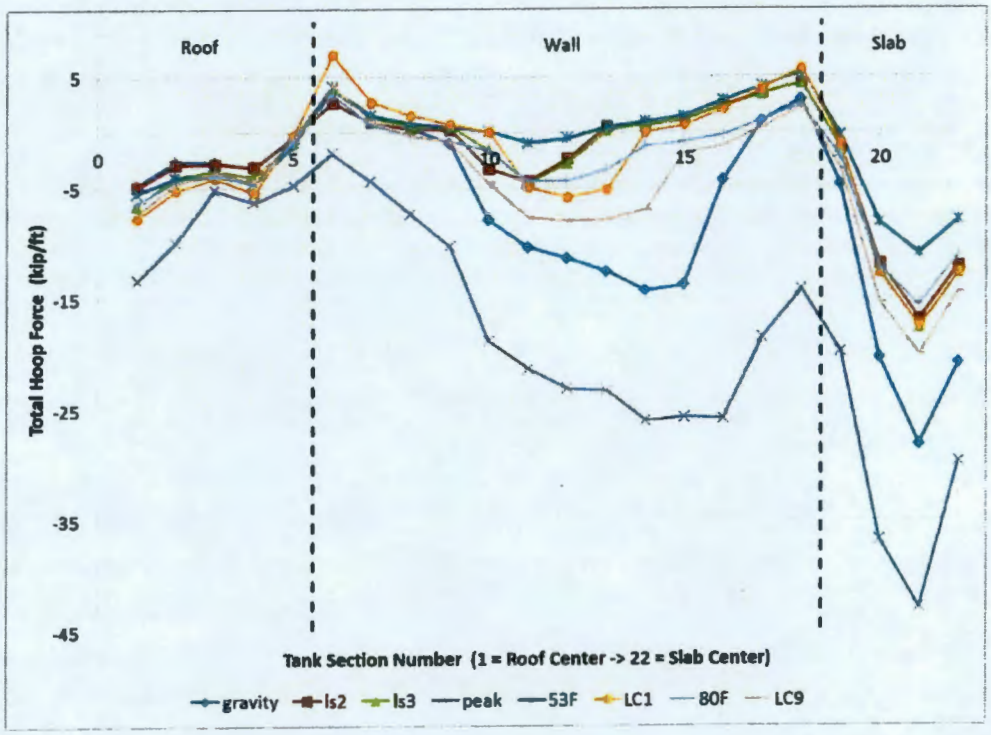

Figure A.5. Total Hoop Force for Run 1

Figure A.6 shows the incremental hoop force. Gravity load adds hoop compression to the roof, low hoop tension in the upper and lower wall and hoop compression to the slab. The waste load has little effect on the roof, and decreases the compressive force in the wall and slab. The addition of the concentrated and uniform surface loads has little effect on the hoop force. The effect of the thermal cycle to peak temperature is to add significant hoop compression to all locations in the tank. As the tank heats up, the surrounding soil resists the tank expansion, resulting in hoop compression. The effect of the thermal cycle through either of the cool-down states is to reduce the hoop compression in all locations. The upper and lower sections of the wall are in hoop tension, as can be seen in Figure A.5. The effect of the load factors for both ACI 349-06 LC1 and LC9 is to add hoop compression to the mid wall and slab with little change to the roof.

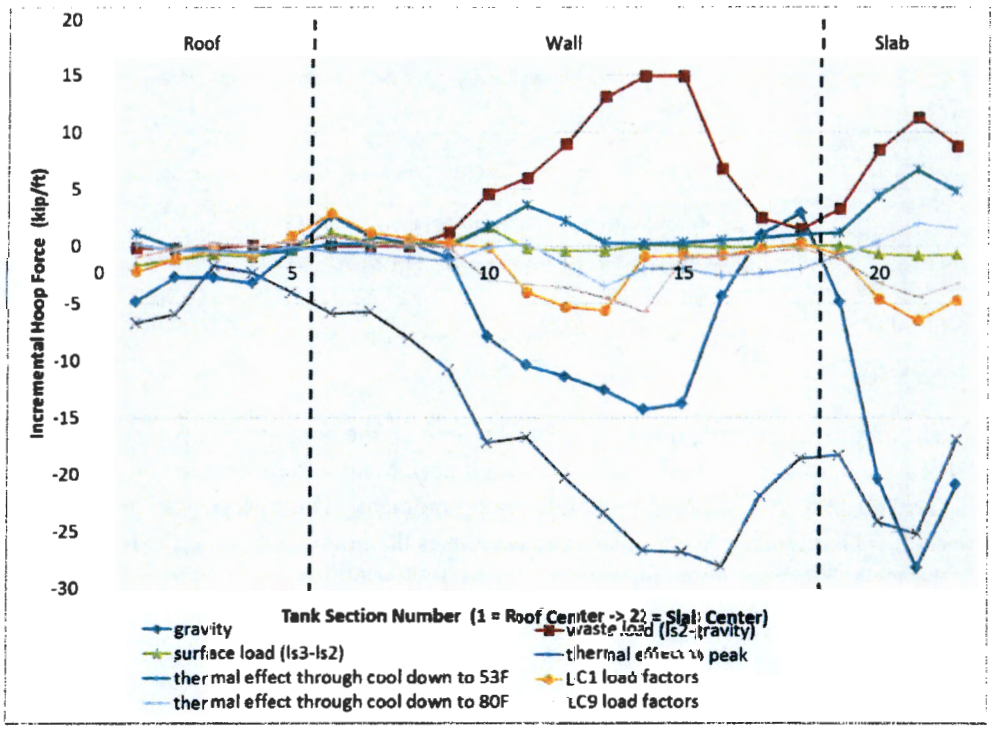

Figure A.6. Incremental Hoop Force for Run 1

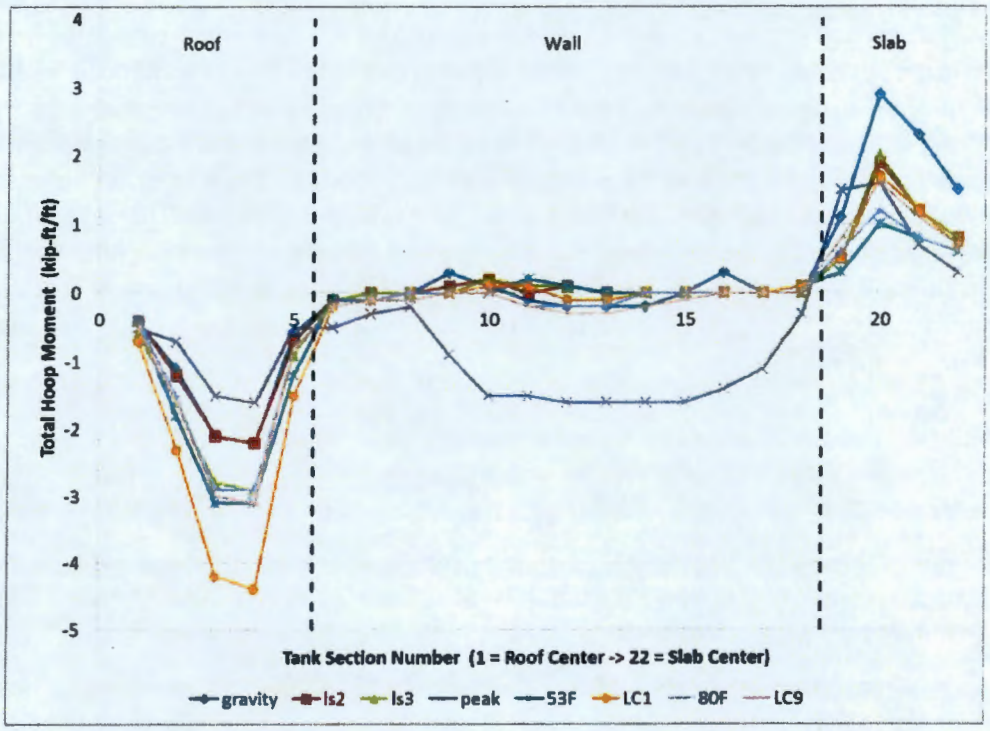

Figure A.7. Total Hoop Moment for Run 1

Figure A.8 shows the incremental hoop moment. In general, the hoop moments on the tank are small in magnitude. Gravity load and the thermal cycle through peak temperature have the largest effect on the hoop moment. The waste load has little effect on the hoop moment. The surface load increases the hoop moment in the roof. The thermal cycle to peak load decreases the hoop moment in the roof and increases the moment in the wall. The cool-down phases and the ACI 349-06 LC1 and LC9 load factors increase the hoop moment in the roof and decreases the hoop moment load in the wall.

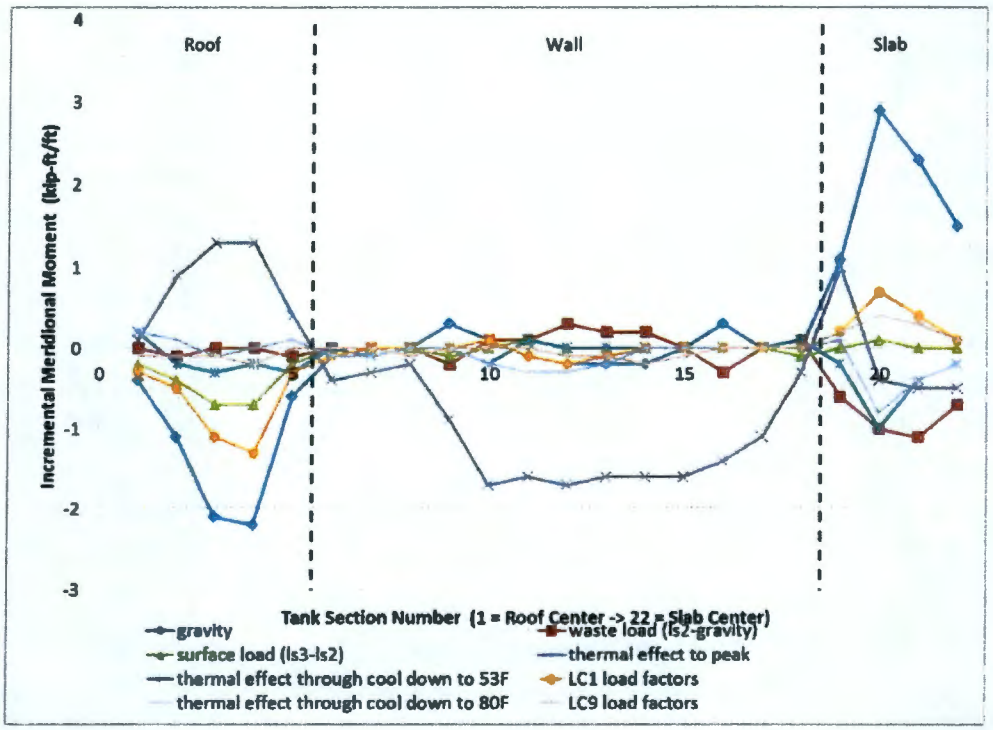

Figure A.8. Incremental Hoop Moment for Run 1

Figure A.9 shows the total shear force is greatest at inner slab. Figure A.10 shows the incremental shear forces. The gravity load has the greatest effect on the shear load in roof, upper and lower wall, and inner slab. The waste load reduces the shear in all locations. The concentrated and uniform surface loads have little effect on the shear throughout the tank. The thermal cycle through peak has minor effects to the shear in most locations and a larger effect on the inner slab. The effect of the thermal cycle through the two cool-down states decreases the shear at the inner slab with little effect elsewhere. The additional load factors for ACI 349-06 LC1 and LC9 increase the shear in the roof and slab.

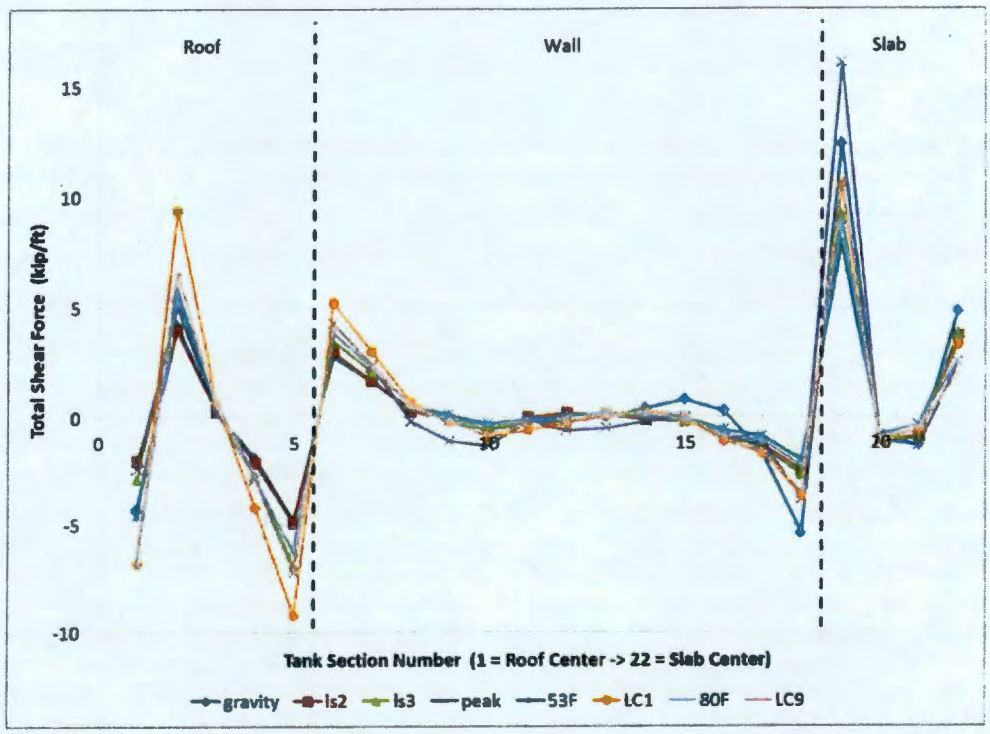

Figure A.9. Total Shear Force for Run 1

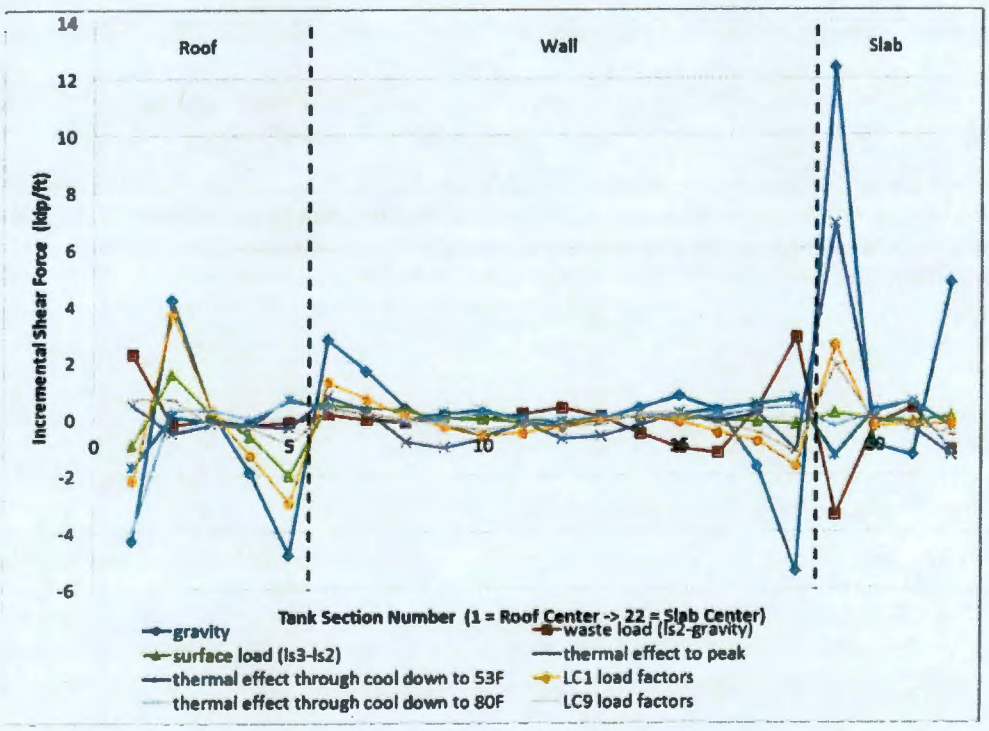

Figure A.10. Incremental Shear Force for Run 1

A.2 Load Effect on Sidewall Pressure

To further understand the effect that each load has, pressures the soil exerts on the tank sidewall are plotted for each load of Run 1.

Figure A.11 shows the sidewall pressures for each load step along with the "at-rest" pressure. The "at-rest" pressure is defined as the at-rest pressure coefficient (0.426) times the weight of the soil above that depth. The middle and lower wall are the most sensitive to the loads, particularly the thermal cycle. Appendix H of the Type II SST AOR (Rinker et al. 2011a) describes the reason for the disparity between the calculated soil pressure and the "at-rest" pressure as, "tank sidewall bending and the haunch carrying some sidewall soil load."

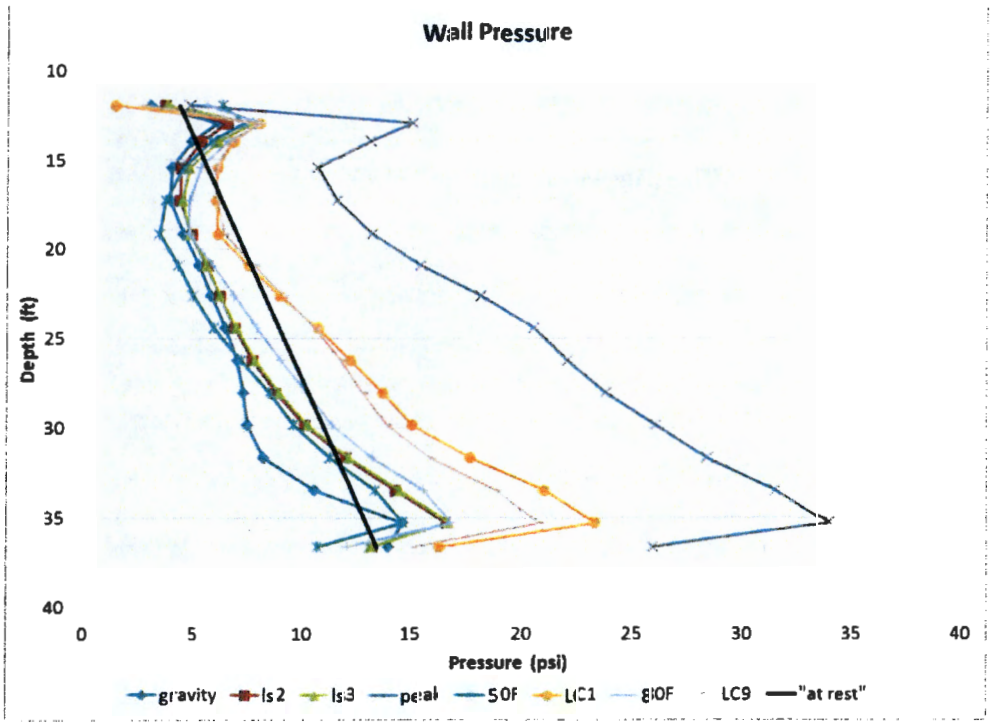

Figure A.11. Pressures on Sidewall due to Different Loads for Run 1

A.3 References

ACI. 2007. American Concrete Institute Code Requirements for Nuclear Safety Related Concrete Structures. ACI 349-06, American Concrete Institute, Farmington Hills, Michigan.

Rinker MW, KI Johnson, SK Bapanapalli, NK Karri, JE Deibler, SP Pilli, CE Guzman-Leong, SE Sanborn, FG Abatt, JA Dewberry, BM Larsen, KL Stoops, and LJ Julyk. 2011a. Single-Shell Tank Integrity Project Analysis of Record: Hanford Type II Single-Shell Tank Thermal and Operating Loads and Seismic Analysis. RPP-RPT-49989, Rev. 0, Pacific Northwest National Laboratory, Richland, Washington.

This page intentionally left blank.

Appendix B

Buckling Calculations in Mathcad™

This page intentionally left blank.

Appendix B

Buckling Calculations in Mathcad™

This appendix presents the concrete shell buckling calculations that were performed using the Mathcad™ software for the Type I single-shell tank analysis of record. Buckling analysis was performed for only the Type I tank wall. The tank roof was not considered since the flat roof is supported by the hatchway and it will not fail by buckling. The results of these calculations are summarized in Chapter 11.0 of this report. The Mathcad™ calculation sheets implement the buckling evaluation methods recommended by Johnson et al. (2010) plus the safety factors recommended by Medwadowski (2004) for the consideration of elastic versus plastic buckling.

B.1 References

Johnson KI, JE Deibler, FG Abatt, and MW Rinker. 2010. *Single-Shell Tank Structural Evaluation Criteria.* RPP-46442, Rev. 0, Pacific Northwest National Laboratory, Richland, Washington.

Medwadowski SJ. 2004. "Buckling of Concrete Shells: An Overview." *Journal of the International Association for Shell and Spatial Structures* 45(1):51-63.

Type I SST - Wall Buckling Evaluation for Bounding Temperature and 11.45-ft Soil Overburden

Type I, Analysis of Record, Wall Buckling Evaluation
Case 1. 11.45-ft Soil, 142-kip Concentrated Load, T=250F, 95/95 Lower Bound Concrete Properties

The following tank buckling evaluation method is described in the main body of the report and in the references provided at the end of this calculation.

Tank Wall Degraded Concrete Properties		**Tank Wall Reinforcing Steel Properties**
Maximum wall temperature during tank history = 250 F		Current maximum temp = 80 F for Type I SSTs
Elastic Modulus (95/95 at Temp)	$E_c := 2.5 \times 10^6 psi$	$E_s := 29.4 \times 10^6 psi$
Concrete Strength (95/95 at Temp), psi	$f_{c_min} := 3568 \cdot psi$	
Concrete Density,	$d_c := 145 \cdot pcf$	
Poisson's Ratio	$\nu := 0.15$	$\nu_s := 0.30$

Tank Geometry - from SST Type I Drawing # D-20

Type I Tank Wall Inner and Outer Radii $r_i := 10ft + 1in = 10.083ft$ $r_o := r_i + 12 \cdot in = 11.083 \cdot ft$

Tank cylinder mid-wall radius of curvature, R_c, inches $R_c := \frac{r_i + r_o}{2} = 10.583 \cdot ft$

Tank minimum wall thickness, t_w, inch $t_w := 12in$

Equivalent Tank Height - including half of Roof and Floor Heights

Flat Roof Thickness $h_d := 12 \cdot in$

Wall Height - bottom of footing to inside roof $h_w := 26ft + 1in = 313 \cdot in$

Dished Floor Depth $h_f := 6 \cdot in$

Equivalent Tank Height, L_{eq} $L_{eq} := h_w + \frac{h_d}{2} + \frac{h_f}{2} = 322 \cdot in$

Tank Cylindrical Wall Buckling (analytical solutions for Theoretical buckling loads are used)

Axial Compression

$$\sigma_{ca} := \frac{1}{\sqrt{3 \cdot (1 - \nu^2)}} \cdot E_c \cdot \left(\frac{t_w}{R_c}\right) = 1.379 \times 10^5 psi \qquad P_{ca} := 2 \cdot \pi \cdot R_c \cdot t_w \cdot \sigma_{ca} = 1.321 \times 10^9 lbf$$

Lateral Uniform Pressure on Tank Wall (Average Soil Pressure)

$h := t_w = 1ft$ $a := R_c = 10.583ft$ $E := E_c = 2.5 \times 10^6 psi$

$$k := \frac{h^2}{12 \cdot a^2} = 7.44 \times 10^{-4} \quad \lambda := \pi \cdot \frac{a}{L_{eq}} = 1.239 \quad \frac{L_{eq}}{a} = 2.535 \quad \frac{a}{h} = 10.583 \quad \beta := \frac{L_{eq}^2}{a \cdot h} = 68$$

Flugge, W., 1960, *Stresses in Shells*, Springer-Verlag, New York, New York.

(page 432, Eqn 20)

$$\varphi_{Flugge}(m,n,\nu,\lambda,k) := \frac{(1-\nu^2)\cdot(n\cdot\lambda)^4 + k\cdot\left[\left[(n\cdot\lambda)^2+m^2\right]^4 - 2\cdot\left[\nu\cdot(n\cdot\lambda)^6 + 3\cdot(n\cdot\lambda)^4\cdot m^2 \ldots + (4-\nu)\cdot(n\cdot\lambda)^2\cdot m^4 + m^6\right] \ldots + 2\cdot(2-\nu)\cdot(n\cdot\lambda)^2\cdot m^2 + m^4\right]}{m^2\cdot\left[(n\cdot\lambda)^2+m^2\right]^2 - m^2\cdot\left[3\cdot(n\cdot\lambda)^2+m^2\right]}$$

$m := 2 \quad n := 2$

Given

$m \geq 2$

$n \geq 1$

$\varphi_{Flugge}(m,n,\nu,\lambda,k) \geq 0$

$P(\nu,\lambda,k) := \text{Minimize}(\varphi_{Flugge}, m, n)$

$m_{min}(\nu,\lambda,k) := \text{round}(P(\nu,\lambda,k)_0)$

$n_{min}(\nu,\lambda,k) := \text{round}(P(\nu,\lambda,k)_1)$

$\varphi_{cr_Flugge}(\nu,\lambda,k) := \varphi_{Flugge}(m_{min}(\nu,\lambda,k), n_{min}(\nu,\lambda,k), \nu, \lambda, k)$

$p_{cr_Flugge}(E,\nu,\lambda,k) := \frac{E}{1-\nu^2}\sqrt{12\cdot k}\cdot\varphi_{cr_Flugge}(\nu,\lambda,k)$

Theoretical Lateral Buckling Pressure, P_{cl} $P_{cl} := p_{cr_Flugge}(E,\nu,\lambda,k) = 2667.6\,psi$

Buckling Load Reduction Factors

α_1 = The Geometric Imperfection Factor

For the Cylindrical wall under uniform lateral pressure $\alpha_{1c_lat} = 0.75$ (Seide, 1981)

For cylindrical wall under axial load $\alpha_{1c_axi} = 1 - 0.9\cdot\left(1 - \exp\left(\frac{-1}{16}\cdot\sqrt{\frac{R}{t}}\right)\right)$

which is valid for $100 \leq \frac{R_c}{t_w} \leq 3000$ and $0.5 \leq \frac{L_{eq}}{R_c} \leq 5$

but $\frac{R_c}{t_w} = 10.583 \quad \frac{L_{eq}}{R_c} = 2.535$

Hence, conservatively assume R/t=100 $\alpha_{1c_axi} := 1 - 0.9\cdot\left(1 - \exp\left(\frac{-1}{16}\sqrt{100}\right)\right) = 0.582$

Recommended Values

$\alpha_{1c_axi} := 0.58$ for axial compression of a cylinder

$\alpha_{1c_lat} := 0.75$ for external lateral pressure

α_2 = The Creep Buckling Load-Reduction Factor

Creep Strain after 67 years at 250F, using Hanford concrete creep model in Johnson et al. (2010), Appendix A

$Tc := 250$ $\quad tim := 67 \cdot 365.25 = 24472\ days$ $\quad mcp := -0.838$

$Xi := 226.09 - 0.00429 \cdot Tc + 147.53 \cdot Tc^{-0.387} - 309.26 \cdot Tc^{-0.044} = 1.906$

Creep Compliance. $CrpCmpl := e^{-3.3} \cdot \frac{Xi \cdot tim^{(mcp+1)}}{(mcp+1)1psi} = 2.231 \frac{1}{psi}$ (1e-6 in/in)/psi stress

Concrete Stress at Mid-Wall, (Weight of Soil+Roof+MidWall) / Wall Area

$Soil := \pi \cdot r_o^2 \cdot 11.45ft \cdot 125 \frac{lbf}{ft^3} = 5.523 \times 10^5 lbf$ $\quad Roof := \pi \cdot r_o^2 \cdot 1ft \cdot 145 \frac{lbf}{ft^3} = 5.596 \times 10^4 lbf$

$MidWall := 2 \cdot \pi \cdot R_c \cdot \frac{26.083}{2} ft \cdot t_w \cdot 145 \frac{lbf}{ft^3} = 1.257 \times 10^5 lbf$

$TWt := Soil + Roof + MidWall = 7.34 \times 10^5 lbf$ $\quad Area := 2 \cdot \pi \cdot r_o \cdot t_w = 69.639 ft^2$ $\quad WallStr := \frac{-TWt}{Area} = -73.2 psi$

Creep Strain at Mid Wall (Creep Compliance x Stress) $\quad Crpstr := CrpCmpl \cdot \frac{WallStr}{1000000} = -1.633 \times 10^{-4} \frac{in}{in}$

Initial Elastic Strain $\quad Elstrain := \frac{WallStr}{E_c} = -2.928 \times 10^{-5}$

C_u = ultimate creep strain / initial elastic strain $\quad C_{ua} := \frac{Crpstr}{Elstrain} = 5.578$ $\quad \alpha_{2a} := \frac{1}{(1 + C_{ua})} = 0.152$

If a creep analysis is not available, Popov and Medwadowski (1981) recommend the following as an estimate of the ultimate creep coefficient, C_u:

$C_u = 4 - 2\log(f_c)$ where f_c is the concrete strength (N/mm^2) at the time of sustained loading.

$f_c := \frac{f_{c\ min}}{\frac{N}{mm^2}} = 24.6$ $\quad C_{ub} := 4 - 2 \cdot \log(f_c) = 1.218$ $\quad \alpha_{2b} := \frac{1}{(1 + C_{ub})} = 0.451$

Use the maximum C_u to obtain minimum creep reduction factor $\quad C_u := \max(C_{ua}, C_{ub}) = 5.578$

$\alpha_2 := \frac{1}{(1 + C_u)} = 0.152$

α_3 = The Buckling Load-Reduction Factor Accounting for Cracking and the Amount and Type of Reinforcement.

E_{C2eol} is the effective concrete modulus in the wall accounting for creep strain and end-of-life degraded concrete modulus, E_{Ceol}.

Use the degraded concrete modulus based on thermal history

$E_{Ceol} := E_c = 2.5 \times 10^6 psi$ $\quad E_{C2eol} := \frac{E_{Ceol}}{(1 + C_u)} = 3.801 \times 10^5 psi$ $\quad n := \frac{E_s}{E_{C2eol}} = 77.352$

Rebar Reinforcement Fractions

Meridional Rebar - from SST Type-I Drawing # D-21

$Bar_m := 8$ Rebar Size (in 1/8th of an inch).

$S_{pm} := 12$ Maximum Bar Spacing (inches) near inner and outer wall surfaces **Mid Height of 12" Thick Wall**

$$A_{sm} := 2 \cdot \left(\frac{Bar_m}{8}\right)^2 \cdot \frac{\pi}{4} \cdot \frac{12}{S_{pm}} = 0.884 \quad \text{Steel Area, in}^2\text{/ft}$$

$$A_c := 12 \cdot \frac{t_w}{in} = 144 \quad \text{Concrete Area, in}^2\text{/ft} \qquad \rho_m := \frac{A_{sm}}{A_c} = 0.00614$$

Hoop Rebar - from SST Type-I Drawing # D-21

$Bar_h := 5$ Rebar Size (in 1/8th of an inch).

$S_{ph} := 12$ Bar Spacing (inches) near inner and outer wall surfaces. **Mid Height of 12" Thick Wall**

$$A_{sh} := 2 \cdot \left(\frac{Bar_h}{8}\right)^2 \cdot \frac{\pi}{4} \cdot \frac{12}{S_{ph}} = 0.614 \quad \text{Steel Area, in}^2\text{/ft} \qquad \rho_h := \frac{A_{sh}}{A_c} = 0.00426$$

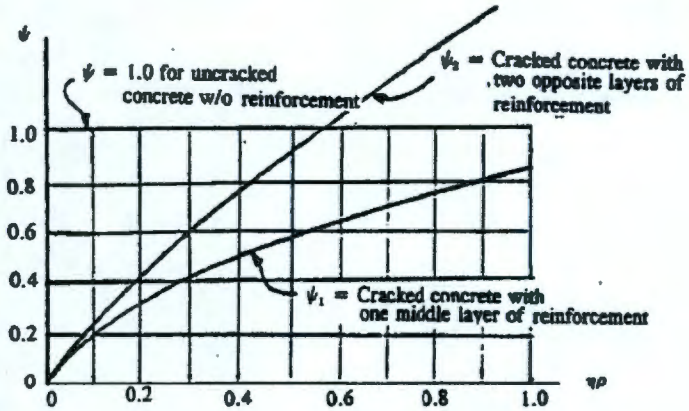

Values of ψ for Effect of Concrete Cracking And Amounts and Type of Reinforcement (Figure 4 of Scordelis 1981).

Must interpolate by eye

From the above plot for cracked concrete with two opposite layers of reinforcement.

Meridional Rebar $n \cdot \rho_m = 0.475$ $\psi_m := 0.92$

Hoop Rebar $n \cdot \rho_h = 0.33$ $\psi_h := 0.65$

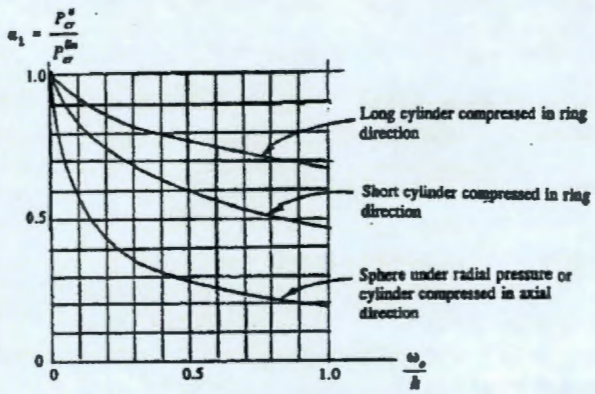

Effect of Geometric Imperfections on Buckling Load (Figure 3 of Scordelis 1981).
ω_0/h factors for different geometries for specified geometric imperfection factor, α_1.

Must interpolate by eye

Tank Wall, Axial Load: Cylinder compressed in axial direction

$\alpha_{1c_axi} := 0.58$ $\omega_{ohc_axi} := 0.1$

Tank Wall, Lateral Pres: Short cylinder compressed in ring direction

$\alpha_{1c_lat} := 0.74$ $\omega_{ohc_lat} := 0.20$

Pacific Northwest National Laboratory
Type I Wall Buckling Evaluation
Case 1. 11.45-ft Soil, 142-kip Concentrated Load,
T=250F, 95/95 Lower Bound Concrete Properties

Page 6 of 13
Date: 7/18/2014 By: K. I. Johnson
Chkd: 8/09/2014 By: N. K. Karri
Revised: 9/09/2014 By: K. I. Johnson

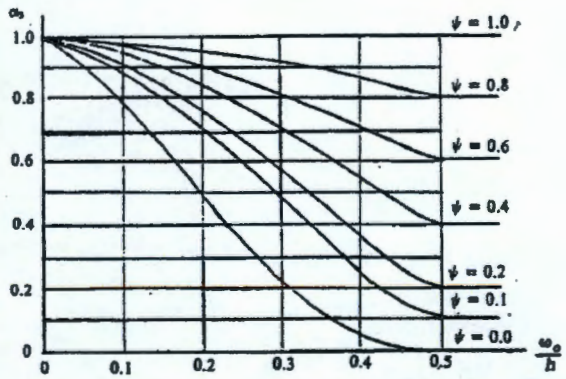

Reduction Factor α_3 for Concrete Cracking and Amount and Type of Reinforcement (Figure 5 of Scordelis 1981)

Must interpolate by eye

Tank Wall, Axial Load: cylinder compressed in axial direction (Meridional Rebar)

$\alpha_{1c_axi} = 0.58$ $\omega_{ohc_axi} = 0.1$ $\psi_m = 0.92$ $\alpha_{3c_axi} = 0.98$

Tank Wall, Lateral Pres: short cylinder compressed in ring direction (Hoop Rebar)

$\alpha_{1c_lat} = 0.74$ $\omega_{ohc_lat} = 0.2$ $\psi_h = 0.65$ $\alpha_{3c_lat} = 0.92$

Calculate $P_3 = \alpha_1\alpha_2\alpha_3 P_{buckle}$ and α_4 for highly loaded nonlinear concrete material effects

Axial Compressive Pressure on Cylindrical Wall, psi

$P_{3c_axi} := \alpha_{1c_axi} \cdot \alpha_2 \cdot \alpha_{3c_axi} \cdot \alpha_{ca} = 11920.4\,psi$ $\quad E_{3c_axi} := 2 \cdot \pi \cdot R_c \cdot t_w \cdot P_{3c_axi} = 1.14 \times 10^8\,lbf$

Ultimate axial force of concrete

Degraded Concrete Strength $f_{c_min} = 3568\,psi$ $\quad E_{ult_axi} := 2 \cdot \pi \cdot R_c \cdot t_w \cdot f_{c_min} = 3.42 \times 10^7\,lbf$

$Raxi(\alpha_4) := (\alpha_4)^2 \left(\frac{P_{3c_axi}}{f_{c_min}}\right)^2 + (\alpha_4 - 1)$ $\quad \alpha_{4axi} := root(Raxi(\alpha_4), \alpha_4, 0.01, 0.99) = 0.258$

Total Axial Load Reduction Factor $\alpha_{dc} := \alpha_{1c_axi} \cdot \alpha_2 \cdot \alpha_{3c_axi} \cdot \alpha_{4axi} = 0.022$

Reduced Axial Wall Buckling Pressure, psi $P_{c_axi_red} := \alpha_{4axi} \cdot P_{3c_axi} = 3073.8\,psi$

Reduced Axial Wall Buckling Force, psi $E_{c_axi_red} := P_{c_axi_red} \cdot 2 \cdot \pi R_c \cdot t_w = 2.943 \times 10^7\,lbf$

$tons := E_{c_axi_red} = 14716 \cdot tonf$

Lateral External Pressure on **Short** Cylindrical Wall, psi

$P_{3c_lat} := \alpha_{1c_lat} \cdot \alpha_2 \cdot \alpha_{3c_lat} \cdot P_{cl} = 276.1\,psi$

Cylinder compressive hoop stress $\sigma_{hoop} := \frac{P_{3c_lat} \cdot R_c}{t_w} = 2922.2\,psi$

$Rlat(\alpha_4) := (\alpha_4)^2 \left(\frac{\sigma_{hoop}}{f_{c_min}}\right)^2 + (\alpha_4 - 1)$ $\quad \alpha_{4lat} := root(Rlat(\alpha_4), \alpha_4, 0.01, 0.99) = 0.685$

Total Laterial Pressure Reduction Factor $\alpha_{dc} := \alpha_{1c_lat} \cdot \alpha_2 \cdot \alpha_{3c_lat} \cdot \alpha_{4lat} = 0.071$

Reduced Lateral Buckling Pressure, Short Wall $P_{c_lat_red} := \alpha_{4lat} \cdot P_{3c_lat} = 189.2\,psi$

Ultimate Lateral Pressure for concrete strength $P_{ult_lat} := f_{c_min} \cdot \frac{t_w}{R_c} = 337.13\,psi$

Applied Loads on the Tank Wall

Axial Compressive Stress at the Mid-Height of the Wall

This includes the total weight of the soil, uniform live load, concentrated live load, and the weight of the roof and wall concrete.

Finite Element Results for Axial Compression at the Mid-Height of the Wall, (F = 20.8 kip/ft)

Meridional Section Force, Loadstep 3, Gravity Loads $E_{c_axi} := 20.8 \frac{kip}{ft} 2 \cdot \pi \cdot R_c = 1.38 \times 10^6\,lbf$

Wall Lateral Earth Pressure calculated as the at rest soil pressure at depth=25.49-ft, Type-I tank ht=27-ft 1-in from bottom of footing to top of flat roof, Soil depth=11.45-ft.

Soil internal friction angle, φ $\varphi := 35\,deg$ $k_o := 1 - \sin(\varphi) = 0.426$

Soil Density, d_s $d_s := 125\,pcf$

Soil Overburden Depth $h_{soil} := 11.45\,ft$ $h_w = 26.083\,ft$ $h_d = 1\,ft$

Soil Depth at Midwall $h_{mid} := \frac{h_w}{2} + h_d + h_{soil} = 25.49\,ft$

Lateral Soil Pressure at Mid-Wall $P_{lat} := k_o \cdot d_s \cdot h_{mid} = 9.4\,psi$

Wall Buckling - Linear Combination of Axial and Lateral Loads

Applied Axial Wall Compression, lbf $F_{c_axi} = 1.383 \times 10^6\,lbf$

Reduced Axial Wall Capacity, lbf $F_{c_axi_red} = 2.943 \times 10^7\,lbf$

Applied Lateral Wall Pressure, psi $P_{lat} = 9.4\,psi$

Reduced Lateral Wall Pressure Capacity, psi $P_{c_lat_red} = 189.2\,psi$

Safety Factors Considering Elastic or Plastic Buckling plus External Pressure and Axial Loads

Per Kollar and Dulacska (1984), different safety factors are needed depending on the type of load (dead or live) and depending on the failure mode (elastic or plastic buckling) and the stability of the post buckled condition. Also the interaction with other loads must be considered.

In the present calculations, Axial Compression is conservatively treated as a live load. External Pressure on the tank cylinder is treated as a dead load. The following appropriate safety factors can then be imposed:

Safety Factor

Elastic buckling $k_{el} = \begin{pmatrix} 3.5 \\ 1.75 \end{pmatrix}$ unstable post-buckling (Axial Compression Load)
stable post-buckling (Wall External Pressure)

Plastic buckling $k_{pl} = \begin{pmatrix} 1.5 \\ 1.7 \end{pmatrix}$ dead loading = Wall Lateral Pressure
live loading = Axial Compression Load

Elastic Buckling Safety Factors for Axial Compression (C) and External Pressure (U) Loads

From the IASS Working Group No. 5, *Recommendations for Reinforced Concrete Shells and Folded Plates*, (IASS, 1979):
For shells that do not experience a reduction in load-carrying capacity in the post-buckling regime, a factor of safety of 1.75 is recommended. For shells that do experience a reduction in the load-carrying capacity in the post-buckling regime, a factor of safety of 3.5 is recommended.

Wall Uniform Axial Compression $SF_{c_axi} := 3.5$ Post Buckling = Reduced Load Capacity

Wall Lateral External Pressure $SF_{c_lat} := 1.75$ Post Buckling = Displacement Controlled Loading, Soil Pressure is Self Relieving

The allowable load for each load type (Axial Compression Load vs. Lateral External Pressure) acting alone can be determined.

using the ***quadratic*** Dunkerley type relation

$$\left(\frac{k_{el}\cdot p_{cr_allow}}{p_{cr_el_upper}}\right)^2 + \left(\frac{k_{pl}\cdot p_{cr_allow}}{p_{pl}}\right)^2 = 1$$

which gives

$$p_{cr_allow} = \frac{p_{cr_el_upper}}{k_{el}}\cdot\sqrt{\frac{1}{1+\left(\frac{k_{pl}}{k_{el}}\cdot\frac{p_{cr_el_upper}}{p_{pl}}\right)^2}} \qquad \lambda = \frac{p_{pl}}{p_{cr_el_upper}} = \frac{p_{ult}}{p_3}$$

or

$$p_{allow_qD}(k_{el}, k_{pl}, p_3, \lambda) := \frac{p_3}{k_{el}}\cdot\sqrt{\frac{1}{1+\left(\frac{k_{pl}}{k_{el}}\cdot\frac{1}{\lambda}\right)^2}}$$

Interaction between Lateral External Pressure and Axial Compression must satisfy the following.

Axial Compression Loads = P_c

Lateral Pressure = P_u

$$\frac{p_{u_applied}}{p_{u_allow}} + \frac{p_{c_applied}}{p_{c_allow}} \le 1$$

Hence, for a given $p_{u_applied}$ the maximum $p_{c_applied}$ is given by

$$p_{c_applied_max} \le p_{c_allow}\cdot\left(1 - \frac{p_{u_applied}}{p_{u_allow}}\right)$$

using the ***quadratic*** Dunkerley type relation for allowable loads

$$p_{c_max}(k_{el_c}, k_{pl_c}, p_{3_c}, \lambda_c, k_{el_u}, k_{pl_u}, p_{3_u}, \lambda_u, p_{u_app}) := \left| \begin{array}{l} p_{c_allow} \leftarrow p_{allow_qD}(k_{el_c}, k_{pl_c}, p_{3_c}, \lambda_c) \\ p_{c_allow}\cdot\left(1 - \dfrac{p_{u_app}}{p_{allow_qD}(k_{el_u}, k_{pl_u}, p_{3_u}, \lambda_u)}\right) \end{array} \right.$$

Method 1.

Substituting the Type I Limit Loads and the Critical Buckling Loads

Axial Compression on Cylinder (C)	External Lateral Pressure (U)	Notes
$k_{el_c} := 3.5$	$k_{el_u} := 1.75$	Axial Post Buckling has Reduced Load Capacity
$k_{pl_c} := 1.7$ (live load)	$k_{pl_u} := 1.5$	Axial = part live, Lateral = dead
$P_{ult_c} := E_{ult_axi} = 3.417 \times 10^7\,lbf$	$P_{ult_u} := P_{ult_lat} = 337.1\,psi$	Axial and Lateral Limit Loads
$P_{3dc} := E_{3c_axi} = 1.141 \times 10^8\,lbf$	$P_{3du} := P_{3c_lat} = 276.1\,psi$	Linear Buckling loads times $\alpha_1\alpha_2\alpha_3$
$\lambda_c := \frac{P_{ult_c}}{P_{3dc}} = 0.299$	$\lambda_u := \frac{P_{ult_u}}{P_{3du}} = 1.221$	Ratio of limit load / reduced elastic buckling load

Applied Axial Force on Walls including Soil, Concrete Wt, Uniform Surface Load $\quad p_{c_app} := E_{c_axi} = 1.383 \times 10^6\,lbf$

Applied Lateral External Pressure on Walls $\quad p_{u_app} := P_{lat} = 9.436\,psi$

The multiple safety factor approach gives:

$p_{c_allow} := p_{allow_qD}(k_{el_c}, k_{pl_c}, P_{3dc}, \lambda_c) = 1.711 \times 10^7 \cdot lbf$ Axial Compression

$p_{u_allow} := p_{allow_qD}(k_{el_u}, k_{pl_u}, P_{3du}, \lambda_u) = 129.135 \cdot psi$ Lateral Pressure

$p_{cmax} := p_{c_max}(k_{el_c}, k_{pl_c}, P_{3dc}, \lambda_c, k_{el_u}, k_{pl_u}, P_{3du}, \lambda_u, p_{u_app}) = 1.586 \times 10^7 \cdot lbf$

Calculate the Demand/Capacity ratio as the linear interaction of the Lateral Pressure and Axial Compression loads divided by their respective allowable loads $\quad R_{combined} := \frac{p_{u_app}}{p_{u_allow}} + \frac{p_{c_app}}{p_{c_allow}} = 0.15$

The Axial Compression load is also a smaller fraction of the maximum value $\quad R_c := \frac{p_{c_app}}{p_{cmax}} = 0.09$

Method 2.

A different approach is recommended by Medwadowski (2004) in "Buckling of Concrete Shells: An Overview," IASS Journal Vol. 45 (2004) n.1, pp 51-63. The point of separation between the buckling mode of failure and the ultimate load failure occurs when

$$\frac{\alpha_1 \cdot p_{cr_lin}}{k_{buckling}} = \frac{p_{ult}}{k_{material}}$$

with safety factors $\quad k_{buckling} := 3.5$

$k_{material} := 1.75$

Hence, the buckling mode of failure governs if

$$\alpha_1 \cdot p_{cr_lin} < \frac{k_{buckling}}{k_{material}} \cdot p_{ult} = 2 \cdot p_{ult} \text{ or } \quad \frac{\alpha_1 \cdot p_{cr_lin}}{p_{ult}} < 2$$

That is, buckling governs when the critical buckling load times the geometric imperfection factor is less than 2 times the ultimate failure load.

so the applied safety factor to be used is $k_{buckling}$ otherwise use $k_{material}$ when $\alpha_1 \cdot p_{cr_lin} > 2 \cdot p_{ult}$

Substituting	Axial Compression Load	External Lateral Pressure
	$p_{cr_lin_c} := P_{ca} = 1.321 \times 10^9\,lbf$	$p_{cr_lin_u} := P_{cl} = 2.668 \times 10^3\,psi$
	$\alpha_{1_c} := \alpha_{1c_axl} = 0.58$	$\alpha_{1_u} := \alpha_{1c_lat} = 0.74$
	$P_{ult_c} = 3.417 \times 10^7\,lbf$	$P_{ult_u} = 337.134\,psi$
	$\frac{\alpha_{1_c} \cdot p_{cr_lin_c}}{P_{ult_c}} = 22.423 \quad > 2$	$\frac{\alpha_{1_u} \cdot p_{cr_lin_u}}{P_{ult_u}} = 5.855 \quad > 2$
so	$k_{pl_c} := k_{material} = 1.75$	$k_{pl_u} := k_{material} = 1.75$
	$k_{el_c} := k_{material} = 1.75$	$k_{el_u} := k_{material} = 1.75$

$p_{c_allow} := p_{allow_qD}(k_{el_c}, k_{pl_c}, P_{3dc}, \lambda_c) = 1.87 \times 10^7 \cdot lbf$ Axial Compression

$p_{u_allow} := p_{allow_qD}(k_{el_u}, k_{pl_u}, P_{3du}, \lambda_u) = 122.064 \cdot psi$ Lateral Pressure

$p_{cmax} := p_{c_max}(k_{el_c}, k_{pl_c}, P_{3dc}, \lambda_c, k_{el_u}, k_{pl_u}, P_{3du}, \lambda_u, p_{u_app}) = 1.726 \times 10^7 \cdot lbf$

Calculate the Demand/Capacity ratio as the linear interaction of the Lateral Pressure (U) and Axial Compression (C) loads divided by their respective allowable loads

$$R_{combined} := \frac{p_{u_app}}{p_{u_allow}} + \frac{p_{c_app}}{p_{c_allow}} = 0.151$$

The Axial Compression load is also a smaller fraction of the maximum value

$$R_c := \frac{p_{c_app}}{p_{cmax}} = 0.08$$

Method 3. (Preferred Approach)

However, if the allowable loads are calculated by $p_{allow}(\alpha_4, p_3, k_{SF}) := \frac{\alpha_4 \cdot p_3}{k_{SF}}$

Axial Compression Load (C)	External Lateral Pressure (U)
$p_{cr_lin_c} = 1.321 \times 10^9\,lbf$	$p_{cr_lin_u} = 2.668 \times 10^3\,psi$
$\alpha_{1_c} = 0.58$	$\alpha_{1_u} = 0.74$
$\zeta_{w_c} := (\omega_{ohc_axl}) = 0.1$	$\zeta_{w_u} := (\omega_{ohc_lat}) = 0.2$
$P_{ult_c} = 3.417 \times 10^7\,lbf$	$P_{ult_u} = 337.134\,psi$
$P_{3dc} = 1.141 \times 10^8\,lbf$	$P_{3du} = 276.11\,psi$
$\alpha_{4dc} := \alpha_{4axl} = 0.258$	$\alpha_{4du} := \alpha_{4lat} = 0.685$
$p_{c_app} = 1.383 \times 10^6\,lbf$	$p_{u_app} = 9.436\,psi$

From Eqns 26b and 22 in Medwadowski "Buckling of Concrete Shells: An Overview," IASS Journal Vol. 45 (2004) n.1, pp 51-63,

$$k_{SF}(\zeta_w, \alpha_1, p_{cr_lin}, p_{ult}) := \begin{cases} 1.75 & \text{if } \alpha_1 \cdot p_{cr_lin} > 2 \cdot p_{ult} \\ 2.5 + \exp(-1.5 \cdot \zeta_w) & \text{otherwise} \end{cases}$$

$k_{SF_c} := k_{SF}(\zeta_{w_c}, \alpha_{1_c}, p_{cr_lin_c}, p_{ult_c}) = 1.75$ Axial Compression

$k_{SF_u} := k_{SF}(\zeta_{w_u}, \alpha_{1_u}, p_{cr_lin_u}, p_{ult_u}) = 1.75$ Lateral Pressure

$p_{c_allow} := p_{allow}(\alpha_{4dc}, p_{3dc}, k_{SF_c}) = 1.682 \times 10^7 \cdot lbf$ Axial Compression

$p_{u_allow} := p_{allow}(\alpha_{4du}, p_{3du}, k_{SF_u}) = 108.099 \cdot psi$ Lateral Pressure

$$p_{c_max} := p_{c_allow} \cdot \left(1 - \frac{p_{u_app}}{p_{u_allow}}\right) = 1.535 \times 10^7 \cdot lbf$$

Calculate the Demand/Capacity ratio as the linear interaction of the Lateral Pressure and Axial Compression loads divided by their respective allowable loads

$$R_{combined} := \frac{p_{u_app}}{p_{u_allow}} + \frac{p_{c_app}}{p_{c_allow}} = 0.17$$

The Axial Compression load is also a smaller fraction of the maximum value

$$R_c := \frac{p_{c_app}}{p_{c_max}} = 0.09$$

Method 3 gives slightly higher D/C ratios than method 2 in this case.

In conclusion, the results given with Method 2 and Method 3 from Medwadowski (2004) are similar to those given by Method 1 using the multiple safety factors recommended by Kollar and Dulacska (1984). The combined Demand/Capacity ratio for the contributions of Lateral External Pressure and Axial Compression loads is 0.17, and the applied Axial Compressive load is a small fraction (0.09) of the maximum allowable axial wall compression.

Therefore, this evaluation shows that the Type I tank wall loaded with 11.45-ft of soil and a concentrated load of 142 kips passes the buckling evaluation criteria.

References

Baker EH, L Kovalevsky, and FL Rish. 1972. *Structural Analysis of Shells*. McGraw-Hill, New York, New York.

Fitch, JR and B Budiansky. 1970. "Buckling and Postbuckling Behavior of Spherical Caps under Axisymmetric Load." AIAA Journal, Vol. 8, No. 4, pp. 686-693.

Flugge, W., 1960, *Stresses in Shells*, Springer-Verlag, New York, New York.

IASS. 1979. *Recommendations for Reinforced Concrete Shells and Folded Plates*. Prepared by the Working Group No. 5 of The International Association for Shell and Spatial Structures (IASS), Stefan J. Medwadowski, Chairman. International Association for Shell and Spatial Structures, Madrid, Spain.

Johnson KI, JE Deibler, FG Abatt and MW Rinker. 2010. *Single Shell Tank Structural Evaluation Criteria*. PNNL-18837, Rev. 1. Pacific Northwest National Laboratory, Richland, Washington.

Kollar L and E Dulacska. 1984. *Buckling of Shells for Engineers*, Wiley-Interscience, John Wiley & Sons, New York, New York.

Medwadowski SJ. 2004. "Buckling of Concrete Shells: An Overview." *Journal of the International Association for Shell and Spatial Structures* 2004, No. 144 pp. 51–63

Popov EP and SJ Medwadowski. 1981. "Stability of Reinforced Concrete Shells: State-of-the-Art Overview." In *Concrete Shell Buckling*, ACI SP-67, American Concrete Institute, Detroit, Michigan.

Scordelis AC. 1981. "Stability of Reinforced Concrete Domes and Hyperbolic Paraboloid Shells." In *Concrete Shell Buckling*, ACI SP-67, American Concrete Institute, Detroit, Michigan.

Appendix C

Details of ACI-349 Demand/Capacity Calculations

This page intentionally left blank.

Appendix C

Details of ACI-349 Demand/Capacity Calculations

This appendix presents the details of the ACI-349 demand to capacity ratios that were calculated for meridional, hoop, and shear in each of the 22 tank sections presented throughout the body of this report. The hoop and meridional combined flexural capacities are determined by following the provisions in ACI-349-06 Section 10. The detailed calculation procedure is described in Section 3.2 of the SST Structural Evaluation Criteria report (Johnson et al. 2010). Assuming a linear strain profile, with a maximum strain in the concrete of 0.003 in/in, the forces and moments for the sections are calculated using a Whitney stress block approximation for the compressive concrete and elastic perfectly plastic behavior for the steel. A complete closed moment-axial force capacity curve (M-P diagram) can be calculated by varying the assumed depth of the neutral axis in the section as well as applying the appropriate strength reduction factors as described in ACI-349-06. Once the capacity interaction diagram is completed, the demand to capacity ratio is defined as the ratio of the length of the vector from the origin to the demand point over the length of the vector (in the same direction as the demand vector) from the origin to the capacity curve. Figure 7.2 illustrates this definition of D/C for the meridional and hoop directions. The through wall shear and in-plane shear capacity calculations are also described in the SST Structural Evaluation Criteria (Johnson et al. 2010). The shear capacity follows the provisions in ACI-349-06 Section 11.

The demand to capacity calculation was automated for all 22 ACI sections using an Excel document and a Mathcad™ document. The Mathcad™ document performs all the ACI-349-06 calculations necessary to develop the complete M-P diagram for capacity in both the hoop and meridional directions as well as the shear capacities. The Excel document contains all the necessary data to perform the calculations in Mathcad™. This data includes:

- Section demands (force, moment and shear), current temperatures, and section locations and thicknesses for the specific load step extracted from the ANSYS® results. Table C.1 shows an example of the section demands, current temperatures, locations, and thicknesses for Run 1 under the peak temperature load step.
- Section properties containing amounts and locations of reinforcing steel. These properties are shown in Tables 7.1 and 7.2.
- Temperature dependent concrete compressive strengths and temperature dependent steel yield strength and modulus. These properties are described in Appendix A of the SST Structural Evaluation Criteria (Johnson et al. 2010).
- Section maximum temperatures used to determine degraded concrete properties.

Table C.1. Example Table of Section Demands

Section	Shear [kips/ft]	F-merid [kips/ft]	M-merid [kips-ft/ft]	F-hoop [kips/ft]	M-hoop [kips-ft/ft]	Tmin [°F]	Tmax [°F]	Tave [°F]	xbar [in]	ybar [in]	sect-thk [in]	IP Shear [kips/ft]
2	-0.6	-10.3	3.3	-9.7	3.6	233.5	244.1	238.4	44	319	12	0
4	-1.3	-9.6	-0.1	-6.4	1.8	225.5	238.0	230.7	89	319	12	0
6	4.4	-21.7	-4.7	-1.1	0.3	207.5	219.9	214.0	127	303	12	0
8	-0.9	-25.3	1.3	-11.8	0.1	234.8	250.0	242.7	127	266	12	0
10	-0.7	-29.4	0.1	-20.3	0.3	239.7	250.0	245.0	127	221	12	0
12	-0.4	-33.2	0.0	-23.4	0.5	243.1	250.0	245.9	127	176	12	0
14	-0.1	-35.9	0.2	-27.1	0.4	241.9	250.0	245.7	127	131	12	0
16	0.4	-37.3	0.2	-30.3	0.4	240.0	250.0	245.6	127	86	12	0
18	-1.9	-37.5	-2.2	-26.8	1.9	236.8	250.0	243.7	127	43	12	0
20	0.8	-18.4	-0.6	-19.1	-0.2	245.0	250.0	247.6	69	1	7	0
22	0.0	-19.6	-0.1	-19.5	-0.2	245.7	250.0	247.9	23	-2	7	0

The Mathcad™ document loads the data from the Excel document and uses this to calculate the hoop, meridional, through wall shear and in-plane shear D/C ratios. While this Mathcad™ document was set up to automatically calculate all 22 sections using Mathcad™'s animate function, the document can also be used to evaluate individual sections. In this appendix, the Mathcad™ calculation sheets for section 5 under unfactored peak temperature loading are presented. This includes the hoop, meridional, through wall shear, and in-plane shear demand to capacity calculations (for axisymmetric runs all of the in-plane shear demands are zero). After these calculations, the resulting D/C ratios, capacity curves, and demand vectors are output into external text files.

The Mathcad™ document performs the D/C calculations in eight sections:

- Load data: Here the data from the Excel document is loaded for all 22 sections including the section properties, temperatures, and demands as well as the temperature dependent concrete and steel properties. Plots of tank geometry, temperature dependent concrete strength, section forces and moments, and temperature dependent steel modulus and yield strength are provided for quick verification that these inputs have been loaded correctly. Finally, the section number to be evaluated is entered into the Mathcad™ document. Alternatively, instead of one section number, "FRAME" can be entered and the animation function can be used to loop through all of the sections.
- Global Parameters: Here, for a given section, the degraded concrete properties and reinforcing steel properties are set based on the maximum temperature experienced by that section and the current temperature of that section respectively. In addition, the section height (thickness), width, and gross area are calculated. In addition, the factor β_1 (the factor for the depth of the compressive stress block)

is assigned somewhere from 0.65-0.85 depending on the concrete compressive strength according to ACI-349-06. Finally, the eccentricity factor α is also set and the axial load above where the strength reduction factor is 0.7 is determined.

- Case-Specific Parameters and Geometry: Here, for a given section, section specific geometry properties (rebar depths, spacings, and areas and location of the plastic centroid) are calculated for both the meridional direction (left side) and circumferential (or hoop) direction (right side) for multiple layers of rebar in either direction. These section specific geometry properties are determined for both positive and negative bending moment in the meridional and circumferential directions. Finally, the pure compression strength reduction factor of 0.7 is applied to determine the maximum compression capacity (Point D) on the diagram.
- Functions: Here, for a given section, functions are set up to calculate the axial force capacity, P, and positive or negative moment capacity, M_{pos} or M_{neg}. These capacities are set up as functions that depend on the neutral axis of strain, the rebar layer depths, the rebar layer areas, the plastic centroid location, the strength reduction factor, and the maximum compression capacity (Point D). The strength reduction factor, following the guidelines of ACI-349-06, is set to 0.7 for P (in compression) greater than $0.1f_c'A_g/0.7$, set to 0.9 for P in tension, and linearly interpolated for values in between.
- Capacity Calculations: Here the capacity functions for P, M_{pos}, and M_{neg}, defined in the previous section are used to develop the complete diagram. First, the maximum possible neutral axis depth is determined. Then, the capacity functions are solved for 250 different neutral axis locations; for each given neutral axis the corresponding capacity axial force and moment are determined. Corresponding angles and vector lengths (from the origin to the capacity point) are determined to compare to the demands later. These 250 different capacity points are used to plot the complete diagrams in Section 8 of the Mathcad™ document described below.
- Demand Calculations: Here the meridional force and moments are used to determine the demand vector angle and length. For the given demand angle and length the capacity functions are solved again. This determines the exact capacity at that demand angle rather than interpolating between the 250 capacity points determined in the previous section. The D/C ratio for the meridional demand is then calculated. This process is repeated in the circumferential direction.
- Shear Demand/Capacity Calculations: This section performs the through wall shear and in-plane shear D/C calculations. The shear capacity equations are from ACI-349-06 Section 11. The specific equation used to calculate the through wall capacity depends on the presence of flexure and axial tension or compression. The strength reduction factor of 0.85 is used to reduce the shear capacities. The through wall shear and in-plane shear D/C ratios are then calculated.
- Results and Output: This section summarizes the D/C ratios in the circumferential, meridional, through wall shear, and in-plane shear directions. The circumferential and meridional capacity curves, demands, and D/C vectors are plotted on one M-P diagram. The D/C ratios are output to a text file. The capacity curves and the demand and capacity vectors are also output to separate text files.

C.1 Example Calculations for Hoop, Meridional, and Shear Demand/Capacity Ratios for Section 5

Pacific Northwest National Laboratory
ACI-349-06 Demand/Capacity Calculation - Section 5 Example

Page 1 of 16
Date: 7/14/2010 By: M.S. Schwendeman
Chkd: 8/2/2010 By: S.E. Sanborn
Revised: 4/12/2014 By: J.E. Deibler

ACI Section Capacity/Demand Calculations
Tank Type II
Michael Schwendeman 7/14/10

SE Sanborn 10/13/10 Rev 4: Knocked down hoop rebar in haunch to 75%, added or logic to Case_c, case 4 to handle 0 moment with theta_c = theta min
SES 1/14/11 Rev 5: Reads in Rev5 excel sheet that counts middle layer of rebar in the haunch sections.
SES 2/3/11 Rev 6: Reads in Rev6 excel sheet that counts middle layer of rebar in sect 18
SES 3/30/11 Rev 7: Added in plane shear D/C for seismic demands
SES 4/25/11 Type III Rev 0: Modified for Type III tank
SES 5/12/11 Type III Rev 1: Reads in Rev1 Excel sheet
SES 5/19/11 Type III Rev 2: Reads in Rev2 Excel sheet
SES 5/20/11 Type III Rev 3: Reads in Rev3 Excel sheet
SES 5/26/11 Type III Rev 4: Reads in Rev4 Excel Sheet
SES 12/17/12 Type IVb Rev0: Set up for Type IVb Excel Sheet
SES 12/31/12 Type IVb Rev1: Reads in Rev1 of Excel Sheet
SES 1/7/2013 Type IVb Rev2: Reads in Rev2 of Excel Sheet
JED 4/12/2014 Type I

Load Data:

Load Section Properties (excel): sectionprops : ACI-Type data.xls

Load Section Temperatures (excel): sectiontempe := ACI-Type data.xls

Load Concrete Compressive Strengths (excel): concretefc := ACI-Type data.xls

Load Bar Number Properties (excel): barprops := ACI-Type data.xls

Load Steel Yield Strengths (excel): steelstrengths := ACI-Type data.xls

Load Steel Modulus (excel): steelmodulus : ACI-Type data.xls

Load ANSYS Results (excel): ANSYS := ACI-Type data.xls

ORIGIN := 1 Defines first vector index as "1" rather than "0"

CALCULATE ALL SECTIONS INSTRUCTIONS:
1) Set Section:=FRAME
2) Find the function APPENDPRN at the bottom of the program
3) Specify a *unique* filename.txt and output vector (best if a horizontal vector beginning with section number) in
APPENDPRN("filename.txt",outputVector)
4) Right-click APPENDPRN and choose "enable evaluation"
5) In Tools>Animation>Record, choose the range of Section numbers using "from" and "to"
6) With the Record Animation window open, drag to highlight the APPENPRN statement
7) Click "Animate" and wait for it to cycle through all the sections
8) When it finishes, click "cancel", close the animation playback window, and open filename.txt to access your data

Pacific Northwest National Laboratory
ACI-349-06 Demand/Capacity Calculation - Section 5 Example

Page 2 of 18
Date: 7/14/2010 By: M.S. Schwendeman
Chkd: 8/2/2010 By: S.E. Sanborn
Revised: 4/12/2014 By: J.E. Deibler

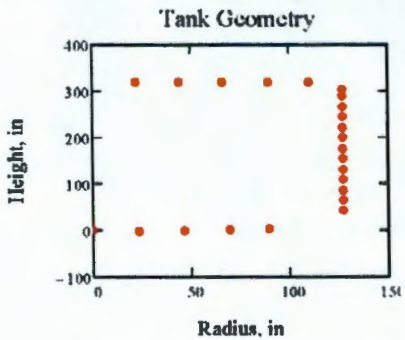

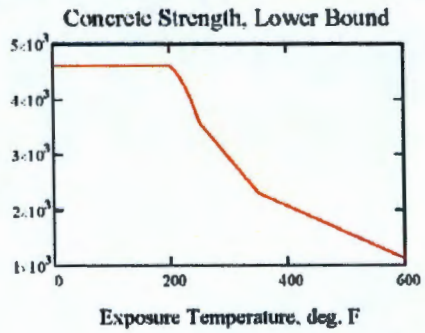

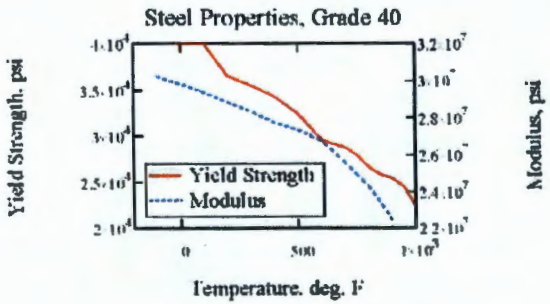

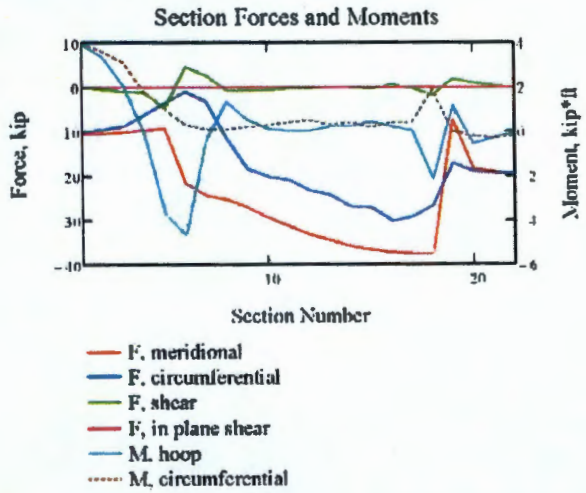

Input Section Number: Section := 5

Global Parameters:

Mechanical Properties:

Concrete: **max concrete temperature:** $T_{max} := \text{vlookup}(\text{Section}, \text{sectiontemps}, 2)_1 = 224.2$

Compressive strength: $f_c := \text{linterp}\left(\text{concretefc}^{\langle 1 \rangle}, \text{concretefc}^{\langle 2 \rangle}, T_{max}\right) \text{psi} = 4.257 \times 10^3 \text{ psi}$

Compressive strain: $\varepsilon_{cu} := 0.003 \frac{\text{in}}{\text{in}}$

Steel: **Grade:** $\text{grade} := \text{vlookup}(\text{Section}, \text{sectionprops}, 6)_1 = 40$

Average Section Temp: $\text{tempAve} := \text{vlookup}(\text{Section}, \text{ANSYS}, 9)_1 = 217$

Yield strength: $f_y := \frac{\text{grade}}{40} \text{linterp}\left(\text{steelstrengths}^{\langle 1 \rangle}, \text{steelstrengths}^{\langle 2 \rangle}, \text{tempAve}\right) 1000 \text{ psi} = 3.633 \times 10^4 \text{ psi}$

Modulus: $E_s := \text{linterp}\left(\text{steelmodulus}^{\langle 1 \rangle}, \text{steelmodulus}^{\langle 2 \rangle}, \text{tempAve}\right) 10^6 \text{ psi} = 2.872 \times 10^7 \text{ psi}$

Yield strain: $\varepsilon_y := \frac{f_y}{E_s} = 1.265 \times 10^{-3}$

Section Geometry

Height: $h := \text{vlookup}(\text{Section}, \text{sectionprops}, 3)_1 \text{ in} = 12 \text{ in}$

Unit width: $b := 12\text{in}$ **Section area:** $A_g := b\,h = 144 \text{ in}^2$

Other Parameters

β_1, using section 10 of ACI 349-06:

$$\beta_1 := \begin{cases} \left[0.85 - \frac{0.05}{1000psi}\left(f_c - 4000psi\right)\right] & \text{if } \left[f_c < 4000psi + (0.85 - 0.65)\frac{1000psi}{0.05}\right] \\ 0.85 & \text{if } \left(f_c < 4000psi\right) \\ 0.65 & \text{otherwise} \end{cases} = 0.8371$$

α, factor to account for small eccentricity of axial load for columns: $\alpha := 0.8$

$$P_{\varphi} := \frac{0.1 f_c A_g}{0.7} = 87.58\ kip$$

Case-Specific Parameters and Geometry:

"mp"=Meridional, positive moment, "mn"=Meridional, negative moment
"cp"=Circumferential, positive moment, "cn"=Circumferential, negative moment

Cycle through all possible bars: $Bars_m := 4$ $j := 1..Bars_m$

+M, meridional

Define vector of relative bar property cell distance for lookup [bar1, bar2, bar3, bar4], with bar1 being the most compressed bar, and bar4 the least: $k_p := (0\ 20\ 30\ 10)^T$

Bar size no.: $sizeNo_{mp_j} := vlookup(Section, sectionprops, 9 + k_{p_j})1$

Depth $d_{mp_j} := vlookup(Section, sectionprops, 10 + k_{p_j})1\ in$

:

Diameter: $d_{b_mp_j} := vlookup(sizeNo_{mp_j}, barprops, 3)1\ in$

Spacing: $s_{p_mp_j} := vlookup(Section, sectionprops, 11 + k_{p_j})1\ in$

Area: $$A_{mp_j} := \begin{cases} \left[\pi\left(\frac{d_{b_mp_j}}{2}\right)^2 \frac{b}{s_{p_mp_j}}\right] & \text{if } s_{p_mp_j} \neq 0 \\ 0 & \text{otherwise} \end{cases}$$

Cycle through possible bars (no fourth bar for circumferential): $Bars_c := 3$ $r := 1..Bars_c$

+M, circumferential

Define vector of relative bar property cell distance for lookup [bar1, bar2, bar3], with bar1 being the most compressed bar, and bar3 the least: $s_p := (0\ 20\ 10)^T$

Bar size no.: $sizeNo_{cp_r} := vlookup(Section, sectionprops, 13 + s_{p_r})1$

Depth $d_{cp_r} := vlookup(Section, sectionprops, 14 + s_{p_r})1\ in$

:

Diameter: $d_{b_cp_r} := vlookup(sizeNo_{cp_r}, barprops, 3)1\ in$

Spacing: $s_{p_cp_r} := vlookup(Section, sectionprops, 15 + s_{p_r})1\ in$

Area: $$A_{cp_r} := \begin{cases} \left[\pi\left(\frac{d_{b_cp_r}}{2}\right)^2 \frac{b}{s_{p_cp_r}}\right] & \text{if } s_{p_cp_r} \neq 0 \\ 0 & \text{otherwise} \end{cases}$$

Pacific Northwest National Laboratory
ACI-349-06 Demand/Capacity Calculation - Section 5 Example

Page 5 of 16
Date: 7/14/2010 By: M.S. Schwendeman
Chkd: 8/2/2010 By: S.E. Sanborn
Revised: 4/12/2014 By: J.E. Deibler

Total Bar Geometry: Total area: $A_{st_m} := \sum A_{mp} = 0.884\ in^2$

Plastic Centroid: $x_{p_mp} := \dfrac{\left[0.85\, b\, f_c \dfrac{h^2}{2} + f_y \sum \overrightarrow{(A_{mp}\, d_{mp})}\right]}{0.85 f_c\, b\, h + f_y \sum A_{mp}} = 6\ in$

-M, meridional

Define vector of relative bar property cell distance for lookup [bar1, bar2, bar3, bar4], with bar1 being the most compressed bar, and bar4 the least: $k_n := (10\ \ 30\ \ 20\ \ 0)^T$

Bar size no.: $sizeNo_{mn_j} := vlookup(Section, sectionprops, 9 + k_{n_j})_1$

Depth $d_{mn_j} := h - \left(vlookup(Section, sectionprops, 10 - k_{n_j})_1\ in\right)$

Diameter: $d_{b_mn_j} := vlookup(sizeNo_{mn_j}, barprops, 3)_1\ in$

Spacing: $s_{p_mn_j} := vlookup(Section, sectionprops, 11 + k_{n_j})_1\ in$

Area: $A_{mn_j} := \begin{cases} \pi \left(\dfrac{d_{b_mn_j}}{2}\right)^2 \dfrac{b}{s_{p_mn_j}} & \text{if } s_{p_mn_j} \neq 0 \\ 0 & \text{otherwise} \end{cases}$

Plastic Centroid: $x_{p_mn} := \dfrac{\left[0.85\, b\, f_c \dfrac{h^2}{2} + f_y \sum \overrightarrow{(A_{mn}\, d_{mn})}\right]}{0.85 f_c\, b\, h + f_y \sum A_{mn}} - 6\ in$

Find Point "D" force value, which serves as upper bound on force capacity

Point D: $\varphi_D := 0.7$ $\quad P_{D_m} := \alpha\, \varphi_D \left[0.85\, f_c \left(A_g - A_{st_m}\right) + f_y\, A_{st_m}\right] - 308.002\ kip$

Total Bar Geometry: Total area: $A_{st_c} := \sum A_{cp} = 0.884\ in^2$

Plastic Centroid: $x_{p_cp} := \dfrac{\left[0.85\, b\, f_c \dfrac{h^2}{2} + f_y \sum \overrightarrow{(A_{cp}\, d_{cp})}\right]}{0.85 f_c\, b\, h + f_y \sum A_{cp}} - 6\ in$

-M, meridional

Define vector of relative bar property cell distance for lookup [bar1, bar2, bar3], with bar1 being the most compressed bar, and bar3 the least: $s_n := (10\ \ 20\ \ 0)^T$

Bar size no.: $sizeNo_{cn_r} := vlookup(Section, sectionprops, 13 + s_{n_r})_1$

Depth $d_{cn_r} := h - \left(vlookup(Section, sectionprops, 14 + s_{n_r})_1\ in\right)$

Diameter: $d_{b_cn_r} := vlookup(sizeNo_{cn_r}, barprops, 3)_1\ in$

Spacing: $s_{p_cn_r} := vlookup(Section, sectionprops, 15 + s_{n_r})_1\ in$

Area: $A_{cn_r} := \begin{cases} \left[\pi \left(\dfrac{d_{b_cn_r}}{2}\right)^2 \dfrac{b}{s_{p_cn_r}}\right] & \text{if } s_{p_cn_r} \neq 0 \\ 0 & \text{otherwise} \end{cases}$

Plastic Centroid: $x_{p_cn} := \dfrac{\left[0.85\, b\, f_c \dfrac{h^2}{2} + f_y \sum \overrightarrow{(A_{cn}\, d_{cn})}\right]}{0.85 f_c\, b\, h + f_y \sum A_{cn}} - 6\ in$

Point D: $P_{D_o} := \alpha\, \varphi_D \left[0.85\, f_c \left(A_g - A_{st_o}\right) - f_y\, A_{st_o}\right] - 308.002\ kip$

Functions:

Moment and force (P) evaluated for given c (neutral axis of strain), d (vector of bar depths), A_s (vector of bar areas), x_p (plastic centroid), P_φ (determines φ factor), and P_D (maximum allowable force).

$$C_c(c) := 0.85\, f_c\, b\, \beta_1\, c$$

$$\varepsilon_s(c,d) := \begin{cases} \varepsilon_{cu}\dfrac{(c-d)}{c} & \text{if } c \neq 0 \\ \text{sign}(-d)\ 1\ 10^{10} & \text{otherwise} \end{cases} \qquad \text{A big number}$$

$$f_s(c,d) := \begin{cases} \min\left(E_s\, \varepsilon_s(c,d), f_y\right) & \text{if } \varepsilon_s(c,d) > 0 \\ \max\left(E_s\, \varepsilon_s(c,d), -f_y\right) & \text{otherwise} \end{cases}$$

$$F_s(c,d,A_s) := \begin{cases} \left(A_s\, f_s(c,d)\right) & \text{if } \beta_1\, c < d \\ \left[A_s\left(f_s(c,d) - 0.85\, f_c\right)\right] & \text{otherwise} \end{cases}$$

$$P_n(c,d,A_s,N) := C_c(c) + \sum_{m=1}^{N} F_s\left(c, d_m, A_{s_m}\right)$$

$$\varphi(c,d,A_s,N,P_\varphi) := \begin{cases} 0.9 & \text{if } P_n(c,d,A_s,N) < 0 \\ 0.7 & \text{if } P_n(c,d,A_s,N) > P_\varphi \\ \left[0.7 + \dfrac{(0.9-0.7)\left(P_\varphi - P_n(c,d,A_s,N)\right)}{P_\varphi}\right] & \text{otherwise} \end{cases}$$

$$M_{pos}(c,d,A_s,x_p,N,P_\varphi) := \varphi(c,d,A_s,N,P_\varphi)\left[C_c(c)\left(x_p - \frac{\beta_1\, c}{2}\right) + \sum_{m=1}^{N}\left[F_s\left(c,d_m,A_{s_m}\right)\left(x_p - d_m\right)\right]\right]$$

$$M_{neg}(c,d,A_s,x_p,N,P_\varphi) := -\varphi(c,d,A_s,N,P_\varphi)\left[C_c(c)\left(x_p - \frac{\beta_1\, c}{2}\right) + \sum_{m=1}^{N}\left[F_s\left(c,d_m,A_{s_m}\right)\left(x_p - d_m\right)\right]\right]$$

$P(c, d, A_s, N, P_\varphi, P_D) := \min(P_{D_\varphi}(c, d, A_s, N, P_\varphi)\ P_n(c, d, A_s, N))$

Capacity Calculations:

Generates capacity curve for vector of c values

Meridional

determine c_{max} for calculations (meridional):

$c_{max_m} := \mathrm{root}(M_{pos}(c, d_{mp}, A_{mp}, x_{p_mp}, Bars_m, P_\varphi) - M_{neg}(c, d_{mn}, A_{mn}, x_{p_mn}, Bars_m, P_\varphi), c, .1\ in, 50in) = 14.392in$

determine c_{max} for calculations (circumferential):

$c_{max_c} := \mathrm{root}(M_{pos}(c, d_{cp}, A_{cp}, x_{p_cp}, Bars_c, P_\varphi) - M_{neg}(c, d_{cn}, A_{cn}, x_{p_cn}, Bars_c, P_\varphi), c, .1in, 50in) = 14.355in$

input desired number of points: $n := 250$

increment: $dc_m := \frac{c_{max_m}}{n-1} = 0.058in$

set up vector of c values for calculations

$i := 1..n$

$c_{m_i} := dc_m \cdot (i-1)$

+M

$P_{mp_i} := P(c_{m_i}, d_{mp}, A_{mp}, Bars_m, P_\varphi, P_{D_m})$

$M_{mp_i} := M_{pos}(c_{m_i}, d_{mp}, A_{mp}, x_{p_mp}, Bars_m, P_\varphi)$

Circumferential

input desired number of points: $n := n$ (see left)

increment: $dc_c := \frac{c_{max_c}}{n-1} = 0.058in$

set up vector of c values for calculations

$i := i$ (see left)

$c_{c_i} := dc_c \cdot (i-1)$

+M

$P_{cp_i} := P(c_{c_i}, d_{cp}, A_{cp}, Bars_c, P_\varphi, P_{D_c})$

$M_{cp_i} := M_{pos}(c_{c_i}, d_{cp}, A_{cp}, x_{p_cp}, Bars_c, P_\varphi)$

-M

$P_{mn_i} := P\left(c_{m_i}, d_{mn}, A_{mn}, Bars_m, P_\varphi, P_{D_m}\right)$

$M_{mn_i} := M_{neg}\left(c_{m_i}, d_{mn}, A_{mn}, x_{p_mn}, Bars_m, P_\varphi\right)$

concatenate +M and -M vectors

$M_m := stack\left(M_{mp}, M_{mn}\right)$

$P_m := stack\left(P_{mp}, P_{mn}\right)$

$i := 1..2n$

Calculate the angles and lengths of the capacity vectors, for comparision with demand vectors:

Angle: $\theta_{m_i} := atan2\left(M_{m_i} kip^{-1} ft^{-1}, P_{m_i} kip^{-1}\right)$

For unit agreement, nondimensionalize forces and moments by reference force of 1 kip and reference length of 1 ft.

Length: $r_{m_i} := \sqrt{\left(P_{m_i} kip^{-1}\right)^2 + \left(M_{m_i} kip^{-1} ft^{-1}\right)^2}$

Define max and min angles

$\theta_{max_m} := \theta_{m_n} - 90\ deg$

$\theta_{min_m} := \theta_{m_1} = -90\ deg$

Create Ouput Matrix of P,M,θ,and r values and sort by θ

$MeridMatrix := augment\left(M_m kip^{-1} ft^{-1}, P_m kip^{-1}, r_m, \theta_m\right)$

$MeridOutput := csort(MeridMatrix, 4)$

-M

$P_{cn_i} := P\left(c_{c_i}, d_{cn}, A_{cn}, Bars_c, P_\varphi, P_{D_c}\right)$

$M_{cn_i} := M_{neg}\left(c_{c_i}, d_{cn}, A_{cn}, x_{p_cn}, Bars_c, P_\varphi\right)$

concatenate +M and -M vectors

$M_c := stack\left(M_{cp}, M_{cn}\right)$

$P_c := stack\left(P_{cp}, P_{cn}\right)$

$i := i$ **(see left)**

Calculate the angles and lengths of the capacity vectors, for comparision with demand vectors:

$\theta_{c_i} := atan2\left(M_{c_i} kip^{-1} ft^{-1}, P_{c_i} kip^{-1}\right)$

For unit agreement, nondimensionalize forces and moments by reference force of 1 kip and reference length of 1 ft.

Length: $r_{c_i} := \sqrt{\left(P_{c_i} kip^{-1}\right)^2 + \left(M_{c_i} kip^{-1} ft^{-1}\right)^2}$

Define max and min angles

$\theta_{max_c} := \theta_{c_n} - 90\ deg$

$\theta_{min_c} := \theta_{c_1} = -90\ deg$

Create Ouput Matrix of P,M,θ,and r values and sort by θ

$CircumMatrix := augment\left(M_c kip^{-1} ft^{-1}, P_c kip^{-1}, r_c, \theta_c\right)$

$CircumOutput := csort(CircumMatrix, 1)$

Demand Calculations:

Meridional Demand:

Force: $P_{u_m} := (\text{vlookup}(\text{Section}, \text{ANSYS}, 3))_1 \text{ kip} = 9.3 \text{ kip}$

Moment: $M_{u_m} := (-\text{vlookup}(\text{Section}, \text{ANSYS}, 4))_1 \text{ kip ft} = 3.8 \text{ kip ft}$

For unit agreement, nondimensionalize forces and moments by reference force of 1 kip and length of 1 ft.

Demand angle and length:

Angle: $\theta_{u_m} := \begin{cases} \text{atan2}\left(M_{u_m} \text{kip}^{-1} \text{ ft}^{-1}, P_{u_m} \text{ kip}^{-1}\right) & \text{if } M_{u_m} \neq 0 \vee P_{u_m} \neq 0 \\ 0 & \text{otherwise} \end{cases} = 67.775°$

Length: $r_{u_m} := \sqrt{\left(P_{u_m} \text{ kip}^{-1}\right)^2 + \left(M_{u_m} \text{ kip}^{-1} \text{ ft}^{-1}\right)^2} = 10.04639$

Ratio: $MtoF_m := \begin{cases} \dfrac{M_{u_m} \text{kip}^{-1} \text{ ft}^{-1}}{P_{u_m} \text{ kip}^{-1}} & \text{if } P_{u_m} \neq 0 \\ 1 & \text{otherwise} \end{cases} = 0.409$

Evaluate based on whether using +M terms (cases 1 and 2) or -M terms (cases 3 and 4) and whether P_u is positive (cases 1 and 3) or negative (cases 2 and 4) or zero (cases 5 and 6)

$$Case_m := \begin{cases} 1 & \text{if } (\theta_{u_m} \leq \theta_{max_m}) \wedge (\theta_{u_m} \geq \theta_{min_m}) \wedge P_{u_m} > 0 = 1 \\ 2 & \text{if } (\theta_{u_m} \leq \theta_{max_m}) \wedge (\theta_{u_m} \geq \theta_{min_m}) \wedge P_{u_m} < 0 \\ 3 & \text{if } (\theta_{u_m} > \theta_{max_m}) \\ 4 & \text{if } (\theta_{u_m} < \theta_{min_m}) \\ 5 & \text{if } P_{u_m} = 0 \wedge M_{u_m} \geq 0 \\ 6 & \text{if } P_{u_m} = 0 \wedge M_{u_m} < 0 \end{cases}$$

Find c_0, where P=0

$c_{0_mp} := root(P(c, d_{mp}, A_{mp}, Bars_m, P_\varphi, P_{D_m}), c, 0, c_{max_m}) = 0.883\,in$

$c_{0_mn} := root(P(c, d_{mn}, A_{mn}, Bars_m, P_\varphi, P_{D_m}), c, 0, c_{max_m}) = 0.883\,in$

solve for the c value that will give the correct angle for comparison with the demand

$$c_{cap_m} := \begin{cases} root(M_{pos}(c, d_{mp}, A_{mp}, x_{p_mp}, Bars_m, P_\varphi)\,kip^{-1}\,ft^{-1} - MtoF_m\,P(c, d_{mp}, A_{mp}, Bars_m, P_\varphi, P_{D_m})\,kip^{-1}, c, c_{0_mp}, c_{max_m}) & \text{if } Case_m = 1 \\ -4.392\,in \\ root(M_{pos}(c, d_{mp}, A_{mp}, x_{p_mp}, Bars_m, P_\varphi)\,kip^{-1}\,ft^{-1} - MtoF_m\,P(c, d_{mp}, A_{mp}, Bars_m, P_\varphi, P_{D_m})\,kip^{-1}, c, 0, c_{0_mp}) & \text{if } Case_m = 2 \\ root(M_{neg}(c, d_{mn}, A_{mn}, x_{p_mn}, Bars_m, P_\varphi)\,kip^{-1}\,ft^{-1} - MtoF_m\,P(c, d_{mn}, A_{mn}, Bars_m, P_\varphi, P_{D_m})\,kip^{-1}, c, c_{0_mn}, c_{max_m}) & \text{if } Case_m = 3 \\ root(M_{neg}(c, d_{mn}, A_{mn}, x_{p_mn}, Bars_m, P_\varphi)\,kip^{-1}\,ft^{-1} - MtoF_m\,P(c, d_{mn}, A_{mn}, Bars_m, P_\varphi, P_{D_m})\,kip^{-1}, c, 0, c_{0_mn}) & \text{if } Case_m = 4 \\ c_{0_mp} & \text{if } Case_m = 5 \\ c_{0_mn} & \text{if } Case_m = 6 \end{cases}$$

Calculate $M_{capacity}$ and $P_{capacity}$ for this angle

$$M_{cap_m} := \begin{cases} M_{pos}(c_{cap_m}, d_{mp}, A_{mp}, x_{p_mp}, Bars_m, P_\varphi) & \text{if } Case_m = 1 \vee Case_m = 2 \vee Case_m = 5 \\ M_{neg}(c_{cap_m}, d_{mn}, A_{mn}, x_{p_mn}, Bars_m, P_\varphi) & \text{otherwise} \end{cases} = 45.21\,kip\,ft$$

$$P_{cap_m} := \begin{cases} P(c_{cap_m}, d_{mp}, A_{mp}, Bars_m, P_\varphi, P_{D_m}) & \text{if } Case_m = 1 \vee Case_m = 2 \vee Case_m = 5 \\ P(c_{cap_m}, d_{mn}, A_{mn}, Bars_m, P_\varphi, P_{D_m}) & \text{otherwise} \end{cases} = 110.645\,kip$$

Find the demand/capacity ratio

$$r_{cap_m} := \sqrt{\left(P_{cap_m}\,kip^{-1}\right)^2 + \left(M_{cap_m}\,kip^{-1}\,ft^{-1}\right)^2} = 119.525$$

$$DCratio_m := \frac{r_{u_m}}{r_{cap_m}} = 0.084$$

Circumferential Demand:

Force: $P_{u_c} := (-\text{vlookup}(\text{Section}, \text{ANSYS}, 5))_1 \text{ kip} = 3.7 \text{ kip}$

Moment : $M_{u_c} := (-\text{vlookup}(\text{Section}, \text{ANSYS}, 6))_1 \text{ kip ft} = -1 \text{ kip ft}$

For unit agreement, nondimensionalize forces and moments by reference force of 1 kip and length of 1 ft.

Demand angle and length:

Angle: $\theta_{u_c} := \begin{cases} \text{atan2}\left(M_{u_c}\,\text{kip}^{-1}\,\text{ft}^{-1}, P_{u_c}\,\text{kip}^{-1}\right) & \text{if } M_{u_c} \neq 0 \vee P_{u_c} \neq 0 \\ 0 & \text{otherwise} \end{cases} = -105.124°$

Length: $r_{u_c} := \sqrt{\left(P_{u_c}\,\text{kip}^{-1}\right)^2 + \left(M_{u_c}\,\text{kip}^{-1}\,\text{ft}^{-1}\right)^2} = 3.833$

Ratio : $MtoF_c := \begin{cases} \dfrac{M_{u_c}\,\text{kip}^{-1}\,\text{ft}^{-1}}{P_{u_c}\,\text{kip}^{1}} & \text{if } P_{u_c} \neq 0 \\ 1 & \text{otherwise} \end{cases} = -0.27$

Evaluate based on whether using +M terms (cases 1 and 2) or -M terms (cases 3 and 4) and whether P_u is positive (cases 1 and 3) or negative (cases 2 and 4) or zero (cases 5 and 6)

$$Case_c := \begin{cases} 1 & \text{if } (\theta_{u_c} < \theta_{max_c}) \wedge (\theta_{u_c} > \theta_{min_c}) \wedge P_{u_c} > 0 \\ 2 & \text{if } (\theta_{u_c} \leq \theta_{max_c}) \wedge (\theta_{u_c} \geq \theta_{min_c}) \wedge P_{u_c} < 0 \\ 3 & \text{if } (\theta_{u_c} > \theta_{max_c}) \\ 4 & \text{if } (\theta_{u_c} < \theta_{min_c}) \vee (\theta_{u_c} = \theta_{min_c}) \wedge (M_{u_c} = 0) \\ 5 & \text{if } P_{u_c} = 0 \wedge M_{u_c} \geq 0 \\ 6 & \text{if } P_{u_c} = 0 \wedge M_{u_c} < 0 \end{cases} = 3$$

Find c_o, where P=0

$c_{0_cp} := \mathrm{root}(P(c, d_{cp}, A_{cp}, Bars_c, P_\varphi, P_{D_c}), c, 0, c_{max_c}) = 0.883\,in$

$c_{0_cn} := \mathrm{root}(P(c, d_{cn}, A_{cn}, Bars_c, P_\varphi, P_{D_c}), c, 0, c_{max_c}) = 0.883\,in$

solve for the c value that will give the correct angle for comparison with the demand

$$c_{cap_c} := \begin{cases} \mathrm{root}(M_{pos}(c, d_{cp}, A_{cp}, x_{p_cp}, Bars_c, P_\varphi)\,kip^{-1}\,ft^{-1} - MtoF_c\,P(c, d_{cp}, A_{cp}, Bars_c, P_\varphi, P_{D_c})\,kip^{-1}, c, c_{0_cp}, c_{max_c}) & \text{if } Case_c = 1 \\ \mathrm{root}(M_{pos}(c, d_{cp}, A_{cp}, x_{p_cp}, Bars_c, P_\varphi)\,kip^{-1}\,ft^{-1} - MtoF_c\,P(c, d_{cp}, A_{cp}, Bars_c, P_\varphi, P_{D_c})\,kip^{-1}, c, 0, c_{0_cp}) & \text{if } Case_c = 2 \\ \mathrm{root}(M_{neg}(c, d_{cn}, A_{cn}, x_{p_cn}, Bars_c, P_\varphi)\,kip^{-1}\,ft^{-1} - MtoF_c\,P(c, d_{cn}, A_{cn}, Bars_c, P_\varphi, P_{D_c})\,kip^{-1}, c, c_{0_cn}, c_{max_c}) & \text{if } Case_c = 3 \\ \mathrm{root}(M_{neg}(c, d_{cn}, A_{cn}, x_{p_cn}, Bars_c, P_\varphi)\,kip^{-1}\,ft^{-1} \quad MtoF_c\,P(c, d_{cn}, A_{cn}, Bars_c, P_\varphi, P_{D_c})\,kip^{-1}, c, 0, c_{0_cn}) & \text{if } Case_c = 4 \\ c_{0_cp} & \text{if } Case_c = 5 \\ c_{0_cn} & \text{if } Case_c = 6 \end{cases} = 7.083\,in$$

Calculate $M_{capacity}$ and $P_{capacity}$ for this angle

$$M_{cap_c} := \begin{cases} M_{pos}(c_{cap_c}, d_{cp}, A_{cp}, x_{p_cp}, Bars_c, P_\varphi) & \text{if } Case_c = 1 \vee Case_c = 2 \vee Case_c = 5 \\ M_{neg}(c_{cap_c}, d_{cn}, A_{cn}, x_{p_cn}, Bars_c, P_\varphi) & \text{otherwise} \end{cases} = 49.628\,kip\,ft$$

$$P_{cap_c} := \begin{cases} P(c_{cap_c}, d_{cp}, A_{cp}, Bars_c, P_\varphi, P_{D_c}) & \text{if } Case_c = 1 \vee Case_c = 2 \vee Case_c = 5 \\ P(c_{cap_c}, d_{cn}, A_{cn}, Bars_c, P_\varphi, P_{D_c}) & \text{otherwise} \end{cases} = 183.624\,kip$$

Find the demand/capacity ratio

$$r_{cap_c} := \sqrt{\left(P_{cap_c}\,kip^{-1}\right)^2 + \left(M_{cap_c}\,kip^{-1}\,ft^{-1}\right)^2} = 190.212$$

$$DCratio_c := \frac{r_{u_c}}{r_{cap_c}} = 0.02$$

$Mangle_m := \begin{pmatrix} 0 \\ M_{cap_m}\,kip^{-1}\,ft^{-1} \end{pmatrix}$ $Mangle_c := \begin{pmatrix} 0 \\ M_{cap_c}\,kip^{-1}\,ft^{-1} \end{pmatrix}$ **For Plotting Vectors**

$Pangle_m := \begin{pmatrix} 0 \\ P_{cap_m}\,kip^{-1} \end{pmatrix}$ $Pangle_c := \begin{pmatrix} 0 \\ P_{cap_c}\,kip^{-1} \end{pmatrix}$

Shear Demand/Capacity Calculations:

Use ACI 349-06 eq. 11-4 to 11-8, using force and moment demand from meridional case, and $d=d_{mp2}$ for positive (and zero) moment and $d=d_{mn2}$ for negative moment (similarly with areas).

Through wall shear calculation

$V_u := vlookup(Section, ANSYS, 2)_1\ kip = -4.8\,kip$

$N_u := \begin{cases} P_{u_m} & \text{if } |P_{u_m}| > 1kip \\ 0 & \text{otherwise} \end{cases} = 9.3\,kip$

$M_u := |M_{u_m}| = 3.8\ kip\ ft$

$d := \begin{cases} d_{mn_{Bars_m}} & \text{if } M_{u_m} \le 0 \\ d_{mp_{Bars_m}} & \text{otherwise} \end{cases} = 9.625\,in$

$A_s := \begin{cases} A_{mn_{Bars_m}} & \text{if } M_{u_m} < 0 \\ A_{mp_{Bars_m}} & \text{otherwise} \end{cases} = 0.442\,in^2$

In-plane shear calculation

$V_{uip} := vlookup(Section, ANSYS, 13)_1\ kip = 0\,kip$

"Shear and Flexure only"

$$Vud_Mu := \begin{cases} \min\left(\left|\frac{V_u\, d}{M_u}\right|, 1\right) & \text{if } M_u \neq 0 \\ 1 & \text{otherwise} \end{cases} = 1$$

calculate $V_u d/M_u$ with maximum value of 1.0

$$\rho_w := \frac{A_s}{b\, d} = 3.825 \cdot 10^{-3}$$

$$V_{c1} := \left(1.9\sqrt{f_c\, psi}^{\frac{1}{2}} + 2500\rho_w\, Vud_Mu\, psi\right) b\, d = 15.423\, kip$$

$$V_{c1_max} := 3.5\, psi^{\frac{1}{2}} \sqrt{f_c}\, b\, d = 26.377\, kip$$

$$V_{c1_min} := 2\, psi^{\frac{1}{2}} \sqrt{f_c}\, b\, d = 15.072\, kip$$

"Shear, Flexure, and Axial Compression

$$M_m := M_u - N_u\left(\frac{4\,h - d}{8}\right) = 0.082\, kip\, ft$$

$$lw := b = 12\, in$$

$$V_{c2_max} := 3.5\, psi^{\frac{1}{2}} \sqrt{f_c}\, b\, d \sqrt{1 + \frac{N_u}{(500psi)\, b\, h}} = 28.028\, kip$$

Also use for M_m<0

$$V_{cip} := 3.3\, psi^{\frac{1}{2}} \sqrt{f_c}\, h\, b - \frac{N_u\, b}{4\, lw} = 33.331\, kip$$

$$V_{c2} := \begin{cases} \left[\left(1.9\sqrt{f_c\, psi}^{\frac{1}{2}} + 2500\, psi\, \rho_w \left|\frac{V_u\, d}{M_m}\right|\right) b\, d\right] & \text{if } M_m \neq 0 \\ V_{c2_max} & \text{otherwise} \end{cases} = 65.909\, kip$$

"Shear, Flexure, and Axial Tension"

$$V_{c3} := 2\,psi^{\frac{1}{2}}\left[1+\frac{N_u}{(500psi)\,b\,h}\right]\sqrt{f'_c}\,b\,d = 17.019\,kip$$

Calculate Shear Capacity:

$$V_c := \begin{cases} \max(V_{c1_min}, \min(V_{c1}, V_{c1_max})) & \text{if } N_u = 0 = 28.028\,kip \\ \min(V_{c2}, V_{c2_max}) & \text{if } N_u > 0 \wedge M_m \geq 0 \\ V_{c2_max} & \text{if } (N_u > 0 \wedge M_m < 0) \\ V_{c3} & \text{otherwise} \end{cases}$$

Factored Shear Capacity:

$$\varphi_{shear} := 0.85$$

$$V_{cu} := \varphi_{shear}\,V_c = 23.824\,kip$$

Shear Demand/Capacity Ratio:

$$DCratio_{shear} := \left|\frac{V_u}{V_c}\right| = 0.201$$

Factored In plane Shear Capacity:

$$V_{cip} := \varphi_{shear}\,V_{cip} = 28.331\,kip$$

Shear Demand/Capacity Ratio:

$$DCratio_{shearip} := \left|\frac{V_{uip}}{V_{cip}}\right| = 0$$

Results and Output:

$DCratio_c = 0.0201$ $DCratio_m = 0.0841$ $DCratio_{shear} = 0.2015$ $DCratio_{shearip} = 0$

$$ratios := \left(Section\ \theta_{u_m}\ \tau_{u_m}\ \tau_{cap_m}\ DCratio_m\ \theta_{u_c}\ \tau_{u_c}\ \tau_{cap_c}\ DCratio_c\ V_u\,kip^{-1}\ V_c\,kip^{-1}\ DCratio_{shear}\ V_{uip}\,kip^{-1}\ V_{cip}\,kip^{-1}\ DCratio_{shearip}\right)$$

Pacific Northwest National Laboratory
ACI-349-06 Demand/Capacity Calculation - Section 5 Example

Page 16 of 16
Date: 7/14/2010 By: M.S. Schwendeman
Chkd: 8/2/2010 By: S.E. Sanborn
Revised: 4/12/2014 By: J.E. Deibler

Section = 5

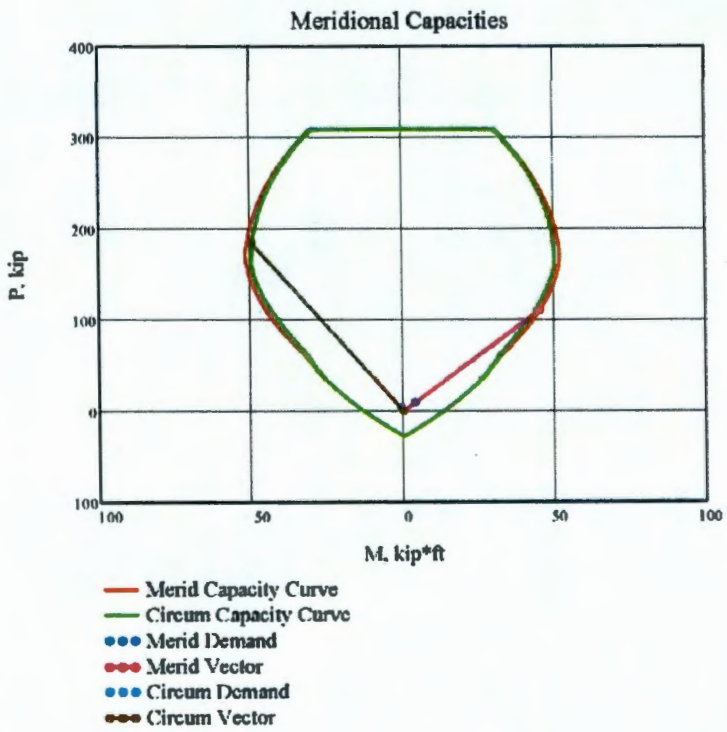

Output/Save Results:

Output := augment(MeridOutput, CircumOutput)

appendd := APPENDPRN("ACItypel_ii6.txt", ratio)

vector := augment($Mangle_m$, $Pangle_m$, $Mangle_c$, $Pangle_c$)

capacityvector.txt

vector

Output

C.2

ACI. 2007. *American Concrete Institute Code Requirements for Nuclear Safety Related Concrete Structures*. ACI 349-06, American Concrete Institute, Farmington Hills, Michigan.

Johnson KI, JE Deibler, FG Abatt, and MW Rinker. 2010. *Single-Shell Tank Structural Evaluation Criteria*. RPP-46442, Rev. 0, Pacific Northwest National Laboratory, Richland, Washington.

Appendix D

External Reviewer Comments and Resolutions

This page intentionally left blank.

Appendix D

External Reviewer Comments and Resolution

September 25, 2014

Jim Castleberry
MS R3-26
Washington River Protection Solutions
PO Box 1500
Richland, WA 99352

Re: Comments and recommendations of Drs. R.P. Kennedy and A.S. Veletsos on the Hanford Type 1 Single-Shell Tank Thermal and Operating Loads and Seismic Analyses (PNNL Report RPP-RPT-49993, Rev. 0 and Becht Document 20906-R-00).

Jim:
We have provided our comments and recommendations on the Analyses of Record (AOR) documents for the period from 2010 to the present. We appreciate the project's diligence and effort in responding to our comments.
Following are our specific comments on the above-referenced documents:

- Both the seismic and the thermal and operating loads (TOLA) analyses presented represent high quality, state of the art studies that are comprehensive and conclusive.
- The analyses indicate that the only location in the tank where the demand exceeds the available capacity is in the bottom slab. We concur with the conclusion that the potential damage of this exceedance will not affect tank integrity.
- The limit load analyses presented indicate that the safety factor for the tanks considered may be close to, or slightly below, the recommended value of 3. However, considering that both this value and the method of analysis used are conservative, we agree that the tanks will be able to support safely higher loads. Additional analyses would naturally be required to assess the adequacy of the safety factors for the increased loads.
- We agree with the conclusion that tank-to-tank interaction studies are not necessary for the Type I tanks.
- The three-dimensional plots of the Demand/Capacity (D/C) ratios presented in Chapter 7 of the PNNL report are difficult to review. For example, Figure 7-34 shows a D/C spike of over 1.0 but it is difficult to determine from it if this occurs in Section 18 or 19. The difficulty is caused by the three-dimensional presentation of the results, the volume of data included in the plots, and the location of the spikes at the 180 degrees location, which is at the back of the plot. It is our view that these plots should be simplified and clarified. We specifically recommend that the variations with distance or (or section number) of the maximum values of the D/C ratios of the horizontal shear in the tank wall and of the vertical shears in the slabs of the roof and base be displayed separately in two-dimensional plots, using a reasonable number of sections in each case. It would also be desirable to present a listing of the critical values at Sections 18 and 19.

<u>Response:</u> Additional plots and tables have been added to Chapter 7 to clearly show the locations and values of the D/C ratios. The results for section 18 at the bottom of the wall and section 19 in the footing are specifically highlighted. The spikes in the ACI shear D/C ratios have been correlated to decreases in the shear capacity as conservatively calculated in the Mathcad™ ACI routine. The shear demand remains nearly constant around the tank, but the shear capacity conservatively decreases with the change in sign of the already low meridional moment.

- The TOLA results in the report are expressed in terms of D/C ratios while the seismic effects are presented as forces and moments. This makes it difficult to crosswalk between the two analyses and to compare results. While we are not concerned about this issue considering that the seismic effects are low, we recommend that a statement be included in the report indicating the small contribution of the seismic effects to the overall effects.

  <u>Response:</u> Sentences have been added in the Executive Summary, Chapter 9, and the Conclusions stating that the seismic loads are small, representing only about 10% of the section capacities. This increases the maximum D/C ratios for the unfactored thermal and operating loads from 0.35 to 0.45.

We appreciate the opportunity to participate in the review of the analyses considered. While we have completed the review of all of the Analyses of Record, we will remain available for any additional project review needs.

Sincerely,

Robert P. Kennedy

Dr. R. P. Kennedy

Dr. A. S. Veletsos

Attachment 1: Seismic Analysis Report

This page intentionally left blank.

Becht Engineering Company, Inc. • Becht Nuclear Services • becht.com

5224 Woodside Executive Court, Aiken, SC 29803 • 803-648-7461
114 Columbia Point Drive, Suite A, Richland, WA 99352 • 509-943-1625

HANFORD TYPE I SINGLE SHELL TANK SEISMIC ANALYSIS

Document No. 20906-R-001

Revision No. 0

F. G. Abatt[1], Ken L. Stoops[2], Brian M. Larsen[3], Larry J. Julyk[1]

10/13/2014

[1]Senior Engineering Advisor, Becht Engineering, Richland, WA
[2]Senior Engineer I, Becht Engineering, Richland, WA
[3]Engineering Advisor, Becht Engineering, Richland, WA

Project Number	Project Name	Client
20906	Type I SST Seismic Analysis	PNNL

Quality Assurance	Open Items	Pre-verified Software Used
NQA-1	No	ANSYS® 13.0

Originator	Verifier	Approver
Ken Stoops Digitally signed by Ken Stoops Date: 2014.10.13 15:38:21 -07'00' Ken Stoops	Brian Larsen cn=Brian Larsen, o=Becht Engineering Company, Inc., ou=Becht Nuclear Services, email=blarsen@becht.com, c=US 2014.10.14 08:18:24 -07'00' Brian Larsen	F. G. Abatt Digitally signed by F. G. Abatt DN: cn=F. G. Abatt, o=Becht Engineering Company, Inc., ou=Becht Nuclear Services, email=gabatt@becht.com, c=US Date: 2014.10.14 08:37:37 -07'00'

Record of Revisions

Revision	Date	Description of Changes
0	10/13/2014	Initial Issue

1.0 Executive Summary

This report documents the seismically induced tank demands for the buried reinforced concrete Type I (55-kgal storage capacity) Single-Shell Tanks (SSTs) located on the Department of Energy (DOE) Hanford Site. A companion report (Johnson et al. 2014a) documents the thermal and operating loads analysis (TOLA) and the demand/capacity ratios for the combined TOLA and seismic demands.

The seismic analyses documented in this report use modern finite element (FE) modeling techniques with ANSYS®[1] version 13.0. The soil-structure interaction (SSI) seismic analysis uses a range of soil properties and evaluates the tank with and without stored waste for the seismic event.

The SSTs are categorized as and evaluated as Performance Category 2 (PC-2) structures, and DOE-STD-1020-2002, Section 2 (DOE 2002), requires that the ground motions for PC-2 shall be developed following the 2000 International Building Code requirements. The Tank Operations Contractor standard (TFC-ENG-STD-06) recognizes the State of Washington Administrative Code (WAC) 51-50-003, which adopted the 2009 edition of the International Building Code at the time that the structural evaluation criteria for the SSTs were developed (Johnson et al: 2010).

Consistent with Johnson et al. (2010), IBC (2009), and DOE (2002), the maximum considered earthquake (MCE) ground motions are defined as the ground motions with a mean annual frequency of exceedance of 4×10^{-4} (2% probability of exceedance in 50 years). In this analysis, the site-specific design response spectra (DRS) for the SST facilities site uses the Rohay and Reidel (2005) Hanford Waste Treatment Plant (WTP) design spectra as a reasonable assessment of the current state of knowledge of the hazard levels at the 200 East and 200 West areas. The 2005 spectra are conservative relative to data documented in Geomatrix (2007), but this choice was made to protect against the chance that Hanford seismic hazard levels could be increased in the near future.

The seismic model input (horizontal and vertical) motions were defined as acceleration time series. These input motions are carefully determined to ensure that they result in far-field surface-level and tank foundation-level responses in the ANSYS® Soil-Structure Interaction (SSI) model that meet or exceed appropriate spectral matching criteria for the design-bases spectra. The resulting input motions are generally conservatively biased. The maximum tank section forces and moments obtained from the SSI analysis are extracted from the seismic finite-element model and presented in this report. These seismic demands are combined with the non-seismic forces and moments to evaluate the tank integrity per the American Concrete Institute (ACI) code in Johnson et al. (2014a).

Additional analysis, documented in Appendix A to this report, is conducted to address the effects of a manhole penetration on the tank seismic induced demands. The effect of the manhole penetration produces small localized demand differences, and its effect on tank structural integrity is considered insignificant.

The Type I SST seismic analysis project is performed under the Becht QA (quality assurance) program (Becht 2013). The Becht QA program is based on ASME NQA-1 2008.

[1] ANSYS® is a registered trademark of ANSYS, Inc., Canonsburg, Pennsylvania.

1.1 Acknowledgments

The authors would like to acknowledge the management support of Washington River Protection Solutions (WRPS) and the funding they provided on behalf of the U.S. Department of Energy's Office of River Protection (ORP) to perform the Single-Shell Tank Analysis of Record (AOR) Project.

Table of Contents

1.0 Executive Summary iii
1.1 Acknowledgments iv
2.0 Introduction 1
2.1 Type I SST Background 1
3.0 Scope 3
4.0 Conclusions 4
5.0 References 5
6.0 Structural Model Description 8
6.1 Model Geometry 9
6.1.1 Model Organization 13
6.1.2 Organization and Identification System 13
6.1.3 Input and Output Files 14
6.1.4 Tank Concrete 16
6.1.5 Concrete Hatchway 20
6.1.6 Soil Model 21
6.2 Model Interfaces 25
6.2.1 Soil/Concrete Tank Interface 27
6.2.2 Concrete Hatchway/Overburden Soil Fill Interface 29
6.2.3 Concrete Hatchway/Concrete Tank Interface 29
6.2.4 At-Rest Soil Pressure at Tank Wall 30
6.2.5 Waste/Concrete Tank Interface 30
6.2.6 Soil-to-Soil Interfaces 31
6.2.7 Soil Arching 31
6.2.8 Soil-to-Roof Contact Stiffness 31
6.3 Material Properties 32
6.3.1 Tank Concrete Properties 32
6.3.2 Waste 34
6.3.3 Soil Properties 35
6.4 Load Conditions 40
6.4.1 Surface Loads 40
6.5 Boundary Conditions 41
6.5.1 Soil Boundary Conditions 41
6.5.2 Tank Boundary Conditions 43
6.5.3 Model Excitation 43
6.5.4 Seismic Input 44
6.6 Post-Processing 44
6.6.1 Concrete Tank Elements 44

6.6.2 Contact Elements 47
6.6.3 Enveloping Process 47
6.7 Run Descriptions 49
6.7.1 Seismic Run Matrix 49
6.7.2 Results Extraction 50
7.0 Soil Column Properties, Base Motion Inputs, and Spectral Matching 51
7.1 Introduction 51
7.2 SHAKE Soil Column Descriptions 51
7.3 Characterization of the SHAKE Soil Columns 52
7.3.1 Amplification Factors for Three Soil Profiles – Horizontal Motion 52
7.3.2 Amplification Factors for Three Soil Profiles – Vertical Motion 54
7.4 Development of Time Histories at the Base of the SSI Profiles to be Used as Input to ANSYS® SSI Models 56
7.5 Generation of Target Spectra Using SHAKE 57
7.6 Description of the ANSYS® Soil Column Models 62
7.6.1 Element Geometry and Layer Thickness 63
7.6.2 Boundary Conditions 67
7.6.3 Seismic Loading 68
7.6.4 ANSYS® Soil Column Material Properties 69
7.7 Calibration of ANSYS® Damping Parameters 69
7.8 Characterization of the ANSYS® Soil Columns Dynamic Response 74
7.8.1 Soil Column Harmonic Analysis – Vertical Excitation 76
7.9 Spectral Matching Methodology and Acceptance Criteria 78
7.9.1 Spectral Matching for the ANSYS® SSI Model with Horizontal Time Histories 79
7.9.2 Spectral Matching for the ANSYS® SSI Model with Vertical Time Histories 85
7.9.3 Spectral Response of the Tank 91
8.0 Seismic Results 94
8.1 Concrete Tank 94
8.1.1 Lower Bound Soil (LBS) 97
8.1.2 Best-Estimate Soil (BES) 103
8.1.3 Upper Bound Soil (UBS) 106
8.1.4 Summary of Seismic Demands 109
8.2 Soil Contact Results 116
9.0 Calculation Verification 119

Table of Contents – Appendices & Attachments

Appendix A — Manhole Penetration A-1
A.1 Introduction A-1
A.2 Type I SST Manhole Penetration Model A-1
A.3 Results A-3
Appendix B — Investigation of a Numerical Anomaly Associated with Specification of Initial Friction Values B-1
B.1 Summary B-1
B.2 Conclusion B-1
B.3 Discovery B-1
B.4 Causation B-3
B.5 Results B-4
Appendix C — Software Quality Assurance and Computer Files C-1

Attachment 1 — Computer Files Att1-1

List of Figures

Figure 2-1 Drawing D-1 (Annotated) Showing Tank Farm Arrangement 2
Figure 6-1. Rendering of Concrete Tank and Hatchway, Cut to Show Internal Details 9
Figure 6-2. Element Plot of Complete Seismic Model for Lower Bound Soil Configuration 10
Figure 6-3. Element Plot of Seismic Model Showing Backfill and Waste Material Properties 10
Figure 6-4. Element Plot of Seismic Model Showing Tank, Waste, Hatchway, and Overburden Soil 11
Figure 6-5. Drawing D-20 (Partial) Showing Symmetry Plane Lines for Hatchway Section Cuts A-A and B-B 12
Figure 6-6. Model Top View of Half-Symmetry Hatchway Orientation at Sections A-A (left) and B-B (right) 12
Figure 6-7. Concrete Tank Profile Showing ACI-Evaluation Section Locations and Associated Tank Elements 17
Figure 6-8. Element Plot of Concrete Tank Profile Showing Shell Element Thickness 18
Figure 6-9. Shell Element Orientation Sketch 18
Figure 6-10. Concrete Tank Profile Showing ACI-Evaluation Section Locations and Seismic Model Element Material Numbers 19
Figure 6-11. Element Plot Showing Tank and Hatchway at Section A-A 20
Figure 6-12. Element Plot Showing Tank and Hatchway at Section B-B 21
Figure 6-13. Model Plot of LBS – Excavated Backfill Soil 22
Figure 6-14. Model Plot of BES – Excavated Backfill Soil 22
Figure 6-15. Model Plot of UBS – Excavated Backfill Soil 23
Figure 6-16. Element Plot Showing Overburden Soil without Hatchway 23
Figure 6-17. Element Plot of LBS Far-Field Soil Layering and Material Property Assignment 24
Figure 6-18. Element Plot of BES Far-Field Soil Layering and Material Property Assignment 25
Figure 6-19. Element Plot of UBS Far-Field Soil Layering and Material Property Assignment 25
Figure 6-20. Element Plot Annotated with Locations of Interfaces in Seismic Model 26
Figure 6-21. Element Plot Showing Interface Elements Real Property Assignment - All Interfaces 27
Figure 6-22. Element Plot Showing Interface Elements Real Property Assignment – Soil-to-Concrete Tank 28
Figure 6-23. Element Plot Showing Interface Elements Real Property Assignment – Hatchway (Section A-A)-to-Overburden 29
Figure 6-24. Element Plot Showing Interface Elements Real Property Assignment – Hatchway (Section A-A)-to-Tank 29
Figure 6-25. Element Plot Showing Interface Elements Real Property Assignment – Waste-to-Concrete Tank 30
Figure 6-26. Element Plot Showing Waste 34
Figure 6-27. Element Plot of Surface Load Elements (Shown Circled, in Green) 41
Figure 6-28. Seismic Model Boundary Conditions – Symmetry Plane and Soil Base 42
Figure 6-29. Seismic Model Boundary Conditions – Slaved Boundary Conditions 42

Figure 6-30. Seismic Model Boundary Condition – Concrete Tank 43
Figure 6-31. ANSYS® SHELL 181 Element Force and Moment Vector Orientations (the Type-I tank orientations are the same as the Type-II tank profile shown) 45
Figure 6-32. Element Plot of Concrete Tank Elements at ACI-Evaluation Sections 46
Figure 7-1. SHAKE91 Lower Bound Amplification Factors from Horizontal Input Motion 53
Figure 7-2. SHAKE91 Best Estimate Amplification Factors from Horizontal Input Motion 53
Figure 7-3. SHAKE91 Upper Bound Amplification Factors from Horizontal Input Motion 54
Figure 7-4. SHAKE91 Lower Bound Amplification Factors from Vertical Input Motion 55
Figure 7-5. SHAKE91 Best Estimate Amplification Factors from Vertical Input Motion 55
Figure 7-6. SHAKE91 Upper Bound Amplification Factors from Vertical Input Motion 56
Figure 7-7. Lower Bound Horizontal Target Spectra 58
Figure 7-8. Lower Bound Vertical Target Spectra 58
Figure 7-9. Best Estimate Horizontal Target Spectra 59
Figure 7-10. Best Estimate Vertical Target Spectra 59
Figure 7-11. Upper Bound Horizontal Target Spectra 60
Figure 7-12. Upper Bound Vertical Target Spectra 60
Figure 7-13. Lower Bound Horizontal Target Spectra at SST Foundation Elevations, with Extrapolated E0 61
Figure 7-14. Lower Bound Vertical Target Spectra at SST Foundation Elevations, with Extrapolated E0 62
Figure 7-15. Elevation View of Typical ANSYS® Soil Column Model 63
Figure 7-16. Top View of ANSYS® Soil Column Model Showing Boundary Conditions 68
Figure 7-17. Mass Proportional Damping vs. Frequency for Alpha=1.0 71
Figure 7-18. Stiffness Proportional Damping vs. Frequency 72
Figure 7-19. Composite Rayleigh Damping for Lower Bound ANSYS® Soil Column 72
Figure 7-20. Composite Rayleigh Damping for Best Estimate ANSYS® Soil Column 73
Figure 7-21. Composite Rayleigh Damping for Upper Bound ANSYS® Soil Column 73
Figure 7-22. SHAKE91 vs. ANSYS® Free Field Horizontal Amplification Factors for Lower Bound Soil 74
Figure 7-23. SHAKE91 vs. ANSYS® Free Field Horizontal Amplification Factors for Best Estimate Soil 75
Figure 7-24. SHAKE91 vs. ANSYS® Free Field Horizontal Amplification Factors for Upper Bound Soil 75
Figure 7-25. SHAKE91 vs. ANSYS® Free Field Vertical Amplification Factors for Lower Bound 76
Figure 7-26. SHAKE91 vs. ANSYS® Free Field Vertical Amplification Factors for Best Estimate 77
Figure 7-27. SHAKE91 vs. ANSYS® Free Field Vertical Amplification Factors for Upper Bound 77
Figure 7-28. Comparison of Lower Bound Horizontal Surface Spectra from the ANSYS® SSI Model 80

Figure 7-29. Comparison of Lower Bound Horizontal Tank Foundation Spectra from the ANSYS® SSI Model 81

Figure 7-30. Comparison of Best Estimate Horizontal Surface Spectra from the ANSYS® SSI Model 82

Figure 7-31. Comparison of Best Estimate Horizontal Tank Foundation Spectra from the ANSYS® SSI Model 83

Figure 7-32. Comparison of Upper Bound Horizontal Surface Spectra from the ANSYS® SSI Model 84

Figure 7-33. Comparison of Upper Bound Horizontal Tank Foundation Spectra from the ANSYS® SSI Model 85

Figure 7-34. Comparison of Lower Bound Vertical Surface Spectra from the ANSYS® SSI Model 86

Figure 7-35. Comparison of Lower Bound Vertical Tank Foundation Spectra from the ANSYS® SSI Model 87

Figure 7-36. Comparison of Best Estimate Vertical Surface Spectra from the ANSYS® SSI Model 88

Figure 7-37. Comparison of Best Estimate Vertical Tank Foundation Spectra from the ANSYS® SSI Model 89

Figure 7-38. Comparison of Upper Bound Vertical Surface Spectra from the ANSYS® SSI Model 90

Figure 7-39. Comparison of Upper Bound Vertical Tank Foundation Spectra from the ANSYS® SSI Model 91

Figure 7.40. Comparison of Horizontal Acceleration Response Spectra for Lower Bound Soil - Tank vs. Far-Field 93

Figure 7.41. Comparison of Vertical Acceleration Response Spectra for Lower Bound Soil - Tank vs. Far-Field 93

Figure 8-1. Element Plot Top View Showing Tank at ACI-Evaluation Sections 1-5 and Hatchway at Section A-A 96

Figure 8-2. Element Plot Top View Showing Tank at ACI-Evaluation Sections 1-5 and Hatchway at Section B-B 96

Figure 8-3. Lower Bound Soil (LBS), Full Tank, Hatchway Section A-A: Concrete Tank Meridional Force (kip/ft.) – Seismic Only 97

Figure 8-4. Lower Bound Soil (LBS), Full Tank, Hatchway Section A-A: Concrete Tank Hoop Force (kip/ft.) – Seismic Only 98

Figure 8-5. Lower Bound Soil (LBS), Full Tank, Hatchway Section A-A: Concrete Tank Meridional Moment (kip ft./ft.) – Seismic Only 99

Figure 8-6. Lower Bound Soil (LBS), Full Tank, Hatchway Section A-A: Concrete Tank Hoop Moment (kip ft./ft.) – Seismic Only 100

Figure 8-7. Lower Bound Soil (LBS), Full Tank, Hatchway Section A-A: Concrete Tank Through-Wall Shear Force (kip/ft.) – Seismic Only 101

Figure 8-8. Lower Bound Soil (LBS), Full Tank, Hatchway Section A-A: Concrete Tank In-Plane Shear Force (kip/ft.) – Seismic Only 102

Figure 8-9. Best Estimate Soil (BES), Full Tank, Hatchway Section A-A: Concrete Tank Meridional Force (kip/ft.) – Seismic Only 103

Figure 8-10. Best Estimate Soil (BES), Full Tank, Hatchway Section A-A: Concrete Tank Hoop Force (kip/ft.) – Seismic Only 103

Figure 8-11. Best Estimate Soil (BES), Full Tank, Hatchway Section A-A: Concrete Tank Meridional Moment (kip ft./ft.) – Seismic Only 104

Figure 8-12. Best Estimate Soil (BES), Full Tank, Hatchway Section A-A: Concrete Tank Hoop Moment (kip ft./ft.) – Seismic Only 104

Figure 8-13. Best Estimate Soil (BES), Full Tank, Hatchway Section A-A: Concrete Tank Through-Wall Shear Force (kip/ft.) – Seismic Only 105

Figure 8-14. Best Estimate Soil (BES), Full Tank, Hatchway Section A-A: Concrete Tank In-Plane Shear Force (kip/ft.) – Seismic Only 105

Figure 8-15. Upper Bound Soil (UBS), Full Tank, Hatchway Section A-A: Concrete Tank Meridional Force (kip/ft.) – Seismic Only 106

Figure 8-16. Upper Bound Soil (UBS), Full Tank, Hatchway Section A-A: Concrete Tank Hoop Force (kip/ft.) – Seismic Only 106

Figure 8-17. Upper Bound Soil (UBS), Full Tank, Hatchway Section A-A: Concrete Tank Meridional Moment (kip ft./ft.) – Seismic Only 107

Figure 8-18. Upper Bound Soil (UBS), Full Tank, Hatchway Section A-A: Concrete Tank Hoop Moment (kip ft./ft.) – Seismic Only 107

Figure 8-19. Upper Bound Soil (UBS), Full Tank, Hatchway Section A-A: Concrete Tank Through-Wall Shear Force (kip/ft.) – Seismic Only 108

Figure 8-20. Upper Bound Soil (UBS), Full Tank, Hatchway Section A-A: Concrete Tank In-Plane Shear Force (kip/ft.) – Seismic Only 108

Figure 8-21. Seismic Results: Concrete Tank Meridional Force (kip/ft.) – Seismic Only 110

Figure 8-22. Seismic Results: Concrete Tank Hoop Force (kip/ft.) – Seismic Only 111

Figure 8-23. Seismic Results: Concrete Tank Meridional Moment (kip ft./ft.) – Seismic Only 112

Figure 8-24. Seismic Results: Concrete Tank Hoop Moment (kip ft./ft.) – Seismic Only 113

Figure 8-25. Seismic Results: Concrete Tank Through-Wall Shear Force (kip/ft.) – Seismic Only 114

Figure 8-26. Seismic Results: Concrete Tank In-Plane Shear Force (kip/ft.) – Seismic Only 115

Figure 8-27. Soil/Concrete Tank Contact Element Normal Pressure in Tank Wall (kip/sq. ft.) – Gravity Only 117

Figure 8-28. Soil/Concrete Tank Contact Element Bounding Normal Pressure – Seismic Only 118

Figure A-1. Element Plot Showing Tank with Manhole Penetration and Hatchway at Section A-A A-2

Figure A-2. Element Plot Angled View Detail Showing Tank with Manhole Penetration A-2

Figure A-3. Element Plot Top View Showing Tank Elements at ACI-Evaluation Sections 1-5 (roof) with Manhole Penetration and Hatchway at Section A-A A-3

Figure A-4a. Manhole Penetration Study: Concrete Tank Meridional Force Surface Plot – Seismic Only A-4

Figure A-4b. Manhole Penetration Study: Concrete Tank Meridional Force Comparison – Seismic Only A-4

Figure A-5a. Manhole Penetration Study: Concrete Tank Hoop Force Surface Plot – Seismic Only A-5

Figure A-5b. Manhole Penetration Study: Concrete Tank Hoop Force Comparison– Seismic Only A-5

Figure A-6a. Manhole Penetration Study: Concrete Tank Meridional Moment Surface Plot – Seismic Only A-6

Figure A-6b. Manhole Penetration Study: Concrete Tank Meridional Moment Comparison – Seismic Only A-6

Figure A-7a. Manhole Penetration Study: Concrete Tank Hoop Moment Surface Plot – Seismic Only A-7

Figure A-7b. Manhole Penetration Study: Concrete Tank Hoop Moment Comparison – Seismic Only A-7

Figure A-8a. Manhole Penetration Study: Concrete Tank Through-Wall Shear Force Surface Plot – Seismic Only A-8

Figure A-8b. Manhole Penetration Study: Concrete Tank Through-Wall Shear Force Comparison – Seismic Only A-8

Figure A-9a. Manhole Penetration Study: Concrete Tank In-Plane Shear Force Surface Plot – Seismic Only A-9

Figure A-9b. Manhole Penetration Study: Concrete Tank In-Plane Shear Force Comparison – Seismic Only A-9

Figure B-1. Seismic Results Over Time Using Zero Initial Friction Coefficients: Concrete Tank Hoop Force (kip/ft.) – Gravity + Seismic B-2

Figure B-2. Seismic Results Over Time Using Zero Initial Friction Coefficients: Concrete Tank Hoop Force (kip/ft.) at Top (Left) and Bottom (Right) of the Wall – Gravity + Seismic B-2

Figure B-3. Seismic Results Over Time Using Small Nonzero Initial Friction Coefficients: Concrete Tank Hoop Force (kip/ft.) at Bottom of the Wall – Gravity + Seismic B-3

Figure B-4. Seismic Results: Concrete Tank Meridional Force (kip/ft.) – Seismic Only B-5

Figure B-5. Seismic Results: Concrete Tank Hoop Force (kip/ft.) – Seismic Only B-5

Figure B-6. Seismic Results: Concrete Tank Meridional Moment (kip ft./ft.) – Seismic Only B-6

Figure B-7. Seismic Results: Concrete Tank Hoop Moment (kip ft./ft.) – Seismic Only B-6

Figure B-8. Seismic Results: Concrete Tank Through-Wall Shear Force (kip/ft.) – Seismic Only B-7

Figure B-9. Seismic Results: Concrete Tank In-Plane Shear Force (kip/ft.) – Seismic Only B-7

List of Tables

Table 6-1. List of Model Components 13
Table 6-2. ANSYS® Model Input File Description (pre-processing phase) 14
Table 6-3. ANSYS® Model Input File Description (solution phase) 15
Table 6-4. ANSYS® Model Input File Description (post-processing phase) 15
Table 6-5. ANSYS® Model Output File Description 16
Table 6-6. Type I SST Hatchway Load (for Half Model) 20
Table 6-7. Summary of Soil-to-Concrete Tank Friction Properties 28
Table 6-8. Fully Cracked Orthotropic Concrete Properties 33
Table 6-9. Seismic Model Waste Properties 34
Table 6-10. Strain Compatible Lower Bound Native Soil Properties 36
Table 6-11. Strain Compatible Best Estimate Native Soil Properties 37
Table 6-12. Strain Compatible Upper Bound Native Soil Properties 38
Table 6-13. Lower Bound Excavated Backfill Soil Properties 39
Table 6-14. Best Estimate Excavated Backfill Soil Properties 39
Table 6-15. Upper Bound Excavated Backfill Soil Properties 40
Table 6-16. Type I SST Concentrated Surface Loads (for Half Model) 41
Table 6-17. Selected ANSYS® SHELL181 Output Quantities and Sequence Numbers 44
Table 6-18. Tank Concrete ACI-Evaluation Section Data Output (Sample Excerpt) 46
Table 6-19. Selected ANSYS® CONTA173 Output Quantities 47
Table 6-20. Seismic Model Run Matrix 49
Table 7-1. SSI Soil Profile Geometry 52
Table 7-2. Maximum Allowable Element Sizes for Lower Bound Soil 64
Table 7-3. Maximum Allowable Element Sizes for Best Estimate Soil 66
Table 7-4. Maximum Allowable Element Sizes for Upper Bound Soil 67
Table 7-5. Soil Column Modal Frequencies for Horizontal Excitation 76
Table 7-6. Soil Column Modal Frequencies for Vertical Excitation 78
Table B-1. Summary of Zero Initial Friction Properties B-3
Table C-1. Computer Listing C-1
Table C-2. Computer Files Directory Listing C-3

Acronyms

ACI	American Concrete Institute
AOR	analysis of record
ASCE	American Society of Civil Engineers
BE	best estimate
BES	best estimate soil
D/C	demand/capacity ratio
DF	damping factor
DOE	U.S. Department of Energy
DRS	design response spectra
ECS	element coordinate system
FCC	fully cracked concrete
FE	finite element
FIRS	foundation input response spectra
GCS	global coordinate system
HSS	high shear stiffness
kip	thousand pounds
ksf	kips per square foot
LB	lower bound
LBS	lower bound soil
MCE	maximum considered earthquake
ORP	DOE Office of River Protection
PNNL	Pacific Northwest National Laboratory
QA	quality assurance
SCOR	soil column outcrop response
SSI	soil-structure interaction
SST	single-shell tank
TOLA	Thermal and Operating Loads Analysis
TTI	tank-to-tank interaction
UB	upper bound
UBS	upper bound soil
WRPS	Washington River Protection Solutions
WTP	Waste Treatment Plant
WAC	Washington Administrative Code

2.0 Introduction

The U.S. Department of Energy (DOE) Office of River Protection (ORP) has determined the need to better understand the structural integrity of the Single Shell Tanks (SSTs) on the Hanford Site in Washington State. To address this need, Pacific Northwest National Laboratory (PNNL) is performing an SST Analysis of Record (AOR) for Washington River Protection Solutions (WRPS). The primary objective of the SST AOR Project is to perform a comprehensive structural AOR for the SSTs in order to understand the existing SST structural integrity that considers both past usage and a postulated design basis earthquake that may occur in the future. PNNL has performed the static analysis of the thermal and operating loads while Becht Engineering Company, Inc. (Becht) was subcontracted to perform the seismic analysis of the SSTs.

The analyses described in this report document the seismic demands for the Type I (55-kgal storage capacity) SSTs. The Type I SSTs are also known as 200-series tanks. A companion report (Johnson et al. 2014a) documents the thermal and operating loads analysis (TOLA) and calculates the demand/capacity (D/C) ratios for combined TOLA and seismic loads per ACI 349 (ACI 2007) requirements.

2.1 Type I SST Background

In response to Hanford's plutonium production, a total of 149 underground tanks were constructed between 1943 and 1964 to contain the nuclear waste in twelve separate tank farms in the 200 East and West areas of the Hanford Site. A total of sixteen (four per farm) underground tanks, each with a nominal 55,000-gallon capacity and 20-foot internal diameter, were built along the edges of four tank farms (B, C, T, and U which also contain the Type II Series 100 SSTs) and are designated as the Type I Series 200 SSTs. The Type I and II tanks are among the oldest SSTs at the Hanford Site. By 1980, discharge operations to all the SSTs ended pursuant with a congressional mandate. Interim stabilization was completed by 2004 when all pumpable supernate and interstitial liquids were removed from all SSTs (Berman 2009).

Each SST is an underground reinforced concrete structure with a welded carbon steel liner extending along the base and cylindrical concrete wall of the SSTs. The Type I tanks have an internal height of approximately 26 feet from the floor to the roof, with the steel liner extending to nearly the full height of the tank. Because the SST steel liners are not structurally attached to the concrete (they provide a leak tight boundary for the stored waste) they are not included in the structural analysis.

Typical center-to-center spacing of the 75-ft internal diameter series 100 SSTs of approximately 100 feet in the Hanford tank farms results in a vault-to-vault minimum distance of approximately 58% of the tank outer radius ($0.58R_o$). The 50 ft. center-to-center spacing between the Type I tanks gives a vault-to-vault spacing of approximately 3 times the tank outer radius (see Figure 2-1 with excerpt from Drawing D-1). The distance between the Type I tanks and the adjacent Type II tanks has a more typical center-to-center spacing of 100 ft. More detailed descriptions and background information on the Type I SSTs can be found in Johnson et al. (2014a).

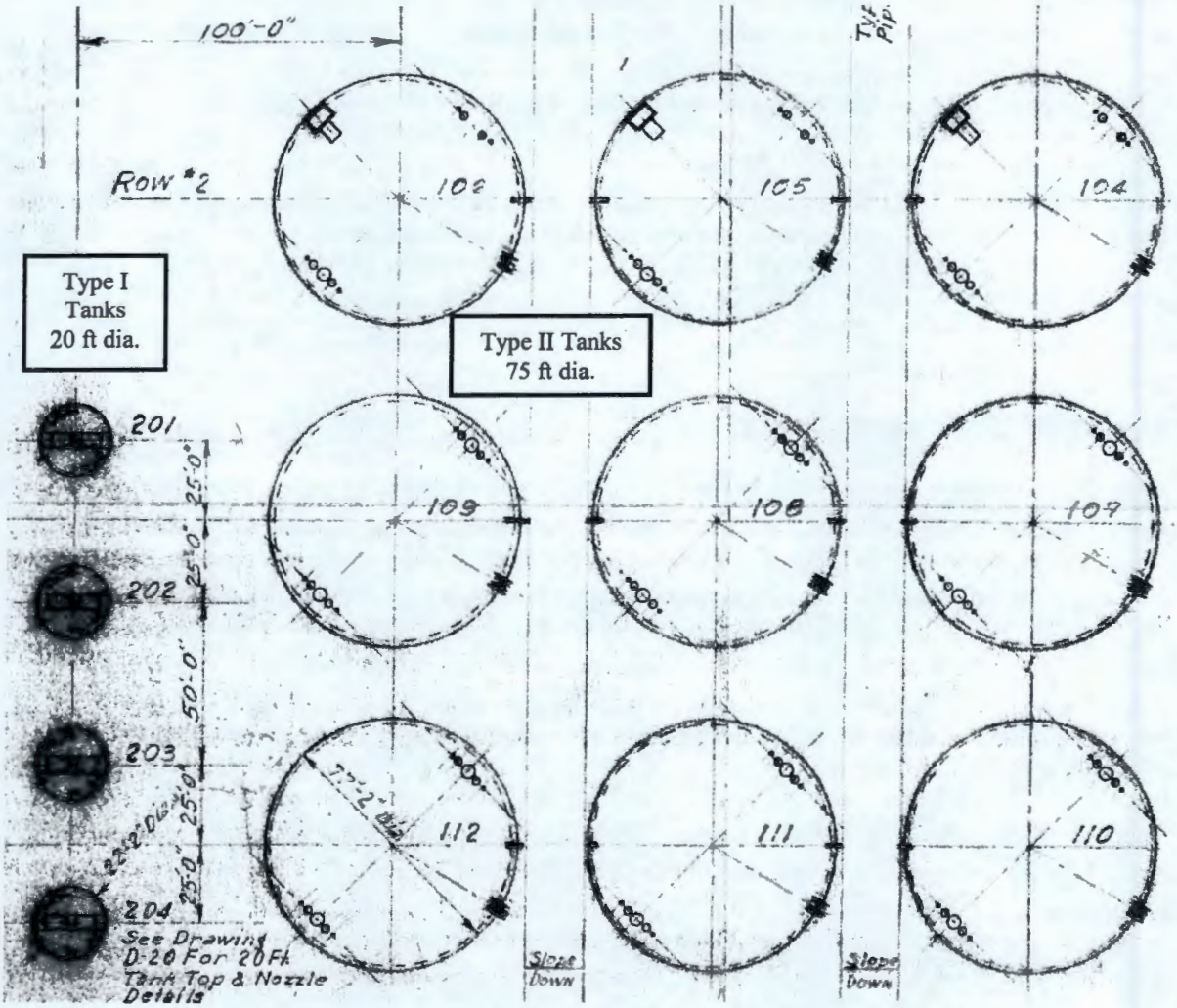

Figure 2-1 Drawing D-1 (Annotated) Showing Tank Farm Arrangement

3.0 Scope

The objective of the Single-Shell Tank Analysis of Record Project is to perform a comprehensive structural analysis of record for each of the four types of Hanford SSTs. This report provides the results of the seismic analysis for the Type I SSTs. A companion report, Johnson et al. (2014a), provides results for the thermal and operating loads analysis and documents the resulting demand-to-capacity ratios to assess the structural integrity of the Type I SSTs.

Similar to the previous SST structural and seismic analyses reported in Rinker et al. (2011a and 2011b) and Johnson et al. (2014c), the current AOR uses a single-tank model in the analysis of the Type I tanks. Hence, it does not directly consider tank-to-tank interaction (TTI). An evaluation of TTI effects for both seismic and thermal and operating loads is documented in Johnson et al. (2014b), which provides the basis for appropriate adjustments to account for TTI in the AOR single-tank model analysis results. Tank-to-tank interaction effects were considered but not specifically evaluated for the Type I tanks because the 50-ft center-to-center spacing gives 3 radii of soil between adjacent tanks. Furthermore, all the D/C ratios are significantly less than 0.8, so adding the maximum $\Delta D/C=0.2$ for tank-to-tank effects would still result in values well below 1.0.

The seismic analysis documented herein assesses the impacts of potentially non-conservative assumptions and changes in Hanford site-specific seismic loading or lack thereof in previous structural analyses of the SSTs prior to the current AOR effort. These assumptions or changes included addressing: updated Hanford site-specific seismic hazard; updated Hanford site-specific variation of backfill and far-field soil properties; the effects of thermally induced concrete material degradation and effective orthotropic concrete cracked section properties; the non-rigid (low frequency) response of the tank roof; the asymmetric seismically induced soil loading; the asymmetric seismically induced waste loading; the application of current methodology for matching the far-field seismic response for both the tank foundation and soil surface-level elevations to corresponding design spectra; and incorporating long time settled "at-rest" soil pressure loading on the outer surface of the concrete wall of the tank as the initial soil pressure loading for the nonlinear concrete-to-soil interfaces that allow potential differential sliding and separation.

The seismic analysis considers interaction of the tank and attached hatchway superstructure with the surrounding soil, and the effects of the tank waste. The SST and the surrounding soil are modeled as a system of finite elements. The depth and width of the soil incorporated into the analysis model are sufficient to obtain accurate analytical results. The analyses required to support the work statement differ from previous analyses of the SSTs in that the soil-structure interaction model includes nonlinear contact surfaces between the tank and the supporting soil. The contained waste is modeled explicitly in order to capture the interaction behavior between the concrete tank and contained waste.

4.0 Conclusions

The results from this report are used as input for calculating the concrete demand-to-capacity ratios under combined thermal and operating and seismic loads to assess tank structural integrity as documented in Johnson et al. (2014a) in accordance with ACI 349 (ACI 2007).

The lower bound soil stiffness profile tends to create the greatest demands overall. In the half-symmetry tank model with the lower bound (softer) soil properties, the inclusion of hatchway section A-A (see Section 6.0 for discussion of tank features) of the massive upper pit structure typically produces greater or similar demands compared to the alternate section B-B. Also, the demands typically have a low sensitivity to the waste. Although the overall sensitivity is typically low, the roof demands are more sensitive to the choice of hatchway orientation, and the wall demands are more sensitive to the presence or level of the waste. The seismically induced demands are further assessed in Johnson et al. (2014a) in terms of demand/capacity ratios under combined TOLA and seismic demands.

This analysis uses a reduced run analysis matrix, relative to the run matrices of possible combinations of configurations included in previous AORs. Evaluations of a full tank with hatchway section A-A clearly shows that the lower bound soil stiffness tends to govern. Based on the limited sensitivity of the seismic demands for other configurations with lower bound soil, the additional best estimate and upper bound soil stiffnesses need not be run as the lower bound soil configuration will continue to govern. Furthermore, the low Type I demand/capacity ratios calculated in Johnson et al. (2014a) provide assurance that the sensitivity of the structural integrity to seismic demands is low. Thus, a reduced run analysis matrix with a single representative base case is sufficient for the evaluation of the Type I SSTs.

The effect of the manhole penetration in the roof produces small localized demand differences. During original construction additional reinforcing steel was provided around the manhole. Because the manhole was part of the original design, and the effects on the concrete demands are small and localized, it is not considered necessary to include the manhole in the baseline model.

5.0 References

ACI 2007, *American Concrete Institute Code Requirements for Nuclear Safety Related Concrete Structures*, ACI 349-06, American Concrete Institute, Farmington Hills, Michigan.

ASCE 2000, *Seismic Analysis of Safety-Related Nuclear Structures and Commentary*, ASCE 4-98, American Society of Civil Engineers, Reston, Virginia.

ASME 2008, *Quality Assurance Requirements for Nuclear Facility Applications*, ASME NQA-1 2008, American Society of Mechanical Engineers, New York, NY.

ANSYS 2010, *User's Manual Version 13.0*, ANSYS, Inc., Canonsburg, PA.

Berman, HS, 2009, *Hanford Single-Shell Tank Integrity Program*, Single-Shell Tank Integrity Project-Workshop, July 29, 2009, WRPS-40224-VA, Richland, Washington.

Becht 2013, *Quality Assurance Manual*, BNS-QAM-1, Becht Engineering Co., Inc., Richland, WA.

DOE 2002, *Natural Phenomena Hazards Design and Evaluation Criteria for Department of Energy Facilities*, DOE-STD-1020-2002, U.S. Department of Energy, Washington, D.C.

DuPont, 1944a, *General Layout*, Drawing D-1, Rev 4, Richland, WA

DuPont, 1944b, *Typical Sections for 20ft Tank*, Drawing D-20, Rev 6, Richland, WA

Geomatrix 2007, *Updated Site Response Analyses for the Waste Treatment Plant*, DOE Hanford Site

IBC 2003, *International Building Code 2003*, International Code Council, Inc.

IBC 2009, *International Building Code 2009*, International Code Council, Inc.

Idriss, IM and Sun, JI, 1992, *User's Manual for SHAKE91 A Computer Program for Conducting Equivalent Linear Seismic Response Analyses of Horizontally Layered Soil Deposits, Program modified based on the original SHAKE program published in December 1972 by Schnabel, Lysmer, and Seed*, Center for Geotechnical Modeling, Department of Civil & Environmental Engineering, University of California, Davis, California, November, 1992.

Hundal TS. 2004a. 241-B Tank Farm Historic Dome Load Record Data. RPP-20446, Rev. 0, COGEMA Engineering Corporation, Richland, Washington.

Hundal TS. 2004b. 241-C Tank Farm Historic Dome Load Record Data. RPP-20449, Rev. 0, COGEMA Engineering Corporation, Richland, Washington.

Hundal TS. 2004c. 241-T Tank Farm Historic Dome Load Record Data. RPP-20452, Rev. 0, COGEMA Engineering Corporation, Richland, Washington.

Hundal TS. 2004d. 241-U Tank Farm Historic Dome Load Record Data. RPP-20455, Rev. 0, COGEMA Engineering Corporation, Richland, Washington.

Johnson, KI, Deibler, JE, Abatt, FG and Rinker, MW, 2010, *Single-Shell Tank Structural Evaluation Criteria*, RPP-RPT-46442, Pacific Northwest National Laboratory, Richland, Washington.

Johnson, KI, Karri, NK, Deibler, JE, Sanborn, SE, Abatt, FG, Stoops, KL, Larsen, BM, and Julyk, LJ, 2014a, *Single-Shell Tank Integrity Project Analysis of Record: Hanford Type I Single-Shell Tank Thermal and Operating Loads and Seismic Analysis,* RPP-RPT-49993, Rev. 0, Pacific Northwest National Laboratory, Richland, Washington.

Johnson, KI, Karri, NK, Bapanapalli, SK, Sanborn, SE, Deibler, JE, Pilli, SP, Abatt, FG, Stoops, KL, Larsen, BM, and Julyk, LJ, 2014b, *Single-Shell Tank Integrity Project Analysis of Record: Tank-to-Tank Interaction Study of the Hanford Single-Shell Tanks,* RPP-RPT-49991, Rev. 0, Pacific Northwest National Laboratory, Richland, Washington.

Johnson, KI, Karri, NK, Bapanapalli, SK, Sanborn, SE, Deibler, JE, Pilli, SP, Abatt, FG, Stoops, KL, Larsen, BM, and Julyk, LJ, 2014c, *Single-Shell Tank Integrity Project Analysis of Record: Hanford Type IV Single-Shell Tank Thermal and Operating Loads and Seismic Analysis,* RPP-RPT-49992, Rev. 0, Pacific Northwest National Laboratory, Richland, Washington.

Mackey TC. 2012. *Analysis of Record Summary for Single-Shell Tanks*. RPP-11802, Rev. 3, CH2M HILL Hanford Group, Inc., Richland, Washington.

McGuire, RK, Silva, WJ, and Costantino, CJ, 2001, *Technical Basis for Revision of Regulatory Guidance on Design Ground Motions: Hazard- and Risk-Consistent Ground Motion Spectra Guidelines:* NUREG/CR-6728, U.S. Nuclear Regulatory Commission, Washington DC.

Nuclear Energy Institute (NEI), 2009, *Consistent Site Response/Soil-Structure Interaction Analysis and Evaluation*, Letter to Mr. Nilesh Chokshi from Russell Bell, dated June 12, 2009.

Rinker, MW, Abatt, FG, Carpenter, BG, and Hendrix, CA, 2006, *Hanford Double-Shell Tank Thermal and Seismic Project – Establishment of Time Domain Soil-Structure Interaction Analysis of a Hanford Double-Shell Tank*, RPP-RPT-28964, Rev. 0, Available online at www.osti.gov.

Rinker, MW, Carpenter, BG, Hendrix, CA, and Abatt, FG, 2008, *Hanford Thermal and Seismic Project – ANSYS Seismic Analysis of Hanford Double-Shell Tanks*, RPP-RPT-28966 Rev. 1, PNNL-15720 Rev. 1, Pacific Northwest National Laboratory, Richland, Washington.

Rinker, MW, Johnson, KI, Bapanapalli, SK, Karri, NK, Deibler, JE, Pilli, SP, Guzman-Leong, CE, Sanborn, SE, Abatt, FG, Dewberry, JA, Larsen, BM, Stoops, KL, and Julyk, LJ, 2011a, *Single-Shell Tank Integrity Project Analysis of Record: Hanford Type II Single-Shell Tank Thermal and Operating Loads and Seismic Analysis*, RPP-RPT-49989, Rev. 0, Pacific Northwest National Laboratory, Richland, Washington.

Rinker, MW, Johnson, KI, Bapanapalli, SK, Karri, NK, Deibler, JE, Pilli, SP, Guzman-Leong, CE, Sanborn, SE, Abatt, FG, Dewberry, JA, Larsen, BM, Stoops, KL, and Julyk, LJ, 2011b, *Single-Shell Tank Integrity Project Analysis of Record: Hanford Type III Single-Shell Tank Thermal and Operating Loads*

and Seismic Analysis, RPP-RPT-49990, Rev. 0, Pacific Northwest National Laboratory, Richland, Washington.

Rohay, AC and Brouns, TM, 2007, *Site-Specific Velocity and Density Model for the Waste Treatment Plant, Hanford, Washington*, PNNL-16652, Report prepared by Pacific Northwest National Laboratory for the U.S. Department of Energy, Office of River Protection, under Contract DE-AC05-76RL01830.

Rohay, AC and Reidel, SP, 2005, *Site-Specific Seismic Site Response Model for the Waste Treatment Plant, Hanford, Washington*, Report prepared by Pacific Northwest National Laboratory for the U.S. Department of Energy, Office of River Protection, under Contract DE-AC05-76RL01830, March.

Schnabel, PB, Lysmer, J, and Seed, HB, 1972, *SHAKE – A Computer Program for Earthquake Response Analysis of Horizontally Layered Sites*, Earthquake Research Center, University of California, Berkeley, California, EERC 72-12.

Shannon and Wilson, Inc, 2000, *Final Report, Geotechnical Investigation, River Protection –Waste Treatment Plant*, Project No. DE-AC06-96RL-13308, Subcontract No. W375-WTSC99-1036, 200 East Area, Hanford Site, Richland, Washington.

Stoops, KL, 2013, *Software Verification Test Results for ANSYS*, Becht Engineering Company, Inc., BNSQA-ANSYS 13.0, Richland, Washington.

6.0 Structural Model Description

This evaluation uses the same methods as the previous AORs of the Type II, Type III, and Type IV SSTs documented in Rinker et al. (2011a and 2011b) and Johnson et al. (2014c). Thus, it is not necessary to repeat all the details of the methodology discussion that are included in the previous reports. Where other studies have been performed supporting the development of this model, these will be referenced as appropriate.

A model of a Hanford Type I SST is created and analyzed in the time domain using version 13.0 of the general-purpose finite element program ANSYS® (ANSYS 2010); specific computers used in this analysis are identified in Appendix C. The seismic model for the Type I tanks is developed from drawing D-20 Rev. 6 (DuPont 1944b) and is representative of the Type I tanks.

The seismic Type I SST geometry is modeled in ANSYS® as a centerline shell model – also known as a mid-thickness shell model. The Type I SST shell model includes orthotropic fully cracked concrete (FCC) stiffness properties determined from the TOLA analysis (Johnson et al. 2014a) as listed here in Section 6.3.1. The fully cracked concrete case is consistent with the no-tension hypothesis described in Section 5.6 of Rinker et al. (2011a). Since the seismic model uses linear concrete properties, the effects of concrete cracking are implemented by applying the fully cracked orthotropic properties developed in the TOLA analysis (Johnson et al. 2014a) for the element shell locations of the seismic model. The FCC properties also include thermal degradation of the concrete modulus.

Three variations of soil have been considered in this analysis to address the soil property uncertainty as recommended by ASCE (2000). These variations are:

- Lower Bound Soil (LBS) properties
- Best Estimate Soil (BES) properties
- Upper Bound Soil (UBS) properties

The model is evaluated for two waste height configurations: an empty tank and a full tank. For the purposes of this evaluation, "full" means that the waste height is 284 inches, which is 95% of the tank wall height. The content of the interim stabilized SSTs consists of saltcake and sludge-like (non-Newtonian high viscosity) material, and is modeled using low stiffness elastic volumetric elements rather than fluid elements. Based on the higher demands from high shear stiffness (HSS) waste in previous AORs, as well as the low overall differences in Type I demands and the low overall Type I demand/capacity ratios (see Johnson et al. 2014a), only the high shear stiffness (HSS) condition is included in this analysis.

The massive upper structure attached to the tank roof (referred to herein as a "hatchway") is a feature common to all Type I SSTs. The hatchway is large relative to the tank, spanning the entire width of the roof, and is integrally attached to the roof (see Figure 6-1). As such, this feature is included in all of the evaluation configurations (previous AORs had only considered tank appurtenances in side studies). The model is evaluated for two hatchway orientations to address the antisymmetry of the hatchway. The

hatchway itself is not evaluated as part of the tank integrity evaluation. See Johnson et al. (2014a) for detailed discussion on the tank integrity evaluation.

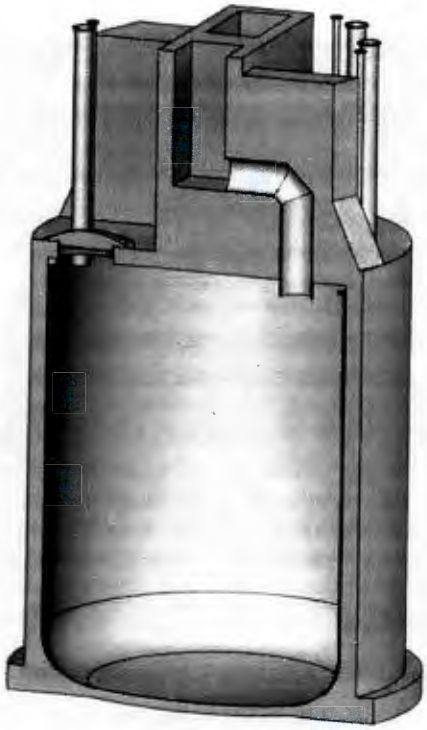

Figure 6-1. Rendering of Concrete Tank and Hatchway, Cut to Show Internal Details

Each configuration is run as a full nonlinear (contact interface elements are the only nonlinear elements in the seismic model) seismic transient including gravity, with an initial gravity-only step to obtain the proper initial soil loading for the soil-to-concrete interface elements which allow potential slippage and/or separation. The difference between the two cases represents the seismic-only effects.

6.1 Model Geometry

A half-symmetry (180°) model of the SST, including the concrete tank and surrounding soil, is developed to evaluate the soil-structure interaction seismic loading on the Type I SST. Details for each part of the model are discussed in the following sections. The complete model, including the SST and surrounding soil, is shown in Figure 6-2.

The global origin is above the center of the model at grade elevation. The x-axis is radial and the positive z-axis points upward. The y-axis completes the right-hand triad, and in a cylindrical coordinate system defines the rotational angle in a counter-clockwise direction. The model is located between the global 0° and 180° angles. Where shown, tank data is presented in a likewise oriented local coordinate system with an origin at the tank footing centerline elevation. The tank and soil mesh is based on 9-degree slices over the half model, for a total of twenty radial slices. Plots of the model are shown in

Figure 6-2 through Figure 6-4 showing the concrete tank, contained waste, hatchway, backfill and overburden soil, and the native and far-field soil. The unit system used in the model is kip, foot, second.

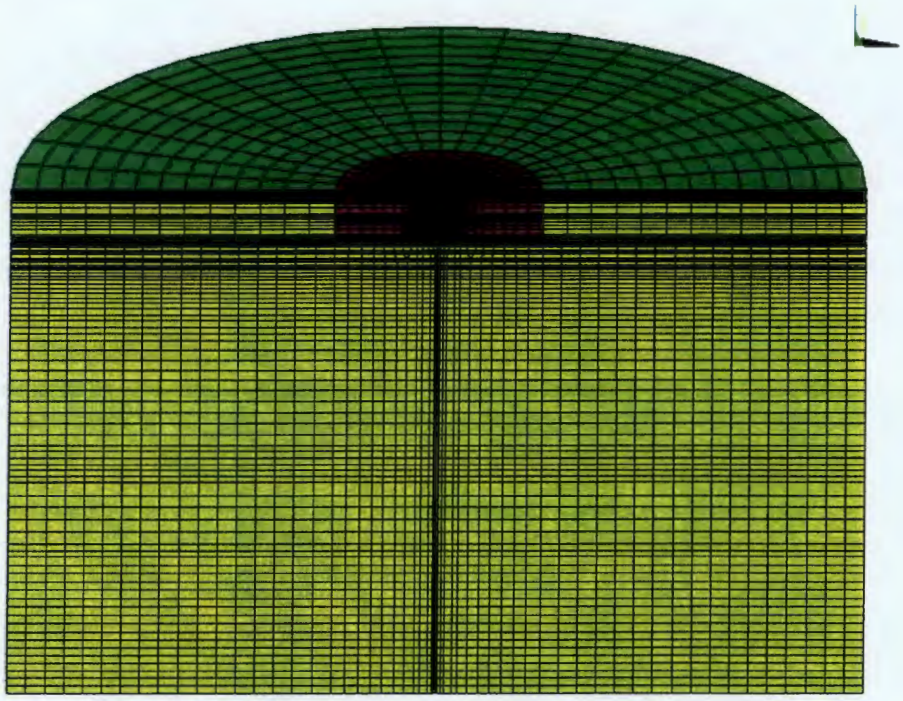

Figure 6-2. Element Plot of Complete Seismic Model for Lower Bound Soil Configuration

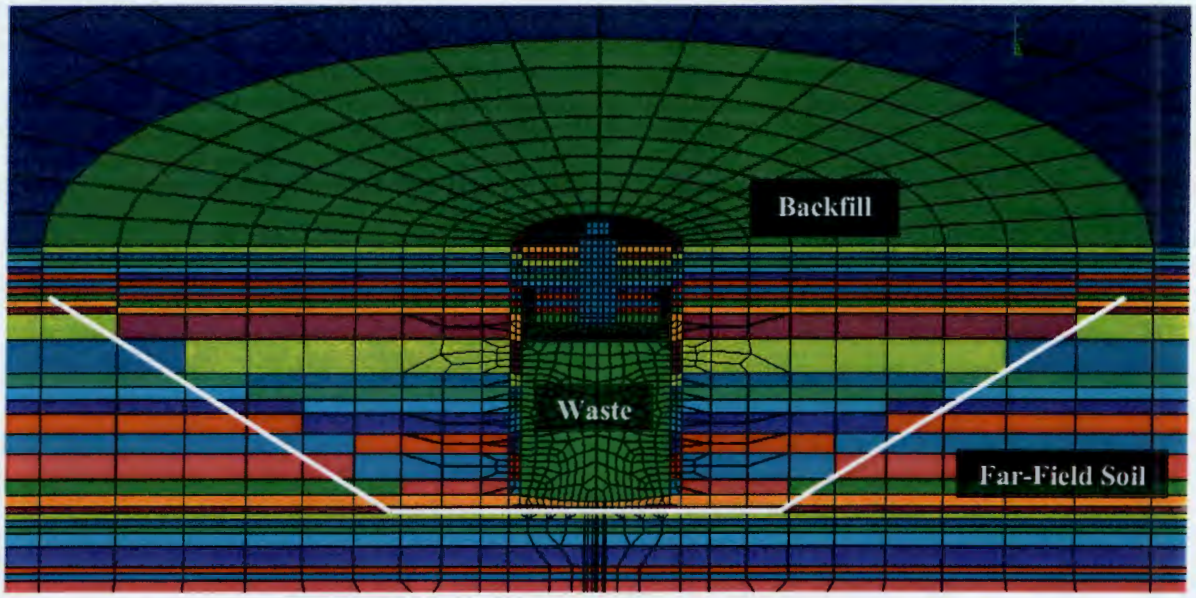

Figure 6-3. Element Plot of Seismic Model Showing Backfill and Waste Material Properties

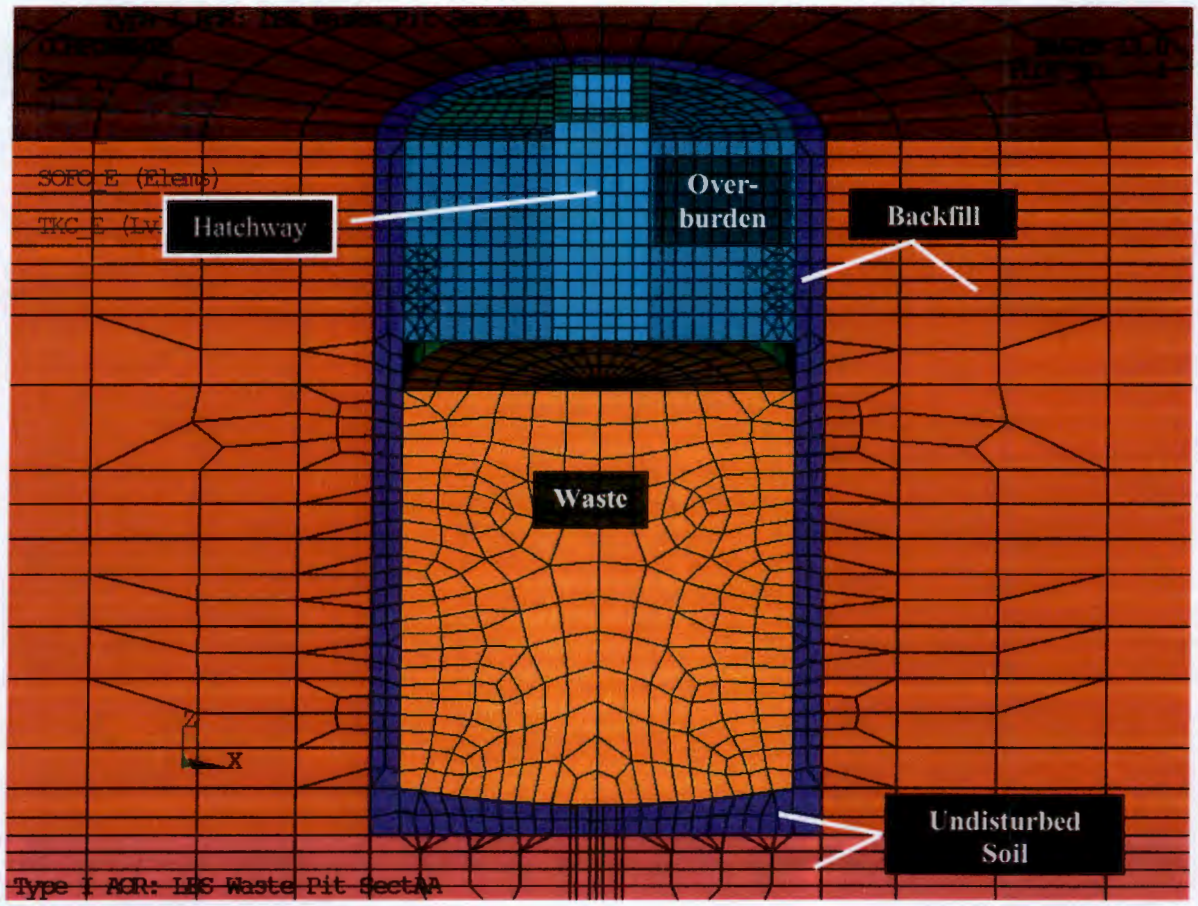

Figure 6-4. Element Plot of Seismic Model Showing Tank, Waste, Hatchway, and Overburden Soil

The hatchway has two-axis symmetry/antisymmetry, in contrast to the axisymmetric tank and soil. The hatchway is described in two basic orientations as shown in Figure 6-5 and Figure 6-6 below, labeled as sections A-A and B-B. (Note that in drawing D-20, the section lines deviate in order to cut through features of interest) The half model symmetry plane is placed along these section lines. For a 3D view of the hatchway, see Figure 6-11.

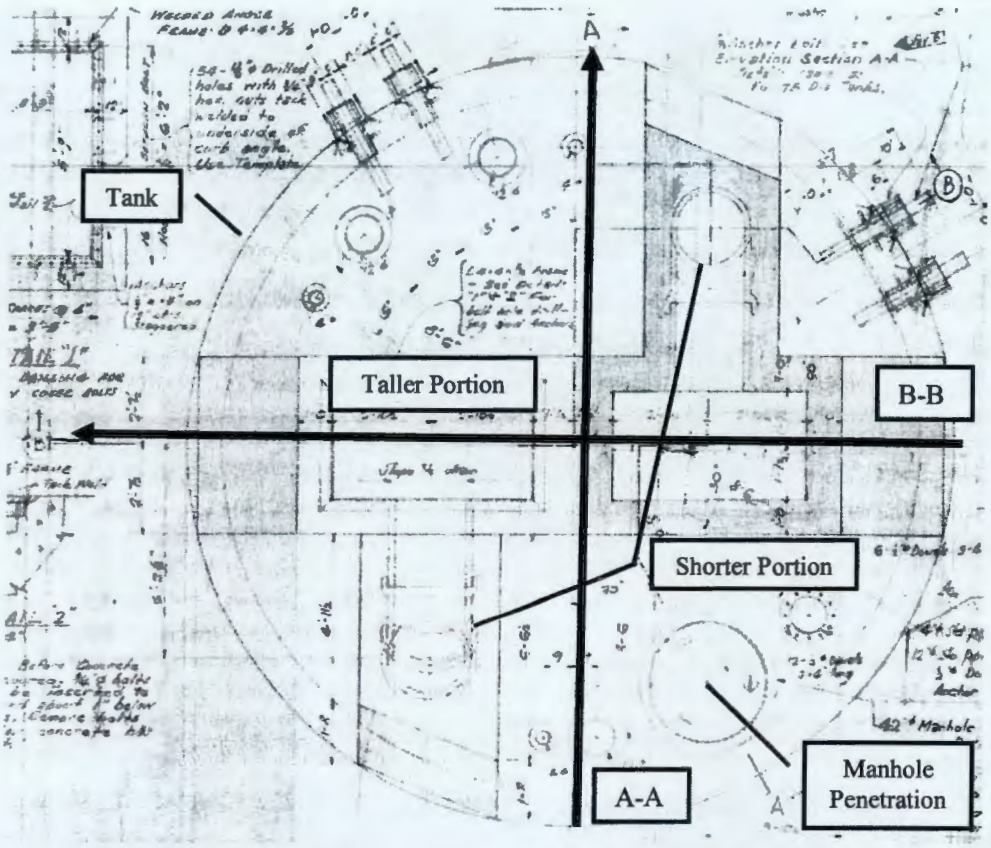

Figure 6-5. Drawing D-20 (Partial) Showing Symmetry Plane Lines for Hatchway Section Cuts A-A and B-B

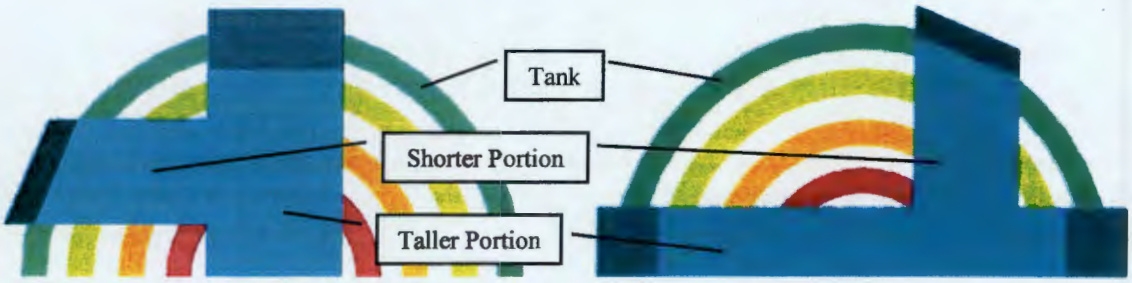

Figure 6-6. Model Top View of Half-Symmetry Hatchway Orientation at Sections A-A (left) and B-B (right)

In section A-A the taller portion of the hatchway is orientated perpendicular to the symmetry plane, and in section B-B the taller portion of the hatchway is oriented parallel to the symmetry plane. From the structural perspective of the tank, the taller portion of hatchway in section A-A spans the roof in the axis perpendicular to the horizontal seismic motion, whereas the taller portion of hatchway in section B-B spans the roof in the axis parallel to the horizontal seismic motion. Both orientations of the hatchway expose a large sidewall face normal to the axis of the seismic motion.

Both hatchway orientations are considered in this analysis because the horizontal seismic motion only acts in a single axis (see Section 6.5.3) of the half-symmetry model. Although the use of the single

symmetry plane (see Section 6.5.2) does not strictly reproduce the full anti-symmetric 3D hatchway geometry, the differences in structural effects resulting from the choice of symmetry (e.g. torsion) are considered to be insignificant, particularly in light of the otherwise low seismic demands and the low overall Type I demand/capacity ratios (see Johnson et al. 2014a).

6.1.1 Model Organization

The model is divided into distinct components, each with its own input file. Each component may be modified and meshed independently to facilitate development of alternate configurations, such as used in the run matrix. The model is progressively defined as each input file is executed. Each input file integrates into the model by reading the model data from preceding input files. The model configuration may be changed by removing or otherwise disabling the input file for individual features. A number of global reference points are also created before geometry generation to define key locations and locate the local coordinate systems used in the component input files.

6.1.2 Organization and Identification System

Where possible, items are organized in a hierarchical manner. Each model component is assigned a tag and a number to easily distinguish its attributes such as coordinate systems, element MAT/REAL/TYPE/SECT properties, from other components (Table 6-1). The tag enables both alphabetic and numeric hierarchical organization. The tag is used in labeling and identifying model components and variables, beginning with the component, then with subcomponent(s), and ending with a letter designating the modeling item (i.e., area, element, etc.). The tag itself is assigned a numeric value so that it can also be used as a variable within numerically organized aspects of the model.

Table 6-1. List of Model Components

Component	Tag	Number
Tank Concrete Roof	TKCD	100
Tank Concrete Sidewall	TKCW	200
Tank Concrete Floor	TKCF	300
Tank Appurtenances	PITS	400
Tank Waste	WAST	500
Soil Fill Overburden (above tank)	SOFO	600
Soil Fill Around tank (immediately surrounding tank)	SOFA	700
Soil Fill Excavated (remaining fill)	SOFE	800
Soil Undisturbed	SOUD	900
Contacts	CONT	1000
Target surfaces	TARG	2000

Elements constituting a given component have attributes beginning with the component number. Contact interface pair real numbers are organized using a hierarchical method as well. For example, element type 1160 is a contact (1xxx) interface element between the tank concrete roof (1xx) and the soil fill overburden (6x). The last digit in the contact number is used to distinguish multiple contact regions that would otherwise result in the same number, according to the hierarchical scheme. For example, the interface between the tank floor and underlying soil is subdivided into the footing and floor center regions.

6.1.3 Input and Output Files

A list of the files used, along with a short description of each file, is provided in Table 6-2 through Table 6-5. The tables address the model parts in the order that they are executed and assembled – tank components first, then the surrounding soil, followed by solution and post-processing phases.

Table 6-2. ANSYS® Model Input File Description (pre-processing phase)

File Name	Use	Description
Assembly.inp	All	Calls other input files for development of model, solution, and post-processing
Plotmacrolib.inp	All	Contains macros for plotting model.
TKCD.inp	Geometry	Creates tank concrete dome (roof) geometry. Uses PNNL ACI-evaluation section cut locations.
TKCW.inp	Geometry	Creates tank concrete sidewall geometry. Uses PNNL ACI-evaluation section cut locations.
TKCF.inp	Geometry	Creates tank concrete floor geometry. Uses PNNL ACI-evaluation section cut locations.
WAST.inp	Geometry	Creates model of waste (optional). Matches surrounding tank geometry.
SOIL_properties.inp	Properties	Defines specific soil material properties and layering. Excavated region and native soil have different material properties. Properties vary by layer.
SOFO.inp	Geometry	Creates soil fill overburden for excavated region above tank. Matches tank roof geometry. Reads soil properties and layers from the SOIL_properties input file.
PITS	Geometry	Creates hatchway (either section A-A or B-B). Matches tank roof geometry. Integrates with SOFO input file to modify surrounding soil fill overburden.
SOFA.inp	Geometry	Creates soil fill for excavated region immediately around tank. Matches tank floor, sidewall, roof, and soil overburden geometry. Encapsulates tank in a regular cylinder for easier interface with surrounding soil. Reads soil properties and layers from the SOIL_properties input file.
SOFE.inp	Geometry	Creates soil fill for excavated region near tank (i.e. out to backfill slope). Matches soil immediately surrounding tank geometry. Reads soil properties and layers from the SOIL_properties input file. Volume contains both excavated and undisturbed soil.
SOUD.inp	Geometry	Creates soil at far-field with undisturbed (native) properties. Matches preceding excavated soil geometry. Reads soil properties and layers from the SOIL_properties input file.
Surface_load.inp	Geometry	Creates surface loads
prepost.inp	All	Prepares model data for post-processing – set up data arrays, select elements at ACI-evaluation sections.
Connect.inp	Geometry	Creates interfaces between model components: • Tank, hatchway, waste, and soil around tank • Soil overburden slip planes • Soil fill and undisturbed soil portions of the model
BC.inp	Geometry	Creates boundary conditions: • Symmetry plane • Slaved (coupled) boundary conditions around exterior of model to control shear behavior • Spar elements at edge of soil model when couples and boundary conditions cannot both be applied to the same node • Places large mass at bottom of model for excitation force
Modify.inp	All	Modifies as-generated tank model. Applies orthotropic tank concrete properties.
Plots.inp	All	Generates model plots.
TKCP.inp	Geometry	Modifies tank roof to add penetration (only used for study in Appendix A)

Table 6-3. ANSYS® Model Input File Description (solution phase)

File Name	Use	Description
Solution.inp	Gravity	Executes static, pseudo-static solution phase of model.
Solution_TH.inp	Seismic	Executes the transient solution.
th-10ms-h.inp	Seismic	Acceleration time series input (horizontal) – tabular data.
th-10ms-v.inp	Seismic	Acceleration time series input (vertical) – tabular data.

Table 6-4. ANSYS® Model Input File Description (post-processing phase)

File Name	Use	Description
post1.inp	Static	Post-processes model static POST1 results. Creates tabular and graphical summaries of results.
postproc.inp	Transient	Post-processes model transient (pseudo-static/time series) POST26 results for tank concrete elements. Creates tabular and graphical summaries of results.
post-cont.inp	Transient	Post-processes model transient (pseudo-static/time series) POST26 results for contact elements. Creates tabular and graphical summaries of results.
subtract_gravity.inp	Seismic	Read in gravity-only results from previous output, subtract gravity from gravity + seismic. Creates tabular and graphical summaries of tank concrete seismic-only results.
subtract_cont.inp	Seismic	Read in gravity-only results from previous output, subtract gravity from gravity + seismic. Creates tabular and graphical summaries of contact seismic-only results.
spectra.inp	Transient	Post-processes response spectra results. Creates tabular and graphical summaries of response spectra results, and compares results to target data.
spectra_target.inp	Transient	Contains SHAKE (Schnabel et al. 1972) target response spectra (horizontal and vertical) for comparison to SSI model results – tabular data.
SC-SPTR-H.txt	Transient	Soil column target response spectra (horizontal) for comparison to SSI model results – tabular data.
SC-SPTR-V.txt	Transient	Soil column target response spectra (vertical) for comparison to SSI model results – tabular data.

Table 6-5. ANSYS® Model Output File Description

File Name	Use	Description
QAoutput.out	General	Run information for QA control and run identification.
Model_GEO_data.OUT	Geometry	Summary of model geometry data: Tank concrete component geometry and ACI-evaluation section data (see Table 6-18 for excerpt) Soil geometry data
Model_MAT_data.OUT	Properties	Summary of model material property data.
Solution.OUT	Transient	Summary of model data, including contact stiffness and mass
TKC1_ACI_angles.OUT	Transient	List of ESOL minimum/maximum results for tank concrete elements.
TKC1_ACI_SUM#.OUT	Transient	Summary of results for tank concrete elements. Used in both gravity and seismic steps, where # is the load step number.
TKC1_ACI_MIN#.OUT	Transient	List of minimum results for tank concrete elements. Used in both gravity and seismic steps, where # is the load step number.
TKC1_ACI_MAX#.OUT	Transient	List of maximum results for tank concrete elements. Used in both gravity and seismic steps, where # is the load step number.
TKC1_ACI_seismic_only_SUM.OUT	Seismic	Summary of seismic-only results for tank concrete elements.
CONT1_ACI_SUM#.OUT	Transient	Summary of results for contact elements. Used in both gravity and seismic steps, where # is the load step number.
CONT1_ACI_MIN#.OUT	Transient	List of minimum results for contact elements. Used in both gravity and seismic steps, where # is the load step number.
CONT1_ACI_MAX#.OUT	Transient	List of maximum results for contact elements. Used in both gravity and seismic steps, where # is the load step number.
CONT1_ACI_seismic_only_SUM.OUT	Seismic	Summary of seismic-only results for contact elements.
SPTR-accel.out	Transient	List of acceleration and response spectra results
SPTR-disp.out	Transient	List of displacement and response spectra results
TKC_TH_POST26_U.OUT	Transient	List of response spectra results related to tank behavior

6.1.4 Tank Concrete

The tank concrete is subdivided into the floor, sidewall, and roof using input files TKCF.inp, TKCW.inp, and TKCD.inp, respectively. The input files contain tank profile geometric coordinates and locations of ACI-evaluation sections. Orthotropic material properties and associated thicknesses are applied separately in input file modify.inp. Because the tank concrete subcomponents are integral, they are merged together using the input file connect.inp.

The Type I SST profile and centerline of the tank initially was created using a 2-D CAD model. The centerline locations from the CAD geometry for the profile were used in the creation of the centerline shell seismic ANSYS® model, shown in Figure 6-7. In all parts, the basic geometry is created first, and then cut to create locations from which concrete forces and moments are extracted and combined with TOLA results to perform an ACI evaluation (Johnson et al. 2014a). These locations are referred to as ACI-evaluation sections. The ACI-evaluation section sequence starts near the center of the roof and moves radially along the roof, down the sidewall, then from the outside to the center of the tank floor. ANSYS® element type SHELL181 (4-node finite strain shell) is chosen to model the tank concrete vault. As described in the ANSYS® 13.0 manual (ANSYS 2010), SHELL181 is suitable for analyzing thin to moderately-thick shell structures. Detailed output quantities are described in Section 6.6. Because the model uses shell elements, the geometry is based on the centerline of the actual geometry. The centerline

geometry is approximate when the section is irregular (e.g., lower knuckle) or has misalignments (e.g., outer footing vs. floor). Figure 6-8 shows the concrete tank shell model with shell thicknesses displayed.

Due to the differences between TOLA and seismic modeling and post-processing methods, some ACI-evaluation sections are at slightly different locations in the TOLA and seismic models because the TOLA model uses results extracted at nodes, and the seismic model uses results from element centroids. This difference is due to the fact that the TOLA model used solid elements to represent the tank and the seismic model uses shell elements. To match the seismic ACI-evaluation section locations as closely as practical with the TOLA model ACI-evaluation section locations, the seismic model uses a mesh that is offset to align the seismic model element centroids with TOLA node locations. A graphical display of the ACI-evaluation section locations and corresponding elements within the tank mesh is shown in Figure 6-7.

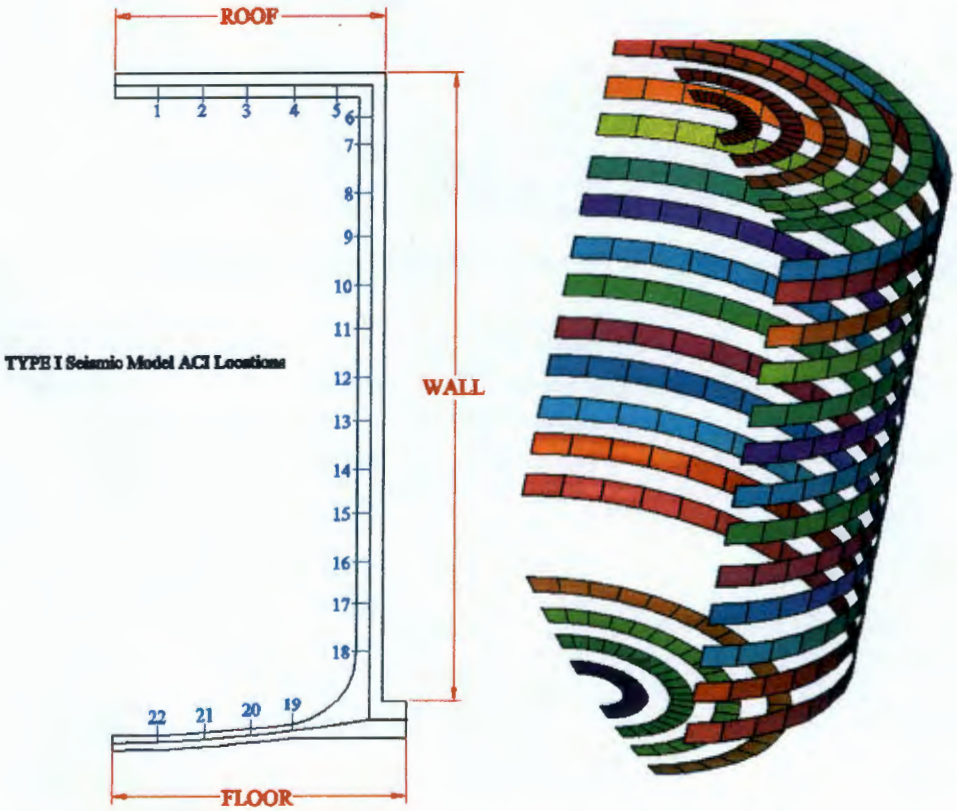

Figure 6-7. Concrete Tank Profile Showing ACI-Evaluation Section Locations and Associated Tank Elements

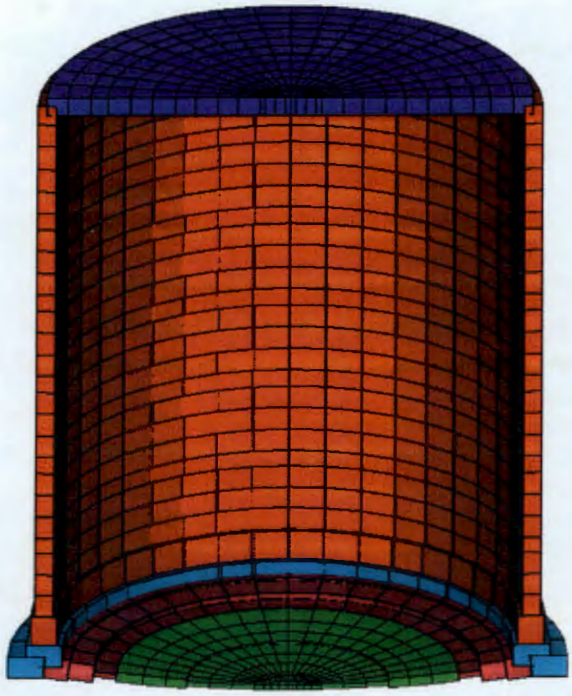

Figure 6-8. Element Plot of Concrete Tank Profile Showing Shell Element Thickness

The tank shell elements are oriented such that the positive element x-axis is aligned in the meridional direction, initially pointing away from the roof center. The element y-axis is aligned in the hoop direction. This orientation allows for extraction of meridional and hoop results and application of orthotropic material properties. Each ring of elements has unique properties defined in order to maximize accuracy and ensure smooth transitions. Shell element orientation is shown in Figure 6-9 and concrete tank material properties are shown in Figure 6-10.

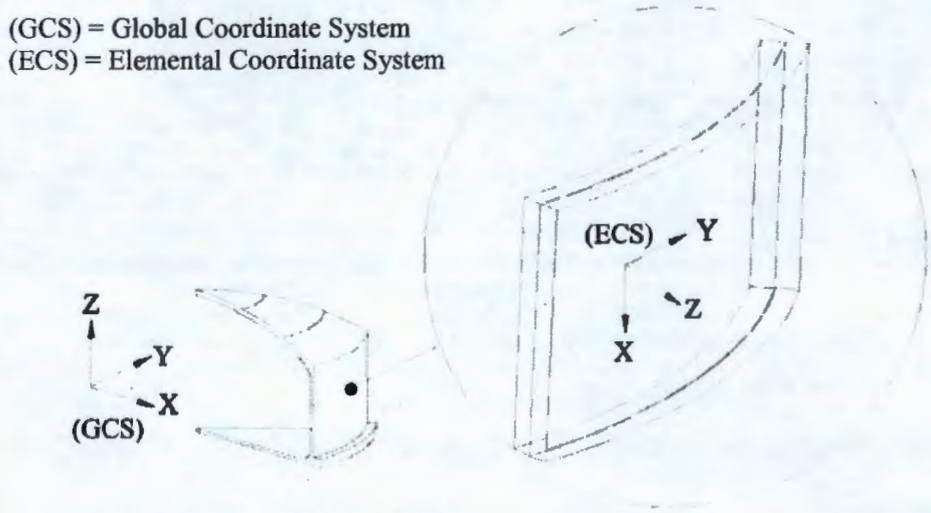

Figure 6-9. Shell Element Orientation Sketch

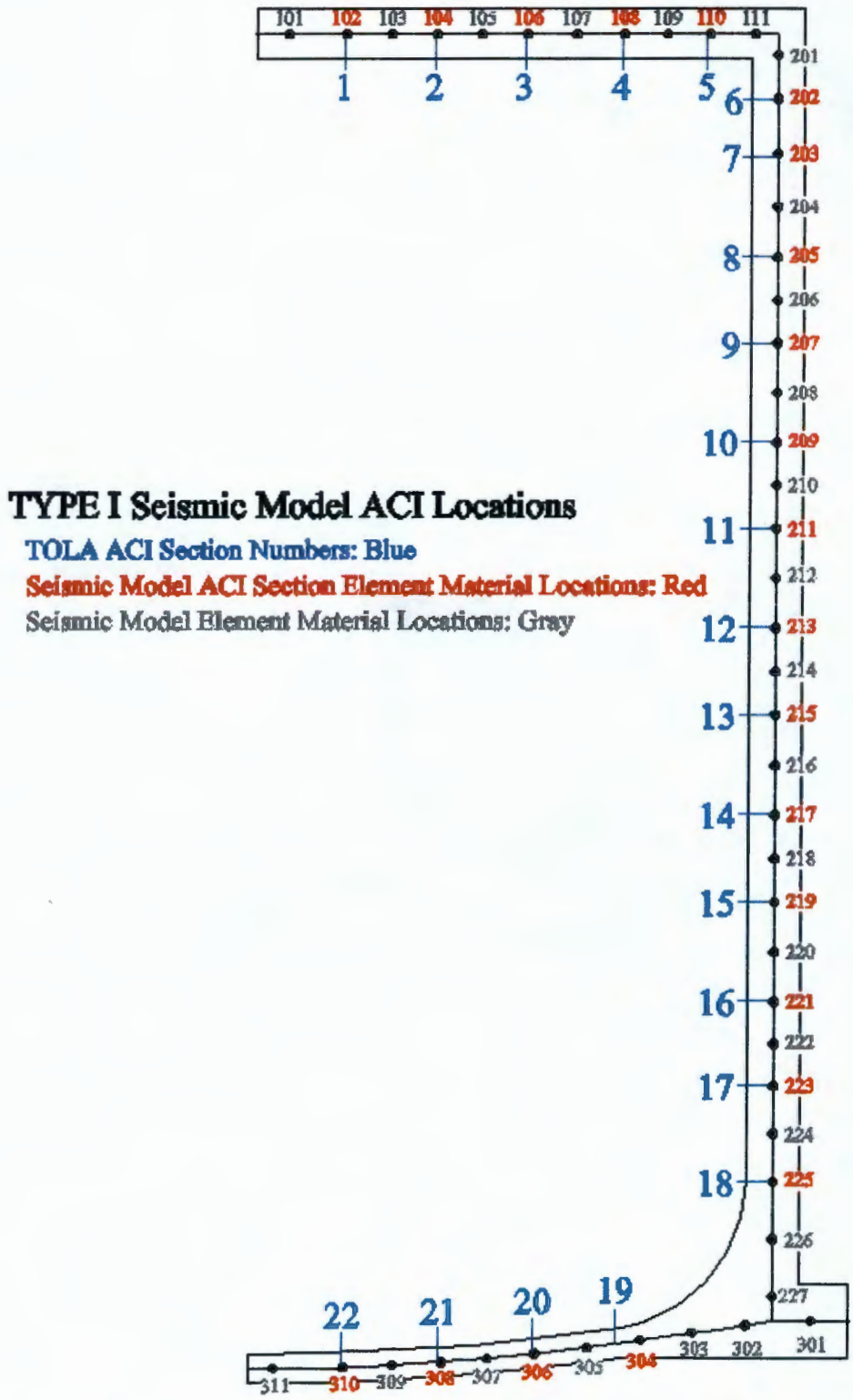

Figure 6-10. Concrete Tank Profile Showing ACI-Evaluation Section Locations and Seismic Model Element Material Numbers

6.1.5 Concrete Hatchway

The hatchway is modeled using ANSYS® SOLID45 elements, which are eight-node elements with three translational degrees-of-freedom at each node. Both orientations (shown in Figure 6-11 and Figure 6-12) are created using input file PITS.inp. The density of the hatchway concrete is adjusted such that the net weight (hatchway weight minus displaced soil weight) of the hatchway is 16 kips (see Hundal 2004a-2004d).

Table 6-6. Type I SST Hatchway Load (for Half Model)

Load Source	Weight
Hatchway	115 kip
Displaced Soil	99 kip
Total Net Load	16 kip

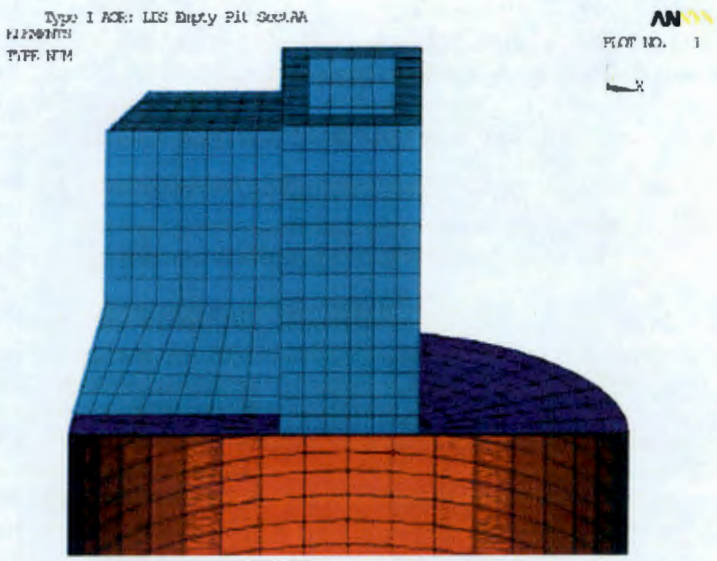

Figure 6-11. Element Plot Showing Tank and Hatchway at Section A-A

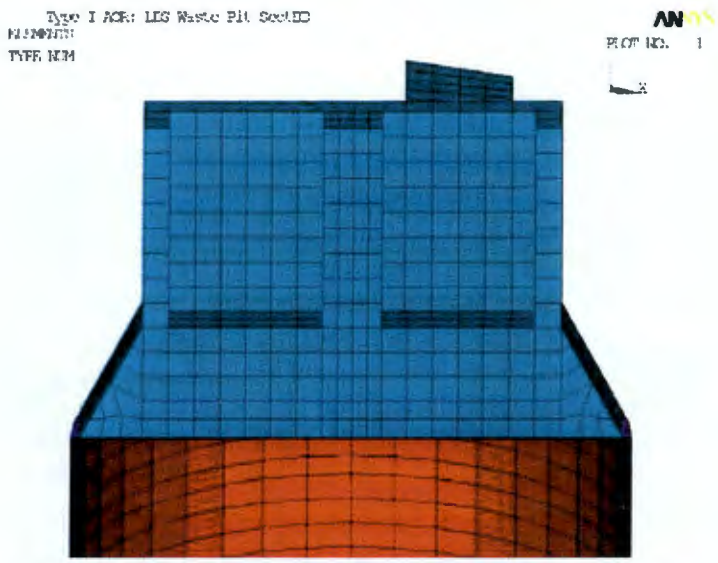

Figure 6-12. Element Plot Showing Tank and Hatchway at Section B-B

6.1.6 Soil Model

The soil model is divided into solid model subcomponents roughly corresponding to the excavated backfill soil and the far-field soil. These subcomponents exist mainly to facilitate model construction and meshing. The appropriate material properties (backfill/far-field) are applied according to the location within the model.

The soil extends to a model outer boundary radius of 320 ft. Soil regions are modeled using ANSYS® SOLID45 linear elastic elements, which are eight-node elements with three translational degrees-of-freedom at each node. The soil mesh transitions to a coarser mesh away from regions of interest, in order to reduce the number of elements.

Three sets of soil properties are considered (as discussed above):

- Lower Bound Soil (LBS)
- Best Estimate Soil (BES)
- Upper Bound Soil (UBS)

Each set of soil properties has different layering, maximum depth, and material properties. To simplify model configuration control, the specific properties and layering are maintained in an input file (SOIL_properties.inp) separate from the remainder of the soil modeling inputs. Thus, the file containing parameters that differ between the soil property sets can be modified independently of other input files. The excavated backfill soil uses the same layering as the native (far-field) soil, except near the floor where layers are combined to prevent poor element aspect ratios and improve mesh consistency (e.g. at the tangent of the floor dish and the horizontal layer divisions). The properties for the two soil subcomponents are used consistently, so that the BES native soil is used with the BES backfill, etc.

6.1.6.1 Excavated Backfill Soil

The excavated soil modeling in this analysis uses the same methodology as the previous analysis (Johnson et al. 2014c). The excavated backfill soil is subdivided into three subgroups – one for soil above the tank (overburden), one for soil immediately surrounding the tank, and another for all remaining backfill. The backfill portion of the soil is developed using the input files SOFO.inp, SOFA.inp, and SOFE.inp. The solid model volumes defined for soil around and below the tank contain soil with both backfill and native soil properties. All soil in these volumes at an elevation below the tank foundation and beyond the backfill excavation slope has native soil properties.

Soil layering and material properties are found in input file SOIL_properties.inp. Figure 6-13 through Figure 6-15 shows the soil material property layering for the excavated backfill soil portion of the model for LBS, BES, and UBS, respectively. The excavated backfill soil layering is the same among all three soil columns.

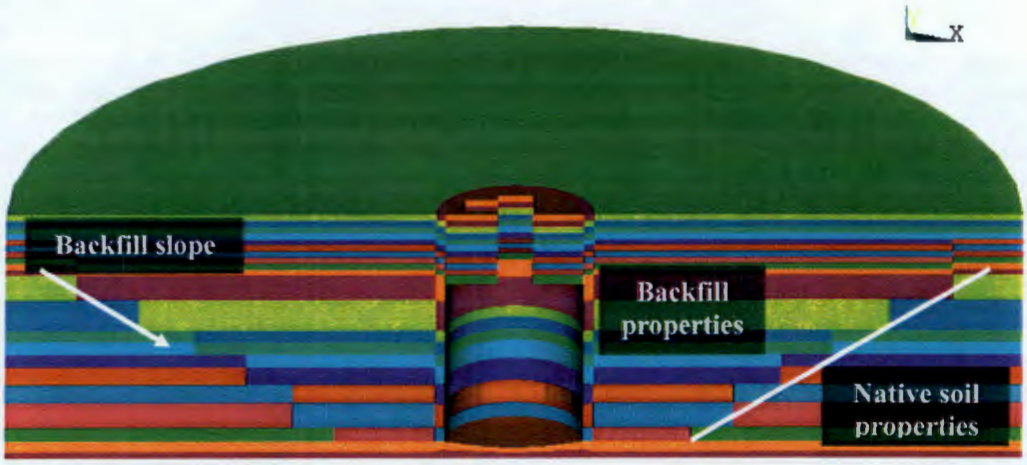

Figure 6-13. Model Plot of LBS – Excavated Backfill Soil

Figure 6-14. Model Plot of BES – Excavated Backfill Soil

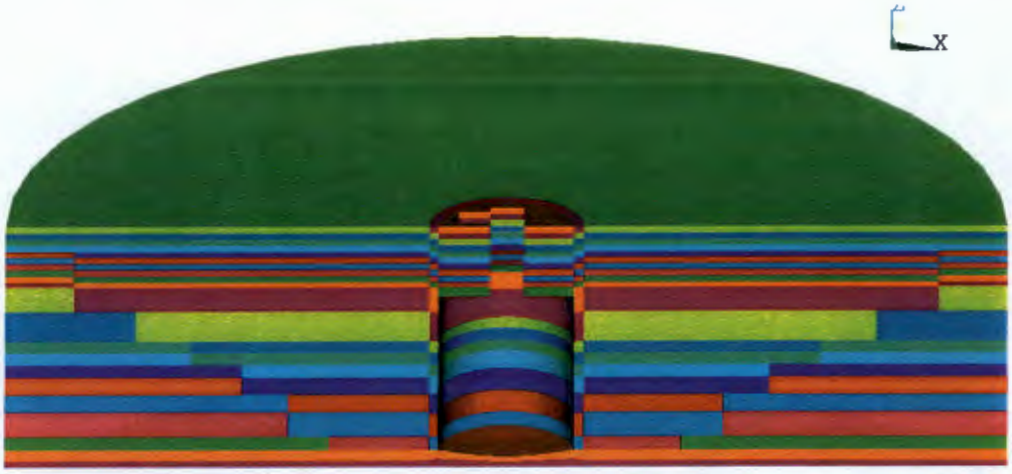

Figure 6-15. Model Plot of UBS – Excavated Backfill Soil

6.1.6.2 Soil Surrounding Hatchway

The overburden soil swept mesh is maintained as regular as possible, except that the presence of the hatchway creates some irregularly shaped volumes that must be free meshed with tetrahedral elements. The soil overburden is shown in Figure 6-16, without the hatchway. To visualize the volume that is removed from the soil, see Figure 6-11 showing the hatchway.

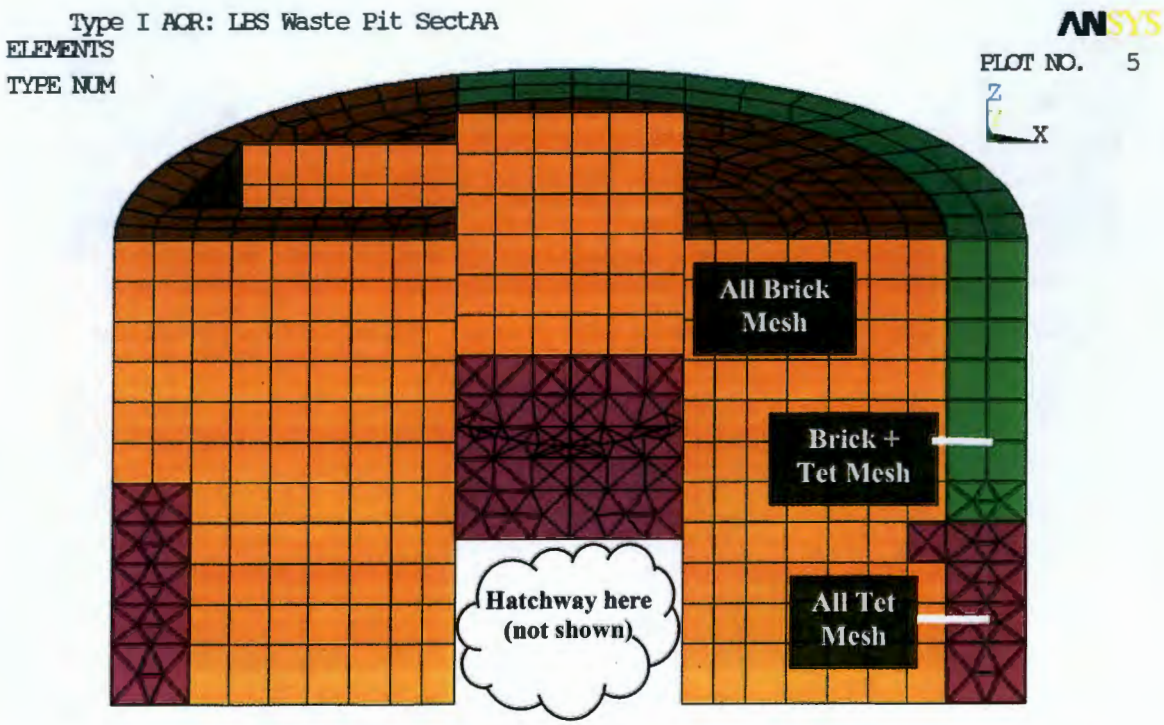

Figure 6-16. Element Plot Showing Overburden Soil without Hatchway

6.1.6.3 Native Soil

The native ("undisturbed") soil region of the model is developed using input file SOUD.inp. The soil layering and material properties are found in input file SOIL_properties.inp. SOLID45 elements are used and the material properties are discussed above. Figure 6-17 through Figure 6-19 shows the soil layering in the native soil portion of the model for LBS, BES, and UBS, respectively. Note the differences in soil depth between the models, which is necessary to meet shear wave velocity requirements at the base (see Section 7.2). Also note the LBS model has a mesh size smaller than the soil layering (see Section 7.6.1).

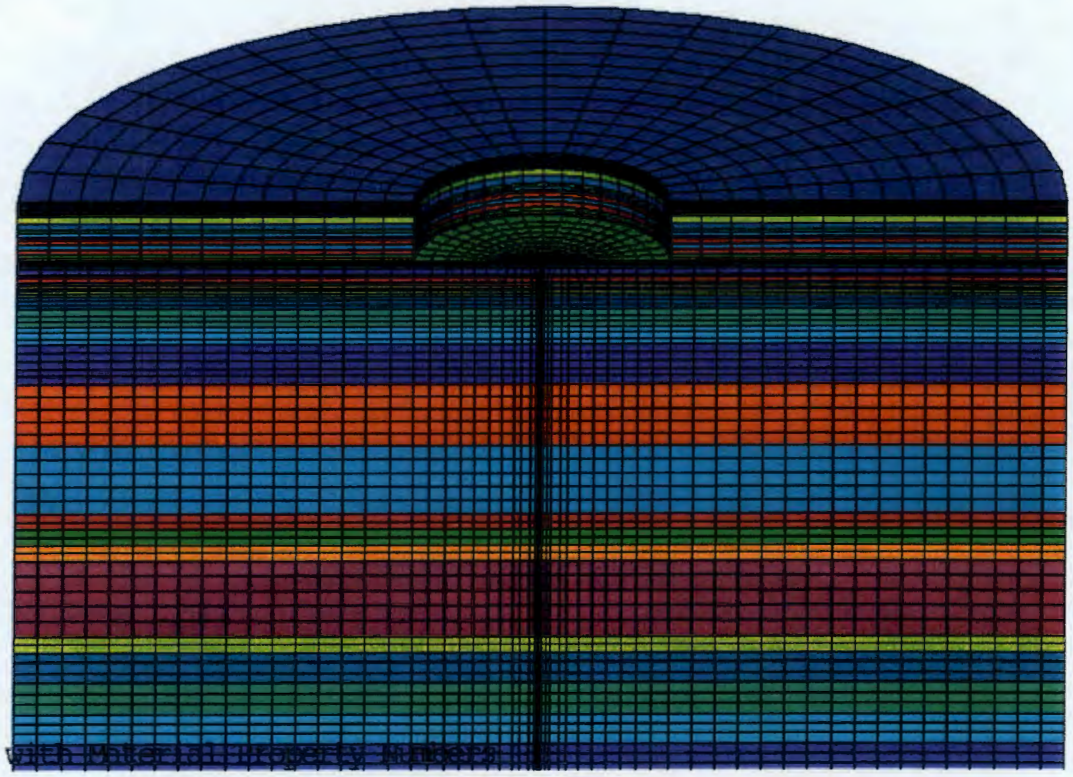

Figure 6-17. Element Plot of LBS Far-Field Soil Layering and Material Property Assignment

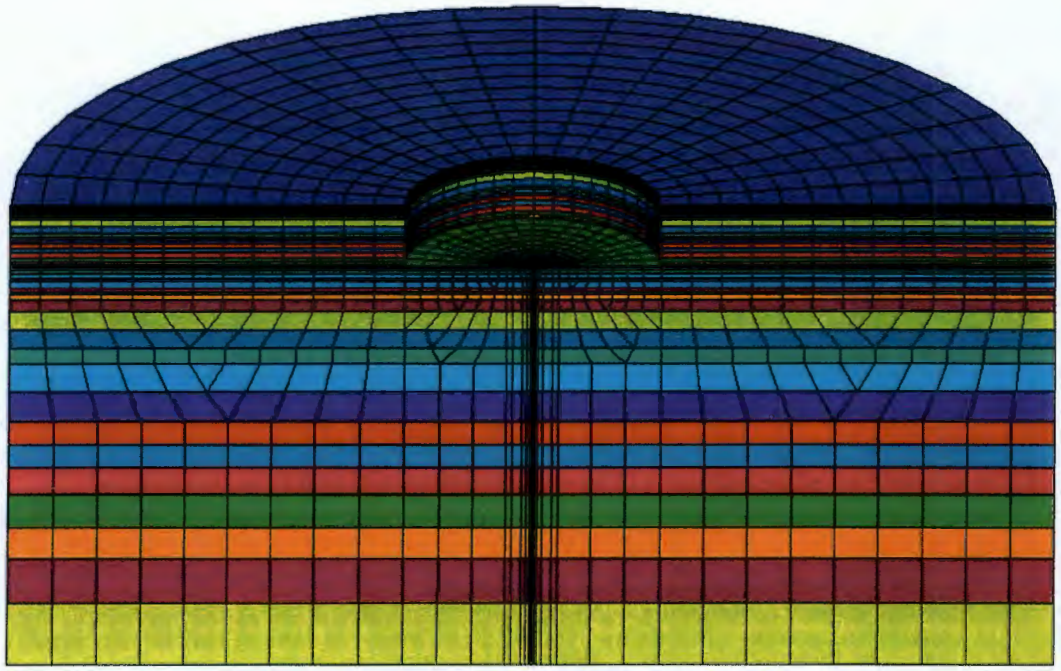

Figure 6-18. Element Plot of BES Far-Field Soil Layering and Material Property Assignment

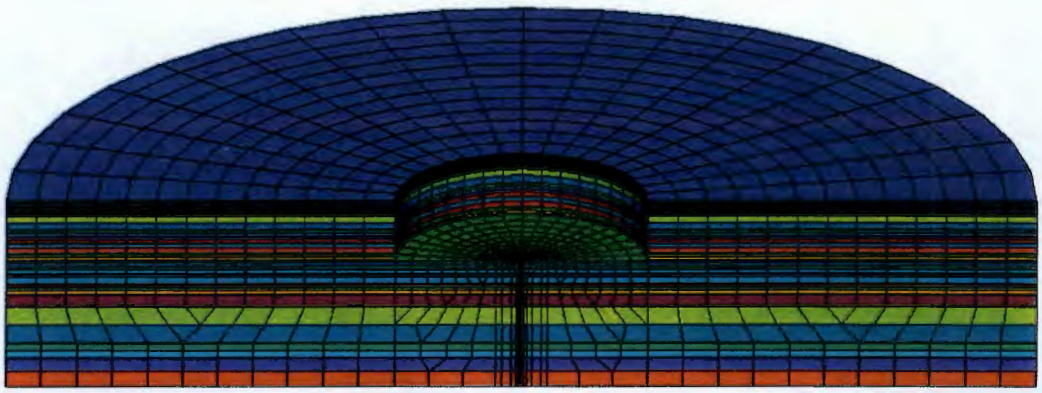

Figure 6-19. Element Plot of UBS Far-Field Soil Layering and Material Property Assignment

6.2 Model Interfaces

The model uses two types of interfaces; nonlinear and linear. Contact surfaces are used where nonlinear behavior is of interest (such as the soil-to-concrete interface). Linear interfaces are used to bond model components together, such as joining independently meshed soil components defined solely for the benefit of the modeling technique. Bonded contacts are simplified to merged nodes wherever possible to reduce model complexity.

The interfaces are applied after the model geometry is created, using the input file connect.inp. Interface elements are overlaid (ESURF command) on the underlying components to create contact/target

surface pairs. Contact interfaces use ANSYS® element types TARGE170 and CONTA173. Where practical, the contact/target surfaces use matching meshes for optimal contact performance.

As shown in Figure 6-20 and Figure 6-21, the following nonlinear interfaces are included in the model:

1. Concrete tank-to-soil interface surrounding the tank
2. Concrete tank-to-waste interface (when waste is present)
3. Hatchway-to-soil interface surrounding the hatchway
4. Soil-to-soil vertical slip planes added to the soil overburden above tank to improve the geostatic and dynamic behavior (minimize potential for soil arching)

The following interface surfaces are linear:

5. Soil-to-soil interface between soil immediately surrounding the tank to other soil
6. Soil-to-soil interface between volume containing the excavated backfill to the surrounding far-field soil
7. Concrete tank roof-to-hatchway (bonded contacts)

Additional details on these interfaces are found in the following sections.

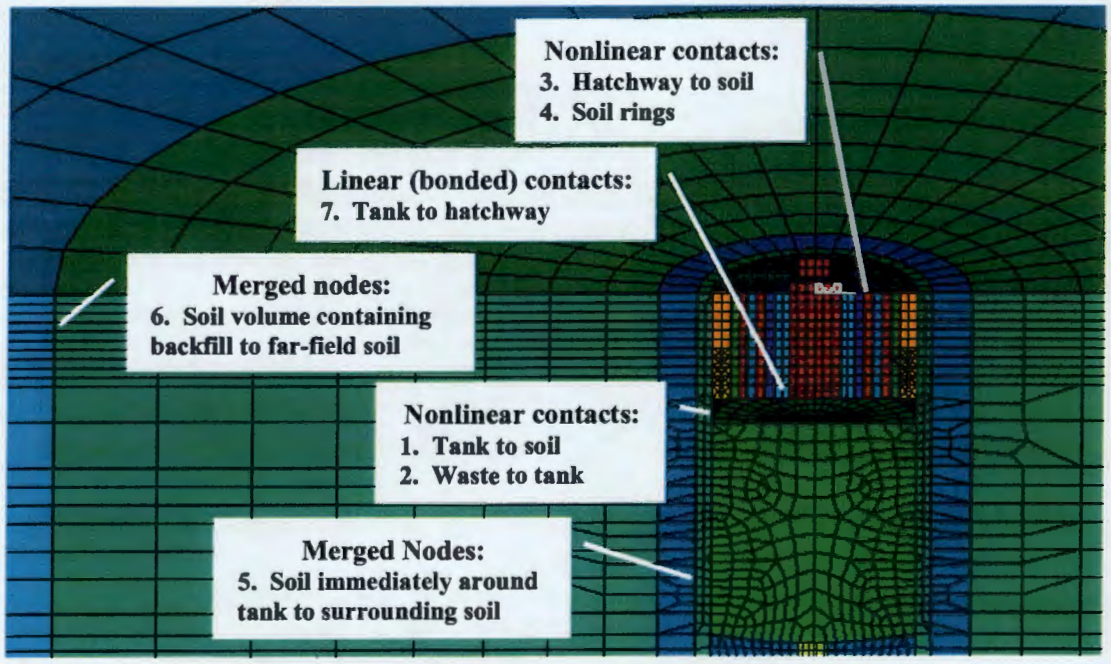

Figure 6-20. Element Plot Annotated with Locations of Interfaces in Seismic Model

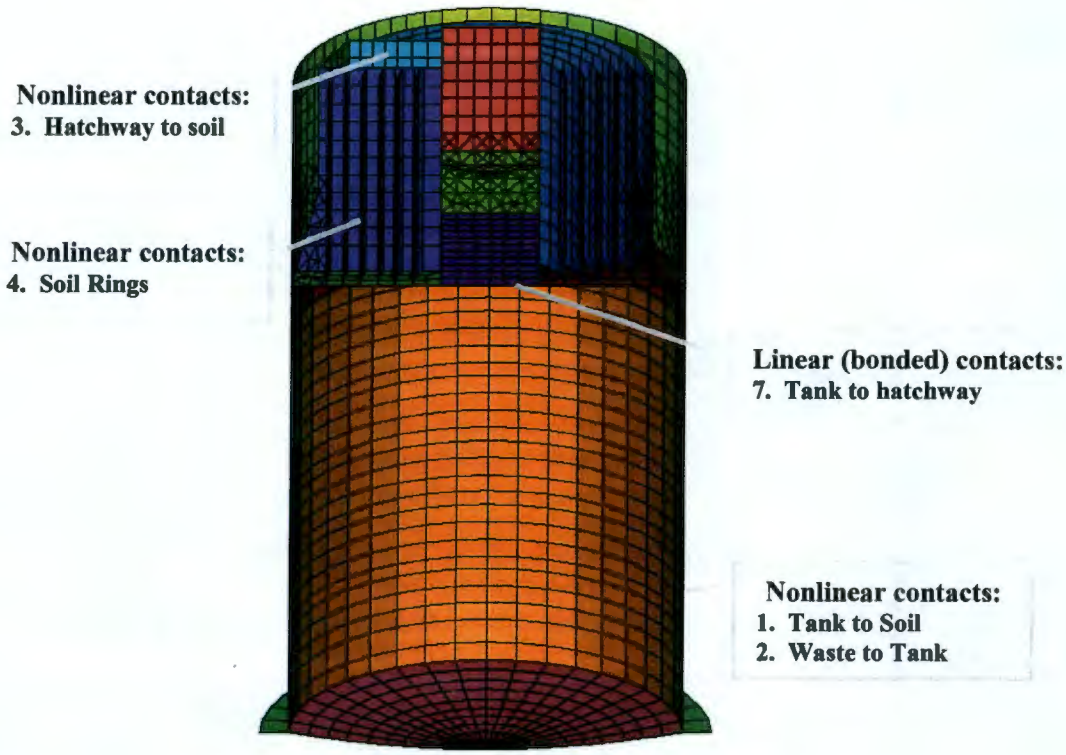

Figure 6-21. Element Plot Showing Interface Elements Real Property Assignment - All Interfaces

6.2.1 Soil/Concrete Tank Interface

A combination of ANSYS® TARGE170 and CONTA173 elements is used to model the interface between the soil and the concrete tank. The presence of this interface surface is important to establish a proper initial geostatic stress state (see Section 6.2.4) and also to allow for the possibility of sliding or separation between the concrete vault and the surrounding soil during seismic loading. The soil is the contact surface and the concrete tank is the target surface. The soil/concrete tank interface elements are shown in Figure 6-22. Portions of this interface are replaced with hatchway-to-soil interface (see Figure 6-24) due to the displacement of soil with the hatchway.

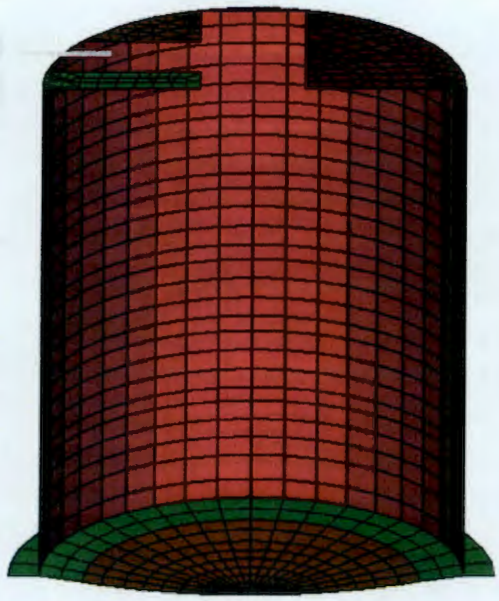

Figure 6-22. Element Plot Showing Interface Elements Real Property Assignment – Soil-to-Concrete Tank

The friction coefficients used in vertically oriented interfaces of the seismic model during the application of dead weight are artificially low in order to prevent the development of unrealistic soil drag-down loads in the sidewall from artificially high friction between the concrete and in-place modeled soil. During construction the loose backfill soil was placed in 6- to 24-inch thick layers and compacted, thus high concrete-to-soil friction induced drag-down loads would not have developed. Hence, the friction coefficients selected for the concrete wall and soil interface are small to minimize the artificial development of high drag-down loads in the initial geostatic analysis of the full in-place modeled backfill soil as gravity is applied.

The roof and wall friction coefficients used during both phases of the seismic analysis are summarized in Table 6-7. These friction values are consistent with the values used in the previous Type IV SST AOR (Johnson et al. 2014c) and the TOLA friction values as discussed in Johnson et al. (2014a), except that the low friction values (previously 0.05) at the wall in the initial gravity step are reduced to zero. The use of zero initial friction values causes an offset in the initial condition as a result of changing from an initial zero value to a nonzero value. The influence of this offset on the seismic demands is evaluated in Appendix B.

Table 6-7. Summary of Soil-to-Concrete Tank Friction Properties

Interface Location	Initial Gravity Step	Seismic Transient
Roof	0.3	0.3
Sidewall	0	0.5
Footing top surface	0.6	0.6
Basemat	0.6	0.6
Hatchway	0	0.5

6.2.2 Concrete Hatchway/Overburden Soil Fill Interface

The concrete-to-soil interface for the hatchway (see Figure 6-23) is modeled similar to the tank wall-to-soil (see Section 6.2.1). To improve solution stability separation of the surfaces is not allowed. A previous appurtenance analysis (Rinker et al. 2011b) found that a reduced coefficient of friction in the gravity step produced a more realistic initial geostatic state. A coefficient of friction of 0.5 (same as the tank wall) is used during the seismic transient. The mesh of the concrete hatchway does not match the mesh of the soil overburden but the contact elements allow proper load transfer. To visualize the volume that this interface surrounds, see Figure 6-11 showing the hatchway.

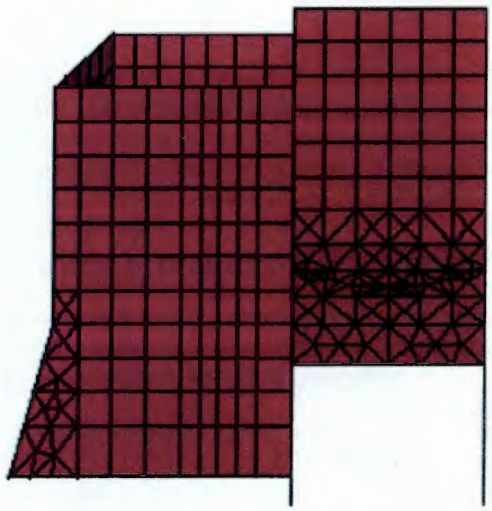

Figure 6-23. Element Plot Showing Interface Elements Real Property Assignment – Hatchway (Section A-A)-to-Overburden

6.2.3 Concrete Hatchway/Concrete Tank Interface

A combination of ANSYS® TARGE170 and CONTA173 elements is used to model the interface between the concrete hatchway and the concrete tank. The concrete roof is the target surface and the concrete hatchway is the contact surface (see Figure 6-24). The contact surfaces are bonded, since the hatchway is physically attached to the roof with rebar. The mesh of the bottom of the concrete hatchway does not match the mesh of the concrete roof but the contact elements allow proper load transfer. To visualize the volume that this interface underlies, see Figure 6-11 showing the hatchway. This interface replaces portions of the tank-to-soil interface (see Figure 6-22) due to the displacement of soil with the hatchway.

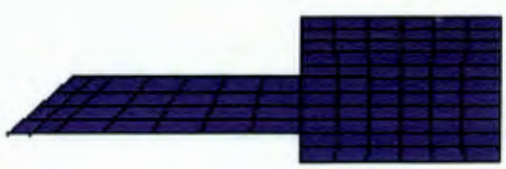

Figure 6-24. Element Plot Showing Interface Elements Real Property Assignment – Hatchway (Section A-A)-to-Tank

6.2.4 At-Rest Soil Pressure at Tank Wall

Initially, the sidewall pressure of the seismic SST model did not follow the linear trend of the long time settled at-rest pressure estimate of 0.5ρgh during gravity loading. To achieve the at-rest pressure profile on the side wall during gravity loading, the contact interference between the soil and the side wall of the tank is adjusted by defining a small initial contact offset using the real constants for ANSYS® CONTA173 elements. This initial contact adjustment allows the gravity-only contact pressure to be approximately the theoretical (long time settled) at-rest pressure of 0.5ρgh for the side wall of the tank. The dead weight contact pressure in Figure 8-27 demonstrates the effectiveness of the at-rest pressure adjustment by showing contact pressure in the wall close to the theoretical at-rest pressure.

The tank wall-to-soil contact uses a reduced contact normal stiffness factor (FKN) of 0.1. A lower contact normal stiffness reduces the sensitivity of the contact pressure, making at-rest pressure calibration smoother. The contact normal stiffness factor used in this analysis is the same as the previous Type IV AOR (Johnson et al. 2014c).

6.2.5 Waste/Concrete Tank Interface

A combination of ANSYS® TARGE170 and CONTA173 elements is used to model the interface between the waste and the concrete tank wall and floor. The presence of this interface is important to establish a realistic relationship between the relatively low-stiffness waste and the concrete tank. The relatively flexible behavior of the waste is best modeled by allowing the waste to move independently of the tank. A frictionless sliding contact surface is used at this interface in order to simulate a yield mechanism for the waste. The surfaces are allowed to slide but not separate. Separation is not permitted due to contact instabilities encountered during previous analyses. The waste is the contact surface and the concrete tank is the target surface. The waste/concrete tank interface elements are shown in Figure 6-25.

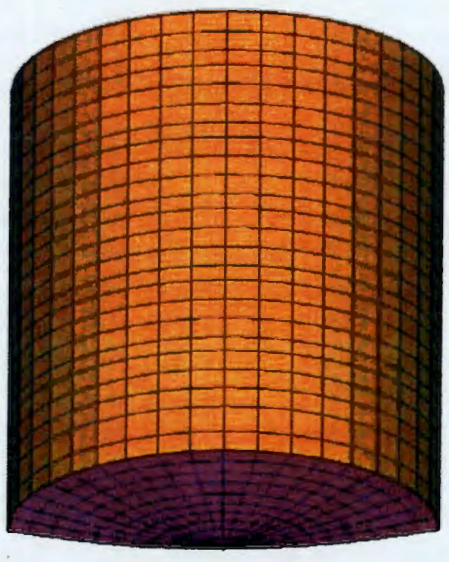

Figure 6-25. Element Plot Showing Interface Elements Real Property Assignment – Waste-to-Concrete Tank

6.2.6 Soil-to-Soil Interfaces

The solid modeling technique used in the creation of the model results in artificial boundaries within the soil. These boundaries are typically between volumes with different mesh patterns or densities. These interfaces are linear, except for the slip planes described below.

Vertical slip planes are inserted into the soil overburden (soil above the roof within the radius of the wall) to prevent or minimize soil arching. More detailed discussion on the development of the vertical slip planes or "soil rings" is presented in the Type III AOR (Rinker et al. 2011b). The locations of the contact surfaces are consistently placed halfway between the ACI-evaluation sections to ensure a more uniform loading. Due to the small number of ACI-evaluation sections in the Type I model vs. previous 75 foot diameter SSTs (thus, few rings), an additional slip plane is placed in between each existing plane, to double the number of rings. To improve solution stability, separation of the surfaces is not allowed. To establish the initial deadweight conditions in the model, a zero coefficient of friction is used, which lets the soil settle consistently with the steady-state roof deformation. A coefficient of friction of 0.2 is used during the seismic transient.

6.2.7 Soil Arching

When linear elastic material properties are used to model the soil, there is potential for developing artificial tensile zones. When the tensile zone is part of a beam type behavior forming a self-supporting condition, the soil is said to be arching. When this occurs there is a potential for soil loads to be transferred away from the tank roof into the surrounding soil. While localized tensile zones (i.e., not forming a continuous arch) will have only a limited impact on the results, excessive arching behavior will result in underestimating the vertical loads on the concrete roof and tank sidewalls. Discussion of soil arching is also found in Rinker et al. 2008.

Arching will not occur where a yield method (e.g., Drucker-Prager as in the TOLA model) or other displacement mechanism is provided. In the seismic model, vertical contact surfaces are inserted into the overburden to create annular rings of soil that are free to displace vertically consistent with the tank roof, but allow the load to be transferred laterally during horizontal motion. This effectively creates a nonlinear yield mechanism that acts in the vertical direction only. A low coefficient of friction is used, thereby ensuring that the majority of the soil load is carried by the tank roof. Studies performed in the Type III AOR (Rinker et al. 2011b) found that the coefficients of friction used here are effective in minimizing the potential for arching.

6.2.8 Soil-to-Roof Contact Stiffness

The overburden soil above the roof has differently sized/placed elements than the elements in the concrete roof. This meshing difference results in localized uneven contact pressure. This is mitigated by softening the contact stiffness to smooth out the loading. However, care is taken to ensure that the contact is not too soft, i.e. creating a nonphysical situation where the soil response becomes decoupled from the roof response. Thus, the contact stiffness for the roof to the soil overburden is verified to ensure that the contact stiffness creates a rigid response (33 Hz or greater). The maximum soil depth at the roof is 11.5 ft.

The following calculation determines the minimum contact stiffness between the soil overburden and the roof:

$$f = \frac{\sqrt{\frac{k}{m}}}{2\pi} \quad \text{Frequency} \tag{6.1}$$

$$f = 33Hz \quad \text{Target Frequency} \tag{6.2}$$

$$\rho = 129\frac{lbm}{ft^3} \quad \text{Soil Density of Backfill (see Section 6.3.3)} \tag{6.3}$$

$$m_{haunch} = 11.5\,ft \cdot (1ft)^2 \cdot \rho = 1183lb \quad \text{Mass of Soil Above the Roof in a 1 ft}^2\text{ Area} \tag{6.4}$$

$$k = (f \cdot 2\pi)^2 \cdot m_{haunch} = 1982\frac{kip}{ft} \quad \text{Contact Stiffness} \tag{6.5}$$

Thus, a contact stiffness between the soil overburden and the roof of 1982 kip/ft. or greater creates an effectively rigid contact at any location on the roof. The actual contact stiffness in the models is confirmed to satisfy this rigid contact condition.

6.3 Material Properties

Material properties are applied using the same methodologies as documented in previous AORs for SST Types II, III, and IV (Rinker et al. 2011a and 2011b and Johnson et al. 2014c.)

6.3.1 Tank Concrete Properties

Since there has been no significant post-construction seismic event experienced by the SSTs, the earthquake is assumed to occur at present day or in the future. Thus, the thermally degraded cracked section concrete properties as determined in the TOLA analysis (Johnson et al., 2014a) are used in the seismic analysis. The tank concrete properties for the seismic analysis include the effects of historical thermal and operating loads. No concrete component (beta) damping properties are applied, as this is conservative and Johnson et al. (2014c) found the tank demands are insensitive to this property since the soil damping dominates.

The tank concrete material properties are applied after the tank geometry and mesh are created. Orthotropic tank concrete properties are applied in the modify.inp input file. Table 6-8 provides orthotropic concrete section properties assuming all sections are fully cracked as obtained from Johnson et al. (2014a). Locations of the material numbers and ACI-evaluation sections are shown in Figure 6-7.

Table 6-8. Fully Cracked Orthotropic Concrete Properties

Concrete Material Number	Eshl Merid (EX) (psi)	Shell Thickness t-shl (in.)	Shell Density, Rho-shl (lb/in^3)	Eshl Hoop (EY) (using merid. thickness) (psi)	Ez (psi)	ν_{mh} (PRXY)	ν_{mz} (PRXZ)	ν_{hz} (PRYZ)	G_{mh} (GXY) (psi)	G_{hz} (GYZ) (psi)	G_{zm} (GXZ) (psi)
101	9.12E+05	9.71	0.1037	9.12E+05	3.26E+06	0.15	0.04	0.04	3.96E+05	6.68E+05	6.68E+05
102	9.12E+05	9.71	0.1037	9.12E+05	3.26E+06	0.15	0.04	0.04	3.96E+05	6.68E+05	6.68E+05
103	9.12E+05	9.71	0.1037	9.12E+05	3.26E+06	0.15	0.04	0.04	3.96E+05	6.68E+05	6.68E+05
104	9.12E+05	9.71	0.1037	9.12E+05	3.26E+06	0.15	0.04	0.04	3.96E+05	6.68E+05	6.68E+05
105	9.12E+05	9.71	0.1037	9.12E+05	3.26E+06	0.15	0.04	0.04	3.96E+05	6.68E+05	6.68E+05
106	9.12E+05	9.71	0.1037	9.12E+05	3.26E+06	0.15	0.04	0.04	3.96E+05	6.68E+05	6.68E+05
107	9.12E+05	9.71	0.1037	9.12E+05	3.26E+06	0.15	0.04	0.04	3.96E+05	6.68E+05	6.68E+05
108	9.12E+05	9.71	0.1037	9.12E+05	3.26E+06	0.15	0.04	0.04	3.96E+05	6.68E+05	6.68E+05
109	9.12E+05	9.71	0.1037	9.12E+05	3.26E+06	0.15	0.04	0.04	3.96E+05	6.68E+05	6.68E+05
110	9.12E+05	9.71	0.1037	2.23E+05	3.26E+06	0.15	0.04	0.01	1.69E+05	2.05E+05	6.68E+05
111	9.12E+05	9.71	0.1037	2.23E+05	3.26E+06	0.15	0.04	0.01	1.69E+05	2.05E+05	6.68E+05
201	9.12E+05	9.71	0.1037	1.55E+05	3.26E+06	0.15	0.04	0.01	1.27E+05	1.46E+05	6.68E+05
202	9.12E+05	9.71	0.1037	3.10E+05	3.26E+06	0.15	0.04	0.01	2.15E+05	2.76E+05	6.68E+05
203	9.12E+05	9.71	0.1037	1.55E+05	3.26E+06	0.15	0.04	0.01	1.27E+05	1.46E+05	6.68E+05
204	9.12E+05	9.71	0.1037	1.55E+05	3.26E+06	0.15	0.04	0.01	1.27E+05	1.46E+05	6.68E+05
205	9.12E+05	9.71	0.1037	1.55E+05	3.26E+06	0.15	0.04	0.01	1.27E+05	1.46E+05	6.68E+05
206	9.12E+05	9.71	0.1037	7.53E+05	3.26E+06	0.15	0.04	0.03	3.63E+05	5.79E+05	6.68E+05
207	9.12E+05	9.71	0.1037	7.53E+05	3.26E+06	0.15	0.04	0.03	3.63E+05	5.79E+05	6.68E+05
208	9.12E+05	9.71	0.1037	7.53E+05	3.26E+06	0.15	0.04	0.03	3.63E+05	5.79E+05	6.68E+05
209	9.12E+05	9.71	0.1037	7.53E+05	3.26E+06	0.15	0.04	0.03	3.63E+05	5.79E+05	6.68E+05
210	9.12E+05	9.71	0.1037	7.53E+05	3.26E+06	0.15	0.04	0.03	3.63E+05	5.79E+05	6.68E+05
211	9.12E+05	9.71	0.1037	7.53E+05	3.26E+06	0.15	0.04	0.03	3.63E+05	5.79E+05	6.68E+05
212	9.12E+05	9.71	0.1037	8.28E+05	3.26E+06	0.15	0.04	0.04	3.80E+05	6.22E+05	6.68E+05
213	9.12E+05	9.71	0.1037	8.28E+05	3.26E+06	0.15	0.04	0.04	3.80E+05	6.22E+05	6.68E+05
214	9.12E+05	9.71	0.1037	8.28E+05	3.26E+06	0.15	0.04	0.04	3.80E+05	6.22E+05	6.68E+05
215	9.12E+05	9.71	0.1037	8.28E+05	3.26E+06	0.15	0.04	0.04	3.80E+05	6.22E+05	6.68E+05
216	9.12E+05	9.71	0.1037	8.28E+05	3.26E+06	0.15	0.04	0.04	3.80E+05	6.22E+05	6.68E+05
217	9.12E+05	9.71	0.1037	9.32E+05	3.26E+06	0.15	0.04	0.04	4.00E+05	6.79E+05	6.68E+05
218	9.12E+05	9.71	0.1037	9.32E+05	3.26E+06	0.15	0.04	0.04	4.00E+05	6.79E+05	6.68E+05
219	9.12E+05	9.71	0.1037	9.32E+05	3.26E+06	0.15	0.04	0.04	4.00E+05	6.79E+05	6.68E+05
220	9.12E+05	9.71	0.1037	9.32E+05	3.26E+06	0.15	0.04	0.04	4.00E+05	6.79E+05	6.68E+05
221	9.12E+05	9.71	0.1037	1.09E+06	3.26E+06	0.15	0.04	0.05	4.26E+05	7.58E+05	6.68E+05
222	9.12E+05	9.71	0.1037	1.09E+06	3.26E+06	0.15	0.04	0.05	4.26E+05	7.58E+05	6.68E+05
223	9.12E+05	9.71	0.1037	1.09E+06	3.26E+06	0.15	0.04	0.05	4.26E+05	7.58E+05	6.68E+05
224	9.12E+05	9.71	0.1037	1.09E+06	3.26E+06	0.15	0.04	0.05	4.26E+05	7.58E+05	6.68E+05
225	9.12E+05	9.71	0.1037	1.09E+06	3.26E+06	0.15	0.04	0.05	4.26E+05	7.58E+05	6.68E+05
226	7.50E+05	13.79	0.1014	6.82E+05	3.26E+06	0.15	0.03	0.03	3.13E+05	5.36E+05	5.77E+05
227	6.35E+05	19.16	0.1022	5.78E+05	3.26E+06	0.15	0.03	0.03	2.65E+05	4.70E+05	5.07E+05
301	5.85E+05	11.65	0.1297	1.68E+06	3.26E+06	0.15	0.03	0.08	3.55E+05	1.01E+06	4.74E+05
302	5.85E+05	11.65	0.1297	1.68E+06	3.26E+06	0.15	0.03	0.08	3.55E+05	1.01E+06	4.74E+05
303	6.61E+05	9.31	0.1268	1.91E+06	3.26E+06	0.15	0.03	0.09	4.02E+05	1.08E+06	5.23E+05
304	9.52E+05	2.65	0.2214	1.05E+06	3.26E+06	0.15	0.04	0.05	4.31E+05	7.39E+05	6.90E+05
305	7.23E+05	5.02	0.1167	5.55E+05	3.26E+06	0.15	0.03	0.03	2.78E+05	4.54E+05	5.61E+05
306	7.24E+05	5.00	0.1168	5.57E+05	3.26E+06	0.15	0.03	0.03	2.78E+05	4.56E+05	5.62E+05
307	7.23E+05	5.01	0.1168	5.55E+05	3.26E+06	0.15	0.03	0.03	2.78E+05	4.54E+05	5.61E+05
308	9.51E+05	2.66	0.2204	1.05E+06	3.26E+06	0.15	0.04	0.05	4.31E+05	7.39E+05	6.89E+05
309	9.51E+05	2.66	0.2210	1.05E+06	3.26E+06	0.15	0.04	0.05	4.31E+05	7.39E+05	6.89E+05
310	9.51E+05	2.66	0.2210	1.05E+06	3.26E+06	0.15	0.04	0.05	4.31E+05	7.39E+05	6.89E+05
311	9.51E+05	2.66	0.2210	1.05E+06	3.26E+06	0.15	0.04	0.05	4.31E+05	7.39E+05	6.89E+05

6.3.2 Waste

All analyses that include waste are run with a waste height of 284 inches, which represents a bounding waste capacity in any Type I SST. The consideration of both an empty and a "full" tank is considered bounding. Waste shear modulus data relevant to the Hanford interim stabilized waste are summarized in Appendix N of Rinker et al. (2011a). Based on the higher demands from high shear stiffness (HSS) waste in previous AORs, as well as the low overall differences in Type I demands and the low overall Type I demand/capacity ratios (see Johnson et al. 2014a), only the HSS waste condition is included in this analysis. The waste is modeled using ANSYS® SOLID45 solid elements. The waste material properties used are given in Table 6-9, and Figure 6-26 shows the waste elements.

Table 6-9. Seismic Model Waste Properties

Waste	Specific Gravity	Poisson's Ratio	Shear Modulus	Young's Modulus
High Shear Stiffness (HSS)	1.7	0.49	146 kip/ft^2	436 kip/ft^2

A Poisson's ratio of 0.49 is consistent with undrained saturated clays/silts/sediments. No additional damping is applied to the waste beyond the global mass-proportional (alpha) damping for the component Rayleigh damping used in ANSYS® for transient analyses.

Figure 6-26. Element Plot Showing Waste

6.3.3 Soil Properties

Far-field soil properties are provided by AMEC Geomatrix and documented in the *Development of Inputs for SSI Analyses of SSTs*, Rev. 0 in Appendix R of Rinker et al. (2011a). The dynamic materials model uses the linear elastic relationship and the shear and compression wave velocities as constants for each soil layer. Backfill soil properties are provided in Appendices O and P in Rinker et al. (2011a). The soil properties used in the models are summarized in the following tables:

- Table 6-10. Strain Compatible Lower Bound Native Soil Properties
- Table 6-11. Strain Compatible Best Estimate Native Soil Properties
- Table 6-12. Strain Compatible Upper Bound Native Soil Properties
- Table 6-13. Lower Bound Excavated Backfill Soil Properties
- Table 6-14. Best Estimate Excavated Backfill Soil Properties
- Table 6-15. Upper Bound Excavated Backfill Soil Properties

Table 6-10. Strain Compatible Lower Bound Native Soil Properties

Elevation (ft)	Damping (in Decimal)	Unit Weight (kip/ft^3)	Strain-Compatible Vs (ft/sec)	Vp (ft/sec)	Poisson's Ratio	Shear Modulus (kip/ft^2)	Modulus of Elasticity (kip/ft^2)	Material Property No.
-1	0.01540	0.106	438	1047.6	0.39	632	1761	901
-2	0.02120	0.106	438	1047.6	0.39	632	1761	902
-3	0.02830	0.106	438	1047.6	0.39	632	1761	903
-4	0.03720	0.106	438	1047.6	0.39	632	1761	904
-5	0.04340	0.106	438	1047.6	0.39	632	1761	905
-6	0.04290	0.106	540	1047.6	0.32	960	2532	906
-7	0.04300	0.106	540	1047.6	0.32	960	2532	907
-8	0.04740	0.106	540	1047.6	0.32	960	2532	908
-9	0.05090	0.106	540	1047.6	0.32	960	2532	909
-10	0.04210	0.106	680	1099.0	0.19	1522	3622	910
-14	0.04350	0.106	680	1099.2	0.19	1522	3623	911
-19	0.04620	0.106	787	2027.4	0.41	2039	5755	912
-21	0.04960	0.106	815	2027.4	0.40	2187	6138	913
-23	0.04990	0.106	860	2027.4	0.39	2435	6770	914
-25	0.05520	0.106	860	2027.4	0.39	2435	6770	915
-28	0.05600	0.106	860	2027.4	0.39	2435	6770	916
-31	0.05710	0.106	900	2313.1	0.41	2666	7524	917
-35	0.05360	0.106	970	2313.1	0.39	3097	8631	918
-37	0.06110	0.106	970	2313.1	0.39	3097	8631	919
-39	0.06140	0.106	970	2313.1	0.39	3097	8631	920
-40	0.05580	0.106	1047	2313.1	0.37	3609	9896	921
-41	0.05580	0.106	1047	2313.1	0.37	3609	9896	922
-42	0.05080	0.106	1089	2313.1	0.36	3904	10600	923
-43	0.05080	0.106	1089	2313.1	0.36	3904	10600	924
-45	0.05080	0.106	1089	2313.1	0.36	3904	10600	925
-48	0.05180	0.106	1089	2313.1	0.36	3904	10600	926
-49	0.05170	0.106	1089	2313.1	0.36	3904	10600	927
-50	0.05170	0.106	1089	2313.1	0.36	3904	10600	928
-54	0.04990	0.106	1089	2313.1	0.36	3904	10600	929
-55	0.05210	0.106	1190	2313.1	0.32	4662	12307	930
-57	0.05210	0.106	1190	2313.1	0.32	4662	12307	931
-59	0.05210	0.106	1190	2313.1	0.32	4662	12307	932
-63	0.05250	0.106	1210	2313.1	0.31	4820	12643	933
-71	0.05650	0.106	1210	2313.1	0.31	4820	12643	934
-82	0.05580	0.106	1210	2313.1	0.31	4820	12643	935
-94	0.06140	0.106	1210	2313.1	0.31	4820	12643	936
-120	0.06430	0.106	1210	2313.1	0.31	4820	12643	937
-160	0.06490	0.106	1210	2313.1	0.31	4820	12643	938
-205	0.08060	0.106	1149	2313.1	0.34	4346	11614	939
-215	0.08060	0.127	1210	2313.1	0.31	5775	15148	940
-225	0.07500	0.127	1210	2313.1	0.31	5775	15148	941
-235	0.07500	0.127	1210	2313.1	0.31	5775	15148	942
-285	0.08320	0.127	1210	2313.1	0.31	5775	15148	943
-295	0.06580	0.135	1560	3470.1	0.37	10203	28025	944
-315	0.06570	0.135	1560	3470.1	0.37	10203	28025	945
-335	0.07030	0.135	1560	3470.1	0.37	10203	28025	946
-355	0.08130	0.135	1400	3470.1	0.40	8217	23055	947
-380	0.05510	0.135	1580	3470.1	0.37	10466	28662	948
-405	0.05880	0.135	1580	3470.1	0.37	10466	28662	949

Table 6-11. Strain Compatible Best Estimate Native Soil Properties

Elevation (ft)	Damping (in Decimal)	Unit Weight (kip/ft^3)	Strain-Compatible Vs (ft/sec)	Vp (ft/sec)	Poisson's Ratio	Shear Modulus (kip/ft^2)	Modulus of Elasticity (kip/ft^2)	Material Property No.
-1	0.011430	0.106	710	1283.3	0.28	1659	4246	901
-2	0.015250	0.106	710	1283.3	0.28	1659	4246	902
-3	0.019600	0.106	710	1283.3	0.28	1659	4246	903
-4	0.022300	0.106	720	1283.3	0.27	1707	4336	904
-5	0.024350	0.106	720	1283.3	0.27	1707	4336	905
-6	0.029730	0.106	720	1283.3	0.27	1707	4336	906
-7	0.028480	0.106	775	1283.3	0.21	1977	4797	907
-8	0.032350	0.106	775	1283.3	0.21	1977	4797	908
-9	0.030730	0.106	775	1283.3	0.21	1977	4797	909
-10	0.029030	0.106	987	1595.0	0.19	3207	7631	910
-14	0.030100	0.106	987	1595.0	0.19	3207	7631	911
-19	0.031750	0.106	1086	1755.0	0.19	3882	9238	912
-21	0.034500	0.106	1158	2483.3	0.36	4414	12016	913
-23	0.035750	0.106	1158	2483.3	0.36	4414	12016	914
-25	0.035950	0.106	1158	2483.3	0.36	4414	12016	915
-28	0.036980	0.106	1158	2483.3	0.36	4414	12016	916
-31	0.037950	0.106	1280	2833.3	0.37	5393	14797	917
-35	0.037800	0.106	1280	2833.3	0.37	5393	14797	918
-37	0.040450	0.106	1280	2833.3	0.37	5393	14797	919
-39	0.040680	0.106	1280	2833.3	0.37	5393	14797	920
-40	0.034850	0.106	1344	2833.3	0.35	5946	16112	921
-41	0.034850	0.106	1344	2833.3	0.35	5946	16112	922
-43	0.035150	0.106	1383	2833.3	0.34	6296	16920	923
-45	0.035150	0.106	1383	2833.3	0.34	6296	16920	924
-48	0.035480	0.106	1416	2833.3	0.33	6600	17604	925
-49	0.033130	0.106	1526	2833.3	0.30	7666	19865	926
-50	0.033130	0.106	1526	2833.3	0.30	7666	19865	927
-55	0.034100	0.106	1526	2833.3	0.30	7666	19865	928
-57	0.034450	0.106	1526	2833.3	0.30	7666	19865	929
-59	0.034450	0.106	1526	2833.3	0.30	7666	19865	930
-62	0.035900	0.106	1526	2833.3	0.30	7666	19865	931
-70	0.037880	0.106	1526	2833.3	0.30	7666	19865	932
-82	0.040400	0.106	1526	2833.3	0.30	7666	19865	933
-94	0.041930	0.106	1526	2833.3	0.30	7666	19865	934
-104	0.032480	0.106	1780	2877.0	0.19	10430	24822	935
-123	0.034250	0.106	1780	4816.7	0.42	10430	29641	936
-143	0.028330	0.106	2424	4816.7	0.33	19343	51468	937
-158	0.018450	0.135	2638	4816.7	0.29	29176	75027	938
-173	0.019100	0.135	2638	4935.2	0.30	29176	75858	939
-192	0.020000	0.135	2638	4935.2	0.30	29176	75858	940
-213	0.020700	0.135	2638	4935.2	0.30	29176	75858	941
-233	0.008130	0.156	3350	6267.3	0.30	54370	141362	942
-213	0.020700	0.135	2638	4935.2	0.30	29176	75858	943
-303	0.008450	0.156	3350	6267.3	0.30	54370	141362	944

Table 6-12. Strain Compatible Upper Bound Native Soil Properties

Elevation (ft)	Damping (in Decimal)	Unit Weight (kip/ft^3)	Strain-Compatible Vs (ft/sec)	Vp (ft/sec)	Poisson's Ratio	Shear Modulus (kip/ft^2)	Modulus of Elasticity (kip/ft^2)	Material Property No.
-1	0.008700	0.106	1089	1760.3	0.19	3904	9291	901
-2	0.010200	0.106	1089	1760.3	0.19	3904	9291	902
-3	0.012200	0.106	1089	1760.3	0.19	3904	9291	903
-4	0.015200	0.106	1089	1760.3	0.19	3904	9291	904
-5	0.016400	0.106	1089	1760.3	0.19	3904	9291	905
-6	0.017700	0.106	1089	1760.3	0.19	3904	9291	906
-7	0.018300	0.106	1089	1760.3	0.19	3904	9291	907
-8	0.016300	0.106	1280	2069.1	0.19	5393	12837	908
-9	0.017700	0.106	1280	2069.1	0.19	5393	12837	909
-10	0.016400	0.106	1280	2069.1	0.19	5393	12837	910
-14	0.019500	0.106	1379	2229.0	0.19	6260	14898	911
-19	0.020900	0.106	1423	3041.0	0.36	6666	18129	912
-21	0.020400	0.106	1423	3041.0	0.36	6666	18129	913
-23	0.022700	0.106	1520	3041.0	0.33	7606	20284	914
-25	0.021000	0.106	1520	3041.0	0.33	7606	20284	915
-28	0.022900	0.106	1630	3041.0	0.30	8746	22713	916
-31	0.020400	0.106	1732	3041.0	0.26	9875	24884	917
-35	0.021700	0.106	1732	3469.7	0.33	9875	26348	918
-37	0.024400	0.106	1732	3469.7	0.33	9875	26348	919
-39	0.026400	0.106	1732	3469.7	0.33	9875	26348	920
-40	0.021200	0.106	1732	3469.7	0.33	9875	26348	921
-41	0.021200	0.106	1732	3469.7	0.33	9875	26348	922
-43	0.019800	0.106	1732	3469.7	0.33	9875	26348	923
-45	0.019800	0.106	1732	3469.7	0.33	9875	26348	924
-48	0.021900	0.106	1950	3469.7	0.27	12518	31774	925
-49	0.022300	0.106	1950	3469.7	0.27	12518	31774	926
-50	0.022300	0.106	1950	3469.7	0.27	12518	31774	927
-55	0.020400	0.106	1950	3469.7	0.27	12518	31774	928
-57	0.021100	0.106	1950	3469.7	0.27	12518	31774	929
-59	0.021100	0.106	1950	3469.7	0.27	12518	31774	930
-62	0.023800	0.106	1950	3469.7	0.27	12518	31774	931
-70	0.023800	0.106	1950	3469.7	0.27	12518	31774	932
-82	0.025400	0.106	1950	3469.7	0.27	12518	31774	933
-94	0.027400	0.106	1950	3469.7	0.27	12518	31774	934
-99	0.015900	0.135	2351	5899.6	0.41	23173	65144	935
-104	0.015900	0.135	2351	5899.6	0.41	23173	65144	936
-113	0.016900	0.135	2351	5899.6	0.41	23173	65144	937
-123	0.016900	0.135	2351	5899.6	0.41	23173	65144	938

Table 6-13. Lower Bound Excavated Backfill Soil Properties

Elevation (ft)	Damping (in Decimal)	Unit Weight (kip/ft^3)	Strain-Compatible Vs (ft/sec)	Poisson's Ratio	Shear Modulus (kip/ft^2)	Modulus of Elasticity (kip/ft^2)	Material Property No.
-1	0.01540	0.129	560	0.28	1256	3216	601, 701, 801
-2	0.02120	0.129	575	0.28	1325	3391	602, 702, 802
-3	0.02830	0.129	590	0.28	1395	3570	603, 703, 803
-4	0.03720	0.129	605	0.28	1466	3754	604, 704, 804
-5	0.04340	0.129	620	0.28	1540	3942	605, 705, 805
-6	0.04290	0.129	635	0.28	1615	4135	606, 706, 806
-7	0.04300	0.129	650	0.28	1693	4333	607, 707, 807
-8	0.04740	0.129	665	0.28	1772	4535	608, 708, 808
-9	0.05090	0.129	680	0.28	1852	4742	609, 709, 809
-10	0.04210	0.129	695	0.28	1935	4954	610, 710, 810
-14	0.04350	0.1227	755	0.28	2172	5561	611, 711, 811
-19	0.04620	0.1122	830	0.28	2400	6145	712, 812
-21	0.04960	0.108	860	0.28	2481	6350	713, 813
-23	0.04990	0.108	880	0.28	2597	6649	714, 814
-25	0.05520	0.108	900	0.28	2717	6955	715, 815
-28	0.05600	0.108	930	0.28	2901	7426	716, 816
-31	0.05710	0.108	960	0.28	3091	7913	717, 817
-35	0.05360	0.108	1000	0.28	3354	8586	718, 818
-37	0.06110	0.108	1020	0.28	3490	8933	719, 819

Table 6-14. Best Estimate Excavated Backfill Soil Properties

Elevation (ft)	Damping (in Decimal)	Unit Weight (kip/ft^3)	Strain-Compatible Vs (ft/sec)	Poisson's Ratio	Shear Modulus (kip/ft^2)	Modulus of Elasticity (kip/ft^2)	Material Property No.
-1	0.01143	0.129	750	0.28	2253	5769	601, 701, 801
-2	0.01525	0.129	770	0.28	2375	6081	602, 702, 802
-3	0.01960	0.129	790	0.28	2500	6401	603, 703, 803
-4	0.02230	0.129	810	0.28	2628	6729	604, 704, 804
-5	0.02435	0.129	830	0.28	2760	7065	605, 705, 805
-6	0.02973	0.129	850	0.28	2894	7410	606, 706, 806
-7	0.02848	0.129	870	0.28	3032	7763	607, 707, 807
-8	0.03235	0.129	890	0.28	3173	8124	608, 708, 808
-9	0.03073	0.129	910	0.28	3318	8493	609, 709, 809
-10	0.02903	0.129	930	0.28	3465	8870	610, 710, 810
-14	0.035750	0.1227	1010	0.28	3887	9951	611, 711, 811
-19	0.035950	0.1122	1110	0.28	4293	10991	712, 812
-21	0.036980	0.108	1150	0.28	4436	11355	713, 813
-23	0.037950	0.108	1177	0.28	4644	11888	714, 814
-25	0.037800	0.108	1203	0.28	4857	12433	715, 815
-28	0.040450	0.108	1243	0.28	5185	13273	716, 816
-31	0.040680	0.108	1283	0.28	5524	14141	717, 817
-35	0.034850	0.108	1337	0.28	5993	15341	718, 818
-37	0.034850	0.108	1363	0.28	6234	15959	719, 819

Table 6-15. Upper Bound Excavated Backfill Soil Properties

Elevation (ft)	Damping (in Decimal)	Unit Weight (kip/ft^3)	Strain-Compatible Vs (ft/sec)	Poisson's Ratio	Shear Modulus (kip/ft^2)	Modulus of Elasticity (kip/ft^2)	Material Property No.
-1	0.008700	0.129	960	0.28	3692	9451	601, 701, 801
-2	0.010200	0.129	988	0.28	3910	10011	602, 702, 802
-3	0.012200	0.129	1016	0.28	4135	10586	603, 703, 803
-4	0.015200	0.129	1044	0.28	4366	11178	604, 704, 804
-5	0.016400	0.129	1072	0.28	4603	11785	605, 705, 805
-6	0.017700	0.129	1100	0.28	4847	12409	606, 706, 806
-7	0.018300	0.129	1128	0.28	5097	13049	607, 707, 807
-8	0.016300	0.129	1156	0.28	5353	13705	608, 708, 808
-9	0.017700	0.129	1184	0.28	5616	14377	609, 709, 809
-10	0.016400	0.129	1212	0.28	5884	15065	610, 710, 810
-14	0.019500	0.1227	1324	0.28	6679	17100	611, 711, 811
-19	0.019500	0.1122	1464	0.28	7468	19118	712, 812
-21	0.020400	0.108	1520	0.28	7749	19837	713, 813
-23	0.022700	0.108	1558	0.28	8141	20842	714, 814
-25	0.021000	0.108	1596	0.28	8543	21871	715, 815
-28	0.022900	0.108	1653	0.28	9164	23461	716, 816
-31	0.020400	0.108	1710	0.28	9807	25107	717, 817
-35	0.021700	0.108	1786	0.28	10698	27388	718, 818
-37	0.024400	0.108	1824	0.28	11158	28566	719, 819

6.4 Load Conditions

The load applied in the seismic model on the roof includes 11.5 ft. of overburden with a soil density of 129 lb/ft^3, which conservatively exceeds the nominal soil load for B, C, T, and U farms.

6.4.1 Surface Loads

A shell element with a unit thickness is added to the surface on a 5-foot-radius circular area over the center of the roof (see Figure 6-27) to create a simulated concentrated load over the tank roof. The surface load is also applied on the hatchway where hatchway horizontal surfaces replace the soil. This method provides a spatially uniform distribution of the surface load. The stiffness of the shell is 40 ksf (approx. 1/100th of the underlying soil) so as to not provide any structural rigidity to the soil or hatchway.

The nominal allowable concentrated load for 200 series SSTs with the maximum allowable soil overburden per Mackey (2012) is 142,000 lbf (71,000 lbf for a half model). The hatchway adds net weight to the roof, therefore this nominal concentrated load on the soil over the center of the tank is reduced by 16 kip due to the addition of hatchway net weight in excess of the displaced soil (see Table 6-16). The density of the shell is adjusted to provide the total load equal to the nominal allowable concentrated load.

The gravity results are subtracted from the gravity plus seismic results to produce seismic-only results, therefore the seismic-only results only retain the inertial effect of the concentrated load. The dead weight contribution is added back in when the seismic-only results are combined with the TOLA results. The surface load is developed using the input file Surface_load.inp.

Table 6-16. Type I SST Concentrated Surface Loads (for Half Model)

Load Source	Net Load
Hatchway [1]	16 kip
Applied Surface Load	55 kip
Total	71 kip

[1] See Table 6-6

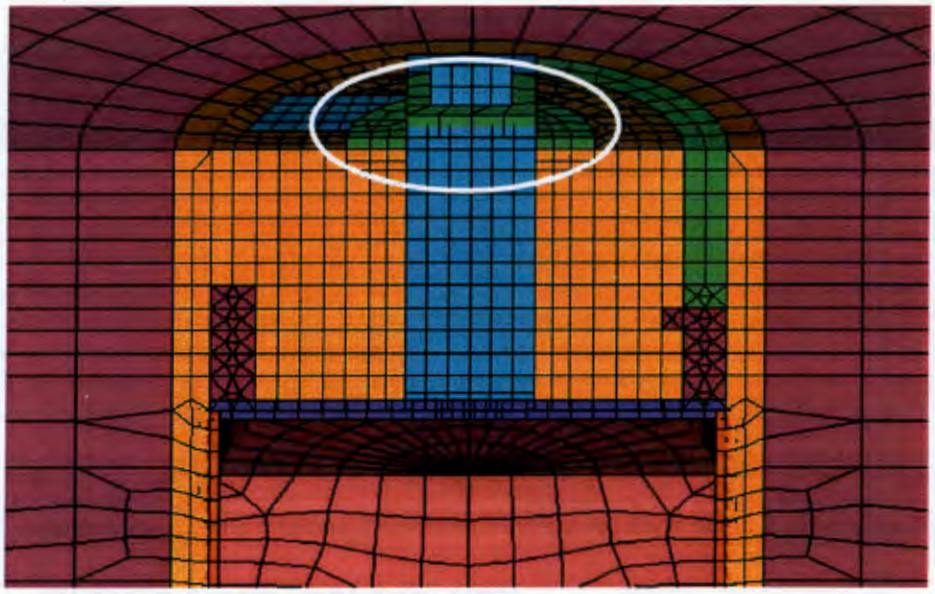

Figure 6-27. Element Plot of Surface Load Elements (Shown Circled, in Green)

6.5 Boundary Conditions

Boundary conditions and supporting elements are developed in input file BC.inp, and are described in the following two sections.

6.5.1 Soil Boundary Conditions

The soil elements support three translational degrees of freedom, thus the nodes on the symmetry plane have translation normal to the symmetry plane set to zero (see Figure 6-28).

At each elevation, all nodes on the outside edge (radius = 320 ft) have been "slaved" to a single node at each layer. Couples are used in each of the three translations to force the soil to behave essentially as a shear beam. This approach is used to create the appropriate conditions for vertically propagating waves to pass through the model (see Figure 6-29) and minimizes wave scattering at the far-field boundary. All nodes at the base of the model are coupled together to create a rigid region in the plane where the seismic excitation is applied. The effectiveness of this approach is documented in Rinker et al. (2006).

ANSYS® LINK8 elements with a high stiffness are used to connect the native soil slaved nodes on each layer to the symmetry plane. These are required because the slaved node of a couple cannot also support an applied boundary condition. Therefore, to maintain the desired soil behavior, the link elements effectively complete the coupling of the symmetry plane node at each layer.

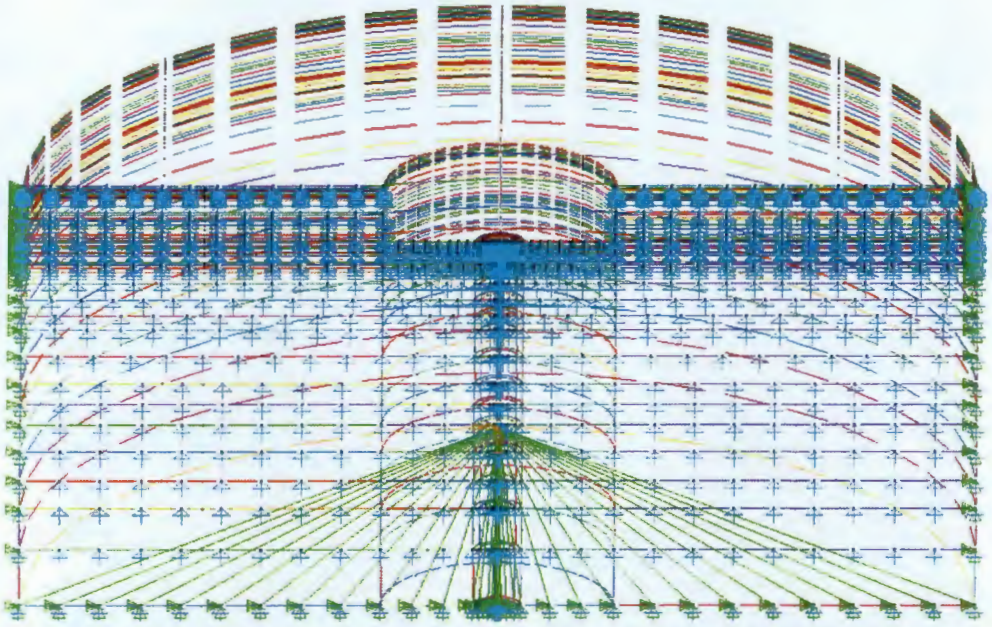

Figure 6-28. Seismic Model Boundary Conditions – Symmetry Plane and Soil Base

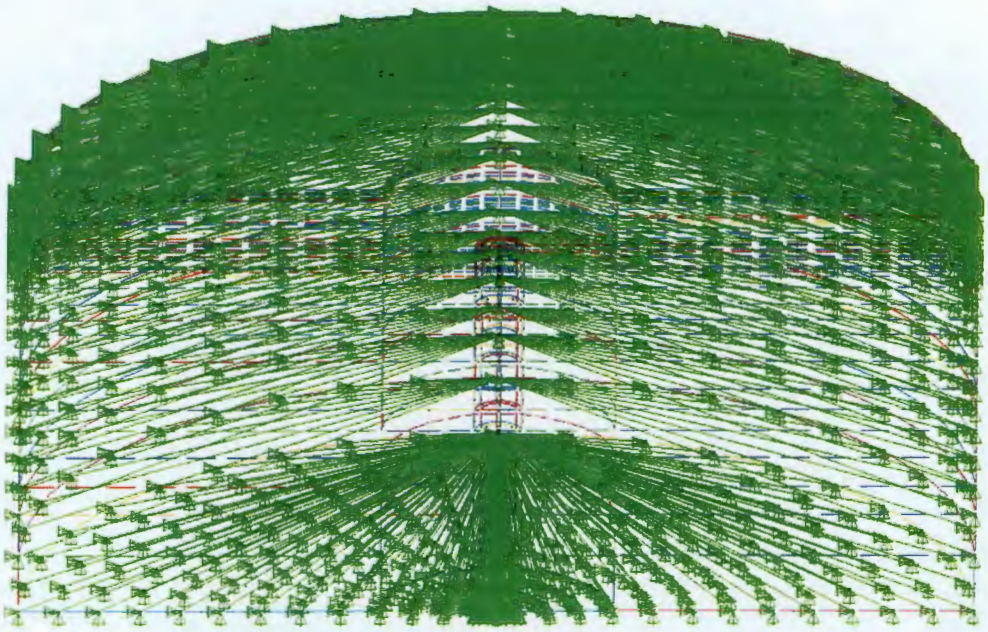

Figure 6-29. Seismic Model Boundary Conditions – Slaved Boundary Conditions

6.5.2 Tank Boundary Conditions

The tank model shell elements support six degrees of freedom; thus, all nodes on the symmetry plane are fixed from translation normal to the symmetry plane and for rotations about the two axes in the symmetry plane as shown in Figure 6-30. Since the hatchway uses solid elements, the boundary conditions on the hatchway are applied for translation normal to the symmetry plane only, the same as the soil.

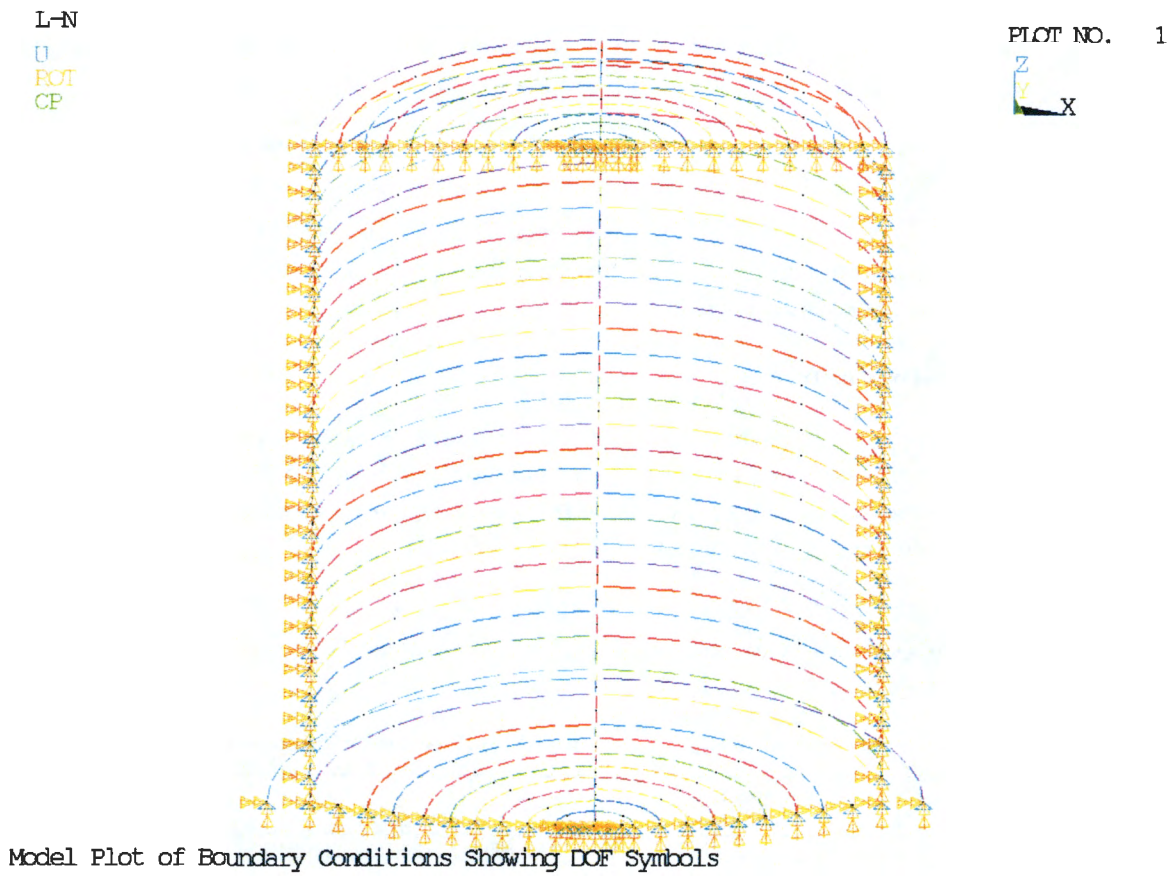

Figure 6-30. Seismic Model Boundary Condition – Concrete Tank

6.5.3 Model Excitation

A large mass element is located at the base of the model and a seismic excitation is applied to that node as a force time series. The use of a large base mass, which is greater than 100 times the mass of the full model, ensures that the input motion is faithfully reproduced in the model. The applied force is the product of the mass of the entire model and the acceleration for that time step of the seismic acceleration time series.

6.5.4 Seismic Input

Seismic inputs are applied using the same methodologies and loading as the previous analyses of SST Types II, III, and IV AORs documented in Rinker et al. (2011a and 2011b) and Johnson et al. (2014c). Discussion of seismic input development and spectra matching is provided in Section 7.0.

Horizontal and vertical input motions have been defined as acceleration time series (Appendix R of Rinker et al. 2011a) for a 40.96 second event consisting of 4,096 data points each (time increment of the seismic input is 0.01 seconds). To reduce computer run times, only the first 2,048 data points are used for the seismic analysis because this is sufficient to completely capture the strong motion of the seismic record.

6.6 Post-Processing

The methods for post-processing described below are typical for all of the seismic runs and studies used with the seismic model. Information about the run configuration (see Section 6.7.1) is recorded in the output files to aid identification and checking.

6.6.1 Concrete Tank Elements

Concrete tank forces and moments at each of the ACI-evaluation sections are extracted from the model in 9-degree slices, according to the coordinate system described in Section 6.1. The ACI-evaluation section sequence starts near the center of the roof and moves radially along the roof, down the sidewall, then from the outside to the center of the tank floor.

As described in the ANSYS® 13.0 manual (ANSYS 2010), the ANSYS® SHELL181 element used for the concrete tank supports the following output used in this analysis (Table 6-17):

Table 6-17. Selected ANSYS® SHELL181 Output Quantities and Sequence Numbers

Output Quantity Name	Item	Sequence Numbers	Description
N11	SMISC	1	Meridional force (per unit length)
N22	SMISC	2	Hoop force (per unit length)
N12	SMISC	3	In-plane shear force (per unit length)
M11	SMISC	4	Meridional moments (per unit length)
M22	SMISC	5	Hoop moments (per unit length)
M12	SMISC	6	Twisting moment – not used
Q13	SMISC	7	Transverse (through-wall) shear force (per unit length)
Q23	SMISC	8	Transverse (through-wall) shear force (per unit length)

Figure 6-31 shows the ANSYS® SHELL181 element force and moment vector and element coordinate system (ECS) relative to the tank model coordinate system. Results for through-wall shear forces are the envelope of SMISC7 and SMISC8. Results are not presented for SMISC6, the element in-plane twisting moment, as this is not used in the ACI evaluation.

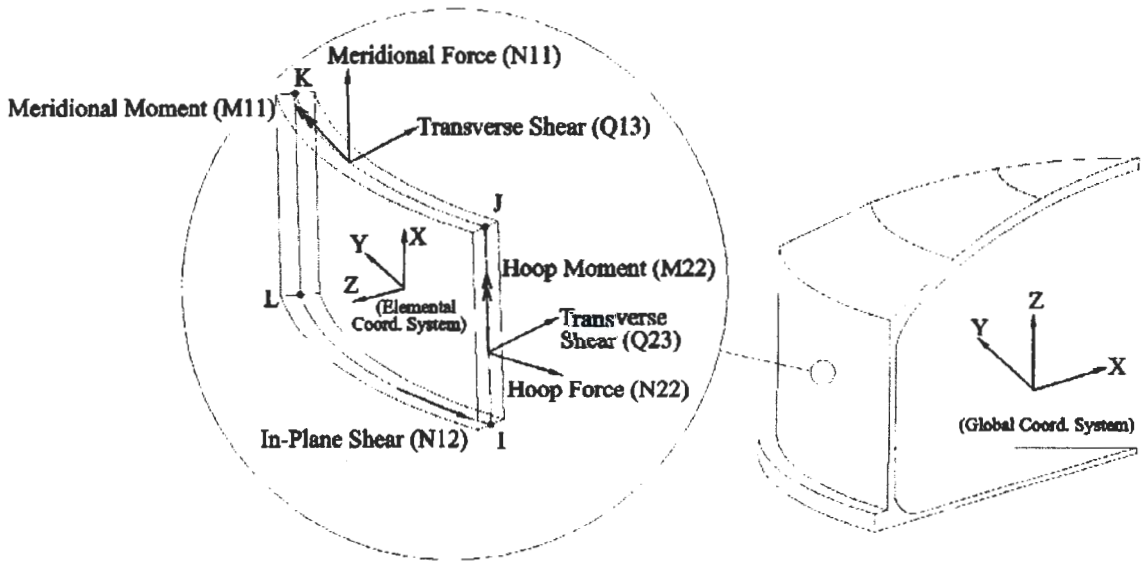

Figure 6-31. ANSYS® SHELL 181 Element Force and Moment Vector Orientations (the Type-I tank orientations are the same as the Type-II tank profile shown)

The elements for post-processing are determined by selecting the elements whose centroids most closely match the locations defined as ACI-evaluation sections. A sample excerpt of the element selection for the first angle slice is shown as Table 6-18. The first four columns (ACI#, LocX/Y/Z) describe the ACI-evaluation sections by sequence number and location. The next four columns (Elem/X/Y/Z) identify the element at that location, and the location of the element centroid. All locations are in a cylindrical coordinate system with its origin at the elevation of the footing centerline. The element path (PathE) is the cumulative sum of each successive element centroid spacing. The vector components of the slope (SlopeX, SlopeZ) and the material property number of the element are reported for checking purposes. The selected elements are shown graphically in Figure 6-32.

Table 6-18. Tank Concrete ACI-Evaluation Section Data Output (Sample Excerpt)

Tank 1 Concrete elements at angle 1 (4.5°) ACI section data

ACI#	LocX	LocY°	LocZ	Elem	ElemX	ElemY	ElemZ	PathE	SlopX	SlopZ	Mat
1	1.83	4.49	25.83	129	1.83	4.50	25.83	22	1.00	0.00	102
2	3.67	4.49	25.83	109	3.67	4.50	25.83	44	1.00	0.00	104
3	5.50	4.49	25.83	89	5.50	4.50	25.83	66	1.00	0.00	106
4	7.44	4.49	25.83	69	7.44	4.50	25.83	89	1.00	0.00	108
5	9.17	4.49	25.83	49	9.17	4.50	25.83	110	1.00	0.00	110
6	10.54	4.49	24.50	249	10.54	4.50	24.50	133	0.00	1.00	202
7	10.54	4.49	23.42	259	10.54	4.50	23.47	145	0.00	1.00	203
8	10.54	4.49	21.42	279	10.54	4.50	21.42	170	0.00	1.00	205
9	10.54	4.49	19.67	299	10.54	4.50	19.67	191	0.00	1.00	207
10	10.54	4.49	17.67	319	10.54	4.50	17.67	215	0.00	1.00	209
11	10.54	4.49	15.92	339	10.54	4.50	15.92	236	0.00	1.00	211
12	10.54	4.49	13.92	359	10.54	4.50	13.92	260	0.00	1.00	213
13	10.54	4.49	12.17	379	10.54	4.50	12.17	281	0.00	1.00	215
14	10.54	4.49	10.17	399	10.54	4.50	10.17	305	0.00	1.00	217
15	10.54	4.49	8.42	419	10.54	4.50	8.42	326	0.00	1.00	219
16	10.54	4.49	6.42	439	10.54	4.50	6.42	350	0.00	1.00	221
17	10.54	4.49	4.73	459	10.54	4.50	4.73	370	0.00	1.00	223
18	10.54	4.49	2.80	479	10.54	4.50	2.80	393	0.00	1.00	225
19	7.91	4.49	-0.46	849	7.91	4.50	-0.39	443	0.00	0.00	304
20	5.78	4.49	-0.70	869	5.78	4.50	-0.65	469	0.00	0.00	306
21	3.90	4.49	-0.85	889	3.90	4.50	-0.82	491	0.00	0.00	308
22	1.93	4.49	-0.94	909	1.93	4.50	-0.92	515	0.00	0.00	310

Model Plot with Material Property Numbers

Figure 6-32. Element Plot of Concrete Tank Elements at ACI-Evaluation Sections

6.6.2 Contact Elements

Soil contact data are extracted from the contact elements overlying the tank ACI-evaluation sections. The location (i.e., mesh) of the soil contact elements is not as strictly controlled as the tank ACI-evaluation section locations, but is of sufficient detail and proximity to show meaningful trends along the tank profile. Just as with the tank elements, ANSYS® determines the contact elements for post-processing by selecting the elements whose centroids most closely match the locations defined as ACI-evaluation sections.

As described in the ANSYS® 13.0 manual (ANSYS 2010), the ANSYS® CONTA173 element used for the contact surfaces supports the following output used in this analysis (Table 6-19):

Table 6-19. Selected ANSYS® CONTA173 Output Quantities

Output Quantity Name	Description
CONT:PRES	Normal contact pressure

6.6.3 Enveloping Process

The transient analysis consists of an initial gravity step plus 2,048 transient time steps. To condense the amount of data that is generated by the transient analysis, the following enveloping process is used:

1. At every element at all ACI-evaluation section locations, the maximum and minimum results are extracted over the entire transient . Built-in ANSYS® post-processing functions are used to determine the maximum and minimum results.

2. To isolate the seismic-only results for each element, gravity is subtracted from the seismic plus gravity results. The minima and maxima results are each subtracted separately to maintain accuracy. Since the seismic-only results are reported as absolute values only, the seismic-only result is the bounding greatest absolute value of each pair of the min/max subtracted results. These partially enveloped results are used in the surface plots to present detailed results around the tank circumference.

3. The above results at each ACI-evaluation section are summarized by determining the bounding results at any angle around the tank. These fully enveloped results are used in the comparison plots to present multiple sets of results in a simplified representational format.

These steps are performed within ANSYS® post-processing using array parameter operations. The results are output in tabular text format. See Section 6.1.3 for a list of output files generated during post-processing.

6.6.3.1 Post-Processing Example

Since the post-processing is a complex process, a simplified example is demonstrated below. These hypothetical results are chosen to demonstrate different mathematical combinations that may be encountered. In this example,

- Angle 1 is completely insensitive to seismic
- Angle 2 experiences fully reversing loads due to seismic with a bias from the constant gravity load
- Angles 3 and 4 experience the same loads as angle 2, but with +/- 10% asymmetry

1. The bounding min/max values in time are determined for each element.

Gravity-only Results	Min	Max
Angle 1	100	100
Angle 2	100	100
Angle 3	100	100
Angle 4	100	100

Gravity + Seismic Results	Min	Max
Angle 1	100	100
Angle 2	90	110
Angle 3	91	91
Angle 4	89	89

2. To isolate the seismic-only results, subtract minimum and maximum gravity-only results from the gravity plus seismic results and report the greatest absolute value of the subtracted values.

Seismic-only Results	Min	Max	Bound
Angle 1	0	0	0
Angle 2	-10	10	10
Angle 3	-9	-9	9
Angle 4	-11	-11	11

3. Final seismic-only bounding value at any angle:

Seismic-only Results	Bound
Any angle	11

6.7 Run Descriptions

See Section 6.3.2 for definition of full tank and high modulus (stiff) waste properties. All seismic runs use orthotropic thermally degraded, fully cracked concrete (FCC) properties as determined in the TOLA analysis (Johnson et al. 2014a) and listed in Table 6-9.

6.7.1 Seismic Run Matrix

The seismic run matrix is listed in Table 6-20. This analysis uses a reduced run matrix relative to the previous AORs. Evaluations of a full tank with hatchway section A-A (runs 1-3 as listed in Table 6-20) show that the lower bound soil configuration tends to govern. Based on the limited sensitivity of the seismic demands for other configurations with lower bound soil (runs 4 & 5 as listed in Table 6-20), the corresponding best estimate and upper bound soil configurations need not be run as the lower bound soil configuration will continue to govern. Furthermore, the low Type I demand/capacity ratios calculated in Johnson et al. (2014a) provide assurance that the sensitivity of the structural integrity to seismic demands is low. Thus, a reduced run matrix with a single representative base case (highlighted in Table 6-21) is sufficient for the evaluation of the Type I SSTs.

Table 6-20. Seismic Model Run Matrix

Run	Soil	Backfill	Time series	Tank Concrete	Waste	Hatchway [1]	At-rest [2]
1	LBS	LB	LBS H + V	FCC	Full stiff (HSS)	Section A-A	Wall
2	BES	BE	BES H + V	FCC	Full stiff (HSS)	Section A-A	Wall
3	UBS	UB	UBS H + V	FCC	Full stiff (HSS)	Section A-A	Wall
4	LBS	LB	LBS H + V	FCC	Full stiff (HSS)	Section B-B	Wall
5	LBS	LB	LBS H + V	FCC	Empty	Section A-A	Wall

H + V = Horizontal + Vertical seismic input
FCC = Fully Cracked concrete.
HSS = High Shear Strength for waste properties.
[1] Refer to Section 6.1 for orientation of hatchway sections
[2] At-rest soil pressure calibration location (see Section 6.2.4)

The tank seismic-only demands from the above seismic runs are presented in Section 8.0 of this report. Based on the overall similarity/insensitivity in the seismic-only demands, demand/capacity ratios (see Johnson et al. 2014a) are only calculated for the governing case of run 1. An additional seismic model configuration is also run to further examine the effect of a 42 in. diameter manhole penetration in the tank roof (see Figure 6-5). Results for the additional penetration run are presented in Appendix A of this report.

6.7.2 Results Extraction

The following data are recorded for the gravity and transient analyses.

• Nodes	Displacements at all locations
• Reactions	None applicable
• Concrete Tank	Element results
• Tank-Soil Contacts	Element results
• Tank-Waste Contacts	None
• Excavated Backfill Soil	Element results (overburden only)
• Native Soil	None
• Hatchway	None
• Waste	None

The following results have been extracted from the analyses.

• Nodes	Displacements and accelerations (see Section 7.9)
• Concrete Tank Elements	Element Forces and Moments (see Section 8.0)

A detailed description of the post-processing methods is found in Section 6.6.

7.0 Soil Column Properties, Base Motion Inputs, and Spectral Matching

7.1 Introduction

The previous chapters described the ANSYS® tank model in detail, but it did not describe the details of the soil columns used for the analysis, the input motions used for the analysis, or the spectral matching performed to confirm that the input motions to the model produced the appropriate free-field responses in the model. The purpose of this chapter is to summarize the SSI profile properties that were developed in the AMEC Geomatrix report in Appendix R of Rinker et al. (2011a), describe the process for developing the input motions to the ANSYS® SSI model, characterize the dynamic SHAKE and ANSYS® soil columns, characterize the dynamic response of the soil in the full ANSYS® SSI model, and perform spectral matching to ensure that the ANSYS® SSI model reproduces an appropriate free-field response.

Three soil columns and their associated properties were defined in the subject AMEC Geomatrix report. The three columns are necessary to address the uncertainty of the soil properties in the SSI analysis. The three soil columns are referred to as the lower bound (LB), best estimate (BE), and upper bound (UB) columns. Each column has a different depth and different dynamic properties. As stated in the subject AMEC Geomatrix report, normally the range in SSI properties is intended to cover the uncertainty in properties at a single site. In this case, that range of properties has been extended to cover the uncertainty in properties and column depths over a broader geographical area represented by the Hanford SST sites.

7.2 SHAKE Soil Column Descriptions

A single set of LB, BE, and UB SSI profiles is specified for analysis of the Hanford SST sites. The LB profile is taken to be the 200 East LB profile because it has lower shear wave velocities and greater depth to a major velocity contrast. The BE profile is chosen to be the 200 West BE profile because it produces higher relative displacements than the 200 East BE profile, representing the larger relative displacements computed for the 200 West LB profile. The UB profile is chosen to be the 200 West UB profile because it clearly represents the stiffest and shallowest soil profile among the SST sites. The SSI profile geometry for each of the soil types is shown in Table 7-1.

Table 6-10 through Table 6-12 in Section 6.3.3 list the final set of LB, BE, and UB SSI profiles used in the SHAKE evaluations. Included in these tables are values of compression wave speeds (V_P) and Poisson's ratio. The compression wave speeds are calculated based on results presented in Rohay and Brouns (2007) with imposition of a minimum Poisson's ratio of 0.19 based on minimum value reported in Shannon and Wilson (2000). Figures 4.9a and 4.9b in the subject AMEC Geomatrix report show the three shear wave velocity profiles.

The base of the SSI profiles is placed in accordance with ASCE (2000) such that the shear wave velocity at the base is greater than or equal to 3,500 ft/s, or else the base is at least three times the maximum foundation dimension below the foundation (approximately 285 ft). The depth of the LB SSI profile is set at 405 ft, with a corresponding shear wave velocity of over 4,000 ft/s, which meets both of

the criteria above. The depth of the BE profile is set at 303 ft, with a corresponding shear wave velocity of 3,350 ft/s, which meets the second criterion above. The depth of the UB profile is set at 123 ft. with a corresponding shear wave velocity of 4,552 ft/s, which meets the first criterion above. In the cases of the LB and UB profiles, the base of the SSI profile corresponds with the first large velocity contrast encountered (e.g., basalt).

Table 7-1. SSI Soil Profile Geometry

Soil Type	Extending Depth	Number of Layers
Lower bound	405 ft	49
Best estimate	303 ft	44
Upper bound	123 ft	38

7.3 Characterization of the SHAKE Soil Columns

7.3.1 Amplification Factors for Three Soil Profiles – Horizontal Motion

SHAKE91 (Idriss and Sun 1992) inputs for the three soil profiles include the soil properties and the final horizontal time histories to compute the amplification of ground motion through the soil column. The amplitude curves show the natural frequencies of the soil column. The following figures show the amplification factors at the surface and the Type II, III, and IV tank foundation levels, which are -41ft. (E1), -49 ft. (E2) and -57 ft. (E3).

Figure 7-1 shows the amplification factors for the full LB soil column computed from SHAKE91. Figure 7-2 shows the amplification factors for the full BE soil column computed with SHAKE91. The natural frequencies of the full soil column are seen at the amplitude peaks. Figure 7-3 shows the amplification factors computed by SHAKE91 for the full UB soil column.

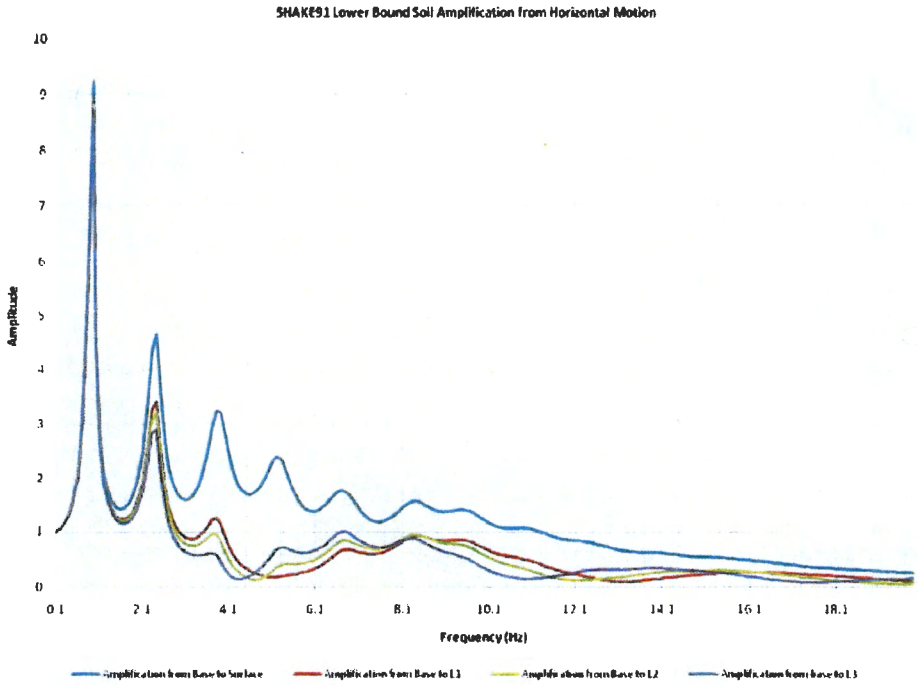

Figure 7-1. SHAKE91 Lower Bound Amplification Factors from Horizontal Input Motion

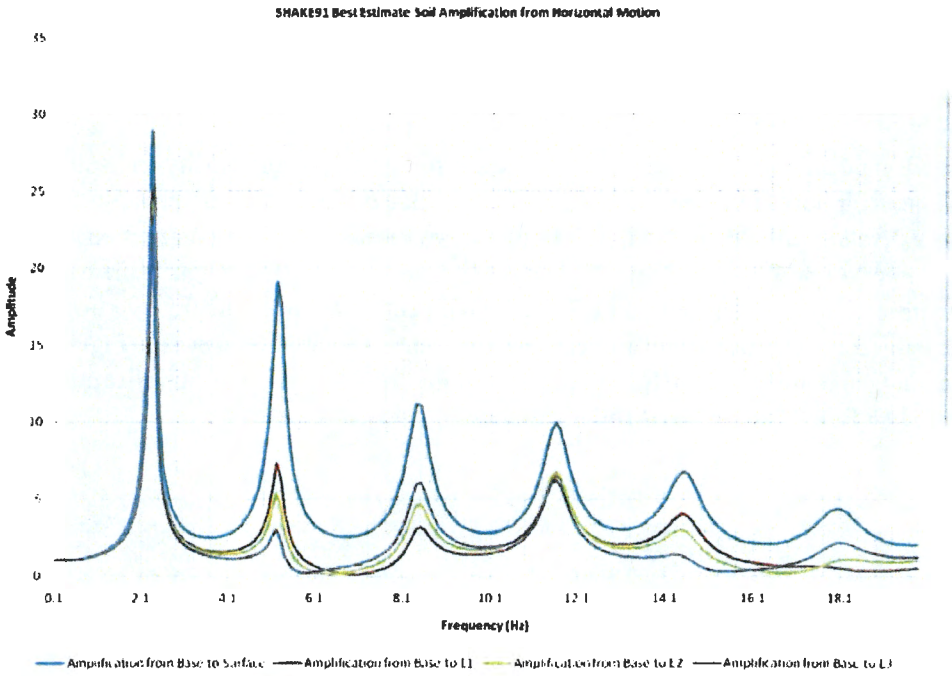

Figure 7-2. SHAKE91 Best Estimate Amplification Factors from Horizontal Input Motion

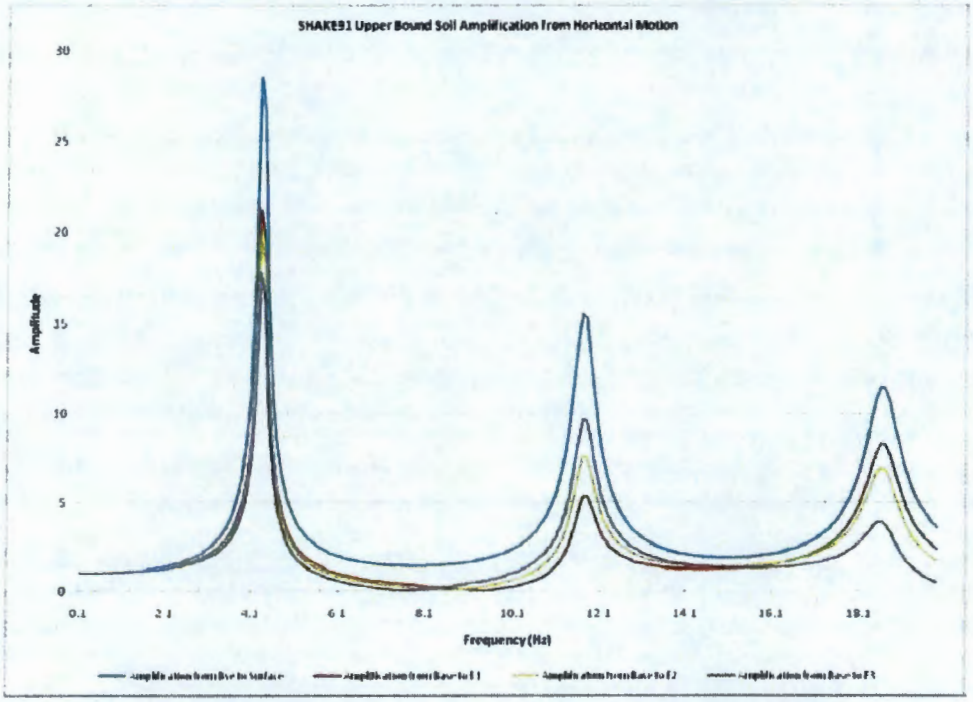

Figure 7-3. SHAKE91 Upper Bound Amplification Factors from Horizontal Input Motion

7.3.2 Amplification Factors for Three Soil Profiles – Vertical Motion

The subsurface horizontal time histories cannot be directly used to represent vertical seismic motion because the vertical control motion is different than the horizontal control motion.

The SHAKE inputs for vertical spectra use the same soil layering, soil density and soil damping as the SHAKE inputs for horizontal spectra. The soil layer velocities are different, namely, compression wave speeds (V_p) values are used instead of the shear wave speeds (V_s). The compression wave speeds values for the three soil profiles are shown in Section 6.3.3 as Table 6-10 through Table 6-12. Figure 7-4 shows the amplification factors for the full LB soil column computed from the final vertical time series. The fundamental frequencies of the full soil column are seen at the amplitude peaks. Figure 7-5 shows the amplification factors for the full BE soil column and Figure 7-6 shows the amplification factors computed by SHAKE91 for the full UB soil column.

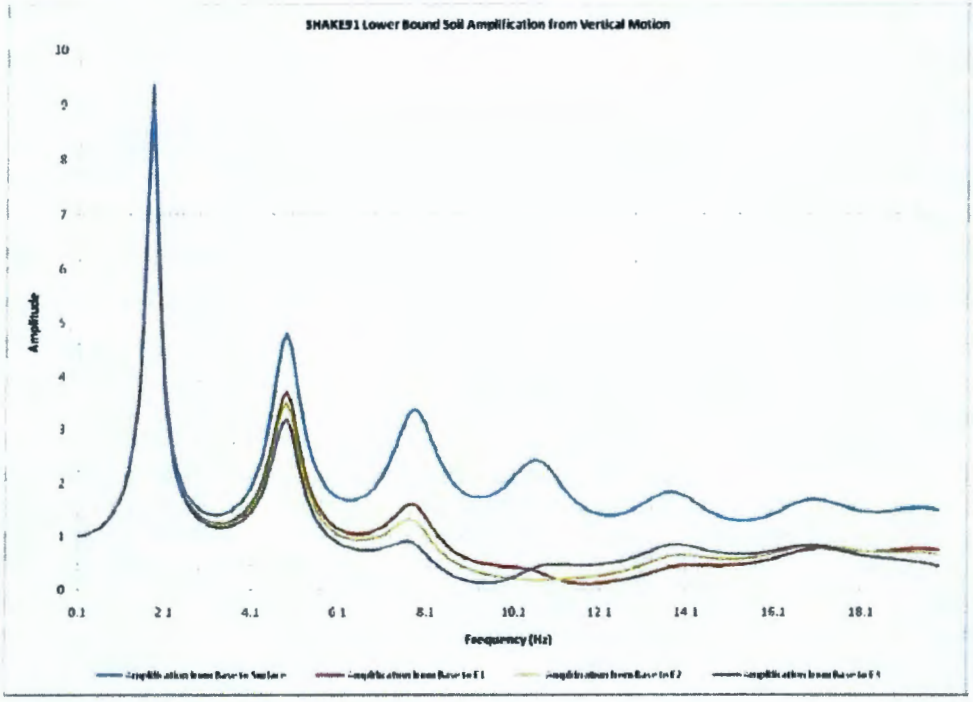

Figure 7-4. SHAKE91 Lower Bound Amplification Factors from Vertical Input Motion

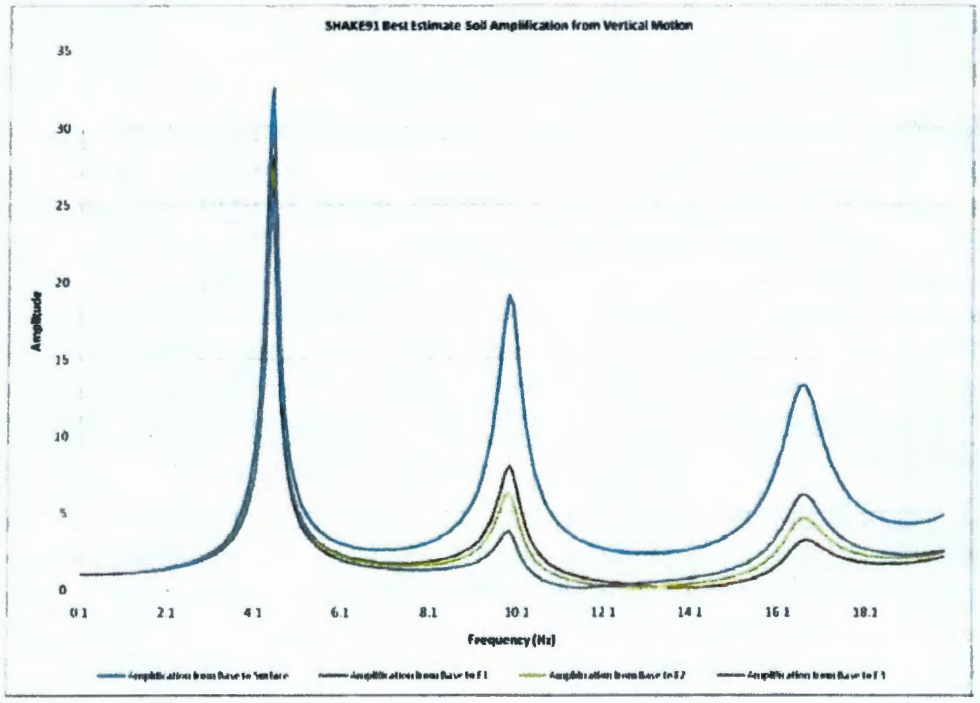

Figure 7-5. SHAKE91 Best Estimate Amplification Factors from Vertical Input Motion

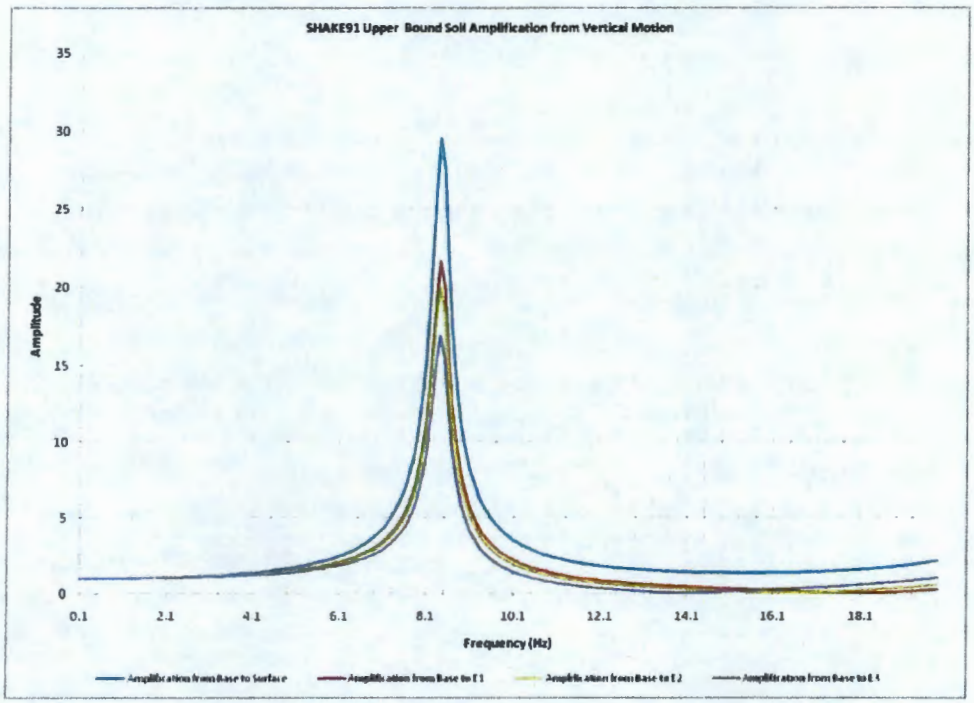

Figure 7-6. SHAKE91 Upper Bound Amplification Factors from Vertical Input Motion

7.4 Development of Time Histories at the Base of the SSI Profiles to be Used as Input to ANSYS® SSI Models

The ANSYS® SSI models require that acceleration time histories be provided as input at the base of the SSI profiles. The time histories were developed in a consistent manner following the guidance presented in Section 3.2.3 of NEI (2009). A more complete description of this process appears in the AMEC Geomatrix report in Appendix R of Rinker et al. (2011a). The first step is to develop soil column outcrop response (SCOR) based foundation input response spectra (FIRS) corresponding to the foundation depths of the various SST types. Acceleration time histories are then spectrally matched for these FIRS. The spectrally matched acceleration time histories are then input into the SSI profiles to compute in-column motions at the three foundation depths and at the base of the SSI profiles using SHAKE. The above steps are performed by AMEC Geomatrix and documented in the AMEC Geomatrix report (Appendix R of Rinker et al. 2011a).

The resulting base motions are then used to compute tank foundation level and surface motions in the ANSYS® SSI models. The computed foundation level and surface motions are compared to the tank foundation level and surface-level targets to ensure that the SSI model is producing adequate levels of ground shaking. Because pseudo-outcrop motions are not available from ANSYS®, the tank foundation-level target is the in-column motion from SHAKE that is consistent with the time series that is spectrally matched to the FIRS at the corresponding elevation.

More explicitly, the procedure for developing the time histories to be used as input to the SSI models consists of the following steps:

1. Specification of design surface spectra.
2. Specification of dynamic properties of the three soil profiles. These are defined in terms of the LB, BE, and UB SSI profiles.

Development of input time histories for the ANSYS® SSI models.

3a. From the site response analyses conducted to develop the soil properties, obtain pseudo-outcrop motions at the tank foundation levels.

3b. Construct FIRS at the tank foundation levels using the results of Step 3a.

3c. Create time histories that are spectrally matched to FIRS at the tank foundation levels.

3d. Deconvolve the tank foundation-level inputs from Step 3c to the base of the SSI profiles using SHAKE, and then extract as in-column motions at the base.

3e. Apply the in-column motions from Step 3d as input to the ANSYS® SSI full models.

3f. Verify that these tank foundation-level spectra and surface spectra from the ANSYS® models meet appropriate matching criteria.

3g. Adjust the time histories as necessary to meet the matching criteria. The outcome of this step is a specific set of input time histories to be used for a specific SSI profile; that is, one set for the LB profile, one set for the BE profile, and one set for the UB profile.

Steps 1, 2, 3a through 3d are documented in the subject AMEC Geomatrix report. Step 3e is performed as part of this evaluation, and steps 3f and 3g are performed jointly by AMEC Geomatrix and Becht and are documented here and in the subject AMEC Geomatrix report.

7.5 Generation of Target Spectra Using SHAKE

Target spectra are produced in SHAKE and are the benchmark for determining if the free-field response in the ANSYS® model is correct. The surface target spectrum for the ANSYS® SSI model is simply the PC-2 surface spectrum documented in the AMEC Geomatrix report in Appendix R of Rinker et al. (2011a). This spectrum is referred to as the surface design response spectra (DRS) and is equal to two-thirds of the site-specific maximum considered earthquake (MCE). The surface spectrum is the same for the LB, BE, and UB profiles.

The initial foundation-level target spectra are probabilistically developed FIRS for each of the three soil columns. A bounding FIRS is defined for each soil column that is the upper bound of the E1, E2, and E3 level FIRS. As mentioned above, pseudo-outcrop motions are not available from ANSYS®, so the actual foundation-level targets used for spectral matching between ANSYS® and SHAKE are the in-column spectra from SHAKE that are consistent with the time series that is spectrally matched to the FIRS at the corresponding elevation.

Figure 7-7 through Figure 7-12 show the target spectra for all three soil profiles as a result of the horizontal and vertical input base motion.

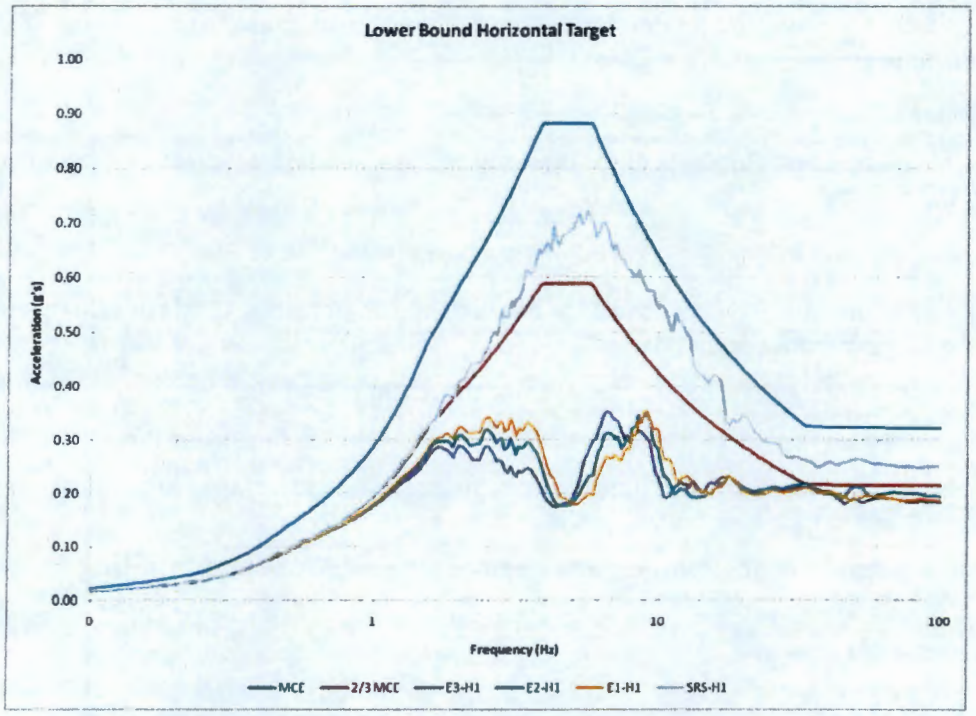

Figure 7-7. Lower Bound Horizontal Target Spectra

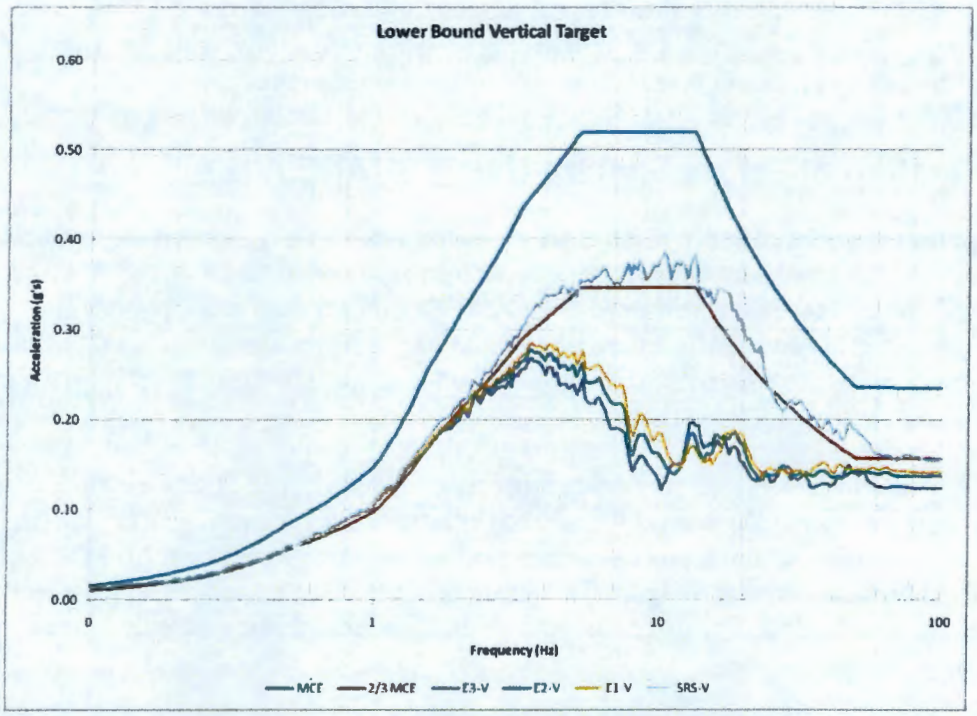

Figure 7-8. Lower Bound Vertical Target Spectra

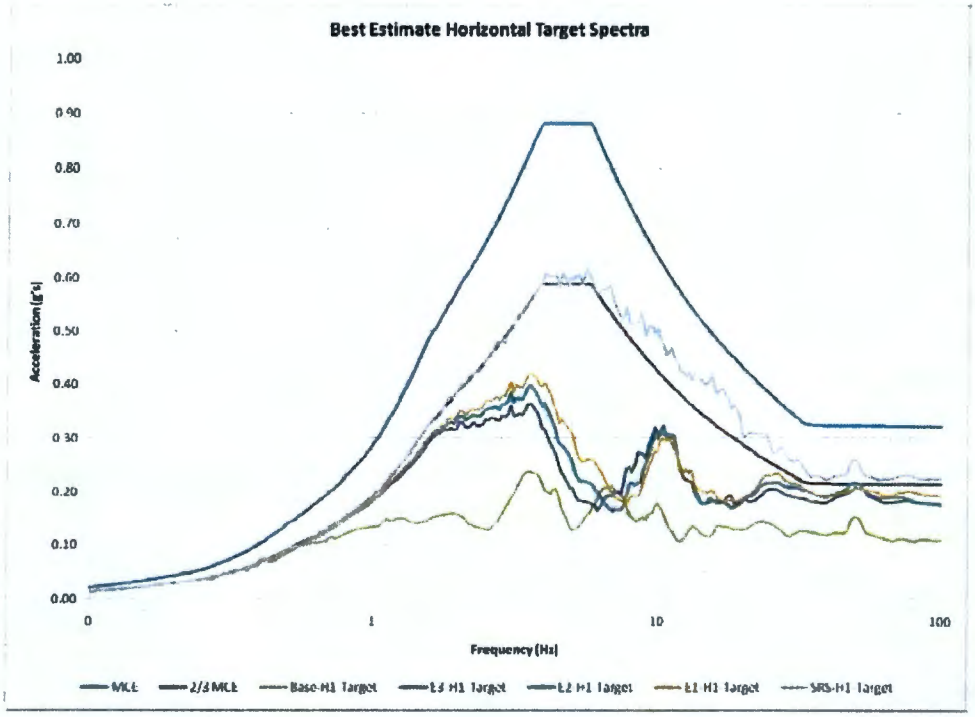

Figure 7-9. Best Estimate Horizontal Target Spectra

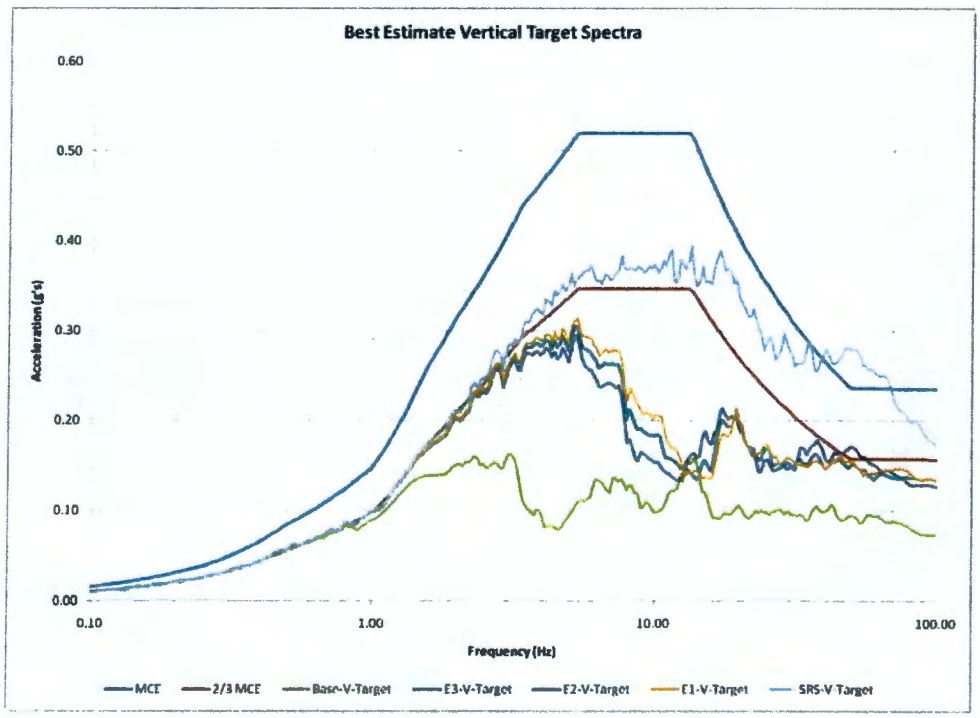

Figure 7-10. Best Estimate Vertical Target Spectra

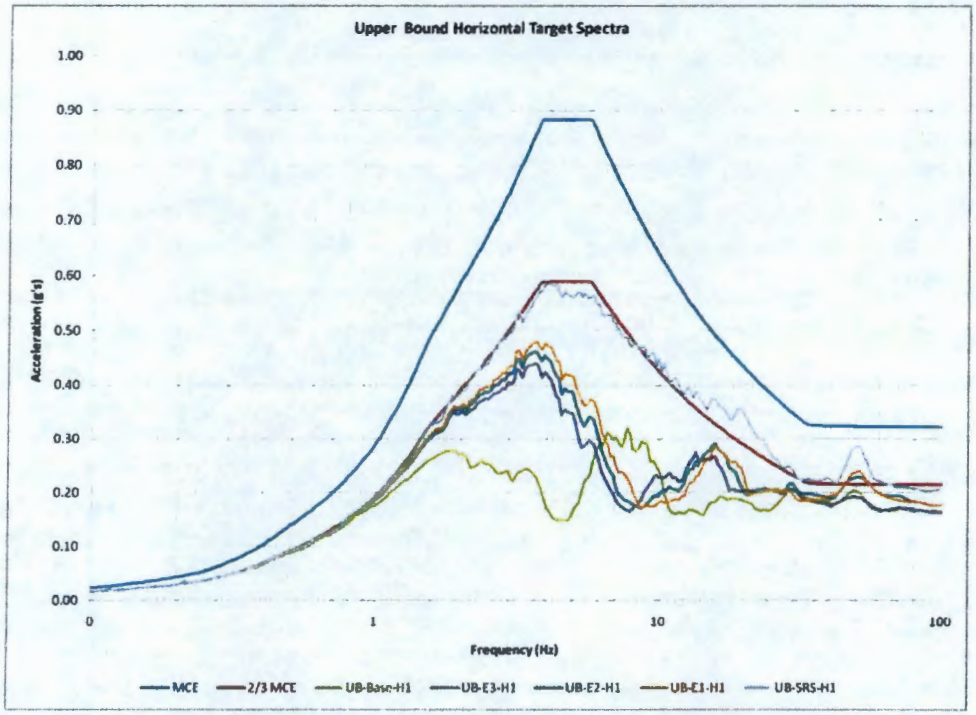

Figure 7-11. Upper Bound Horizontal Target Spectra

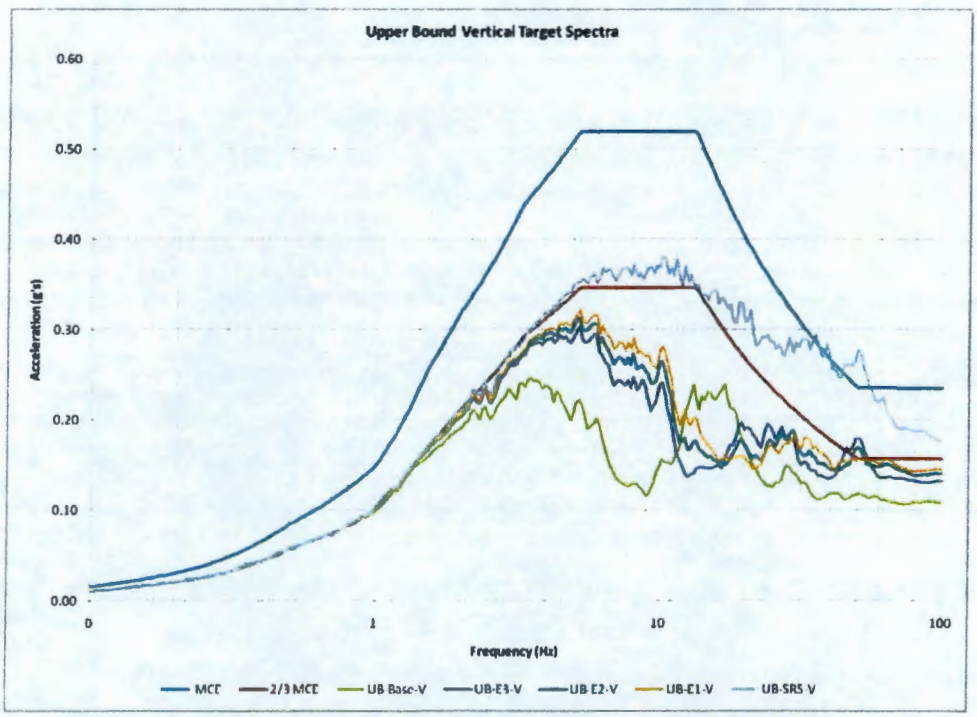

Figure 7-12. Upper Bound Vertical Target Spectra

The target spectra provided in Appendix R of Rinker at .al. (2011a) were at elevations of -57 ft. (E3), -49 ft. (E2), and -43 ft. (E1), corresponding to the foundation elevations of the Type IV, Type III, and Type II tanks, respectively. Target spectra were not provided at the foundation elevation of the Type I tanks, which is 37 ft. below grade. However, because the soil properties are roughly linear within tank foundation elevations, a new Type I target spectra was extrapolated from the existing targets. To be consistent with the existing labeling scheme, the Type I foundation elevation target spectra is designated "E0". To demonstrate the effectiveness of the extrapolation method, the lower bound target spectra are compared in Figure 7-13 and Figure 7-14. As expected, the E0 target (shown in black) continues the trend of the other tank foundation elevation targets (shown increasingly darker toward surface).

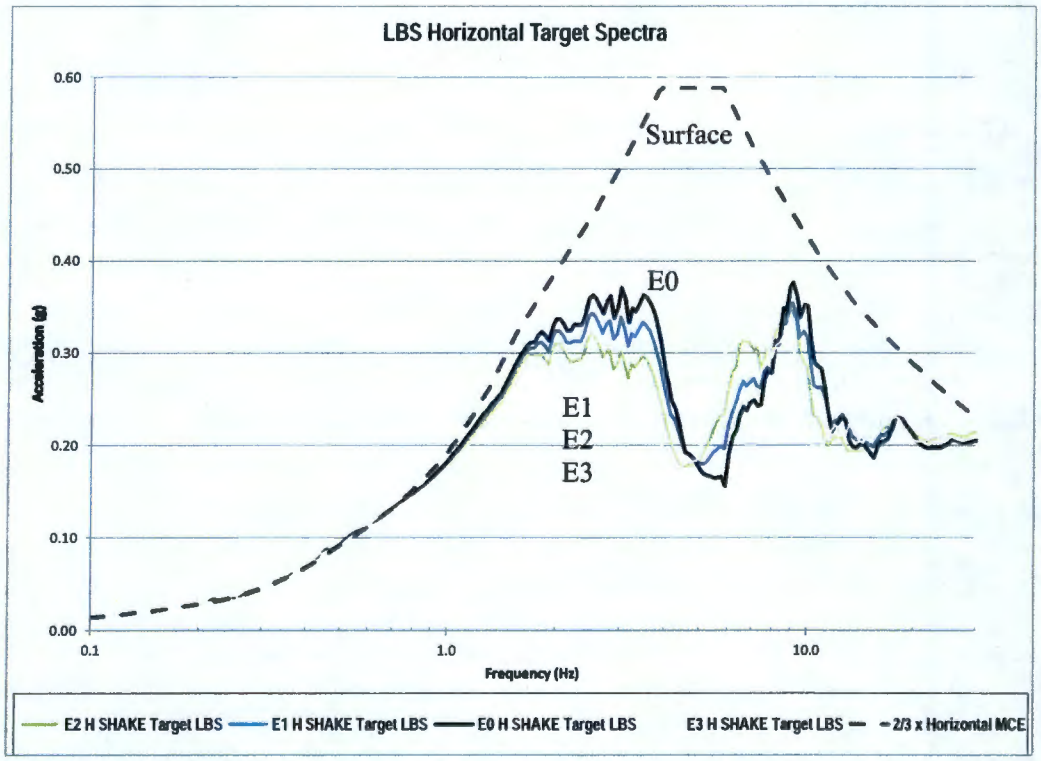

Figure 7-13. Lower Bound Horizontal Target Spectra at SST Foundation Elevations, with Extrapolated E0

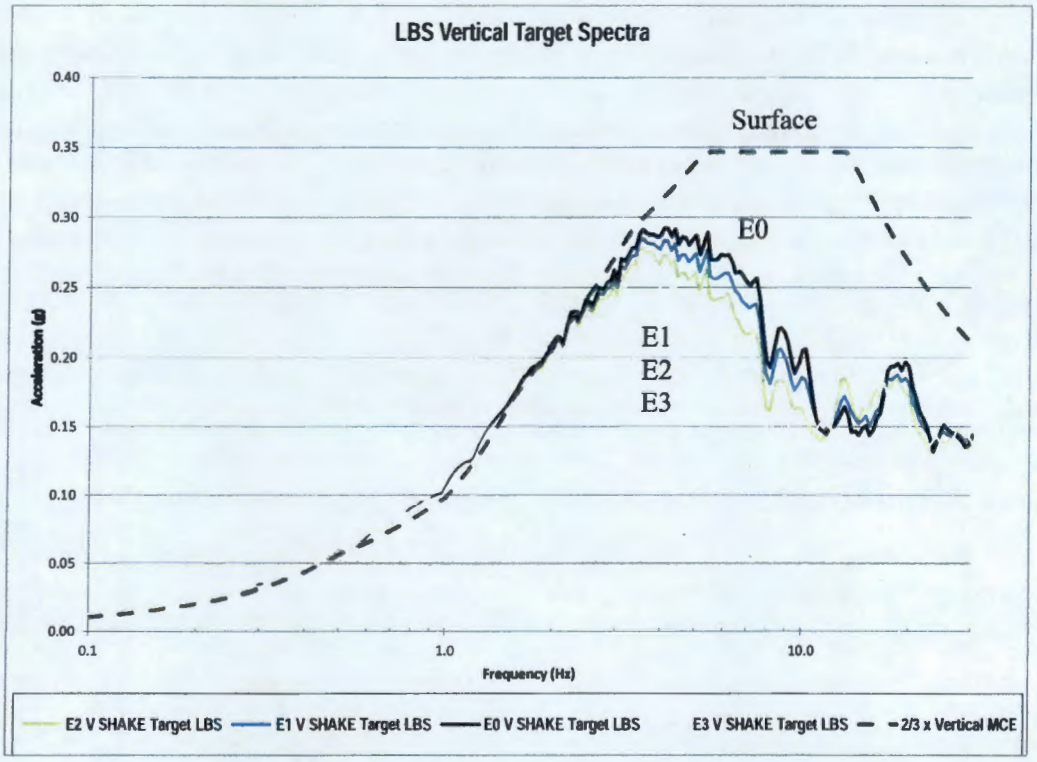

Figure 7-14. Lower Bound Vertical Target Spectra at SST Foundation Elevations, with Extrapolated E0

7.6 Description of the ANSYS® Soil Column Models

As stated in the introduction to this chapter, it is necessary to perform spectral matching between the ANSYS® SSI models and the SHAKE models to determine if the free-field response is adequately reproduced in the ANSYS® models. As an intermediate step, simplified soil column models are generated in ANSYS®, the appropriate dynamic properties are assigned, the Rayleigh damping parameters are established, and spectral matching is checked. This step serves the purpose of establishing damping parameters and spectral matching in simpler models than the full ANSYS® SSI models. This saves time while demonstrating that ANSYS® can adequately reproduce the target free-field response. The final spectral matching with the full SSI model is then performed as a confirmatory step.

The ANSYS® column is 40 ft. wide by 10 ft. wide and has the depth of the individual soil profile being considered (LB, BE, or UB). The individual soil column depths are listed in Table 7-1. The soil column models have four elements across the width and one element through the lateral thickness. The ANSYS® soil column model uses ANSYS® SOLID45 elements for the soil and incorporates strain compatible elastic properties for the soil. The ANSYS® soil column model is shown in Figure 7-15.

Solid elements are used to model the soil layers, where each layer is assigned unique soil properties including the elastic modulus, the density, Poisson's ratio and soil layer damping known as beta damping. The elastic modulus for each layer is calculated from the strain compatible shear modulus using the relationship shown in Section 7.6.4. The shear wave speeds, densities, and Poisson's ratios are given

from the SHAKE models described in Section 7.2. The elastic (extensional) modulus (E) is determined from the elastic relations shown below.

Shear Modulus: $$G = \rho \cdot V_S^2 \quad (7.1)$$

Modulus of Elasticity: $$E = 2G(1+\upsilon) \quad (7.2)$$

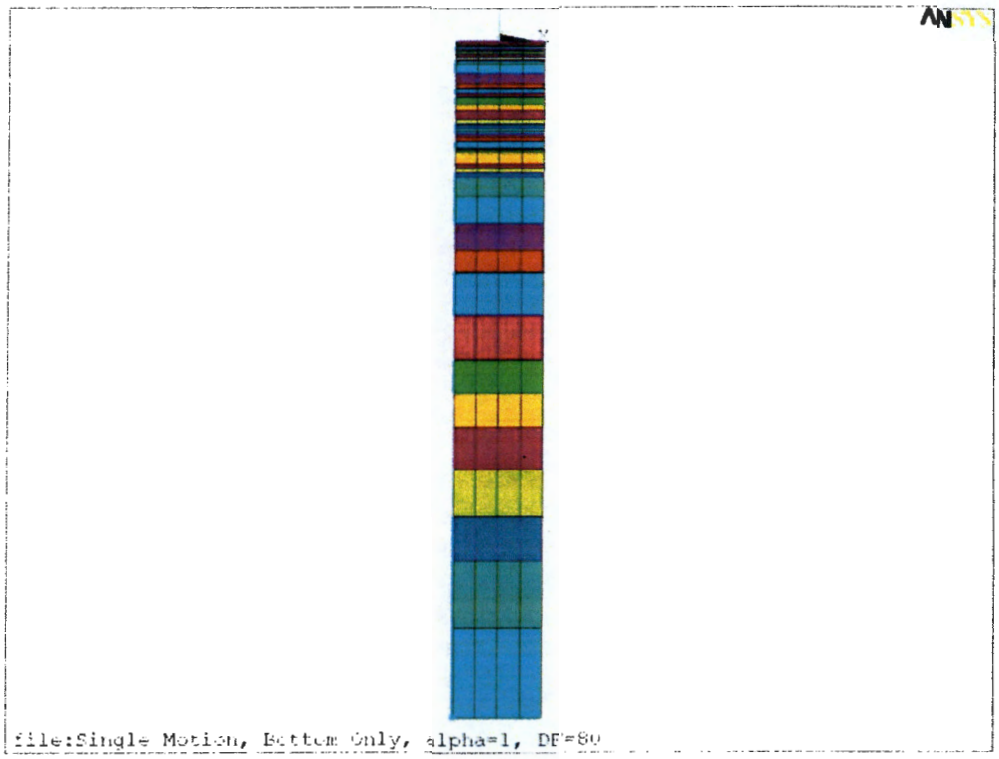

Figure 7-15. Elevation View of Typical ANSYS® Soil Column Model

7.6.1 Element Geometry and Layer Thickness

For a finite element model to effectively represent seismic wave propagation, the resolution of the mesh must be sufficient to transmit the highest frequency of interest.

The relationship between element size and cutoff frequencies for LB, BE, and UB soil profiles are shown in Table 7-2 through Table 7-4, respectively. In addition to the element vertical thicknesses used in the model, the tables display the maximum element vertical thicknesses consistent with having five, eight, or ten elements per wavelength based on a cutoff frequency of 25 Hz. The SSI profile layering is documented in the AMEC Geomatrix report in Appendix R of Rinker et al. (2011a). However, in the ANSYS® model, some layers are subdivided in order to be consistent with the above considerations to obtain maximum passing frequencies and in a few cases layers are merged for convenience. The tables show the actual layer thickness and the subdivided layer thickness in the last two columns.

The LB soil column spectra at the surface and tank foundation did not consistently match with the target spectra despite adjustments of damping parameters and time histories. Several layer thicknesses exceeded 10 feet, the maximum element thickness consistent with the 1/5th wavelength guideline. Layers 35–49 have soil layers that are greater than 10 feet thick and these layers are subdivided so that there are ten elements per wavelength at the 25 Hz cutoff frequency. In addition, Layers 33–34 that are adjacent to Layer 35 are also subdivided.

Table 7-2. Maximum Allowable Element Sizes for Lower Bound Soil

Layer Number	Vs (ft/sec)	Vp (ft/sec)	Cutoff Wave Length (ft)	Maximum Allowable Element Thickness (ft)			Actual Element Thickness (ft)	Mesh Refinements Thickness (ft)
				1/5th Wave Length	1/8th Wave Length	1/10th Wave Length		
1	438	1047	18	4	2	2	1	1.0
2	438	1047	18	4	2	2	1	1.0
3	438	1047	18	4	2	2	1	1.0
4	438	1047	18	4	2	2	1	1.0
5	438	1047	18	4	2	2	1	1.0
6	540	1047	22	4	3	2	1	1.0
7	540	1047	22	4	3	2	1	1.0
8	540	1047	22	4	3	2	1	1.0
9	540	1047	22	4	3	2	1	1.0
10	680	1099	27	5	3	3	1	1.0
11	680	1099	27	5	3	3	4	4.0
12	787	2027	31	6	4	3	5	5.0
13	815	2027	33	7	4	3	2	2.0
14	860	2027	34	7	4	3	2	2.0
15	860	2027	34	7	4	3	2	2.0
16	860	2027	34	7	4	3	3	3.0
17	900	2313	36	7	5	4	3	3.0
18	970	2313	39	8	5	4	4	4.0
19	970	2313	39	8	5	4	2	2.0
20	970	2313	39	8	5	4	2	2.0
21	1047	2313	42	8	5	4	1	1.0
22	1047	2313	42	8	5	4	1	1.0
23	1089	2313	44	9	5	4	1	1.0
24	1089	2313	44	9	5	4	1	1.0
25	1089	2313	44	9	5	4	2	2.0
26	1089	2313	44	9	5	4	3	3.0
27	1089	2313	44	9	5	4	1	1.0
28	1089	2313	44	9	5	4	1	1.0
29	1089	2313	44	9	5	4	4	4.0
30	1190	2313	48	10	6	5	1	1.0
31	1190	2313	48	10	6	5	2	2.0
32	1190	2313	48	10	6	5	2	2.0

Table 7-2. (contd)

Layer Number	Vs (ft/sec)	Vp (ft/sec)	Cutoff Wave Length (ft)	Maximum Allowable Element Thickness (ft)			Actual Element Thickness (ft)	Mesh Refinements Thickness (ft)
				1/5th Wave Length	1/8th Wave Length	1/10th Wave Length		
33	1210	2313	48	10	6	5	4	2 elements 2.0-ft
34	1210	2313	48	10	6	5	8	3 elements 2.67-ft
35	1210	2313.	48	10	6	5	11	3 elements 3.67-ft
36	1210	2313	48	10	6	5	12	3 elements 4.0-ft
37	1210	2313	48	10	6	5	26	5 elements 5.20-ft
38	1210	2313	48	10	6	5	40	5 elements 8.0-ft
39	1149	2313	46	9	6	5	45	5 elements 9.0-ft
40	1210	2313	48	10	6	5	10	2 elements 5.0-ft
41	1210	2313	48	10	6	5	10	2 elements 5.0 ft
42	1210	2313	48	10	6	5	10	2 elements 5.0 ft
43	1210	2313	48	10	6	5	50	5 elements 10.0-ft
44	1560	3470	62	12	8	6	10	2 elements 5.0-ft
45	1560	3470	62	12	8	6	20	3 elements 6.67-ft
46	1560	3470	62	12	8	6	20	3 elements 6.67-ft
47	1400	3470	56	11	7	6	20	3 elements 6.67-ft
48	1580	3470	63	13	8	6	25	4 elements 6.25-ft
49	1580	3470	63	13	8	6	25	4 elements 6.25-ft
		Mode Value			10	6	5	-

A sensitivity analysis is performed for the BE soil column because Layers 32–44 have thicknesses that exceed the 1/5th wavelength guideline. The results showed slightly higher accelerations at peak acceleration points and slightly lower accelerations than the lowest acceleration points. It is concluded that mesh refinements did not improve spectral matching between the SHAKE and the ANSYS® soil column model. Therefore, no further mesh adjustments are implemented.

Table 7-3. Maximum Allowable Element Sizes for Best Estimate Soil

Layer Number	Vs (ft/sec)	Vp (ft/sec)	Cut-off Wave Length (ft)	Maximum Allowable Element Thickness (ft)			Actual Element Thickness (ft)
				1/5th Wave Length	1/8th Wave Length	1/10th Wave Length	
1	710	1283	28	6	4	3	1.0
2	710	1283	28	6	4	3	1.0
3	710	1283	28	6	4	3	1.0
4	720	1283	29	6	4	3	1.0
5	720	1283	29	6	4	3	1.0
6	720	1283	29	6	4	3	1.0
7	775	1283	31	6	4	3	1.0
8	775	1283	31	6	4	3	1.0
9	775	1283	31	6	4	3	1.0
10	987	1595	39	8	5	4	1.0
11	987	1595	39	8	5	4	4.0
12	1086	1755	43	9	5	4	5.0
13	1158	2483	46	9	6	5	2.0
14	1158	2483	46	9	6	5	2.0
15	1158	2483	46	9	6	5	2.0
16	1158	2483	46	9	6	5	3.0
17	1280	2833	51	10	6	5	3.0
18	1280	2833	51	10	6	5	4.0
19	1280	2833	51	10	6	5	2.0
20	1280	2833	51	10	6	5	2.0
21	1344	2833	54	11	7	5	1.0
22	1344	2833	54	11	7	5	1.0
23	1383	2833	55	11	7	6	2.0
24	1383	2833	55	11	7	6	2.0
25	1416	2833.	57	11	7	6	3.0
26	1526	2833	61	12	8	6	1.0
27	1526	2833	61	12	8	6	1.0
28	1526	2833	61	12	8	6	5.0
29	1526	2833	61	12	8	6	2.0
30	1526	2833	61	12	8	6	2.0
31	1526	2833	61	12	8	6	3.0
32	1526	2833	61	12	8	6	8.0
33	1526	2833	61	12	8	6	12.0
34	1526	2833	61	12	8	6	12.0
35	1780	2877	71	14	9	7	10.0
36	1780	4816	71	14	9	7	19.0
37	2424	4816	97	19	12	10	20.0
38	2638	4816	106	21	13	11	15.0
39	2638	4935	106	21	13	11	15.0
40	2638	4935	106	21	13	11	19.0
41	2638	4935	106	21	13	11	21.0
42	3350	6267	134	27	17	13	20.0
43	3350	6267	134	27	17	13	30.0
44	3350	6267	134	27	17	13	40.0
Mode Value				12	8	6	--

Table 7-4. Maximum Allowable Element Sizes for Upper Bound Soil

Layer Number	Vs (ft/sec)	Vp (ft/sec)	Cutoff Wave Length (ft)	Maximum Allowable Element Thickness (ft)			Actual Element Thickness (ft)
				1/5th Wave Length	1/8th Wave Length	1/10th Wave Length	
1	1089	1760	44	9	5	4	1.0
2	1089	1760	44	9	5	4	1.0
3	1089	1760	44	9	5	4	1.0
4	1089	1760	44	9	5	4	1.0
5	1089	1760	44	9	5	4	1.0
6	1089	1760	44	9	5	4	1.0
7	1089	1760	44	9	5	4	1.0
8	1280	2069	51	10	6	5	1.0
9	1280	2069	51	10	6	5	1.0
10	1280	2069	51	10	6	5	1.0
11	1379	2229	55	11	7	6	4.0
12	1423	3041	57	11	7	6	5.0
13	1423	3041	57	11	7	6	2.0
14	1520	3041	61	12	8	6	2.0
15	1520	3041	61	12	8	6	2.0
16	1630	3041	65	13	8	7	3.0
17	1732	3041	69	14	9	7	3.0
18	1732	3469	69	14	9	7	4.0
19	1732	3469	69	14	9	7	2.0
20	1732	3469	69	14	9	7	2.0
21	1732	3469	69	14	9	7	1.0
22	1732	3469	69	14	9	7	1.0
23	1732	3469	69	14	9	7	2.0
24	1732	3469	69	14	9	7	2.0
25	1950	3469	78	16	10	8	3.0
26	1950	3469	78	16	10	8	1.0
27	1950	3469	78	16	10	8	1.0
28	1950	3469	78	16	10	8	5.0
29	1950	3469	78	16	10	8	2.0
30	1950	3469	78	16	10	8	2.0
31	1950	3469	78	16	10	8	3.0
32	1950	3469	78	16	10	8	8.0
33	1950	3469	78	16	10	8	12.0
34	1950	3469	78	16	10	8	12.0
35	2351	5899	94	19	12	9	5.0
36	2351	5899	94	19	12	9	5.0
37	2351	5899	94	19	12	9	9.0
38	2351	5899	94	19	12	9	10.0
Mode Value				16	10	8	--

7.6.2 Boundary Conditions

Rinker et al. (2006) demonstrated that the best results were achieved when so-called "slaved" boundary conditions were applied. Accordingly, slaved boundary conditions are applied to the lateral boundaries of the ANSYS® SSI full model and the ANSYS® soil column models. At each elevation, the nodes on the exterior lateral faces (faces with ±x-direction normal) are coupled such that the horizontal (±x-direction) and vertical (±z-direction) displacements are the same at a given elevation. These

boundary conditions support the horizontal shear and vertical compression modes associated with vertically propagating shear and compression waves, but do not allow displacements that are not consistent with the soil behavior.

All nodes in the soil column models are constrained against out-of-plane (y-direction) motion. In the case of horizontal seismic input (±x-direction), the bottom of the models is fixed vertically. In the case of vertical seismic input (±z-direction), the base of the models is fixed in both horizontal directions, but is free vertically.

Consistent with Rinker et al. (2006), the boundary constraints of the soil column meet the ASCE-4 (2000) guidance on boundary conditions (Section C3.3.3.3): "*When vertically propagating waves are used, horizontal roller boundaries are used for shear waves, and vertical roller boundaries are specified for compression waves.*"

The nodes at each soil layer are coupled instead of fixing vertical displacements to allow for vertically propagating compression waves. The coupling includes horizontal displacements and allows for shear wave displacements. Therefore, coupling the exterior model nodes results in the same condition as given in ASCE-4 (2000), but allows both vertical and horizontal excitation of the model simultaneously. The boundary conditions of the ANSYS® soil column model are shown in Figure 7-16.

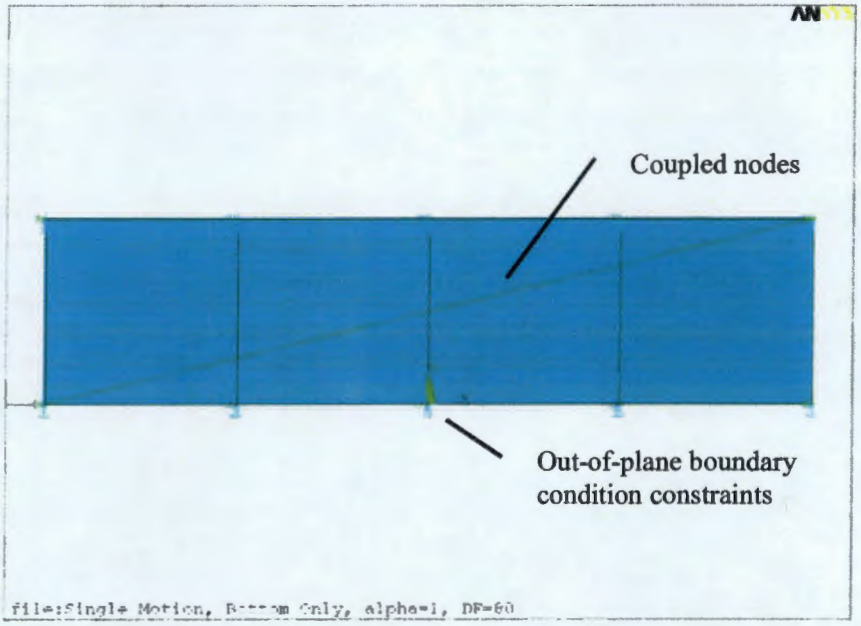

Figure 7-16. Top View of ANSYS® Soil Column Model Showing Boundary Conditions

7.6.3 Seismic Loading

The base excitation for the soil models is determined from the output acceleration time series from the SHAKE model at various elevations corresponding to the base of the soil column models for each soil type.

Acceleration time series input is applied to the ANSYS® model as a force time series at a large mass at the base of the model. The base mass is simulated with an ANSYS® MASS21 element having a mass approximately 1,000 times greater than the total mass of the tank and soil model, thus simulating seismic ground motion. The nodes at the bottom of the ANSYS® model are coupled together to form a rigid region effectively providing a single point force time series input to the soil column.

7.6.4 ANSYS® Soil Column Material Properties

The soil properties used in the ANSYS® models are linear elastic, isotropic properties. These properties are developed based on the linear elastic relationships and the strain-compatible shear and compression wave velocities. The strain-compatible dynamic soil properties used in the ANSYS® models are summarized in Table 6-10 through Table 6-12.

7.7 Calibration of ANSYS® Damping Parameters

The full time-integration algorithm for structural analysis in ANSYS® utilizes a Rayleigh damping formulation consisting of mass and stiffness proportional damping parameter coefficients α and β, respectively. In the ANSYS® soil column model, each soil layer is assigned a unique stiffness proportional (beta) damping coefficient value. Mass proportional (alpha) damping is also employed in the ANSYS® model, although the alpha damping parameter is limited to a global application in the model rather than on an element-by-element basis.

In this evaluation, the effects of changing both the alpha and beta terms are evaluated with respect to the ability to match the soil column behavior from SHAKE to ANSYS® computed spectra. A wide range of both alpha and beta terms were initially tested; however, only the final values are presented here.

Values for mass proportional (alpha) damping coefficient ranged from 0.3 to 2.0. After testing, an alpha damping coefficient value of 1.0 resulted in the best match for all three soil columns.

In contrast to mass proportional damping, which is applied globally to the model, stiffness proportional (beta) damping can be applied to specific materials, and therefore can be defined in an almost unlimited number of combinations. For simplicity, beta damping is varied uniformly across the model by using a single scaling factor on the damping values taken from SHAKE. Specifically, damping values output by SHAKE are assigned to each material layer in ANSYS® and then divided by the scaling factor (DF) to define the beta damping coefficient value for each layer.

For example, if the damping for the soil layer is 2.0% of critical damping, the material damping property applied in ANSYS® would be (0.02)/DF. Studies were run varying the DF value from 25 to 100. A DF value of 40 is the best match for the lower bound soil column. A DF value of 80 resulted in the best match for the best estimate and upper bound soil columns.

Varying alpha has a significant effect on lower frequencies, but does not significantly affect the composite damping over the full range of frequencies of interest (0–20 Hz). Varying the DF factor (and therefore beta damping coefficient) affects primarily the composite damping at higher frequencies. To evaluate the performance of the ANSYS® soil column model, response spectra are extracted at the soil surface and at the Type II, III, and IV tank foundation levels (-43-ft, -49-ft, and -57-ft).

Damping parameters alpha and DF are selected by matching response spectra between ANSYS® and SHAKE without explicitly considering a target frequency or target composite damping. However, it is informative to relate the selected parameters to the critical damping level as a function of frequency. The relationship between the mass proportional damping parameter alpha, the critical damping level, and frequency is straightforward since a single value of alpha is applied globally.

$$\xi_a = \frac{\alpha}{4\pi f} = \frac{1.0}{4\pi f} \tag{7.3}$$

The relationship between stiffness proportional damping and frequency is slightly more complicated because the stiffness proportional damping parameter DF depends on the frequency-independent damping from the SHAKE analysis. The stiffness proportional damping in ANSYS® is entered layer-by-layer by dividing the frequency independent critical damping ratio reported from SHAKE by the parameter DF. This results in layer-by-layer frequency dependent stiffness proportional damping in ANSYS®.

$$\xi_{\beta i} = \xi_{\beta i}(\xi_{SHAKEi}, f) \tag{7.4}$$

For a given frequency-independent critical damping ratio from SHAKE, the stiffness dependent critical damping ratio can be calculated as a function of frequency through the following equations:

$$\beta_i = \frac{\xi_{SHAKEi}}{DF} \tag{7.5}$$

and

$$\xi_{\beta i} = \pi \beta_i f = \pi \left(\frac{\xi_{SHAKEi}}{DF} \right) f \tag{7.6}$$

where DF equals 40 for the lower bound soil column and DF equals 80 for the best estimate and upper bound soil columns.

Figure 7-17 shows the percent critical damping as a function of frequency ranging from 0.1–20 Hz using an alpha value of 1.0. The mass proportional damping curve shown in Figure 7-17 is applicable to all soil profiles because the value of alpha coefficient does not change for any of the soil profiles. Figure 7-18 shows the stiffness proportional damping as a function of frequency for typical SHAKE damping values.

Figure 7-19 shows the composite Rayleigh damping for the LB soil profile. The fundamental frequency of the LBS column is shown as 0.9 Hz and the frequency of the fifth mode is 13.6 Hz. This frequency range establishes an important frequency range for quantifying the composite damping for the soil. Similarly, Figure 7-20 shows the composite Rayleigh damping for the BE soil profile. The fundamental frequency of the BE column is shown as 2.3 Hz and the frequency of the fifth mode is 14.4 Hz. Figure 7-21 shows the composite damping for the UB soil profile. In this case the fundamental mode is at 4.3 Hz and the third mode is at 18.7 Hz.

The important point in Figure 7-19, Figure 7-20, and Figure 7-21 is that in each case, the composite damping in the frequency range of interest is between the minimum and maximum damping specified in SHAKE. That is, the values of alpha and beta resulting from optimizing the spectral matching process correspond to physically realistic values for the critical damping in each of the soil columns in physically meaningful frequency ranges.

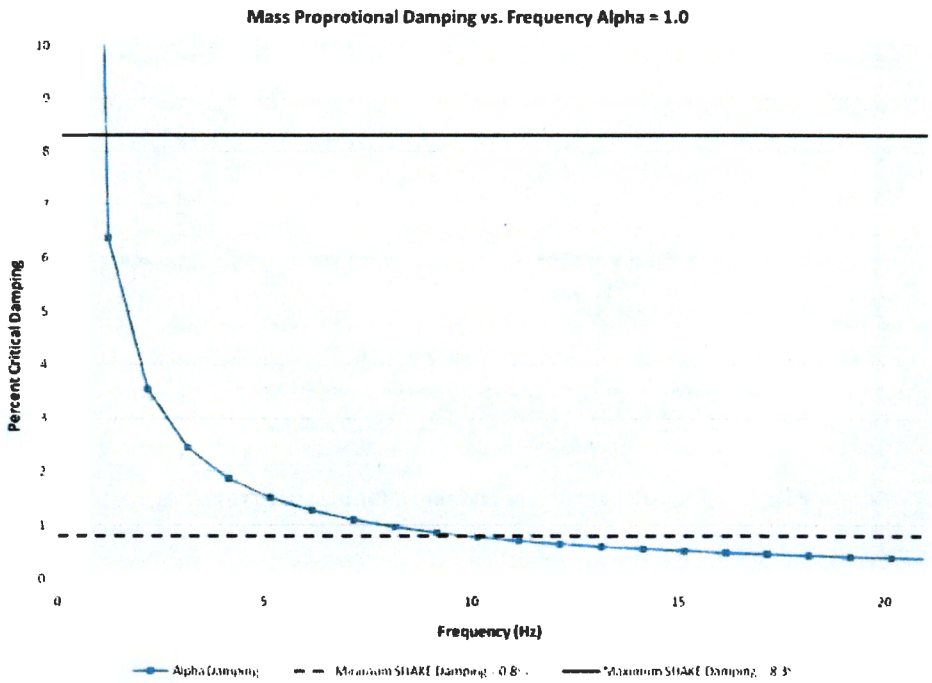

Figure 7-17. Mass Proportional Damping vs. Frequency for Alpha=1.0

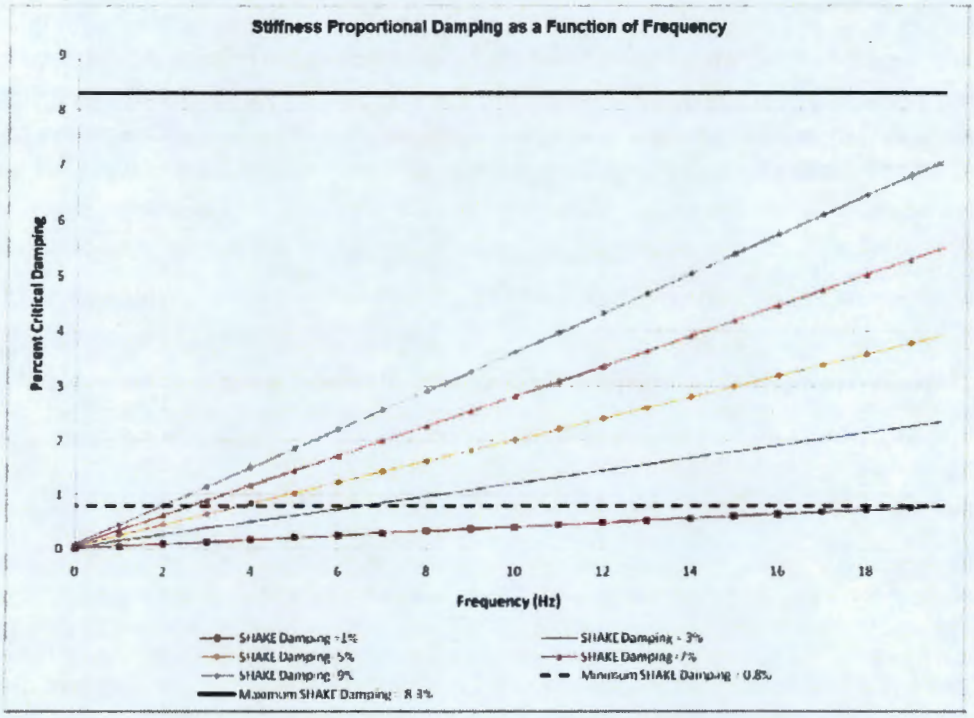

Figure 7-18. Stiffness Proportional Damping vs. Frequency

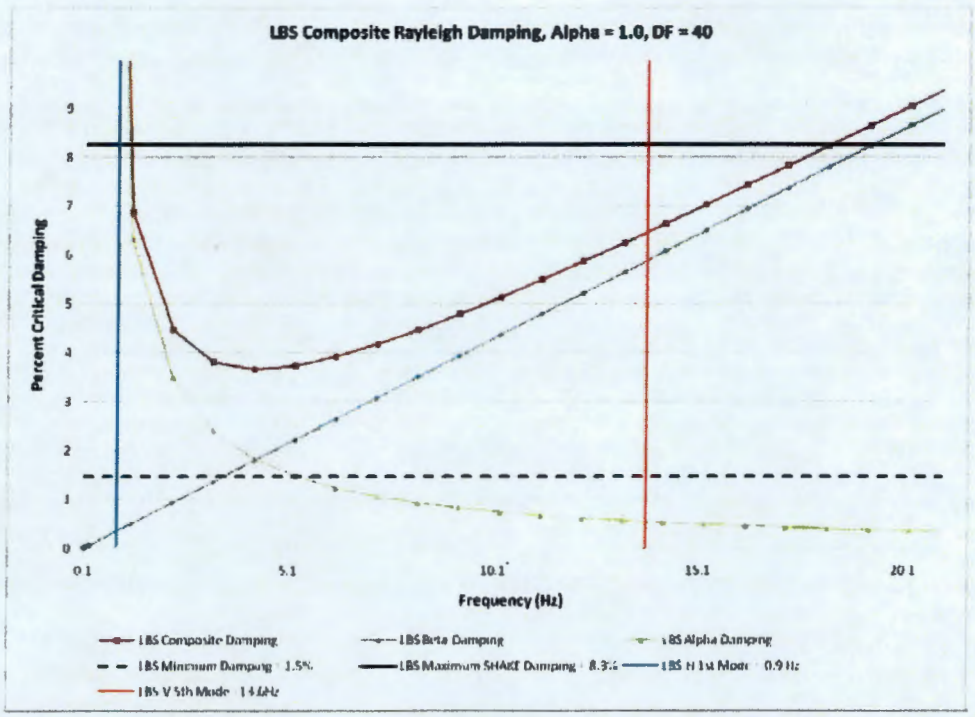

Figure 7-19. Composite Rayleigh Damping for Lower Bound ANSYS® Soil Column

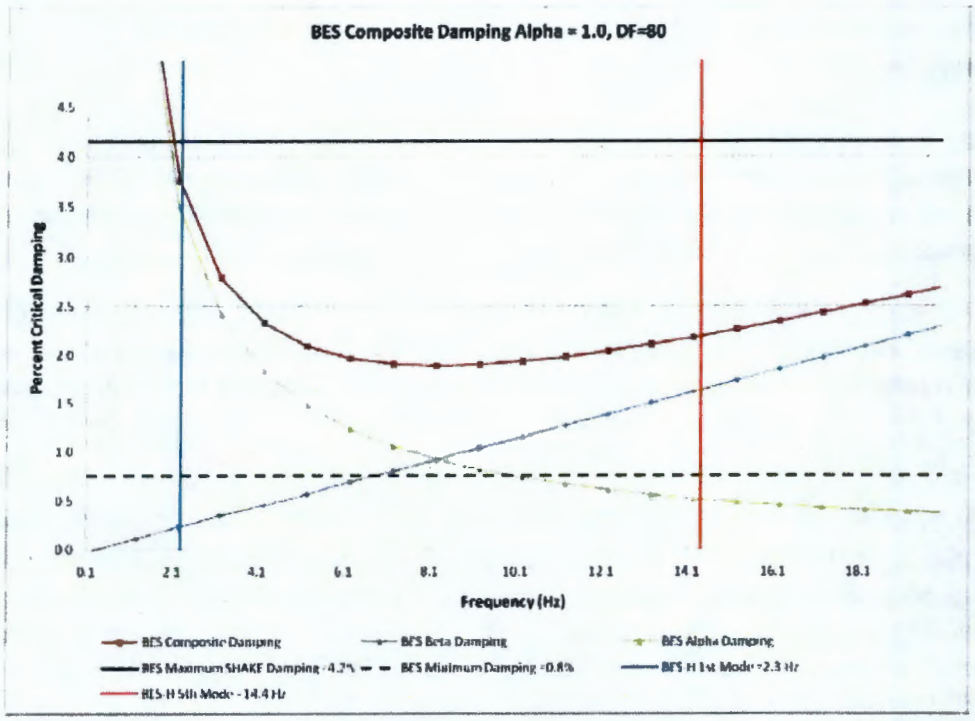

Figure 7-20. Composite Rayleigh Damping for Best Estimate ANSYS® Soil Column

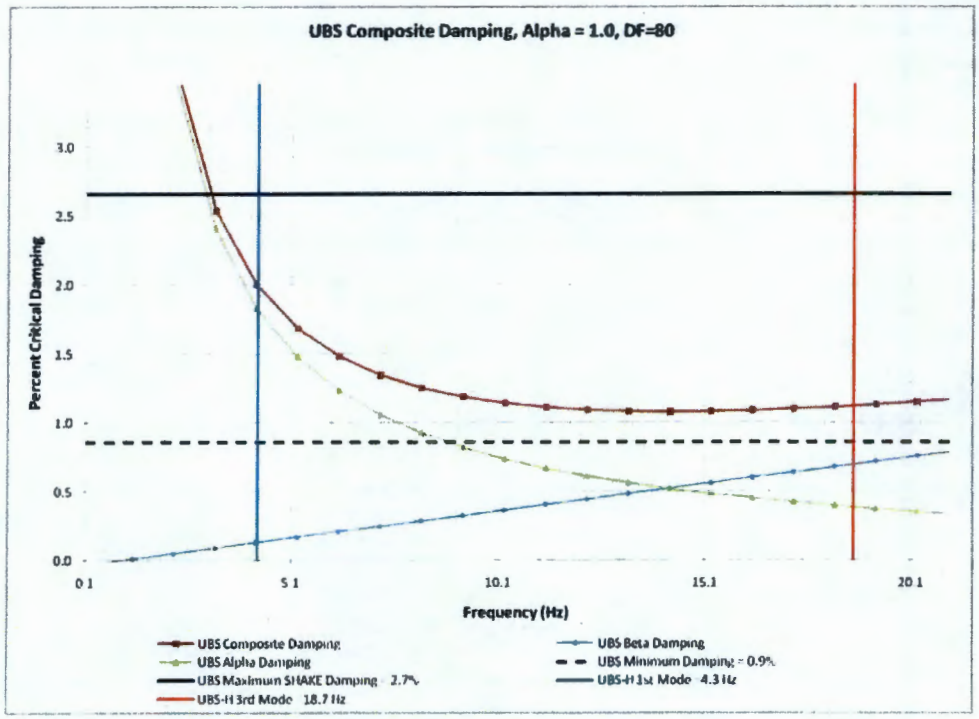

Figure 7-21. Composite Rayleigh Damping for Upper Bound ANSYS® Soil Column

7.8 Characterization of the ANSYS® Soil Columns Dynamic Response

Using the three soil profiles, a harmonic analysis of each soil type is performed in ANSYS® to benchmark the soil column, provide insight for the alpha/beta optimization used in the time domain evaluations, ensure that the boundary conditions are appropriate, and verify that the isotropic material properties used in ANSYS® are correct.

The amplification factors shows the amplification of the base motion to the surface of the Type II, III, or IV tank foundations (-43 ft, -49 ft, and -57 ft). The lower bound soil column depth is 405 ft., the best estimate full column soil depth is 303 ft, and the upper bound soil column depth is 123 ft. Full soil column amplification factors from ANSYS® and SHAKE91 are compared to show reasonable matches at each elevation.

The SHAKE91 models include layer-by-layer constant damping. The ANSYS® harmonic analysis omits the individual material layer damping and incorporates a constant damping ratio applied globally. Good matches between SHAKE91 and ANSYS® amplitude spectra result for the LB and BE columns when the damping ratio in ANSYS® is set to 5.5% and 3.5% of critical, respectively. Similarly, the upper bound amplitude spectra agree well between SHAKE91 and ANSYS® when a constant damping ratio of 2.3% of critical is specified in the ANSYS® harmonic analysis.

Figure 7-22 through Figure 7-24 show the SHAKE91 and ANSYS® horizontal amplification factors for the LB, BE, and UB soil columns. The peak amplifications from the SHAKE91 and ANSYS® results are in good agreement. Table 7-5 summarizes the natural frequencies of the three soil columns for horizontal excitation.

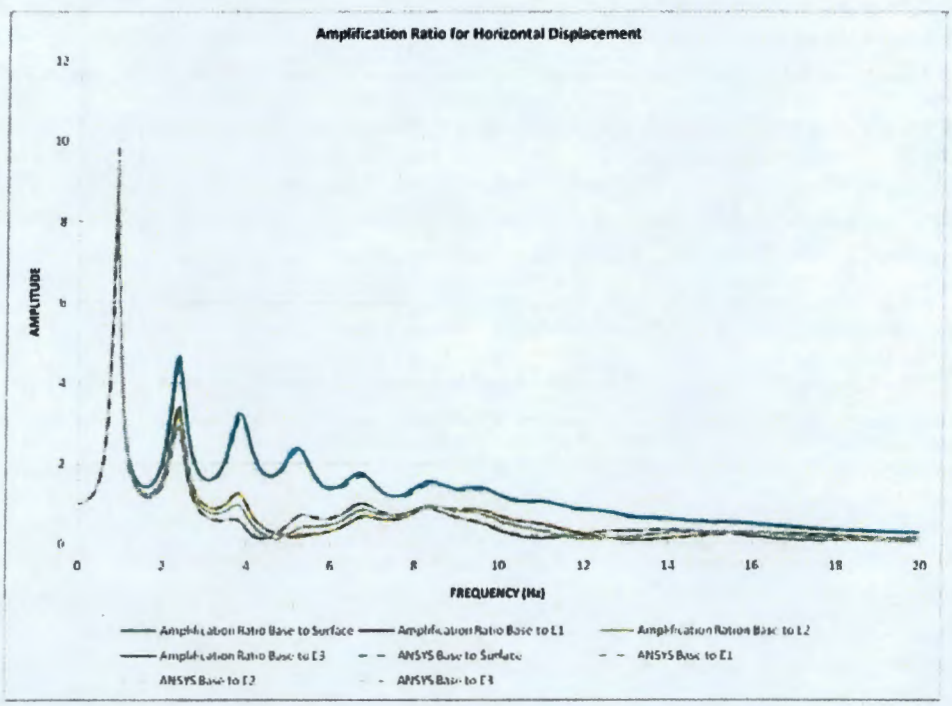

Figure 7-22. SHAKE91 vs. ANSYS® Free Field Horizontal Amplification Factors for Lower Bound Soil

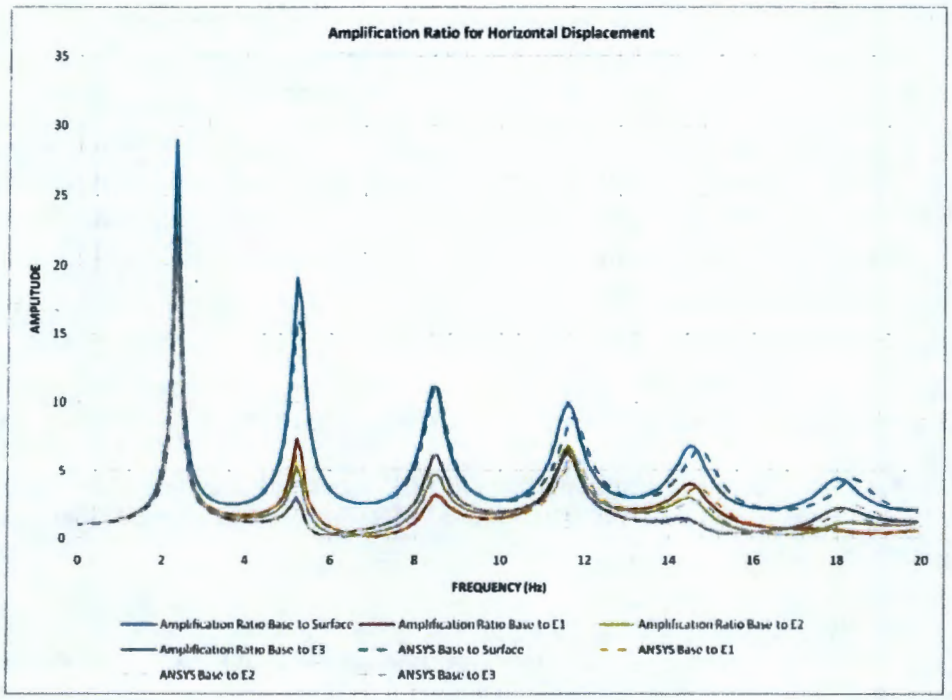

Figure 7-23. SHAKE91 vs. ANSYS® Free Field Horizontal Amplification Factors for Best Estimate Soil

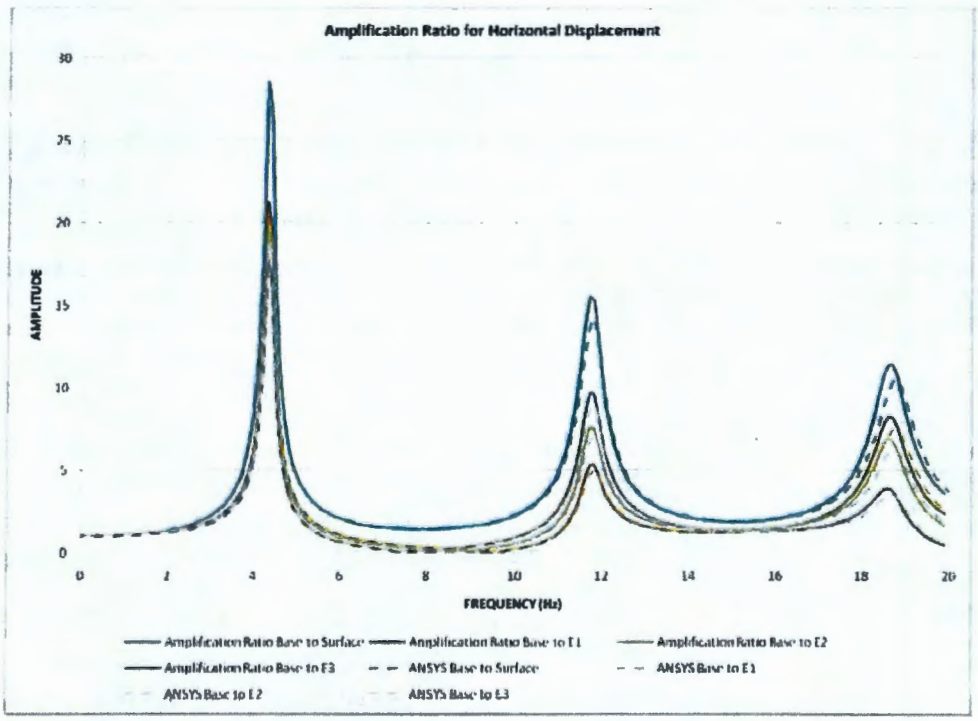

Figure 7-24. SHAKE91 vs. ANSYS® Free Field Horizontal Amplification Factors for Upper Bound Soil

Table 7-5. Soil Column Modal Frequencies for Horizontal Excitation

Mode	Modal Frequency (Hz)					
	Lower Bound Soil		Best Estimate Soil		Upper Bound Soil	
	SHAKE91	ANSYS®	SHAKE91	ANSYS®	SHAKE91	ANSYS®
1	0.9	0.9	2.3	2.3	4.3	4.3
2	2.4	2.4	5.2	5.2	11.7	11.8
3	3.8	3.9	8.5	8.5	18.7	18.8
4	5.2	5.2	11.6	11.7	--	--
5	6.7	6.7	14.5	14.7	--	--

7.8.1 Soil Column Harmonic Analysis – Vertical Excitation

Ultimately, the seismic excitations are applied to ANSYS® models as force time series based on acceleration time series determined via SHAKE. Although the horizontal and vertical input motions are different, the soil column properties remain the same for the two directions.

Figure 7-25 through Figure 7-27 show the SHAKE91 and ANSYS® vertical amplification factors for the LB, BE, and UB columns. Table 7-6 summarizes the natural frequencies of the three soil columns for vertical excitation.

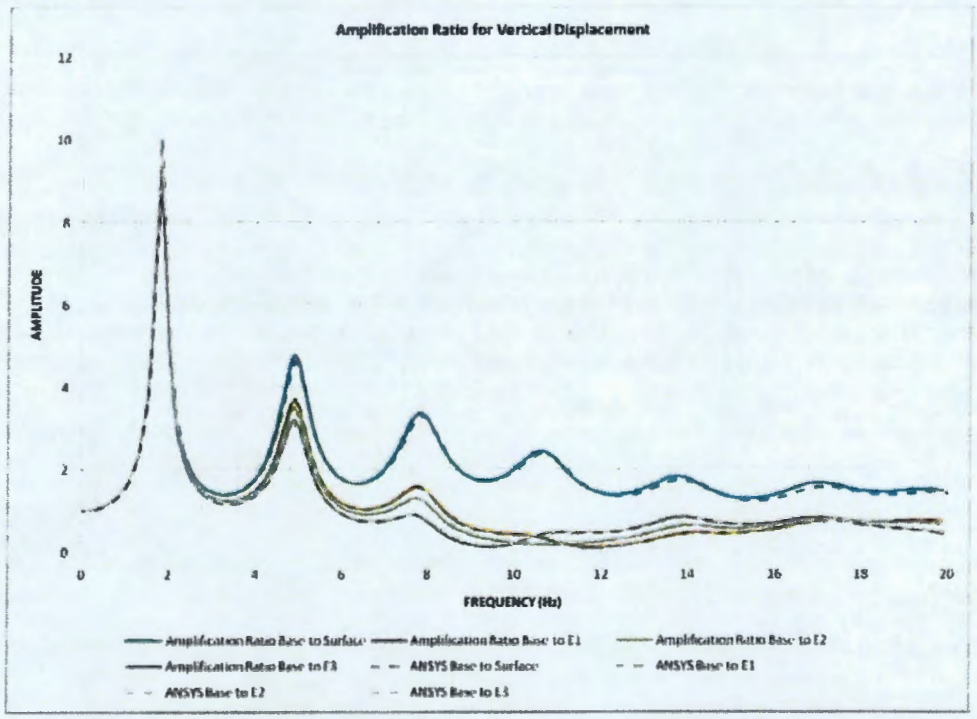

Figure 7-25. SHAKE91 vs. ANSYS® Free Field Vertical Amplification Factors for Lower Bound

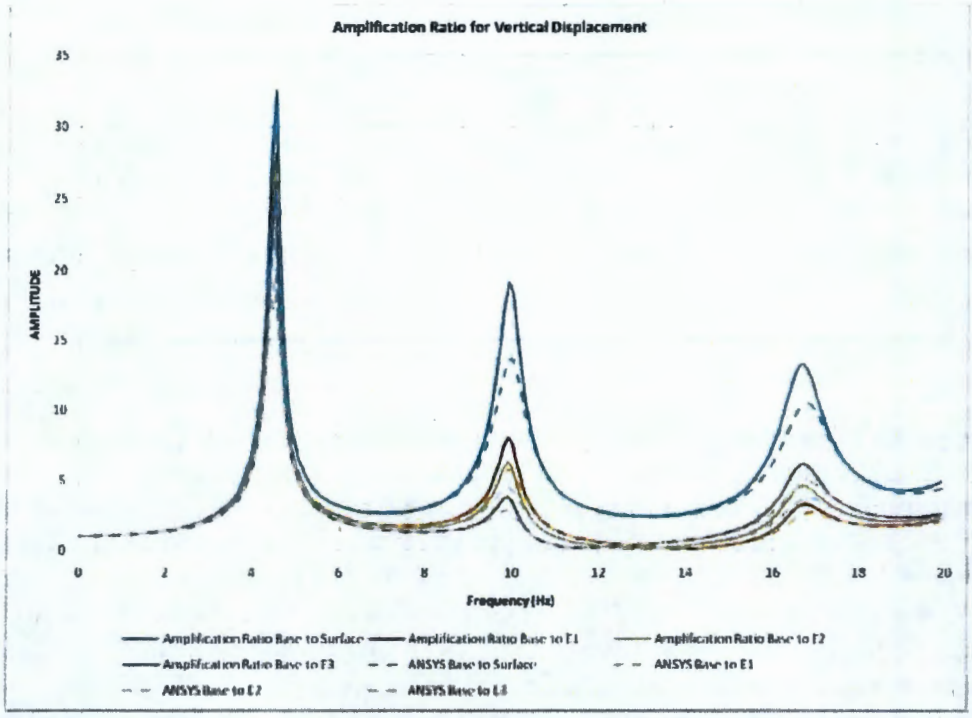

Figure 7-26. SHAKE91 vs. ANSYS® Free Field Vertical Amplification Factors for Best Estimate

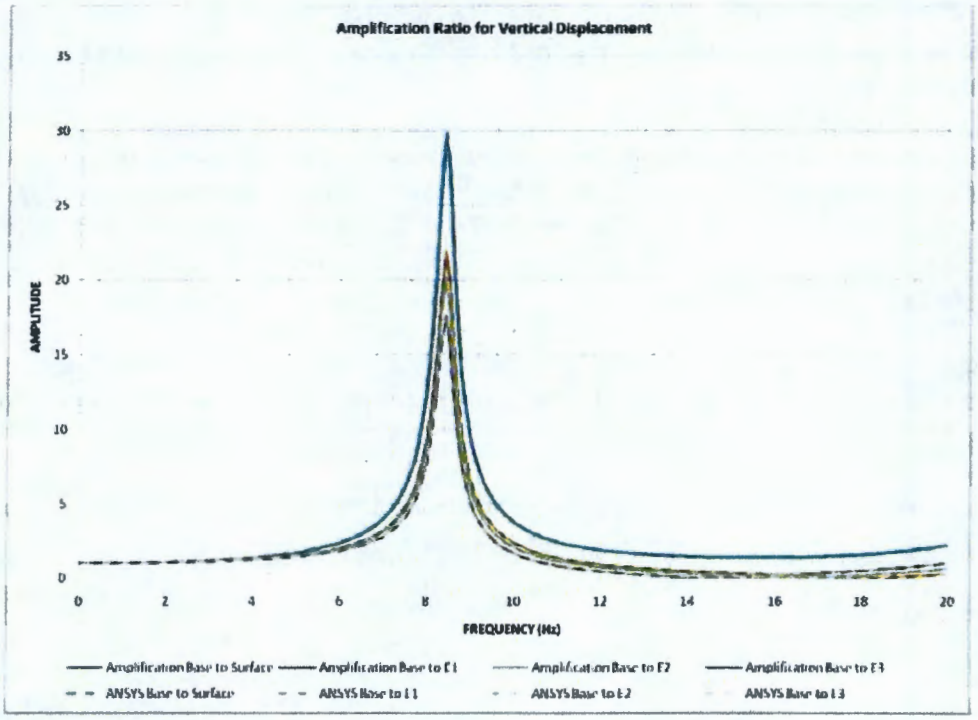

Figure 7-27. SHAKE91 vs. ANSYS® Free Field Vertical Amplification Factors for Upper Bound

Table 7-6. Soil Column Modal Frequencies for Vertical Excitation

Mode	Modal Frequency (Hz)					
	Lower Bound Soil		Best Estimate Soil		Upper Bound Soil	
	SHAKE91	ANSYS®	SHAKE91	ANSYS®	SHAKE91	ANSYS®
1	1.8	1.8	4.5	4.5	8.4	8.4
2	4.9	4.9	9.9	9.9	--	--
3	7.8	7.9	16.7	16.8	--	--
4	10.6	10.7	--	--	--	--
5	13.8	13.8	--	--	--	--

7.9 Spectral Matching Methodology and Acceptance Criteria

As described in the AMEC Geomatrix report in Appendix R of Rinker et al. (2011a), smooth target spectra have been developed at the surface and at the tank foundation levels using SHAKE. The surface target spectrum is the DRS (2/3 of the site-specific MCE) and the tank foundation-level target spectra are the three FIRS described previously, there is one FIRS for each SSI profile and for each tank foundation level. Because the SSI evaluation is performed using ANSYS®, it must be verified that the spectral matching is preserved at the tank foundation level and at the surface in the ANSYS® SSI model when the base time series are input to the SSI models. As stated in Section 7.4, the tank foundation-level targets for ANSYS® are the in-column spectra that are compatible with the time series that are spectrally matched to the FIRS. Although the only one bounding FIRS is used for each soil column, when the spectrally matched motion is deconvolved to the base in SHAKE and convolved back up in ANSYS®, the process results in nine in-column targets to be considered in ANSYS®. That is, one target for each tank foundation elevation for each SSI profile.

The time series spectrally matched to the target response spectra shown in the subject Geomatrix report were input as pseudo-outcrop motion into SHAKE91 and the in-column motions at the Type II, III, and IV foundation elevations E1, E2, and E3 as well as the in-column motion at the base of the SSI profiles were obtained. The motions at the base of the SSI profiles were then baseline corrected and applied as input to the ANSYS® SSI models.

The acceptance criteria for spectral matching are that the in-column spectra at each tank foundation level for each of the three soil columns should individually match the target (in-column) spectra from SHAKE according to the criteria below from McGuire et al. (2001) for a mean-based fit.

- Comparison between the time series response spectrum and the target response spectrum is made for 300 frequencies spaced uniformly in log frequency, 100 frequencies per log decade.
- The 5% damped response spectrum of the acceleration time series shall not fall more than 10% below the target response spectrum at any one frequency.
- The spectral ordinates for no more than 9 adjacent frequencies shall lie below the target spectrum.

At the surface, the same criteria are applied to the upper bound envelope of the three surface spectra corresponding to the three SSI profiles. Any deficiencies in the ANSYS® motions are noted. If

significant valleys were present in the ANSYS® spectra over narrow frequency ranges, they were minimized as described below. If only a minor broad-banded adjustment is required, the time series could simply be scaled uniformly. Although some modifications to the time series at the base of the SSI profiles were made to minimize significant narrow-banded valleys, no corrections were made to reduce peaks in the ANSYS® spectra.

To minimize significant valleys in the ANSYS® spectra relative to the target spectra, the base time series was modified by adjusting the appropriate FIRS target spectrum smoothly upward in the frequency range where the ANSYS® motions were deficient, and a new spectrally matched time series was obtained. This modified time series was then input into SHAKE91 and deconvolved to obtain a new base input motion for ANSYS®. The process was repeated until the response spectra for the ANSYS® in-column motions at the three tank foundation levels and at the surface adequately matched the response spectra for the SHAKE91 in-column motions obtained using the initial spectrally matched time series. This process was repeated separately for the LB, BE, and UB runs. It is important to understand that the adjustment to the target FIRS was done only within SHAKE simply for generating a modified time series. The target FIRS used for spectral matching in ANSYS® remained unaltered. This iterative process was followed for both the horizontal and vertical input motions.

The test of the input motions is the response of the full ANSYS® SSI models to those motions. To check this response and compare the spectra to the targets, the ANSYS® SSI models are used to compute motions at the lateral boundary of the models (intended to simulate the free-field motion) at the surface and at the Type I tank foundation elevation (E0), which is at elevation -37 ft. The surface spectra and (in-column) foundation spectra are extracted from ANSYS® and compared to the DRS and in-column targets developed in SHAKE.

The spectral matching results for the full ANSYS® SSI model are presented below for the three soil columns and two directions of motion. Due to the substantial similarities in the results, all configurations within the same soil column are shown on the same plot. At the surface, the plot shows the smooth surface spectrum (2/3 of the horizontal MCE), the SHAKE surface spectrum (the legend shows this as 'Target'), and the ANSYS® surface spectrum (Surface). The plot also shows the ratio of the ANSYS® spectrum to the target as a percentage. The surface target is defined as the deterministic SHAKE surface spectrum. The tank foundation-level plot shows the in-column SHAKE target spectrum (Target), the ANSYS® SSI model spectrum (E0), and the ratio of the two curves.

7.9.1 Spectral Matching for the ANSYS® SSI Model with Horizontal Time Histories

The conclusion from this section is that adequate spectral matching has been achieved between the ANSYS® SSI model and the target spectra generated by SHAKE in the frequency range of 0.1 to 30.0 Hz for both the surface and tank foundation elevations. Adequate spectral matching between the ANSYS® SSI model and target spectra for the LB soil profile at the tank foundation elevation has a slightly smaller frequency range of 0.1 to 24 Hz. In general, there is a conservative bias in the input time histories.

7.9.1.1 Spectral Results for Lower Bound Soil Column

Figure 7-28 shows the ANSYS® surface spectra from the ANSYS® SSI model along with the SHAKE surface spectrum and the smooth target spectrum for the LB soil profile. The ratio of the ANSYS® to SHAKE spectra is greater than 1.0 from 0.15 to 30 Hz and is greater than 0.9 between 0.1 and 30.0 Hz.

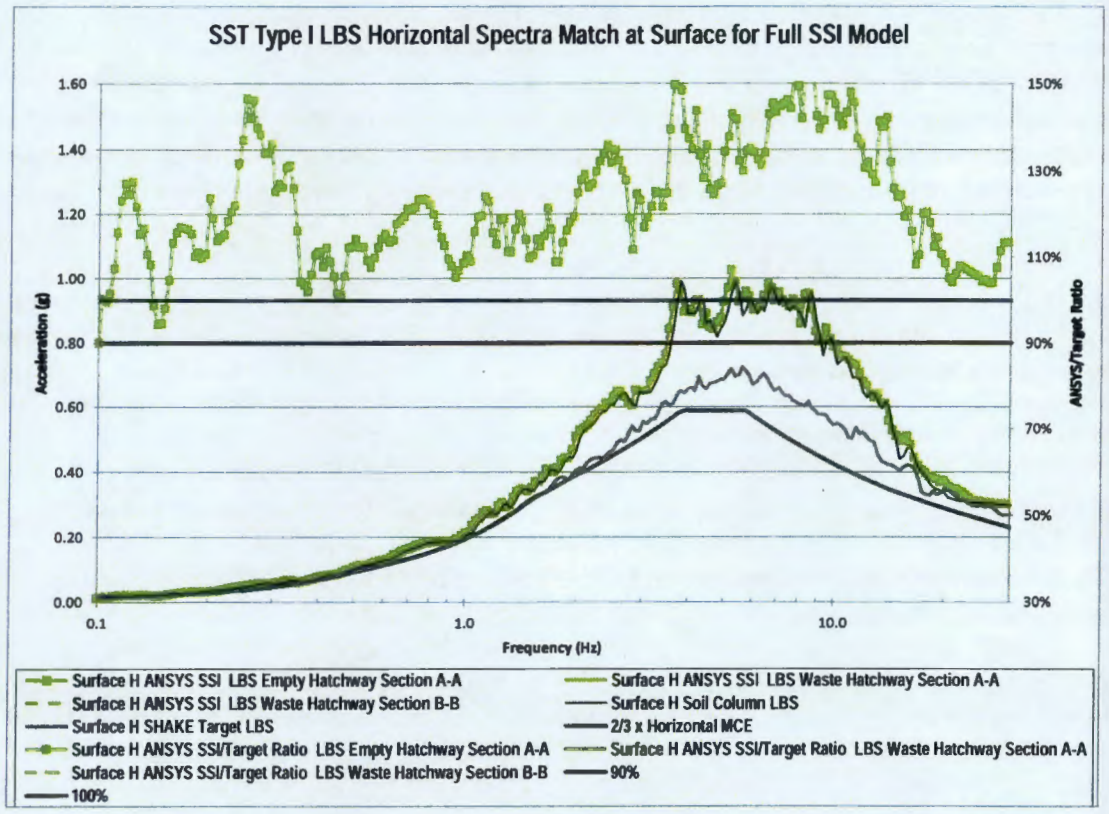

Figure 7-28. Comparison of Lower Bound Horizontal Surface Spectra from the ANSYS® SSI Model

Figure 7-29 shows the ANSYS® SSI model foundation level response spectra and the SHAKE in-column target spectrum for the LB soil profile. The ratio of the ANSYS® to SHAKE spectra is greater or equal to 1.0 from 0.15 to 17 Hz and is greater than 0.9 between 0.1 and 24 Hz.

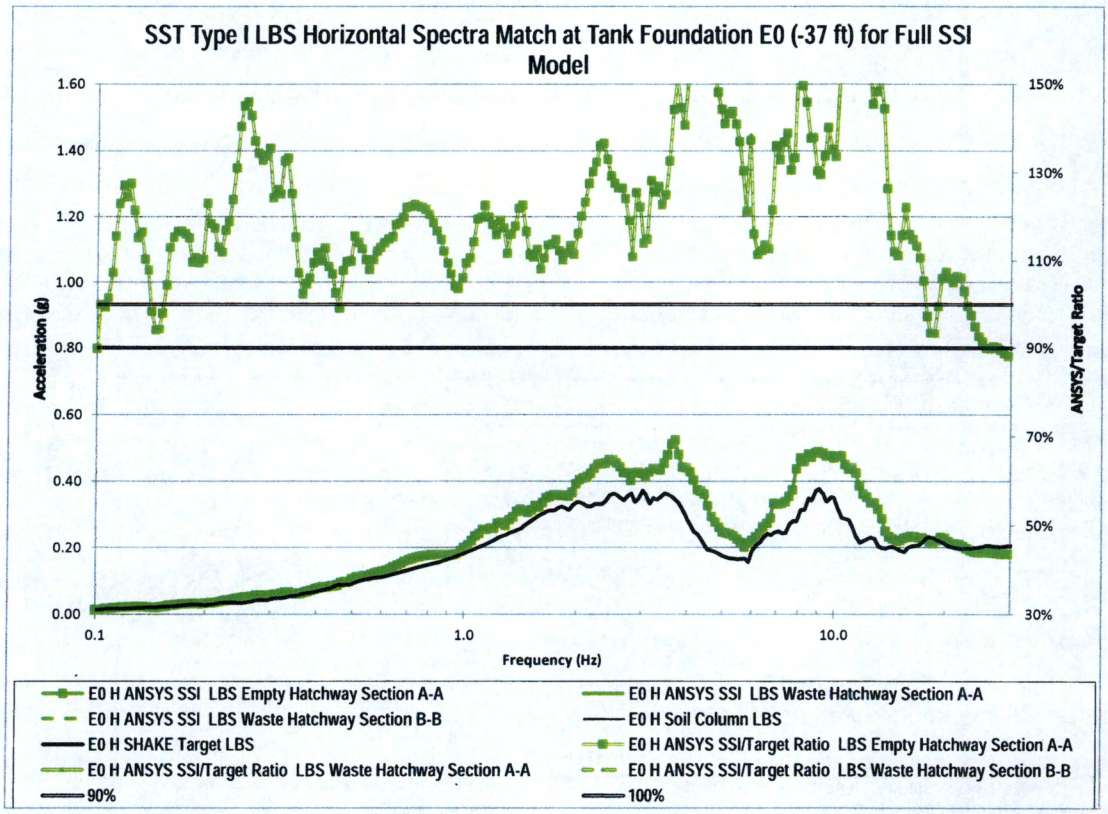

Figure 7-29. Comparison of Lower Bound Horizontal Tank Foundation Spectra from the ANSYS® SSI Model

7.9.1.2 Spectral Results for Best Estimate Soil Column

Figure 7-30 shows the ANSYS® surface spectra from the ANSYS® SSI model along with the SHAKE surface spectrum and the smooth target spectrum for the BE soil profile. The ratio of the ANSYS® to SHAKE spectra is greater than 1.0 from 0.17 to 30 Hz and is greater than 0.9 from 0.1 to 30 Hz.

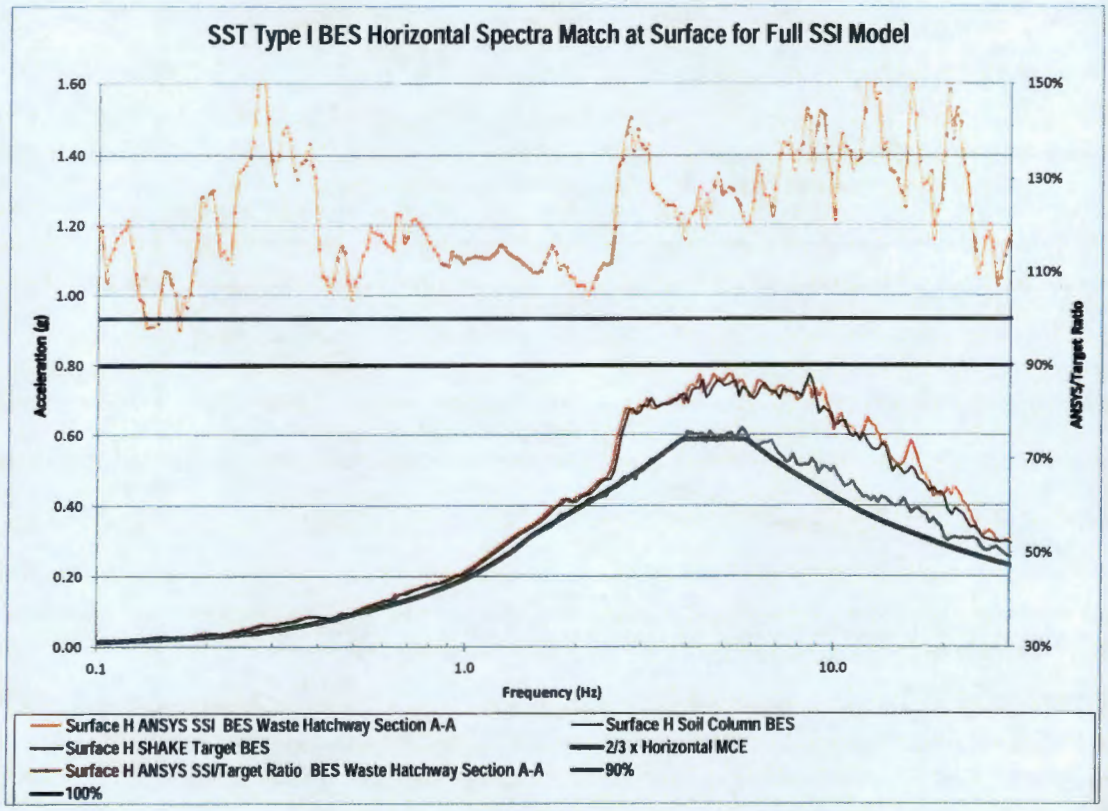

Figure 7-30. Comparison of Best Estimate Horizontal Surface Spectra from the ANSYS® SSI Model

Figure 7-31 shows the ANSYS® SSI model foundation level response spectra and the SHAKE in-column target spectrum for the BE soil profile. The ratio of the ANSYS® to SHAKE spectra is greater than 1.0 from 0.1 to 30 Hz except for a few isolated points above 0.95, and is greater than 0.9 from 0.1 to 30 Hz.

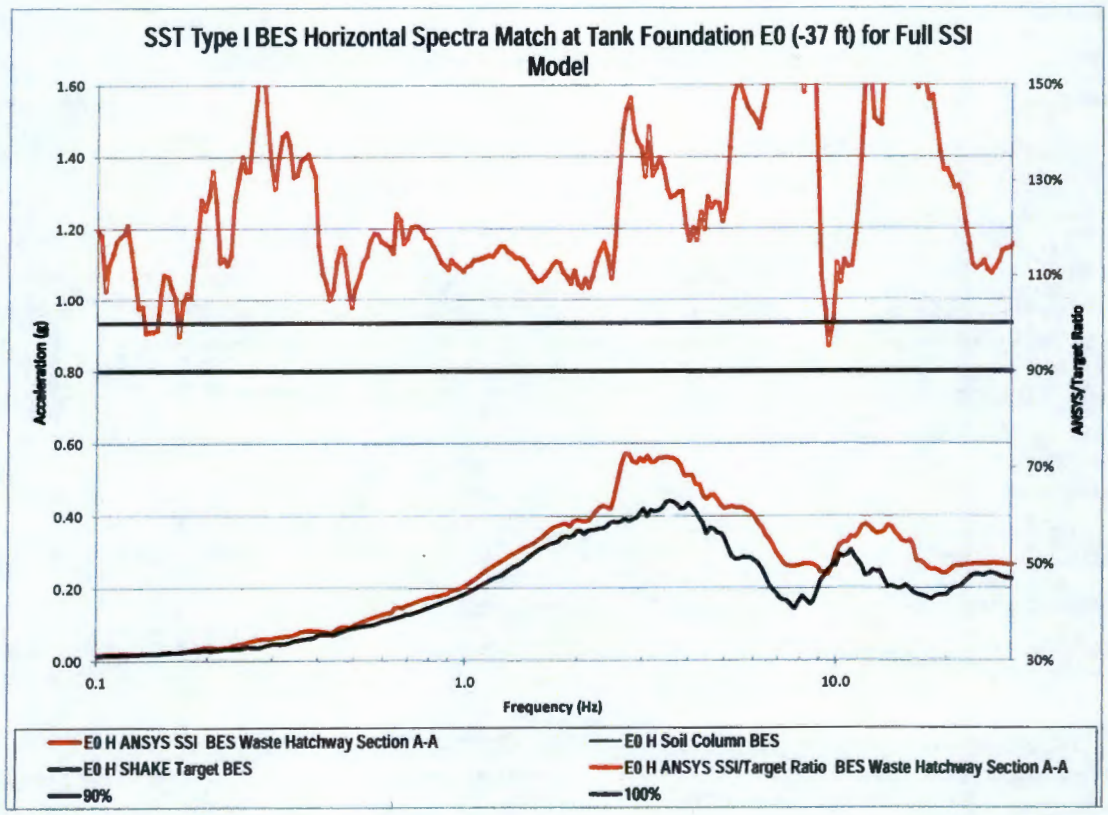

Figure 7-31. Comparison of Best Estimate Horizontal Tank Foundation Spectra from the ANSYS® SSI Model

7.9.1.3 Spectral Results for Upper Bound Soil Column

Figure 7-32 shows the ANSYS® surface spectra from the ANSYS® SSI model along with the SHAKE surface spectrum and the smooth target spectrum for the UB soil profile. The ratio of the ANSYS® to SHAKE surface spectra is greater than 1.0 from 0.1 to 30 Hz.

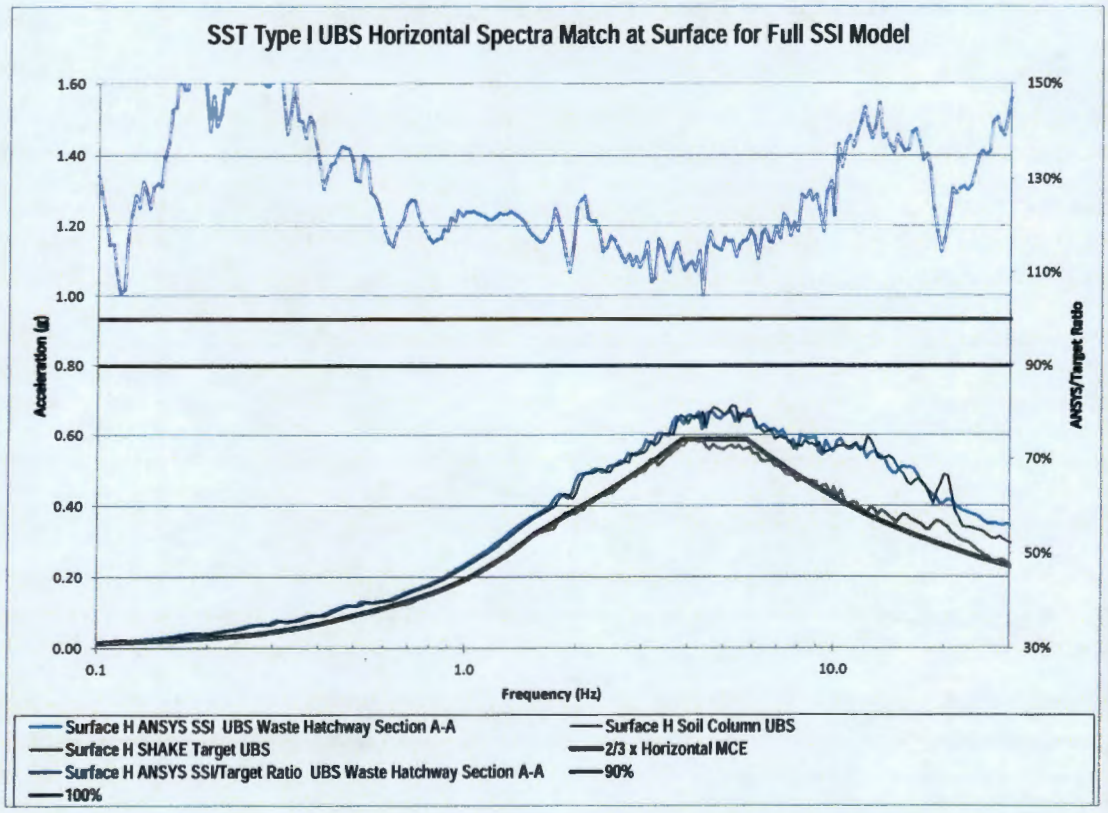

Figure 7-32. Comparison of Upper Bound Horizontal Surface Spectra from the ANSYS® SSI Model

Figure 7-33 shows the ANSYS® SSI model foundation level response spectra and the SHAKE in-column target spectrum for the UB soil profile. The ratio of the ANSYS® to SHAKE spectra is greater than 1.0 from 0.1 to 30 Hz.

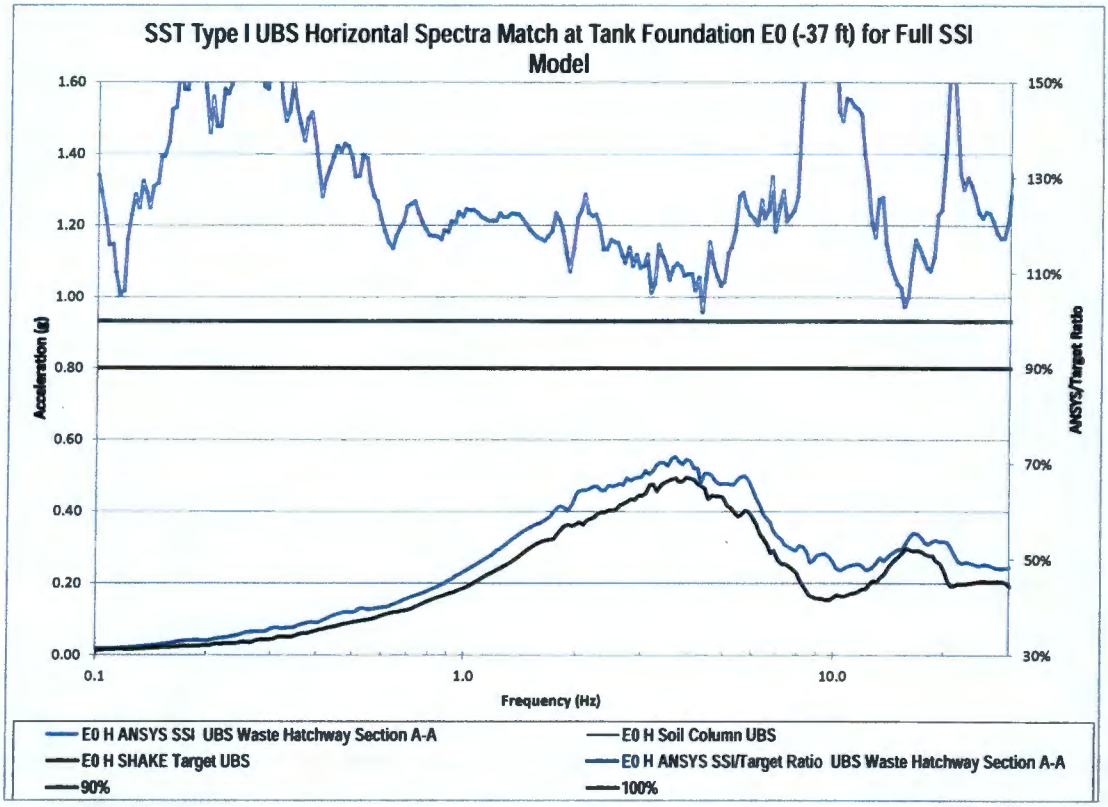

Figure 7-33. Comparison of Upper Bound Horizontal Tank Foundation Spectra from the ANSYS® SSI Model

7.9.2 Spectral Matching for the ANSYS® SSI Model with Vertical Time Histories

The previous section described the spectral matching between the ANSYS® SSI model and SHAKE for horizontal input motions. This section repeats that process for the vertical input motion.

The conclusion from this section is that adequate spectral matching has been achieved between the ANSYS® SSI model and the target spectra generated by SHAKE in the frequency range of 0.1 to 30 Hz for both the surface and tank foundation elevations. In general, there is a conservative bias in the input time histories.

7.9.2.1 Spectral Results for Lower Bound Soil Column

Figure 7-34 shows the ANSYS® surface spectra from the ANSYS® SSI model along with the SHAKE surface spectrum and the smooth target spectrum for the LB soil profile. The ratio of the ANSYS® to SHAKE spectra is equal to or greater than 1.0 between 0.1 and 30.0 Hz.

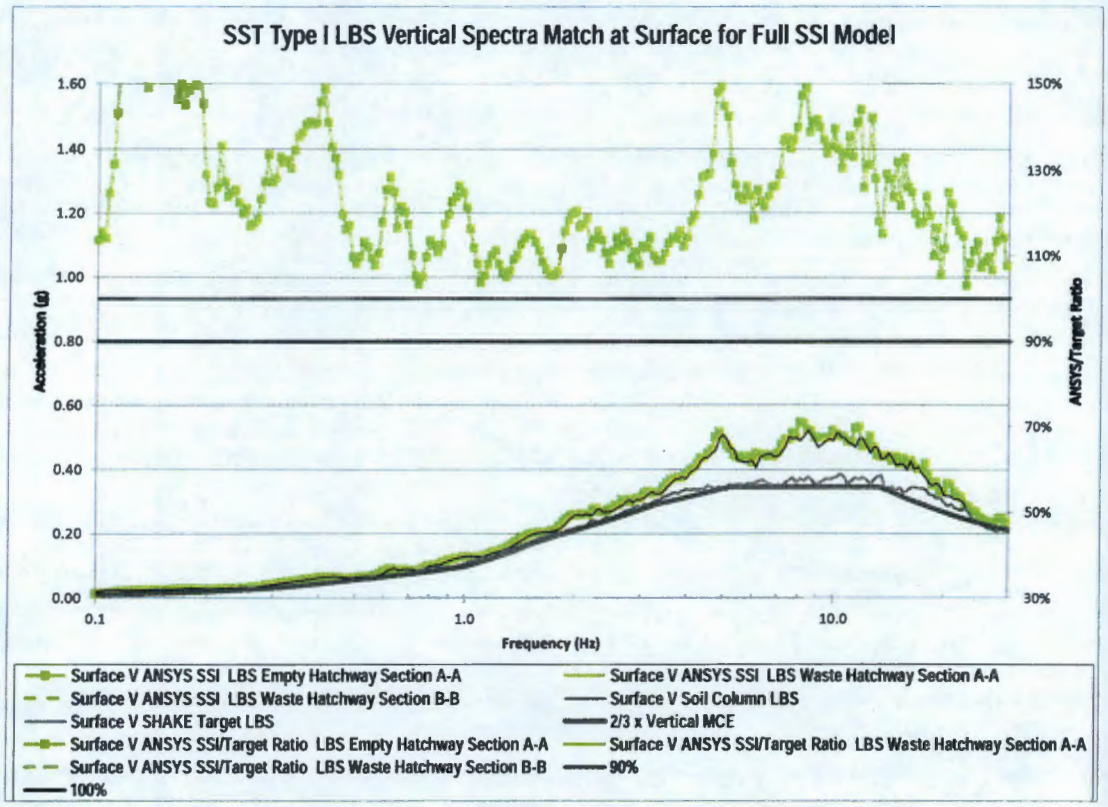

Figure 7-34. Comparison of Lower Bound Vertical Surface Spectra from the ANSYS® SSI Model

Figure 7-35 shows the ANSYS® SSI model foundation level response spectra and the SHAKE in-column target spectrum for the LB soil profile. The ratio of the ANSYS® to SHAKE spectra is greater than 0.9 from 0.1 to 30 Hz, and greater than 1.0 except for a group of less than 10 points between 17 and 20 Hz.

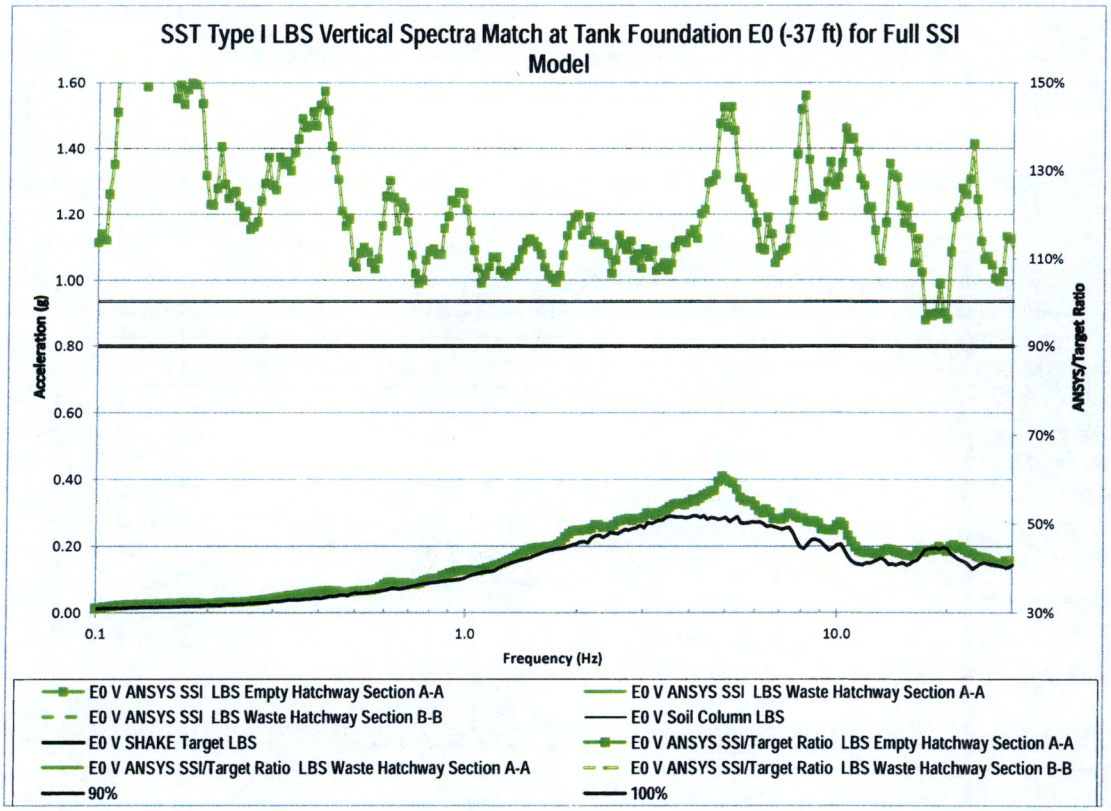

Figure 7-35. Comparison of Lower Bound Vertical Tank Foundation Spectra from the ANSYS® SSI Model

7.9.2.2 Spectral Results for Best Estimate Soil Column

Figure 7-36 shows the ANSYS® surface spectra from the ANSYS® SSI model along with the SHAKE surface spectrum and the smooth target spectrum for the BE soil profile. The ratio of the ANSYS® to SHAKE spectra is equal to or greater than 1.0 from 0.1 to 30 Hz.

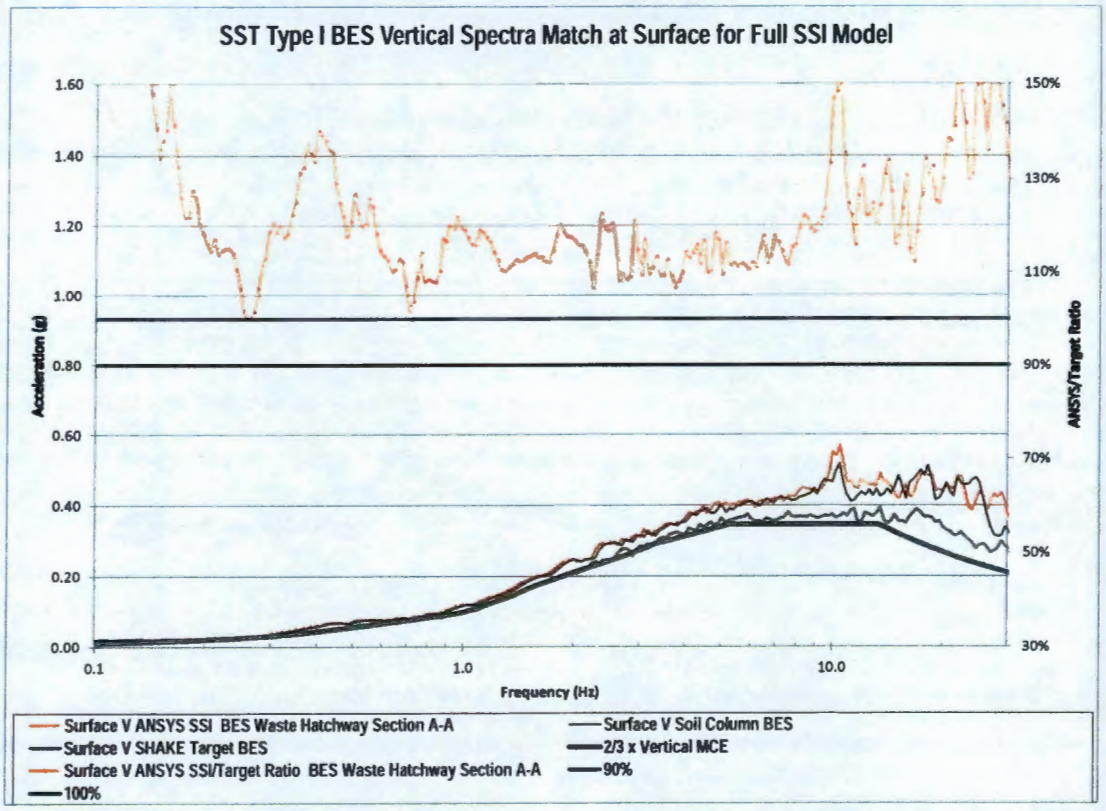

Figure 7-36. Comparison of Best Estimate Vertical Surface Spectra from the ANSYS® SSI Model

Figure 7-37 shows the ANSYS® SSI model foundation level response spectra and the SHAKE in-column target spectrum for the BE soil profile. The ratio of the ANSYS® to SHAKE spectra is equal to or greater than 1.0 except for a few points at 0.97 at approximately 17 Hz.

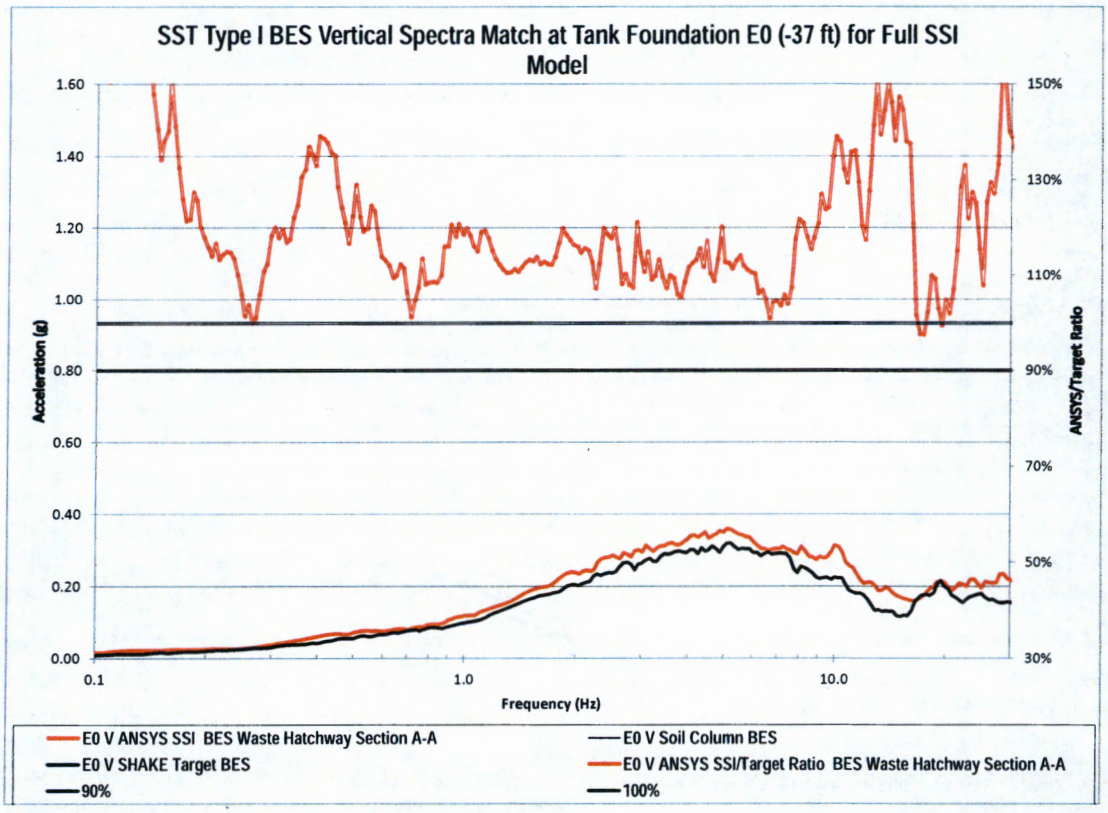

Figure 7-37. Comparison of Best Estimate Vertical Tank Foundation Spectra from the ANSYS® SSI Model

7.9.2.3 Spectral Results for Upper Bound Soil Column

Figure 7-38 shows the ANSYS® surface spectra from the ANSYS® SSI model along with the SHAKE surface spectrum and the smooth target spectrum for the UB soil profile. The ratio of the ANSYS® to SHAKE spectra is greater than 1.0 between 0.1 and 30 Hz.

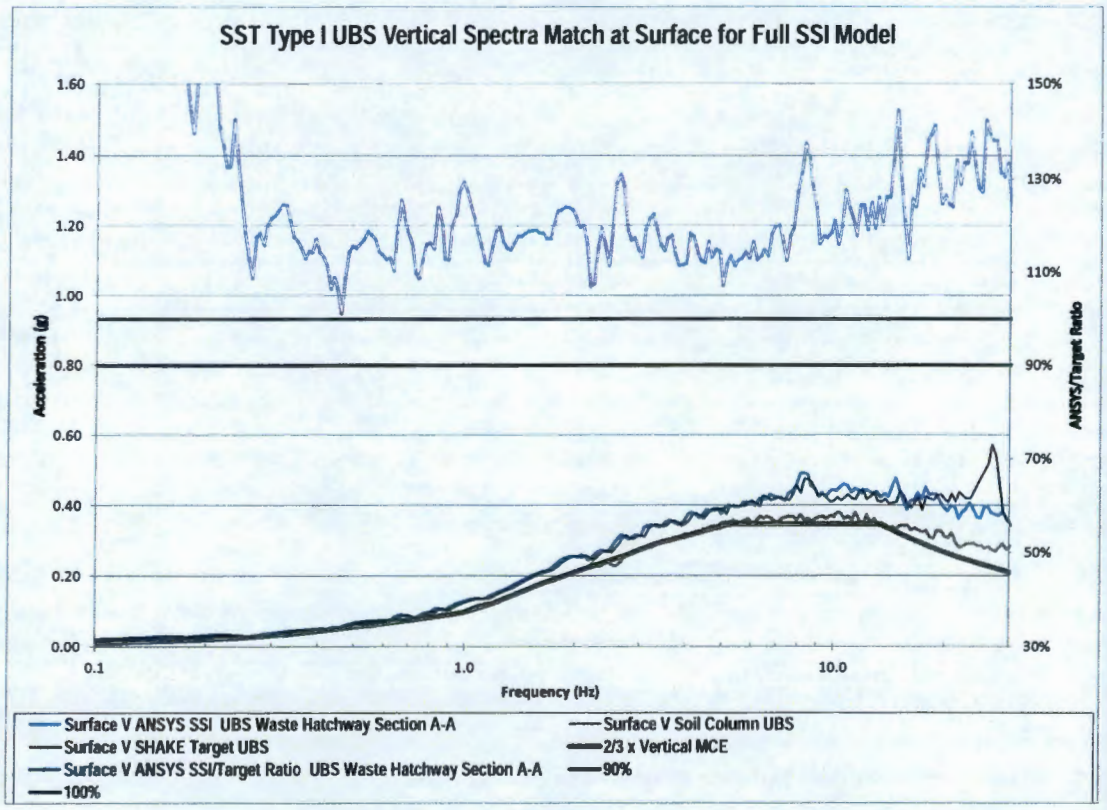

Figure 7-38. Comparison of Upper Bound Vertical Surface Spectra from the ANSYS® SSI Model

Figure 7-39 shows the ANSYS® SSI model foundation level response spectra and the SHAKE in-column target spectrum for the UB soil profile. The ratio of the ANSYS® to SHAKE spectra is greater than 1.0 between 0.1 and 30 Hz.

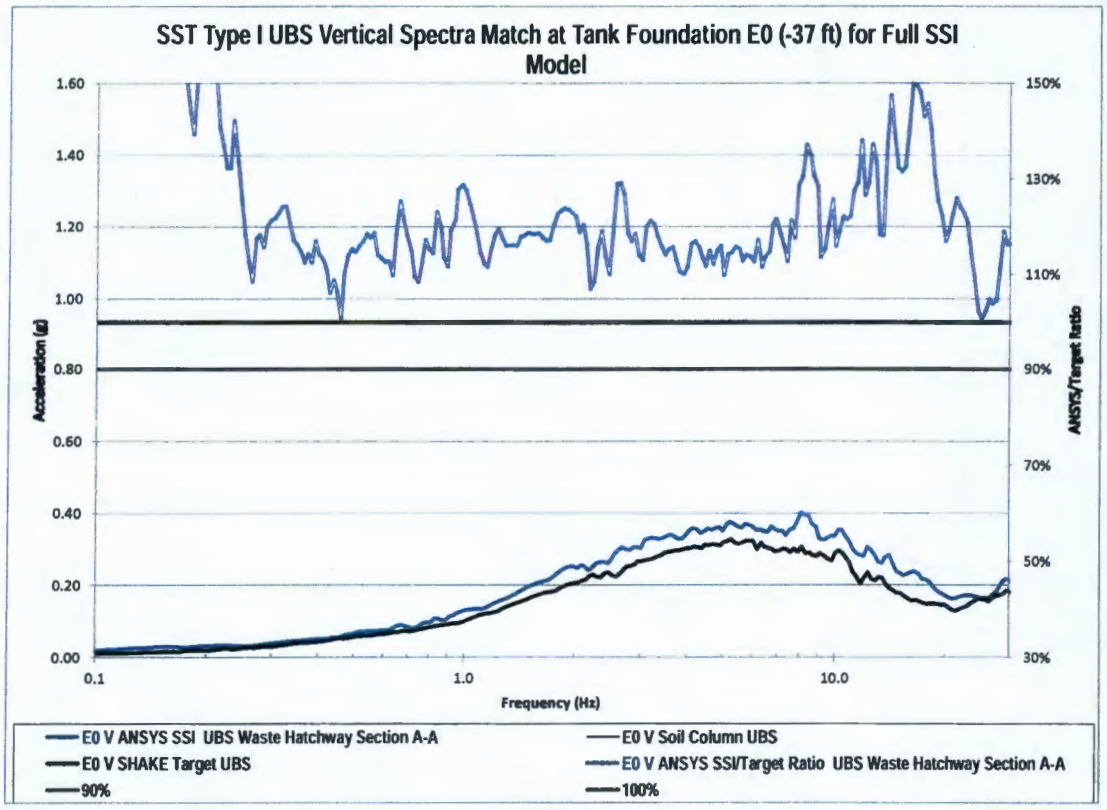

Figure 7-39. Comparison of Upper Bound Vertical Tank Foundation Spectra from the ANSYS® SSI Model

7.9.3 Spectral Response of the Tank

The in-structure spectral response of the tank is presented here in order to identify important structural modes of the tank. This analysis uses the same spectral response methodology as described in the Type IV AOR (Johnson et al. 2014c). These results are presented as supporting information only, since concrete damping is not applied as described in Section 6.1.4, thus eliminating the need to calibrate model properties to the tank frequency response. For simplicity, only results for the representative case (see Section 6.7) are presented here. Note that the in-structure spectral response of the tank is not subject to the requirements previously presented for the far-field soil response.

The in-structure acceleration response spectra from the tank response are extracted from the analysis runs to identify the dominant frequencies of the tank response. Five locations are considered; the tank footing, tank roof at sidewall (i.e. haunch), tank roof center, far-field soil at the foundation elevation, and far-field soil at the roof elevation. The tank footing location is taken on the symmetry plane to capture any rocking motion. For computation of the in-structure spectra, a consistent 5% spectral damping is used. The structural modes of the tank itself are revealed by a strong amplification in the tank in-structure spectra that is not present in the far-field soil spectra.

The in-structure response spectra are shown in Figure 7.40 through Figure 7.41. The horizontal spectra shows that the tank generally moves consistent with the soil column, thus there are no significant horizontal tank modes in the frequency range up to 30 Hz. The vertical in-structure spectra at the roof clearly show an amplified response of the roof center at 10 Hz, and broadly above 20 Hz. In comparison to the in-structure response spectra seen in the Type IV AOR (Johnson et al. 2014c), the Type I response is less amplified and occurs at a higher frequency. These differences are generally expected given the presence of the hatchway attached to the tank roof.

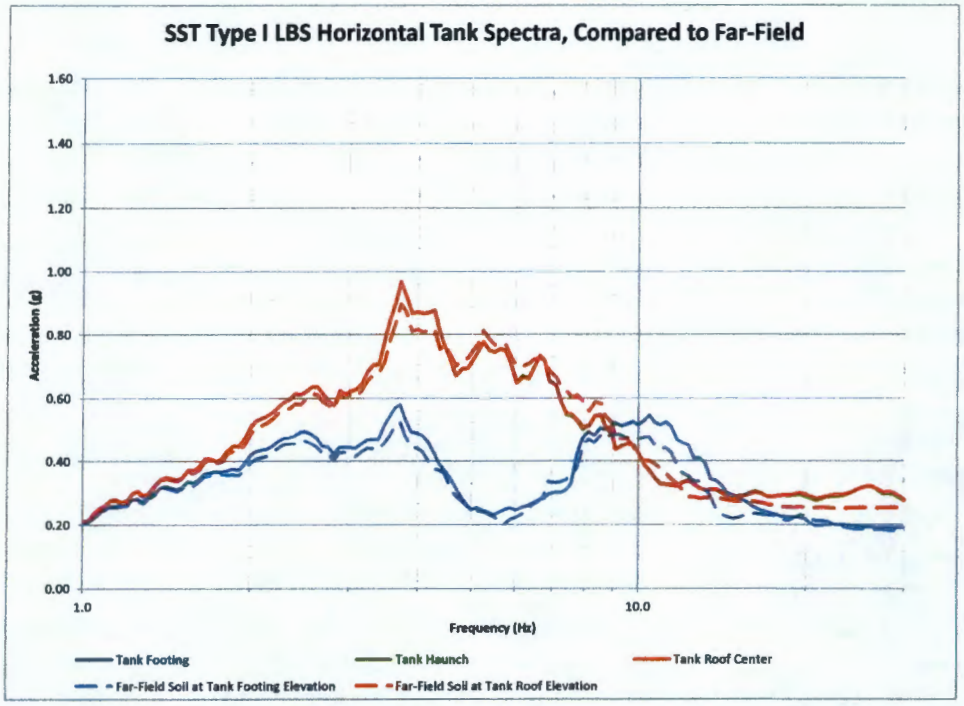

Figure 7.40. Comparison of Horizontal Acceleration Response Spectra for Lower Bound Soil - Tank vs. Far-Field

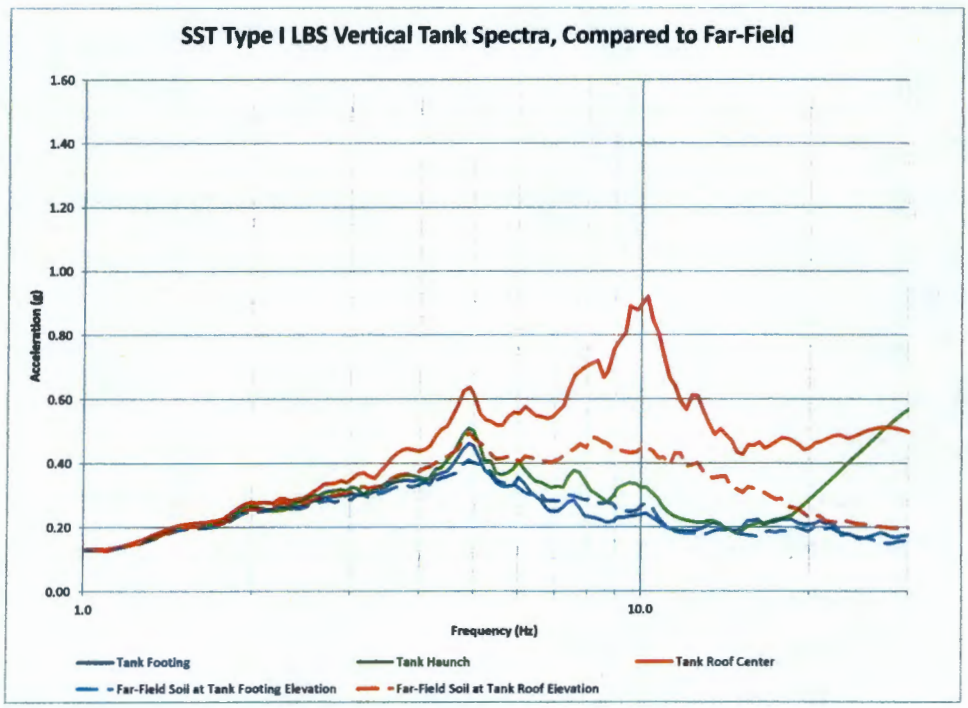

Figure 7.41. Comparison of Vertical Acceleration Response Spectra for Lower Bound Soil - Tank vs. Far-Field

8.0 Seismic Results

The results show significant variance around the circumference of the tank as a result of the irregularly shaped hatchway, especially in and near the tank roof. To aid with physical interpretation, the results from selected individual configurations are shown as partially enveloped surface plots (i.e. showing results for all ACI-evaluation sections around the circumference from 0° to 180°), and the approximate location of the hatchway is indicated for reference. The surface plot results are for the full tank, hatchway section A-A configuration for each soil case. The subsequent comparison plots present fully enveloped results from all of the run matrix cases. Keep in mind that the surface plots reveal localized responses, whereas the fully enveloped plots present only the bounding results, which may occur at different circumferential locations on the tank. For example, localized demand increases resulting from the irregularly shaped hatchway may mask more general (i.e. axisymmetric) tank behavior.

The results should not be interpolated across the discontinuities at the roof/wall and wall/floor junctions, therefore a gap is shown in the results plots at these locations.

8.1 Concrete Tank

Concrete tank resultant forces and moments are extracted from the model using the post-processing methods described in Section 6.6. The forces and moments are plotted against the ACI-evaluation section sequence that starts near the center of the roof and moves radially along the roof, down the sidewall, then from the outside to the center of the tank floor. The seismic-only load is the difference between the full transient loading and initial gravity loading. As the tank floor is not critical to tank structural integrity, it will not be highlighted in the following discussions.

Concrete force/moment surface plots are grouped in sets for each soil profile as follows:

- Figure 8-3. Lower Bound Soil (LBS), Full Tank, Hatchway Section A-A: Concrete Tank Meridional Force (kip/ft.) – Seismic Only
- Figure 8-4. Lower Bound Soil (LBS), Full Tank, Hatchway Section A-A: Concrete Tank Hoop Force (kip/ft.) – Seismic Only
- Figure 8-5. Lower Bound Soil (LBS), Full Tank, Hatchway Section A-A: Concrete Tank Meridional Moment (kip ft./ft.) – Seismic Only
- Figure 8-6. Lower Bound Soil (LBS), Full Tank, Hatchway Section A-A: Concrete Tank Hoop Moment (kip ft./ft.) – Seismic Only
- Figure 8-7. Lower Bound Soil (LBS), Full Tank, Hatchway Section A-A: Concrete Tank Through-Wall Shear Force (kip/ft.) – Seismic Only
- Figure 8-8. Lower Bound Soil (LBS), Full Tank, Hatchway Section A-A: Concrete Tank In-Plane Shear Force (kip/ft.) – Seismic Only
- Figure 8-9. Best Estimate Soil (BES), Full Tank, Hatchway Section A-A: Concrete Tank Meridional Force (kip/ft.) – Seismic Only

- Figure 8-10. Best Estimate Soil (BES), Full Tank, Hatchway Section A-A: Concrete Tank Hoop Force (kip/ft.) – Seismic Only
- Figure 8-11. Best Estimate Soil (BES), Full Tank, Hatchway Section A-A: Concrete Tank Meridional Moment (kip ft./ft.) – Seismic Only
- Figure 8-12. Best Estimate Soil (BES), Full Tank, Hatchway Section A-A: Concrete Tank Hoop Moment (kip ft./ft.) – Seismic Only
- Figure 8-13. Best Estimate Soil (BES), Full Tank, Hatchway Section A-A: Concrete Tank Through-Wall Shear Force (kip/ft.) – Seismic Only
- Figure 8-14. Best Estimate Soil (BES), Full Tank, Hatchway Section A-A: Concrete Tank In-Plane Shear Force (kip/ft.) – Seismic Only
- Figure 8-15. Upper Bound Soil (UBS), Full Tank, Hatchway Section A-A: Concrete Tank Meridional Force (kip/ft.) – Seismic Only
- Figure 8-16. Upper Bound Soil (UBS), Full Tank, Hatchway Section A-A: Concrete Tank Hoop Force (kip/ft.) – Seismic Only
- Figure 8-17. Upper Bound Soil (UBS), Full Tank, Hatchway Section A-A: Concrete Tank Meridional Moment (kip ft./ft.) – Seismic Only
- Figure 8-18. Upper Bound Soil (UBS), Full Tank, Hatchway Section A-A: Concrete Tank Hoop Moment (kip ft./ft.) – Seismic Only
- Figure 8-19. Upper Bound Soil (UBS), Full Tank, Hatchway Section A-A: Concrete Tank Through-Wall Shear Force (kip/ft.) – Seismic Only
- Figure 8-20. Upper Bound Soil (UBS), Full Tank, Hatchway Section A-A: Concrete Tank In-Plane Shear Force (kip/ft.) – Seismic Only

Discussion of local influence of the hatchway is presented alongside the LBS partially enveloped surface plots. Following the surface plots are additional fully enveloped plots of each force/moment presenting all configurations on one plot in order to identify overall trends in the demands. Discussion of overall trends is presented alongside these comparison plots.

For reference, the tank concrete elements (see Section 6.6.1) at ACI-evaluation sections 1-5 (i.e. roof) are shown with the hatchway in Figure 8-1 and Figure 8-2. Note that ACI-evaluation section 1 (near the center) is always completely covered by the taller portion of the hatchway.

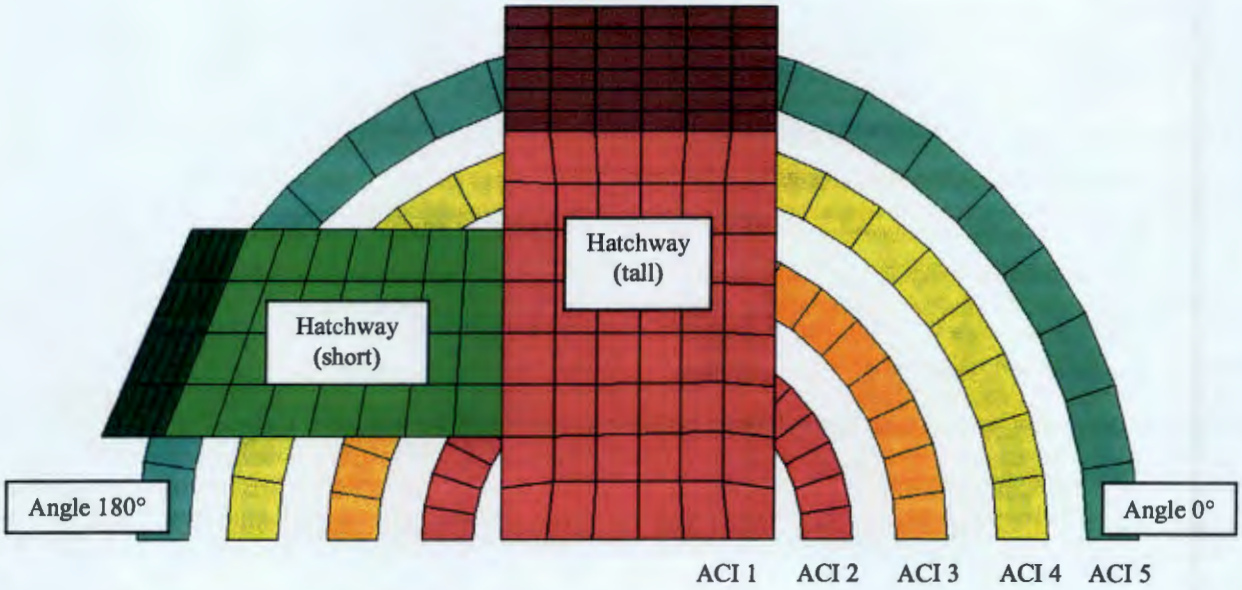

Figure 8-1. Element Plot Top View Showing Tank at ACI-Evaluation Sections 1-5 and Hatchway at Section A-A

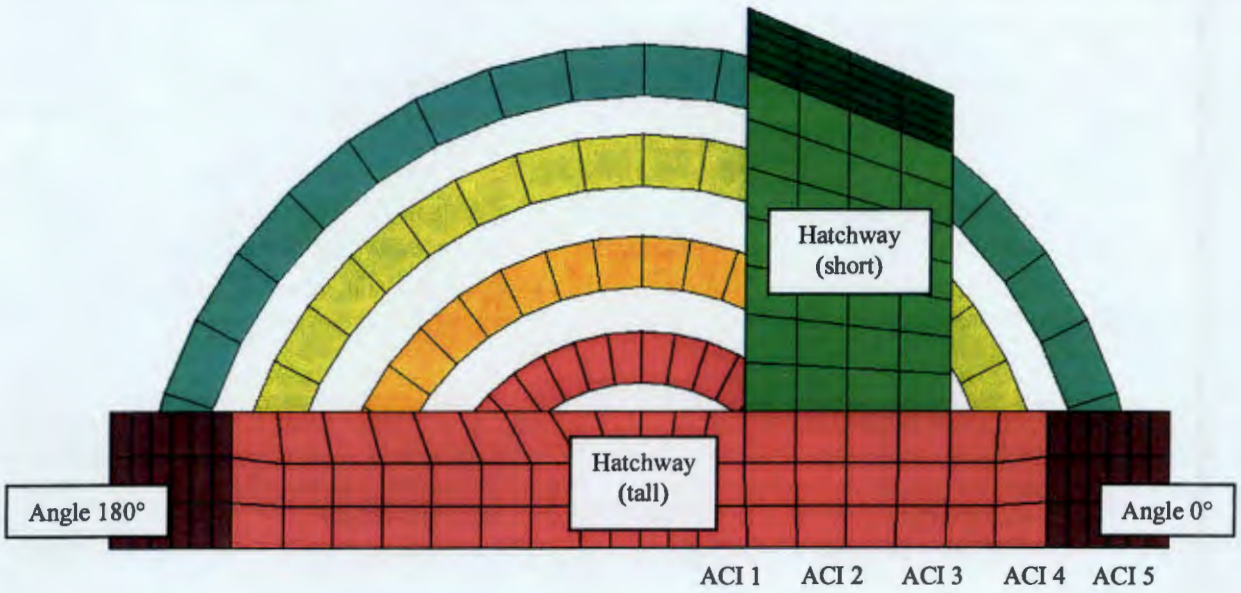

Figure 8-2. Element Plot Top View Showing Tank at ACI-Evaluation Sections 1-5 and Hatchway at Section B-B

8.1.1 Lower Bound Soil (LBS)

This representative case is used for demand/capacity evaluation in Johnson et al. (2014a). The following figures show the force and moment demands as colored contour ranges (listed below the plots) for the ACI section numbers (the horizontal axis) and the angle locations around the tank perimeter (the vertical axis).

The seismic-only meridional forces in Figure 8-3 show that the demands at the top of the wall are increased by proximity to the hatchway, but the influence diminishes toward the bottom of the wall. The demands at the roof are insensitive to the presence of the hatchway.

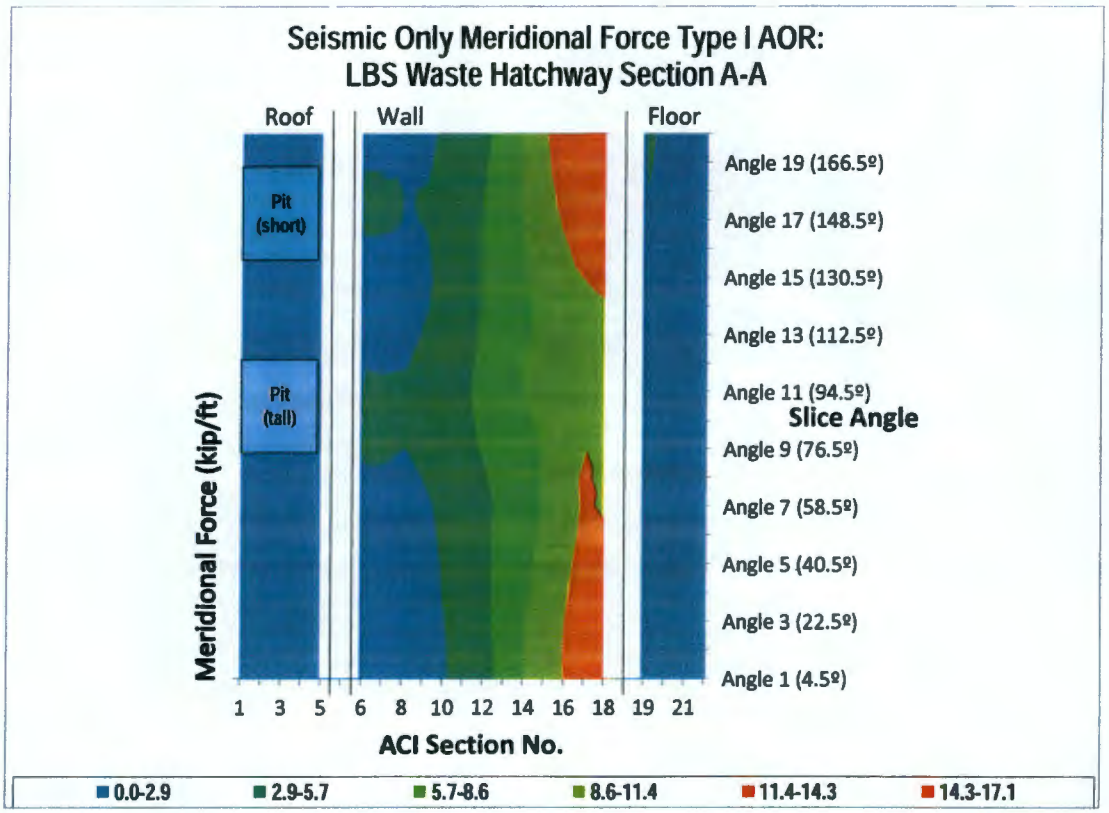

Figure 8-3. Lower Bound Soil (LBS), Full Tank, Hatchway Section A-A: Concrete Tank Meridional Force (kip/ft.) – Seismic Only

The seismic-only hoop forces in Figure 8-4 show that the demands have a low sensitivity to proximity to the hatchway.

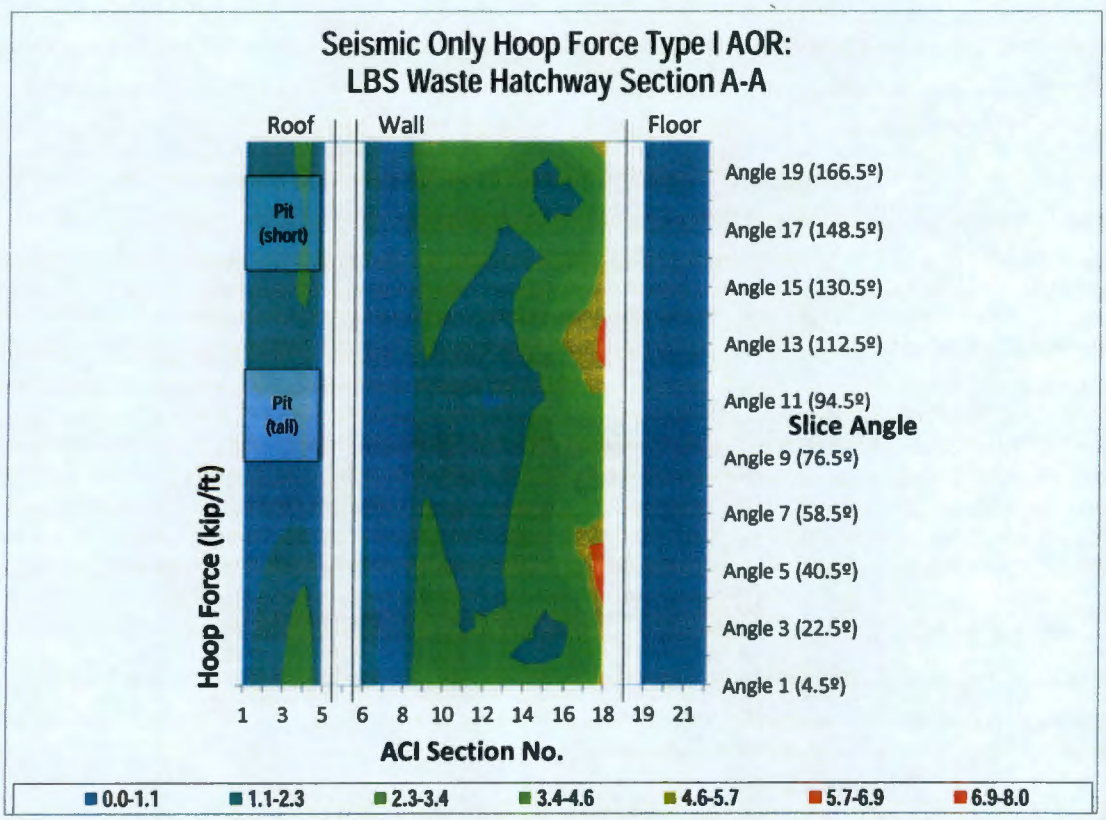

Figure 8-4. Lower Bound Soil (LBS), Full Tank, Hatchway Section A-A: Concrete Tank Hoop Force (kip/ft.) – Seismic Only

The seismic-only meridional moments in Figure 8-5 show that the demands at the roof are decreased by proximity to the hatchway, but the top of the wall shows sharp local increases. This local peak load corresponds to the stiffest load path beneath the hatchway and the tank. The influence of the hatchway does not extend beyond the top of the wall. The greatest demands in the roof are seen where the soil bears upon the roof.

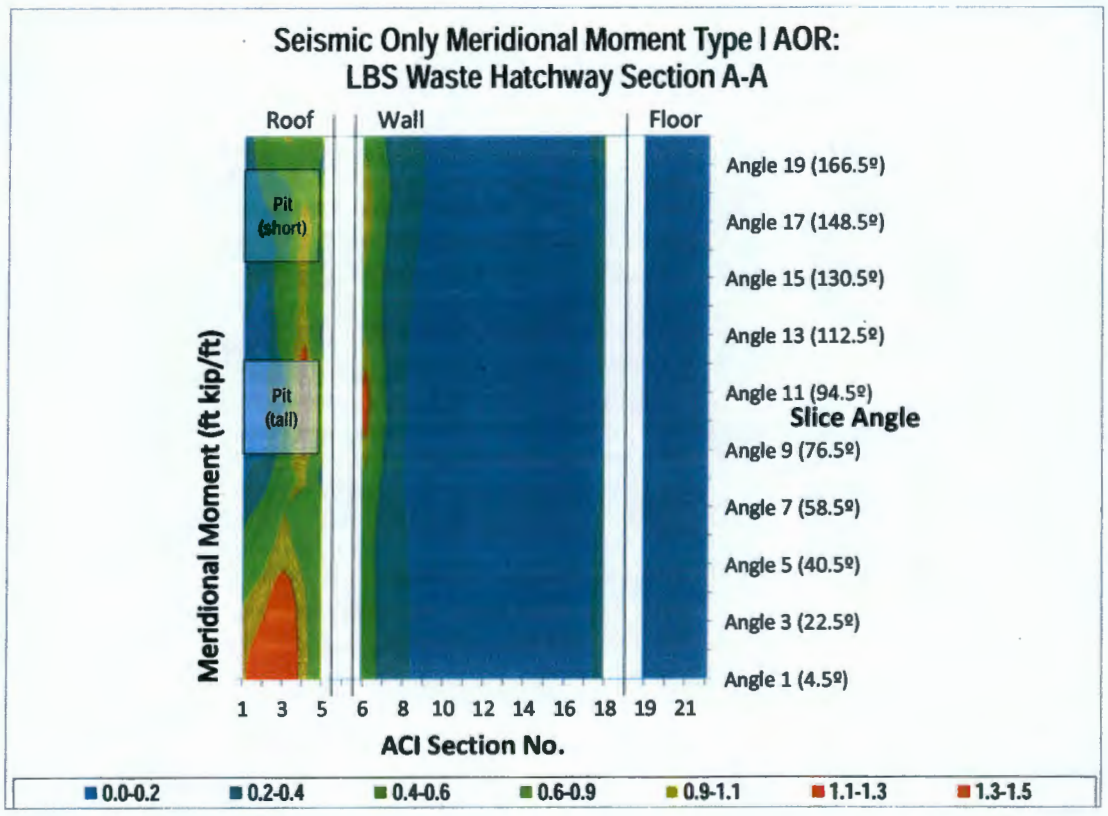

Figure 8-5. Lower Bound Soil (LBS), Full Tank, Hatchway Section A-A: Concrete Tank Meridional Moment (kip ft./ft.) – Seismic Only

The seismic-only hoop moments in Figure 8-6 show that the demands at the roof are increased by proximity to the hatchway, but the influence does not extend beyond the roof. The greatest demands in the roof are seen beneath the hatchway.

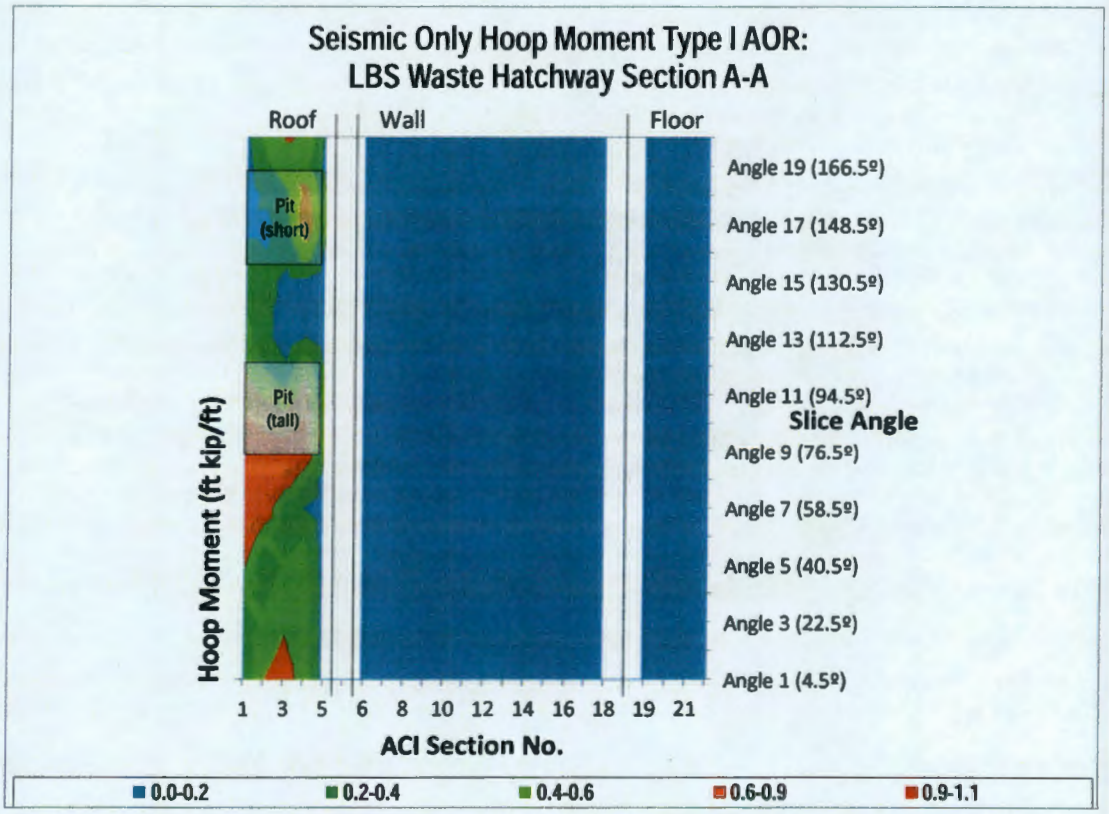

Figure 8-6. Lower Bound Soil (LBS), Full Tank, Hatchway Section A-A: Concrete Tank Hoop Moment (kip ft./ft.) – Seismic Only

The seismic-only through-wall shear forces in Figure 8-7 show that the demands at the roof are decreased by proximity to the hatchway, except at the top of the wall where the demands show sharp local increases. This local peak load corresponds to the stiffest load path beneath the hatchway and the tank. Elsewhere, the greatest demands in the roof are seen where the soil bears upon the roof, furthest from the wall. The influence of the hatchway does not extend beyond the top of the wall.

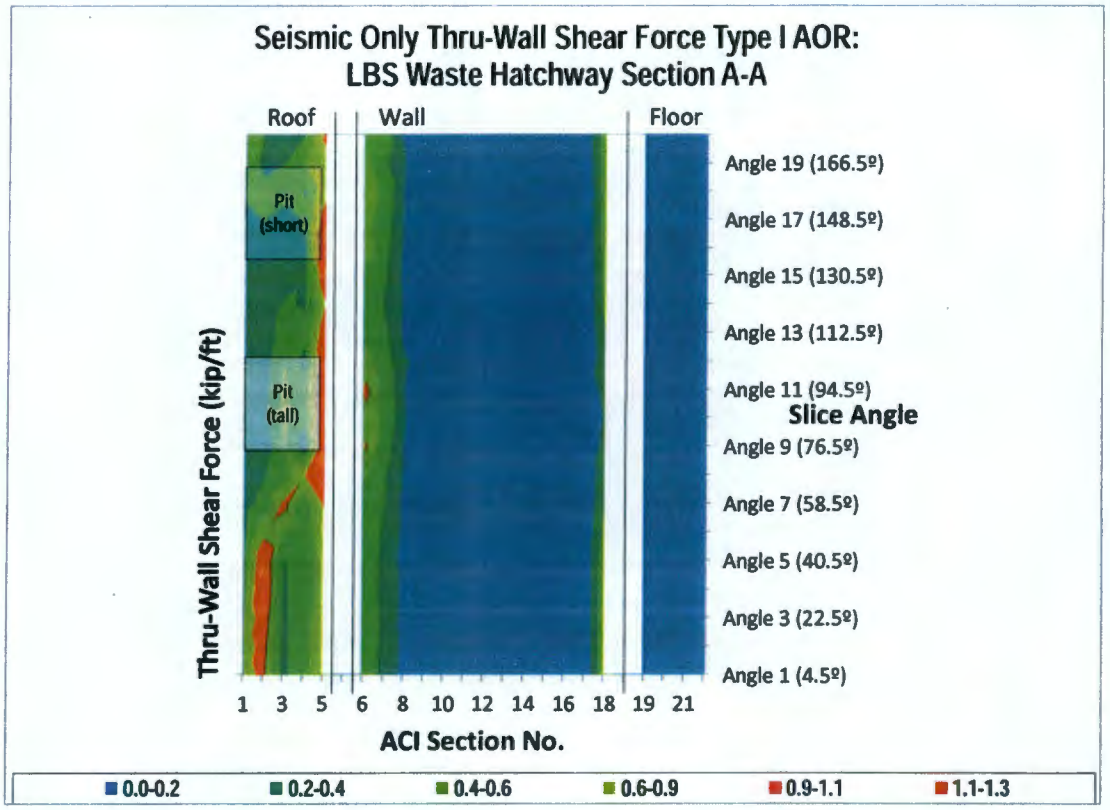

Figure 8-7. Lower Bound Soil (LBS), Full Tank, Hatchway Section A-A: Concrete Tank Through-Wall Shear Force (kip/ft.) – Seismic Only

The seismic-only in-plane shear forces in Figure 8-8 show that the demands have a low sensitivity to proximity to the hatchway.

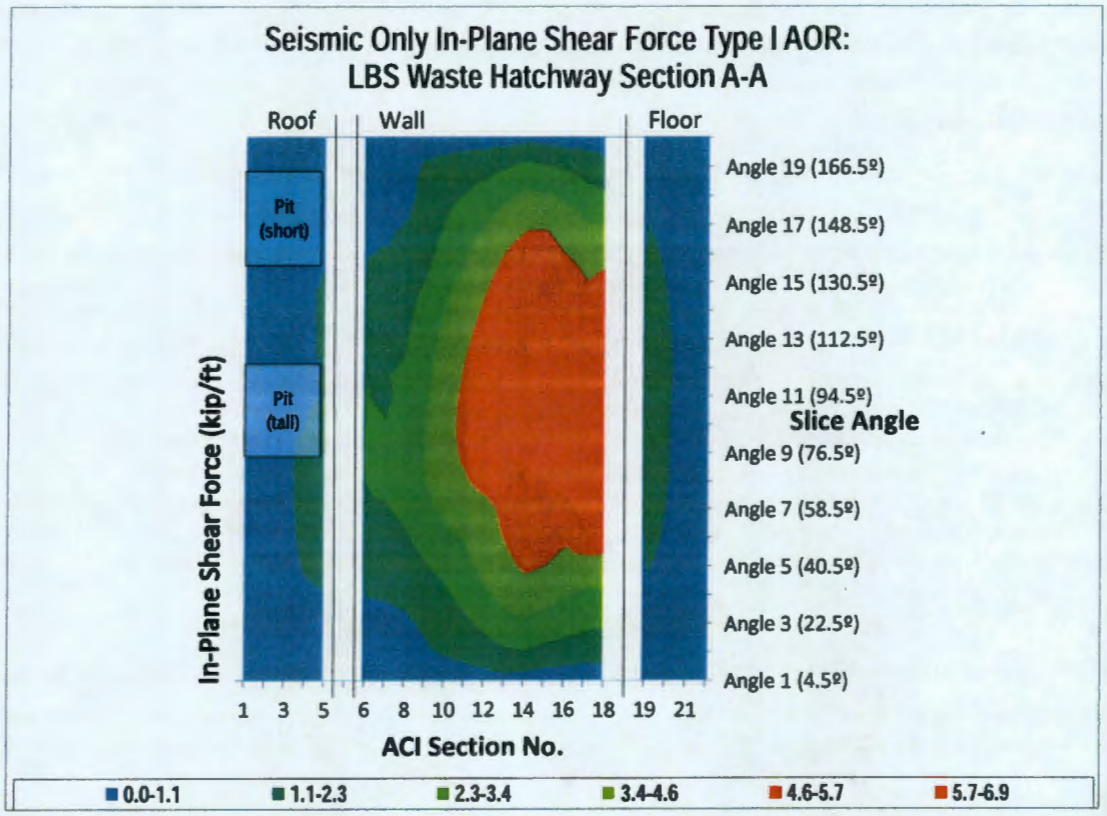

Figure 8-8. Lower Bound Soil (LBS), Full Tank, Hatchway Section A-A: Concrete Tank In-Plane Shear Force (kip/ft.) – Seismic Only

8.1.2 Best-Estimate Soil (BES)

The influence of the hatchway on the seismic-only demands is similar to that discussed in Section 8.1.1.

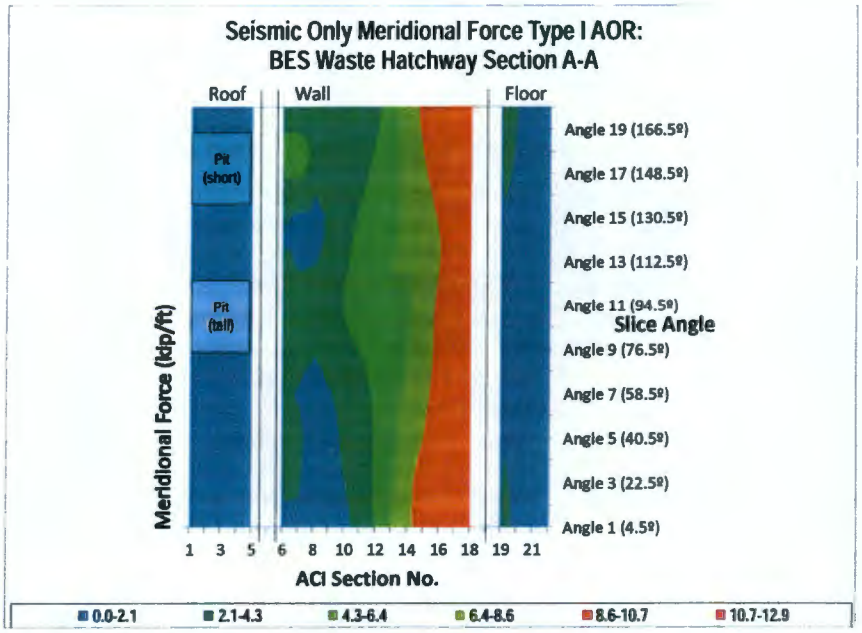

Figure 8-9. Best Estimate Soil (BES), Full Tank, Hatchway Section A-A: Concrete Tank Meridional Force (kip/ft.) – Seismic Only

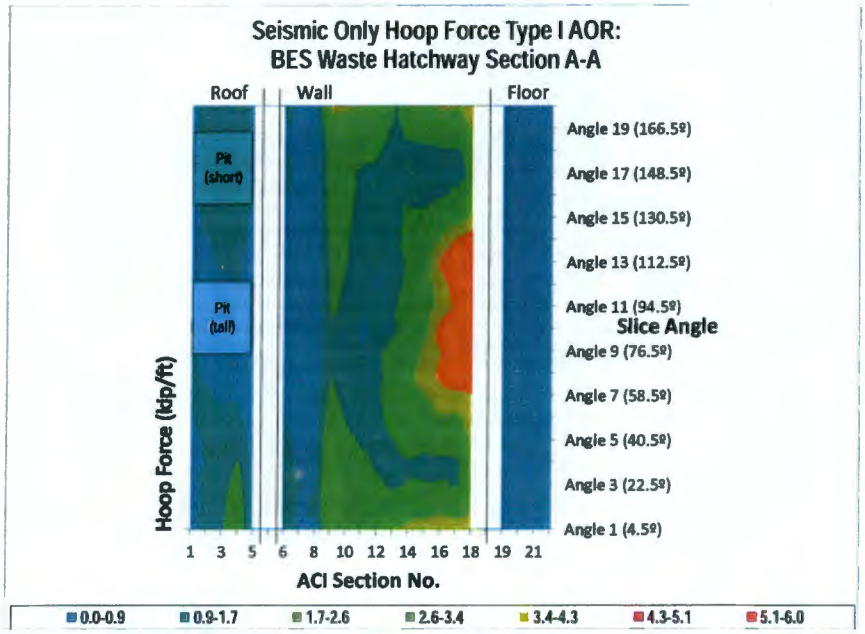

Figure 8-10. Best Estimate Soil (BES), Full Tank, Hatchway Section A-A: Concrete Tank Hoop Force (kip/ft.) – Seismic Only

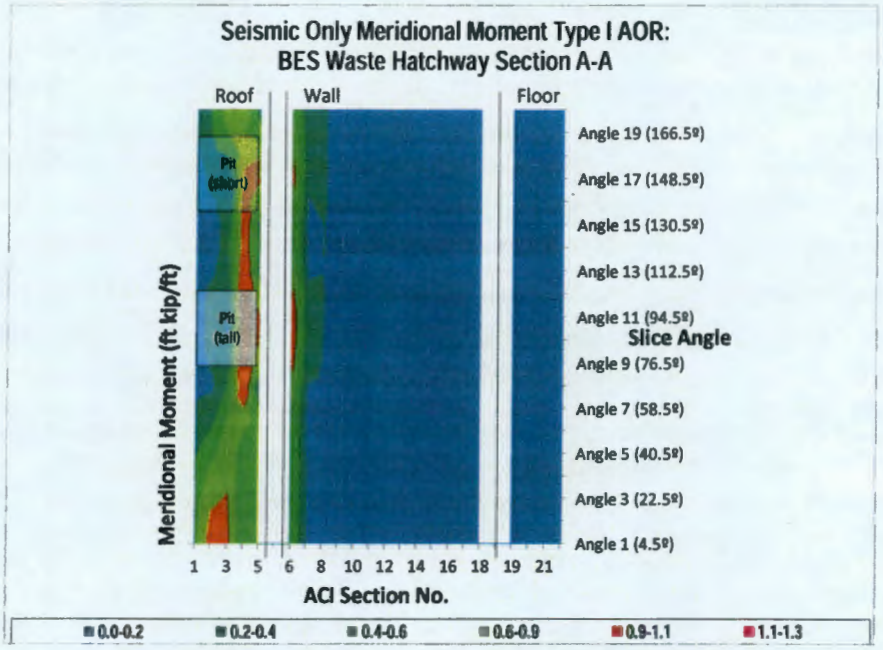

Figure 8-11. Best Estimate Soil (BES), Full Tank, Hatchway Section A-A: Concrete Tank Meridional Moment (kip ft./ft.) – Seismic Only

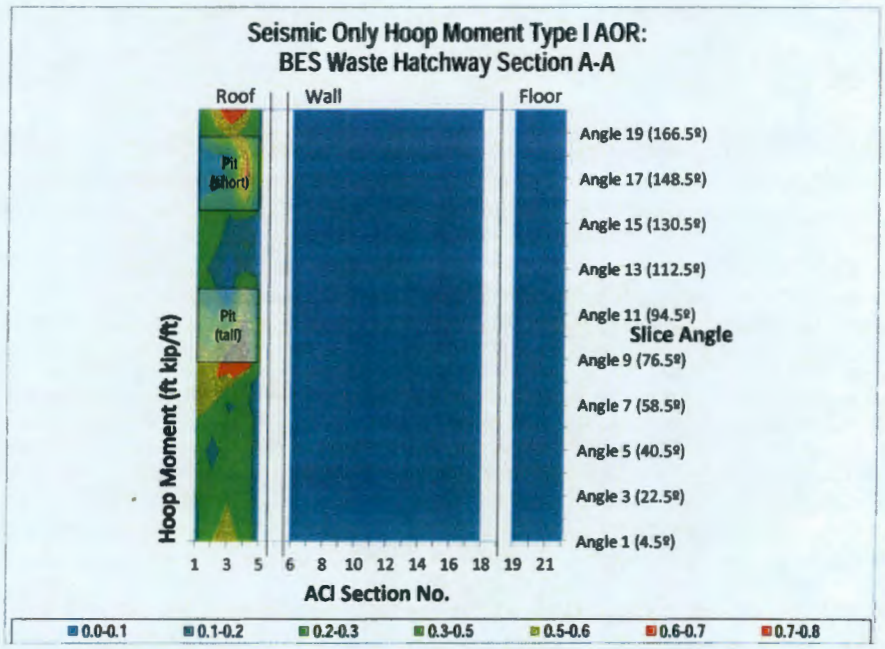

Figure 8-12. Best Estimate Soil (BES), Full Tank, Hatchway Section A-A: Concrete Tank Hoop Moment (kip ft./ft.) – Seismic Only

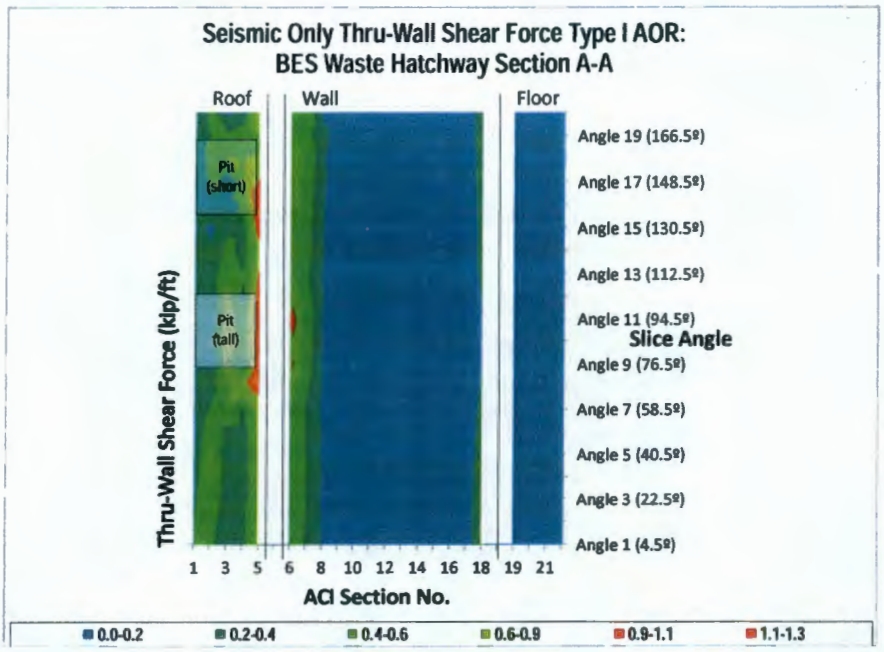

Figure 8-13. Best Estimate Soil (BES), Full Tank, Hatchway Section A-A: Concrete Tank Through-Wall Shear Force (kip/ft.) – Seismic Only

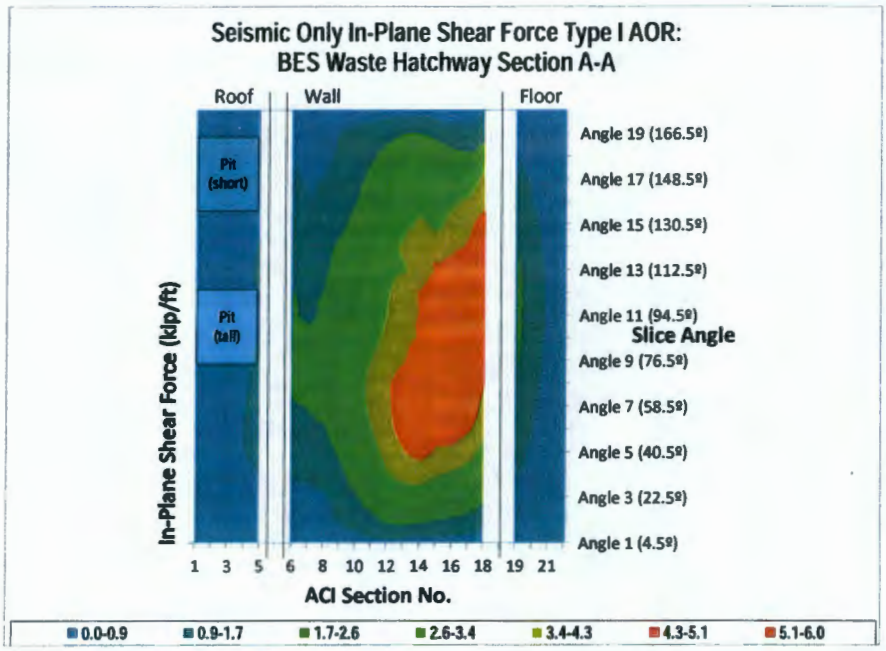

Figure 8-14. Best Estimate Soil (BES), Full Tank, Hatchway Section A-A: Concrete Tank In-Plane Shear Force (kip/ft.) – Seismic Only

8.1.3 Upper Bound Soil (UBS)

The influence of the hatchway on the seismic-only demands is similar to that discussed in Section 8.1.1.

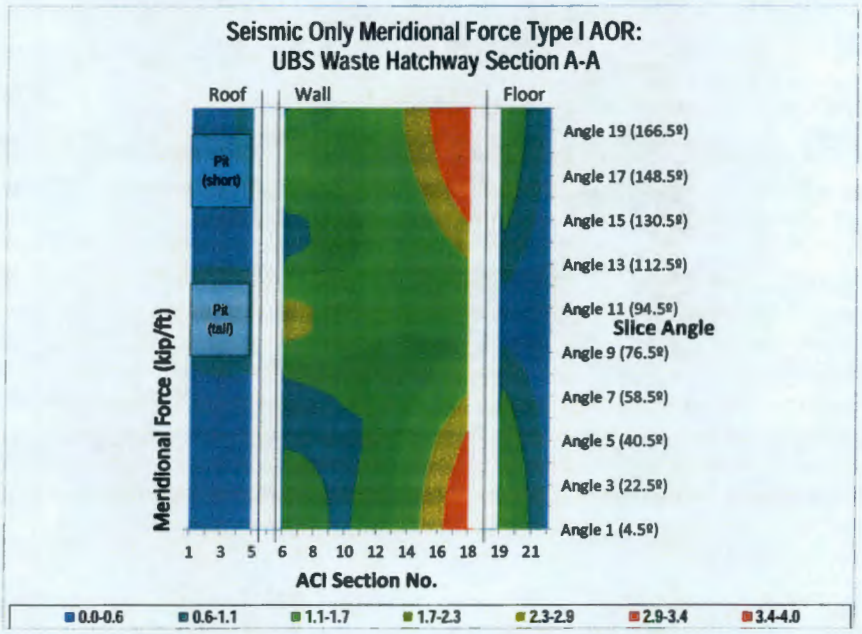

Figure 8-15. Upper Bound Soil (UBS), Full Tank, Hatchway Section A-A: Concrete Tank Meridional Force (kip/ft.) – Seismic Only

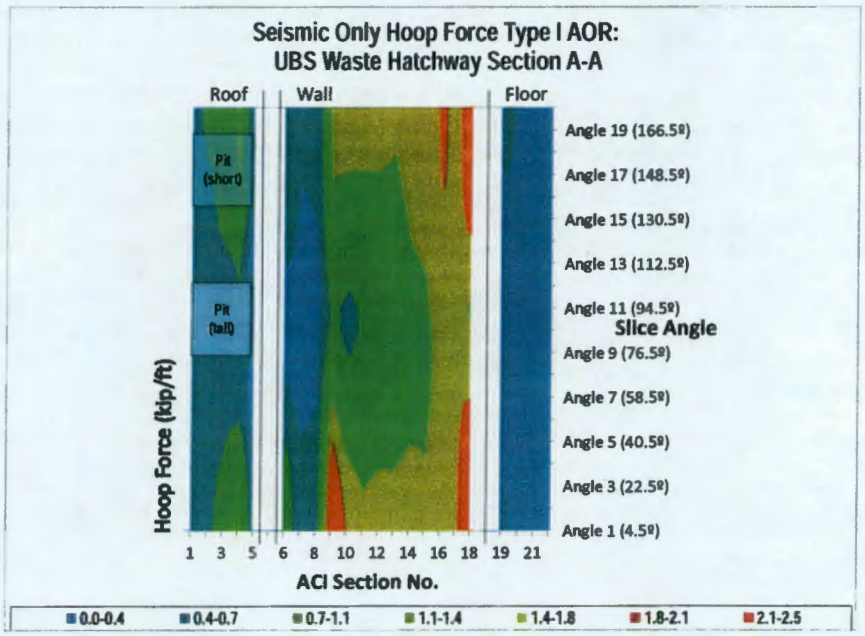

Figure 8-16. Upper Bound Soil (UBS), Full Tank, Hatchway Section A-A: Concrete Tank Hoop Force (kip/ft.) – Seismic Only

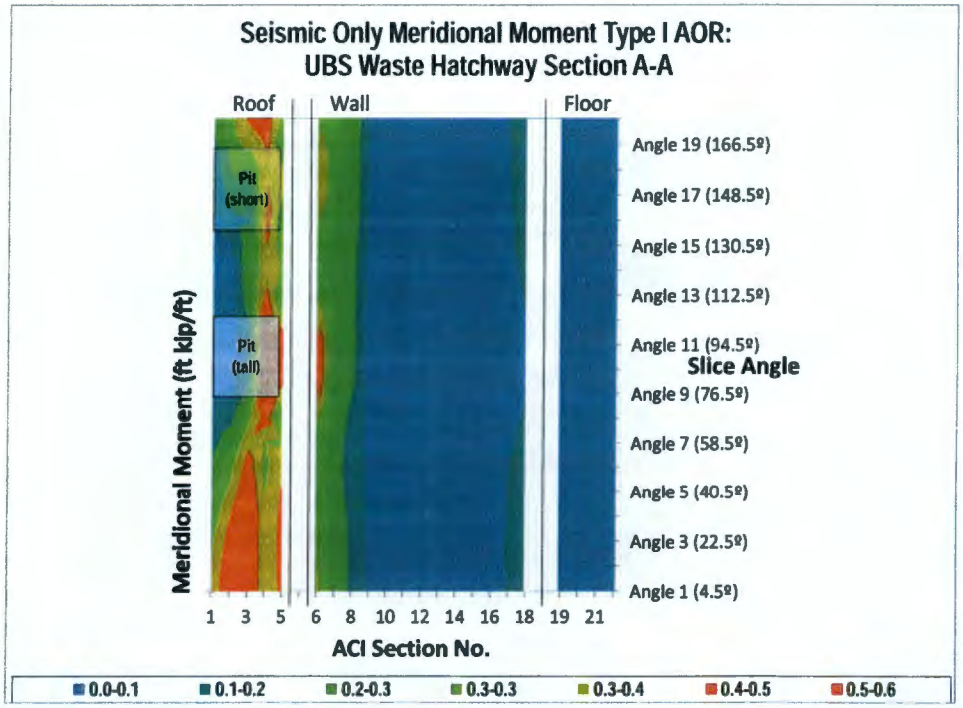

Figure 8-17. Upper Bound Soil (UBS), Full Tank, Hatchway Section A-A: Concrete Tank Meridional Moment (kip ft./ft.) – Seismic Only

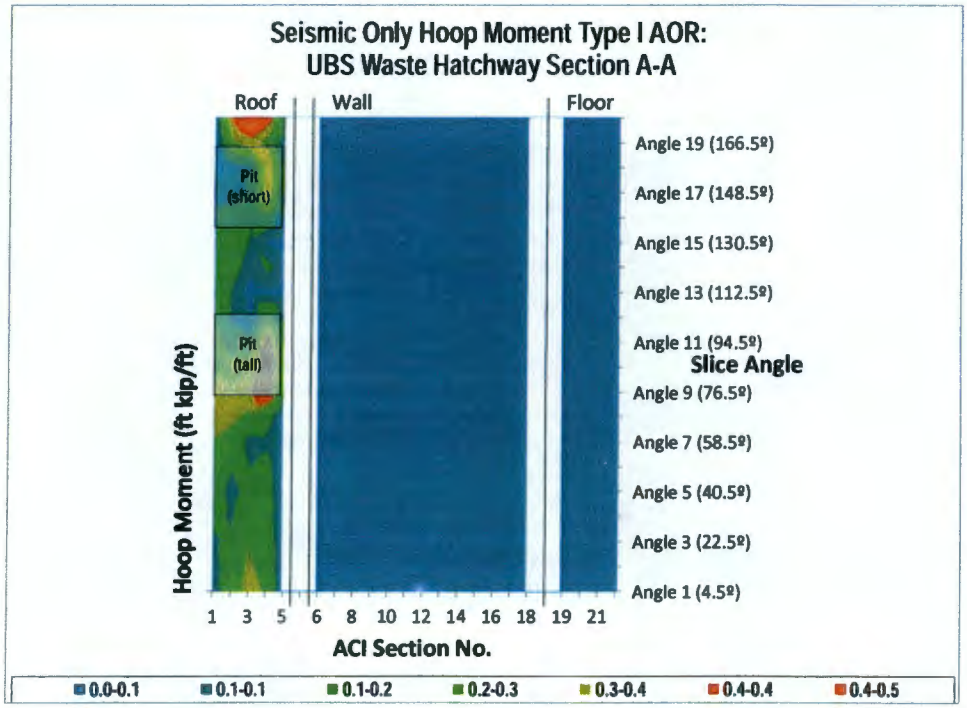

Figure 8-18. Upper Bound Soil (UBS), Full Tank, Hatchway Section A-A: Concrete Tank Hoop Moment (kip ft./ft.) – Seismic Only

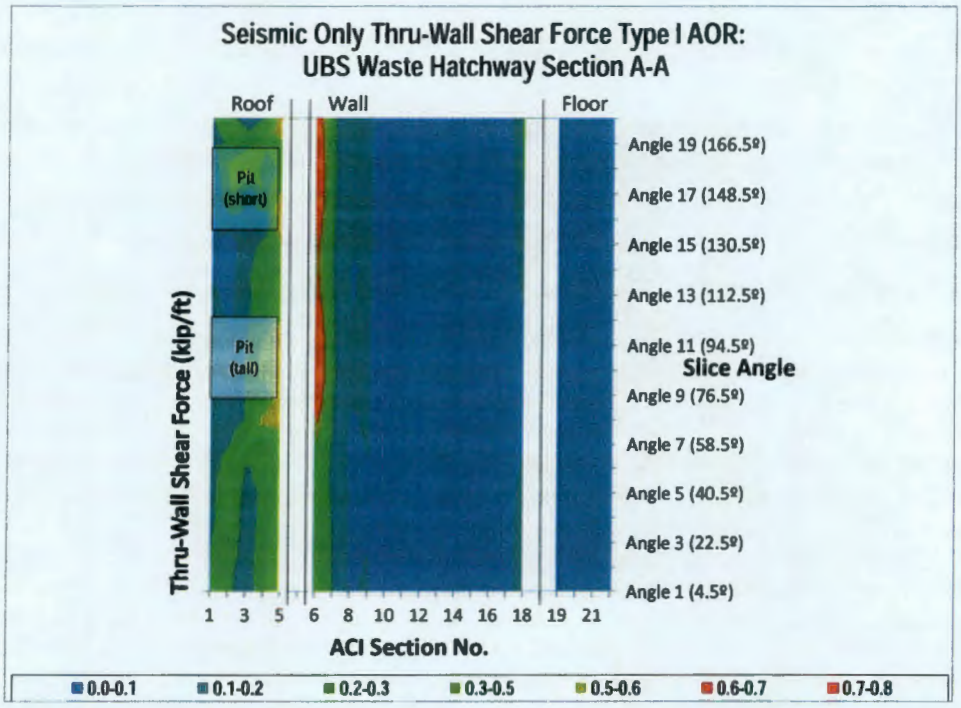

Figure 8-19. Upper Bound Soil (UBS), Full Tank, Hatchway Section A-A: Concrete Tank Through-Wall Shear Force (kip/ft.) – Seismic Only

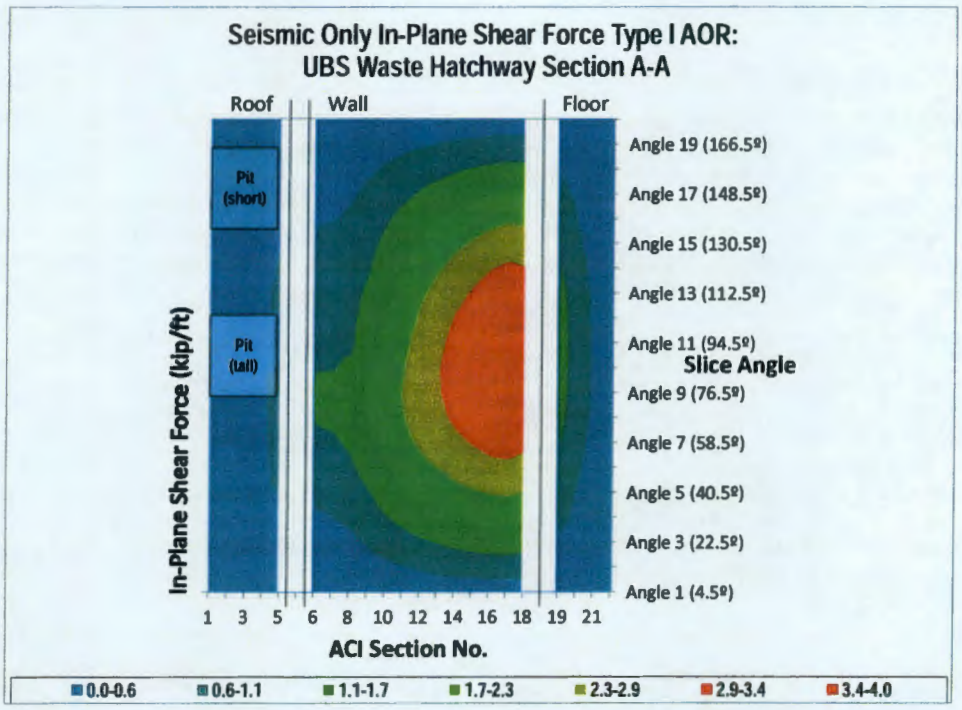

Figure 8-20. Upper Bound Soil (UBS), Full Tank, Hatchway Section A-A: Concrete Tank In-Plane Shear Force (kip/ft.) – Seismic Only

8.1.4 Summary of Seismic Demands

Figure 8-3 through Figure 8-20 show concrete demands for each of the soil cases. Figure 8-21 through Figure 8-26 show the enveloped maximum values around the tank perimeter and they include all run matrix cases on one plot in order to identify overall trends in the demands. The representative case used for demand/capacity evaluation (see Section 6.7.1, surface plots in Section 8.1.1) is uniquely marked in black for easy reference.

The seismic forces (excluding through-wall shear forces) show maximum values generally increasing toward the lower part of the wall. The seismic moments and in-plane shear forces show maximum values in the roof, typically with a smaller secondary peak at the bottom of the wall. All seismic demands in the floor are small relative to other locations.

The seismic-only demands typically show that the demands are sorted by soil profiles, with softer soil (LBS) increasing demands and stiffer soil (UBS) having the lowest demands. The seismic meridional and hoop forces have a limited region (only a couple of points) in the wall where the stiffer soil governs. Other than these notable but limited exceptions, the lower bound soil profile is governing. Within the lower bound (lower stiffness) soil configurations, hatchway section A-A (Figure 6-12) typically produces greater or similar demands compared to section B-B (Figure 6-13), and the demands typically have a low sensitivity to the presence of the waste. In some cases, such as meridional force in the roof, other configurations are significantly greater than the representative case from a relative demand perspective, but the demands there overall are too small to be significant from a structural integrity perspective. Although the overall sensitivity is typically low, the roof demands are more sensitive to the choice of hatchway orientation, and the wall demands are more sensitive to the presence or level of the waste.

The seismic-only meridional forces in Figure 8-21 show that the demands are typically driven by soil profiles, with softer soil increasing demands and stiffer soil having the lowest demands. The seismic-only meridional forces have several ACI-evaluation sections in the upper wall where the stiffer soil governs. Within the lower bound soil configurations, hatchway section A-A produces greater demands than section B-B in the wall. Section B-B governs in the roof, but the demands in the roof are all too low to be structurally significant. Within the lower bound soil configurations, the demands are insensitive to the presence of the waste.

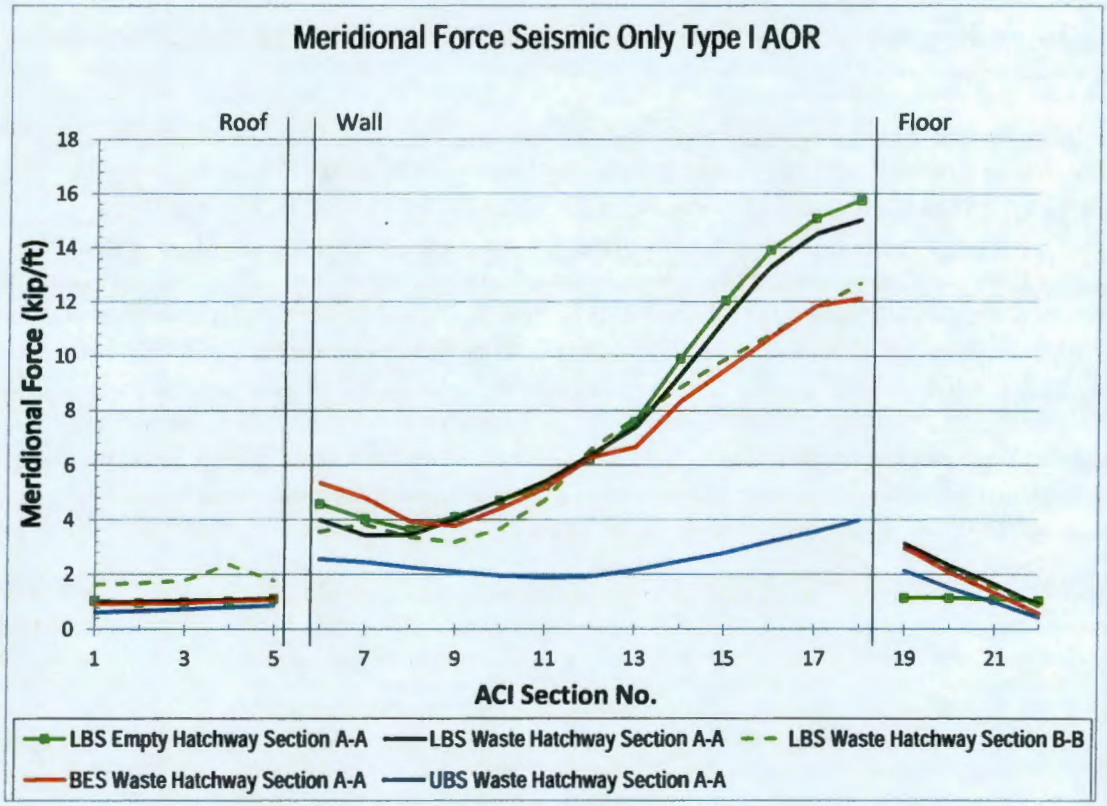

Figure 8-21. Seismic Results: Concrete Tank Meridional Force (kip/ft.) – Seismic Only

The seismic-only hoop forces in Figure 8-22 show that the demands are typically driven by soil profiles, with softer soil increasing demands and stiffer soil having the lowest demands. The seismic-only hoop forces have several ACI-evaluation sections in the middle of the wall where the stiffer soil governs. Within the lower bound soil configurations, hatchway section A-A produces greater demands than section B-B, except for several ACI-evaluation sections in the lower wall. Within the lower bound soil configurations, the demands are only sensitive to the presence of the waste near the middle of the wall.

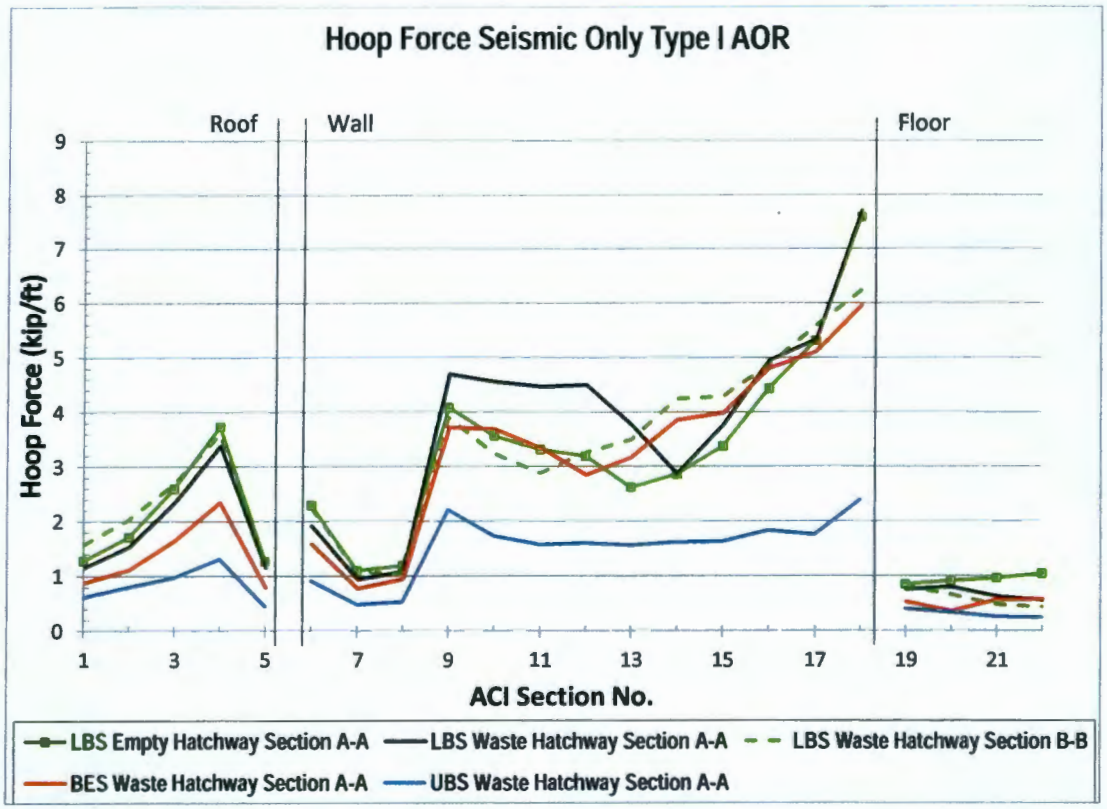

Figure 8-22. Seismic Results: Concrete Tank Hoop Force (kip/ft.) – Seismic Only

The seismic-only meridional moments in Figure 8-23 show that the demands are typically driven by soil profiles, with softer soil increasing demands and stiffer soil having the lowest demands. Within the lower bound soil configurations, the demands are insensitive to the hatchway section except in the center of the roof, where hatchway section A-A is greater. The demands in the wall are relatively small and closely grouped when compared to the demands in the roof. Within the lower bound soil configurations, the demands have a low sensitivity to the presence of the waste.

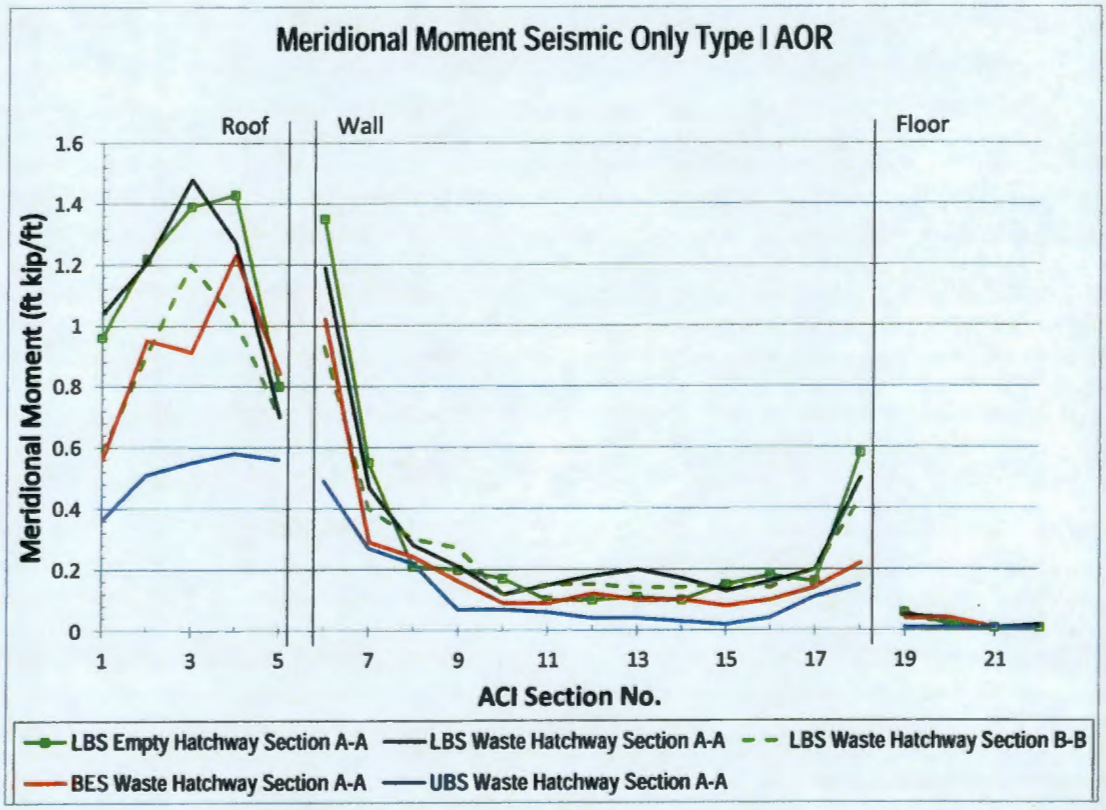

Figure 8-23. Seismic Results: Concrete Tank Meridional Moment (kip ft./ft.) – Seismic Only

The seismic-only hoop moments in Figure 8-24 show that the demands are typically driven by soil profiles, with softer soil increasing demands and stiffer soil having the least demands. Within the lower bound soil configurations, the demands are insensitive to the hatchway section except in the center of the roof, where hatchway section A-A is greater. The demands in the wall are relatively small and closely grouped when compared to the demands in the roof. Within the lower bound soil configurations, the demands are insensitive to the presence of the waste.

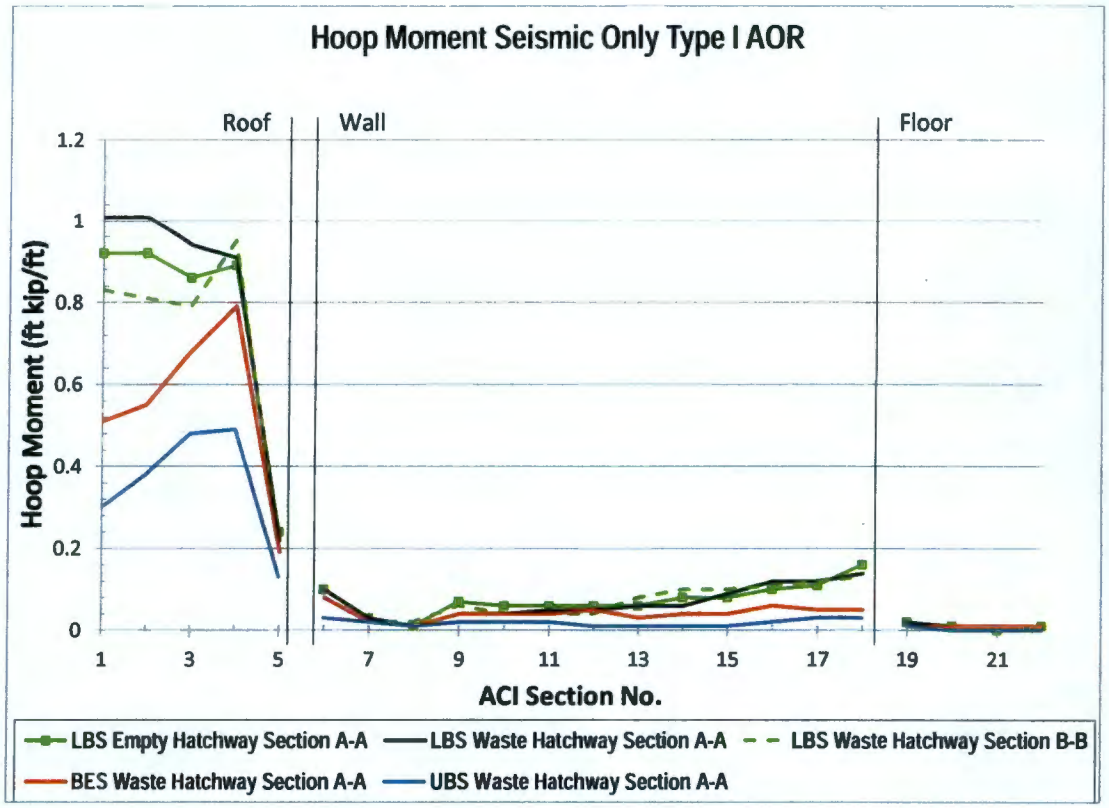

Figure 8-24. Seismic Results: Concrete Tank Hoop Moment (kip ft./ft.) – Seismic Only

The seismic-only through-wall shear forces in Figure 8-25 show that the demands are typically driven by soil profiles, with softer soil increasing demands and stiffer soil having the lowest demands. Within the lower bound soil configurations, the demands are insensitive to the hatchway section except in the center of the roof, where hatchway section A-A is greater. The demands in the wall are relatively small and closely grouped when compared to the demands in the roof. Within the lower bound soil configurations, the demands are insensitive to the presence of the waste.

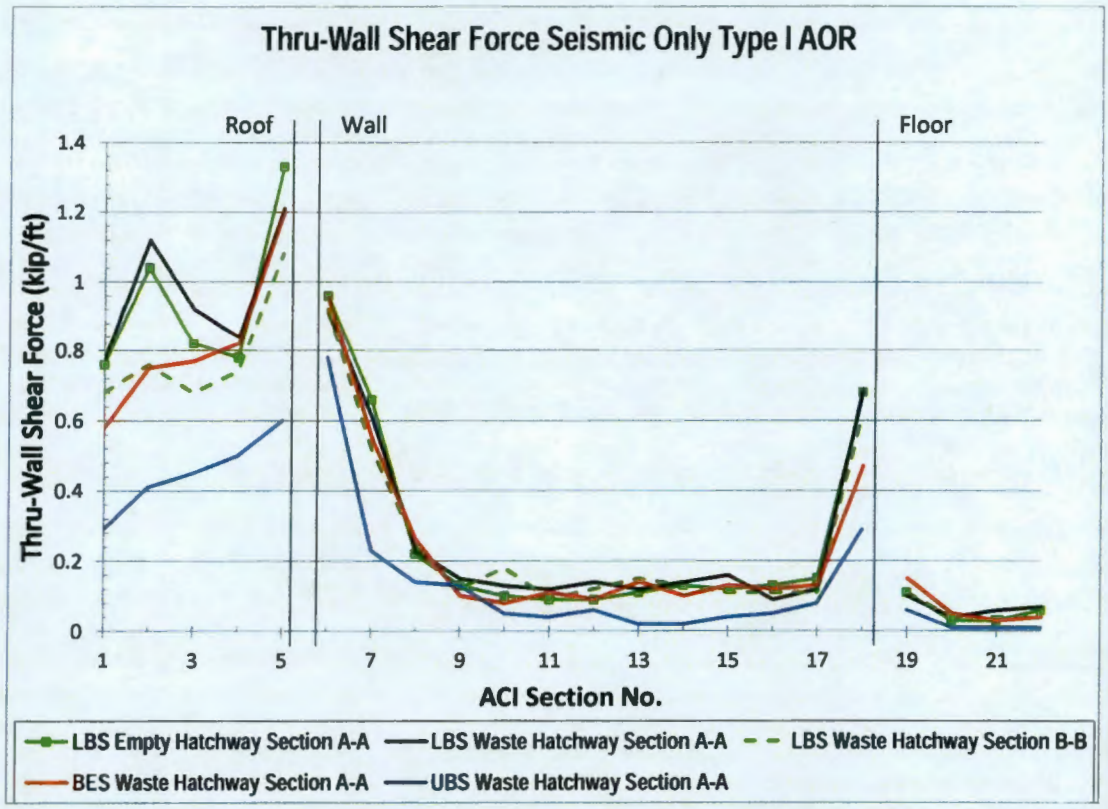

Figure 8-25. Seismic Results: Concrete Tank Through-Wall Shear Force (kip/ft.) – Seismic Only

The seismic-only in-plane shear forces in Figure 8-26 show that the demands are typically driven by soil profiles, with softer soil increasing demands and stiffer soil having the lowest demands. Within the lower bound soil configurations, the demands have a low sensitivity to the hatchway section. Within the lower bound soil configurations, the demands have a low sensitivity to the presence of the waste, with small differences increasing toward the bottom of the wall.

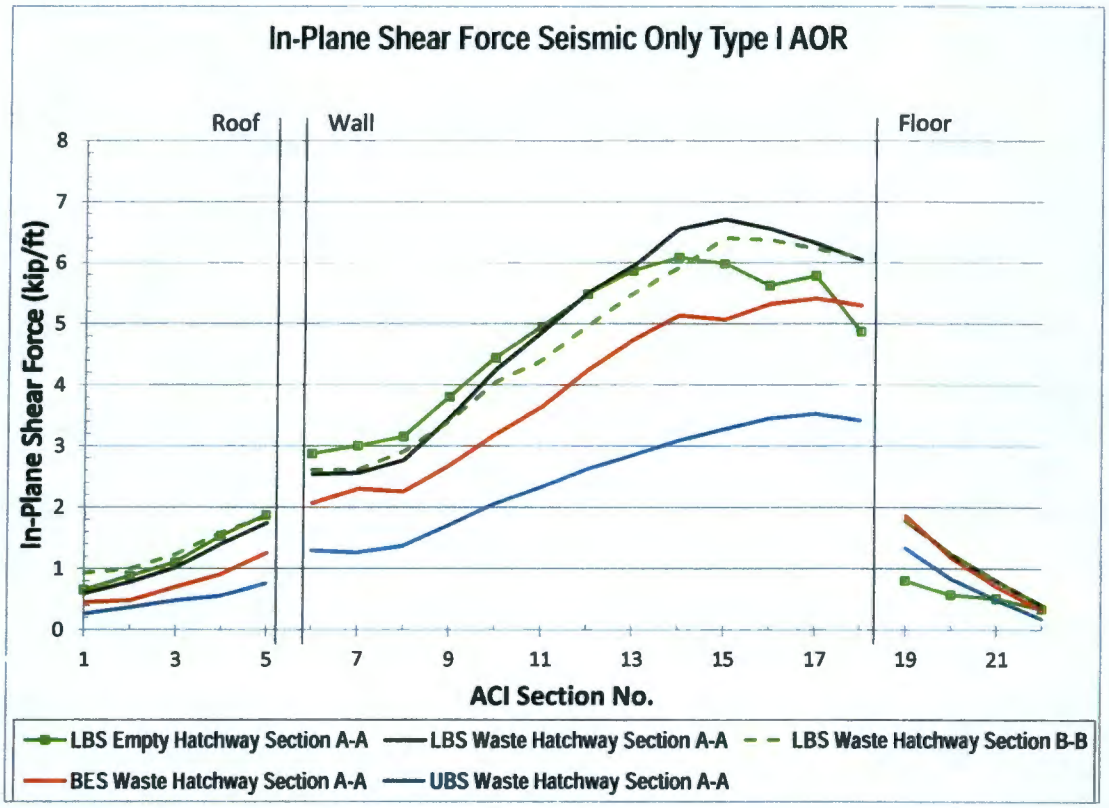

Figure 8-26. Seismic Results: Concrete Tank In-Plane Shear Force (kip/ft.) – Seismic Only

8.2 Soil Contact Results

Tank-to-soil contact results are post-processed using the same methods as for the concrete tank forces and moments. The contact results are plotted against the ACI-evaluation section sequence that starts near the center of the roof and moves radially along the roof, down the sidewall, then from the outside to the center of the tank floor. Contact results plots are as follows:

- Figure 8-27. Soil/Concrete Tank Contact Element Normal Pressure in Tank Wall (kip/sq. ft.) – Gravity Only
- Figure 8-28. Soil/Concrete Tank Contact Element Bounding Normal Pressure – Seismic Only

The contact pressure gravity results are included to demonstrate the effectiveness of the at-rest adjustments in the wall. For more details, see Section 6.2.

Contact pressures show maximum values in the roof and the footing for all load configurations, as expected. Gravity-only contact pressures follow the theoretical at-rest pressure profile due to the slip planes in the soil overburden above the roof and the manual adjustment in the wall (see Section 6.2.4). For seismic-only contact pressure in the wall, the full tank configurations tend to have greater pressures than the empty tank configurations.

The gravity-only soil/concrete tank contact element normal pressures in Figure 8-27 all follow the theoretical at-rest profile in the wall. Small variations occur at the top of the wall as a result of local effects from the hatchway.

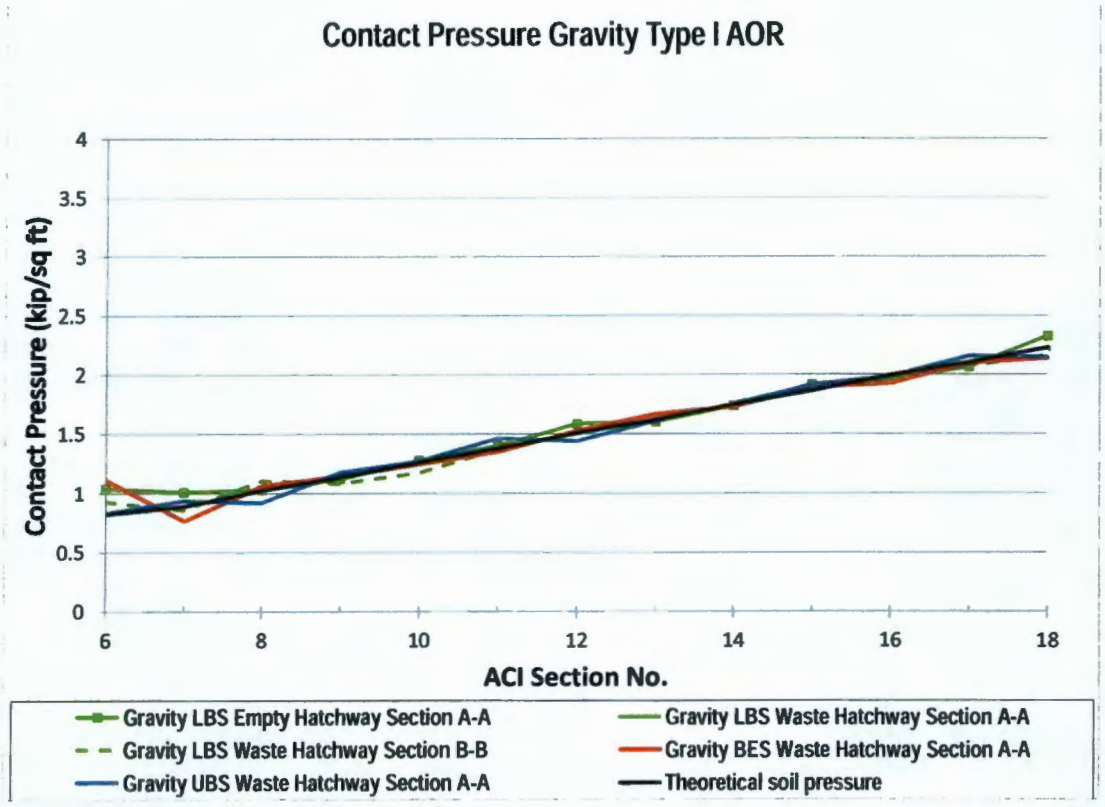

Figure 8-27. Soil/Concrete Tank Contact Element Normal Pressure in Tank Wall (kip/sq. ft.) – Gravity Only

The seismic-only soil/concrete contact element bounding normal pressure in Figure 8-28 shows clear sensitivity to the waste configuration at the wall, with the greatest demands for full tank and the least demands for an empty tank. The roof has a low sensitivity to the presence of the waste.

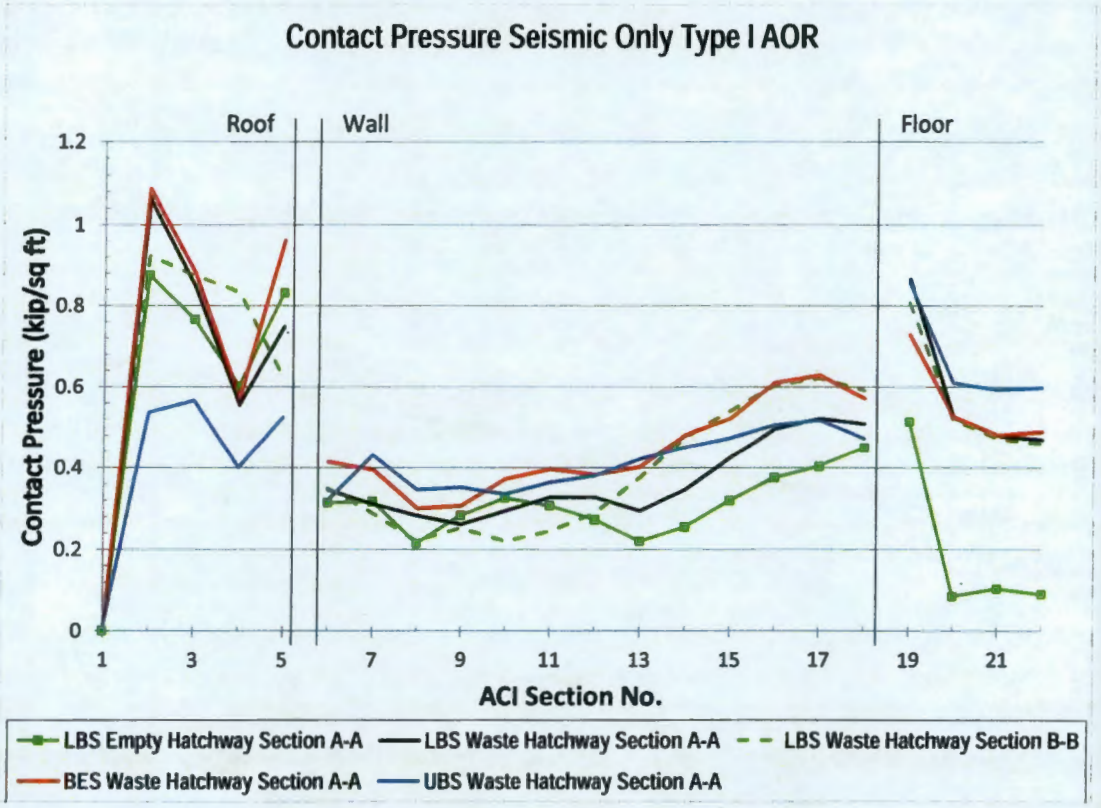

Figure 8-28. Soil/Concrete Tank Contact Element Bounding Normal Pressure – Seismic Only

9.0 Calculation Verification

Verifier: Brian Larsen cn=Brian Larsen, o=Becht Engineering Company, Inc., ou=Becht Nuclear Services, email=blarsen@becht.com, c=US 2014.10.14 08:16:54 -07'00'

	Verification Method	Verification Scope
☒	Line-by-Line Review	Entire calculation.
☐	Alternate Calculations	

Line-by-Line Review Checklist

	Verification Attribute	Yes	N/A	No(1)
1	Coversheet complete and page count correct?	X		
2	Revision is alpha if there are open items?		X	
3	Calculation headers complete?	X		
4	Attachments are listed and included?	X		
5	Calculation objective clearly stated?	X		
6	Scope (boundaries) of calculation clearly stated?	X		
7	Open items clearly stated?		X	
8	Design criteria clear and complete?	X		
9	Input drawings and specifications listed in references with revision or edition number?	X		
10	Applicable codes, standards listed in references with revision or edition number?	X		
11	Input parameters are in accordance with references, reasonable or conservative?	X		
12	Geometry, sizes, properties are in accordance with references or conservative?	X		
13	Input loads and load combinations in accordance with references or conservative?	X		
14	Formulas and software used appropriate and within their range of applicability?	X		
15	References include the computer program verification document?	X		
16	Software version is consistent with V&V, and valid for the computer used?	X		
17	Results clearly stated, and reasonable?	X		

Notes:
1. If "No" is selected then an explanation is provided in the following verifier comments.

Verifier Comments (If Necessary)

#	Location	Comment
1	n/a	ANSYS input files common to multiple runs (e.g. tank concrete material properties) were compared for consistency. ANSYS input files common to previous AORs (e.g. soil properties) were compared to previous AORs for consistency.

Appendix A — Manhole Penetration

A.1 Introduction

The Type I tank design includes a 42 in. diameter manhole penetration (see Figure 6-5). The effect of the manhole on concrete tank demands is investigated because the manhole diameter is 18% of the tank radius, which may cause significant change in local demands.

A.2 Type I SST Manhole Penetration Model

The Type I SST manhole penetration model development is the same as the Type I SST baseline seismic model (see Section 6.0) except for the addition of a hole in the roof (see Figure A-1). The manhole penetration hole is inserted into the Lower Bound Soil (LBS) full tank with hatchway section A-A (baseline) model tank roof via input file TKCP.inp. The location of the manhole is taken from drawing D-20 (see detail in Figure 6-5). The penetration analysis is not performed for all the material property combinations as it is not part of the Type I SST main evaluation.

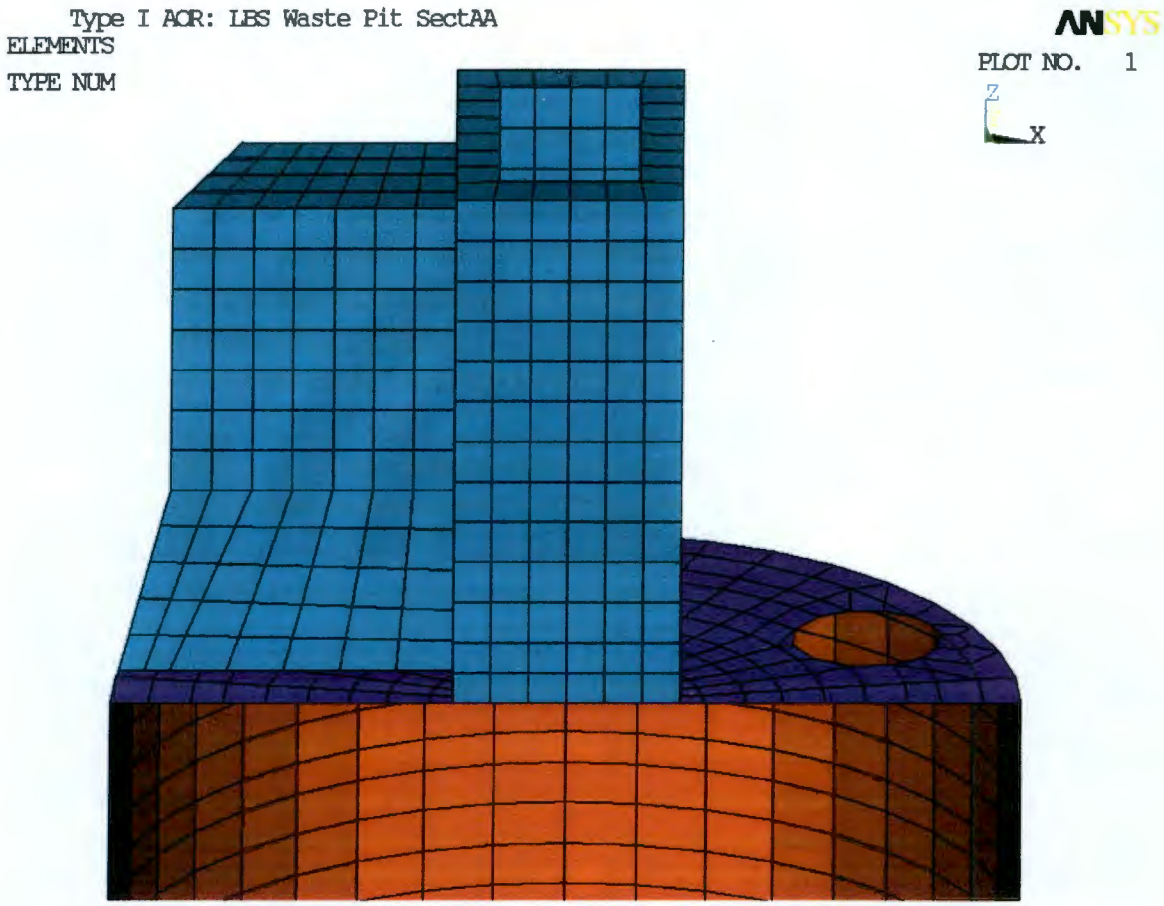

Figure A-1. Element Plot Showing Tank with Manhole Penetration and Hatchway at Section A-A

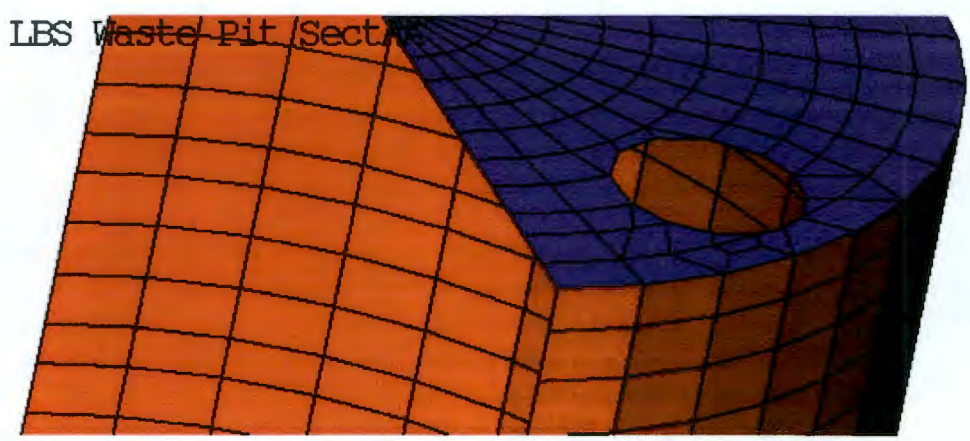

Figure A-2. Element Plot Angled View Detail Showing Tank with Manhole Penetration

As described in Section 6.6.1, tank concrete demands are taken from the elements *nearest* the ACI-evaluation section location as shown in Figure A-3. Elements at ACI-evaluation section locations that are inside the penetration (i.e. not present) are skipped entirely in postprocessing.

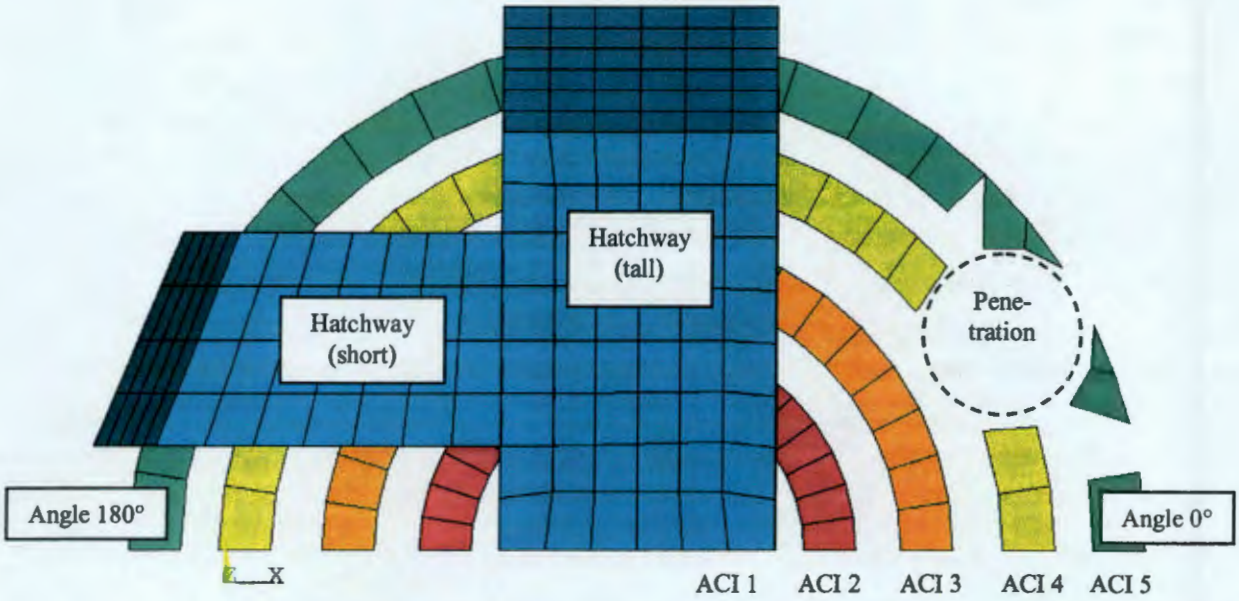

Figure A-3. Element Plot Top View Showing Tank Elements at ACI-Evaluation Sections 1-5 (roof) with Manhole Penetration and Hatchway at Section A-A

A.3 Results

Concrete tank force and moment results are extracted from the model using the post-processing methods described in Section 6.6. The forces and moments are plotted against the ACI-evaluation section sequence that starts near the center of the roof and moves radially along the roof, down the sidewall, then from the outside to the center of the tank floor. Forces and moments have been enveloped circumferentially for the two-dimensional plots (Figure A-4b through Figure A-9b). As the tank floor is not critical to tank structural integrity, it will not be highlighted in the following discussions.

The effects of the manhole penetration are seen in spatial demands shown on the surface plots (Figure A-4 through Figure A-9a), and by fully enveloped comparison to the baseline model without the manhole penetration (Figure A-4b through Figure A-9b). For ease of reference, the location of the manhole penetration is identified on the surface plots.

The presence of the manhole penetration produces a different roof response and a redistribution of demand relative to the baseline model without penetration. Small localized increases in demands are seen in the roof, but there are no significant changes in the demands elsewhere. During original construction additional reinforcing steel was provided around the manhole. Because the manhole was part of the original design, and the effects on the concrete demands are small and localized, it is not considered necessary to include the manhole in the baseline model.

The localized effects of the penetration are too small to be seen in the surface plot (Figure A-4a), and insignificant localized differences are seen in the enveloped plot (Figure A-4b).

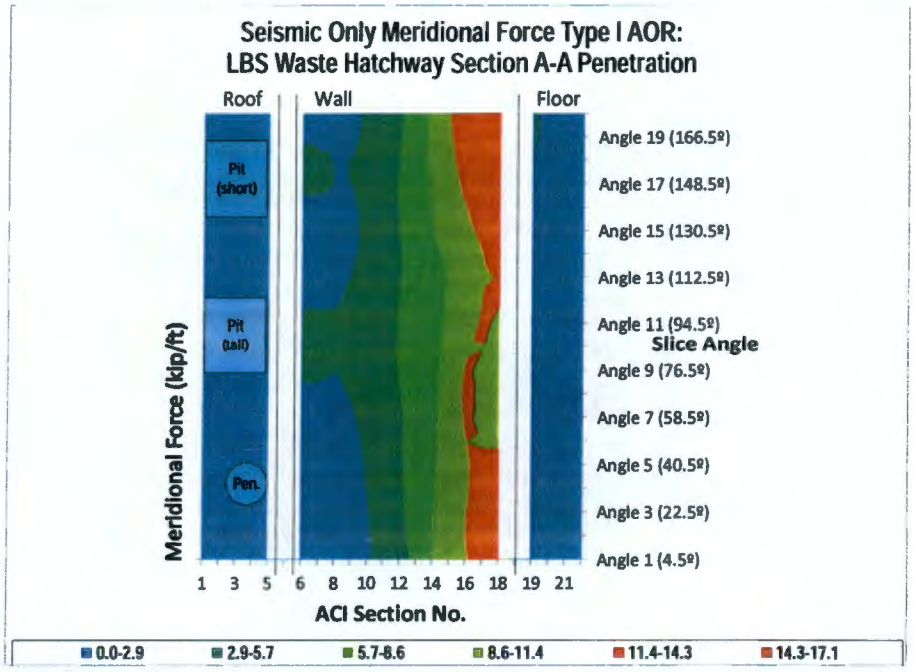

Figure A-4a. Manhole Penetration Study: Concrete Tank Meridional Force Surface Plot – Seismic Only

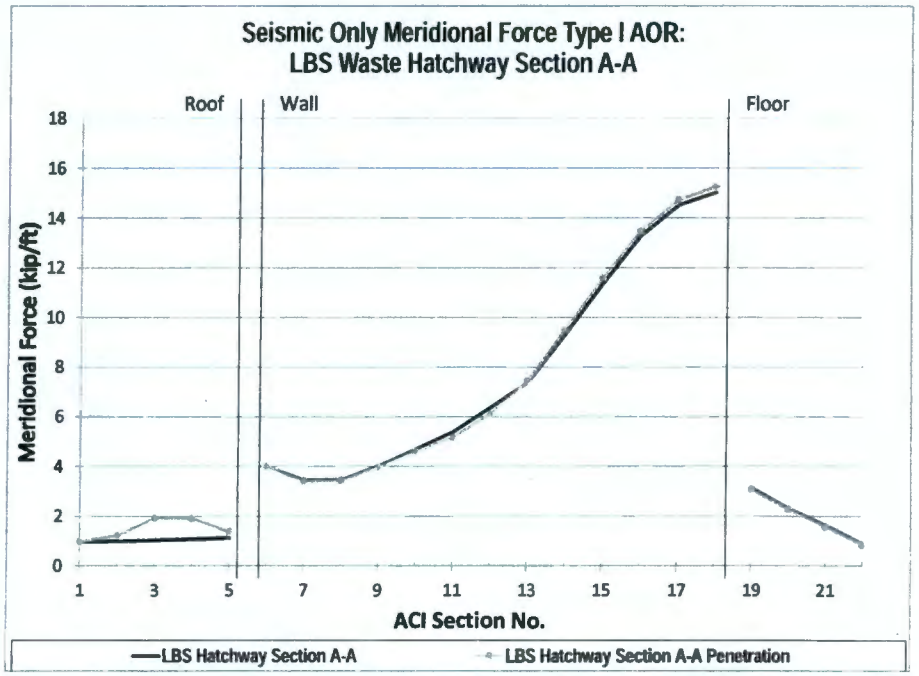

Figure A-4b. Manhole Penetration Study: Concrete Tank Meridional Force Comparison – Seismic Only

The localized effects of the penetration are barely visible in the surface plot (Figure A-5a), and insignificant localized differences are seen in the enveloped plot (Figure A-5b).

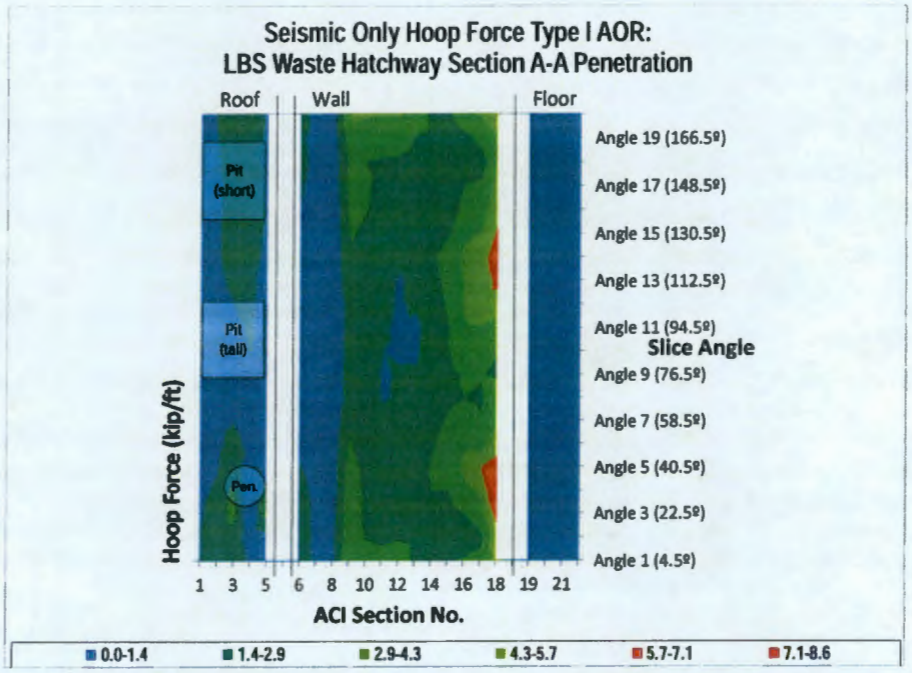

Figure A-5a. Manhole Penetration Study: Concrete Tank Hoop Force Surface Plot – Seismic Only

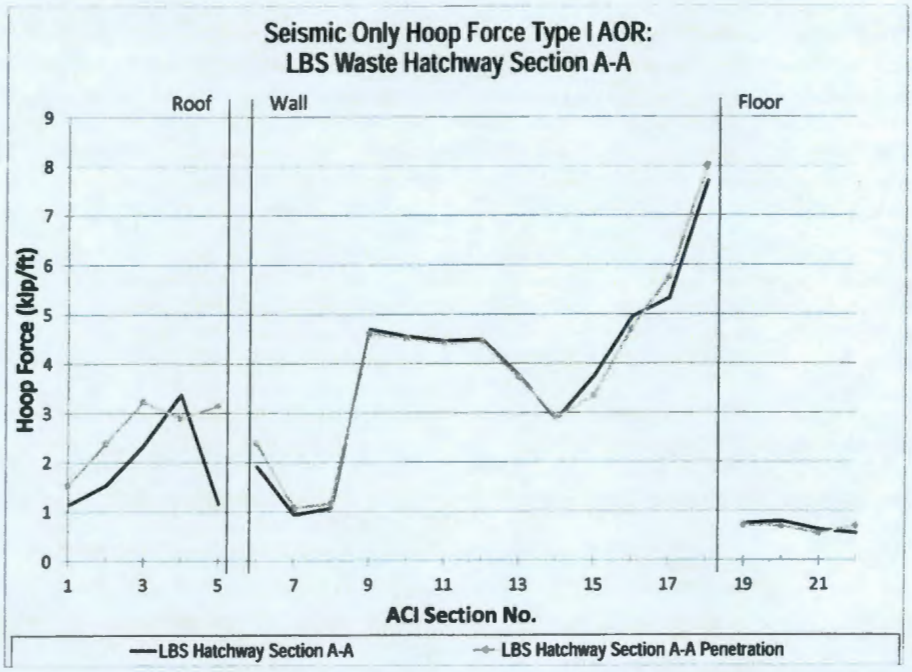

Figure A-5b. Manhole Penetration Study: Concrete Tank Hoop Force Comparison– Seismic Only

The localized effects of the penetration are clearly visible in the surface plot (Figure A-6a), but these local effects are only a small increase as seen in the enveloped plot (Figure A-6b).

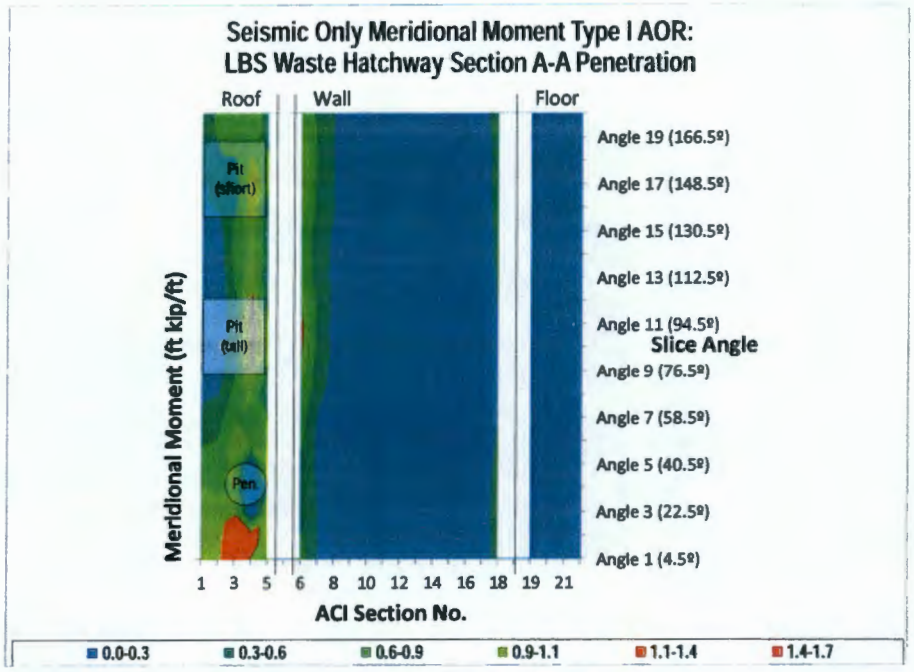

Figure A-6a. Manhole Penetration Study: Concrete Tank Meridional Moment Surface Plot – Seismic Only

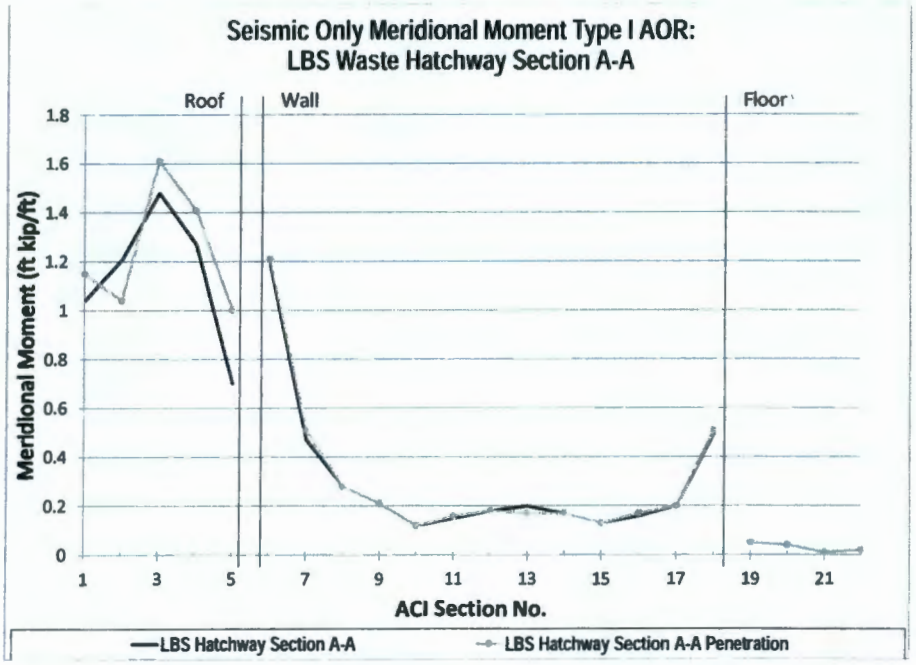

Figure A-6b. Manhole Penetration Study: Concrete Tank Meridional Moment Comparison – Seismic Only

The localized effects of the penetration are too small to be seen in the surface plot (Figure A-7a), and insignificant localized differences are seen in the enveloped plot (Figure A-7b).

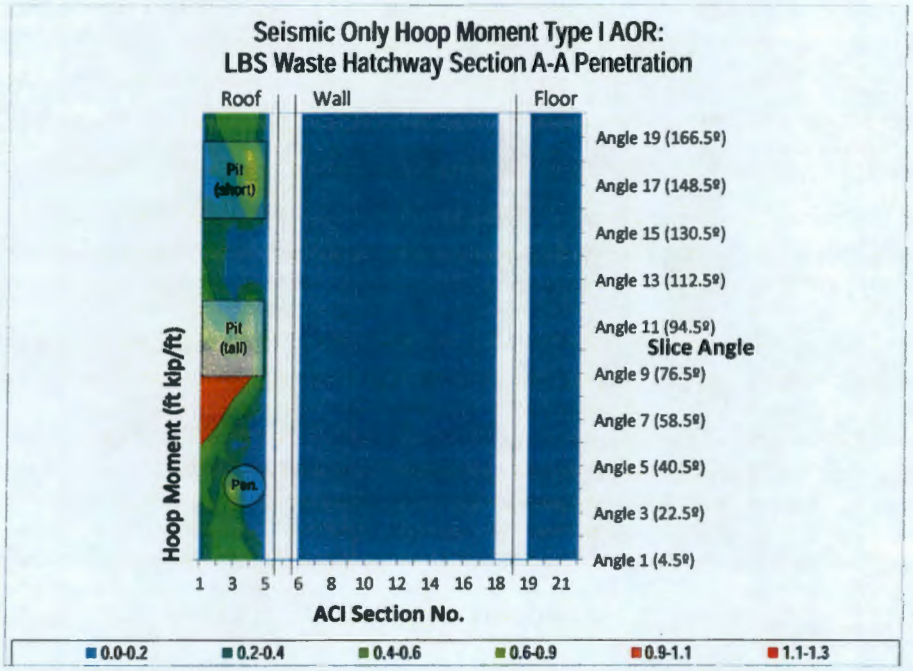

Figure A-7a. Manhole Penetration Study: Concrete Tank Hoop Moment Surface Plot – Seismic Only

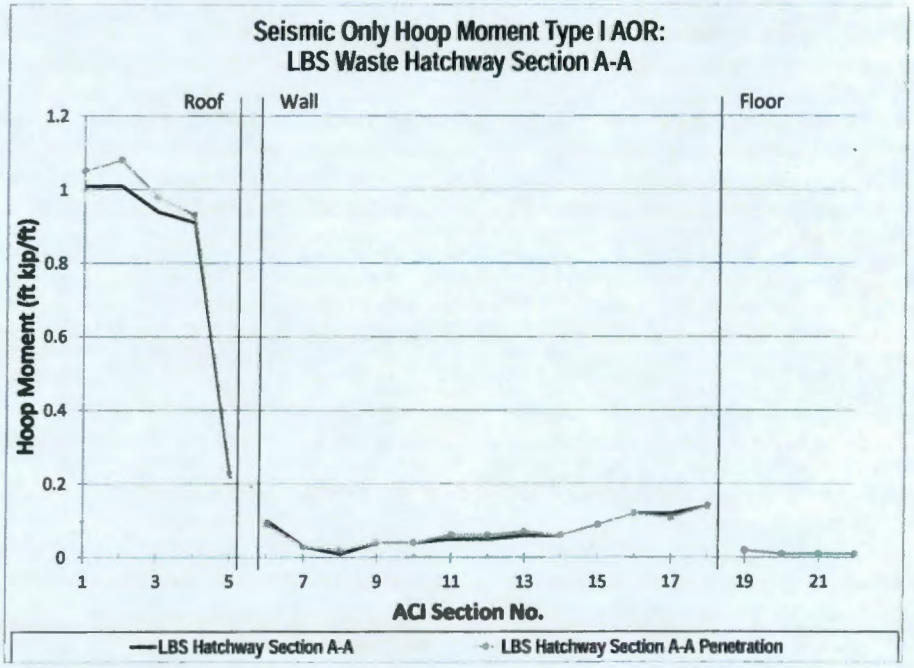

Figure A-7b. Manhole Penetration Study: Concrete Tank Hoop Moment Comparison – Seismic Only

The localized effects of the penetration are clearly visible in the surface plot (Figure A-8a), but these local effects are only a small increase as seen in the enveloped plot (Figure A-8b).

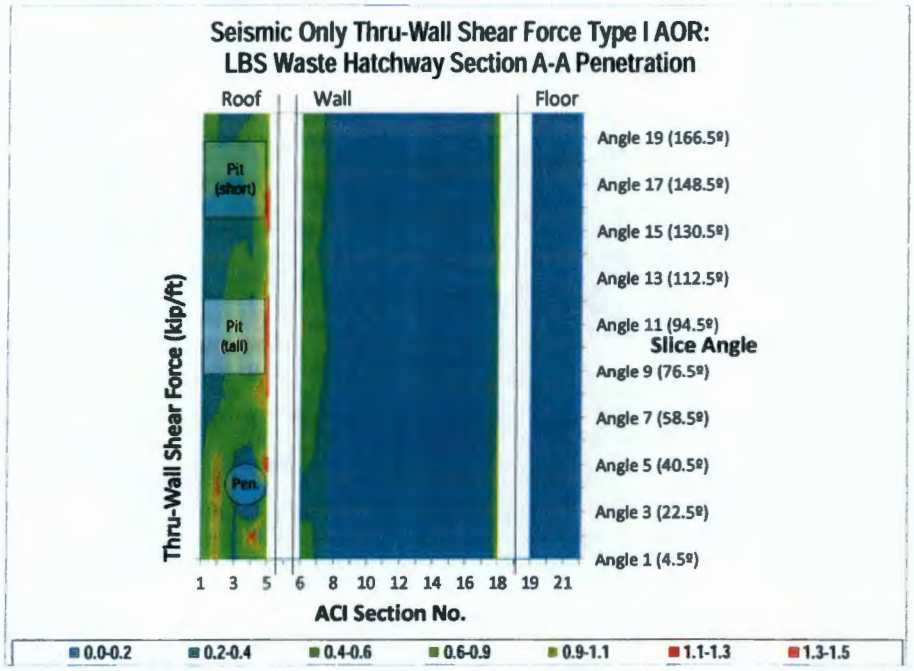

Figure A-8a. Manhole Penetration Study: Concrete Tank Through-Wall Shear Force Surface Plot – Seismic Only

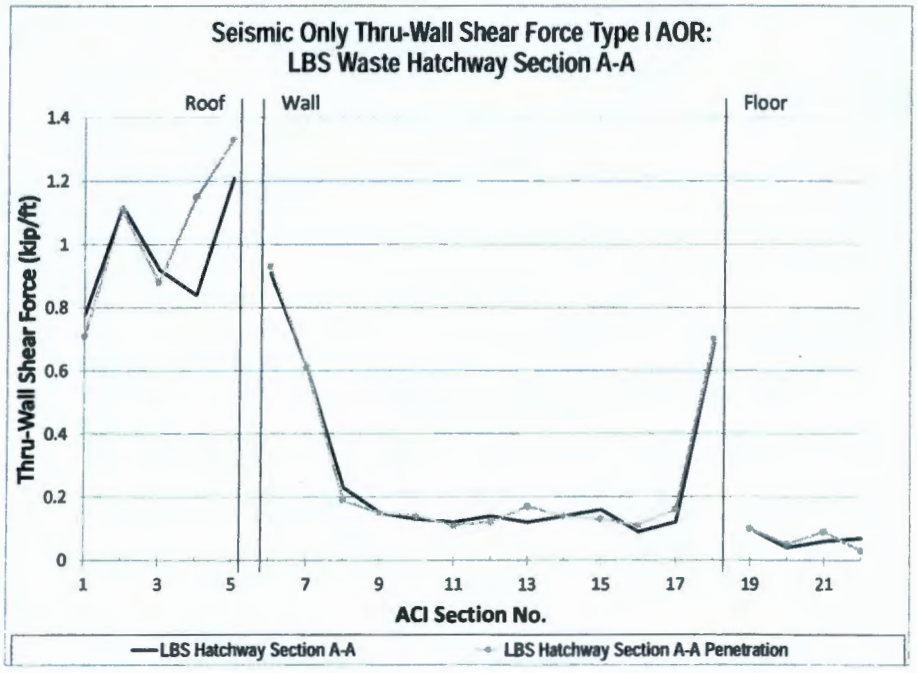

Figure A-8b. Manhole Penetration Study: Concrete Tank Through-Wall Shear Force Comparison – Seismic Only

The localized effects of the penetration are clearly visible in the surface plot (Figure A-9a), but these local effects are only a small increase as seen in the enveloped plot (Figure A-9b).

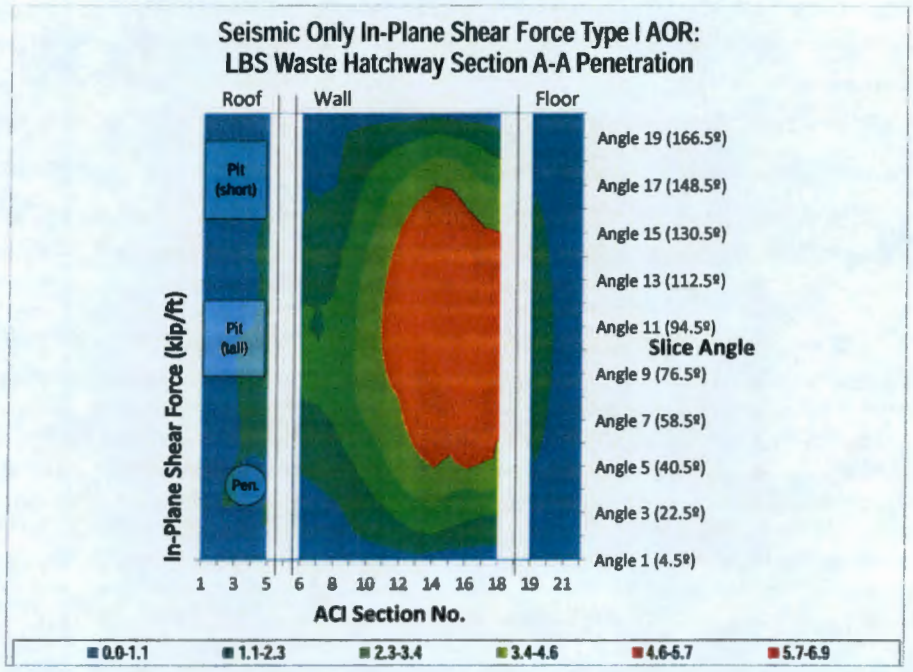

Figure A-9a. Manhole Penetration Study: Concrete Tank In-Plane Shear Force Surface Plot – Seismic Only

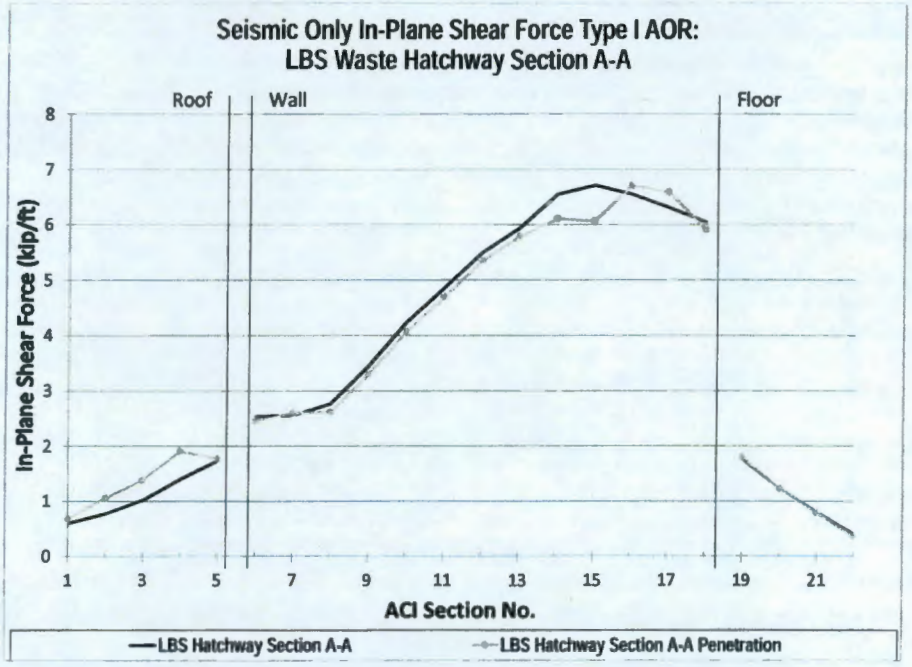

Figure A-9b. Manhole Penetration Study: Concrete Tank In-Plane Shear Force Comparison – Seismic Only

Appendix B — Investigation of a Numerical Anomaly Associated with Specification of Initial Friction Values

B.1 Summary

Review of the Type I seismic results revealed that all of the models have a brief period of oscillation in the demands following the dead weight solution. In some cases, the oscillation leads to initial values at the beginning of the seismic transients that are different than the original dead weight solution. Investigation revealed that the oscillation is triggered by the change from zero initial friction coefficients used for the dead weight solution to nonzero friction coefficients used for the transient seismic solution. The friction coefficients in question are for vertical contact surfaces (including tank wall to soil), as summarized in Table 6-7.

Replacing the initial zero friction value with a small nonzero value (as used in previous AORs) eliminates the oscillation and resulting offset in demands from the dead weight solution. The resulting seismic-only demand profiles using the small nonzero initial friction coefficients are similar in shape to the original results, but the use of a small nonzero initial friction coefficient reduces the magnitude of the demand. The original results using the zero initial friction coefficients are therefore conservative. Because of the low tank D/C ratios and the small overall effect on the analyses, it is judged to be acceptable to use the original results rather than re-perform all of the computer runs.

B.2 Conclusion

A re-run of seismic run matrix case 1 (used for D/C calculation in Johnson et al. 2014a) with a nonzero initial friction shows demands that are consistently lower or approximately equal to the existing results. Thus, the existing results in Section 8.0 lead to conservative tank D/C ratios in Johnson et al. (2014a).

B.3 Discovery

Review of the Type I seismic results revealed that all of the models have a brief period of oscillation in the demands following the dead weight solution (see Figure B-1). The oscillation occurs before the tank responds to any seismic input. However, in some cases, particularly for meridional and hoop forces toward the bottom of the wall, the oscillation settles to a value different than the converged dead weight solution, thus introducing an offset in the demands. In other words, the initial values at the beginning of the seismic transients are different than the original dead weight solution.

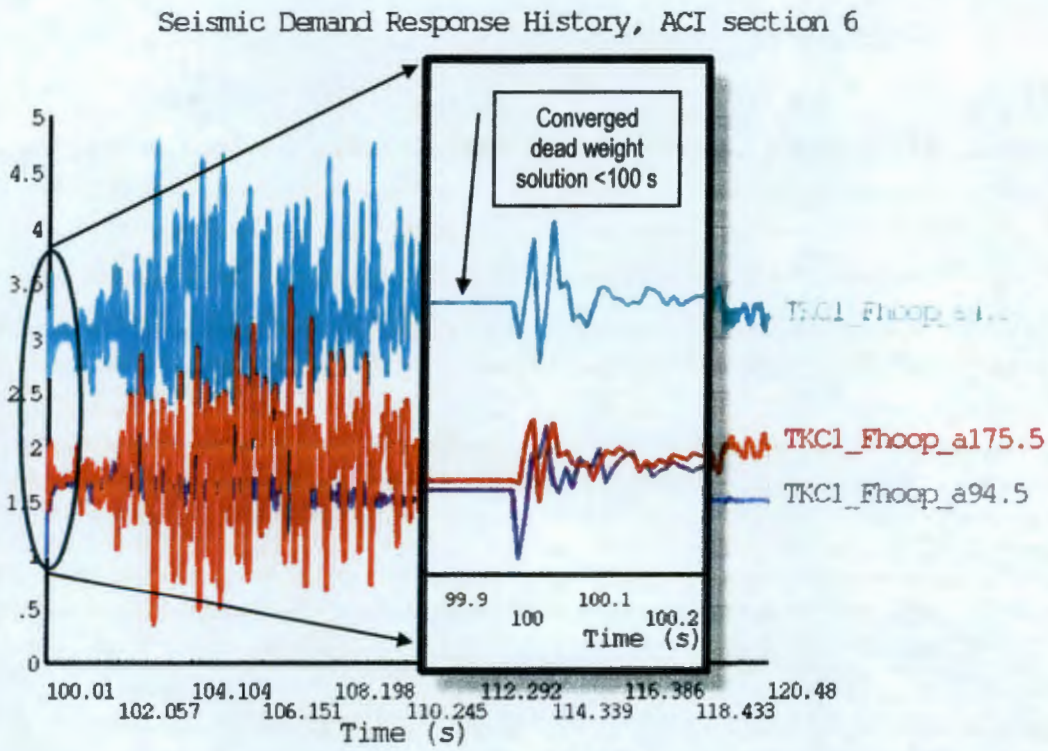

Figure B-1. Seismic Results Over Time Using Zero Initial Friction Coefficients: Concrete Tank Hoop Force (kip/ft.) – Gravity + Seismic

The offset is shown in Figure B-2 from a short test run without seismic excitation, designed to more clearly reveal the oscillation. The demands at the top of the wall (ACI-evaluation section #6) settle close to the initial deadweight value, but the demands at the bottom of the wall (ACI-evaluation section #18) settle to a significant offset from the initial deadweight value. The offset is significant for meridional and hoop forces, but is small for the moments and shear forces.

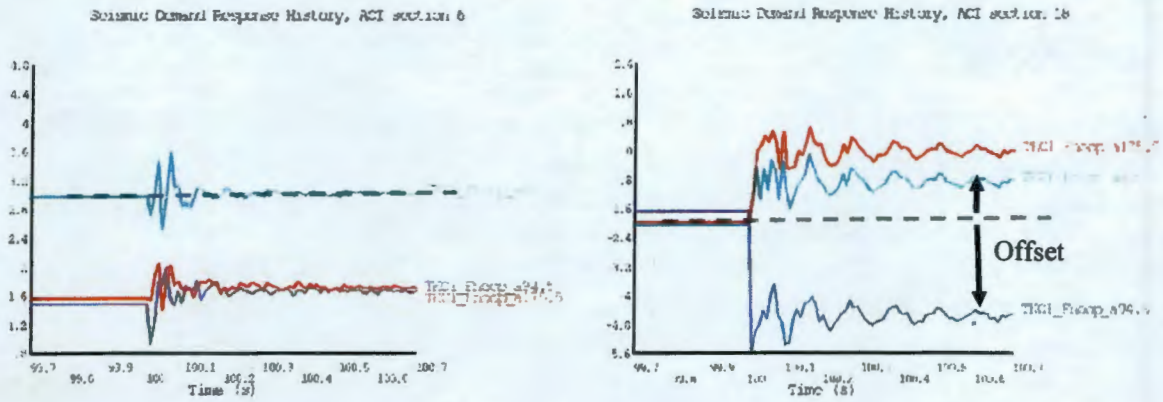

Figure B-2. Seismic Results Over Time Using Zero Initial Friction Coefficients: Concrete Tank Hoop Force (kip/ft.) at Top (Left) and Bottom (Right) of the Wall – Gravity + Seismic

B.4 Causation

Investigation revealed that the oscillation is triggered by the change in the coefficients of friction at the beginning of the seismic transient. More specifically, a change from a *zero* initial value to a *nonzero* value (see Table 6-7). In previous AORs, low coefficients of friction were used during the initial dead weight solution to prevent unrealistic soil drag-down loads on vertical surfaces, as described in Section 6.2.1. However, in the Type I AOR, the low coefficient of friction is changed to zero. Replacing the initial zero friction value with a small value (as used in previous AORs) eliminates the oscillation (see Figure B-3). Although this change is physically inconsequential, it clearly has a numeric significance within the ANSYS solution (e.g. introduces new solution matrix terms). Consequently, its effect on the seismic demands must be evaluated.

Table B-1. Summary of Zero Initial Friction Properties

Interface Location	Initial Gravity Step (Zero)	Initial Gravity Step (Nonzero)	Seismic Transient
Tank wall to soil	0	0.005	0.5
Hatchway to soil	0	0.05	0.5
Soil to soil (above tank)	0	0.05	0.2

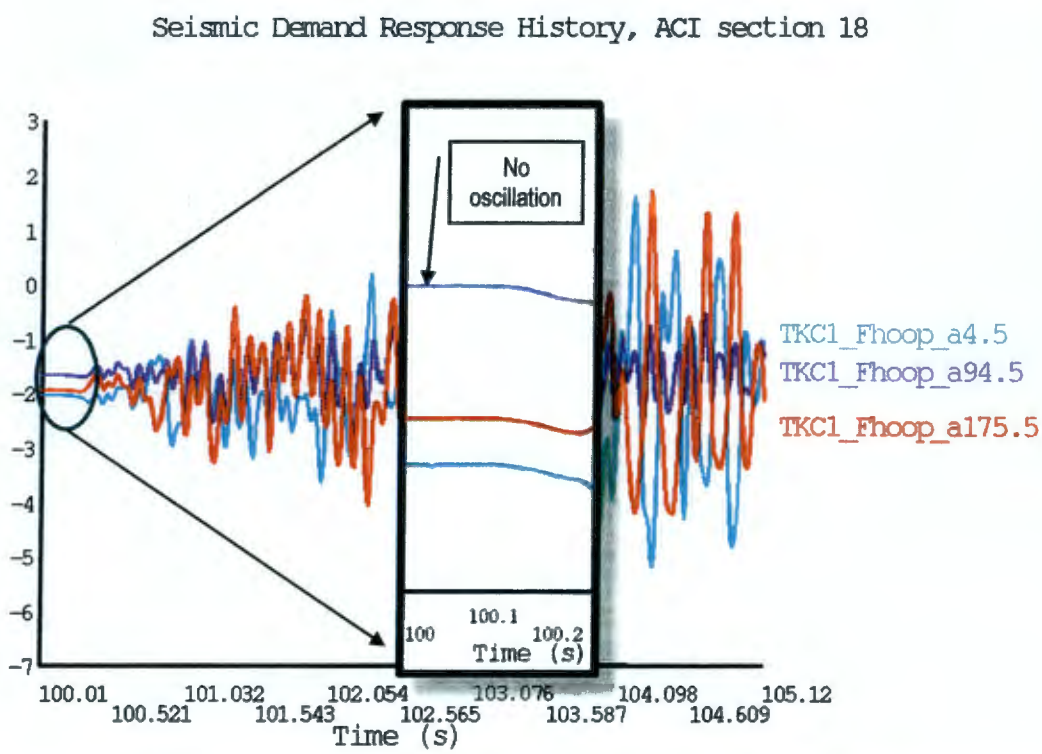

Figure B-3. Seismic Results Over Time Using Small Nonzero Initial Friction Coefficients: Concrete Tank Hoop Force (kip/ft.) at Bottom of the Wall – Gravity + Seismic

B.5 Results

Seismic run matrix case 1 (used for D/C calculation in Johnson et al. 2014a), is re-run with a small nonzero initial friction. The existing results with zero initial friction are compared to the results with small nonzero initial friction in Figure B-4 through Figure B-9.

To expedite resolution, the re-run is performed using only the first 512 steps of seismic transient run. The first 512 transient steps are sufficient to capture the initial oscillation (when present) and the strongest motion portion of the seismic excitation. For consistency in the comparison, the post-processing on the existing zero friction run was revised to include only the first 512 transient steps.

Concrete tank force and moment resultants are extracted from the model using the post-processing methods described in Section 6.6. The forces and moments are plotted against the ACI-evaluation section sequence that starts near the center of the roof and moves radially along the roof, down the sidewall, then from the outside to the center of the tank floor. Forces and moments have been enveloped circumferentially.

The post-processing algorithm is designed to be conservative and includes any offset as increased seismic-only demands. Thus, elimination of the offset will reduce the seismic-only demands. The meridional and hoop forces show the largest reduction in demand, as they are the demands with the most significant offsets following the oscillation, particularly in the wall. Reduction in the meridional and hoop moments and through-wall shear forces are most clearly seen in the roof, and the moment and though-wall shear demands in the wall are typically already low enough that the differences are considered insignificant. In-plane shear forces show a slight *increase* in demand with nonzero initial friction, but the differences are all too small to be considered significant.

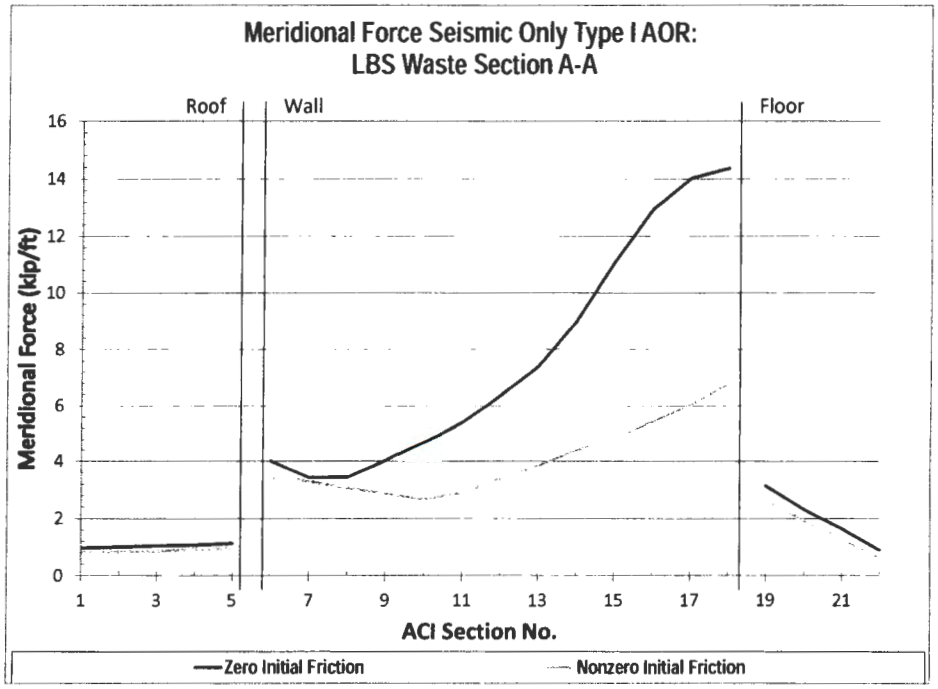

Figure B-4. Seismic Results: Concrete Tank Meridional Force (kip/ft.) – Seismic Only

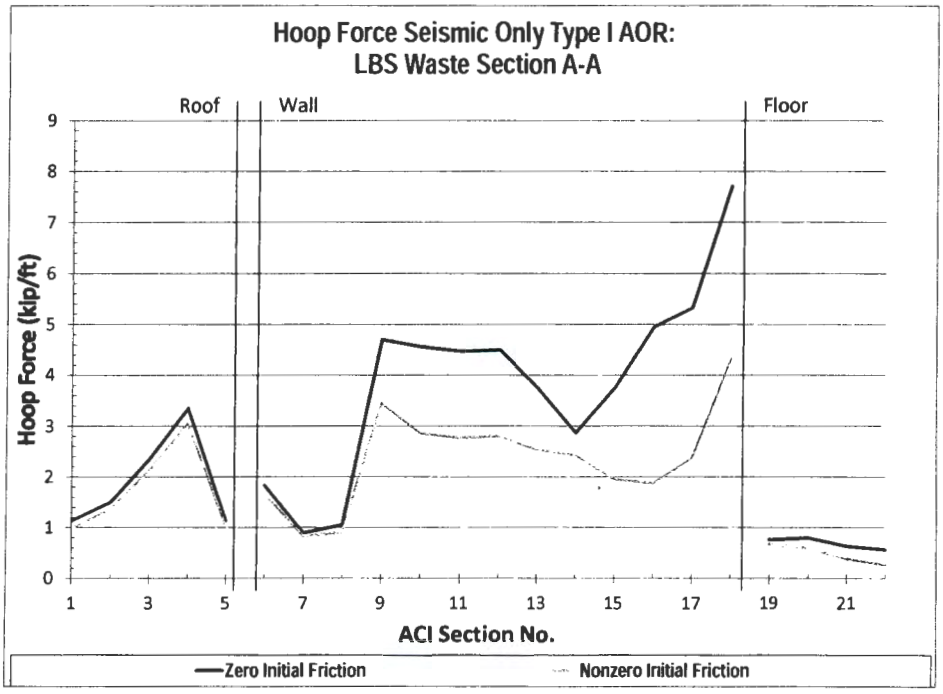

Figure B-5. Seismic Results: Concrete Tank Hoop Force (kip/ft.) – Seismic Only

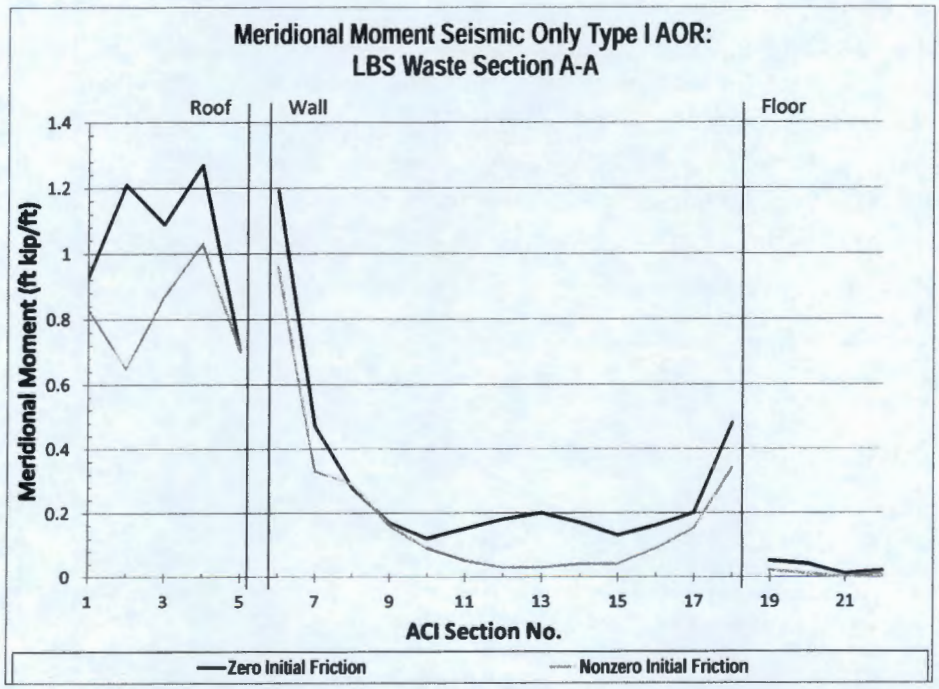

Figure B-6. Seismic Results: Concrete Tank Meridional Moment (kip ft./ft.) – Seismic Only

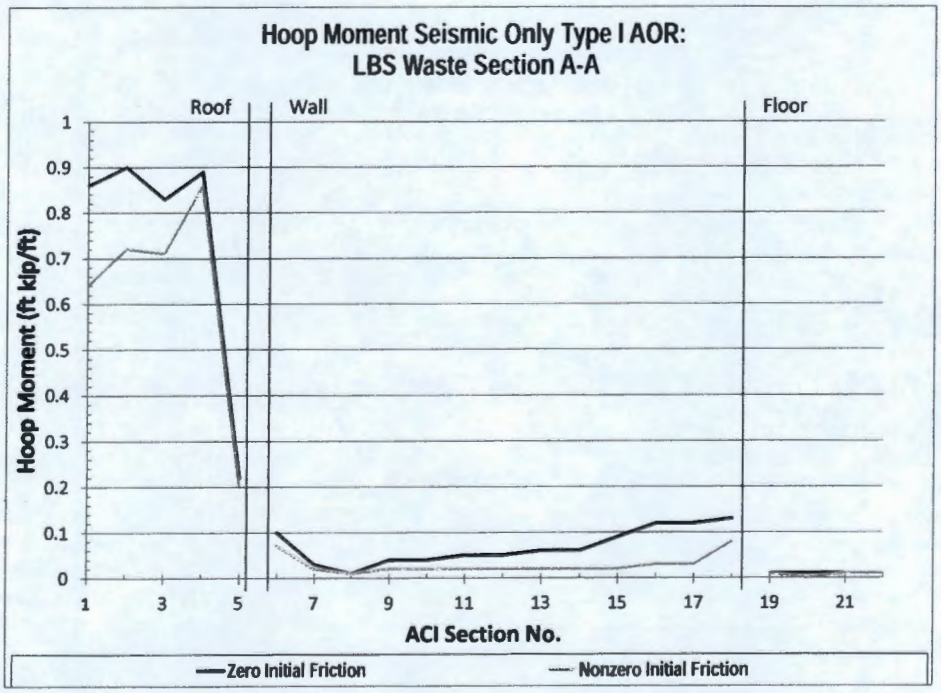

Figure B-7. Seismic Results: Concrete Tank Hoop Moment (kip ft./ft.) – Seismic Only

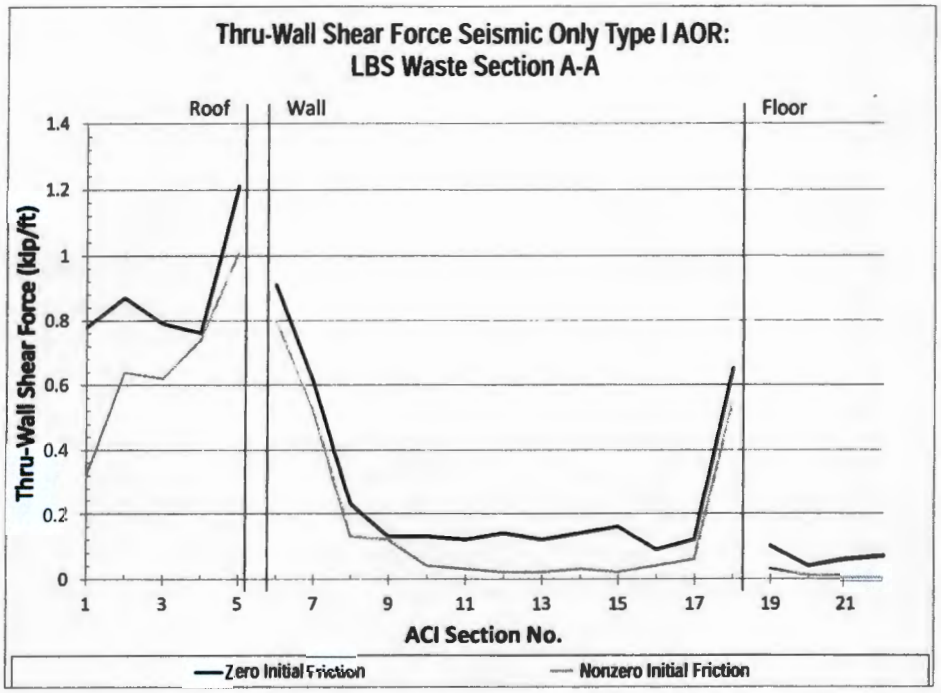

Figure B-8. Seismic Results: Concrete Tank Through-Wall Shear Force (kip/ft.) – Seismic Only

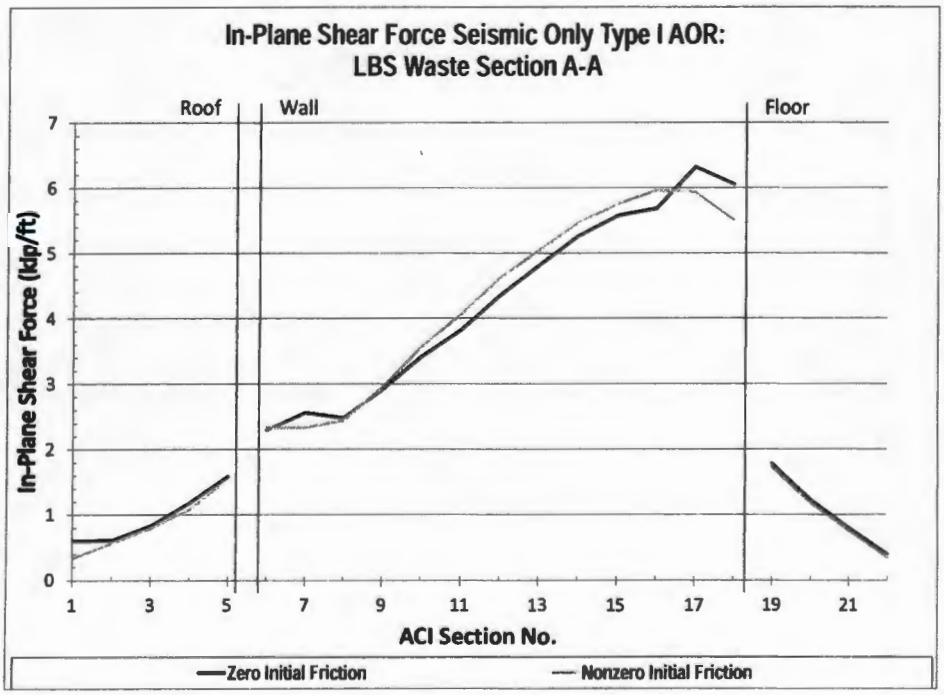

Figure B-9. Seismic Results: Concrete Tank In-Plane Shear Force (kip/ft.) – Seismic Only

Appendix C — Software Quality Assurance and Computer Files

The Type I SST seismic analysis project is performed under the Becht QA (quality assurance) program (Becht 2013). PNNL has formally audited Becht as an NQA-1 supplier (subcontractor) and found the Becht QA program acceptable for use on the SST project. The Becht QA program is based on ASME NQA-1 2008.

ANSYS® 13.0 is used to perform the analyses in this calculation report. This version of software has been validated and verified for use on the computer that ran the analysis, according to Becht QA Manual "Requirement 11" and associated QA procedures. The software test report is documented in Stoops (2013). The in-use test was performed satisfactorily to verify adequacy of the controlled computer configuration in which the final analysis runs were performed. The workstations used in this analysis are listed in Table C-1.

Table C-1. Computer Listing

Name	Description	Serial No.	Physical Address
WE17166	Dell 2x Xeon X5570 2.93 GHz W7 Ent x64	47JBVK1	00-23-AE-AD-33-6A
WE20497	Dell 2x Xeon X5680 3.33 GHz W7 Ent x64	2SRD8P1	BC-30-5B-A2-61-84
WE25411	Dell Xeon E5-1620 3.6 GHz W7 Ent x64	6XPSQW1	90-B1-1C-87-AC-38
WE26071	Dell Xeon E5-1620 3.6 GHz W7 Ent x64	2FK37Y1	B8-CA-3A-97-E2-CA
Superfortress	Dell Xeon W3565 3.2 GHz W7 Pro x64	D0KSPN1	B8-AC-6F-99-EB-7B

A summary of the files used, along with a short description of each file, are provided in Section 6.1.3 as Table 6-2 through Table 6-5. These input/output files, individually listed in Table C-2 are electronically attached as part of this document. These input/output files are provided to PNNL as a specific project deliverable. The output files from each ANSYS run include information identifying the software and workstation used. The most comprehensive identifying information is found in the file "QAoutput.out".

Each ANSYS input file used in the analysis was reviewed during calculation verification (see Section 9.0). The following is a summary of the process used for setting up and checking the runs:

- Each run matrix case is created and placed in individual folders.
- Files are cross-compared between each run. Some are expected to match, and some are expected to differ – these expectations must be met or otherwise justified.
- Files that are consistent across the whole project (such as soil properties) are compared to previously checked files from past tasks. Some data, such as soil properties are also checked against the tables given in previous final reports.
- The "output" of the files is checked using an appropriate method. Typically, by checking the model (dimensions, properties, etc.) generated by the input files.
- Additionally, the results (e.g. tank demands) are cross-compared across the run matrix to see overall trends.

Table C-2. Computer Files Directory Listing

Date	Time	Size	File Name
Directory of L:\Projects\20000's\20906\QA\Documents\ANSYS\2014-7-10 BES waste HSS sectAA			
05/27/2011	01:03 PM	30,502	spectra_target (LBS).inp
07/11/2014	08:30 AM	72,522	connect.inp
05/27/2014	08:29 AM	28,811	postproc.inp
05/27/2011	01:03 PM	30,500	spectra_target.inp
05/09/2014	11:15 AM	8,072	BC.inp
07/11/2014	09:26 AM	26,863	post-cont.inp
05/13/2014	12:05 PM	26,285	SOFE.inp
07/02/2014	04:25 PM	39,430	SOFA.inp
05/02/2014	08:49 AM	23,722	SOIL_properties (BES SST).inp
06/17/2014	02:34 PM	36,633	SOFO.inp
06/18/2014	03:01 PM	8,888	solution.inp
05/27/2011	01:03 PM	37,532	th-10ms-v.inp
06/04/2014	01:23 PM	23,724	TKCW.inp
05/27/2011	01:03 PM	30,201	spectra_target (UBS).inp
05/02/2014	08:48 AM	21,419	SOIL_properties (UBS SST).inp
05/29/2014	03:45 PM	5,161	!TKCP.inp
05/27/2011	01:03 PM	37,544	th-10ms-h.inp
05/27/2011	01:03 PM	37,545	th-10ms-h (LBS SST).inp
05/27/2011	01:03 PM	30,500	spectra_target (BES).inp
05/27/2011	01:03 PM	37,532	th-10ms-v (LBS SST).inp
07/03/2014	08:36 AM	15,862	PITS.inp
05/21/2014	12:56 PM	32,971	!TKC_properties.inp
06/24/2014	04:16 PM	20,394	prepost.inp
06/24/2014	03:29 PM	14,372	subtract_gravity.inp
07/02/2014	10:26 AM	12,291	WAST.inp
12/31/2013	02:41 PM	2,191	postproc_soil_strain.inp
04/30/2014	07:54 AM	23,730	SOIL_properties.inp
07/01/2014	12:13 PM	110,380	spectra.inp
05/31/2014	12:00 PM	11,521	subtract_cont.inp
05/27/2011	01:03 PM	37,545	th-10ms-h (UBS SST).inp
05/27/2014	01:46 PM	30,002	post1.inp
07/10/2014	10:41 AM	41,342	plotmacrolib.inp
05/05/2014	01:14 PM	25,754	SOIL_properties (LBS SST).inp
07/11/2014	09:30 AM	20,501	plots.inp
06/04/2014	01:23 PM	27,656	TKCD.inp
05/27/2011	01:03 PM	37,531	th-10ms-v (UBS SST).inp
06/18/2014	02:55 PM	9,076	solution_TH.inp
07/02/2014	04:42 PM	18,872	assembly.inp
07/03/2014	09:43 AM	5,778	Surface_load.inp
05/27/2011	01:03 PM	37,532	th-10ms-v (BES SST).inp

Date	Time	Size	File Name
06/04/2014	01:23 PM	25,635	TKCF.inp
06/13/2014	02:26 PM	11,822	Modify.inp
05/27/2011	01:03 PM	37,544	th-10ms-h (BES SST).inp
06/17/2014	08:58 AM	31,202	SOUD.inp
Directory of L:\Projects\20000's\20906\QA\Documents\ANSYS\2014-7-10 BES waste HSS sectAA			
03/24/2011	11:00 AM	21,123	UB-SPTR-V.txt
03/24/2011	11:00 AM	21,121	BE-SPTR-V.txt
03/24/2011	11:02 AM	21,115	SC-SPTR-H.txt
03/24/2011	11:00 AM	21,121	SC-SPTR-V.txt
03/24/2011	11:00 AM	21,424	LB-SPTR-V.txt
03/24/2011	11:02 AM	21,115	BE-SPTR-H.txt
03/24/2011	11:02 AM	21,113	UB-SPTR-H.txt
03/24/2011	11:02 AM	21,416	LB-SPTR-H.txt
Directory of L:\Projects\20000's\20906\QA\Documents\ANSYS\2014-7-10 BES waste HSS sectAA			
07/27/2014	02:01 PM	54,932	TKC1_ACI_MAX2049.OUT
07/16/2014	01:56 PM	54,795	CONT1_ACI_MIN1.OUT
07/16/2014	01:52 PM	51,727	TKC1_ACI_SUM1_POST1.OUT
07/27/2014	02:11 PM	54,795	CONT1_ACI_MIN2049.OUT
07/27/2014	02:01 PM	1,050,658	TKC_ACI_angles2049.OUT
07/16/2014	01:56 PM	54,932	TKC1_ACI_MAX1.OUT
07/27/2014	01:37 PM	432,132	SPTR-disp.out
07/27/2014	02:11 PM	55,226	CONT1_ACI_SUM2049.OUT
07/16/2014	01:56 PM	1,149,281	CONT1_ACI_angles1.OUT
07/27/2014	02:01 PM	54,932	TKC1_ACI_SUM2049.OUT
07/16/2014	01:55 PM	1,050,658	TKC_ACI_angles1.OUT
07/16/2014	01:56 PM	54,501	TKC1_ACI_MIN1.OUT
07/16/2014	01:55 PM	66,067	solution.out
07/16/2014	01:51 PM	32,496	mplist.out
07/27/2014	01:37 PM	460,788	SPTR-accel.out
07/16/2014	01:56 PM	55,226	CONT1_ACI_SUM1.OUT
07/27/2014	02:11 PM	50,537	CONT1_ACI_SUM_seismic_only.OUT
07/16/2014	01:51 PM	13,165	elist.out
07/16/2014	01:52 PM	429,196	CONT_angles_1_POST1.OUT
07/27/2014	01:27 PM	2,664	QAoutput.out
07/27/2014	01:37 PM	62,734	TKC_TH_POST26_U.OUT
07/16/2014	01:56 PM	54,932	TKC1_ACI_SUM1.OUT
07/16/2014	01:51 PM	55,238	Model_MAT_data.out
07/27/2014	02:11 PM	1,149,281	CONT1_ACI_angles2049.OUT
07/16/2014	01:43 PM	158,246	Model_GEO_data.OUT
07/27/2014	02:11 PM	55,226	CONT1_ACI_MAX2049.OUT
07/27/2014	02:11 PM	51,256	TKC1_ACI_SUM_seismic_only.OUT
07/16/2014	01:52 PM	52,189	CONT1_ACI_SUM1_POST1.OUT

Date	Time	Size	File Name
07/16/2014	01:52 PM	617,073	TKC1_ACI_angles_1_POST1.OUT
07/27/2014	02:01 PM	54,501	TKC1_ACI_MIN2049.OUT
07/16/2014	01:56 PM	55,226	CONT1_ACI_MAX1.OUT
07/16/2014	01:51 PM	17,654	real.out
Directory of L:\Projects\20000's\20906\QA\Documents\ANSYS\2014-7-10 UBS waste HSS sectAA			
05/27/2011	01:03 PM	30,502	spectra_target (LBS).inp
07/11/2014	08:30 AM	72,517	connect.inp
05/27/2014	08:29 AM	28,811	postproc.inp
05/27/2011	01:03 PM	30,201	spectra_target.inp
05/09/2014	11:15 AM	8,072	BC.inp
07/11/2014	09:26 AM	26,863	post-cont.inp
05/13/2014	12:05 PM	26,285	SOFE.inp
07/02/2014	04:25 PM	39,430	SOFA.inp
05/02/2014	08:49 AM	23,722	SOIL_properties (BES SST).inp
06/17/2014	02:34 PM	36,633	SOFO.inp
06/18/2014	03:01 PM	8,888	solution.inp
05/27/2011	01:03 PM	37,531	th-10ms-v.inp
06/04/2014	01:23 PM	23,724	TKCW.inp
05/27/2011	01:03 PM	30,201	spectra_target (UBS).inp
05/02/2014	08:48 AM	21,419	SOIL_properties (UBS SST).inp
05/29/2014	03:45 PM	5,161	!TKCP.inp
05/27/2011	01:03 PM	37,545	th-10ms-h.inp
05/27/2011	01:03 PM	37,545	th-10ms-h (LBS SST).inp
05/27/2011	01:03 PM	30,500	spectra_target (BES).inp
05/27/2011	01:03 PM	37,532	th-10ms-v (LBS SST).inp
07/03/2014	08:36 AM	15,862	PITS.inp
05/21/2014	12:56 PM	32,971	!TKC_properties.inp
06/24/2014	04:16 PM	20,394	prepost.inp
06/24/2014	03:29 PM	14,372	subtract_gravity.inp
07/02/2014	10:26 AM	12,291	WAST.inp
12/31/2013	02:41 PM	2,191	postproc_soil_strain.inp
05/02/2014	08:48 AM	21,419	SOIL_properties.inp
07/01/2014	12:13 PM	110,380	spectra.inp
05/31/2014	12:00 PM	11,521	subtract_cont.inp
05/27/2011	01:03 PM	37,545	th-10ms-h (UBS SST).inp
05/27/2014	01:46 PM	30,002	post1.inp
07/10/2014	10:41 AM	41,342	plotmacrolib.inp
05/05/2014	01:14 PM	25,754	SOIL_properties (LBS SST).inp
07/11/2014	09:30 AM	20,501	plots.inp
06/04/2014	01:23 PM	27,656	TKCD.inp
05/27/2011	01:03 PM	37,531	th-10ms-v (UBS SST).inp
06/18/2014	02:55 PM	9,076	solution_TH.inp
07/02/2014	04:42 PM	18,872	assembly.inp
07/03/2014	09:43 AM	5,778	Surface_load.inp

Date	Time	Size	File Name
05/27/2011	01:03 PM	37,532	th-10ms-v (BES SST).inp
06/04/2014	01:23 PM	25,635	TKCF.inp
06/13/2014	02:26 PM	11,822	Modify.inp
05/27/2011	01:03 PM	37,544	th-10ms-h (BES SST).inp
06/17/2014	08:58 AM	31,202	SOUD.inp
Directory of L:\Projects\20000's\20906\QA\Documents\ANSYS\2014-7-10 UBS waste HSS sectAA			
03/24/2011	11:00 AM	21,123	UB-SPTR-V.txt
03/24/2011	11:00 AM	21,121	BE-SPTR-V.txt
03/24/2011	11:02 AM	21,113	SC-SPTR-H.txt
03/24/2011	11:00 AM	21,123	SC-SPTR-V.txt
03/24/2011	11:00 AM	21,424	LB-SPTR-V.txt
03/24/2011	11:02 AM	21,115	BE-SPTR-H.txt
03/24/2011	11:02 AM	21,113	UB-SPTR-H.txt
03/24/2011	11:02 AM	21,416	LB-SPTR-H.txt
Directory of L:\Projects\20000's\20906\QA\Documents\ANSYS\2014-7-10 UBS waste HSS sectAA			
08/07/2014	03:34 PM	54,932	TKC1_ACI_MAX2049.OUT
07/27/2014	02:29 PM	54,795	CONT1_ACI_MIN1.OUT
07/27/2014	02:25 PM	51,727	TKC1_ACI_SUM1_POST1.OUT
08/07/2014	03:43 PM	54,795	CONT1_ACI_MIN2049.OUT
08/07/2014	03:34 PM	1,050,658	TKC_ACI_angles2049.OUT
07/27/2014	02:29 PM	54,932	TKC1_ACI_MAX1.OUT
08/07/2014	03:12 PM	432,132	SPTR-disp.out
08/07/2014	03:43 PM	55,226	CONT1_ACI_SUM2049.OUT
07/27/2014	02:29 PM	1,149,281	CONT1_ACI_angles1.OUT
08/07/2014	03:34 PM	54,932	TKC1_ACI_SUM2049.OUT
07/27/2014	02:29 PM	1,050,658	TKC_ACI_angles1.OUT
07/27/2014	02:29 PM	54,501	TKC1_ACI_MIN1.OUT
07/27/2014	02:29 PM	66,068	solution.out
07/27/2014	02:25 PM	31,524	mplist.out
08/07/2014	03:12 PM	460,788	SPTR-accel.out
07/27/2014	02:29 PM	55,226	CONT1_ACI_SUM1.OUT
08/07/2014	03:43 PM	50,537	CONT1_ACI_SUM_seismic_only.OUT
07/27/2014	02:25 PM	13,165	elist.out
07/27/2014	02:25 PM	429,196	CONT_angles_1_POST1.OUT
08/07/2014	03:04 PM	2,664	QAoutput.out
08/07/2014	03:12 PM	62,734	TKC_TH_POST26_U.OUT
07/27/2014	02:29 PM	54,932	TKC1_ACI_SUM1.OUT
07/27/2014	02:24 PM	53,726	Model_MAT_data.out
08/07/2014	03:43 PM	1,149,281	CONT1_ACI_angles2049.OUT
07/27/2014	02:17 PM	157,748	Model_GEO_data.OUT
08/07/2014	03:43 PM	55,226	CONT1_ACI_MAX2049.OUT
08/07/2014	03:43 PM	51,256	TKC1_ACI_SUM_seismic_only.OUT

Date	Time	Size	File Name
07/27/2014	02:25 PM	52,189	CONT1_ACI_SUM1_POST1.OUT
07/27/2014	02:25 PM	617,073	TKC1_ACI_angles_1_POST1.OUT
08/07/2014	03:34 PM	54,501	TKC1_ACI_MIN2049.OUT
07/27/2014	02:29 PM	55,226	CONT1_ACI_MAX1.OUT
07/27/2014	02:25 PM	17,654	real.out
Directory of L:\Projects\20000's\20906\QA\Documents\ANSYS\2014-7-10 LBS waste HSS sectAA			
05/27/2011	01:03 PM	30,502	spectra_target (LBS).inp
07/11/2014	08:30 AM	72,487	connect.inp
05/27/2014	08:29 AM	28,811	postproc.inp
05/27/2011	01:03 PM	30,502	spectra_target.inp
05/09/2014	11:15 AM	8,072	BC.inp
07/11/2014	09:26 AM	26,863	post-cont.inp
05/13/2014	12:05 PM	26,285	SOFE.inp
07/02/2014	04:25 PM	39,430	SOFA.inp
05/02/2014	08:49 AM	23,722	SOIL_properties (BES SST).inp
06/17/2014	02:34 PM	36,633	SOFO.inp
06/18/2014	03:01 PM	8,888	solution.inp
05/27/2011	01:03 PM	37,532	th-10ms-v.inp
06/04/2014	01:23 PM	23,724	TKCW.inp
05/27/2011	01:03 PM	30,201	spectra_target (UBS).inp
05/02/2014	08:48 AM	21,419	SOIL_properties (UBS SST).inp
05/29/2014	03:45 PM	5,161	!TKCP.inp
05/27/2011	01:03 PM	37,545	th-10ms-h.inp
05/27/2011	01:03 PM	37,545	th-10ms-h (LBS SST).inp
05/27/2011	01:03 PM	30,500	spectra_target (BES).inp
05/27/2011	01:03 PM	37,532	th-10ms-v (LBS SST).inp
07/03/2014	08:36 AM	15,862	PITS.inp
05/21/2014	12:56 PM	32,971	!TKC_properties.inp
06/24/2014	04:16 PM	20,394	prepost.inp
06/24/2014	03:29 PM	14,372	subtract_gravity.inp
07/02/2014	10:26 AM	12,291	WAST.inp
12/31/2013	02:41 PM	2,191	postproc_soil_strain.inp
05/05/2014	01:14 PM	25,754	SOIL_properties.inp
07/01/2014	12:13 PM	110,380	spectra.inp
05/31/2014	12:00 PM	11,521	subtract_cont.inp
05/27/2011	01:03 PM	37,545	th-10ms-h (UBS SST).inp
05/27/2014	01:46 PM	30,002	post1.inp
07/10/2014	10:41 AM	41,342	plotmacrolib.inp
05/05/2014	01:14 PM	25,754	SOIL_properties (LBS SST).inp
07/11/2014	09:30 AM	20,501	plots.inp
06/04/2014	01:23 PM	27,656	TKCD.inp
05/27/2011	01:03 PM	37,531	th-10ms-v (UBS SST).inp
06/18/2014	02:55 PM	9,076	solution_TH.inp
07/02/2014	04:42 PM	18,872	assembly.inp

Date	Time	Size	File Name
07/03/2014	09:43 AM	5,778	Surface_load.inp
05/27/2011	01:03 PM	37,532	th-10ms-v (BES SST).inp
06/04/2014	01:23 PM	25,635	TKCF.inp
06/13/2014	02:26 PM	11,822	Modify.inp
05/27/2011	01:03 PM	37,544	th-10ms-h (BES SST).inp
06/17/2014	08:58 AM	31,202	SOUD.inp
Directory of L:\Projects\20000's\20906\QA\Documents\ANSYS\2014-7-10 LBS waste HSS sectAA			
03/24/2011	11:00 AM	21,123	UB-SPTR-V.txt
03/24/2011	11:00 AM	21,121	BE-SPTR-V.txt
03/24/2011	11:02 AM	21,416	SC-SPTR-H.txt
03/24/2011	11:00 AM	21,424	SC-SPTR-V.txt
03/24/2011	11:00 AM	21,424	LB-SPTR-V.txt
03/24/2011	11:02 AM	21,115	BE-SPTR-H.txt
03/24/2011	11:02 AM	21,113	UB-SPTR-H.txt
03/24/2011	11:02 AM	21,416	LB-SPTR-H.txt
Directory of L:\Projects\20000's\20906\QA\Documents\ANSYS\2014-7-10 LBS waste HSS sectAA			
07/30/2014	03:59 AM	54,894	TKC1_ACI_MAX2049.OUT
07/16/2014	01:48 PM	54,763	CONT1_ACI_MIN1.OUT
07/16/2014	01:43 PM	51,689	TKC1_ACI_SUM1_POST1.OUT
07/30/2014	04:04 AM	54,763	CONT1_ACI_MIN2049.OUT
07/30/2014	03:59 AM	1,050,658	TKC_ACI_angles2049.OUT
07/16/2014	01:48 PM	54,894	TKC1_ACI_MAX1.OUT
07/30/2014	03:54 AM	432,094	SPTR-disp.out
07/30/2014	04:04 AM	55,188	CONT1_ACI_SUM2049.OUT
07/16/2014	01:48 PM	1,149,281	CONT1_ACI_angles1.OUT
07/30/2014	03:59 AM	54,894	TKC1_ACI_SUM2049.OUT
07/16/2014	01:48 PM	1,050,658	TKC_ACI_angles1.OUT
07/16/2014	01:48 PM	54,469	TKC1_ACI_MIN1.OUT
07/16/2014	01:48 PM	66,068	solution.out
07/16/2014	01:42 PM	33,306	mplist.out
07/30/2014	03:55 AM	460,750	SPTR-accel.out
07/16/2014	01:48 PM	55,188	CONT1_ACI_SUM1.OUT
07/30/2014	04:04 AM	50,537	CONT1_ACI_SUM_seismic_only.OUT
07/16/2014	01:42 PM	13,165	elist.out
07/16/2014	01:43 PM	429,158	CONT_angles_1_POST1.OUT
07/30/2014	03:50 AM	2,600	QAoutput.out
07/30/2014	03:55 AM	62,696	TKC_TH_POST26_U.OUT
07/16/2014	01:48 PM	54,894	TKC1_ACI_SUM1.OUT
07/16/2014	01:42 PM	56,498	Model_MAT_data.out
07/30/2014	04:04 AM	1,149,281	CONT1_ACI_angles2049.OUT
07/16/2014	01:35 PM	158,661	Model_GEO_data.OUT
07/30/2014	04:04 AM	55,188	CONT1_ACI_MAX2049.OUT

Date	Time	Size	File Name
07/30/2014	04:04 AM	51,224	TKC1_ACI_SUM_seismic_only.OUT
07/16/2014	01:43 PM	52,151	CONT1_ACI_SUM1_POST1.OUT
07/16/2014	01:43 PM	617,035	TKC1_ACI_angles_1_POST1.OUT
07/30/2014	03:59 AM	54,469	TKC1_ACI_MIN2049.OUT
07/16/2014	01:48 PM	55,188	CONT1_ACI_MAX1.OUT
07/16/2014	01:42 PM	17,654	real.out
Directory of L:\Projects\20000's\20906\QA\Documents\ANSYS\2014-7-10 LBS waste HSS sectAA pen			
05/27/2011	01:03 PM	30,502	spectra_target (LBS).inp
07/11/2014	08:30 AM	72,487	connect.inp
05/27/2014	08:29 AM	28,811	postproc.inp
05/27/2011	01:03 PM	30,502	spectra_target.inp
05/09/2014	11:15 AM	8,072	BC.inp
07/11/2014	09:26 AM	26,863	post-cont.inp
05/13/2014	12:05 PM	26,285	SOFE.inp
07/02/2014	04:25 PM	39,430	SOFA.inp
05/02/2014	08:49 AM	23,722	SOIL_properties (BES SST).inp
06/17/2014	02:34 PM	36,633	SOFO.inp
06/18/2014	03:01 PM	8,888	solution.inp
05/27/2011	01:03 PM	37,532	th-10ms-v.inp
05/29/2014	03:45 PM	5,161	TKCP.inp
06/04/2014	01:23 PM	23,724	TKCW.inp
05/27/2011	01:03 PM	30,201	spectra_target (UBS).inp
05/02/2014	08:48 AM	21,419	SOIL_properties (UBS SST).inp
05/27/2011	01:03 PM	37,545	th-10ms-h.inp
05/27/2011	01:03 PM	37,545	th-10ms-h (LBS SST).inp
05/27/2011	01:03 PM	30,500	spectra_target (BES).inp
05/27/2011	01:03 PM	37,532	th-10ms-v (LBS SST).inp
07/03/2014	08:36 AM	15,862	PITS.inp
05/21/2014	12:56 PM	32,971	!TKC_properties.inp
06/24/2014	04:16 PM	20,394	prepost.inp
06/24/2014	03:29 PM	14,372	subtract_gravity.inp
07/02/2014	10:26 AM	12,291	WAST.inp
07/31/2014	02:20 PM	20,548	prepost1.inp
12/31/2013	02:41 PM	2,191	postproc_soil_strain.inp
05/05/2014	01:14 PM	25,754	SOIL_properties.inp
07/01/2014	12:13 PM	110,380	spectra.inp
05/31/2014	12:00 PM	11,521	subtract_cont.inp
05/27/2011	01:03 PM	37,545	th-10ms-h (UBS SST).inp
05/27/2014	01:46 PM	30,002	post1.inp
07/10/2014	10:41 AM	41,342	plotmacrolib.inp
05/05/2014	01:14 PM	25,754	SOIL_properties (LBS SST).inp
07/11/2014	09:30 AM	20,501	plots.inp
06/04/2014	01:23 PM	27,656	TKCD.inp
05/27/2011	01:03 PM	37,531	th-10ms-v (UBS SST).inp

Date	Time	Size	File Name
06/18/2014	02:55 PM	9,076	solution_TH.inp
08/05/2014	02:05 PM	28,830	postproc1.inp
07/02/2014	04:42 PM	18,872	assembly.inp
07/03/2014	09:43 AM	5,778	Surface_load.inp
05/27/2011	01:03 PM	37,532	th-10ms-v (BES SST).inp
06/04/2014	01:23 PM	25,635	TKCF.inp
06/13/2014	02:26 PM	11,822	Modify.inp
05/27/2011	01:03 PM	37,544	th-10ms-h (BES SST).inp
06/17/2014	08:58 AM	31,202	SOUD.inp
Directory of L:\Projects\20000's\20906\QA\Documents\ANSYS\2014-7-10 LBS waste HSS sectAA pen			
03/24/2011	11:00 AM	21,123	UB-SPTR-V.txt
03/24/2011	11:00 AM	21,121	BE-SPTR-V.txt
03/24/2011	11:02 AM	21,416	SC-SPTR-H.txt
03/24/2011	11:00 AM	21,424	SC-SPTR-V.txt
03/24/2011	11:00 AM	21,424	LB-SPTR-V.txt
03/24/2011	11:02 AM	21,115	BE-SPTR-H.txt
03/24/2011	11:02 AM	21,113	UB-SPTR-H.txt
03/24/2011	11:02 AM	21,416	LB-SPTR-H.txt
Directory of L:\Projects\20000's\20906\QA\Documents\ANSYS\2014-7-10 LBS waste HSS sectAA pen			
08/05/2014	02:37 PM	55,183	TKC1_ACI_MAX2049.OUT
08/05/2014	02:29 PM	55,052	CONT1_ACI_MIN1.OUT
07/16/2014	01:44 PM	51,698	TKC1_ACI_SUM1_POST1.OUT
08/05/2014	02:44 PM	55,052	CONT1_ACI_MIN2049.OUT
08/05/2014	02:37 PM	2,089,571	TKC_ACI_angles2049.OUT
08/05/2014	02:29 PM	55,183	TKC1_ACI_MAX1.OUT
07/31/2014	04:22 AM	432,098	SPTR-disp.out
08/05/2014	02:44 PM	55,477	CONT1_ACI_SUM2049.OUT
08/05/2014	02:29 PM	2,275,114	CONT1_ACI_angles1.OUT
08/05/2014	02:37 PM	55,183	TKC1_ACI_SUM2049.OUT
08/05/2014	02:29 PM	2,089,571	TKC_ACI_angles1.OUT
08/05/2014	02:29 PM	54,758	TKC1_ACI_MIN1.OUT
07/16/2014	01:49 PM	66,068	solution.out
07/16/2014	01:43 PM	33,306	mplist.out
07/31/2014	04:22 AM	460,759	SPTR-accel.out
08/05/2014	02:29 PM	55,477	CONT1_ACI_SUM1.OUT
07/31/2014	04:35 AM	50,542	CONT1_ACI_SUM_seismic_only.OUT
07/16/2014	01:43 PM	13,165	elist.out
07/16/2014	01:44 PM	425,817	CONT_angles_1_POST1.OUT
07/31/2014	04:15 AM	2,608	QAoutput.out
07/31/2014	04:22 AM	62,700	TKC_TH_POST26_U.OUT
08/05/2014	02:29 PM	55,183	TKC1_ACI_SUM1.OUT
07/16/2014	01:43 PM	56,498	Model_MAT_data.out

Date	Time	Size	File Name
08/05/2014	02:44 PM	2,275,114	CONT1_ACI_angles2049.OUT
08/05/2014	02:29 PM	249,555	Model_GEO_data.OUT
08/05/2014	02:44 PM	55,477	CONT1_ACI_MAX2049.OUT
07/31/2014	04:35 AM	51,233	TKC1_ACI_SUM_seismic_only.OUT
07/16/2014	01:44 PM	52,160	CONT1_ACI_SUM1_POST1.OUT
07/16/2014	01:44 PM	612,854	TKC1_ACI_angles_1_POST1.OUT
08/05/2014	02:37 PM	54,758	TKC1_ACI_MIN2049.OUT
08/05/2014	02:29 PM	55,477	CONT1_ACI_MAX1.OUT
07/16/2014	01:43 PM	17,654	real.out
Directory of L:\Projects\20000's\20906\QA\Documents\ANSYS\2014-7-10 LBS empty sectAA			
05/27/2011	01:03 PM	30,502	spectra_target (LBS).inp
07/11/2014	08:30 AM	72,465	connect.inp
05/27/2014	08:29 AM	28,811	postproc.inp
05/27/2011	01:03 PM	30,502	spectra_target.inp
05/09/2014	11:15 AM	8,072	BC.inp
07/11/2014	09:26 AM	26,863	post-cont.inp
05/13/2014	12:05 PM	26,285	SOFE.inp
07/02/2014	04:25 PM	39,430	SOFA.inp
05/02/2014	08:49 AM	23,722	SOIL_properties (BES SST).inp
06/17/2014	02:34 PM	36,633	SOFO.inp
06/18/2014	03:01 PM	8,888	solution.inp
05/27/2011	01:03 PM	37,532	th-10ms-v.inp
06/04/2014	01:23 PM	23,724	TKCW.inp
05/27/2011	01:03 PM	30,201	spectra_target (UBS).inp
05/02/2014	08:48 AM	21,419	SOIL_properties (UBS SST).inp
05/29/2014	03:45 PM	5,161	!TKCP.inp
05/27/2011	01:03 PM	37,545	th-10ms-h.inp
05/27/2011	01:03 PM	37,545	th-10ms-h (LBS SST).inp
05/27/2011	01:03 PM	30,500	spectra_target (BES).inp
05/27/2011	01:03 PM	37,532	th-10ms-v (LBS SST).inp
07/03/2014	08:36 AM	15,862	PITS.inp
05/21/2014	12:56 PM	32,971	!TKC_properties.inp
06/24/2014	04:16 PM	20,394	prepost.inp
06/24/2014	03:29 PM	14,372	subtract_gravity.inp
12/31/2013	02:41 PM	2,191	postproc_soil_strain.inp
05/05/2014	01:14 PM	25,754	SOIL_properties.inp
07/01/2014	12:13 PM	110,380	spectra.inp
05/31/2014	12:00 PM	11,521	subtract_cont.inp
05/27/2011	01:03 PM	37,545	th-10ms-h (UBS SST).inp
05/27/2014	01:46 PM	30,002	post1.inp
07/10/2014	10:41 AM	41,342	plotmacrolib.inp
05/05/2014	01:14 PM	25,754	SOIL_properties (LBS SST).inp
07/11/2014	09:30 AM	20,501	plots.inp
06/04/2014	01:23 PM	27,656	TKCD.inp

Date	Time	Size	File Name
05/27/2011	01:03 PM	37,531	th-10ms-v (UBS SST).inp
06/18/2014	02:55 PM	9,076	solution_TH.inp
07/02/2014	04:42 PM	18,872	assembly.inp
07/03/2014	09:43 AM	5,778	Surface_load.inp
07/02/2014	10:26 AM	12,291	!WAST.inp
05/27/2011	01:03 PM	37,532	th-10ms-v (BES SST).inp
06/04/2014	01:23 PM	25,635	TKCF.inp
06/13/2014	02:26 PM	11,822	Modify.inp
05/27/2011	01:03 PM	37,544	th-10ms-h (BES SST).inp
06/17/2014	08:58 AM	31,202	SOUD.inp
Directory of L:\Projects\20000's\20906\QA\Documents\ANSYS\2014-7-10 LBS empty sectAA			
03/24/2011	11:00 AM	21,123	UB-SPTR-V.txt
03/24/2011	11:00 AM	21,121	BE-SPTR-V.txt
03/24/2011	11:02 AM	21,416	SC-SPTR-H.txt
03/24/2011	11:00 AM	21,424	SC-SPTR-V.txt
03/24/2011	11:00 AM	21,424	LB-SPTR-V.txt
03/24/2011	11:02 AM	21,115	BE-SPTR-H.txt
03/24/2011	11:02 AM	21,113	UB-SPTR-H.txt
03/24/2011	11:02 AM	21,416	LB-SPTR-H.txt
Directory of L:\Projects\20000's\20906\QA\Documents\ANSYS\2014-7-10 LBS empty sectAA			
08/02/2014	03:49 AM	54,890	TKC1_ACI_MAX2049.OUT
07/16/2014	01:51 PM	54,759	CONT1_ACI_MIN1.OUT
07/16/2014	01:44 PM	51,685	TKC1_ACI_SUM1_POST1.OUT
08/02/2014	03:54 AM	54,759	CONT1_ACI_MIN2049.OUT
08/02/2014	03:49 AM	1,050,658	TKC_ACI_angles2049.OUT
07/16/2014	01:51 PM	54,890	TKC1_ACI_MAX1.OUT
08/02/2014	03:44 AM	432,090	SPTR-disp.out
08/02/2014	03:54 AM	55,184	CONT1_ACI_SUM2049.OUT
07/16/2014	01:51 PM	1,149,281	CONT1_ACI_angles1.OUT
08/02/2014	03:49 AM	54,890	TKC1_ACI_SUM2049.OUT
07/16/2014	01:51 PM	1,050,658	TKC_ACI_angles1.OUT
07/16/2014	01:51 PM	54,465	TKC1_ACI_MIN1.OUT
07/16/2014	01:51 PM	63,105	solution.out
07/16/2014	01:44 PM	32,750	mplist.out
08/02/2014	03:44 AM	460,746	SPTR-accel.out
07/16/2014	01:51 PM	55,184	CONT1_ACI_SUM1.OUT
08/02/2014	03:55 AM	50,537	CONT1_ACI_SUM_seismic_only.OUT
07/16/2014	01:44 PM	11,860	elist.out
07/16/2014	01:44 PM	429,154	CONT_angles_1_POST1.OUT
08/02/2014	03:37 AM	2,592	QAoutput.out
08/02/2014	03:44 AM	62,692	TKC_TH_POST26_U.OUT
07/16/2014	01:51 PM	54,890	TKC1_ACI_SUM1.OUT

Date	Time	Size	File Name
07/16/2014	01:43 PM	55,796	Model_MAT_data.out
08/02/2014	03:54 AM	1,149,281	CONT1_ACI_angles2049.OUT
07/16/2014	01:35 PM	158,369	Model_GEO_data.OUT
08/02/2014	03:54 AM	55,184	CONT1_ACI_MAX2049.OUT
08/02/2014	03:55 AM	51,220	TKC1_ACI_SUM_seismic_only.OUT
07/16/2014	01:44 PM	52,147	CONT1_ACI_SUM1_POST1.OUT
07/16/2014	01:44 PM	617,031	TKC1_ACI_angles_1_POST1.OUT
08/02/2014	03:49 AM	54,465	TKC1_ACI_MIN2049.OUT
07/16/2014	01:51 PM	55,184	CONT1_ACI_MAX1.OUT
07/16/2014	01:44 PM	17,396	real.out
Directory of L:\Projects\20000's\20906\QA\Documents\ANSYS\2014-7-10 LBS waste HSS sectBB			
05/27/2011	01:03 PM	30,502	spectra_target (LBS).inp
07/11/2014	08:30 AM	72,666	connect.inp
05/27/2014	08:29 AM	28,811	postproc.inp
05/27/2011	01:03 PM	30,502	spectra_target.inp
05/09/2014	11:15 AM	8,072	BC.inp
07/11/2014	09:26 AM	26,863	post-cont.inp
05/13/2014	12:05 PM	26,285	SOFE.inp
07/02/2014	04:25 PM	39,430	SOFA.inp
05/02/2014	08:49 AM	23,722	SOIL_properties (BES SST).inp
06/17/2014	02:34 PM	36,633	SOFO.inp
06/18/2014	03:01 PM	8,888	solution.inp
05/27/2011	01:03 PM	37,532	th-10ms-v.inp
06/04/2014	01:23 PM	23,724	TKCW.inp
05/27/2011	01:03 PM	30,201	spectra_target (UBS).inp
05/02/2014	08:48 AM	21,419	SOIL_properties (UBS SST).inp
05/29/2014	03:45 PM	5,161	!TKCP.inp
05/27/2011	01:03 PM	37,545	th-10ms-h.inp
05/27/2011	01:03 PM	37,545	th-10ms-h (LBS SST).inp
05/27/2011	01:03 PM	30,500	spectra_target (BES).inp
05/27/2011	01:03 PM	37,532	th-10ms-v (LBS SST).inp
07/03/2014	08:37 AM	15,861	PITS.inp
05/21/2014	12:56 PM	32,971	!TKC_properties.inp
06/24/2014	04:16 PM	20,394	prepost.inp
06/24/2014	03:29 PM	14,372	subtract_gravity.inp
07/02/2014	10:26 AM	12,291	WAST.inp
12/31/2013	02:41 PM	2,191	postproc_soil_strain.inp
05/05/2014	01:14 PM	25,754	SOIL_properties.inp
07/01/2014	12:13 PM	110,380	spectra.inp
05/31/2014	12:00 PM	11,521	subtract_cont.inp
05/27/2011	01:03 PM	37,545	th-10ms-h (UBS SST).inp
05/27/2014	01:46 PM	30,002	post1.inp
07/10/2014	10:41 AM	41,342	plotmacrolib.inp
05/05/2014	01:14 PM	25,754	SOIL_properties (LBS SST).inp

Date	Time	Size	File Name
07/11/2014	09:30 AM	20,501	plots.inp
06/04/2014	01:23 PM	27,656	TKCD.inp
05/27/2011	01:03 PM	37,531	th-10ms-v (UBS SST).inp
06/18/2014	02:55 PM	9,076	solution_TH.inp
07/02/2014	04:42 PM	18,872	assembly.inp
07/03/2014	09:43 AM	5,778	Surface_load.inp
05/27/2011	01:03 PM	37,532	th-10ms-v (BES SST).inp
06/04/2014	01:23 PM	25,635	TKCF.inp
06/13/2014	02:26 PM	11,822	Modify.inp
05/27/2011	01:03 PM	37,544	th-10ms-h (BES SST).inp
06/17/2014	08:58 AM	31,202	SOUD.inp
Directory of L:\Projects\20000's\20906\QA\Documents\ANSYS\2014-7-10 LBS waste HSS sectBB			
03/24/2011	11:00 AM	21,123	UB-SPTR-V.txt
03/24/2011	11:00 AM	21,121	BE-SPTR-V.txt
03/24/2011	11:02 AM	21,416	SC-SPTR-H.txt
03/24/2011	11:00 AM	21,424	SC-SPTR-V.txt
03/24/2011	11:00 AM	21,424	LB-SPTR-V.txt
03/24/2011	11:02 AM	21,115	BE-SPTR-H.txt
03/24/2011	11:02 AM	21,113	UB-SPTR-H.txt
03/24/2011	11:02 AM	21,416	LB-SPTR-H.txt
Directory of L:\Projects\20000's\20906\QA\Documents\ANSYS\2014-7-10 LBS waste HSS sectBB			
07/30/2014	04:27 AM	54,894	TKC1_ACI_MAX2049.OUT
07/16/2014	06:17 PM	54,763	CONT1_ACI_MIN1.OUT
07/16/2014	06:11 PM	51,689	TKC1_ACI_SUM1_POST1.OUT
07/30/2014	04:32 AM	54,763	CONT1_ACI_MIN2049.OUT
07/30/2014	04:27 AM	1,050,658	TKC_ACI_angles2049.OUT
07/16/2014	06:17 PM	54,894	TKC1_ACI_MAX1.OUT
07/30/2014	04:24 AM	432,094	SPTR-disp.out
07/30/2014	04:32 AM	55,188	CONT1_ACI_SUM2049.OUT
07/16/2014	06:17 PM	1,149,821	CONT1_ACI_angles1.OUT
07/30/2014	04:27 AM	54,894	TKC1_ACI_SUM2049.OUT
07/16/2014	06:17 PM	1,050,658	TKC_ACI_angles1.OUT
07/16/2014	06:17 PM	54,469	TKC1_ACI_MIN1.OUT
07/16/2014	06:17 PM	61,682	solution.out
07/16/2014	06:11 PM	33,306	mplist.out
07/30/2014	04:24 AM	460,750	SPTR-accel.out
07/16/2014	06:17 PM	55,188	CONT1_ACI_SUM1.OUT
07/30/2014	04:32 AM	50,537	CONT1_ACI_SUM_seismic_only.OUT
07/16/2014	06:11 PM	13,165	elist.out
07/16/2014	06:11 PM	429,158	CONT_angles_1_POST1.OUT
07/30/2014	04:20 AM	2,600	QAoutput.out
07/30/2014	04:24 AM	62,696	TKC_TH_POST26_U.OUT

Date	Time	Size	File Name
07/16/2014	06:17 PM	54,894	TKC1_ACI_SUM1.OUT
07/16/2014	06:10 PM	56,498	Model_MAT_data.out
07/30/2014	04:32 AM	1,149,821	CONT1_ACI_angles2049.OUT
07/16/2014	06:04 PM	158,661	Model_GEO_data.OUT
07/30/2014	04:32 AM	55,188	CONT1_ACI_MAX2049.OUT
07/30/2014	04:32 AM	51,224	TKC1_ACI_SUM_seismic_only.OUT
07/16/2014	06:11 PM	52,151	CONT1_ACI_SUM1_POST1.OUT
07/16/2014	06:11 PM	617,035	TKC1_ACI_angles_1_POST1.OUT
07/30/2014	04:27 AM	54,469	TKC1_ACI_MIN2049.OUT
07/16/2014	06:17 PM	55,188	CONT1_ACI_MAX1.OUT
07/16/2014	06:11 PM	17,654	real.out
Directory of L:\Projects\20000's\20906\QA\Documents\ANSYS\2014-7-10 LBS waste HSS sectAA (initial friction)			
05/27/2011	01:03 PM	30,502	spectra_target (LBS).inp
08/12/2014	12:40 PM	72,483	connect.inp
05/27/2014	08:29 AM	28,811	postproc.inp
05/27/2011	01:03 PM	30,502	spectra_target.inp
05/09/2014	11:15 AM	8,072	BC.inp
07/11/2014	09:26 AM	26,863	post-cont.inp
05/13/2014	12:05 PM	26,285	SOFE.inp
07/02/2014	04:25 PM	39,430	SOFA.inp
05/02/2014	08:49 AM	23,722	SOIL_properties (BES SST).inp
06/17/2014	02:34 PM	36,633	SOFO.inp
06/18/2014	03:01 PM	8,888	solution.inp
05/27/2011	01:03 PM	37,532	th-10ms-v.inp
06/04/2014	01:23 PM	23,724	TKCW.inp
05/27/2011	01:03 PM	30,201	spectra_target (UBS).inp
05/02/2014	08:48 AM	21,419	SOIL_properties (UBS SST).inp
05/29/2014	03:45 PM	5,161	!TKCP.inp
05/27/2011	01:03 PM	37,545	th-10ms-h.inp
05/27/2011	01:03 PM	37,545	th-10ms-h (LBS SST).inp
05/27/2011	01:03 PM	30,500	spectra_target (BES).inp
05/27/2011	01:03 PM	37,532	th-10ms-v (LBS SST).inp
07/03/2014	08:36 AM	15,862	PITS.inp
05/21/2014	12:56 PM	32,971	!TKC_properties.inp
06/24/2014	04:16 PM	20,394	prepost.inp
06/24/2014	03:29 PM	14,372	subtract_gravity.inp
07/02/2014	10:26 AM	12,291	WAST.inp
12/31/2013	02:41 PM	2,191	postproc_soil_strain.inp
05/05/2014	01:14 PM	25,754	SOIL_properties.inp
07/01/2014	12:13 PM	110,380	spectra.inp
05/31/2014	12:00 PM	11,521	subtract_cont.inp
05/27/2011	01:03 PM	37,545	th-10ms-h (UBS SST).inp
05/27/2014	01:46 PM	30,002	post1.inp

Date	Time	Size	File Name
07/10/2014	10:41 AM	41,342	plotmacrolib.inp
05/05/2014	01:14 PM	25,754	SOIL_properties (LBS SST).inp
07/11/2014	09:30 AM	20,501	plots.inp
06/04/2014	01:23 PM	27,656	TKCD.inp
05/27/2011	01:03 PM	37,531	th-10ms-v (UBS SST).inp
06/18/2014	02:55 PM	9,076	solution_TH.inp
07/10/2014	11:13 AM	18,872	assembly.inp
07/03/2014	09:43 AM	5,778	Surface_load.inp
05/27/2011	01:03 PM	37,532	th-10ms-v (BES SST).inp
06/04/2014	01:23 PM	25,635	TKCF.inp
06/13/2014	02:26 PM	11,822	Modify.inp
05/27/2011	01:03 PM	37,544	th-10ms-h (BES SST).inp
06/17/2014	08:58 AM	31,202	SOUD.inp
Directory of L:\Projects\20000's\20906\QA\Documents\ANSYS\2014-7-10 LBS waste HSS sectAA (initial friction)			
03/24/2011	11:00 AM	21,123	UB-SPTR-V.txt
03/24/2011	11:00 AM	21,121	BE-SPTR-V.txt
03/24/2011	11:02 AM	21,416	SC-SPTR-H.txt
03/24/2011	11:00 AM	21,424	SC-SPTR-V.txt
03/24/2011	11:00 AM	21,424	LB-SPTR-V.txt
03/24/2011	11:02 AM	21,115	BE-SPTR-H.txt
03/24/2011	11:02 AM	21,113	UB-SPTR-H.txt
03/24/2011	11:02 AM	21,416	LB-SPTR-H.txt
Directory of L:\Projects\20000's\20906\QA\Documents\ANSYS\2014-7-10 LBS waste HSS sectAA (initial friction)			
08/12/2014	03:55 PM	54,782	CONT1_ACI_MIN1.OUT
08/12/2014	03:50 PM	51,708	TKC1_ACI_SUM1_POST1.OUT
08/16/2014	01:07 AM	54,488	TKC1_ACI_MIN513.OUT
08/16/2014	01:07 AM	54,913	TKC1_ACI_MAX513.OUT
08/12/2014	03:55 PM	54,913	TKC1_ACI_MAX1.OUT
08/16/2014	01:05 AM	170,993	SPTR-disp.out
08/12/2014	03:55 PM	1,149,281	CONT1_ACI_angles1.OUT
08/12/2014	03:55 PM	1,050,658	TKC_ACI_angles1.OUT
08/16/2014	01:07 AM	1,050,658	TKC_ACI_angles513.OUT
08/12/2014	03:55 PM	54,488	TKC1_ACI_MIN1.OUT
08/12/2014	03:55 PM	68,641	solution.out
08/12/2014	03:49 PM	33,678	mplist.out
08/16/2014	01:05 AM	199,649	SPTR-accel.out
08/12/2014	03:55 PM	55,207	CONT1_ACI_SUM1.OUT
08/16/2014	01:09 AM	1,149,281	CONT1_ACI_angles513.OUT
08/16/2014	01:07 AM	54,913	TKC1_ACI_SUM513.OUT
08/16/2014	01:09 AM	50,537	CONT1_ACI_SUM_seismic_only.OUT

Date	Time	Size	File Name
08/12/2014	03:49 PM	13,165	elist.out
08/12/2014	03:50 PM	429,177	CONT_angles_1_POST1.OUT
08/16/2014	01:04 AM	2,638	QAoutput.out
08/16/2014	01:06 AM	62,715	TKC_TH_POST26_U.OUT
08/12/2014	03:55 PM	54,913	TKC1_ACI_SUM1.OUT
08/16/2014	01:09 AM	54,782	CONT1_ACI_MIN513.OUT
08/12/2014	03:49 PM	56,498	Model_MAT_data.out
08/12/2014	03:43 PM	158,661	Model_GEO_data.OUT
08/16/2014	01:09 AM	55,207	CONT1_ACI_SUM513.OUT
08/16/2014	01:09 AM	51,243	TKC1_ACI_SUM_seismic_only.OUT
08/12/2014	03:50 PM	52,170	CONT1_ACI_SUM1_POST1.OUT
08/16/2014	01:09 AM	55,207	CONT1_ACI_MAX513.OUT
08/12/2014	03:50 PM	617,054	TKC1_ACI_angles_1_POST1.OUT
08/12/2014	03:55 PM	55,207	CONT1_ACI_MAX1.OUT
08/12/2014	03:49 PM	17,654	real.out

Pacific Northwest
NATIONAL LABORATORY

Proudly Operated by Battelle *Since 1965*

U.S. DEPARTMENT OF
ENERGY

902 Battelle Boulevard
P.O. Box 999
Richland, WA 99352
1-888-375-PNNL (7665)
www.pnl.gov